NEW MEXICO DEPARTMENT OF TRANSPORTATION

# RESEARCH BUREAU

Innovation in Transportation

# Laboratory Dynamic Modulus of Asphalt Mixes and Resilient Modulus of Soils Throughout New Mexico for the Implementation of Mechanistic Empirical Pavement Design Guide (MEPDG)

## PART 1: Laboratory Dynamic Modulus of Asphalt Mixes

Prepared by:
University of New Mexico
Albuquerque, NM 87131

Prepared for:
New Mexico Department of Transportation
Research Bureau
7500B Pan American Freeway NE
Albuquerque, NM 87109

In Cooperation with:
The US Department of Transportation
Federal Highway Administration

**Report NM11MSC-01**

AUGUST 5, 2013

**FINAL REPORT**

**Project No. NM11MSC-01**

# LABORATORY DYNAMIC MODULUS OF ASPHALT MIXES AND RESILIENT MODULUS OF SOILS THROUGHOUT NEW MEXICO FOR THE IMPLEMENTATION OF MECHANISTIC EMPIRICAL PAVEMENT DESIGN GUIDE (MEPDG)

## PART 1: LABORATORY DYNAMIC MODULUS OF ASPHALT MIXES

**Report Submitted to**
Research Bureau
New Mexico Department of Transportation
7500B Pan American Freeway NE, PO Box 94690
Albuquerque, NM 87199-4690
(505)-841-9145

**Prepared by**
Rafiqul A. Tarefder, Ph.D., P.E., Associate Professor and Regents' Lecturer
Mekdim T. Weldegiorgis, Graduate Research Assistant

Department of Civil Engineering
University of New Mexico
Albuquerque, N.M. 87131

University of New Mexico
August 05, 2013

## SUMMARY PAGE

| | | | |
|---|---|---|---|
| **1. Report No.**<br>NM11MSC-01- Final Report | | **2. Recipient's Catalog No.** | |
| **3. Title and Subtitle**<br>Laboratory Dynamic Modulus of Asphalt Mixes and Resilient Modulus of Soils throughout New Mexico for the Implementation of Mechanistic Empirical Pavement Design Guide<br>Part1: Laboratory Dynamic Modulus of Asphalt Mixes | | **4. Report Date**<br>August 5, 2013 | |
| **5. Author(s):**<br>Mekdim T. Weldegiorgis and Rafiqul A. Tarefder | | **6. Performing Organization Report No.**<br>456-325F | |
| **7. Performing Organization Name and Address**<br>University of New Mexico, Department of Civil Engineering, MSC01 1070, 1 University of New Mexico, Albuquerque, NM 87131 | | **8. Performing Organization Code**<br>456A<br>**9. Contract/Grant No.**<br>456-325 | |
| **10. Sponsoring Agency Name and Address**<br>Research Bureau, 7500B Pan American Freeway,<br>PO Box 94690, Albuquerque, NM 87199-4690 | | **11. Type of Report and Period Covered**<br>Final Report<br>September 1,2010 – July 31, 2013<br>**12. Sponsoring Agency Code** | |
| **13. Supplementary Notes**<br>The research project is funded by NMDOT in cooperation with the FHWA | | | |
| **14. Abstract**<br>This report presents dynamic modulus (*E**) testing results conducted on three plant produced and two laboratory prepared asphalt mixes. The AASHTO TP 62-07 test standard is followed for *E** testing. *E** mastercurves are developed for all mixes. The *E** mastercurve plots show that Superpave (SP) SP II mixes have higher dynamic modulus than SP III mixes. The SP-IV mix exhibits lowest dynamic modulus. The accuracy of test results is insured through independent assurance (IA) tests. One-way analysis of variance (ANOVA) shows that there is no significant difference in *E** data obtained from two different laboratories. This confirms that the data reported in this report are accurate. Viscosity based Witczak model, dynamic shear modulus based Witczak model, and the Hirsch model are employed to predict dynamic moduli from mix information. All three models are found to underpredict measured *E** values of New Mexico mixes. Model predictions differs from laboratory *E** values significantly at high temperatures. An attempt is made in this study to modify the viscosity based Witczak model by giving more emphasis on mix volumetric variables. The modified model shows significant improvements in prediction accuracy over the viscosity based Witczak model. This study recommends the use of mix master curves as well as modified (by UNM) viscosity based Witczak model in the design pavements using Mechanistic Empirical Pavement Design Guide (MEPDG), now called DARWin-ME, in New Mexico. | | | |
| **15. Key Words**<br>Complex Dynamic Modulus, Asphalt Mixtures, Phase Angle, Master Curve | | **16. Distribution Statement**<br>*Available from NMDOT Research Bureau* | |
| **17. Security Classi. of the Report**<br>None | **18. Security Classi. of this page**<br>None | **19. Number of Pages**<br>330 | **20. Price**<br>N/A |

## PREFACE

The research report herein determines the dynamic modulus of asphalt mixes for the state of New Mexico. These dynamic moduli are input for MEPDG at level 2 analyses for New Mexico Department of Transportation.

## NOTICE

The United States government and the State of New Mexico do not endorse products or manufacturers. Trade or manufactures' names appear herein solely because they are considered essential to the object of this report. This information is available in alternative accessible formats. To obtain an alternative format, contact the NMDOT Research Bureau, 7500B Pan American Freeway NE, PO Box 94690, Albuquerque, NM 87199-4690, (505)-841-9145

## DISCLAIMER

This report presents the results of research conducted by the authors and does not necessarily reflect the views of the New Mexico Department of Transportation. This report does not constitute a standard or specification.

## ACKNOWLEDGEMENTS

The authors would like to express their sincere gratitude and appreciation to Jeff Mann, Pavement Design Section Head of NMDOT, for being the advocate of this project and his regular support, sponsorship, and suggestions. The authors would like to thank Bob Meyers, previously Materials Bureau Chief and currently, Geotechnical Section Manager, NMDOT Materials Bureau, for his sponsorship and support for this project. The UNM research team appreciates the valuable service and time of the Project Manager Mr. Virgil Valdez for this project.

The UNM research team would like to thank the Project Technical panel for their valuable suggestions during the quarterly meeting. Special thanks go to several Project Panel members namely, James Gallegos, Manager, Asphalt Section, NMDOT Materials Bureau, Parveez Anwar, State Asphalt Engineer, NMDOT Materials Bureau, and Bryce Simons, NMDOT Materials Testing Engineer, Kelly Montoya, Pavement Design Engineer, and Robert McCoy, previously Pavement Exploration Section Head, now Research Implementation Engineer for their assistance and suggestions for this project.

This project is funded by the New Mexico Department of Transportation (NMDOT)'s Research Bureau. The authors would like to thank the research Bureau Chief, Scott McClure for his support, and Administrator, Dee Billingsley for her fine accounting and reimbursements. The authors would like to thank several members and personnel at UNM for their support. Special thanks go Rebekah Lucero, UNM Civil Engineering accountant.

# TABLE OF CONTENTS

SUMMARY PAGE ..... ii
PREFACE ..... ii
NOTICE ..... iii
DISCLAIMER ..... iii
TABLE OF CONTENTS ..... v
LIST OF TABLES ..... ix
LIST OF FIGURES ..... x

**Chapter 1 ..... 1**

1.1. Research Need and Significance ..... 1
1.2. Objective ..... 2
1.3. Report Organization ..... 2
1.4. Reference ..... 2

**Chapter 2 ..... 2-1**

2.1. Viscoelastic Materials ..... 2-1
2.2. Dynamic Modulus ..... 2-2
2.3. Temperature dependent behavior of viscous materials ..... 2-3
2.4. Application of Viscoelasticity in Asphalt Concrete studies ..... 2-4
2.5. Factors Affecting Dynamic Modulus of Asphalt Concrete ..... 2-5
2.6. Laboratory Test Methods for Asphalt Concrete Dynamic Modulus $\mathbf{E}^*$ ..... 2-6
2.6.1. AASHTO TP62 - Standard Method of Test for Determining Dynamic Modulus of Hot-Mix Asphalt Concrete Mixtures ..... 2-7
2.6.2. ASTM D3479-79 - Standard Test Method for Dynamic Modulus of Asphalt mixtures 2-7
2.6.3. Confined Dynamic Modulus Testing Protocol ..... 2-7
2.6.4. Simplified Dynamic Modulus Testing Protocol ..... 2-8
2.6.5. Dynamic Shear Modulus $\mathbf{G}^*$ test / Simple shear (SST) test ..... 2-8
2.6.6. Indirect Tension test ..... 2-9
2.6.7. Hollow cylinder tensile test (HCT) ..... 2-9
2.7. Models to Predict Asphalt Concrete E* ..... 2-9
2.7.1. Viscosity based Witczak Predictive Model ..... 2-10
2.7.2. Dynamic Shear Modulus based Witczak Predictive Model ..... 2-10
2.7.3. Hirsch Model ..... 2-11
2.7.4. Application of Witczak and Hirsh Models ..... 2-12
2.7.5. Universal Material Model ..... 2-13
2.7.6. Stress-Dependent Stiffness Predictive Equation ..... 2-13
2.7.7. Neural-Network Models ..... 2-14

2.7.8. References....2-14

**Chapter 3....3-18**

3.1. Introduction....3-18
3.2. Objective....3-18
3.3. Test matrix....3-18
3.4. Test Apparatus....3-19
3.4.1. Dynamic Modulus Testing System....3-19
3.4.2. Gyratory Compactor....3-19
3.4.3. Coring Machine....3-19
3.4.4. Diamond Cutting Edge Eet Saw....3-19
3.4.5. Loading Button Fixer....3-20
3.5. Sample collection and Fabrication....3-20
3.5.1. Sample Collection....3-20
3.5.2. Sieve Analysis Test (AASHTO T-27)....3-20
3.5.3. Asphalt content (AASHTO T-308)....3-21
3.5.4. Theoretical Maximum Gravity (**Gmm**) (AASHTO-T-209)....3-21
3.5.5. Sample Compaction (AASHTO T-312)....3-21
3.5.6. Bulk Specific Gravity (**Gmb**) (AASHTO T-166)....3-22
3.5.7. Percent Air Void Determination (Volumetric calculation)....3-22
3.5.8. Air Void Uniformity Check....3-22
3.5.9. **E** ∗ Test Specimen Geometric Requirements....3-22
3.6. Test Setup....3-23
3.7. Test Procedure....3-23
3.8. Test results and Analysis....3-24
3.8.1. Raw Data....3-24
3.8.2. Stress and Strain Data....3-25
3.8.3. Dynamic Modulus Data Analysis and Presentation....3-26
3.8.4. Time Temperature Superposition Principle (TTSP)....3-26
3.8.5. Shift Factor Functions....3-27
3.8.6. Master Curve....3-28
3.9. Dynamic Modulus Results for SPIII with PG 70-22 (Plant Mix)....3-30
3.10. Dynamic Modulus Results of SPIII Mix with PG 64-22 (Laboratory Mix)....3-30
3.11. Dynamic Modulus Results of SPII Mix with PG 64-22 (Plant Mix)....3-31
3.12. Dynamic Modulus Results of SPII Mix with PG 70-22 (Laboratory Mix)....3-31
3.13. Dynamic Modulus Results of SPIV Mix with PG 70-22 (Commercial Mix)....3-32
3.14. Comparison of SP-II, SPIII and SP-IV dynamic modulus data....3-32
3.15. Conclusions....3-32
3.16. Reference....3-33

**Chapter 4....4-71**

4.1. Introduction....4-71
4.2. Objective....4-72
4.3. Methodology....4-73
4.4. E*-Test Matrix....4-74

4.5. Results and Discussion ....4-74
4.5.1. E*-Trend Plots ....4-74
4.5.2. Coefficient of Variation (COV) Plots ....4-75
4.5.3. Within-Laboratory Consistency k-statistic Plots ....4-76
4.5.4. Between-Laboratory Consistency h-statistic Plots ....4-77
4.5.5. Mastercurve Comparison ....4-78
4.5.6. One-way ANOVA Analysis ....4-78
4.5.7. Repeatability Analysis ....4-79
4.5.8. Reproducibility Analysis ....4-80
4.6. Conclusions ....4-81
4.7. Reference ....4-81

**Chapter 5 ....5-107**

5.1. Introduction ....5-107
5.2. Objective ....5-107
5.3. Viscosity Based Witczak Model ....5-107
5.4. Analysis Method ....5-108
5.5. Application of Viscosity ($\boldsymbol{\eta}$) based Witczak Model using Default *A* and *VTS* values ....5-108
5.6. Level-3 $\mathbf{E}*$ Mastercurve prediction in MEPDG ....5-109
5.7. Application of Viscosity ($\boldsymbol{\eta}$) Based Witczak Model using Actual *A* and *VTS* values ....5-109
5.8. Level-2 $\mathbf{E}*$ Mastercurve Prediction in MEPDG ....5-110
5.9. Past Performance Evaluation of $\boldsymbol{\eta}$-based Witczak Model ....5-110
5.10. Maneuvering MEPDG inputs for Level-3 $\mathbf{E}*$ Mastercurve Predictions ....5-111
5.11. Modification of $\boldsymbol{\eta}$-based Witczak model ....5-112
5.12. Performance evaluation using Goodness of Fit Statistic ....5-115
5.12.1. Prediction Capacity of Modified $\boldsymbol{\eta}$-Based Model ....5-115
5.12.2. Frequency Distribution of Residuals ....5-116
5.13. Model Sensitivity Analysis ....5-116
5.13.1. Model Sensitivity to $\mathbf{Va}$ ....5-117
5.13.2. Model Sensitivity to $\mathbf{Veff}$ ....5-117
5.13.3. Model Sensitivity to $\boldsymbol{\rho 200}$ ....5-118
5.14. Conclusions ....5-118
5.15. References ....5-119

**Chapter 6 ....6-139**

6.1. Introduction ....6-139
6.2. Objectives ....6-139
6.3. Dynamic Shear Modulus Based Witczak Predictive Model ....6-139
6.4. Analysis Method ....6-140
6.4.1. Application of G* Based Model Using Default *A* and *VTS* Values Of MEPDG 6-140
6.4.2. Application of G* Based Model Using Actual *A* and *VTS* Values of MEPDG6-141
6.4.3. Application of G*-based model by using $\mathbf{G}*$ and $\boldsymbol{\delta}$ Mastercurves ....6-142

6.5. Conclusions ..... 6-144
6.6. References ..... 6-144

**Chapter 7 ..... 7-153**

7.1. Introduction ..... 7-153
7.2. Objectives ..... 7-153
7.3. Hirsch Model ..... 7-153
7.4. Analysis Method ..... 7-154
7.4.1. Application of Hirsch model using Default A and VTS values of MEPDG ... 7-154
7.4.2. Application of Hirsch model using Actual A and VTS determine through DSR testing ..... 7-155
7.4.3. Application of Hirsh Model by using $\mathbf{G}*$ and $\boldsymbol{\delta}$ Mastercurves ..... 7-156
7.5. Conclusion ..... 7-156
7.6. References ..... 7-156

**Chapter 8 ..... 8-164**

8.1. General ..... 8-164
8.2. Conclusions ..... 8-164
8.3. Recommendations ..... 8-166

**APPENDIX A ..... 168**
**APPENDIX B ..... 181**
**APPENDIX C ..... 194**
**APPENDIX D ..... 207**
**APPENDIX E ..... 220**
**APPENDIX F ..... 233**
**APPENDIX G ..... 258**

# LIST OF TABLES

Table 3.1: Test Matrix for Dynamic Modulus ..... 3-35

Table 3.2: Asphalt Content Test Results ..... 3-36

Table 3.3: Theoretical Maximum Specific Gravity Test ..... 3-37

Table 3.4: Recommended Handling Temperatures ..... 3-38

Table 3.5: Bulk Specific Gravity Test ..... 3-39

Table 3.6: Percentage Air Voids Test ..... 3-40

Table 3.7: Air Void Uniformity Check ..... 3-41

Table 4.1: Test Matrix for Dynamic Modulus ..... 4-83

Table 4.2: ANOVA Analysis Results ..... 4-84

Table 5.1: Average Percent Difference between Witczak predicted and tested E* data ... 5-121

Table 5.2: DSR test Results for PG 64-22 and PG 70-22 ..... 5-121

Table 5.3: Original and Optimized Mix Variables for MEPDG Level-3 Analysis ..... 5-122

Table 5.4: Goodness of Fit of the Modified $\eta$-based Model ..... 5-122

Table 5.5: Average Percent Difference between Witczak predicted and tested E* data ... 5-123

Table 6.1: Average Percent Difference between Witczak Predicted and Measured E* Data Using Default *A* and *VTS* Values ..... 6-145

Table 6.2: Average Percent Difference between Witczak predicted and Tested *E** Data Using Actual *A* and *VTS* Values ..... 6-145

Table 6.3: Mastercurve Parameters for Binders (Ref. Temp = 21 °c) ..... 6-145

Table 7.1: Average Percent Difference between Hirsch Predicted and Measured *E** Data Using Default *A* and *VTS* Values ..... 7-158

Table 7.2: Average Percent Difference between Hirsch Predicted and Tested E* Data Using Actual A and VTS Values ..... 7-158

## LIST OF FIGURES

Figure 3.1: Servo-Hydraulic Testing System ..... 3-42

Figure 3.2: Linear Variable Differential Transformers (LVDTs) Mounted On Specimen 3-42

Figure 3.3: Gyratory Compactor ..... 3-43

Figure 3.4: Asphalt Coring Machine ..... 3-43

Figure 3.5: Lab Specimen Saw ..... 3-44

Figure 3.6: Automatic Positioning Fixture ..... 3-44

Figure 3.7: Rock Flatness Gauge ..... 3-45

Figure 3.8: straightedge and feeler gauge for Waviness check ..... 3-45

Figure 3.9: Sieve analysis for SP-II and SP-III mixes ..... 3-46

Figure 3.10: Typical stress, strain vs. Time Plot at Temperature (-10°C) ..... 3-47

Figure 3.11: Comparison Master Curves with %AV for SP-III with PG 70-22 ..... 3-48

Figure 3.12: Isothermal Plot for Average of SP-III, PG 70-22 ..... 3-48

Figure 3.13: Isochronal Plot for Average of SP-III, PG 70-22 ..... 3-49

Figure 3.14: Master Curve for Average of SP-III, PG 70-22 ..... 3-49

Figure 3.15: Shift Factor for Average of SP-III, PG 70-22 ..... 3-50

Figure 3.16: Cole and Cole Plot for Average of SP-III, PG 70-22 ..... 3-50

Figure 3.17: Black Space Plot for Average of SP-III, PG 70-22 ..... 3-51

Figure 3.18: Loss Tangent Plot for Average of SP-III, PG 70-22 ..... 3-51

Figure 3.19: Comparison Master Curves for SP-III, PG 64-22 Test Results ..... 3-52
Figure 3.20: Isothermal Plot for Average of SP-III, PG 64-22..... 3-52
Figure 3.21: Isochronal Plot for Average of SP-III, PG 64-22..... 3-53
Figure 3.22: Master Curve for Average of SP-III, PG 64-22 ..... 3-53
Figure 3.23: Shift Factor for Average of SP-III, PG 64-22 ..... 3-54
Figure 3.24: Cole and Cole Plot for Average of SP-III, PG 64-22..... 3-55
Figure 3.25: Black Space Plot for Average of SP-III, PG 64-22..... 3-55
Figure 3.26: Loss Tangent Plot for Average of SP-III, PG 64-22 ..... 3-56
Figure 3.27: Comparison Master Curves for SP-II, PG 64-22 Test Results..... 3-57
Figure 3.28: Isothermal Plot for Average of SP-II, PG 64-22..... 3-57
Figure 3.29: Isochronal Plot for Average of SP-II, PG 64-22 ..... 3-58
Figure 3.30: Master Curve for Average of SP-II, PG 64-22..... 3-58
Figure 3.31: Shift Factor for Average of SP-II, PG 64-22..... 3-59
Figure 3.32: Cole and Cole Plot for Average of SP-II, PG 64-22 ..... 3-59
Figure 3.33: Black Space Plot for Average of SP-II, PG 64-22 ..... 3-60
Figure 3.34: Loss Tangent Plot for Average of SP-II, PG 64-22 ..... 3-60
Figure 3.35: Comparison Master Curves for SP-II, PG 70-22 Test Results..... 3-61
Figure 3.36: Isothermal Plot for Average of SP-II, PG 70-22..... 3-61
Figure 3.37: Isochronal Plot for Average of SP-II, PG 70-22 ..... 3-62
Figure 3.38: Master Curve for Average of SP-II, PG 70-22..... 3-63
Figure 3.39: Shift Factor for Average of SP-II, PG 70-22..... 3-63
Figure 3.40: Cole and Cole Plot for Average of SP-II, PG 70-22 ..... 3-64
Figure 3.41: Black Space Plot for Average of SP-II, PG 70-22 ..... 3-64
Figure 3.42: Loss Tangent Plot for Average of SP-II, PG 70-22 ..... 3-65

Figure 3.43: Comparison of Master Curves for SP-IV, PG 70-22 Test Results ..... 3-66

Figure 3.44: Isothermal Plot for Average of SP-IV, PG 70-22 ..... 3-66

Figure 3.45: Isochronal Plot for Average of SP-IV, PG 70-22 ..... 3-67

Figure 3.46: Master Curve for Average of SP-IV, PG 70-22 ..... 3-67

Figure 3.47: Shift Factor for Average of SP-IV, PG 70-22 ..... 3-68

Figure 3.48: Cole and Cole Plot for Average of SP-IV, PG 70-22 ..... 3-68

Figure 3.49: Black Space Plot for Average of SP-IV, PG 70-22 ..... 3-69

Figure 3.50: Loss Tangent Plot for Average of SP-IV, PG 70-22 ..... 3-69

Figure 3.51: Comparison Master Curves for SP-II, SP-III and SP-IV Test Results ..... 3-70

Figure 4.1: (a-d) Concepts of Precision and Accuracy. ..... 4-85

Figure 4.2 (a-e) $E^*$- Trend Plots as A Function of Frequency and Temperature. ..... 4-88

Figure 4.3 (a-e) Coefficient of Variation (COV) Plots. ..... 4-91

Figure 4.4 (a-e) Within-Laboratory Consistency ($k$-Statistic) Plots. ..... 4-94

Figure 4.5 (a-e) Between Laboratories $h$-statistic Plots. ..... 4-97

Figure 4.6 (a-e) Mastercurve Plots ..... 4-100

Figure 4.7 (a-e) Repeatability Analysis of $E^*$-Results From UNM and AMEC Laboratories. ..... 4-103

Figure 4.8 (a-e) Reproducibility Analysis of $E^*$-Results From UNM and AMEC Laboratories. ..... 4-106

Figure 5.1(a-e): $\boldsymbol{\eta}$-based Witczak model predicted vs. Laboratory Measured $\boldsymbol{E^*}$ ..... 5-125

Figure 5.2: Scatter Plot for $\eta$-Based Witczak Model Predicted Vs. Laboratory Measured $E^*$ Data ..... 5-126

Figure 5.3: Trend of Prediction % Error For $\eta$-Based Witczak Model ..... 5-127

Figure 5.4: MEPDG Level-3 Mastercurve Prediction vs. Mastercurve Developed for Laboratory $\boldsymbol{E^*}$ Test Results ..... 5-128

Figure 5.5: DSR Test Results and A and VTS Relationship for PG 64-22 ..... 5-129

Figure 5.6: DSR Test Results and A and VTS Relationship for PG 70-22 ..... 5-130

Figure 5.7: Scatter Plot for $\eta$-Based Witczak Model Prediction Using Actual *A* And *VTS* Developed Through Laboratory DSR Test ..... 5-131

Figure 5.8: MEPDG Level-2 Mastercurve Prediction vs. Mastercurve Developed for Laboratory $E*$ Test Results ..... 5-132

Figure 5.9: MEPDG Level-3 Mastercurve Predictions Using Optimized Mix Data Vs. Mastercurve Developed for Laboratory $E*$ Test Results ..... 5-133

Figure 5.10: Predicted Vs. Measured Scatter Plot ..... 5-134

Figure 5.11: Scatter Plot for New Modified Model ..... 5-135

Figure 5.12: Trend of Prediction % Errors for New Modified Model ..... 5-136

Figure 5.13: Frequency Distribution of *E** Residuals ..... 5-137

Figure 5.14: Sensitivity Analysis for the New Modified Model ..... 5-138

Figure 6.1: Scatter Plot for $\mathbf{G}*$-Based Witczak Model Prediction Using Default *A* and *VTS* Values From MEPDG. ..... 6-146

Figure 6.2: Trend of Prediction % error for $G*$-based Witczak model using default A and VTS values from MEPDG. ..... 6-147

Figure 6.3: Scatter Plot For $G*$-Based Witczak Model Prediction Using Actual *A* and *VTS* Values Determined From Laboratory DSR Test. ..... 6-148

Figure 6.4: Trend of Prediction % Error for $G*$-Based Witczak Model Using Default *A* and *VTS* Values from MEPDG ..... 6-149

Figure 6.5: *G** and Phase Angle Mastercurves For PG 64-22 ..... 6-150

Figure 6.6: G* and Phase angle mastercurves for PG 70-22 ..... 6-151

Figure 6.7: Scatter Plot for G $*$-Based Witczak Model Prediction Using *G** and Phase Angle Mastercurves. ..... 6-152

Figure 7.1: Scatter Plot for Hirsch Model Prediction Using Default *A* And *VTS* Values From MEPDG. ..... 7-159

Figure 7.2: Trend of Prediction % Error for Hirsch Model Using Default *A* And *VTS* Values From MEPDG. ..... 7-160

Figure 7.3: scatter plot for Hirsch model prediction using actual *A* and *VTS* values determined from laboratory DSR test. ..... 7-161

Figure 7.4: Trend of Prediction % Error for Hirsch Model Using Default *A* and *VTS* Values From MEPDG ..... 7-162

Figure 7.5: Scatter plot for Hirsch model prediction using G* and Phase angle mastercurves. ..... 7-163

# Chapter 1

# Introduction

## 1.1. Research Need and Significance

The current state of practice for mix design of Hot Mix Asphalt (HMA) in USA is Superpave, which sets specification and performance tests of HMA recommended by the Strategic Highway Research Program (SHRP). Superpave assures good performances of compacted HMA through volumetric mix design and material selection without going through strength and stiffness tests. However, the use of volumetrics to assess mix performance is highly dependent on experience and subjective to local environmental conditions (Brown et al. 2001). Recently National Cooperative Highway Research Program (NCHRP) made an effort to include dynamic modulus test as a simple performance test. The dynamic modulus is selected because of its ability to capture the viscoelastic nature of asphalt concrete as a function of temperature and loading rate in the stress-strain plots. The recent findings of NCHRP suggest that the dynamic modulus ($E^*$) is one of the best indicators for the rutting and fatigue cracking of asphalt mixtures and therefore, $E^*$ is incorporated in the recently developed Mechanistic Empirical Pavement Design Guide (MEPDG), also known as DARWin-ME (Pellinen 2001; Witczak 2007).

MEPDG considers dynamic modulus as the most important material characterization parameter among the design inputs (ARA Inc. 2004). In MEPDG, mechanistic methods are employed to determine the stress and strains, and empirical methods to predict pavement distresses. Therefore, in both state-of-the art asphalt mix design and pavement design procedures, dynamic modulus testing is very important for material characterization. The main advantage of using dynamic modulus is that it is possible to guarantee Superpave volumetric performance and predict pavement structural response in design using a single $E^*$ value. This brings significant benefits to the state highway agencies because only one test equipment and/or test method is required for both asphalt volumetric mixture design and pavement responses such as rutting and fatigue cracking prediction.

There is a long history of the use of $E^*$ parameter by many researchers such as: Shook et al., 1969; Kallas, 1970; Bohn et al., 1970; Cragg and Pell, 1971; Yeager and Wood, 1975; Majidzadeh et al., 1979; Akhter and Witczak, 1985; Miller et al., 1983; Witczak and Fonseca, 1996. In the past, $E^*$ is used by mainly researchers. The use of $E^*$ as a fundamental martial property in design of pavements in state highway departments is quite new and recent. The New Mexico Department of Transportation (NMDOT) has recently adopted MEPDG for its pavement design. The MEPDG software provides default values of $E^*$ at level-3, which is a national average values. However, there are insufficient data with which to judge how well the default $E^*$ values represent typical New Mexico asphalt mixes. This gap of knowledge of $E^*$ values of typical New Mexico mixes is a major obstacle to the implementation of the MEPDG Guide in New Mexico.

This research attempts to develop *E** master curves of three New Mexico mixes for improved MEPDG analysis at level-2 by the NMDOT pavement designers.

### 1.2. Objective

The primary objectives of this study are to:

- Conduct dynamic modulus test on three plant produced asphalt mixes. Later, this study added two laboratory mixes that uses the same aggregate gradation of the plant mixes but different binder type.
- Apply Witczak and Hirsh models to predict the dynamic modulus from mix information and determine prediction accuracy.

### 1.3. Report Organization

This report comprises of eight chapters. Chapter 1 presents the research needs and objectives. Chapter 2 provides literature review on dynamic modulus testing and available predictive models. In Chapter 3, the materials, specimen fabrication, the experimental program and dynamic modulus test results are discussed. Chapter 4 presents the independent assurance test results and associated statistical analysis. Chapter 5, Chapter 6 and Chapter 7 present the application of viscosity based Witczak model, Dynamic shear modulus based Witczak model, and Hirsh model, respectively. In addition, a discussion on the model predictiion errors and their effects on pavement performance and a modified *E** model with emphasis on mix properties are included in Chapter 7. In Chapter 8, conclusions are made to list the findings of this research and future research recommendations.

### 1.4. Reference

Brown, R., Kandhal, P., and Zhang, J. (2001). "Performance Testing for Hot Mix Asphalt." NCAT Report No. 2001-05A, National Center for Asphalt Technology, Auburn, AL.

Pellinen, T. K. (2001). "Investigation of the use of Dynamic modulus as an indicator of Hot-Mix Asphalt performance." PhD. Dissertation, Arizona State University.

Witczak, M.W. (2007). "Specification Criteria for Simple Performance Tests for Rutting." NCHRP Report 580, Transportation Research Board Ishington, D.C.

ARA Inc., EREC Consultants Division (2004). "MEPDG Design Guide for New & Rehabilitated Pavements (Final Report), Part 2- Design Inputs, Chapter 2, Material Characterization for the Asphalt Material Group", NCHRP Project 1-37A, www.trb.org/mepdg/guide.htm

Shook, J.F., B.F. Kallas, and B.F. McLeod. (1969) “Factors Influencing Dynamic Modulus of Asphalt Concrete,” Journal of Association of Asphalt Paving Technologists, Vol. 38.

Kallas, B.F. (1970) “Dynamic Modulus of Asphalt Concrete in Tension and Tension-Compression,” Journal of Association of Asphalt Paving Technologists, Vol. 39.

Bohn, A.O., P. Ullidtz, and R. Stubstad. (1970). “The Dynamic Modulus of Asphalt Concrete Surfaces.” Dansk Vejtidsskrift, Vol. 47.

Cragg, R. and P.S. Pell. (1971) “The Dynamic Stiffness of Bituminous Road Materials,” Journal of Association of Asphalt Paving Technologists, Vol. 40.

Yeager L.L. and L.E. Wood. (1975) “Recommended Procedure for Determining the Dynamic Modulus of Asphalt Mixtures.” Transportation Research Record: Journal of the Transportation Research Board, No. 549, TRB, National Research Council, Ishington, D.C.

Majidzadeh, K., S. Khedr, and M. El-Mojarrush. (1979) “Evaluation of Permanent Deformation in Asphalt Concrete Pavements.” Transportation Research Record: Journal of the Transportation Research Board, No. 715, TRB, National Research Council, Ishington, D.C.

Akhter, G.F. and M.W. Witczak. (1985) “Sensitivity of Flexible Pavement Performance to Bituminous Mix Properties.” In Transportation Research Record: Journal of the Transportation Research Board, No. 1036, TRB, National Research Council, Ishington, D.C.

Miller J.S., J. Uzan, and M.W. Witczak. (1983) “Modification of the Asphalt Institute Bituminous Mix Modulus Predictive Equation.” Transportation Research Record: Journal of the Transportation Research Board, No. 911, TRB, National Research Council, Ishington, D.C.

Witczak, M.W. and O.A. Fonseca. (1996) “Revised Predictive Model for Dynamic Modulus of Asphalt Mixtures.” Transportation Research Record: Journal of the Transportation Research Board, No. 1540, TRB, National Research Council, Ishington, D.C.

# Chapter 2

# Literature Review

## 2.1. Viscoelastic Materials

Viscoelastic materials exhibit both viscous and elastic deformations under load. When stress is applied on viscoelastic materials, they resist shear flow. Viscoelastic materials exhibit time dependent deformation. Unlike viscous materials, elastic materials deform instantaneously and return to their original position when the stress is removed. The mechanism of elasticity is usually as a result of bond stretching along crystallographic planes whereas viscosity is the result of diffusion of atoms or molecules inside an amorphous material. The response of viscoelastic materials has elastic and viscous components. The viscosity of the viscoelastic material results in a strain rate that depends on time. Unlike elastic materials viscoelastic materials lose energy upon loading and unloading. In the strain stress curve of viscoelastic materials hysteresis is observed with the area of the loop equal to the lost energy during the loading cycle (Meyers and Chawla 1999).

Viscous component of strain in viscoelastic material depends on strain rate, which depends on time. This strain, due to molecular rearrangements, causes a backup stress in the material. When the stress is removed the back stress makes the material to recover to its original form. The strain rate dependency on time gives the prefix Visco- and the full recovery of the material gives the suffix –elasticity, together called viscoelasticity (McCrum et al. 2003).

There are three types of viscous responses to applied stress: linear, nonlinear, and plastic. If the strain rate is linearly proportional to the stress the response is linear and the material is classified as Newtonian material. When the material shows nonlinear response, it becomes Non-Newtonian fluid. When the stress is independent of the strain rate the material exhibits plastic deformation. Viscoelastic materials are those for which the relationship between stress and strain depends on time. If a constant stress is applied on a viscoelastic material, the response strain increases with time and the resulting phenomena is called creep. On the other hand, if the strain is held constant, the response stress decreases with time and this behavior is referred to as relaxation. The above mentioned two phenomena indicate that for viscoelastic materials, the effective stiffness depends on the rate of application of the load. Moreover, if cyclic loading is applied on viscoelastic materials a hysteresis loop develops. This indicates that the occurrence of a phase lag between the application of load and the response which result in mechanical energy dissipation (Meyers and Chawla 1999).

## 2.2. Dynamic Modulus

Viscoelastic property of a material can be represented using different functions. Among these functions, the creep function, the relaxation function, and dynamic function are most common. Studying Viscoelasticity by conducting the dynamic modulus analysis involves application of an oscillatory force (stress) to a material and measuring the resulting displacement (strain). In purely elastic materials, the stress and strain occur in phase, so that the response of one occurs simultaneously with the other. In purely viscous materials, there is a phase difference between stress and strain, where strain lags stress by 90 degree phase lag. In viscoelastic materials, the behavior is somewhere in between that of purely viscous and purely elastic materials, exhibiting some phase lag less than that for purely viscous materials. Stress and strain in a viscoelastic material can be represented using Eq. (2.1) and (2.2) (Meyers and Chawla 1999):

Strain:

$$\varepsilon = \varepsilon_o \sin(t\omega) \tag{2.1}$$

Stress:

$$\sigma = \sigma_o \sin(t\omega + \delta) \tag{2.2}$$

where $\omega$ is frequency of strain oscillation; $t$ is time and $\delta$ is phase lag between stress and strain.

Dynamic modulus is the property of viscoelastic materials. It is the ratio of stress to strain under oscillatory loading. The dynamic modulus can be decomposed into storage and loss moduli. The storage modulus measures the stored energy, which represent the elastic portion of the response. Loss modulus in viscoelastic materials measures the energy dissipated as heat representing the viscous portion. Mathematically, storage and loss modulus are expressed as shown in Eq. (2.3) and (2.4) (Meyers and Chawla 1999).

Storage modulus:

$$E' = \frac{\sigma_o}{\varepsilon_o} cos\, \delta \tag{2.3}$$

Loss modulus:

$$E'' = \frac{\sigma_o}{\varepsilon_o} sin\, \delta \tag{2.4}$$

Phase angle:

$$tan\, \delta = \frac{E''}{E'} \tag{2.5}$$

The complex modulus can be expressed in terms of storage and loss modulus using Eq. (2.6).

$$E^* = E' + iE'' \tag{2.6}$$

where $i$ is the imaginary unit.

For linear viscoelastic material, the relationship between stress and strain under continuous sinusoidal loading is defined by dynamic modulus. The dynamic modulus is defined mathematically as the ratio of peak dynamic stress ($\sigma_o$) and the peak recoverable axial strain ($\varepsilon_o$) (Tashman 2004).

$$|E^*| = \frac{\sigma_0}{\varepsilon_0} \tag{2.7}$$

where $|E^*|$ is dynamic modulus, $\sigma_o$ is peak dynamic stress and $\varepsilon_o$ is peak recoverable axial strain.

The dynamic modulus test is typically conducted at different temperatures and frequencies to establish a master curve representing the values of the dynamic modulus over a range of temperatures and frequencies (AASHTO TP 62-07).

Storage modulus is related to the applied maximum strain which relates the applied strain with the stress response as the storage modulus. This part of the modulus as explained above is in phase with the applied stain. On the other hand the loss modulus is the part of the modulus that is out of phase by 90 degrees. This modulus is related to the width of the ellipse which is proportional to the magnitude of the phase angle. This relationship of the loss modulus with the phase angle shows that the loss modulus is directly related with the internal friction in the viscoelastic materials.

### 2.3. Temperature dependent behavior of viscous materials

The major variable in solving viscoelasticity problems is viscosity ($\eta$). The inverse of viscosity is fluidity ($\varphi$). The values for both variables depend on temperature. A materials resistance to flow (viscosity) decreases as the temperature increases. In other words the materials fluidity increases as temperature increases. Deformation in viscoelastic materials is not a result of atomic displacement on crystallographic planes; rather it is a continuous rearrangement or diffusion of atoms or molecules with time under constant stress. The speed of this molecular diffusion depends on temperature. If the effect of temperature is the same all over the material volume on increasing the diffusion process then the relationship between moduluses at two different temperatures can be expressed by the following equation. If the viscoelastic material has the same modulus at corresponding elongated or shortened time with a change in temperature then the equation given below holds true and the material is referred as thermorheologically simple and rule of time-temperature superposition holds true. Plotting the viscoelastic moduli with respect to log time or log frequency forces the temperature change to

correspond to a horizontal shift on the log time or log frequency axis. Moreover, the shift factor is dependent on temperature and material. The one curve produced by using this time temperature shifting Principe form many curves is called master curve and an example is shown in following figure. (Meyers and Chawla 1999, Lakes 2009).

$$E(t,T) = E(\zeta, T_0) \tag{2.8}$$

$$\zeta = \frac{t}{a_T(T)} \tag{2.9}$$

where: $\zeta$ is reduced time, $T_0$ is reference temperature, $a_T(T)$ is shift factor, E is modulus.

### 2.4. Application of Viscoelasticity in Asphalt Concrete studies

To design a pavement using the elastic layer theory, one needs to have modulus and Poisson's ratio as an input. For mechanistic empirical structural pavement design guide (MEPDG), dynamic modulus is used as the stiffness parameter. Moreover, the dynamic modulus is also one of the selected variables to characterize hot mix asphalt mixtures (Kim 2009).

Both asphalt mix and asphalt binder properties affect the performance of HMA. The MEPDG incorporates this important performance-based material characteristic by developing master curve for $|E^*|$ of asphalt mix that defines the time-temperature dependency. There are three input levels in the MEPDG. In the Level 3 MEPDG input level predictive equations are used to estimate the dynamic modulus and no laboratory $|E^*|$ testing is required. Similarly at Level 2 design predictive equations calibrated with local materials are used as inputs. Level 1 MEPDG input requires site specific material laboratory *E** test results for mastercurve development. In addition, laboratory testing is also required for asphalt binder in Level 1 analysis (Cross et al. 2009).

Inspired by Superpave specifications, Kim et al (2009), gives two performance indicators for asphalt mixtures. A rutting performance indicator given as

$$\frac{|E^*|}{\sin\varphi} \tag{2.10}$$

And fatigue cracking indicator expressed as

$$|E^*| \sin\varphi \tag{2.11}$$

where $\varphi$ is the phase angle of the mix and

The correlation between rutting and the above rutting indicator in Eq. (2.10) have a coefficient of determination ($R^2$) equal to 0.91. However, this factor is not selected as an indicator of rutting potential in asphalt mixtures because of the unstable behavior of the phase angle with increasing temperature for asphalt mixes. For asphalt mixtures, the

phase angle is seen to increase with temperature up to some level and then then it decreases. The possible explanation of this picking effect is elastic response of aggregate skeleton that becomes significant at high temperatures. Because of this the above rutting factor is deemed to be inconsistent (Kim 2009).

### 2.5. Factors Affecting Dynamic Modulus of Asphalt Concrete

- Rate of loading

The stiffness of asphalt concrete gets higher as the rate of loading increases (Kim, 2009).

- Temperature

The stiffness of asphalt concrete decreases as the temperature increases (Kim, 2009).

- Age

Asphalt aging results in an increase of the stiffness however the brittle fracture susceptibility also increases with aging (Kim, 2009).

- Moisture

The effect of moisture and temperature on the stiffness; of asphalt concrete is similar. Both high moisture and high temperature result in plastic flow which is accompanied with decrease in the stiffness (Kim, 2009).

- Modulus of binder

Dynamic modulus asphalt concrete has a direct relationship with modulus of binder. In a study conducted by Shu and Huang (2008) the dynamic modulus of asphalt concrete is shown to increase with increasing binder modulus.

- Modulus of aggregate

Dynamic modulus asphalt concrete is also found to have a direct relationship with aggregate modulus. In the investigation of Shu and Huang (2008), it is observed that the value of dynamic modulus continually increased with increasing binder modulus however the increase in the dynamic modulus is limited for increase of aggregate modulus. Even if the aggregate modulus is increased, the dynamic modulus of the asphalt concrete is found to reduce beyond a thresh hold aggregate modulus of 5000MPa. This is taken by the authors to show the dynamic modulus of asphalt concrete is governed by the modulus of the binder.

- Asphalt content

The dynamic modulus of asphalt concrete is found to decrease with increasing binder content. The underlying cause of this phenomenon might be the increasing lubrication

effect as the binder as the content increases leasing to over lubrication resulting in reduction of the dynamic modulus. This indicates that lower level the asphalt content is one effective way of increasing the dynamic modulus (Shu and Huang 2008)

- Air voids

Shu and Huang (2008) and Kim (2009) observed that higher air void content leads to lower value in the dynamic modulus. It is also observed that not only the amount of air voids but also their size and distribution have significant effect on the dynamic modulus. Kim (2009) described the effect of small well-dispersed air voids in the mix as "micro crack arresters". They indicate that well-dispersed air voids provide enough volume for the asphalt to expand into at high temperatures and too much air will accelerate the growth of micro cracks on the other hand too little air will cause bleeding and promote large plastic deformations. On the other hand, too much air provides suitable access for both air and water into the interior of an asphalt concrete layer that is acting as a catalyst for aging and moisture damage. In conclusion the authors recommend having better control of air void content and size by making sure small and thoroughly distributed air voids to enhance the stiffness of asphalt concrete mix.

## 2.6. Laboratory Test Methods for Asphalt Concrete Dynamic Modulus $|E^*|$

Dynamic modulus tests are conducted by applying sinusoidal stress and measuring strain or the vice versa. The collected data from this method allows one to determine the complex modulus of the material. Moreover, the test is conducted repeatedly by changing the temperature and frequency to capture the transitions corresponding to molecular motions.

There are several methods to determine the dynamic modulus of a martial. These methods vary based on test control methods and test load application. The test control types can also be classified in to two as: stress controlled and strain controlled. In stress controlled test a specified load is applied and resulting displacements are measured. In stain controlled tests, precise strain amount is applied onto specimens and stress is measured. The types of loads that can be applied include axial forces, torsion and shear. In addition the testing procedure can be classified as temperature sweep, frequency sweep, or stress amplitude sweep. In the temperature sweep testes, the dynamic modulus is measured by changing the sample temperature and keeping the test frequency constant. For frequency sweep tests, the temperature is kept constant and loading frequency is varied. Another variation of the testing procedure is to gradually increase the loading amplitude (Menard 1999).

Dynamic modulus test on asphalt concrete is conducted man in both stress and stain (displacement) controlled test modes and by applying axial and shear load. Kim et al (2009) employed dynamic modulus $|E^*|$ test, and the shear modulus $|G^*|$ test for asphalt concrete. However, the provisional test standard in the American Association of State Highway and Transportation Officials is AASSHTO TP-62, which is a uniaxial dynamic testing procedure. Now, this test is fully developed AASHTO T 342.

### 2.6.1. AASHTO TP62 - Standard Method of Test for Determining Dynamic Modulus of Hot-Mix Asphalt Concrete Mixtures

The AASHTO TP 62-07 test standard is mostly similar to the original ASTM test however the temperature and frequency range is widened to include 15 to 55 °C and 25 to 0.1 Hz. The total test series recommended in this test consists of testing at five different temperatures which are -10, 4.4, 21.1, 37.8, and 54.4 ºC (14, 40, 70, 100, and 130 ºF) and six frequency sweep tests with loading frequencies of 0.1, 0.5, 1.0, 5, 10, and 25 Hz at each temperature. The AASHTO TP 62-07 is used to determine the dynamic modulus and phase angle which makes this test method superior than ASTM D 3497 which is described below.

### 2.6.2. ASTM D3479-79 - Standard Test Method for Dynamic Modulus of Asphalt mixtures

This test method is adopted as a standard by the American Society of Testing and Materials (ASTM) in 1979. The test standard is named "Test Method for Dynamic Modulus of Asphalt Concrete Mixtures" ASTM D 3497-79. This a load controlled testing, in which the load is kept constant throughout the frequency sweep. The procedure is performed over a range of temperature and loading frequencies. The test serious is a temperature sweep of at 41, 77 and 104 ºF (5, 25, and 40 ºC) and loading frequencies of 1, 4, and 16 Hz for each temperature. Uniaxial compressive haversine load between 0 and 241 kPa applied in the test series. The load level is decreased to as the temperature is increased to avoid damaging the specimen and to keep the specimen in the linear viscoelastic range. As for the test specimen, it should be prepared to have a height to diameter ratio greater than two.

### 2.6.3. Confined Dynamic Modulus Testing Protocol

Confined dynamic modulus test follows the same test procedure as that of AASHTO TP 62. The only difference is confinement pressure. Typical confining pressures applied on the order of 138 kPa and 206 kPa. Due to the additional complexity of testing, confined dynamic modulus tests are difficult to perform than unconfined dynamic modulus tests. Nevertheless, confined dynamic modulus test is found to be better to categorize and contrast the field performance of the different mixtures of dense-, gap-, and open-graded mixtures (Sotil et al. 2004, Sotil 2003 and Pellinen 2001).

Sotil et al. (2004) conducted confined dynamic modulus tests and found that the unconfined and confined dynamic modulus test results have a linear relationship with the applied bulk stress and are almost parallel regardless of the confinement level. Moreover, they have developed a simple method by which confined dynamic modulus test result values can be predicted from unconfined dynamic modulus test results. However, they have recommended for the method to be further validated with testing programs for a wide range of mixtures including conventional and modified asphalt mixtures.

Alternatively, Seo et al. (2007) compared the dynamic moduli determined from unconfined and confined axial compression tests on specific mixture and determined that the effect of confinement is significant at a high temperature and/or low loading frequency. They showed that as the temperature increases or loading frequency decreases, the asphalt binder becomes softer and the effect of confinement on the aggregate structure becomes more significant which makes the asphalt–aggregate mixture more resistant to stress and, thus, resulting in a greater dynamic modulus for the triaxial test than the uniaxial test. In addition, the comparison between two different mixes showed that the effect of confinement is greater for the mix that has larger aggregate particles.

### 2.6.4. Simplified Dynamic Modulus Testing Protocol

The AASHTO TP62 test procedure requires testing at least two replicate specimens at five temperatures 14°F, 40°F, 70°F, 100°F, and 130°F (−10°C, 4.4°C, 21.1°C, 37.8°C, and 54.4°C) and. and six loading rates of 25, 10, 5, 1.0, 0.5, and 0.1 Hz to develop a master curve. Bonaquist and Christensen (2005) observed that there is a large amount of overlap in the measured data from this test method that is not needed for the development of the master curve. With that drive they have come up with an alternative testing protocol which requires testing at only three temperatures 40°F, 70°F, and 115°F (4.4°C, 21.1°C, and 46.1°C), and four rates of loading 10, 1, 0.1, and 0.01 Hz. The master curve obtained from this procedure is also shown to be comparable with that of the standard test.

The modification done by Bonaquist and Christensen (2005) is to estimate the maximum dynamic modulus using the Hirsch model and use it in the master curve relationship presented below. This eliminates the need of testing at low temperature.

$$\log(E^*) = \delta + \frac{(\text{Max} - \delta)}{1 + e^{\beta + \gamma\left\{\log(\omega) + c\left[10^{A + VTS \log T_R} - \log\left(\eta_{70_{RTFOT}}\right)\right]\right\}}} \tag{2.12}$$

where: $E^*$ is dynamic modulus; $\delta$ is minimum value of $E^*$; Max is specified limiting maximum modulus; $\omega$ is loading frequency; $\beta$, $\gamma$ and c are fitting parameters; $\eta$ is viscosity, cP; $T_R$ is temperature, Rankin; A is regression intercept; VTS is regression slope of viscosity–temperature susceptibility and $\eta_{70_{RTFOT}}$ is viscosity at reference temperature of 70°F (21.1°C) and rolling thin-film oven (RTFO) aging.

Using maximum binder modulus in the Hirsch model the range for maximum mixture modulus is estimated to be from about 3,000,000 (20.6 GPa) for mixtures with very high VMA and low VFA to about 3,800,000 (26.2 GPa) for mixtures with low VMA and high VFA (Bonaquist and Christensen 2005).

### 2.6.5. Dynamic Shear Modulus$|G^*|$ test / Simple shear (SST) test

The SHRP research program developed shear frequency sweep test and it is performed using the simple shear tester (SST). “The test protocol is first introduced as SHRP

Designation M-003: Standard Method of Test for Determining the Shear Stiffness Behavior of Modified and Unmodified Hot Mix Asphalt with Superpave Shear Test Device. Later the test protocol is adopted by the American Association of State Highway and Transportation Officials (AASHTO) as a Provisional Standard: AASHTO Designation: TP7-94" (Kim 2009).

The SST test is conducted by applying a shear load to a specimen with a diameter of 150 mm and 50 mm height. The specimen is glued on top and bottom to platens and shearing action is applied from the bottom. The test is stain controlled with a maximum applied stress of 100 micro stains. The test temperatures are 4, 20 and 40°C. At each temperature a sinusoidal shear stain is applied with maximum frequency of 10 Hz and minimum frequency of 0.1 Hz. while the shear strain is applied sufficient compressive or tensile load is also applied to keep the specimen height constant (Kim 2009).

### 2.6.6. Indirect Tension test

Kim et al (2009) derived a relationship to determine dynamic modulus from indirect test (IDT) test data. The main motivation for this work is the luck of field cores meeting sample size requirements for dynamic modulus test. The AASHTO TP-62 test procedure for dynamic modulus test requires a sample with 150mm height. This is often impossible to get from field coring since most pavements are constructed with less than a few inches thickness. This greatly reduces the use of dynamic modulus testing for investigating pavement condition. However, with the linear viscoelastic solution derived by Kim et al (2009), it is possible to conduct the IDT test and derive dynamic modulus data ($|E^*|$).

### 2.6.7. Hollow cylinder tensile test (HCT)

Buttlar et al. (2002) explored the feasibility of using the HCT to obtain the dynamic modulus of asphalt concrete and found that the HCT device related well with dynamic modulus measurements obtained with uniaxial compression testing apparatus at 0°C and 20°C. In addition, the Witczak dynamic modulus predictive equation results are found to be in reasonably accurate agreement with the test results of the HCT. The Hollow cylinder tester (HCT) is developed with a desire to have an alternative test for the indirect tensile test (IDT). The test is conducted by applying pressure to the internal wall of a hollow cylindrical specimen using flexible membrane. The applied pressure produces hoop stress on the wall of hallow cylindrical specimen. By implementing closed form solutions for thick walled cylinders the tensile strength and creep compliance is calculated from the raw measurements. The stain is either measured by the use stain gauges or directly calculated from the volume change of the cavity. The specimen size is 115mm height by 150mm outside diameter and 106mm inside diameter.

## 2.7. Models to Predict Asphalt Concrete E*

The dynamic modulus of asphalt is selected as a key input parameter in the AASHTO 2002 Mechanistic Empirical Pavement Design Guide (MEPDG) and it is one of the most promising simple performance tests available. However, running the dynamic modulus

test is costly and time consuming and numerous models to predict it have been developed throughout the years.

### 2.7.1. Viscosity based Witczak Predictive Model

This model used the viscosity of binders as the main input parameter to capture the effect of binders. For developing this model 2750 dynamic modulus measurements from 205 different asphalt mixtures are tested in the laboratories of the Asphalt Institute, the University of Maryland, and the Federal Highway Administration. According to the developers, the model can predict the dynamic modulus of mixtures using both modified and conventional asphalt cements (Garcia and Thompson 2007).

$$\begin{aligned}\log|E^*| &= -1.249937 + 0.029232\rho_{200} - 0.001767(\rho_{200})^2 - 0.002841\rho_4 \\ &- 0.058097V_a - 0.802208\left(\frac{V_{beff}}{V_{beff}+V_a}\right) \\ &+ \frac{3.871977 - 0.0021\rho_4 + 0.003958\rho_{38} - 0.000017(\rho_{38})^2 + 0.00547\rho_{34}}{1 + e^{(-603313 - 0.313351\log(f) - 0.393532\log(\eta))}}\end{aligned} \quad (2.13)$$

where: $|E^*|$ is dynamic modulus, $10^5$psi; $\eta$ is bitumen viscosity, $10^6$ Poise; f is loading frequency, Hz; $V_a$ is air void content, %; $V_{beff}$ is effective bitumen content, % by volume; $\rho_{34}$ is cumulative % retained on the 19-mm (3/4-in.) sieve; $\rho_{38}$ is cumulative % retained on the 9.5-mm (3/8-in.) sieve; $\rho_4$ is cumulative % retained on the 4.76-mm (No. 4) sieve; $\rho_{200}$ is % passing the 0.075-mm (No. 200) sieve.

$$\eta = \left(\frac{G^*}{\omega}\right)\left(\frac{1}{\sin(\delta)}\right)^{a_0 + a_1*\omega + a_2\omega^2} \quad (2.14)$$

where: $\eta$ is binder viscosity, cP; G* is binder shear modulus, Pa; $\omega$ is angular frequency used to measure G* and $\delta$, rad/sec; $\delta$ is binder phase angle, degree; $a_0$ = 3.639216; $a_1$= 0.131373; $a_2$ = -0.000901.

### 2.7.2. Dynamic Shear Modulus based Witczak Predictive Model

This model uses dynamic shear modulus test results as a parameter instead of viscosity. The model is also developed with larder database of dynamic modulus data. 7400 data points from 346 HMA mixtures are used to develop this revised version of the Witczak E* predictive model (Garcia and Thompson 2007).

$$\log|E^*| = -0.349 +$$

$$0.754(|G_b^*|^{-0.0052}) * \begin{pmatrix} 6.65 - 0.032\rho_{200} + 0.0027(\rho_{200})^2 - 0.011\rho_4 \\ -0.0001(\rho_4)^2 + 0.006\rho_{38} - 0.00014(\rho_{38})^2 \\ -0.08V_a - 1.06\left(\frac{V_{beff}}{V_{beff}+V_a}\right) \end{pmatrix} +$$

$$\frac{2.558 + 0.032V_a + 0.713\left(\frac{V_{beff}}{V_{beff}+V_a}\right) + 0.0124\rho_{38} + 0.0001(\rho_{38})^2 + 0.00 - 0.0098\rho_{34}}{1 + e^{(-0.7814 - 0.5785\log|G^*| - 0.8834\log(\delta_b))}} \quad (2.15)$$

where: $|E^*|$ is dynamic modulus, psi; $\rho_{200}$ is % (by weight of total aggregate) passing the 0.075-mm (No. 200) sieve; $\rho_4$ is cumulative % (by weight) retained on the 4.76-mm (No. 4) sieve; $\rho_{34}$ is cumulative % (by weight) retained on the 19-mm (3/4-in.) sieve; $\rho_{38}$ is cumulative % (by weight) retained on the 9.5-mm (3/8-in.) sieve; $V_a$ is air void content (by volume of the mix), %; $V_{beff}$ is effective binder content (by volume of the mix), %; $|G^*|$ is dynamic shear modulus of binder, psi; $\delta_b$ is phase angle of binder associated with $|G^*|$, degree.

### 2.7.3. Hirsch Model

The Hirsch model is developed using the mixtures for composite materials. This makes the model a rational method of predicting dynamic modulus (Garcia and Thompson 2007).

$$|E^*| = P_c\left[4{,}200{,}000 * \left(1 - \frac{VMA}{100}\right) + 3|G^*|\left(\frac{VFA * VMA}{10{,}000}\right)\right] + (1 + P_c)\left[\frac{1 - \frac{VMA}{100}}{4{,}200{,}000} + \frac{VMA}{VFA * 3 * |G^*|}\right]^{-1} \quad (2.16)$$

$$P_c = \frac{\left(20 + \frac{VFA * 3 * |G_b^*|}{VMA}\right)^{0.58}}{650 + \left(\frac{VFA * 3 * |G_b^*|}{VMA}\right)^{0.58}} \quad (2.17)$$

where: $|E^*|$ is dynamic modulus, psi; $|G_b^*|$ is binder dynamic modulus, psi; VMA is voids in the mineral aggregate, %; VFA is voids filled with asphalt, %; $P_c$ is aggregate contact factor.

### 2.7.4. Application of Witczak and Hirsh Models

Clyne et al., (2003) in the University of Minnesota implemented the Witczak model to predict master curves of MN/DOT hot mix asphalts (HMA). The experience from MN/DOT shows that the Witczak equation can predict the dynamic modulus test results very well for some mixes and not very well for other mixes. Among the mixes for MN/DOT, the Witczak predictive equations fit the test data for two mixtures very well and under predicted the test data for the other two mixtures. Another study conducted by Christensen et al. (2003) did comparison of the predicted data with test results using Hirsh and Witczak equations. The findings indicate that the Hirsch model as well as the Witczak model produces reasonable estimates of the dynamic modulus. However, the results found from the Witczak predictive equation are found to give less values than the test results. Birgisson et al. (2005) at the University of Florida also used the 2002 Witczak predictive equation to predict the dynamic modulus of Florida asphalt mixtures. In conclusion of this study the Witczak predictive equation is found to underpredict measured data but reliable dynamic modulus estimates can be found provided that a correction factor is applied to the predicted dynamic modulus values. Kim et al. (2005) in North Carolina State University have investigated the accuracy of the Witczak and Hirsch predictive models by calculating the percent of error (the difference between the measured and predicted E* divided by the measured E*) at each frequency and temperature combination and then averaging for different frequencies at the same temperature for each mixture. The findings in the study imply that the 2000 Witczak equation predicts better at cooler temperatures than at warmer temperatures. However, the model is found to underpredict the measured data in most cases. With regards to the Hirsch model, similar predictive power is observed as the Witczak model for 35°C and 54.4°C, but for 10°C its performance is found to be very poor. At the University of Maryland Schwartz (2005) employed sensitivity and validation analysis to evaluate the accuracy of Witczak predictive equation. In conclusion of this study the Witczak model is found to produce good prediction suitable enough for design and performance prediction of asphalt pavements. However, the model is found to lack in predicting the performance variation of different mixes under varying design conditions like temperature, gradation and so forth. Tran and Hall (2005) at the University of Arkansas performed dynamic modulus tests to evaluate the Witczak predictive equation on mixes prepared from two different aggregate sources. The coefficient of determination test statistic is used to evaluate how well the predictive equation estimates the measured dynamic modulus. In conclusion of the study, the Witczak predictive equation is found to give good correlation ($R^2$ of 0.70 – 0.89) to the measured dynamic modulus values. The results are unrer predicting mostly though. Mohammad et al. (2005) at Louisiana Transportation Research Center (LTRC) also studied the Witczak and the Hirsch models by comparing the predicted and the measured E* data. Testing is done in two different laboratories namely the FHWA mobile laboratory and the LTRC laboratory. The final result showed that there is a good agreement between the predicted values from the two models and the measured data. Moreover, the overall measured E* data is found to be higher in value compared with the predicted E* data. Last but not least Dongré et al., (2005) measured dynamic modulus asphalt mixtures from five pavement construction sites across the

United States and compared with the corresponding E* predicted using the Witczak and the Hirsch models. The general trend found from this study indicates that binder data from RTFO aging condition predicts E* values relatively close to the measured data for both Witczak and Hirsch models. Moreover, it is found that Witczak model over-predicts E* values below 100,000 psi while the Hirsh model does the same for E* values below 50,000 psi. For this reason the study recommends to use measured E* values if the anticipated values are below the above mentioned values. In addition to this, the Witczak model as well as the Hirsch model are found to lose accuracy if the volumetric and binder content deviate from the mix design levels. The study recommends that both models should be refined to more accurately predict E* values from production samples.

### 2.7.5. Universal Material Model

The stiffness of the hot mix asphalt (HMA) varies as a function of test temperature and loading frequency. However, the applied stress levels also affect the measured modulus values. A stress-dependent mastercurve can be developed using the approach suggested by Witczak and Uzan for unbound materials. The model form to fit a stress dependent mastercurve of a mix is described given under (Kim 2009).

$$6\log|E^*| = \delta + \frac{\alpha - \delta}{1 + e^{(\beta - \gamma\log(\xi))}} \tag{2.18}$$

$$\delta = \left[(k_1 P_a)\left(\frac{\theta}{p_a}\right)^{k_2}\left(\frac{\tau_{oct}}{p_a}\right)^{k_3}\right] \tag{2.19}$$

where $\log|E^*|$ is log of stress-dependent dynamic modulus; $p_a$ is atmospheric pressure; $\theta$ is bulk stress; $\tau_{oct}$ is octahedral shear stress; $k_i$ is regression coefficients; $\alpha, \beta, \gamma$ are regression coefficients for Sigmoidal function; $\xi$ is reduced frequency

The stress dependency is incorporated into the equilibrium modulus value, that is, parameter $\delta$ in the mastercurve, instead of incorporating it into the shift factors. The calibrated model coefficients for the studied mixtures are $k_1 = -0.0124$, $k_2 = -0.5906$, $k_3 = 0.54011$, and $\alpha = 1.395045$, $\beta = 0.4644119$, and $\gamma = -0.04893$ . Both the bulk stress and octahedral shear stress had an effect on the modulus values as the coefficients $k_2$ and $k_3$ indicate (Kim 2009).

### 2.7.6. Stress-Dependent Stiffness Predictive Equation

A stress dependent dynamic modulus model is also presented in Kim (2009). The model can be used to predict dynamic modulus for unconfined linear viscoelastic stress case, however, for the model to work properly the user must use a minimum bulk stress value of 21 kPa and octahedral shear stress value of 9.9 kPa.

$$6\log|E^*| = \delta + A + \frac{\alpha - (\delta + A) + a_4 G_a + a_5 VFA}{1 + e^{(\beta - \gamma\log(f) - c\log(\eta))}} \tag{2.20}$$

$$A = a_0 + a_1 G_a + a_2 VFA + a_3 \log(\eta) \quad (2.21)$$

$$\delta = \left[ (k_1 P_a) \left( \frac{\theta}{p_a} \right)^{k_2} \left( \frac{\tau_{oct}}{p_a} \right)^{k_3} \right] \quad (2.22)$$

$$G_a = \frac{p_{200} + p_4 + p_{3/8} + p_{3/4}}{4} \quad (2.23)$$

where $\log|E^*|$is log of stress-dependent dynamic modulus ($10^6$ kPa); $\delta$ is equilibrium modulus; $G_a$ is average gradation ( passing %); VFA is void filled with asphalt (volume %); $\eta$ is binder viscosity($10^6$ P); f is frequency (Hz); $a_i$ are regression coefficients; $p_a$is atmospheric pressure; $\theta$ is bulk stress kPa ; $\tau_{oct}$ is octahedral shear stress kPa ; $k_i$ is regression coefficients; $\alpha, \beta, \gamma$ are regression coefficients for Sigmoidal function; $\xi$ is reduced frequency; $p_{200}$is passing 0.074 mm (%); $p_4$ is passing 4.36 mm (%); $p_{3/8}$ is passing 9.5 mm (%); $p_{3/4}$is passing 19 mm (%)

### 2.7.7. Neural-Network Models

Ceylan et al. (2009) developed a new method of predicting HMA dynamic modulus by means of artificial neural network (ANN) and reported that the ANN models predictions have made significant prediction accuracy at high and low temperatures with less prediction bias. The ANN model developed by Ceylan et al. (2009) is a four-layered feed forward back propagation model. The ANN architecture has one input, two hidden and one output layer. All input variables used for the development of the Witczak model are used as an input in the ANN model and the sole out of the ANN model is dynamic modulus. Input database used for the ANN models is also the same as that used by Witczak. However, instead of using all the data for prediction as in the regression analysis, input data are divided in to training and testing sets. The training data subset is used to train the back-propagation ANN model, and the testing data subset is used to examine the statistical accuracy of the developed ANN model. Finally, after a lot of trials for the best network architecture, the 8-30-30-1 architecture (eight inputs, 30 and 30 hidden neurons, and one output neuron, respectively), is chosen as the best architecture for predicting *E** of AC.

### 2.7.8. References

AASHTO. (2005). “Standard Method of test for Determining the dynamic modulus of Hot-Mix Asphalt Concrete Mixtures.” AASHTO TP 62-03, Ishington, D.C.

ASTM International (2003). “Standard Tests Method for Dynamic Modulus of Asphalt Mixtures.” ASTM D3497-79 (Reapproved 2003). ASTM International, 100 Barr Harbor Drive, PO Box C700, West Conshohocken, PA 19428-2959, United States.

Birgisson, B., Sholar, G., and Roque, R. (2005). "Evaluation of Predicted Dynamic Modulus for Florida Mixtures." 84th Annual Meeting of the Transportation Research Board, Paper No. 05-1309, Ishington D.C.

Bonaquist, R. and Christensen, D. W. (2005). "Practical Procedure for Developing Dynamic Modulus Master Curves for Pavement Structural Design." Transportation Research Record: Journal of the Transportation Research Board, No. 1929, Transportation Research Board of the National Academies, Ishington, D.C., 2005, pp. 208–217.

Brown, R., Kandhal, P., and Zhang, J. (2001). "Performance Testing for Hot Mix Asphalt." NCAT Report No. 2001-05A, National Center for Asphalt Technology, Auburn, AL.

Buttlar W.G., Bauer J.M., Sherman D. S. (2002). "Dyanmic Modulus of Asphalt Concrete with Hollow Cylinder Tensile Tester". Transportation Research Records, 1789, Paper vo 02-4112

Ceylan, H., Schwartz, C. W., Kim, S., and Gopalakrishnan, K. (2009). "Accuracy of Predictive Models for Dynamic Modulus of Hot-Mix Asphalt." Journal of Materials in Civil Engineering, Vol. 21, No. 6, 286-293

Clyne T. R. et al. (2003) "Dynamic and Resilient Modulus of Mn/Dot Asphalt Mixtures", Final Report, Department of Civil Engineering, University of Minnesota, 500 Pillsbury Dr. S.E., Minneapolis, MN 55455-0116.

Christensen, D.W., Pellinen, T.K., and Bonaquist, R.F. (2003). "Hirsch Model for Estimating the Modulus of Asphalt Concrete." Journal of the Association of Asphalt Paving Technologists, Volume 72, Lexington, KY.

Cross, S. et al. (2009). "Development of Flexible Pavement Database for Local Calibration of MEPDG" Annual report for FY 2009 (ODOT SPR No. 2209 (job piece 01946(52)), Oklahoma Department of Transportation, 200 N.E. 21st Street, Oklahoma City, Oklahoma 73105.

Dongré, R., Myers, L., D'Angelo, J., Paugh, C., and Gudimettla, J. (2004). "Field Evaluation of Witczak and Hirsch Models for Predicting Dynamic Modulus of Hot-Mix Asphalt." Pre-Print of the Journal of the Association of Asphalt Paving Technologists, Volume 74, 2005.

Garcia, G., and Thompson, M., (2007). "HMA dynamic modulus - Temperature relations" Research Report FHWA-ICT-07-006, Illinois Center for Transportation, Department of Civil and Environmental Engineering, University of Illinois, 205 North Mathews – MC-250 Urbana, IL 61801.

Huang, Y. H. (2004) “Pavement Analysis and Design.” Pearson Education, Inc., Upper Saddle River, New Jersey, 76-90

Kim, R. Y., (2009). “Modelling of Asphalt Concrete” American society of Civil Engineers, 1801 Alexander bell Drive, Reston, VA, USA

Kim, Y.R., King, M., and Momen, M. (2005). “Typical Dynamic Moduli Values of Hot Mix Asphalt in North Carolina and Their Prediction.” 84th Annual Meeting of the Transportation Research Board, Paper No. 05-2568, Ishington D.C.

Lakes R. S. (2009). “Viscoelastic materials”. Cambridge University Press. Avenue of Americas, NY, USA

McCrum, Buckley, and Bucknell (2003): "Principles of Polymer Engineering," 117-176. Menard, Kevin P. (1999). “Dynamic Mechanical Analysis: A Practical Introduction” CRC Press

Meyers and Chawla (1999): "Mechanical Behavior of Materials," 98-103.

Pellinen, T. K. Investigation of the Use of Dynamic Modulus as an Indicator of Hot-Mix Asphalt Performance. Ph.D. dissertation. Arizona State University, Tempe, 2001.

Portela, E. L., Coutinho, R. P., Junior, E. P., Holanda, Á. S. (2009), “Thermo-Mechanical Analysis of Asphalt Pavements.” Federal University of Ceará – Department of Transportation Engineering Campus do Pici , Bl. 703, 60455-760, Fortaleza, Ceará, Brazil

Schwartz, C. W. (2005). “Evaluation of the Witczak Dynamic Modulus Prediction Model.” 84th Annual Meeting of the Transportation Research Board, Paper No. 05-2112, Ishington D.C.

Seo, Y., El-Haggan, O., King, M., Lee, S. J., and Kim, Y. R. (2007). “Air Void Models for the Dynamic Modulus, Fatigue Cracking, and Rutting of Asphalt Concrete.” Journal of Materials in Civil Engineering, Vol. 19, No. 10.

Sotil, A.(2003). “Material Characterization of Asphalt Rubber Mixtures Using the Dynamic Modulus Test. Master’s thesis. Arizona State University, Tempe, 2003.

Sotil, A., Kaloush, K. E., and Witczak, M. W. (2004) “Reduced Confined Dynamic Modulus Testing Protocol for Asphalt Mixtures.” Transportation Research Record: Journal of the Transportation Research Board, No. 1891, TRB, National Research Council, Ishington, D.C., 2004, pp. 153–162.

Tashman, L. and Elangovan, M. A. (2004). “Dynamic Modulus Test – Laboratory Evaluation and Future Implementation in the State of Ishington.” Final research report, Ishington State University (WSU), Transportation Research Center (TRAC), Pullman, WA 99164-2910.

Tran, N.H., and Hall, K.D. (2005). "Evaluating the Predictive Equation in Determining Dynamic Moduli of Typical Asphalt Mixtures Used in Arkansas." Pre-Print of the Journal of the Association of Asphalt Paving Technologists, Volume 74, 2005.

# Chapter 3

# Dynamic Modulus Testing for New Mexico Asphalt Mixes

## 3.1. Introduction

This chapter is dedicated to martial description, sample preparation, and dynamic modus testing of New Mexico asphalt mixes. In this study the dynamic modulus testing is used to characterize the mechanical properties of asphalt concrete in the linear viscoelastic range. Dynamic modulus is a well-used material property for viscoelastic material; however its use in the asphalt industry is relatively new. The provisional standard TP-62 "Standard Method of Test for Determining Dynamic Modulus of Hot-Mix Asphalt Concrete Mixtures" from the American Association of State Highway and Transportation Officials (AASHTO) is used in this study as a guide to conduct the tests.

## 3.2. Objective

The objectives of this study are to:

- Determine dynamic modulus values for New Mexico asphalt mixes
- Develop mastercurves of New Mexico Asphalt mixes

## 3.3. Test matrix

In this study dynamic modulus ($E^*$) test is performed on specimens prepared from five different asphalt mixtures. Three of the asphalt mixtures are plant mixed superpave mixes and the other two are laboratory mixtures. The plant mixes are SP-II mix with binder grade PG 64-22, SP-III asphalt mix with PG 70-22, and SP-IV mix with binder grade PG 70-22, while the laboratory mixes are SP-III mix with PG 64-22 and SP-II with binder PG 70-22. In dynamic modulus testing, the asphalt samples are exposed to a sinusoidal compressive loading and resulting deformation and phase angles are measured. Tests are performed at five temperatures and six loading frequencies under each testing temperature. The applied loads are selected depending on the temperature and frequency to insure the specimen remained in the linear viscoelastic rage.

The minimum test matrix that is required to be completed on this study is testing for six frequencies (25, 10, 5, 1, 0.5, 0.1 Hz) with corresponding cycles of 200, 200, 100, 20, 15, and 15 each applied at five temperatures ( 14, 40, 70, 100, 130 °F) for each specimen. This gives a total of 30 dynamic modulus test results per specimen. The test matrix is also presented in Table 3.1.

## 3.4. Test Apparatus

### 3.4.1. Dynamic Modulus Testing System

The pavement laboratory in the department of civil engineering is equipped with GCTS ATM-025 Servo-Hydraulic testing system capable for performing Dynamic modulus test which is presented in .1. The equipment is also capable of indirect tensile test, flow time and flow number tests just by changing some of the accessories. The machine is capable of producing controlled haversine compressive loading up to 100 Hz frequency. The top actuator has a dynamic load capacity of 25 kN and a stock of the top actuator 100 mm. The system is also equipped with an environmental chamber capable of controlling temperature over the range of -30 °C to +150 °C. The system has its own air conditioning unit and the temperature in the chamber can be controlled with an accuracy of ±0.5 °C. The GCTS ATM-025 is controlled with a digital servo controller GCTS designation SCON-2000. The SCON-2000 is capable of controlling even when the interface computer is shut down. It has a capacity of controlling up 24 sensors. The control system has a maximum of 6Hz loop rate and 300 kHz conversion rate between channels. Figure shows the SCON 2000 controller. The system can be connected to two load cells. For dynamic modulus testing top actuator is connected with a load cell that is capable of measuring loads up to 25kN. However, or indirect tensile test there is a need for more load capacity and the bottom actuator is used with a load cell that has a maximum capacity of 100kN. The resolution of the top actuator load cell is 5N. Spring loaded LVDTs are used for conducting the dynamic modulus testing in this study. The deformation range of these LVDTs is ± 0.5mm and the resolution is 0.0025mm. Figure 3.2 shows two LVDTs mounted on a specimen.

### 3.4.2. Gyratory Compactor

A pine gyrator compactor is used to compact the asphalt mixtures. The gyratory compactor is calibrated for internal angle accuracy. Associated equipment (draft ovens, molds etc…) are also available in for compacting laboratory specimens in accordance with AASHTO TP4. The pine gyratory compactor available is shown in Figure 3.3.

### 3.4.3. Coring Machine

A GCTS coring machine (ACD-150) is used for coring. The machine is water cooled and it can be fit with diamond edged drilling barrels for drilling out 100 mm (4 in) diameter test specimens. The coring rate is pressure controlled and the drilling motor is electric controlled. The drilling motor has a 1.5HP and adjustable spindle speeds. The coring machine with an illustrative cored specimen is shown in Figure 3.4.

### 3.4.4. Diamond Cutting Edge Eet Saw

Figure 3.5 shows the Lab specimen saw that is used to cut specimens. The GCTS designation for the saw is RLS-3HA. The saw system is equipped with 3HP electric

motor, diamond edge cutting blade, pressure controlled automatic feed and a specimen holding setup. It is also completely covered in a rectangular hood for safety.

### 3.4.5. Loading Button Fixer

GCTS Automatic Positioning Fixture (GPF-100) is used to fix loading buttons to the final specimen. Figure 3.6 shows the picture of the automatic positioning system with one sample in the process of fixing LVDT mounting buttons.

## 3.5. Sample collection and Fabrication

### 3.5.1. Sample Collection

With aim of collecting Superpave HMA mixes that are widely used in the design and construction of roads in the state of New Mexico, two Superpave HMA mixes are collected from an actual construction site. The Asphalt mix collection is undertaken in cooperation with the New Mexico Department of Transportation research bureau.

SP-III and SP-II Superpave asphalt mixes sampling is conducted from the Materials Plant for Tramway Blvd to Benallio road reconstruction project. The Project is widening of I-25 from two to three lanes each way from Tramway Boulevard on Albuquerque's north side to the southern exit at Bernalillo with a total length of 7.7 miles. These mixes are prepared in the mixing pant and sampling is performed from windrows of the actual pavement construction as per the requirements of AASHTO T-168. SP-IV mix is collected at a later date from a commercial mix at Lafarge Mix plant in Albuquerque.

In addition to the mix collection virgin aggregates, binders and recycled asphalt samples are also collected. The aggregates source for SP-II and SP-III mixes is the Santo Domingo Pit located in Sandoval County and for SP-IV mix a combination of pits in Bernalillo County are utilized. Sampling of these aggregates is done according to AASHTO T-2. The main source of RAP for SP-II and SP-III mixes is milling from the old I-25 road. Sampling of RAP is also done according to AASHTO T-2 from the RAP pile present in the mix plant. Binder samples for the two binder grades PG 70-22 and PG 64-22 are also collected.

For proper analysis of test results and preparation of specimens, determining the Asphalt mix properties at hand is important. Therefore, Theoretical maximum gravity**,** Asphalt content test and Sieve analysis test are conducted using AASHTO recommended standards. Moreover, for each compacted sample the bulk specific gravity and air void content is determined.

### 3.5.2. Sieve Analysis Test (AASHTO T-27)

Aggregate distribution of the SP-II, SP-III and SP-IV mix aggregates is studied as per the requirements of AASHTO T-27. Samples are obtained by burning off respective SP-II,

SP-III and SP-IV asphalt mix samples. The results are plotted in 0.45 powers Gradation Chart as presented in Figure 3.9.

### 3.5.3. Asphalt content (AASHTO T-308)

Asphalt content test for all plant mixes is also conducted as per the requirements AASHTO T-308. The average asphalt content is found to be 4.61% for SP-III plant mix, 4.42% for SP-II plant mix and 6.27% for SP-IV mix. Table 3.2 shows asphalt content test results.

### 3.5.4. Theoretical Maximum Gravity ($G_{mm}$) (AASHTO-T-209)

The theoretical maximum specific gravity of the mixes is determined using mass determination in air method outlined in AASHTO T-209. Testing Apparatus used for this test include: vacuum Pump, Balance, Vacuum flask, Vacuum gauge, water bath and drying oven. The volumetric flask is standardized over the range of water bath temperatures likely to be encountered and a water bath with temperature control is used to keep the water at constant temperature. A number of replicate tests are conducted to check for operator precision and the average result is also compared with data provided in the specification sheet. The results are found acceptable both for single operator precision as well as multi laboratory precision. Table 3.3 provides theoretical maximum gravity test results for the five types of asphalt mixtures used in this study.

### 3.5.5. Sample Compaction (AASHTO T-312)

Superpave Gyratory Compactor (SGC) is used to compact samples as per the recommendations of AASHTO T-312 and current mix design methods. The SGC is a preferred method of compaction for dynamic modulus sample preparation since it is the best available laboratory method to produce samples with similar characteristics as field.

The required sample size to conduct dynamic modulus test is 100 mm in diameter and 150 mm in height as specified adopted in the AASHTO TP-62. This sample size will produce dynamic modulus measurements that are not influenced by end effects and aggregate size (Kim 2009). However, to insure uniform air voids, the final specimen is extracted out of an oversize compacted sample with a 150mm diameter and 170 mm height.

The pine Gyratory compaction machine is used to compact a 150mm diameter and 170 mm height sample. The compaction temperature used to achieve a viscosity of 280±30 is selected according to the binder grade used and the handling temperature shown in Table 3.4. Several trial gyratory specimens are prepared with the aim of achieving 5.5±0.5% air void for the inside core. The compaction is controlled using minimum height of 170mm (6.7in) and the maximum number of gyrations equal to 160. Compacting the 170mm x 150mm sample at 10.5% air void is found to give the desired air void for the inside core. The sample used for compaction is about 6500gm. Compacted samples are cooled off and

left for about 16hrs to gain strength before coring a 4 inch diameter. Table 3.4 gives the required compaction and mixing temperatures for mixtures used in this study.

### 3.5.6. Bulk Specific Gravity ($G_{mb}$) (AASHTO T-166)

Bulk specific gravity is determined for all samples according to the AASHTO T-166. Bulk specific gravity and theoretical maximum gravity are required to determine the air void of compacted asphalt mixtures. The bulk specific gravity of each sample used for dynamic modulus testing is presented in Table 3.5.

### 3.5.7. Percent Air Void Determination (Volumetric calculation)

To determine the air voids in the sample theoretical maximum gravity ($G_{mm}$) and Bulk Specific gravity ($G_{mb}$) of the samples are utilized as using the air void relation given in Eq. (3.1). Sample air voids ($\%Av$) of all samples used for dynamic modulus test are provided in Table 3.6.

$$\%Av = \left(1 - \frac{G_{mb}}{G_{mm}}\right) * 100 \qquad (3.1)$$

### 3.5.8. Air Void Uniformity Check

The air voids of three samples are checked for uniformity. The air voids of the top and bottom section are compared with the middle section air void to determine the significance of the difference. The test results and statistical analysis calculations are presented in Table 3.7. As can be seen from the analysis the air voids of the top and bottom sections are not significantly different from the middle section. This indicates that the cored sample has uniform air void distribution throughout.

### 3.5.9. $E^*$ Test Specimen Geometric Requirements

The samples prepared for dynamic modulus should meet geometry requirements in addition to the desired air void. Geometric parameters mentioned to be checked for specific requirements in the AASHTO TP-62 provisional standard are sample diameter, height, end perpendicularity and waviness.

The diameters of each specimen at the middle, top and bottom sections along two axes 90 degree apart are recorded. The means and standard deviations are calculated and compared with the AASHTO TP 62-07 requirements; which states that the average of recorded diameters should be between 100 and 104 mm. In addition, the standard deviation for the average should not be greater than 2.5mm.

The ends of all samples are checked for perpendicularity and waviness requirements right before testing as well. Perpendicularity is checked at two perpendicular axes of both top and bottom ends by using the rock flatness gauge shown in Figure 3.7. Waviness is checked by using a straightedge and feeler gauge shown in Figure 3.8. The AASHTO

recommended tolerance for waviness is 0.05 mm across three axes 120 degrees apart. Moreover, the specimen end should not depart from perpendicular to the axis of the specimen by more than 1.0°.

### 3.6. Test Setup

Different test setup techniques have been used in the past and currently the use of spring loaded LVDTs are recommended in the AASHTO TP-62. This instrumentation can be used for both confined and unconfined conditions since it does not interfere with the membrane around the specimen for confined testing. AASHTO TP-62 recommends to measure deformation at a minimum of two locations 180° apart and by increasing the LVDTs to three locations located 120° apart the required number of replicates for testing is reduced. For testing in this study two LVDTs are used as shown in Figure 3.2.

LVDT mounting buttons are glued to the specimen using five minute epoxy. The gauge length is maintained to be 100mm and the Automatic Positioning Fixture is used to fix LVDT mounting buttons 50mm away from the mid height of the specimen. This helps to maintain consistent position for all LVDTs on the specimen. Moreover, end treatments are used instead of capping between specimen ends and platens. Even though, Capping is recommended in the ASTM test standard for dynamic modulus, Witczak et al. (2000) recommends avoiding capping and using friction-reducing treatments between the specimen ends and the platens. Moreover, recommended end treatments in the AASHTO TP-62 provisional test standard is to use a sandwich of two 0.5-mm-thick latex sheets separated with silicone or vacuum grease.

### 3.7. Test Procedure

First Axial LVDTs are attached to the specimen and adjusted to extend up to at least the middle of the linear range to make sure that enough of the range is available for the accumulation of compressive permanent deformation. Then specimen is conditioned to reach to the desired temperature. This is achieved by keeping the specimen in the environmental chamber and allowing it to equilibrate to the specified testing temperature. A dummy specimen with a thermocouple mounted at the center is also used to monitor the specimen temperature. Minimum recommended temperature equilibrating time in the AASHTO standard is also strictly followed.

The specimen is centered with the hydraulic load actuator visually in order to avoid eccentric loading and then a contact load equal to 5 percent of the dynamic load is applied. Then eccentricity is checked at the conditioning stage by applying 50 percent of the required load and observing the response from the LVDTs. The position of the specimen is moved and adjusted very carefully to balance the LVDT measurements. Then, once the deformations are uniform, the full haversine loading is applied to the specimen. The full dynamic load is adjusted to produce axial strains of about 55 microstrains. The AASHTO recommended stain range is between 50 and 150 microstrain. The testing dynamic load increases as the stiffness increases which in turn

increases as the temperature decreases. The general range recommended for the entire dynamic modulus test over all temperatures is between 15 and 2800 kPa (2 and 400 psi).

Two minute rest period between frequencies in the frequency sweep is applied during testing. This is mainly because the controller used cannot produce continuous frequency sweeps and each frequency is programmed separately in such a manner that there will be some lag time or rest period between each frequency. According to kim et al (2009), even though applying rest period helps to prevent specimen from heating up too much during cyclic testing the application of rest period allows some of the transient strains to recover during testing which may have some effect on the measured modulus values and selection of suitable data analysis methods.

Dynamic modulus testing is conducted at -10, 4, 20, 40, and 54 °C (14, 40, 70, 100 and 130°F) at loading frequencies of 0.1, 0.5, 1.0, 5, 10, and 25 Hz at each temperature. Testing is conducted starting at the lowest temperature. Within each temperature testing is conducted staring at the highest frequency and proceeding to the lowest frequency. Therefore, the last frequency and temperature combination is the highest temperature with the lowest frequency. This combination of test temperature and frequency is recommended in the AASHTO TP-62 for constructing the master curve.

## 3.8. Test results and Analysis

### 3.8.1. Raw Data

The data collected using the SCON 2000 data acquisition system are the time, axial force and the displacements of the linear variable differential transducers (LVDT). Even though the system is capable of collecting and storing the entire set of data form the test start to end, to reduce load on the system and increase efficiency, the stored data is only for the last five cycles. Therefore, time is the time period from the last to five cycles to the end of the testing time for each frequency. The axial force is the vertical load applied on the specimen. This is measured using the attached load cell.

The displacements of the two LVDTs is recorded and stored separately. However, for the calculation of strain the average of the two is taken. The axial gage length of the LVDTs is100 mm and two LVDTs are mounted on a specimen surface. Before the tests are performed, the height and diameter for each specimen are measured and the top and bottom specimen areas are calculated. Moreover the AASHTO requirements for specimen geometry are checked for the perpendicularity, waviness and accuracy of dimensions. Then actual stress under which the specimen is exposed to for each test condition is calculated dividing the axial force by the calculated area of the specimen. In same fashion, the displacements from the LVDTs are divided by the axial gage length to get the actual axial strain. The complex dynamic modulus tests is performed under five test temperatures:-10°C, 4°C, 21°C, 37°C, and 54°C and for each temperatures tests are done for five frequencies: 25 Hz, 10 Hz, 5 Hz, 0.5 Hz, and 0. 1 Hz. Then for each test temperature and frequency combination data points are collected and stored for the last five cycles. This produces a large amount of raw data.

To deal with such large amount of data, the GCTS software provides a data organization scheme by which the data is organized into project, sample and specimen folders. Data is organized by classifying each of the replicate specimens in one project folder. Within a project folder, a separate sample folder is created. However instead of creating one sample folder for one sample, replicate sample folders are created for each sample and test temperature combinations. This is done to facilitate test data retrieving as easy as possible. Within each sample folder, data files are named by specimen type and number. It is important to note that the specimen names are test data files. Therefore, with in each sample folder the data files are created for each test sample-temperature combination. With each sample folders all trial test data files are stored. Each data file collects the required data for all frequencies under the test temperature. The data is arranged from 25 Hz and ends at 0.1 Hz for each of the test temperatures. Figure 3.10 is typical stress and strain versus time plots on a GCTS CATS software interface.

### 3.8.2. Stress and Strain Data

The data obtained from the complex modulus test is quite extensive. The stress and strain data obtained from feedback signal is not perfectly sinusoidal. This is because of the test equipment limitations. The noise in sine feedback signal wave imposed with transient recoverable and permanent deformation data affects the computed modulus and phase angle values. Many analysis methods are mentioned in kim et al (2009), however, the data analysis is done according to the AASHTO TP-62 analysis method. To conduct the analysis, The GCTS software is used which is an implementation of the AASHTO TP-62 analysis method. The AASHTO TP-62 employs a method to transform and fit the discrete time-stress data and time strain data to a sinusoidal function. Then dynamic modulus values are calculated by determining the stress amplitude and strain amplitude from the fitted sinusoidal curve. The phase angle is determined by determining the difference of the phase angles of the strain and stress sinusoidal fit curves. All calculations are made from the last five loading cycles.

- The peak stress ($\sigma_o$) is defined as:

$$\sigma_o = \frac{\bar{P}}{A} \tag{3.2}$$

$where$: $\bar{P}$ is average of the last five load amplitudes; $A$ is area of the specimen

- Recoverable axial strain ($\varepsilon_o$) is defined as :

$$\varepsilon_o = \frac{\bar{\Delta}}{GL} \tag{3.3}$$

$where$: $\bar{\Delta}$ is average of the last five deformation amplitudes; $GL$ is gauge length

- Dynamic Modulus $|E^*|$ is defined as:

$$|E^*| = \frac{\sigma_o}{\varepsilon_o} \tag{3.4}$$

- Phase angle $(\phi)$ is defined as:

$$\phi = \frac{t_i}{t_p} * 360 \tag{3.5}$$

$where$: $t_i$ is average lag between a cycle of stress and strain (sec); $t_p$ is average time for stress cycle (sec).

### 3.8.3. Dynamic Modulus Data Analysis and Presentation

Dynamic modulus data can be presented with Isothermal and Isochronal curves, mastercurves, Cole and Cole pane plots, Black space plots and dissipated energy approach. Isothermal and Isochronal curves are important to check the trends of the data and identify errors readily. The mastercurve is a representation of dynamic modulus data in one smooth curve in frequency/time domain by using time temperature superposition principle. Cole and Cole pane plots have the storage modulus in the real axis and the loss modulus in the imaginary axis. The Cole and Cole plane plots are useful for analysis and interpretation of dynamic modulus data at intermediate to low temperatures. For analysis of data at high temperature it is recommended to use the Black space plots. Black space plots are plots of the dynamic modulus in logarithm scale on the abscissa and the phase angel in arithmetic scale on the ordinate axis. The dissipated energy approach basically makes use of loss tangent plots to study the presence of elastic response in the material. In this approach the loss tangent is plotted against reduced frequency or frequency (Pellinen, 2001).

### 3.8.4. Time Temperature Superposition Principle (TTSP)

Time temperature superposition principle is applied on the dynamic modulus data collected from tests conducted at different frequencies and temperature. By applying TTSP dynamic modulus data at different temperatures are moved horizontally on the loading time scale of loafing frequency scale to produce one smooth curve dependent only on loading frequency or time. The amount by which dynamic modulus data is shifted to fit in a smooth curve at a reference temperature is referred to as shift factor$a(T)$. Shifting is achieved by dividing the loading time in the time domain or multiplying the loading frequency in the frequency domain by the shift factor to get the reduced time or reduced frequency. The smooth curve that is developed by shifting the dynamic modulus data is referred to as master curve. The master curve can be developed

for any reference temperature chosen arbitrarily. At the reference temperature the shift factor is one or its logarithm is zero. The use of TTSP to develop master curve have two advantages: the first and foremost is it reduces the three dimensional data (dynamic modulus, loading time/frequency and temperature) in to two dimensional data by eliminating the temperature variable. This makes it easy to compare test results conducted at different conditions. The other advantage is the possibility of interpolation to get intermediate data within the test data range (Kim 2009).

$$f_r = f * a(T) \tag{3.6}$$

$$\log(f_r) = \log(f) + \log[a(T)] \tag{3.7}$$

The above two equations can also be expressed as:

$$t_r = \frac{t}{a(T)} \tag{3.8}$$

$$\log(t_r) = \log(t) - \log[a(T)] \tag{3.9}$$

### 3.8.5. Shift Factor Functions

Different shift factor functions have been used to fit the shift factors trend. Among these, the Arrhenius equation and the Williams, Landel, and Ferry (WLF) equation are used to implement the time temperature principle for both asphalt binders and asphalt concrete test data (Kim 2009).

- Arrhenius equation

The Arrhenius equation is represented by the following equation. Different values ranging from $44kJ/mol$ to $205kJ/mol$ are reported in the literature for the activation energy of asphalt binders. $C$ is also reported to have values of $10920K$, $13060K$ and $7680K$ (Rowe and Sharrock 2010).

$$\log a_t = C\left(\frac{1}{T} - \frac{1}{T_{ref}}\right) = \frac{E_a}{2.203 * R}\left(\frac{1}{T} - \frac{1}{T_{ref}}\right) \tag{3.10}$$

where C is a material constant (K); $E_a$ is the activation energy ($J/mol$); R is the ideal gas constant ($8.314\ \frac{J}{mol} * K$) ; T is the experimental temperature (K); $T_{ref}$ is the reference temperature and the value 2.303 is the natural logarithm of the number 10.

- Williams, Landel, and Ferry (WLF) equation

Rowe and Sharrock (2010) recommend using the WLF equation near the glassy temperature($T_g$) of the material. The WLF equation is given in the following equation:

$$\log a_t = \frac{-C_1(T - T_{ref})}{C_2 + (T - T_{ref})} \tag{3.11}$$

*where*: $C_1$ and $C_2$ are constants that depend on the material properties and reference temperature.

- Modified Kaelble equation

On the other hand, Rowe and Sharrock (2010) develop an alternative equation to fit shift factors. The function they developed is given as follows:

$$\log a_T = -C_1 * \left( \frac{(T - T_d)}{C_2 + |T - T_d|} - \frac{\left(T_{ref} - T_d\right)}{C_2 + \left|T_{ref} - T_d\right|} \right) \tag{3.12}$$

- Second degree polynomial

Another function that is available for fitting the shift factor data is a second degree polynomial as given in the following equation;

$$\log a_T = aT^2 + bT + c \tag{3.13}$$

### 3.8.6. Master Curve

As described by Kim (2009), the generalized power law, polynomial fitting functions, piecewise fitting of polynomial functions and piecewise fitting of polynomial functions supplemented with cubic spline method have been used to develop creep and relaxation mastercurve. The function that is predominantly used for developing mastercurve for dynamic modulus data covering a wide range of temperatures is the sigmoid function. The sigmoidal function is given in the equation below. Parameter $\gamma$ in the equation is indicates how steepness of the function that is how fast the modulus is changing from the minimum value to the maximum and parameter $\beta$ shows the horizontal position at which the rate of change of modulus changes form positive to negative. The parameter $\delta$ on the other hand is associated with the minimum value of asphalt mix modulus which is caused by high temperatures. At high temperatures the modulus of the binder becomes insignificant and aggregate interlock starts to play a significant role in the compressive stiffness. This behavior of asphalt mix is captured by the parameter $\delta$. The highest mix modulus which is associated with binder modulus at very low temperature is represented in the sigmoidal function by the sum of parameters $\delta$ and $\alpha$, $\delta + \alpha$. This highest modulus is also referred to as glassy modulus.

$$\log(|E^*|) = \delta + \frac{\alpha}{1 + e^{\beta - \gamma \log(t_r)}} \tag{3.14}$$

$where\ |E^*|$ is dynamic modulus; $t_r$ is reduced frequency; $\delta$ is minimum modulus value; $\alpha$ is span of modulus values; $\beta, \gamma$ are shape parameters.

There are different methods that can be used to fit the sigmoidal function to shifted dynamic modulus data. Witczak and sotil (2004) have investigated a variety of methods and recommended to optimize all four parameters of the sigmoidal function together with the three coefficients of the polynomial shift factor function. This method is only dependent on dynamic modulus experiment and the form of the shift function is not forced to the mastercurve. Kim (2009), pointed out the problem of experimental error of the test data being absorbed by shift factors as a drawback of this method. The sigmoidal function of the mastercurve can be fitted using Solver Function in the Excel spreadsheets program. However, Kim (2009) recommends being cautious about fitting data with insufficient temperature range. The method recommended to avoid bias is to confine the asymptotic high and low modulus values to assumed proper modulus values.

- Experimental E* Master Curve fitting steps

The following procedure adopted from Witczak and Sotil (2004) is used to develop the master curve. All calculations can be performed using MS excel spread sheet.

Step 1: Determine the Logarithm of test frequency and dynamic modulus

Step 2: Choose the reference temperature. For example 21 ° C reference temperature can be chosen.

Step 3: Give initial estimate of shift factors for each temperature case and program excel with if statement to change the values for each temperature in the iteration process. Dynamic modulus test in this study is conducted at five temperatures, -10° C, 4° C, 21° C, 37° C, 54° C. An initial log shift factor of 1 is chosen for all test temperatures and it is expected to see the shift factor value for the reference temperature to change to zero and values at other temperatures change to negative and positive values accordingly. Program MS-excel is used to determine the log reduced frequency. The following equations used in the MS-excel program.

$$a(t) = \frac{f_T}{f_{T_o}} \tag{3.15}$$

$$fr = f_T = a(t) * f_{T_o} \tag{3.16}$$

$$\log(fr) = \log\{a(t)\} + \log\left(f_{T_o}\right) \tag{3.17}$$

Step 4: Choose initial values for the master curve parameters. A symmetrical sigmoid function is chosen for the mastercurve fitting in this study and initial value of one is used for the parameters α, β, γ and δ.

$$\log(|E^*|) = \delta + \frac{\alpha}{1 + e^{\beta+\gamma \log(fr)}} \tag{3.18}$$

Step 5: Calculate the coefficient of determination. To evaluate the goodness of fit for the iteration results of the solver function it is required to minimize the sum of error squared values and the final result goodness of fit can be evaluated by the coefficient of determination given in the following equation.

$$R^2 = 1 - \frac{SS_{err}}{SS_{tot}} = \frac{\sum_i^n (y_i - \bar{y})^2}{\sum_i^n (y_i - f_i)^2} \tag{3.19}$$

where $R^2$ = Coefficient of determination; $y_i$ = Data set has values; $f_i$ = Modelled value; $\bar{y} = \frac{\sum_i^n y_i}{n}$

### 3.9. Dynamic Modulus Results for SPIII with PG 70-22 (Plant Mix)

The dynamic modulus test result on six samples prepared from SP-III mix with binder grade of PG 70-22 is presented in tabular and graphic form in Appendix A. A summarized depiction of all data represented by mastercurves developed for each test is shown in Figure 3.11. The test results from the six samples are averaged and Figure 3.12 is an Isothermal representation of and Figure 3.13 is isochronal plot of the average data. As can be seen from the Isothermal and isochronal Curves the trend of dynamic modulus is found to be decreasing with increasing temperature and increasing with increasing frequency. Then, the master curve is developed for the average of all test results and presented in Figure 3.14. Experimental fitting of the sigmoid function has shown very good fit to the shifted data. Polynomial function is used to fit the shift factor results and it is shown in Figure 3.15. In addition, Cole and Cole plane, back space, and loss tangent plots are provided in Figure 3.16, Figure 3.17 and Figure 3.18 to supplement and check quality of data. Form the Cole and Cole plane plot it can be seen that the dynamic modulus results follow a single trend which indicate the consistency in those data. Black space plot of the data shows the data at high temperatures follow one trend indicating good quality. The loss tangent plot showed low energy dissipation at lower temperatures indicating higher elastic response. Moreover, loss modulus is found to decrease with both increasing temperature and decreasing frequency. This indicates that the elastic response of the mix starts to decrease as the temperature increases and frequency decreases. At very high temperature though, 54°C, the trend reverses and loss tangent increases as the frequency increased. This indicates that at higher temperature the aggregate interlock effect becomes more significant.

### 3.10. Dynamic Modulus Results of SPIII Mix with PG 64-22 (Lab Mix)

Dynamic modulus tests are also conducted on specimens compacted from laboratory prepared SP-III hot mix asphalt mixes. For this mix the aggregate gradation is kept the same as SP-III plant mix and the binder grade is changed to PG 64-22. Dynamic modulus tests are conducted on six specimens prepared from this mix and all the results are given

in Appendix B. Mastercurves of all six specimens is summarized in Figure 3.19. the results are averaged and the tends of dynamic modulus with temperature and frequency are analyzed using isothermal and isochronal plots as presented in Figure 3.20 and Figure 3.21 respectively. The averaged results showed trends that are similar with the previous SP-III Plant mix. The dynamic modulus reduced as temperature is increased and increased with increasing loading frequency. The mastercurve for this mix is presented in Figure 3.22 and polynomial shift factor fit plot in Figure 3.23. The Cole and Cole plane plot, the Black space plot and the Loss tangent plot are presented in Figure 3.24, Figure 3.25 and Figure 3.26 respectively.

### 3.11. Dynamic Modulus Results of SPII Mix with PG 64-22 (Plant Mix)

The dynamic modulus test results on six specimens of plant mixed SP-II HMA with binder grade of PG 64-22 is presented in tabular and graphic form in Appendix C. the summery of all test results is given in master curve format in Figure 3.27. The trend analysis is done using Isothermal and Isochronal plots as presented in Figure 3.28 and Figure 3.29 respectively. The dynamic moduli tend with respect to temperature as well as with respect to frequency are found to agree with previous results from literature. Dynamic modulus curve fit and associated shift factor fit equations are developed and the respective plots are shown in Figure 3.30 and Figure 3.31. Moreover, Cole and Cole plane, black space and loss tangent plots are used to supplement the analysis and are presented in Figure 3.32, Figure 3.33 and Figure 3.34 respectively. The Cole and Cole plane as well as the Black space plots for this mix show good data quality as per the visual analysis undertaken.

### 3.12. Dynamic Modulus Results of SPII Mix with PG 70-22 (Lab Mix)

Another SP-II mix is also prepared in the laboratory with binder grade PG 70-22. Dynamic modulus test results on six specimens are presented in tabular and graphic form in Appendix D. Individual mastercurves developed for each sample tested from this mix are presented in a single plot in Figure 3.35. Isothermal and isochronal plots are developed to check tends with respect to temperature and frequency. As can be seen form Figure 3.36 and Figure 3.37, the dynamic modulus showed a decreasing tend with temperature and increasing trend with increasing frequency. The dynamic modulus mastercurve is developed and presented in Figure 3.38 and the associated shift factor tend line is followed in Figure 3.39. The Cole and Cole plane plot has shown dynamic modulus results at low temperatures are following one trend line in Figure 3.40. However, the results at higher temperatures are following one trend line in Figure 3.41. Similar trend of low damping ratio at low temperature, increasing of loss tangent with increasing temperature up to intermediate temperatures and decrease of damping ratio with decreasing frequency is observed in the loss tangent plot presented in Figure 3.42.

### 3.13. Dynamic Modulus Results of SPIV Mix with PG 70-22 (Commercial Mix)

Dynamic modulus tests on six specimens are conducted for the SP-IV mix with binder grade of PG 70-22. The test results for all tests are presented in tabular and graphic form in Appendix E. A summarized depiction of all data represented by mastercurves developed for each test is shown in Figure 3.43. The test results from the four samples are averaged and Figure 3.44 is an Isothermal representation of and Figure 3.45 is isochronal plot of the average data. As can be seen from the Isothermal and isochronal Curves the trend of dynamic modulus trend is found to be decreasing with increasing temperature and increasing with increasing frequency. The master curve is developed for the average of all test results and presented in Figure 3.46. Experimental fitting of the sigmoid function has shown very good fit to the shifted data. Polynomial function is used to fit the shift factor results and it is shown in Figure 3.47. In addition, Cole and Cole plane, back space, and loss tangent plots are provided in Figure 3.48, Figure 3.49 and Figure 3.50 to supplement and check quality of data. Form the Cole and Cole plane plot and Black space plot show that the data at low and high temperatures follow one trend indicating good quality. The loss tangent plot showed low energy dissipation at lower temperatures indicating higher elastic response of SP-IV mix at low temperatures.

### 3.14. Comparison of SP-II, SPIII and SP-IV dynamic modulus data

The average dynamic modulus master curves of all plant and laboratory produced mixes is presented in one plot in Figure 3.51. The plot shows that the average mastercurve of SP-II and SP-III mixes, regardless of plant or laboratory produced are found to be close to each other and the SP-IV mix exhibited lower dynamic modulus than all other mixes at lower reduced frequencies (which represents intermediate and high temperatures). The average mastercurve for SP-II mix with PG 64-22 is found to have greatest stiffness over the entire frequency and temperature range and the SP-III mix is intermediate between SP-II and SP-IV mixes.

### 3.15. Conclusions

The study presented in this chapter can be summarized as follows:

- The dynamic modulus test results increase with increasing loading frequency and decrease with increasing temperature for all mixes as presented the isothermal plots.
- The effect of change in loading frequency becomes more significant with increasing temperature for all mixes as presented by the isochronal plots.
- The data quality of dynamic modulus tests conducted very consistent with good repeatability. Low temperatures and high temperature data analysis using Cole and Cole plots and Black space plots confirms good quality of data.
- The sigmoidal function used to fit the mastercurve is found to provide a very good fit to the laboratory testing data.

- Visual observations of dynamic modulus mastercurve plots shows that SPII mixes have higher dynamic modulus than SPIII mixes. SP-IV mix exhibits lowest dynamic modulus.
- The loss modulus is found minimum at the low temperature. Loss modulus increases as the temperature increases up to a point at which the loss modulus of asphalt concrete reaches to a pick value as the temperature is increased. Any increase beyond this point shows a decrease in loss modulus which might indicate the effect of aggregate interlock at high temperatures and phase angle effect of binder.

## 3.16. Reference

American Association of State Highway and Transportation Officials (AASHTO). (2011). "Standard Method of Test for Determining Dynamic Modulus of Hot-Mix Asphalt Concrete Mixtures: TP-62-07." AASHTO Provisional Standards.

American Association of State Highway and Transportation Officials (AASHTO). (2011). "Standard Practice for Sampling Bituminous Paving Mixtures: T-168-03." AASHTO Standards.

American Association of State Highway and Transportation Officials (AASHTO). (2011). "Gyratory Compaction: TP-4." AASHTO Provisional Standards.

American Association of State Highway and Transportation Officials (AASHTO). (2011). "Standard Practice for Sampling aggregates: T-2." AASHTO Standards.

American Association of State Highway and Transportation Officials (AASHTO). (2011). "Determining The Asphalt Binder Content of Hot Mix Asphalt (HMA) By The Ignition Method: T-308." AASHTO Standards.

American Association of State Highway and Transportation Officials (AASHTO). (2011). "Theoretical Maximum Specific Gravity and Density of Bituminous Paving Mixtures: T-209." AASHTO Standards.

American Association of State Highway and Transportation Officials (AASHTO). (2011). "Bulk Specific Gravity of Compacted Asphalt Mixtures Using Saturated Surface-Dry Specimens: T-166." AASHTO Standards.

Witczak, M. W., Bonaquist, R., Von Quintus, H., and Kaloush, K. (2000). "Specimen Geometry and Aggregate Size Effects in Uniaxial Compression and Constant Height Shear Test." Journal of the Association of Asphalt Paving Technologists, Vol. 69, 733–793.

Kim, R. Y., (2009). "Modelling of Asphalt Concrete" American society of Civil Engineers, 1801 Alexander bell Drive, Reston, VA 20191-4400, 65-95.

Pellinen, T. K. (2001). “Investigation of the Use of Dynamic Modulus as an Indicator of Hot-Mix Asphalt Performance”. Ph.D. dissertation. Arizona State University, Tempe.

Witczak M. W. and sotil A. (2004). “A Recommended Methodology for Developing Dynamic Modulus E* Master Curves from Nonlinear Optimization”. Arizona State University, Tempe.

Rowe and Sharrock (2010). “Alternate Shift Factor Relationship for Describing the Temperature Dependency of the Visco-Elastic Behavior of Asphalt Materials”. Journal of the Transportation Research Board, pp 125-135

Witczak M. W., Andrei D., Mirza W. (1999). “Development of the 2002 Guide for the Design of New and Rehabilitated Pavement Structures APPENDIX CC-4: Development of a Revised Predictive Model for the Dynamic (Complex) Modulus of Asphalt Mixtures”. NCHRP 1-37 A, University of Maryland, College Park, MD 20740.

Table 3.1: Test Matrix for Dynamic Modulus

| Test Matrix Parameters | HMA Mixture Type | | | | |
|---|---|---|---|---|---|
| | SP-II plant | SP-III plant | SP-II lab | SP-III lab | SP-IV plant |
| PG Binder Grade | PG 64-22 | PG 70-22 | PG 70-22 | PG 64-22 | PG 70-22 |
| Test Frequency (Hz) | 25, 10, 5, 1, 0.5, 0.1 | | | | |
| Corresponding Cycle to Test Frequency | 200, 200, 100, 20, 15, 15 | | | | |
| Test Temperature (°C) | -10, 4, 21, 37, 54 | | | | |
| Required Number of replicate samples | Six | Six | Six | Six | Six |

Table 3.2: Asphalt Content Test Results

| Mix type | Sample wt. (gm) | Wight loss (gm) | Percent Loss (%) | Calibrated Asphalt Content (%) | Average AC (%) |
|---|---|---|---|---|---|
| SP-II | 1649 | 92.7 | 5.62 | 4.42 | |
| SP-II | 1720 | 97.4 | 5.66 | 4.46 | 4.42 |
| SP-II | 1530 | 85.2 | 5.57 | 4.37 | |
| SP-III | 1306 | 75.3 | 5.77 | 4.57 | |
| SP-III | 1423 | 85 | 5.97 | 4.77 | 4.61 |
| SP-III | 1329 | 75.6 | 5.69 | 4.49 | |
| SP-IV | 1917 | 121 | 6.92 | 6.31 | |
| SP-IV | 1959 | 120 | 6.23 | 6.13 | 6.27 |
| SP-IV | 1902 | 121 | 6.03 | 6.36 | |

Table 3.3: Theoretical Maximum Specific Gravity Test

| Mix type | Sample No. | $G_{mm}$ | Average $G_{mm}$ |
|---|---|---|---|
| SP-II with PG 64-22 | 1 | 2.445 | 2.439 |
| | 2 | 2.432 | |
| SP-II with PG 70-22 | 1 | 2.416 | 2.437 |
| | 2 | 2.422 | |
| | 3 | 2.453 | |
| SP-III with PG 70-22 | 1 | 2.430 | 2.431 |
| | 2 | 2.431 | |
| | 3 | 2.422 | |
| | 4 | 2.439 | |
| SP-III with PG 64-22 | 1 | 2.400 | 2.417 |
| | 2 | 2.429 | |
| | 3 | 2.428 | |
| | 4 | 2.421 | |
| | 5 | 2.412 | |
| SP-IV with PG 70-22 | 1 | 2.386 | 2.383 |
| | 2 | 2.377 | |
| | 3 | 2.386 | |

Table 3.4: Recommended Handling Temperatures

| Superpave Mix Design | SP-II | SP-III | SP-IV |
|---|---|---|---|
| Binder Grade | PG 64-22 | PG 70-22 | PG 70-22 |
| RAP content (%) | 15 | 15 | 15 |
| Mixing Temperature (° F) | 311 | 339 | 318 |
| Molding Temperature (° F) | 289 | 312 | 295 |
| Lay down Temperature (° F) | 289 +/- 22 | 312 +/- 22 | 295 +/- 22 |
| Lab Compaction Temperature (° F) | 289 +/- 4 | 312 +/- 4 | 295 +/- 4 |

Table 3.5: Bulk Specific Gravity Test

| Sample No. | Mix type | Wt. in air (gm) | Wt. in water (gm) | Wt. Surface Dry (gm) | Water absorbed (%) | Gmb |
|---|---|---|---|---|---|---|
| 1 | SP-II with PG 64-22 | 2760.8 | 1578.6 | 2772.4 | 0.972 | 2.313 |
| 2 | | 2772.4 | 1573.9 | 2774.5 | 0.175 | 2.309 |
| 3 | | 2752.2 | 1562 | 2758.7 | 0.543 | 2.300 |
| 4 | | 2759.2 | 1572.8 | 2763.5 | 0.361 | 2.317 |
| 5 | | 2688.7 | 1532.5 | 2693.4 | 0.405 | 2.316 |
| 6 | | 2780.2 | 1573.6 | 2786.3 | 0.503 | 2.293 |
| 1 | SP-II with PG 70-22 | 2680.9 | 1523 | 2701.3 | 1.731 | 2.275 |
| 2 | | 2656.6 | 1501.7 | 2673.1 | 1.409 | 2.268 |
| 3 | | 2701.0 | 1540 | 2729.1 | 2.363 | 2.271 |
| 4 | | 2731.1 | 1559.1 | 2759.1 | 2.333 | 2.276 |
| 5 | | 2742.9 | 1557.7 | 2756.9 | 1.167 | 2.287 |
| 6 | | 2710 | 1529.6 | 2717.5 | 0.631 | 2.281 |
| 1 | SP-III with PG 70-22 | 2787.7 | 1577.9 | 2794 | 0.518 | 2.292 |
| 2 | | 2777.7 | 1575.9 | 2794 | 1.338 | 2.280 |
| 3 | | 2820.2 | 1606.8 | 2828.3 | 0.663 | 2.309 |
| 4 | | 2737.8 | 1542.7 | 2745.3 | 0.624 | 2.277 |
| 5 | | 2737.6 | 1546.7 | 2741 | 0.285 | 2.292 |
| 6 | | 2791.2 | 1569.4 | 2795.9 | 0.383 | 2.276 |
| 1 | SP-III with PG 64-22 | 2766 | 1569.6 | 2775.9 | 0.821 | 2.293 |
| 2 | | 2752.5 | 1565.6 | 2760.7 | 0.686 | 2.303 |
| 3 | | 2732.5 | 1555.6 | 2740.7 | 0.692 | 2.306 |
| 4 | | 2734.8 | 1560.4 | 2751.9 | 1.435 | 2.295 |
| 5 | | 2705.8 | 1545.4 | 2725.8 | 1.694 | 2.292 |
| 6 | | 2756.8 | 1575.3 | 2772.5 | 1.311 | 2.303 |
| 1 | SP-IV with PG 70-22 | 2684.5 | 1503 | 2697.5 | 1.088 | 2.247 |
| 2 | | 2723.6 | 1518.3 | 2729.8 | 0.512 | 2.248 |
| 3 | | 2716.6 | 1527.3 | 2726.9 | 0.859 | 2.265 |
| 4 | | 2732.1 | 1533.3 | 2739.9 | 0.646 | 2.264 |
| 5 | | 2639 | 1471 | 2647 | 0.680 | 2.244 |
| 6 | | 2698.4 | 1512.2 | 2705.7 | 0.612 | 2.261 |

Table 3.6: Percentage Air Voids Test

| Sample No. | Mix type | Air Void (%) |
|---|---|---|
| 1 | SP-II with PG 64-22 | 5.2 |
| 2 | | 5.3 |
| 3 | | 5.7 |
| 4 | | 5.0 |
| 5 | | 5.0 |
| 6 | | 6.0 |
| 1 | SP-II with PG 70-22 | 5.7 |
| 2 | | 6.0 |
| 3 | | 5.9 |
| 4 | | 5.7 |
| 5 | | 5.2 |
| 6 | | 5.5 |
| 1 | SP-III with PG 70-22 | 5.2 |
| 2 | | 5.7 |
| 3 | | 5.0 |
| 4 | | 5.8 |
| 5 | | 5.2 |
| 6 | | 5.8 |
| 1 | SP-III with PG 64-22 | 6.0 |
| 2 | | 5.6 |
| 3 | | 5.5 |
| 4 | | 5.9 |
| 5 | | 6.0 |
| 6 | | 5.6 |
| 1 | SP-IV with PG 70-22 | 5.8 |
| 2 | | 5.8 |
| 3 | | 5.1 |
| 4 | | 5.1 |
| 5 | | 5.9 |
| 6 | | 5.1 |

Table 3.7: Air Void Uniformity Check

| Sample No | Mix type | Core No | Wt. in air (gm) | Wt. in water (gm) | Wt. Surface Dry (gm) | Water absorbed (%) | $G_{mb}$ | $G_{mm}$ | Air void (%) |
|---|---|---|---|---|---|---|---|---|---|
| 26 | SPIII | Top section | 824.6 | 467.4 | 827.3 | 0.750 | 2.291 | 2.43 | 5.712 |
| | | Middle section | 947.9 | 537.1 | 949.3 | 0.340 | 2.300 | 2.43 | 5.366 |
| | | Bottom section | 818.4 | 461.9 | 823.6 | 1.438 | 2.263 | 2.43 | 6.887 |
| 24 | SPIII | Top section | 909.2 | 512.5 | 910.5 | 0.327 | 2.284 | 2.43 | 5.991 |
| | | Middle section | 819.6 | 465.8 | 821.5 | 0.534 | 2.304 | 2.43 | 5.177 |
| | | Bottom section | 868.3 | 495.5 | 871.3 | 0.798 | 2.311 | 2.43 | 4.916 |
| 8 | SPIII | Top section | 857.7 | 481.1 | 860.4 | 0.712 | 2.261 | 2.43 | 6.944 |
| | | Middle section | 849.6 | 478.5 | 851.5 | 0.509 | 2.278 | 2.43 | 6.266 |
| | | Bottom section | 866.5 | 489.3 | 868.8 | 0.606 | 2.283 | 2.43 | 6.038 |
| | | | | | | mean Top section | 2.279 | | 6.216 |
| | | | | | | mean Middle section | 2.294 | | 5.603 |
| | | | | | | mean Bottom section | 2.285 | | 5.947 |
| | | | | | | variance Top section | 0.000 | | 0.417 |
| | | | | | | variance Middle section | 0.000 | | 0.338 |
| | | | | | | variance Bottom section | 0.001 | | 0.977 |
| | | | | | | mean of top section is equal to mean of middle section test statistic < 2.78, means they are equal | 1.221 | | 1.221 |
| | | | | | | mean of bottom section is equal to mean of middle section test statistic < 2.78, means they are equal | 0.520 | | 0.520 |

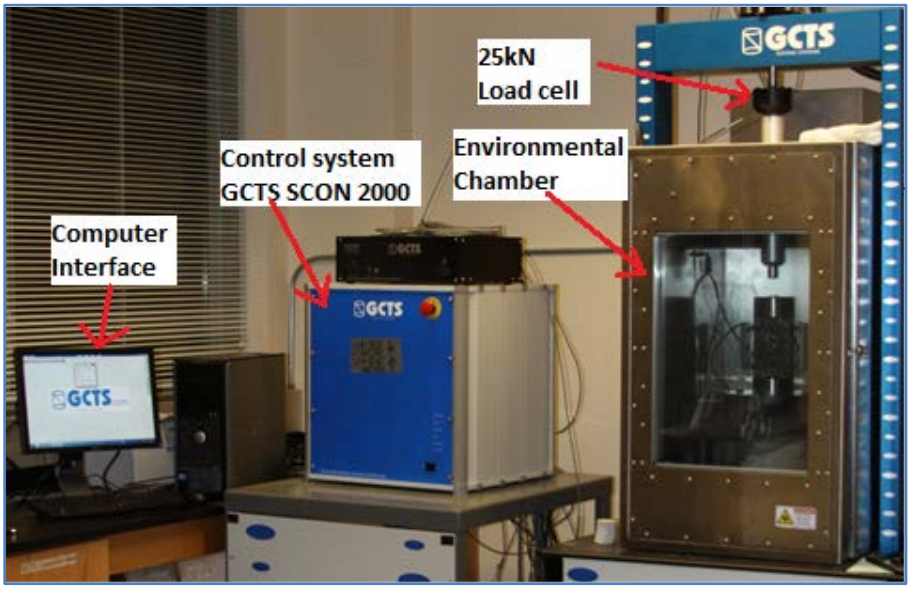


Figure 3.1: Servo-Hydraulic Testing System

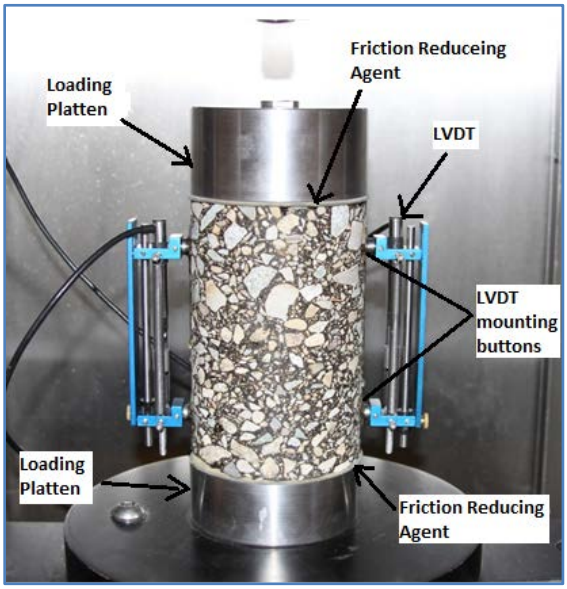


Figure 3.2: Linear Variable Differential Transformers (LVDTs) Mounted On Specimen

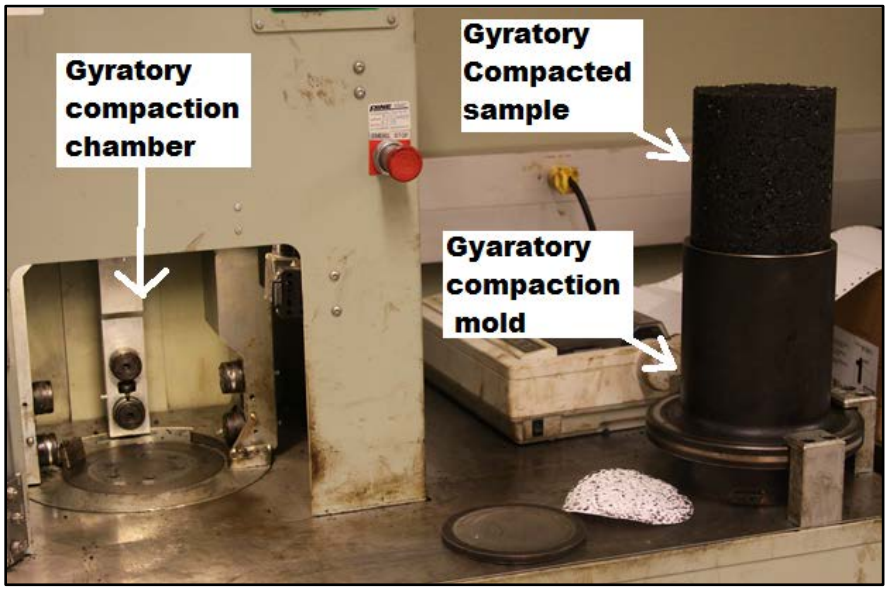


Figure 3.3: Gyratory Compactor

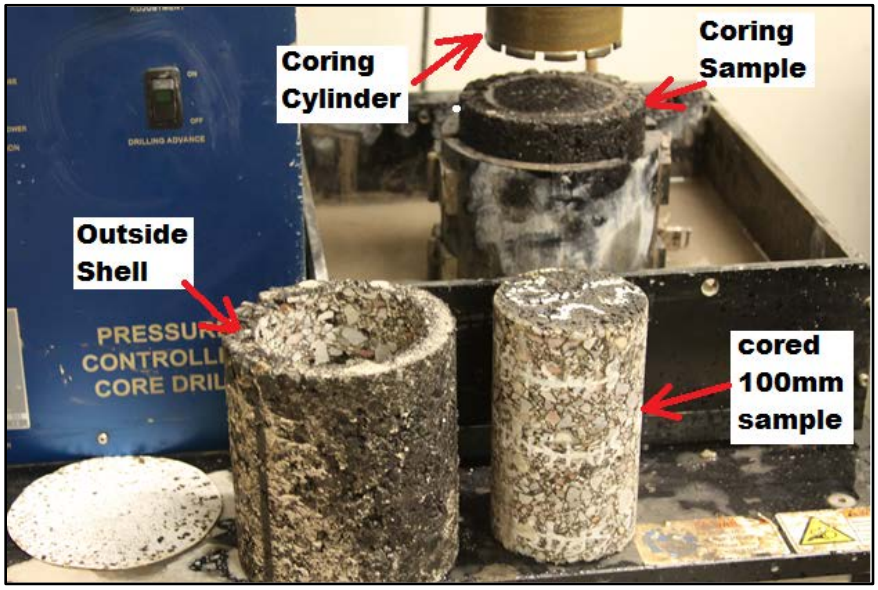


Figure 3.4: Asphalt Coring Machine

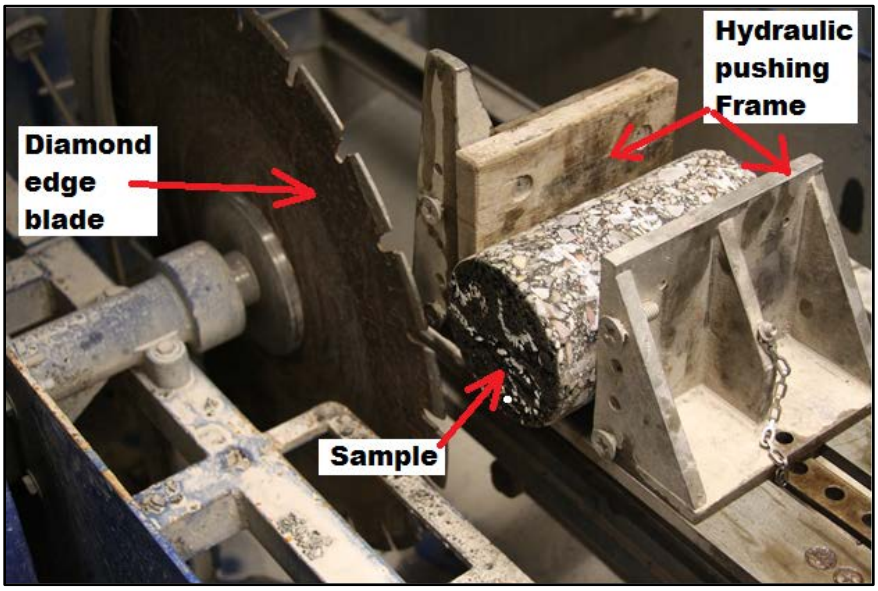


Figure 3.5: Lab Specimen Saw

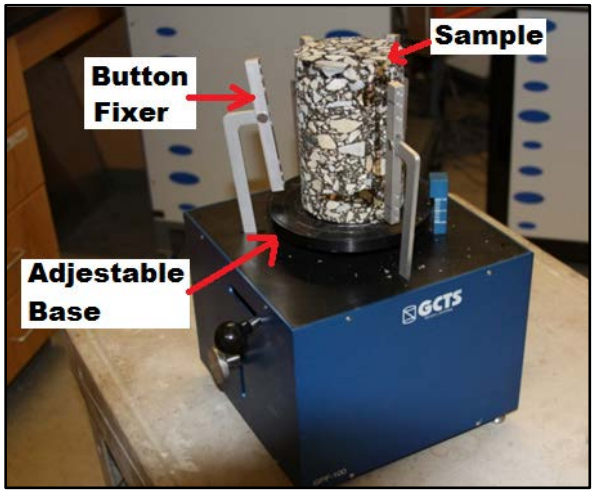


Figure 3.6: Automatic Positioning Fixture

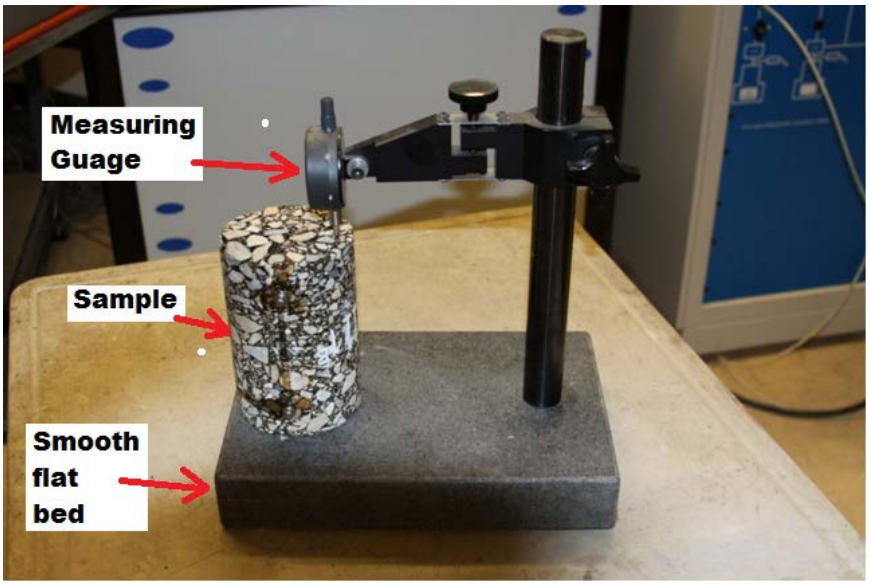


Figure 3.7: Rock Flatness Gauge

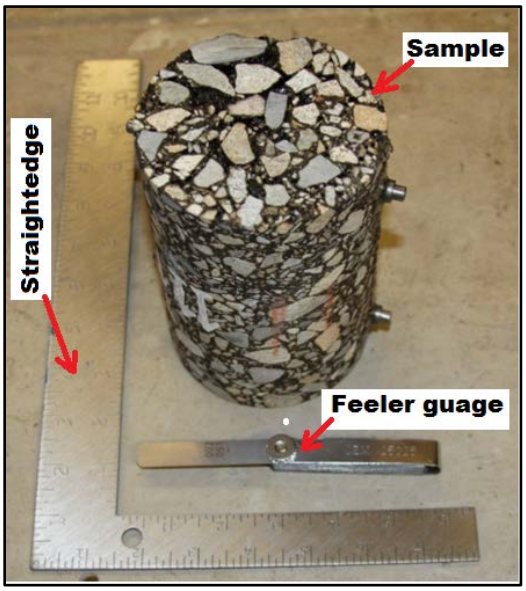


Figure 3.8: straightedge and feeler gauge for Waviness check

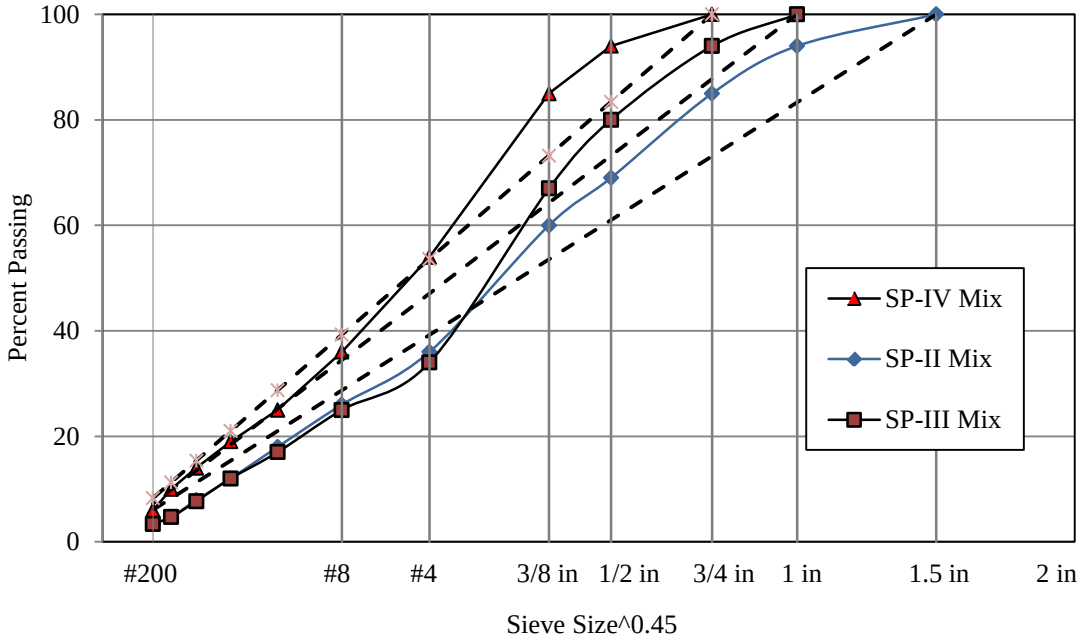


Figure 3.9: Sieve analysis for SP-II and SP-III mixes

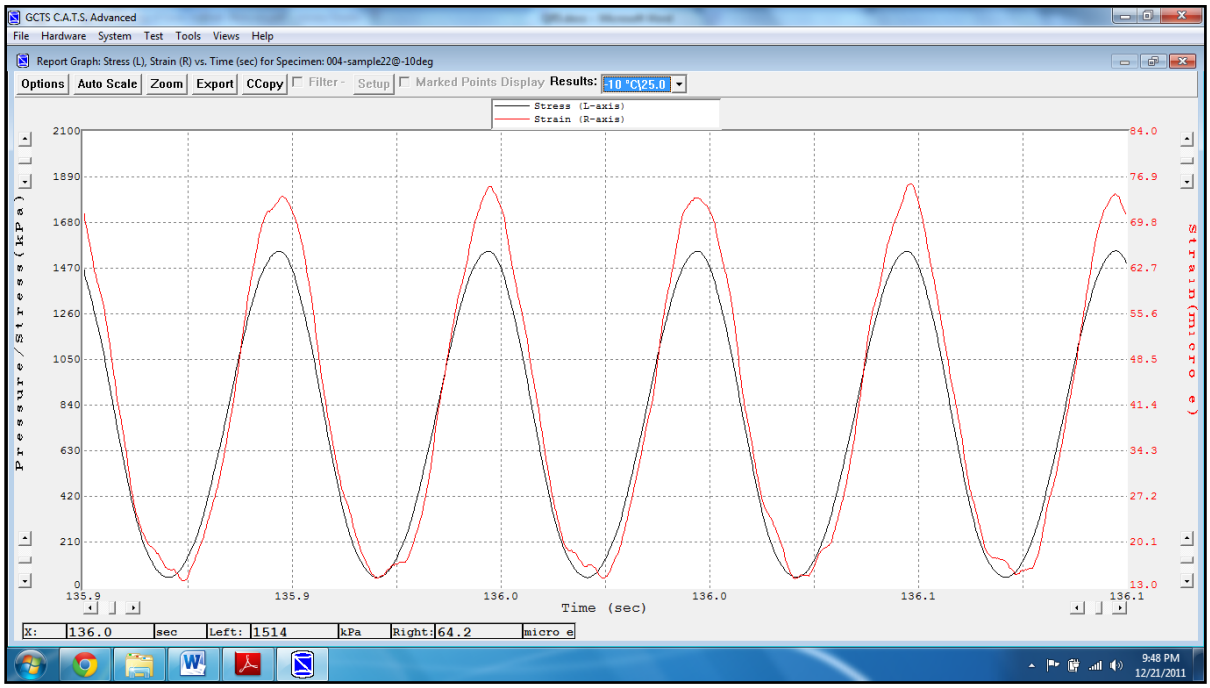


Figure 3.10: Typical stress, strain vs. Time Plot at Temperature (-10°C)

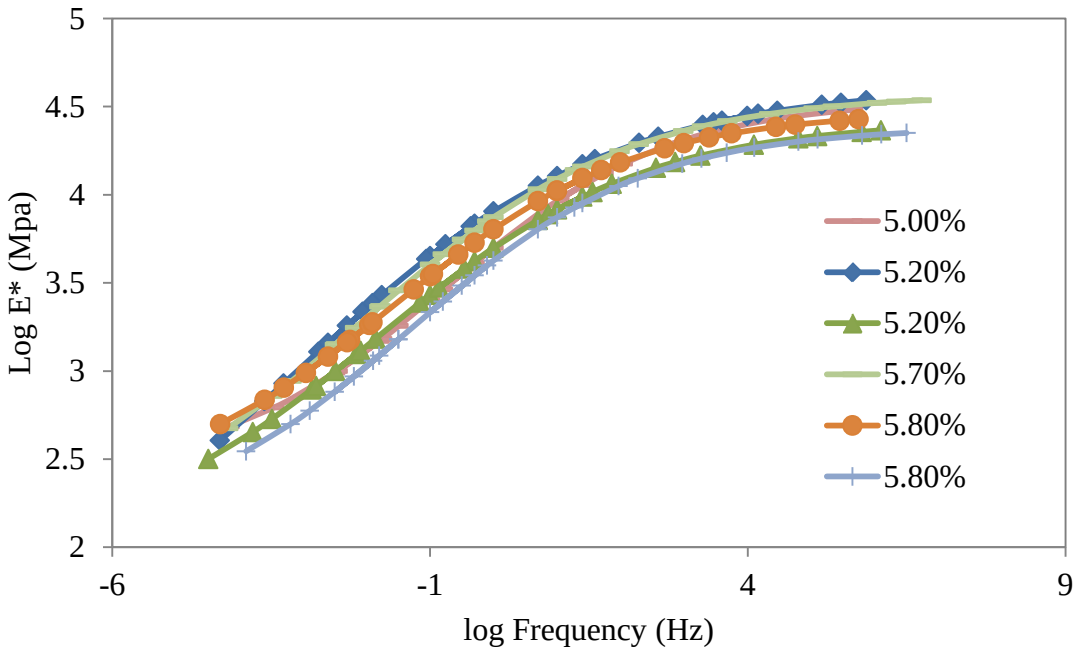


Figure 3.11: Comparison Master Curves with %AV for SP-III with PG 70-22

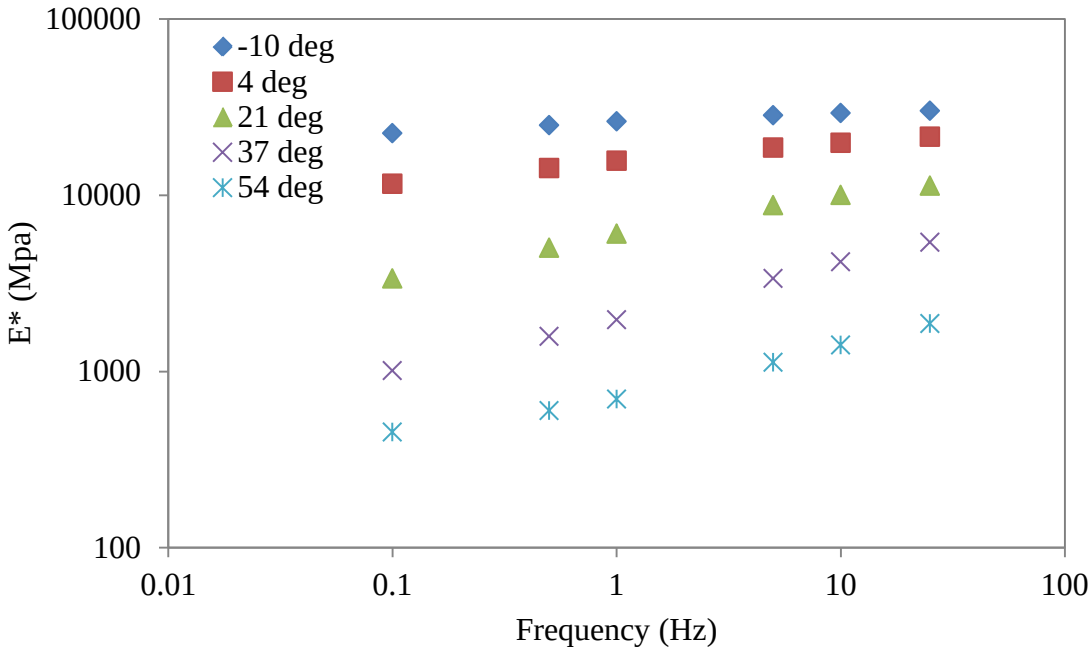


Figure 3.12: Isothermal Plot for Average of SP-III, PG 70-22

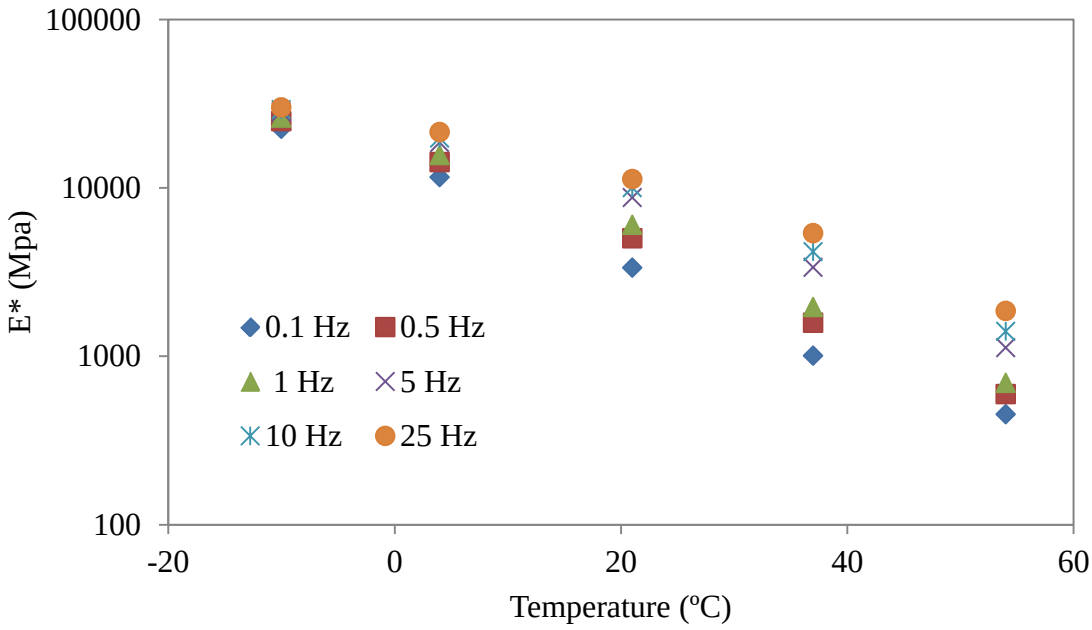


Figure 3.13: Isochronal Plot for Average of SP-III, PG 70-22

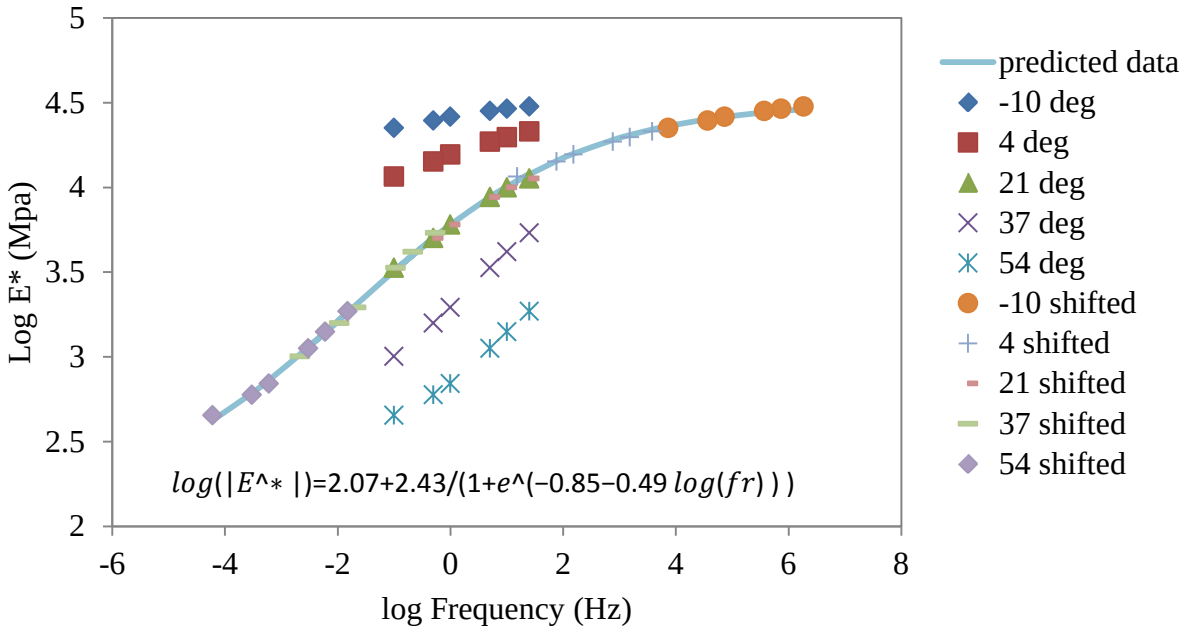


Figure 3.14: Master Curve for Average of SP-III, PG 70-22

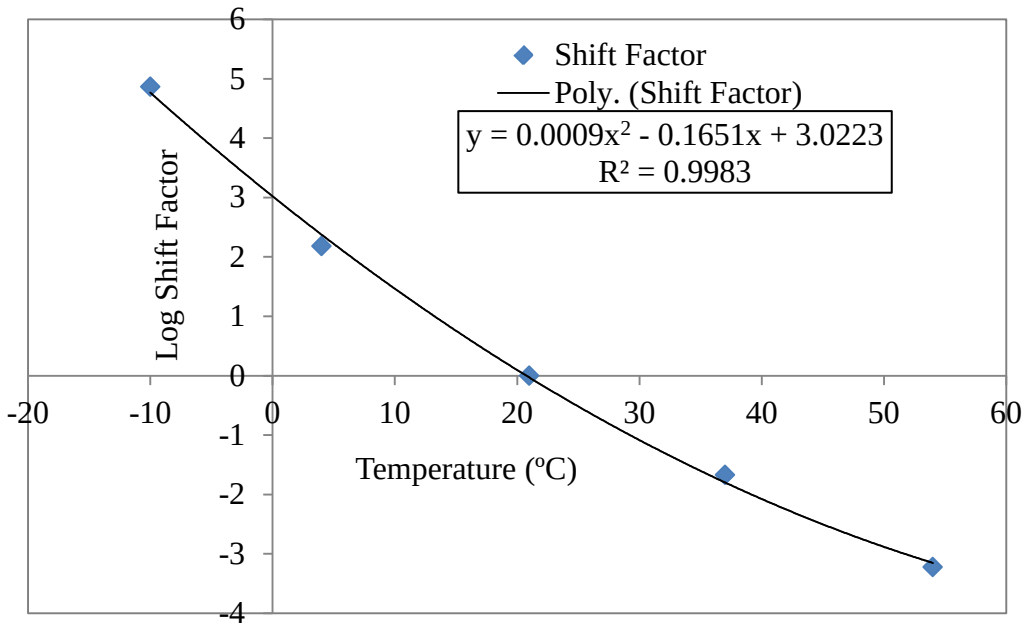


Figure 3.15: Shift Factor for Average of SP-III, PG 70-22

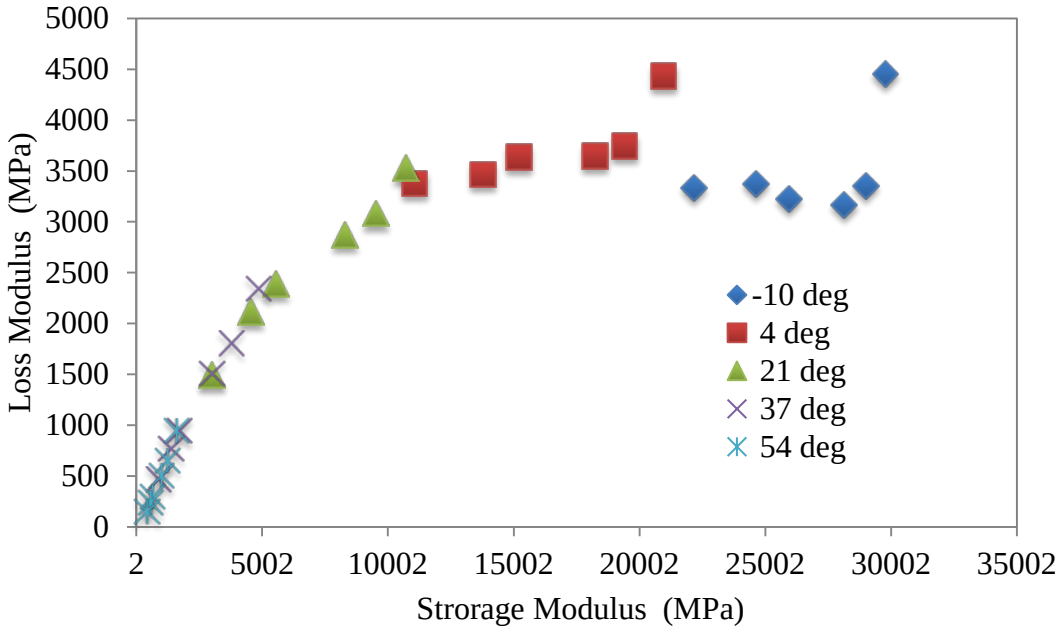


Figure 3.16: Cole and Cole Plot for Average of SP-III, PG 70-22

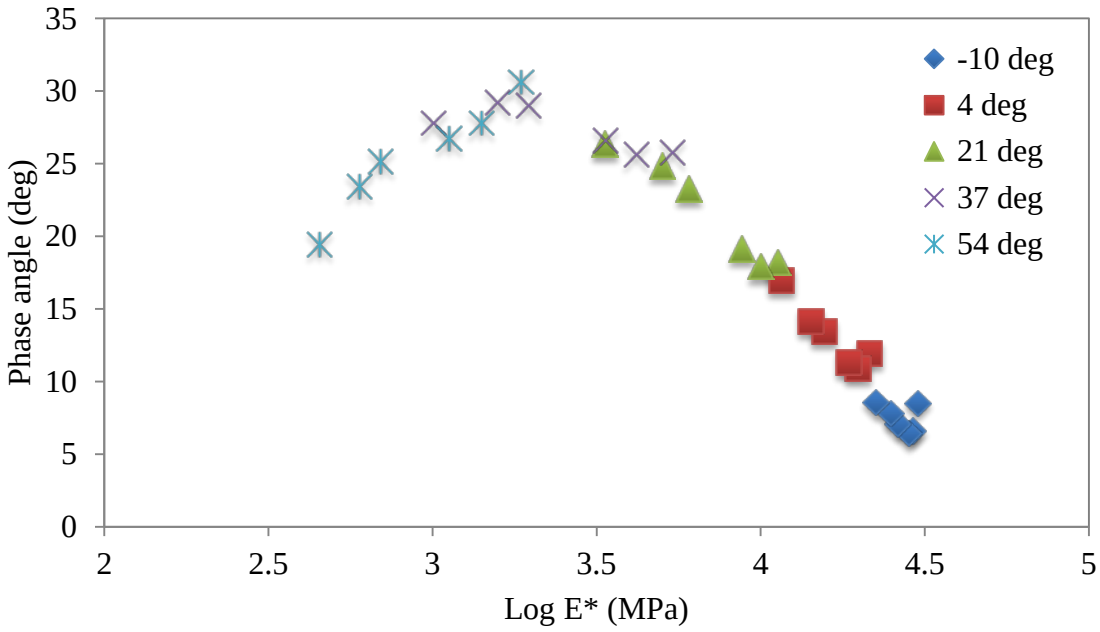


Figure 3.17: Black Space Plot for Average of SP-III, PG 70-22

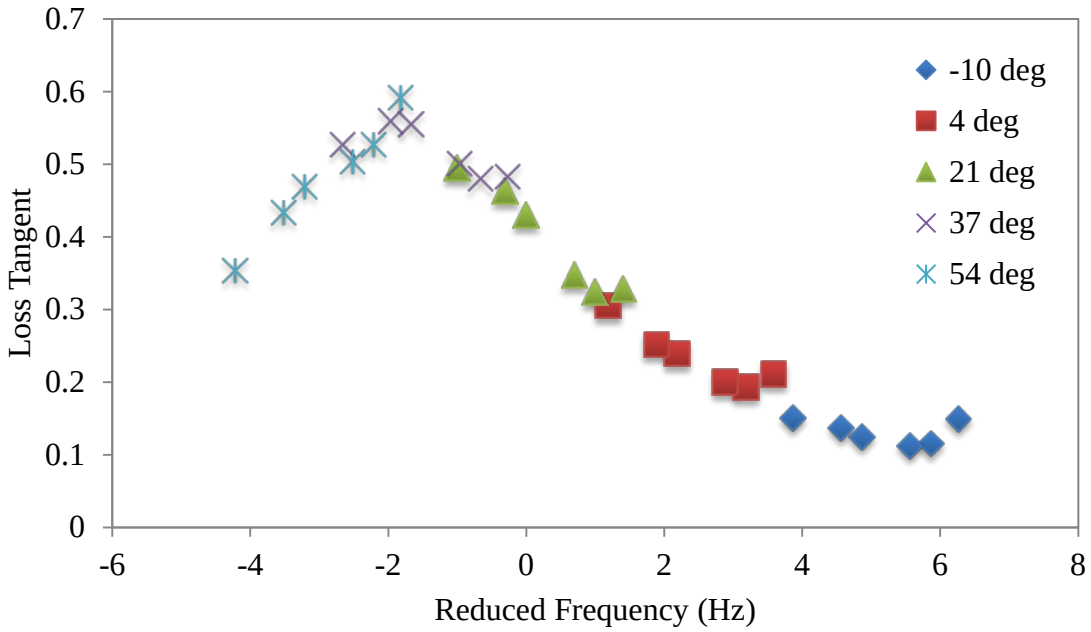


Figure 3.18: Loss Tangent Plot for Average of SP-III, PG 70-22

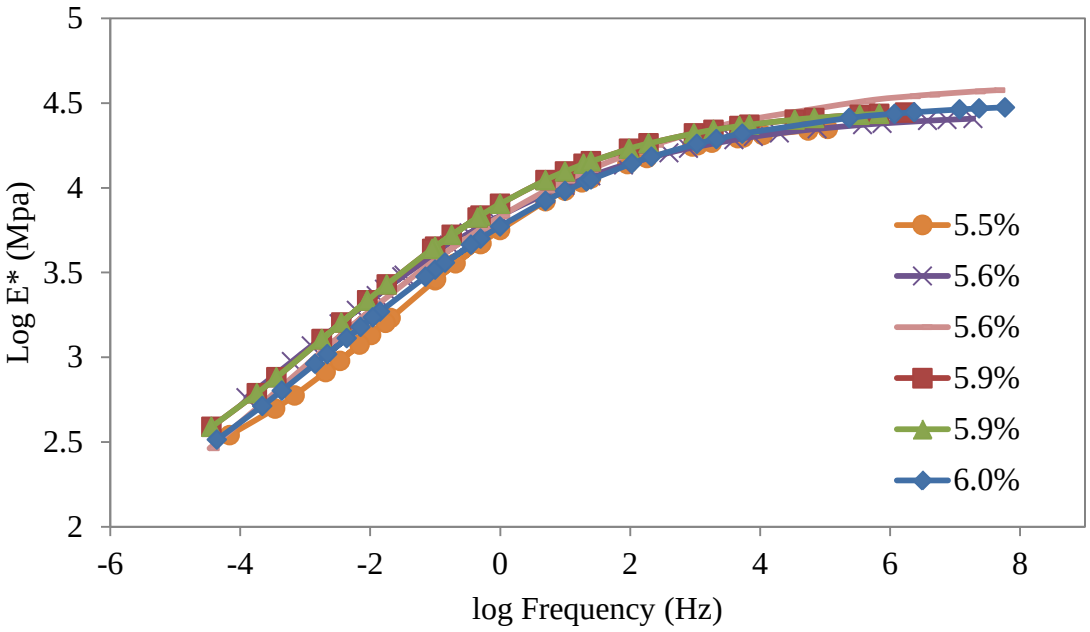


Figure 3.19: Comparison Master Curves for SP-III, PG 64-22 Test Results

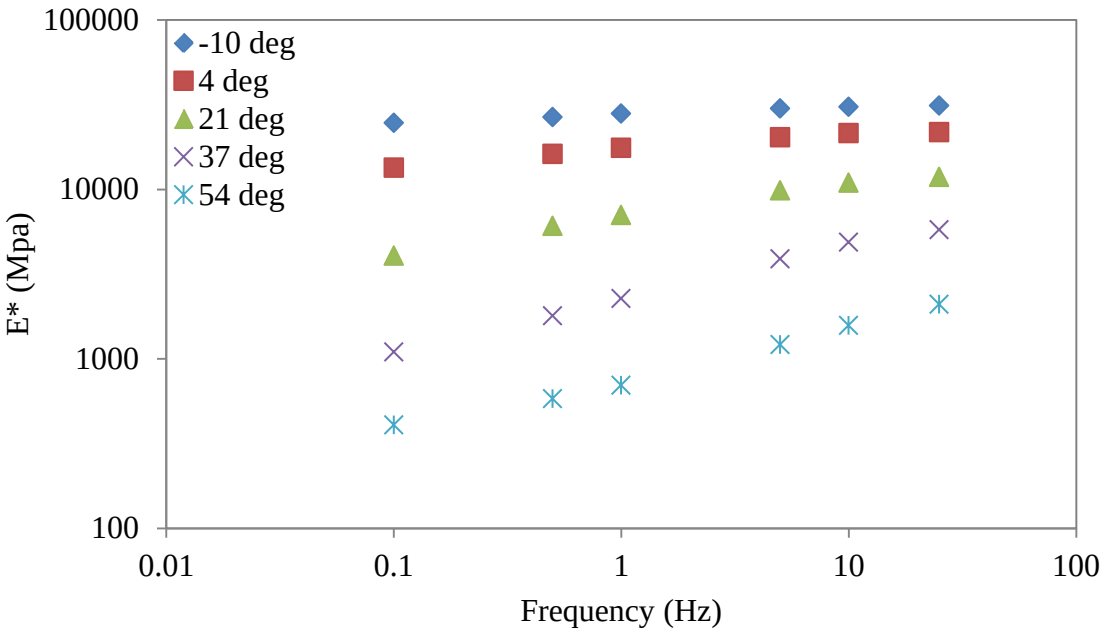


Figure 3.20: Isothermal Plot for Average of SP-III, PG 64-22

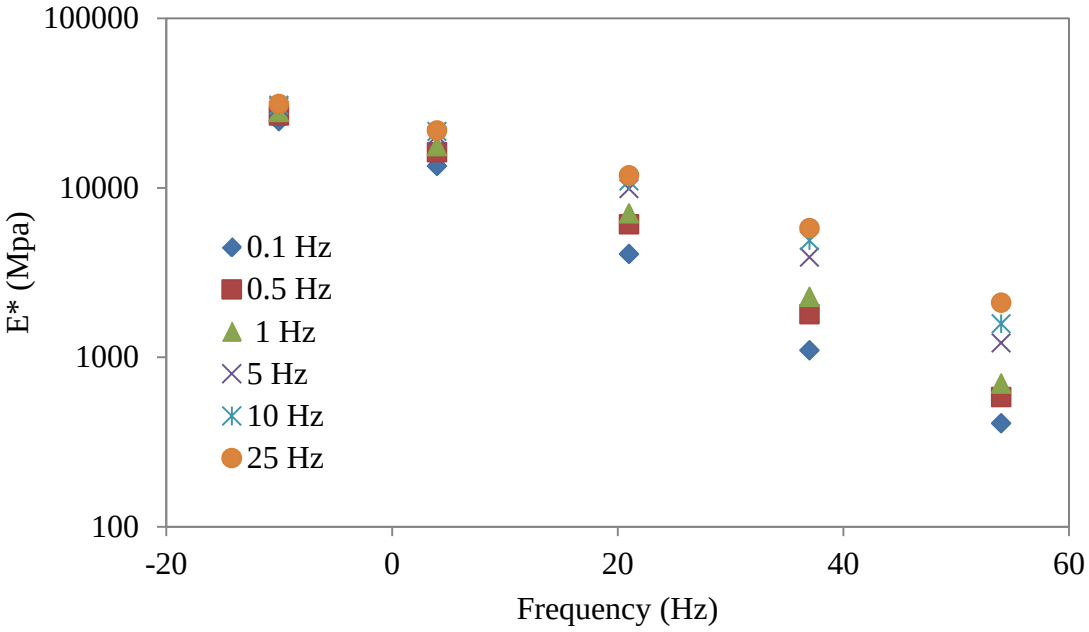


Figure 3.21: Isochronal Plot for Average of SP-III, PG 64-22

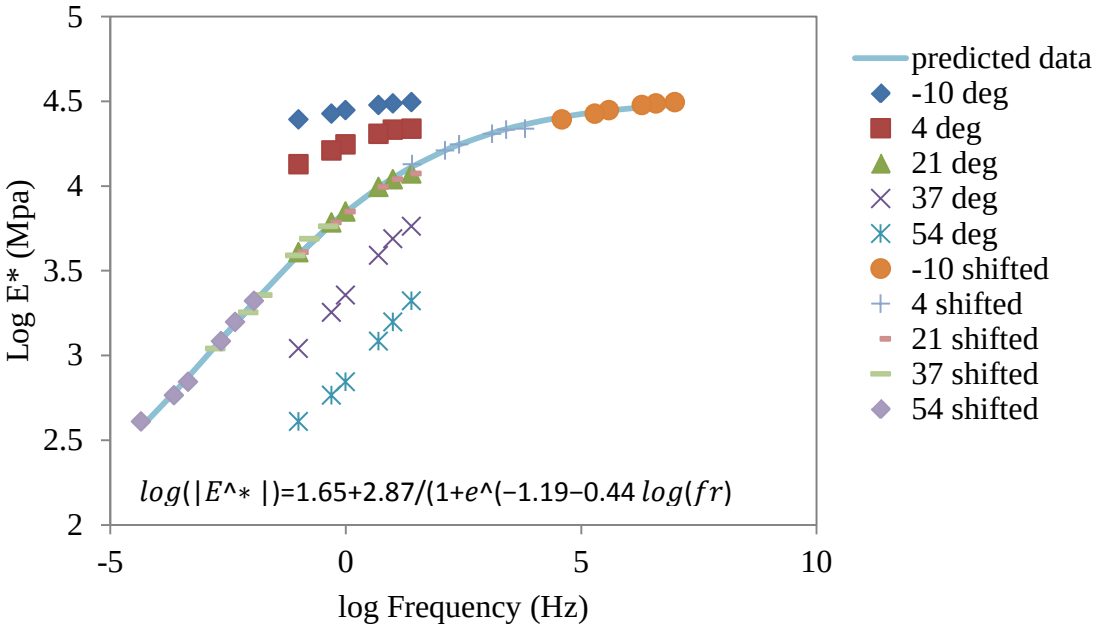


Figure 3.22: Master Curve for Average of SP-III, PG 64-22

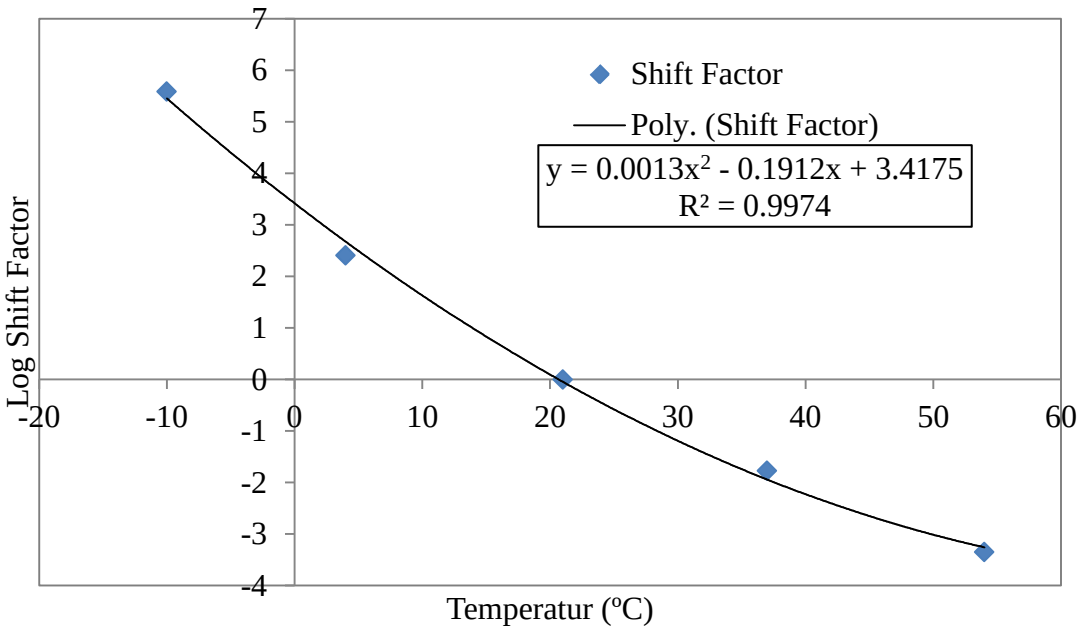


Figure 3.23: Shift Factor for Average of SP-III, PG 64-22

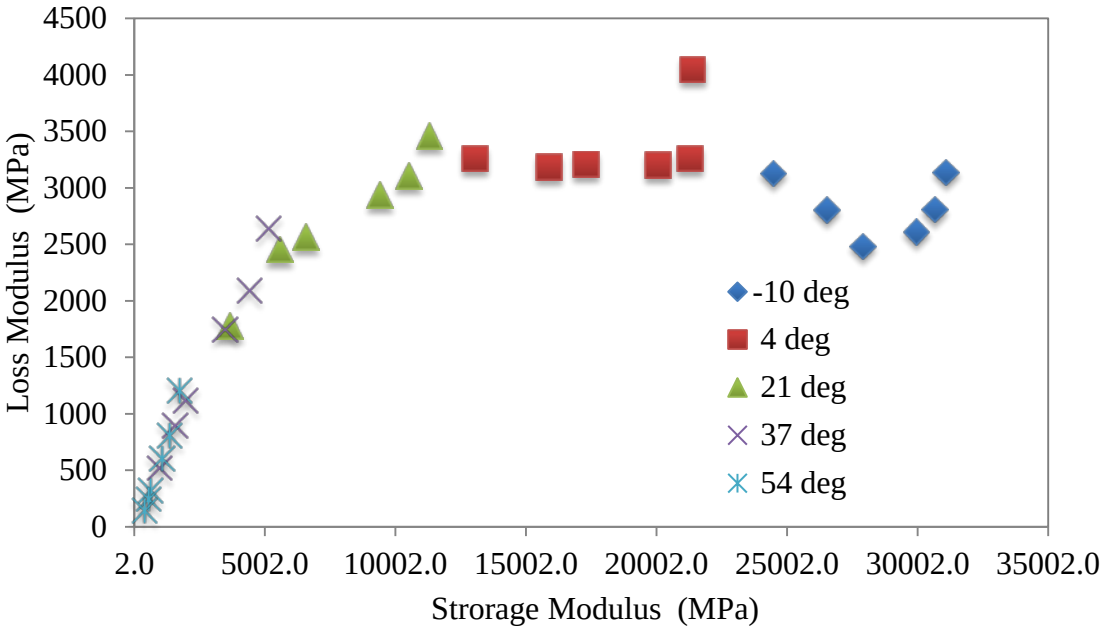


Figure 3.24: Cole and Cole Plot for Average of SP-III, PG 64-22

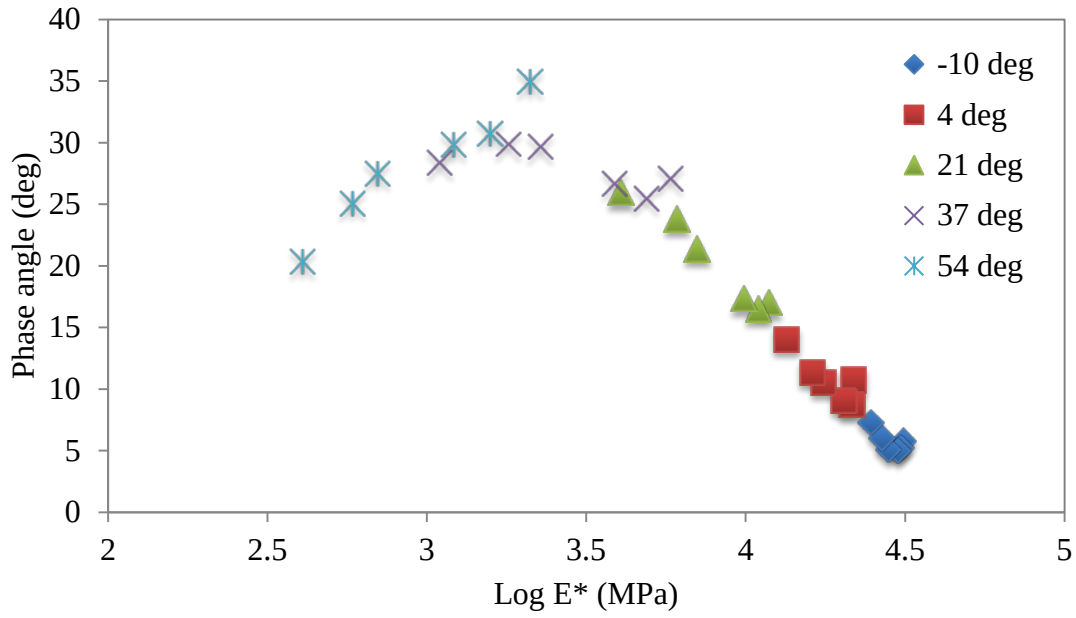


Figure 3.25: Black Space Plot for Average of SP-III, PG 64-22

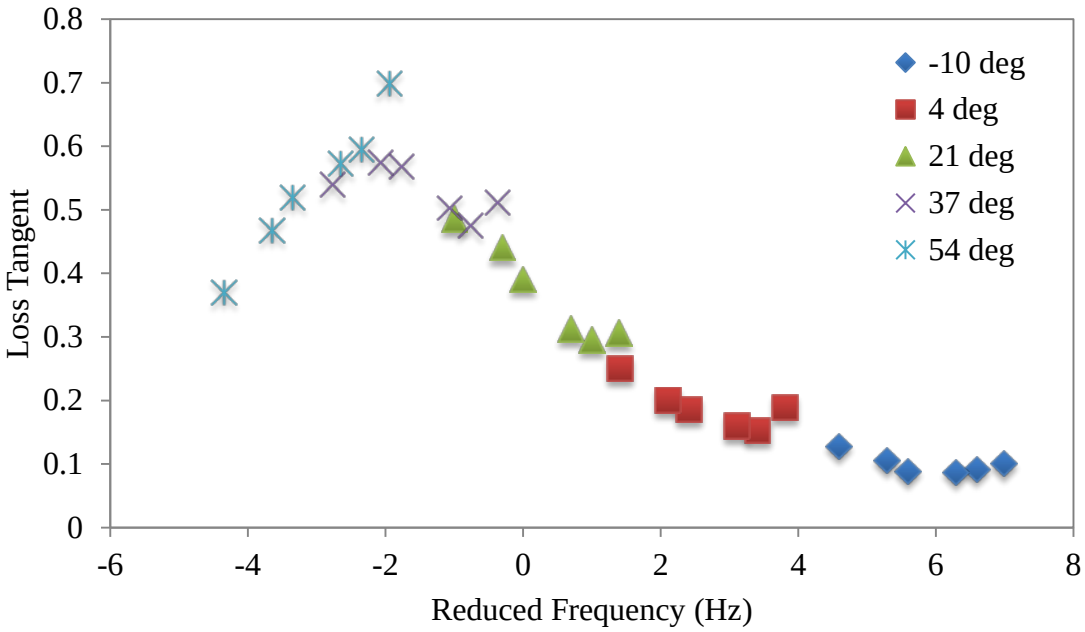


Figure 3.26: Loss Tangent Plot for Average of SP-III, PG 64-22

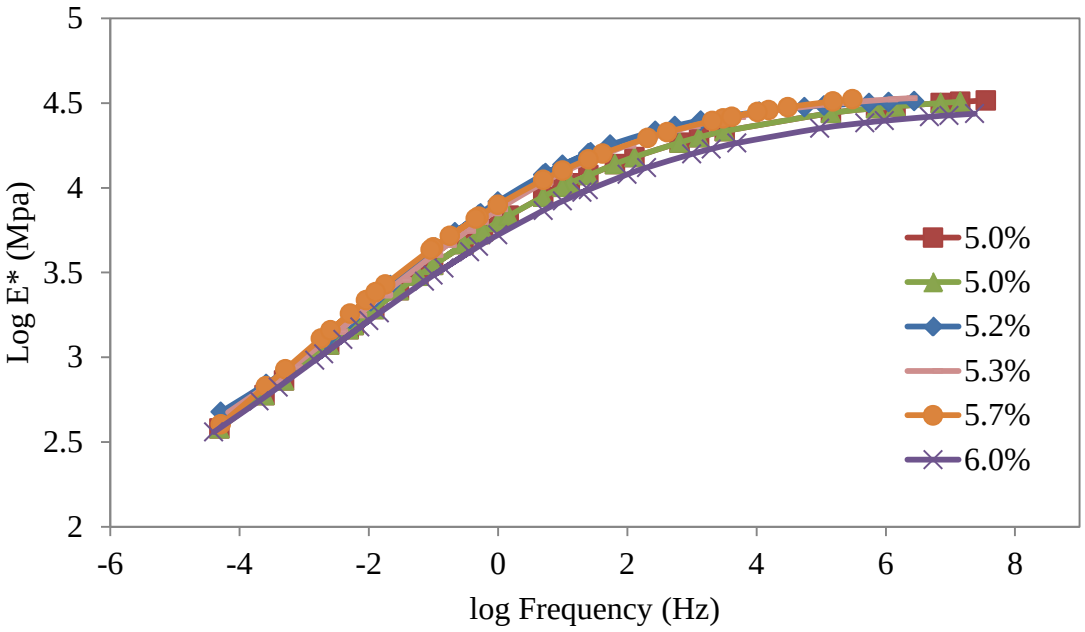


Figure 3.27: Comparison Master Curves for SP-II, PG 64-22 Test Results

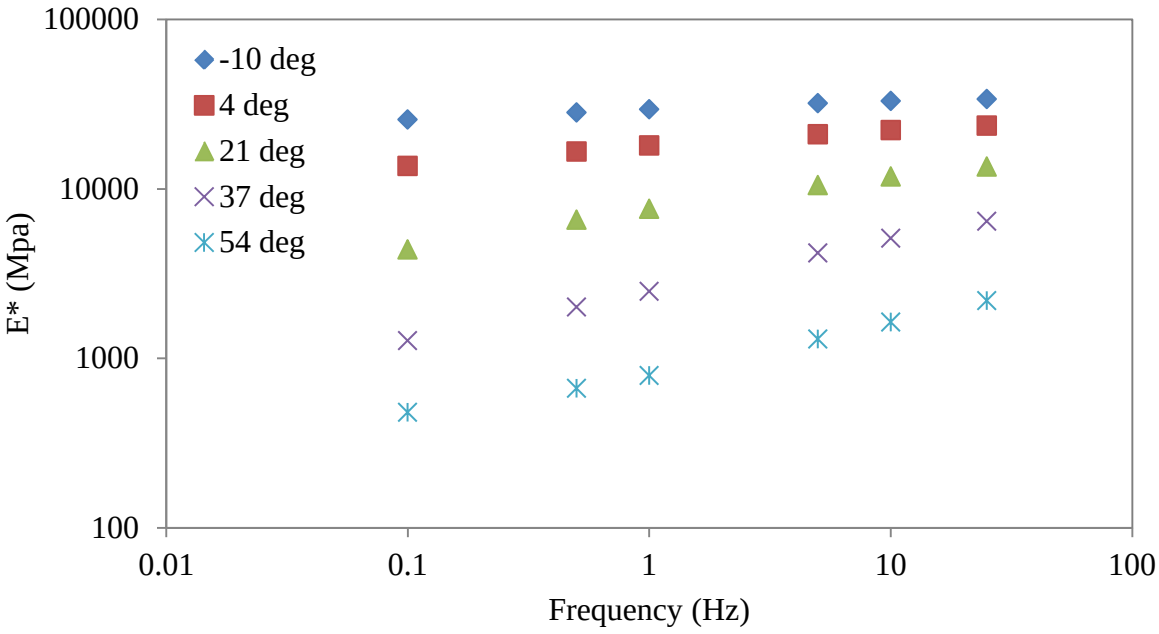


Figure 3.28: Isothermal Plot for Average of SP-II, PG 64-22

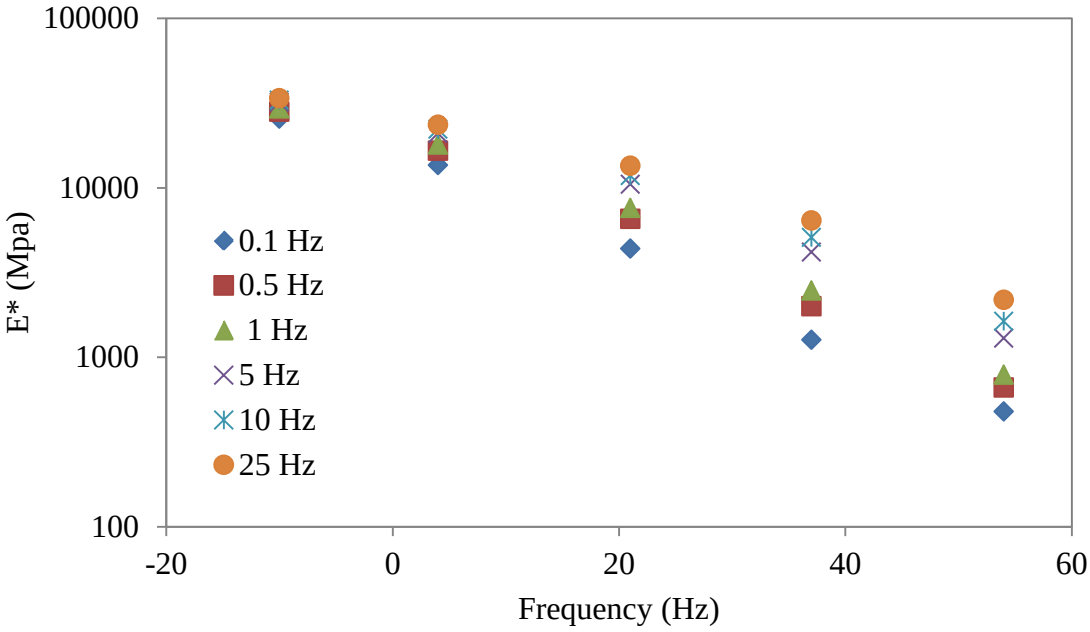


Figure 3.29: Isochronal Plot for Average of SP-II, PG 64-22

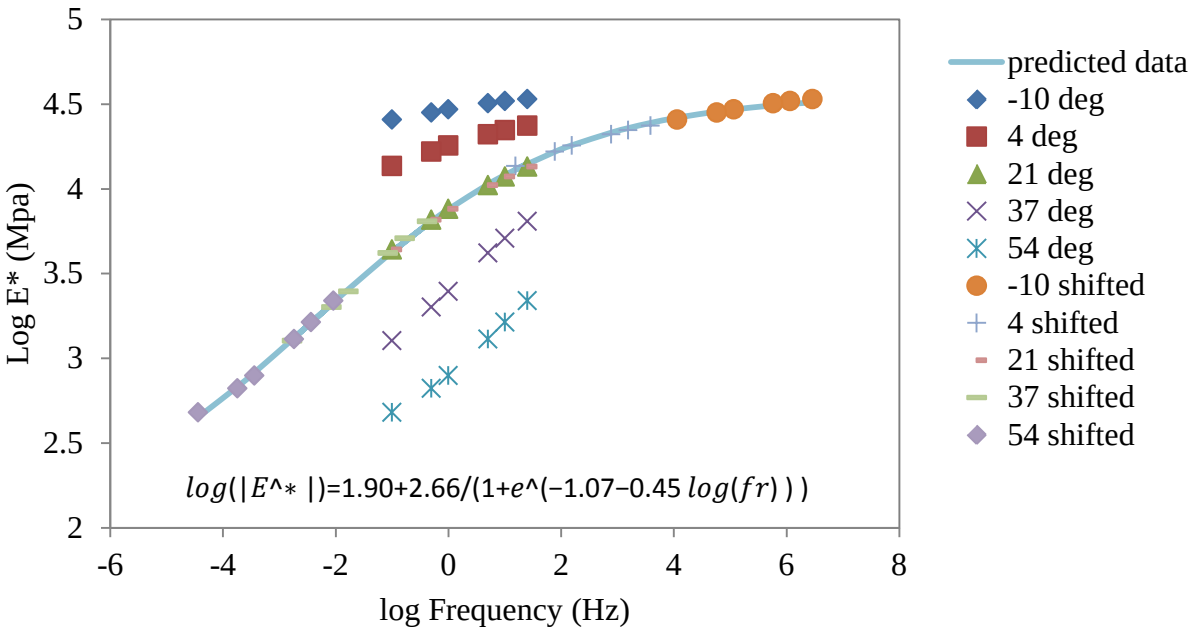


Figure 3.30: Master Curve for Average of SP-II, PG 64-22

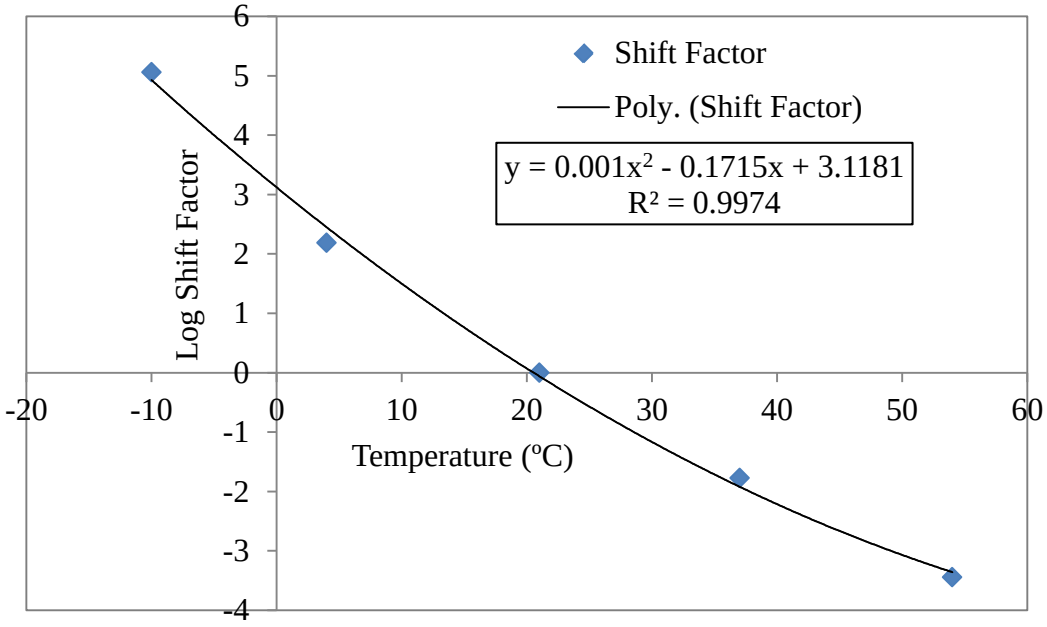


Figure 3.31: Shift Factor for Average of SP-II, PG 64-22

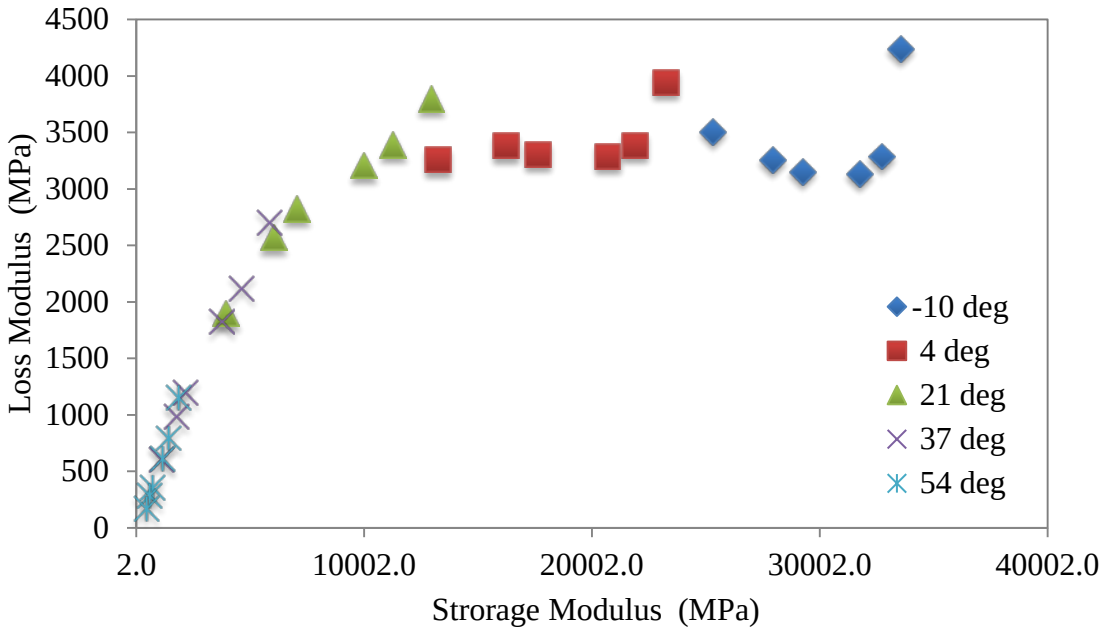


Figure 3.32: Cole and Cole Plot for Average of SP-II, PG 64-22

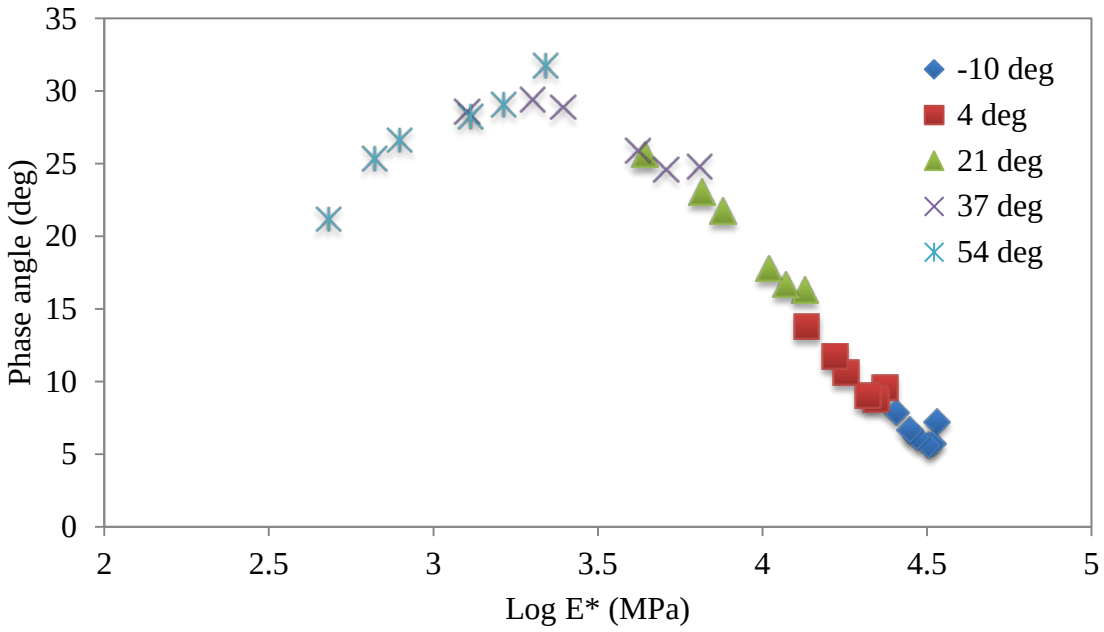


Figure 3.33: Black Space Plot for Average of SP-II, PG 64-22

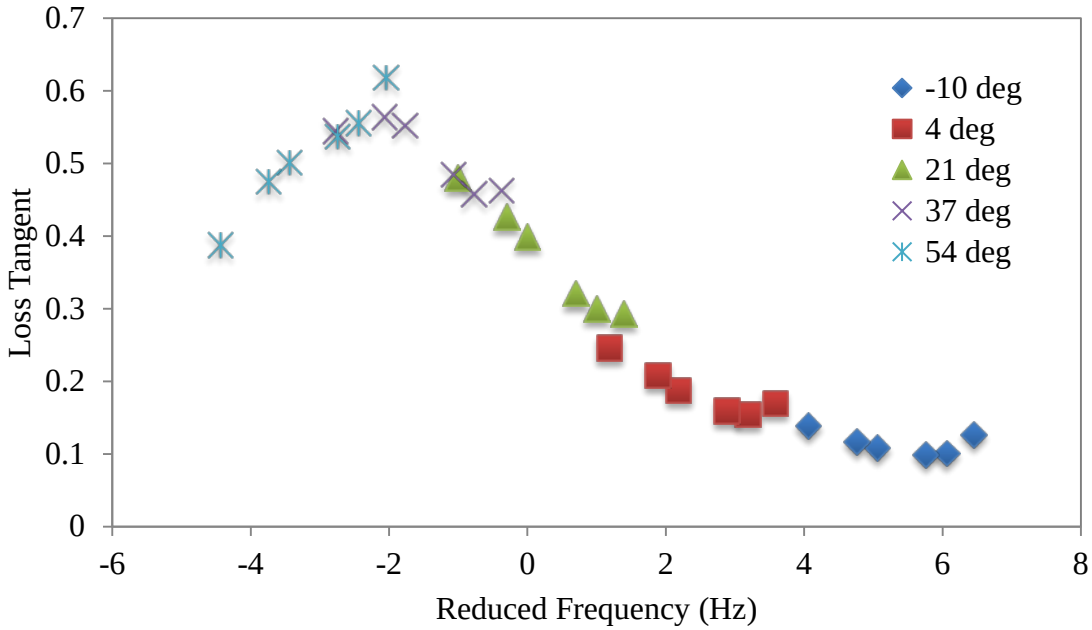


Figure 3.34: Loss Tangent Plot for Average of SP-II, PG 64-22

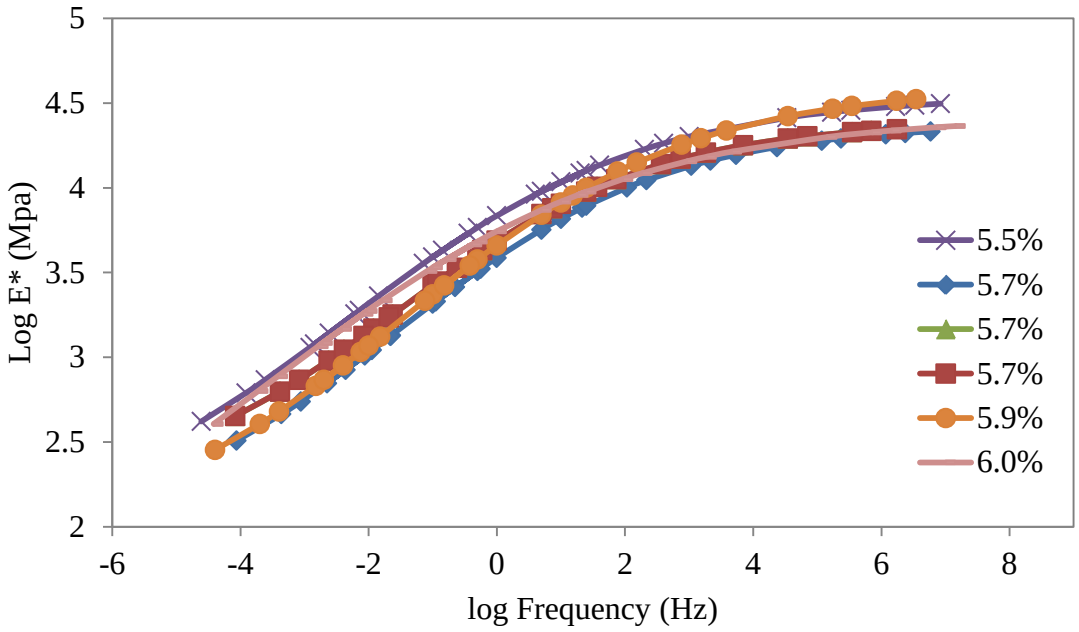


Figure 3.35: Comparison Master Curves for SP-II, PG 70-22 Test Results

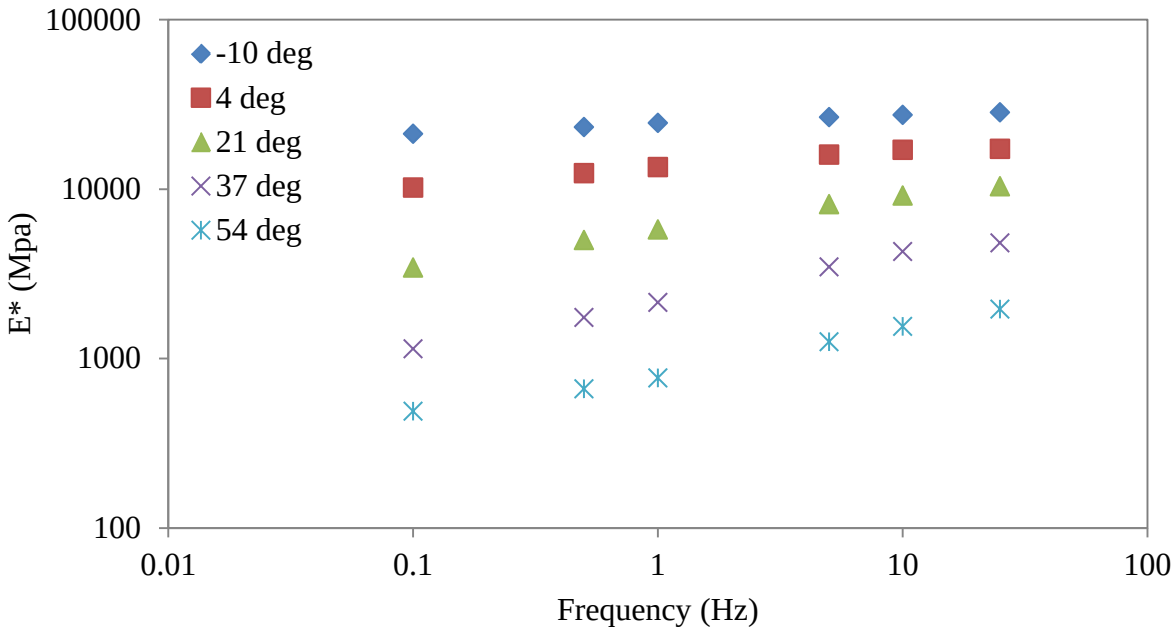


Figure 3.36: Isothermal Plot for Average of SP-II, PG 70-22

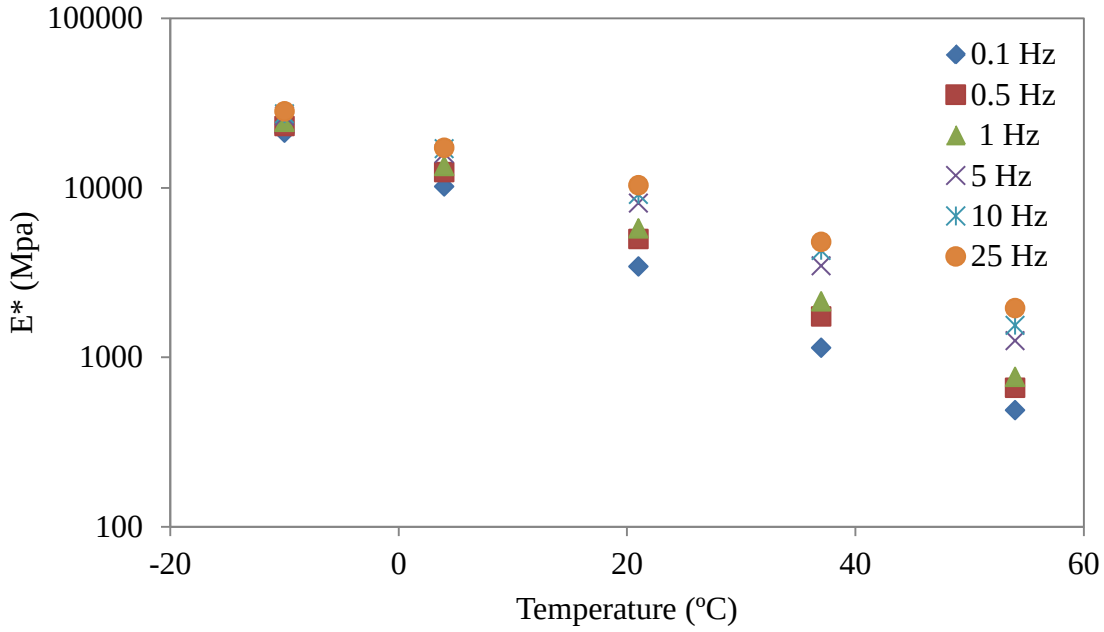


Figure 3.37: Isochronal Plot for Average of SP-II, PG 70-22

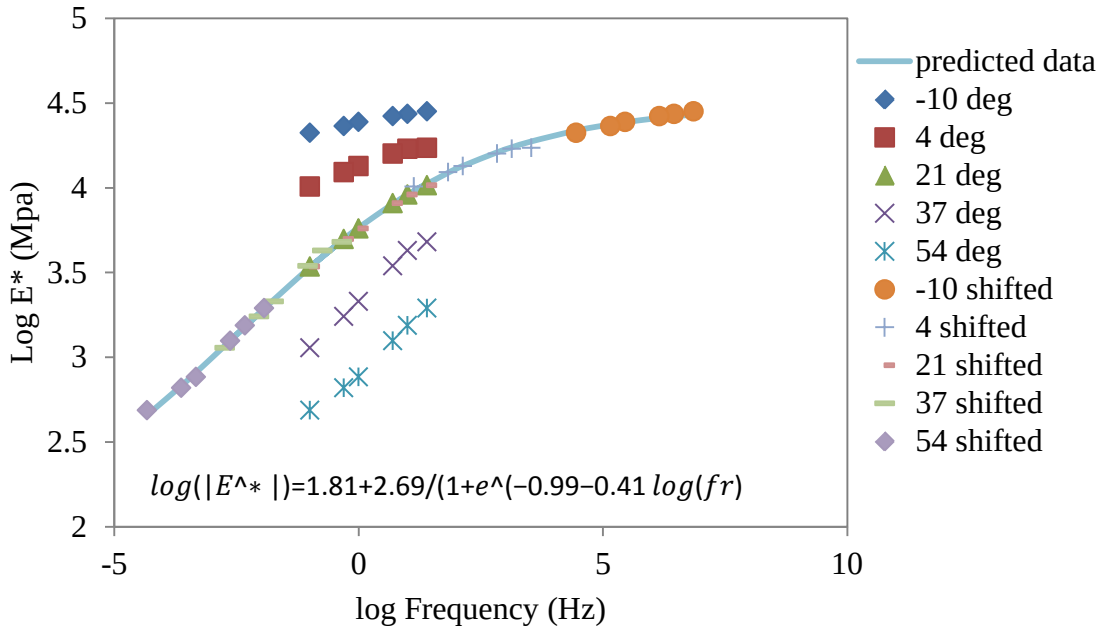


Figure 3.38: Master Curve for Average of SP-II, PG 70-22

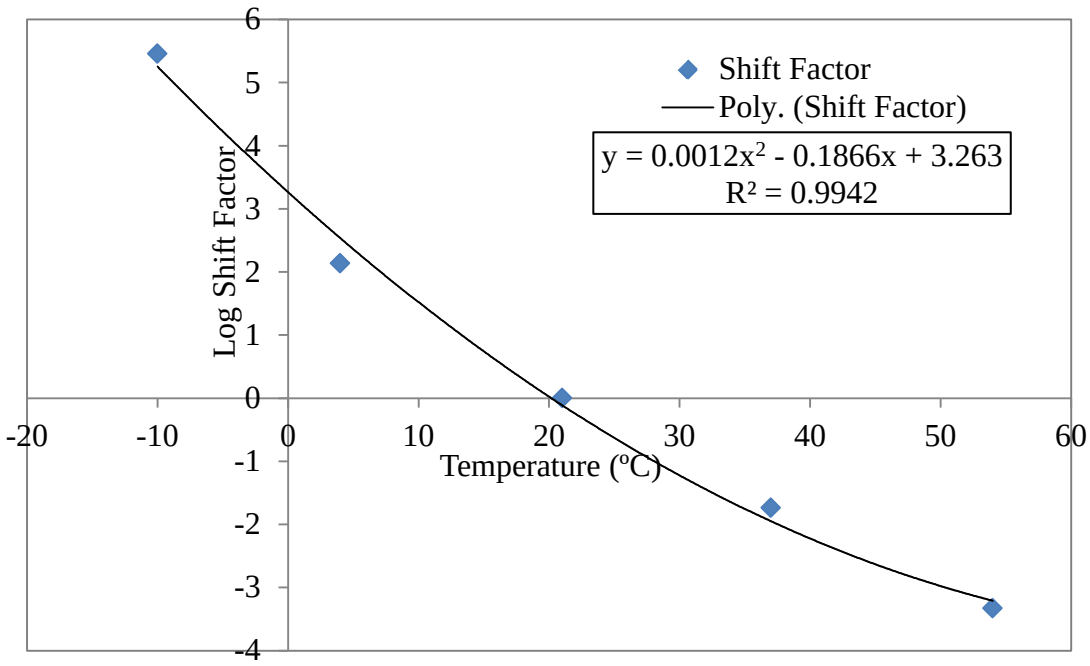


Figure 3.39: Shift Factor for Average of SP-II, PG 70-22

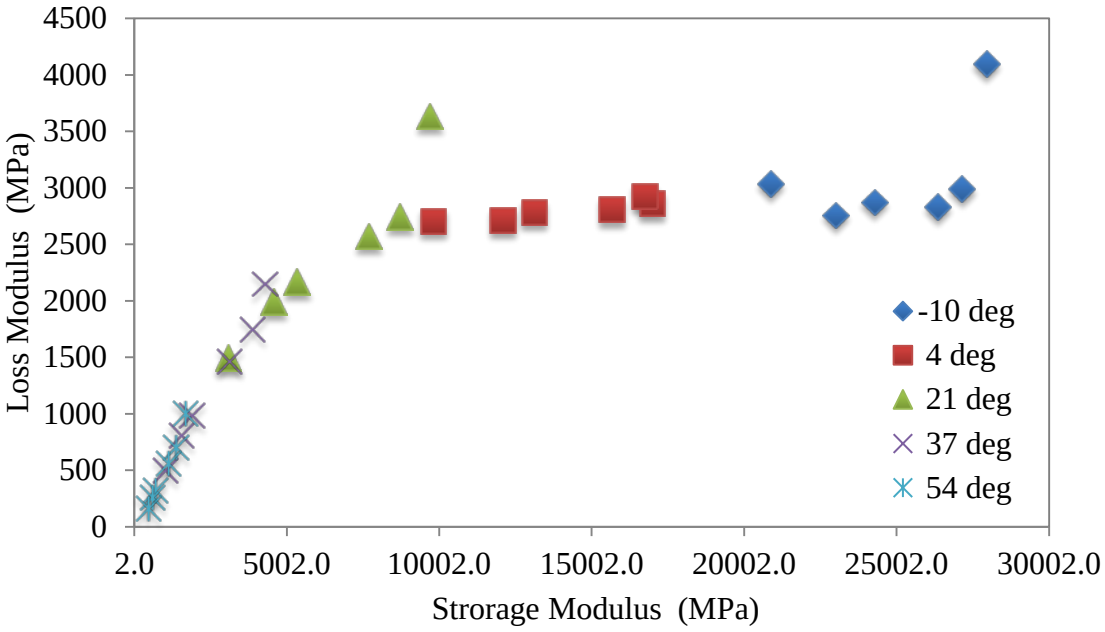


Figure 3.40: Cole and Cole Plot for Average of SP-II, PG 70-22

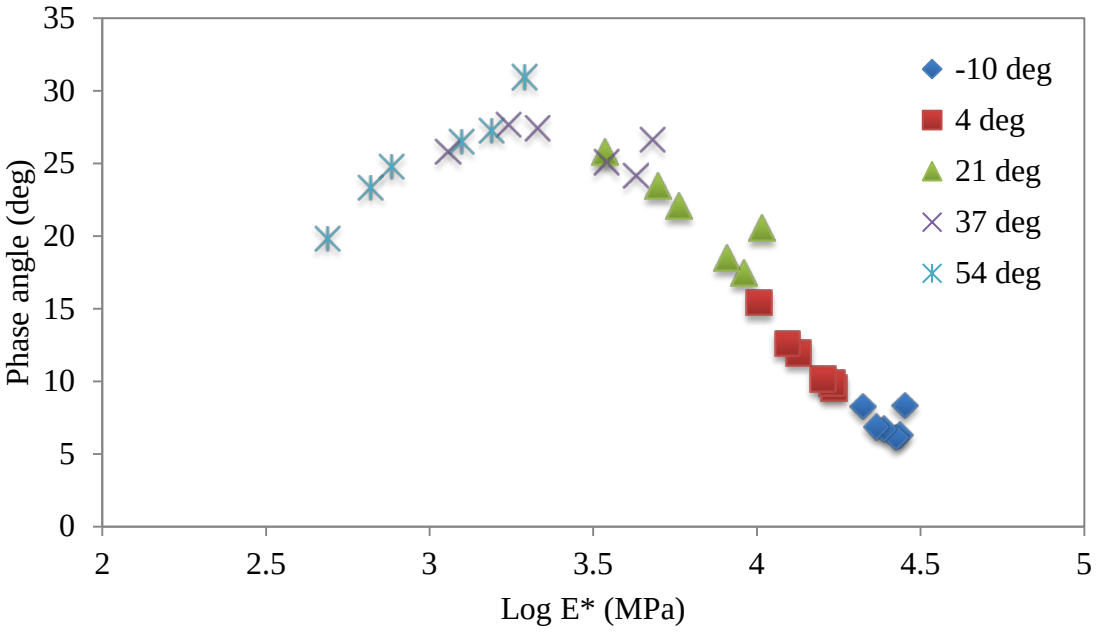


Figure 3.41: Black Space Plot for Average of SP-II, PG 70-22

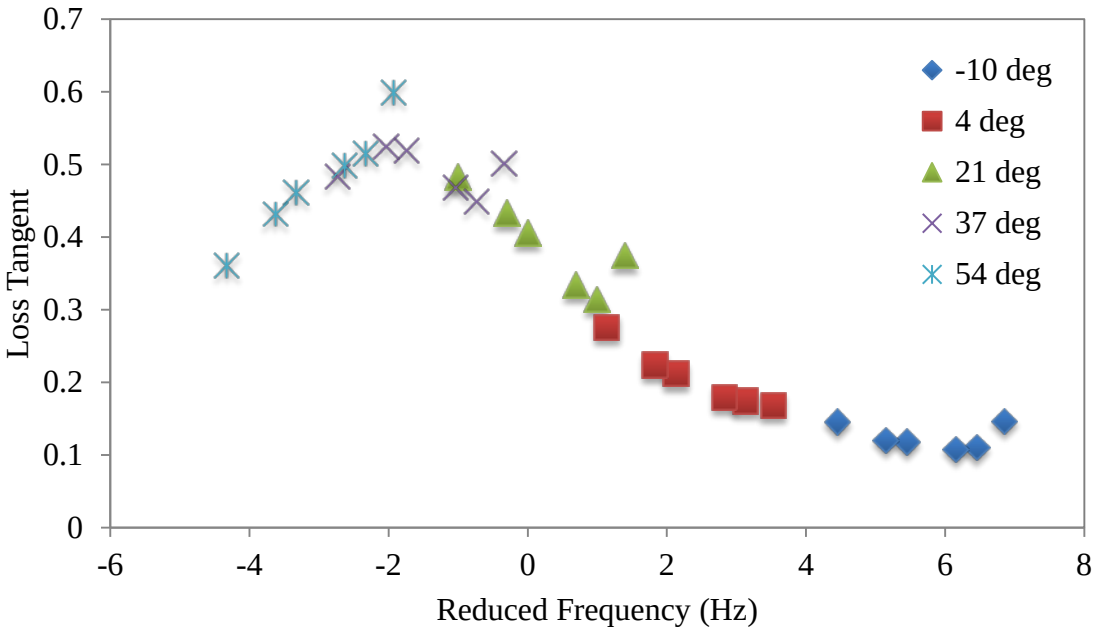


Figure 3.42: Loss Tangent Plot for Average of SP-II, PG 70-22

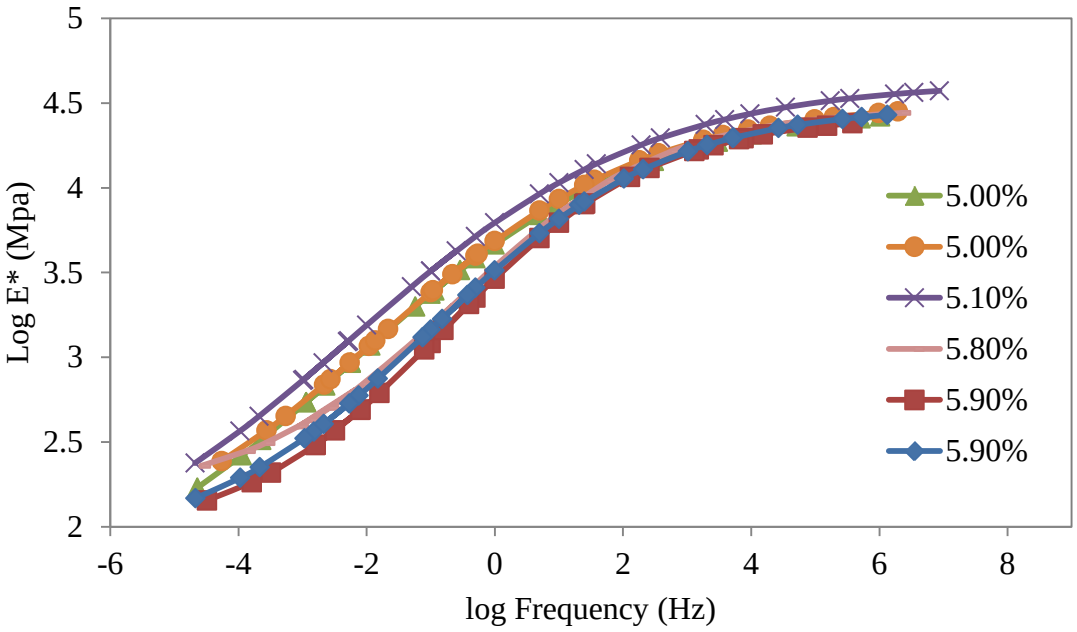


Figure 3.43: Comparison of Master Curves for SP-IV, PG 70-22 Test Results

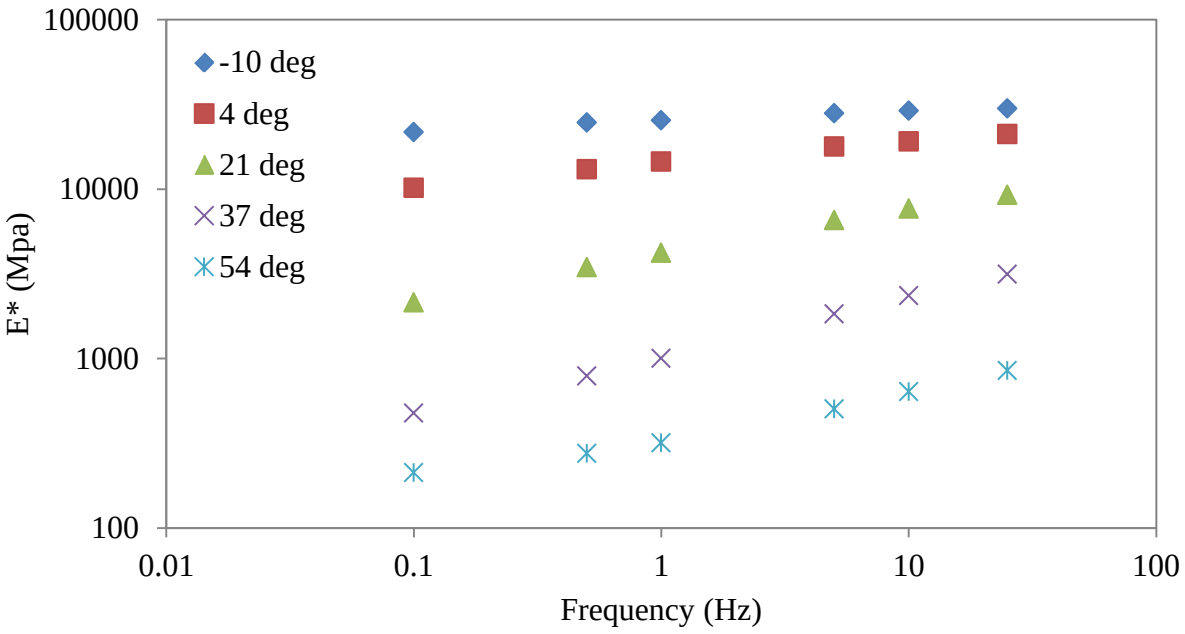


Figure 3.44: Isothermal Plot for Average of SP-IV, PG 70-22

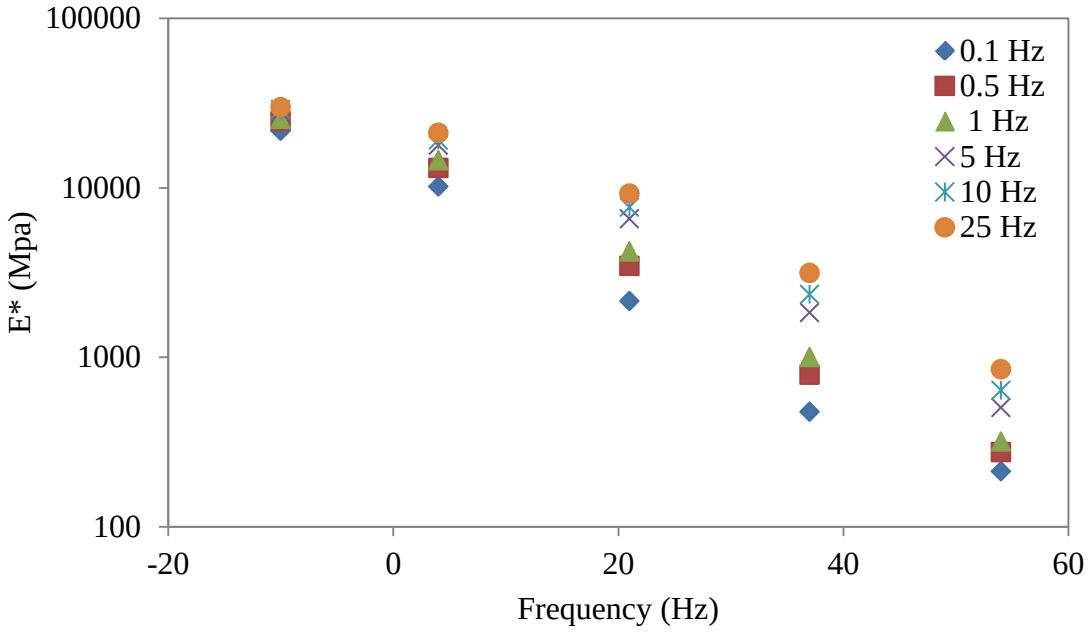


Figure 3.45: Isochronal Plot for Average of SP-IV, PG 70-22

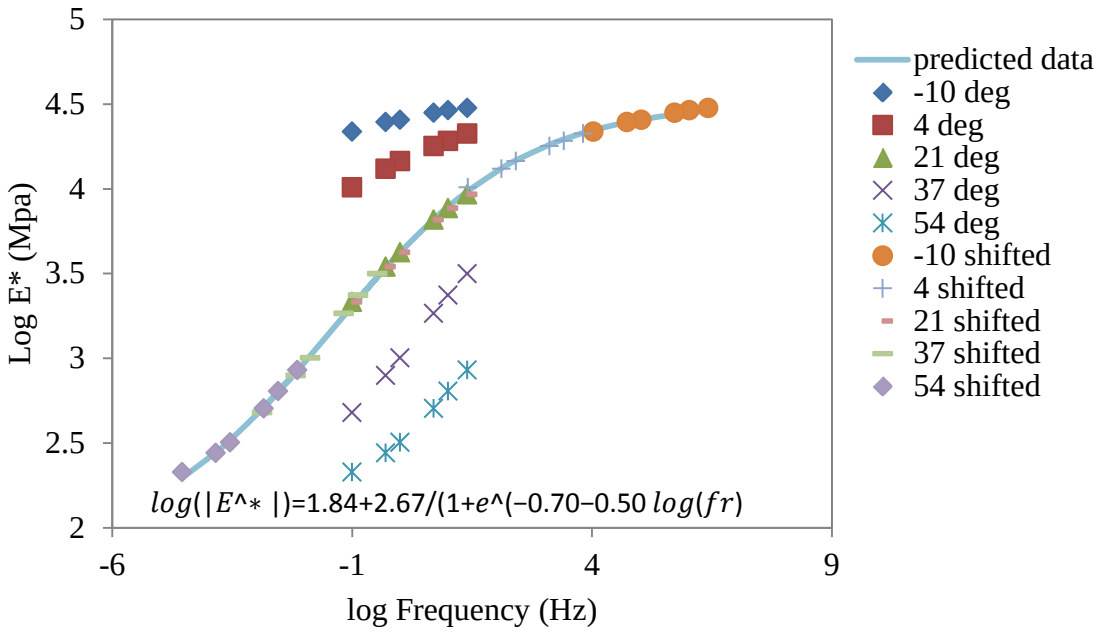


Figure 3.46: Master Curve for Average of SP-IV, PG 70-22

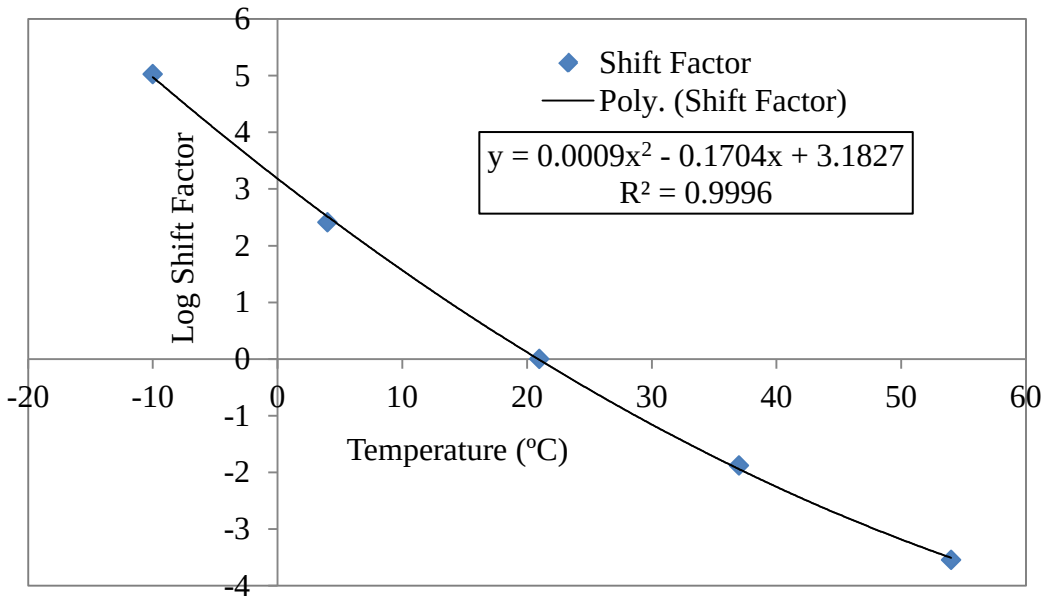


Figure 3.47: Shift Factor for Average of SP-IV, PG 70-22

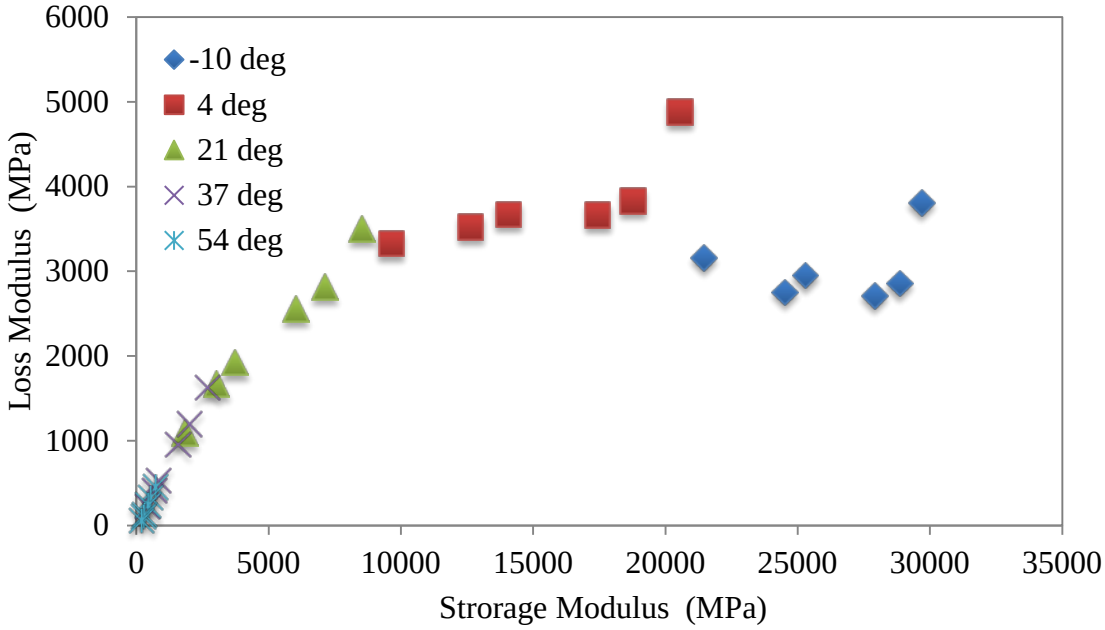


Figure 3.48: Cole and Cole Plot for Average of SP-IV, PG 70-22

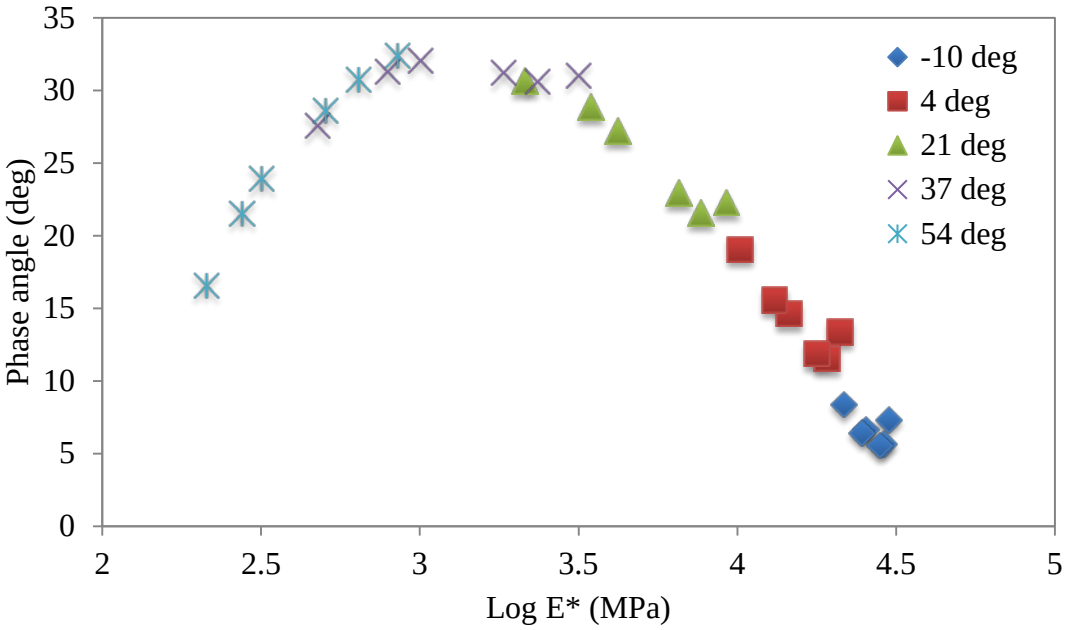


Figure 3.49: Black Space Plot for Average of SP-IV, PG 70-22

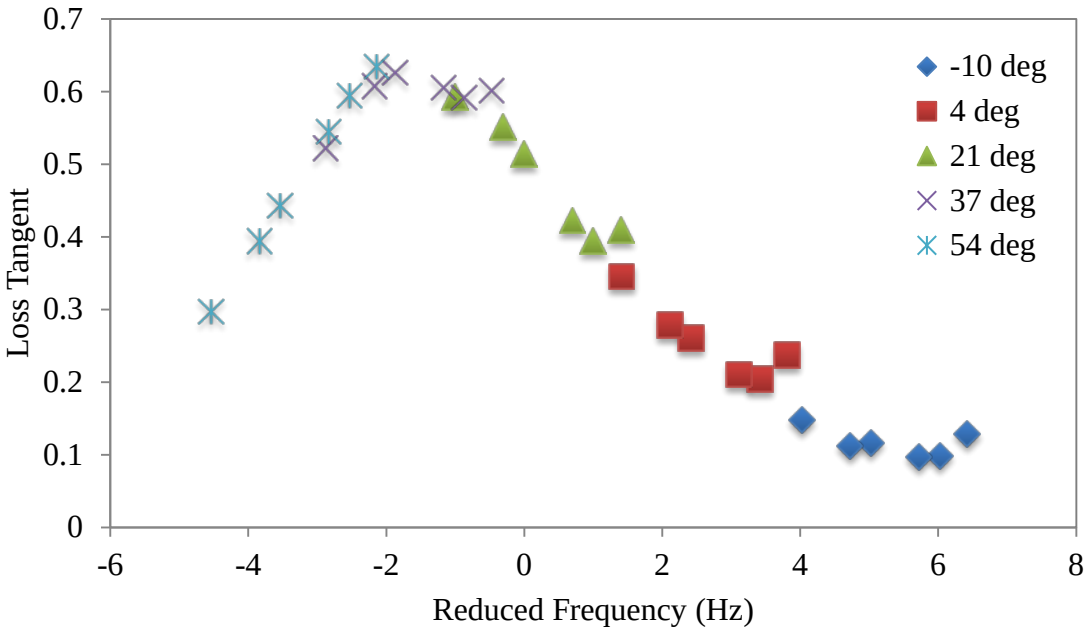


Figure 3.50: Loss Tangent Plot for Average of SP-IV, PG 70-22

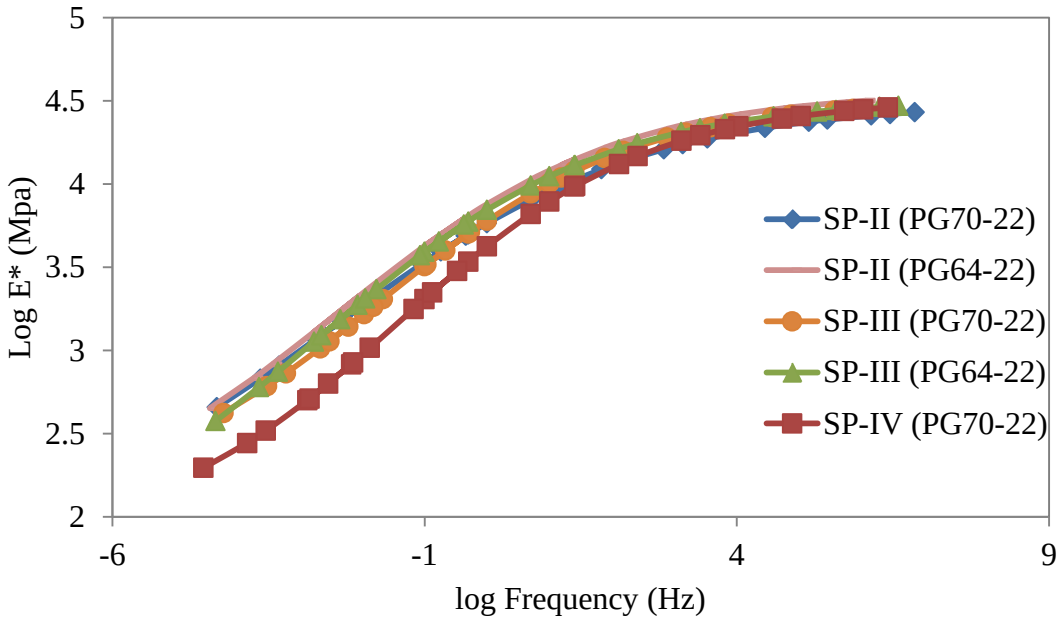


Figure 3.51: Comparison Master Curves for SP-II, SP-III and SP-IV Test Results

# Chapter 4

# Precision Study for Dynamic Modulus Testing of Asphalt Concrete Using Independent Assurance Testing

## 4.1. Introduction

Typical *E**-testing is conducted at a five temperatures and six loading frequencies resulting in a large amount of data per test. Test results may vary and therefore independent assurance (IA) testing is attempted to understand the precision of test results and identify probable causes of variations.

To this day, a limited number of studies have been conducted to establish the precision statement for *E**-testing. Phase VI of NCHRP Project 9-29, conducted by Bonaquist in 2011 (Bonaquist 2011), is the most recent study on the precision of *E**-testing. The study presented the precision statement for *E**-tests conducted with the Asphalt Mixture Performance Tester (AMPT). Precision statements are developed following the recommendation of ASTM E691 Standard (2012). Eight laboratories participated in conducting the *E**-testing. All *E**-testing in the laboratories is performed following the recommendation of AASHTO TP 79 (AASHTO 2009a). Specimens are prepared from loose asphalt mix at each of the eight laboratories as per the recommendation of AASHTO PP 60 (AASHTO 2009b). To investigate the significance of variation on *E**-test results from sample preparation at different laboratories; supplementary samples are prepared at a single laboratory and distributed for testing. *E**-testing is conducted on three replicate samples at 7% air void at each laboratory and the test temperatures are limited to 4, 20 and 40 ºC. Consistency analysis performed on all samples indicated very good consistency at 95% confidence. The critical within-laboratory consistency statistic (*k*-statistic) is determined to be 3.3 and 3.1 for samples from loose mix and prefabricated samples respectively. The critical interlaboratory consistency statistic (*h*-statistic), on the other hand, is found to be 1.2 and 2.1 for samples from loose mix and prefabricated samples respectively. The trend of coefficient of variation (COV) is also investigated and a maximum of 35% COV is observed, but most COVs are found to be below 15% for both sample preparation conditions.

Repeatability of *E**-test is found to be affected by the Nominal Maximum Aggregate Size (NMAS) and stiffness of the mix. It is found that the repeatability COV for *E**-test worsened as the NMAS decreased and the stiffness increased. Reproducibility of *E**-test results, on the other hand, are found to be affected only by stiffness of the mix. Reproducibility is found to improve with an increase in stiffness (dynamic modulus) of the asphalt concrete (AC). Bonaquist (2011) developed the relationship between repeatability and reproducibility with mix stiffness and NMAS, which are presented in Eq. (4.1) and Eq. (4.2). The repeatability COV is found to be around 7% at higher stiffness values and as the stiffness decreased, the repeatability COV increased reaching a value of 24%. The reproducibility COV for the *E**-testing is found to be approximately

10% at high stiffness conditions and as the stiffness decreased, the reproducibility COV increased to values as high as 47% (Bonaquist 2011).

$$s_r\% = \left[29.8e^{(0.014*NMAS)}\right] * |E^*|^{-\left[0.189e^{(0.012*NMAS)}\right]} \quad (4.1)$$

where $s_r\%$ is repeatability COV for $|E^*|$, %; NMAS is nominal maximum aggregate size, mm, and $|E^*|$ is average dynamic modulus, MPa.

$$s_R\% = 223.81 * |E^*|^{-[0.312]} \quad (4.2)$$

where $s_R\%$ is reproducibility COV for $|E^*|$, %, and $|E^*|$ is average dynamic modulus, MPa.

Bennert and Williams (2009) at Center for Advanced Infrastructure & Transportation (CAIT) preformed another study on the precision of *E**-testing. The study is part of the *E**-testing research performed for New Jersey Department of Transportation (NJDOT). Seven laboratories participated by conducting *E**-testing following the recommendations of AASHTO TP 62-07 (2007). The round-robin testing program is performed on two Superpave mixes fabricated using binder grade PG 64-22. *E**-testing is conducted on three replicate samples for each mix at the five temperatures and six testing frequencies. Then, test data is evaluated and precision statements are developed following the ASTM E691standard (2012) procedure. COV determined for the *E**-data of all laboratories over all temperatures and frequencies ranged from 7.7% to 43.5% with an average of 25.7%. However, COV determined for each laboratory separately averaged to 11.9%. Precision statements are developed using percentage precision statistics, one-sigma limit in present (1s%) and two-sigma limit in percent (D2s%). The 1s% is determined to be 13.03% and 26.89% for single operator and multi-laboratory precision, respectively, while the D2s% are determined to be 36.47% and 75.3% for single operator and multi-laboratory precision respectively. Moreover, *E**-variability is found to increase with increasing testing frequency (Bennert and Williams 2009).

As of this writing, only these two studies on the precision of *E**-testing are found. There is a wide variation between the precision statements of the two studies, which indicates the need for more precision studies on *E**-testing. To this end, this study evaluates the precision of *E**-testing conducted on typical New Mexico asphalt mixes through an Independent Assurance (IA) testing program.

### 4.2. Objective

Specific objectives of this study are to:

- Evaluate the precision and accuracy of *E**-testing conducted for New Mexico mixes through IA testing
- Conduct statistical analysis to determine the precision and accuracy of the E*-testing program. Statistical analysis include k-statistic, h-statistic, one-way analysis of variance (ANOVA), repeatability and reproducibility analysis

### 4.3. Methodology

In this study, the precision and accuracy of *E**-testing are evaluated using an IA testing program. Precision is defined as the closeness of the *E**-test results under similar testing conditions. Close test results within laboratories indicate precise testing; on the other hand, close test results between laboratories indicate accurate material property determination. Therefore, close *E**-testing from two laboratories indicates that the true material property is captured accurately through the testing procedure. The concepts of precision and accuracy are shown pictorially in Figure 3.18(a-d). To determine the precision and accuracy, statistical analysis is performed. Statistical analyses performed for precision study are *k*-statistic and repeatability analyses while the accuracy of the testing program is evaluated through *h*-statistic, ANOVA and reproducibility analyses.

Within-laboratory consistency statistic (*k*-statistic) is defined as the ratio of the standard deviation in one laboratory to the average standard deviation of all laboratories (ASTM E691 2012). In this study the *k*-statistic is used to compare test variability within each laboratory.

Between-laboratory consistency statistic (*h*-statistic) is defined as the ratio of the deviation of one laboratory average from the average of all laboratories to the standard deviation of the averages of each laboratory (ASTM E691 2012). In this study, the *h*-statistic is used to show how the average *E**-test results from the two laboratories compare with each other.

ANOVA is a statistical tool used to evaluate the difference between two averages and the variation in the process of collection of data for each average (Kottegoda 2008). In this study, ANOVA analysis is used to evaluate the variance between the two laboratories to determine if there is a significant difference in the testing procedure adopted by each laboratory.

Repeatability is defined as closeness of the test results from a single laboratory using one test procedure on one specific material by a single operator using the same test machine (ASTM E691 2012). The repeatability study is conducted to evaluate the variation of test results in a single laboratory to establish a repeatability limit for a test procedure. In this study, repeatability limits established by both Bonaquist (2011) and Bennert and Williams (2009) are compared with the *E**-test data ranges of each laboratory.

Reproducibility is defined as the closeness of test results conducted at different laboratories using one test procedure on a single material by different operators and test machines (ASTM E691 2012). Reproducibility limits determined by Bonaquist (2011) and Bennert and Williams (2009) are utilized to evaluate the accuracy of *E**-testing in this study.

### 4.4. E*-Test Matrix

Extensive *E**-testing is conducted in UNM Pavement Laboratory and the IA test facility AMEC Environment & Infrastructure, Inc. (AMEC). IA testing is performed on a minimum of two specimens for each mix. All samples for IA testing are prepared in the UNM laboratory and shipped to the AMEC laboratory for testing. Design test matrix for the study is shown in Table 4.1.

All Five Superpave asphalt mixes are used in this study, which are designated as SP-II (PG 64-22), SP-II (PG 70-22), SP-III (PG 64-22), SP-III (PG 70-22) and SP-IV (PG 70-22). The designations of mixes are based on the maximum nominal aggregate size and binder grade utilized. For example, the maximum aggregate size and binder PG-grade for SP-II (PG 64-22) mix is 25 mm and PG 64-22 while the maximum aggregate size of SP-III (PG 70-22) mix is 19 mm mixed with a binder grade of PG 70-22. The NMAS for SP-IV mixes is 12.5 mm. All asphalt mixes contain recycled asphalt pavement. Three of the mixes are collected from an actual mixing plant and the other two mixes are produced in UNM's laboratory using the same gradation of mixes but changing binder grades. The five mixes utilized in this study with their respective descriptions are presented below:

- SP-II (PG 64-22) Superpave mix with NMAS of 25 mm and binder grade of PG 64-22 binder (Plant mix)
- SP-II (PG 70-22) Superpave mix with NMAS of 25 mm and binder grade of PG 70-22 binder (Laboratory mix)
- SP-III (PG 64-22) Superpave mix with NMAS of 19 mm and binder grade of PG 64-22 binder (Plant mix)
- SP-III (PG 70-22) Superpave mix with NMAS of 19 mm and binder grade of PG 70-22 binder (Laboratory mix)
- SP-IV (PG 70-22) Superpave mix with NMAS of 12.5 mm and binder grade of PG 70-22 binder (Plant mix)

### 4.5. Results and Discussion

Dynamic modulus test results from AMEC laboratories are analyzed and dynamic modulus mastercurves are also developed for each sample. Appendix F provides the results. To determine whether there is significant variation between UNM and AMEC *E**-results, statistical analysis is conducted. To match the number of specimens for the analysis, two samples having the closest air voids to samples used for IA testing are utilized. Analysis of data collected from each laboratory is performed using *E**-trend plots, COV plots, within-laboratory consistency (*k*-statistic) plots, between-laboratory (*h*-statistic) plots, one-way ANOVA, and repeatability and reproducibility analyses.

#### 4.5.1. E*-Trend Plots

Figure 4.2(a) to Figure 4.2(e) presents *E**-trend plots as a function of temperature and frequency for test results of the five mixes. The trend plot for all samples tested in both laboratories shows that the dynamic moduli are similar for all samples tested in both

laboratories, indicating that temperature and frequency effects are similar in both laboratories for all mixes tested. The UNM average and AMEC average $E^*$-data overlap for all five test temperatures and six test frequencies suggesting the data obtained from the two laboratories is very similar.

### 4.5.2. Coefficient of Variation (COV) Plots

The COV is defined as the ratio of standard deviation to the average expressed in percentage as shown in Eq. (4.3) (ASTM C670 2010).

$$COV = \frac{\sigma}{\mu} * 100 \tag{4.3}$$

where $COV$ is COV (%), $\sigma$ is standard deviation, $\mu$ is average.

The COVs for UNM laboratory and AMCE laboratory test data are computed for all testing temperature and frequency combinations. The results are presented in a graphical format in Figure 4.3(a) to Figure 4.3(e). Comparison of the COV plots from the two laboratories shows that the COV values of both laboratories are relatively similar. The average and range of COV values determined for each mix type are as follows:

- Figure 4.3 (a): SP-II (PG 64-22) – COV range 0% – 22 % with an average of 13 % for UNM laboratory and range 1% – 27 % with an average of 16 % for AMEC laboratory
- Figure 4.3 (b): SP-II (PG 70-22) – COV range 0% – 24 % with an average of 12 % for UNM laboratory and range 0% – 21 % with an average of 8 % for AMEC laboratory
- Figure 4.3 (c): SP-III (PG 64-22) – COV range 0% – 22 % with an average of 10 % for UNM laboratory and range 8% – 37 % with an average of 20 % for AMEC laboratory
- Figure 4.3 (d): SP-III (PG 70-22) – COV range 0% – 17 % with an average of 6 % for UNM laboratory and range 9% – 30 % with an average of 16 % for AMEC laboratory
- Figure 4.3 (e): SP-IV (PG 70-22) – COV range 1% – 38 % with an average of 9 % for UNM laboratory and range 0% – 29 % with an average of 9 % for AMEC laboratory

Over all, COV values computed for UNM laboratory are relatively smaller than COV values determined for AMEC laboratory. An average COV value computed for $E^*$-results of all mixes at UNM laboratory is found to be 10% while the corresponding average COV value determined for AMEC laboratory is 14%. This might suggest that there is some variability in the testing process adopted by these laboratories and further analysis of is required.

### 4.5.3. Within-Laboratory Consistency k-statistic Plots

The *k*-statistic is computed using Eq. (4.4) (ASTM E691 2012).

$$k = \frac{s}{\sqrt{\sum_1^P \frac{s^2}{P}}} \tag{4.4}$$

where*: k* is within-laboratory consistency statistic, *s* is within-laboratory standard deviation, and *p* is number of laboratories in the interlaboratory study.

The within-laboratory consistency statistic, *k*, is an indicator of the variability in one laboratory as compared to the combined variability in all laboratories. *k*-statistic always assumes a positive value. A value of 1.0 for *k*-statistic indicates the average within-laboratory variability of both laboratories. When the computed *k*-statistic for a specific laboratory is less than 1.0, it indicates that the within-laboratory variability for that laboratory is less than the average variability of all laboratories in the study. Similarly, *k*-statistic greater than 1.0 indicates that within-laboratory variability for that laboratory is more than the average within-laboratory variability of both laboratories involved.

Figure 4.4(a) to Figure 4.4(e) presents a graphical presentation of the *k*-statistic computed for UNM and AMEC laboratories by mix type. Comparison of *k*-statistic plots from the two laboratories shows that the within-laboratory variability of both laboratories is relatively similar. The average and range of *k*-statistic values determined for each mix type are as follows:

- Figure 4.4(a): SP-II (PG 64-22) – *k*-statistic range 0 – 1.4 with an average of 0.9 for UNM laboratory and range 0.1 – 1.4 with an average of 0.9 for AMEC laboratory
- Figure 4.4 (b): SP-II (PG 70-22) – *k*-statistic range 0 – 1.4 with an average of 1 for UNM laboratory and range 0.1 – 1.4 with an average of 0.9 for AMEC laboratory
- Figure 4.4 (c): SP-III (PG 64-22) – *k*-statistic range 0 – 1.0 with an average of 0.5 for UNM laboratory and range 1 – 1.4 with an average of 1.3 for AMEC laboratory
- Figure 4.4 (d): SP-III (PG 70-22) – *k*-statistic range 0 – 1.1 with an average of 0.4 for UNM laboratory and range 0.9 – 1.4 with an average of 1.3 for AMEC laboratory
- Figure 4.4 (e): SP-IV (PG 70-22) – *k*-statistic range 0.2 – 1.4 with an average of 1.0 for UNM laboratory and range 0.1 – 1.4 with an average of 0.8 for AMEC laboratory

The average *k*-statistic value computed for UNM's laboratory is found to be 0.8 while the corresponding average *k*-statistic value determined for AMEC's laboratory is 1.0. This indicates that the within-laboratory variability from both laboratories is very similar. The

fact that both values are very close to 1.0 indicates that testing conducted in both laboratories is precise.

### 4.5.4. Between-Laboratory Consistency h-statistic Plots

The *h*-statistic is computed using Eq. (4.5) given below (ASTM E691 2012).

$$h = \frac{\bar{x} - \bar{\bar{X}}}{\sqrt{\sum_1^p \frac{\left(\bar{x} - \bar{\bar{X}}\right)^2}{(p-1)}}} \tag{4.5}$$

where *h* is between-laboratory consistency statistic; $\bar{x}$ is laboratory average, $\bar{\bar{X}}$ is average of the laboratory averages, and *p* is number of laboratories in the interlaboratory study.

The between-laboratory consistency statistic, *h*-statistic, is used to compare average test results of a specific laboratory with the overall average test results of all laboratories involved in the interlaboratory study. The overall average test results from all laboratories in the study are represented by *h*-statistic equal to "0.0". For averages of individual laboratories, the *h*-statistic can assume positive and negative values. Positive *h*-statistic indicates that the average values of that particular laboratory are higher than the overall average while a negative value for h statistic correspondingly indicates an average value less than the overall average of all laboratories (ASTM E691 2012, Sholar et.al. 2001).

Figure 4.5(a-e) presents the *h*-statistic for both UNM and AMEC laboratories for all mixes tested in this study. Comparison of *h*-statistic plots from the two laboratories suggests that the *E**-results from both laboratories are relatively similar with average UNM laboratory results being less than corresponding values obtained from AMEC. The average and range of *h*-statistic values determined for each mix type are as follows:

- Figure 4.5 (a): SP-II (PG 64-22) – *h*-statistic range -0.71 – 0.71 with an average of 0.28 for UNM laboratory and range -0.71 – 0.71 with an average of 0.28 for AMEC laboratory
- Figure 4.5 (b): SP-II (PG 70-22) – *h*-statistic range -0.71 – 0.71 with an average of -0.66 for UNM laboratory and range -0.71 – 0.71 with an average of 0.66 for AMEC laboratory
- Figure 4.5 (c): SP-III (PG 64-22) – *h*-statistic range -0.71 – 0.71 with an average of -0.66 for UNM laboratory and range -0.71 – 0.71 with an average of 0.66 for AMEC laboratory
- Figure 4.5 (d): SP-III (PG 70-22) – *h*-statistic range -0.71 – 0.71 with an average of -0.52 for UNM laboratory and range -0.71 – 0.71 with an average of 0.52 for AMEC laboratory
- Figure 4.5 (e): SP-IV (PG 70-22) – *h*-statistic range -0.71 – 0.71 with an average of 0.05 for UNM laboratory and range -0.71 – 0.71 with an average of -0.05 for AMEC laboratory

The average *h*-statistic values computed for UNM laboratory is found to be -0.3 while the corresponding average *h*-statistic value determined for AMEC laboratory is 0.3. This indicates that the averages of both laboratories are close to the overall average and the accuracy of testing in both laboratories is good.

### 4.5.5. Mastercurve Comparison

*E**-test data are collected at five temperatures and six frequencies. That means the *E**-data should actually be plotted in three-dimensional plots to visualize the effect of temperature and frequency. However, *E**-data can be presented in two-dimensional plots using mastercurves at a specific reference temperature. The *E**-data collected for each sample at different temperatures and frequencies is converted into a mastercurve for the purpose of comparing the *E**-data at a reference temperature of 21 ºC. The sigmoidal function shown in Eq. (4.6) is used to fit the individual *E**-data to the mastercurve.

$$\log(|E^*|) = \delta + \frac{\alpha}{1+e^{\beta-\gamma\log(f_r)}} \tag{4.6}$$

*where*: $\delta$ is the minimum value of $|E^*|$; $\delta + \alpha$ is the maximum value of $|E^*|$; $\beta$, $\gamma$ are parameters describing the shape of the sigmoidal function; $f_r$ is reduced frequency of loading at reference temperature.

Figure 4.6(a-e) presents the *E**-mastercurves developed for all samples tested from each mix. It can be observed from Figure 4.6 that the trend of mastercurves for all samples is very similar within each mix. Comparison of *E**-values from different samples at each reduced frequency might indicate some variation, however, the difference between the *E**-mastercurves does not look significant from the visual inspection. To investigate the interlaboratory variation more clearly, mastercurves are also developed for the average *E**-test results of each laboratory. The mastercurves for average AMEC and UNM *E**-test results for each mix suggest no significant difference between the average *E**-results of AMEC and UNM laboratories.

### 4.5.6. One-way ANOVA Analysis

One-way ANOVA is conducted to test the equality of means of *E**-data collected from the two laboratories. One-way ANOVA analysis is performed for each temperature and frequency combination cases of all mixes at a 5% significance level. The null and alternative hypotheses are formulated as follows:

Null hypothesis: - The mean *E** computed from UNM laboratory is the same as the mean *E** determined from AMEC laboratory (i.e. the variance caused by testing at the two different laboratories is insignificant), as in Eq. (4.7).

$$\mu_{|E^*_{UNM}|} = \mu_{|E^*_{AMEC}|} \tag{4.7}$$

Alternative Hypothesis: - *E**-test results from UNM and AMEC laboratories have different means, as in Eq. (4.8).

$$\mu_{|E^*_{UNM}|} \neq \mu_{|E^*_{AMEC}|} \quad (4.8)$$

Significance Level: - A significance level of 0.05 is selected for this study. (i.e., the probability of being wrong to reject the null hypothesis is 5 %.)

Test Statistic: - The test statistic for ANOVA analysis is F-statistic. The F-statistic for each temperature and frequency combination is calculated and presented in Table 4.2. The F-critical value is found to be 18.5.

If the F-statistic ≥ F-critical, then we will reject the null hypothesis.

If the F-statistic < F -critical, then we do not reject the null hypothesis.

P-value: - the P-value represents the probability of obtaining an F-statistic value that is equal or more assuming the null hypothesis is true. Computed P-values for each test temperature and frequency combinations for each mix are presented in Table 4.2.

If the P-value < 0.05, then we will reject the null hypothesis.

If the P-value ≥ 0.05, then we do not reject the null hypothesis.

From Table 3, it can be seen that the F-statistic is always below the F-critical value. Considering the fact that all F-statistic data is well below the F-critical value, the null hypothesis is accepted leading to the conclusion that the means of the *E**-data collected from the UNM and AMEC laboratories is the same. On the same note, the P-values are always well above the critical value of 5% which dictates to accept the null hypothesis. The F-test and P-value analysis both confirm the equality of the *E**-results from the two laboratories, which indicates that variance caused by conducting the tests at AMEC and UNM laboratories is insignificant.

### 4.5.7. Repeatability Analysis

The repeatability limit for *E**-test results is the maximum acceptable range between replicate test results in a single laboratory. It is determined by multiplying the repeatability COV with the appropriate factor dependent on the number of test results (ASTM C670 2010). Bonaquist (2011) determined the repeatability COVs to be dependent on NMAS and *E**-values of the mix. Bonaquist (2011) also found that *E**-testing at low temperatures shows less variability with a repeatability COV close to 7%. As the stiffness of AC decreases, however, the repeatability COV increases exponentially. Bennert and Williams (2009), on the other hand, developed general precision statements, which are not a function of any mix variables. They determined the COV for repeatability to be 13.03%. The multiplying factor for two replicate samples is $2\sqrt{2}$. The average and maximum range values are determined for each mix type as follows:

- SP-II (PG 64-22) – maximum range 31 with an average of 19 for UNM laboratory and range 27 with an average of 16 for AMEC laboratory
- SP-II (PG 70-22) – maximum range 33 with an average of 17 for UNM laboratory and range 29 with an average of 12 for AMEC laboratory
- SP-III (PG 64-22) – maximum range 31 with an average of 13 for UNM laboratory and range 53 with an average of 28 for AMEC laboratory
- SP-III (PG 70-22) – maximum range 24 with an average of 8 for UNM laboratory and range 43 with an average of 23 for AMEC laboratory
- SP-IV (PG 70-22) – maximum range 53 with an average of 12 for UNM laboratory and range 40 with an average of 12 for AMEC laboratory

Repeatability analysis results are presented in Figure 4.7(a) to Figure 4.7(e). Acceptable ranges for repeatability along with computed ranges of *E**-test data for each mix tested in UNM and AMCE are presented. It can be observed that the acceptable ranges (d2s% limits) determined using the functions developed by Bonaquist (2011) are lower than the d2s% limits specified by Bennert and Williams (2009). Moreover, for all mixtures tested in this study, the *computed E**-ranges are found to be below the Bennert and Williams (2009) limit and in most cases higher than Bonaquist (2011) limits. This indicates acceptable repeatability of *E**-testing in UNM and AMEC laboratories.

### 4.5.8. Reproducibility Analysis

The reproducibility limit is the maximum allowable difference between the averages of test results obtained from the different laboratories. The reproducibility limit is also calculated by multiplying the reproducibility COV with an appropriate factor from Table 1 of ASTM C670 (2010) and dividing it by the square root of the number of samples used to calculate the averages (ASTM C670). Bonaquist (2011) determined the reproducibility COVs to be dependent on *E**-values of the mix and found that the reproducibility COV is close to 10% for *E**-testing at low temperatures and as the stiffness of AC decreases, the reproducibility COV increases. Bennert and Williams (2009), on the other hand, determined reproducibility COV to be 26.89%. The multiplication factor for two replicate tests is determined to be 2. The average and maximum range values for UNM and AMEC test results are determined for each mix type as follows:

- Figure 4.8 (a): SP-II (PG 64-22) – maximum range 28 with an average of 10
- Figure 4.8 (b): SP-II (PG 70-22) – maximum range 44 with an average of 25
- Figure 4.8 (c): SP-III (PG 64-22) – maximum range 24 with an average of 13
- Figure 4.8 (d): SP-III (PG 70-22) – maximum range 29 with an average of 16
- Figure 4.8 (e): SP-IV (PG 70-22) – maximum range 43 with an average of 15

Reproducibility analysis for UNM and AMEC test results is presented in Figure 4.8(a) to Figure 4.8(e). Reproducibility limits using the functions developed by Bonaquist (2011) and general limits provided by Bennert and Williams (2009) are presented along with the range for averages of UNM and AMEC *E**-results. Similar to the repeatability analysis, the limits for reproducibility computed using Bonaquist (2011) are less than the

reproducibility limits provided by Bennert and Williams (2009). In addition, it can be observed from Figure. 8(a-e) that the reproducibility statistic computed for the two laboratories is, in most cases, below d2s% limits specified by both round-robin studies. This indicates acceptable reproducibility of *E**-results between UNM and AMEC laboratories.

### 4.6. Conclusions

This study is conducted to determine the precision of *E**-testing preformed in UNM pavement laboratory through IA testing. The results from both laboratories are investigated through statistical analysis. In addition, repeatability and reproducibility analysis is performed based on previous round-robin studies conducted in the past. From this study, the following conclusions can be made:

- COV plots indicate that the results from UNM and AMEC laboratories are very similar.
- Within-laboratory consistency (*k*-statistic) plots suggest that the within-laboratory variability from UNM and AMEC laboratories are close to each other, indicating good precision of testing in each laboratory.
- Between-laboratory consistency (*h*-statistic) plots suggest that the average *E**-value determined from UNM and the average *E**-value determined from AMEC laboratory testing are close to each other indicating good accuracy.
- One-way ANOVA analysis is performed for each temperature and frequency testing condition. The results indicate no significant difference in the means as well as the variances for testing at UNM and AMEC laboratories, which indicates good accuracy of testing in both laboratories.
- Repeatability analysis of selected test results indicate acceptable repeatability of *E**-testing in UNM and AMEC laboratories. This indicates good precision testing in both laboratories.
- Reproducibility analysis of selected test results indicate acceptable reproducibility of *E**-testing in UNM and AMEC laboratories, which indicates good accuracy of test results.
- IA testing is a good and economical way to evaluate the accuracy and precision of *E**-testing of a specific laboratory.

### 4.7. Reference

AASHTO Standard TP 62-07 (2007). "Standard Method of Test for Determining Dynamic Modulus of Hot Mix Asphalt (HMA)." *AASHTO Standard Specifications.* Ishington, D.C.

AASHTO Standard TP 79 (2009). "Determining the Dynamic Modulus and Flow Number for Hot Mix Asphalt (HMA) Using the Asphalt Mixture Performance Tester (AMPT)." *AASHTO Standard Specifications*. Ishington, D.C.

AASHTO Standard PP 60 (2009). "Preparation of Cylindrical Performance Test Specimens Using the Superpave Gyratory Compactor (SGC)." *AASHTO Standard Specifications*. Ishington, D.C.

ASTM Standard C670 (2010). "Standard Practice for Preparing Precision and Bias Statements for Test Methods For Construction Materials." *American Society for Testing and Materials (ASTM) Standards*. West Conshohocken, PA.

ASTM Standard E691 (2012). "Standard Practice for Conducting an Interlaboratory Study to Determine the Precision of a Test Method." *ASTM Standards*. West Conshohocken, PA.

Bennert T. and Williams S. G. (2009). " Precision of AASHTO TP62-07 for use in mechanistic-empirical pavement design guide for flexible pavements." *J. of the Transportation Research Board (TRB)*, 2127, 115–126.

Bonaquist, R. (2011). "NCHRP Report 702: Precision of the Dynamic Modulus and Flow Number Tests Conducted with the Asphalt Mixture Performance Tester." TRB of the National Academies, Ishington, D.C.

Kottegoda, N. T. (2008). *Applied statistics for civil and environmental engineers*. Blackwell Pub., Malden, MA.

Sholar, G. A., Musselman, J. A., Page, G. C., Upshaw, P. B., and Moseley, H. L. (2001). "Precision Statements for the Ignition Oven Using Plant-Produced Mix." Research Report- FL/DOT/SMO/01-445, Florida Department of Transportation, State Materials Office, Gainesville, FL.

Table 4.1: Test Matrix for Dynamic Modulus

| Laboratories | Asphalt Mixes | Replicate Samples | Test Frequency (Hz) | Test Temperature (°C) |
|---|---|---|---|---|
| (Two) | (Five) | (two) | (six) | (five) |
| UNM-Lab | SP-II (PG 64-22) | | 25 | -10 |
| AMEC-Lab | SP-II (PG 70-22) | | 10 | 4 |
| | SP-III (PG 64-22) | | 5 | 21 |
| | SP-III (PG 70-22) | | 1 | 37 |
| | SP-IV (PG 70-22) | | 0.5 | 54 |
| | | | 0.1 | |

Table 4.2: ANOVA Analysis Results

| Temp. | Freq. | SP-2 (PG64-22) | | SP-2 (PG70-22) | | SP-3 (PG64-22) | | SP-3 (PG70-22) | | SP-4 (PG70-22) | |
|---|---|---|---|---|---|---|---|---|---|---|---|
| (ºC) | (Hz) | F-stat | P-value | F-stat | P-value | F-stat | P-value | F-stat | P-value | F-stat | P-value |
| -10 | 25 | 2.902 | 0.231 | 0.001 | 0.976 | 0.176 | 0.716 | 4.730 | 0.162 | 0.033 | 0.873 |
| | 10 | 3.729 | 0.193 | 0.001 | 0.982 | 0.208 | 0.693 | 7.680 | 0.109 | 0.087 | 0.795 |
| | 5 | 3.534 | 0.201 | 0.009 | 0.933 | 0.207 | 0.694 | 6.784 | 0.121 | 0.110 | 0.771 |
| | 1 | 4.255 | 0.175 | 0.009 | 0.933 | 0.131 | 0.752 | 4.259 | 0.175 | 0.166 | 0.723 |
| | 0.5 | 4.270 | 0.175 | 0.020 | 0.900 | 0.261 | 0.660 | 4.266 | 0.175 | 0.189 | 0.706 |
| | 0.1 | 3.765 | 0.192 | 0.010 | 0.929 | 0.162 | 0.726 | 3.047 | 0.223 | 0.230 | 0.679 |
| 4 | 25 | 0.218 | 0.687 | 3.640 | 0.197 | 0.552 | 0.535 | 6.208 | 0.130 | 14.995 | 0.061 |
| | 10 | 0.181 | 0.712 | 6.334 | 0.128 | 0.338 | 0.620 | 8.053 | 0.105 | 12.953 | 0.069 |
| | 5 | 0.194 | 0.703 | 6.283 | 0.129 | 0.321 | 0.628 | 8.731 | 0.098 | 13.130 | 0.068 |
| | 1 | 0.110 | 0.772 | 6.523 | 0.125 | 0.218 | 0.686 | 7.694 | 0.109 | 8.060 | 0.105 |
| | 0.5 | 0.052 | 0.840 | 5.210 | 0.150 | 0.273 | 0.654 | 7.637 | 0.110 | 9.717 | 0.089 |
| | 0.1 | 0.013 | 0.919 | 5.247 | 0.149 | 0.191 | 0.705 | 3.854 | 0.189 | 9.126 | 0.094 |
| 21 | 25 | 0.053 | 0.839 | 0.012 | 0.923 | 2.696 | 0.242 | 1.761 | 0.316 | 3.818 | 0.190 |
| | 10 | 0.004 | 0.953 | 0.092 | 0.790 | 1.600 | 0.333 | 1.505 | 0.345 | 4.586 | 0.166 |
| | 5 | 0.018 | 0.907 | 0.171 | 0.719 | 1.424 | 0.355 | 1.580 | 0.336 | 11.382 | 0.078 |
| | 1 | 0.102 | 0.780 | 0.013 | 0.918 | 1.666 | 0.326 | 1.685 | 0.324 | 0.062 | 0.826 |
| | 0.5 | 0.085 | 0.798 | 0.043 | 0.855 | 1.039 | 0.415 | 1.709 | 0.321 | 0.027 | 0.886 |
| | 0.1 | 0.118 | 0.764 | 0.041 | 0.858 | 1.465 | 0.350 | 1.319 | 0.370 | 0.025 | 0.888 |
| 37 | 25 | 0.387 | 0.597 | 0.012 | 0.923 | 0.691 | 0.493 | 0.448 | 0.572 | 0.010 | 0.930 |
| | 10 | 0.157 | 0.730 | 5.160 | 0.151 | 0.306 | 0.636 | 0.308 | 0.635 | 0.020 | 0.900 |
| | 5 | 0.111 | 0.771 | 3.587 | 0.199 | 0.989 | 0.425 | 0.253 | 0.665 | 8.974 | 0.096 |
| | 1 | 0.018 | 0.907 | 6.134 | 0.132 | 1.095 | 0.405 | 0.136 | 0.748 | 8.874 | 0.097 |
| | 0.5 | 0.073 | 0.813 | 6.537 | 0.125 | 0.887 | 0.446 | 0.012 | 0.923 | 3.173 | 0.217 |
| | 0.1 | 0.184 | 0.710 | 12.232 | 0.073 | 0.548 | 0.536 | 0.008 | 0.936 | 0.438 | 0.576 |
| 54 | 25 | 1.300 | 0.372 | 0.452 | 0.571 | 7.812 | 0.108 | 0.236 | 0.675 | 0.191 | 0.705 |
| | 10 | 0.718 | 0.486 | 0.016 | 0.911 | 4.848 | 0.159 | 0.000 | 0.987 | 5.124 | 0.152 |
| | 5 | 0.581 | 0.525 | 0.001 | 0.983 | 5.820 | 0.137 | 0.004 | 0.955 | 0.730 | 0.483 |
| | 1 | 0.013 | 0.918 | 0.112 | 0.769 | 2.102 | 0.284 | 0.302 | 0.638 | 0.888 | 0.445 |
| | 0.5 | 0.087 | 0.795 | 0.741 | 0.480 | 0.925 | 0.438 | 0.887 | 0.446 | 1.339 | 0.367 |
| | 0.1 | 0.789 | 0.468 | 3.498 | 0.202 | 0.078 | 0.806 | 0.620 | 0.513 | 1.649 | 0.328 |

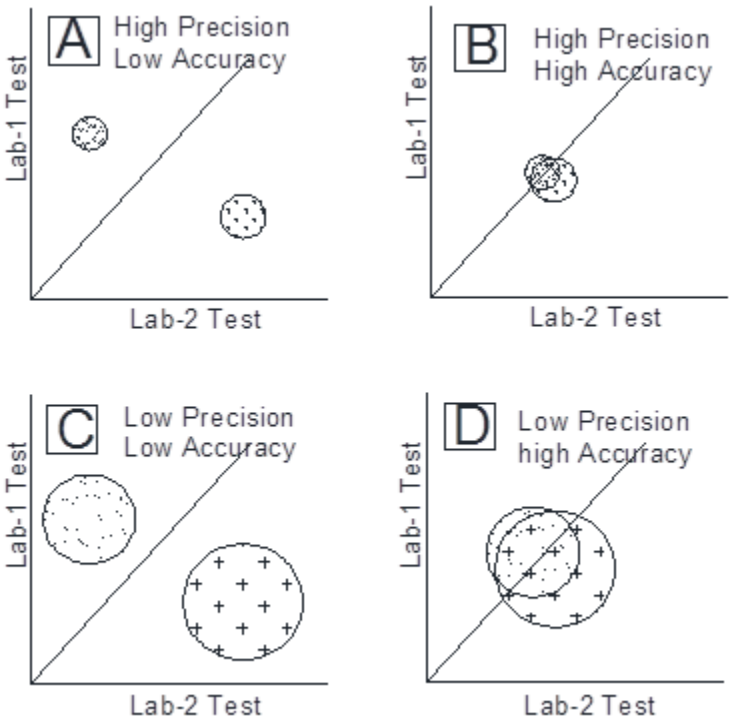


Figure 4.1: (a-d) Concepts of Precision and Accuracy.

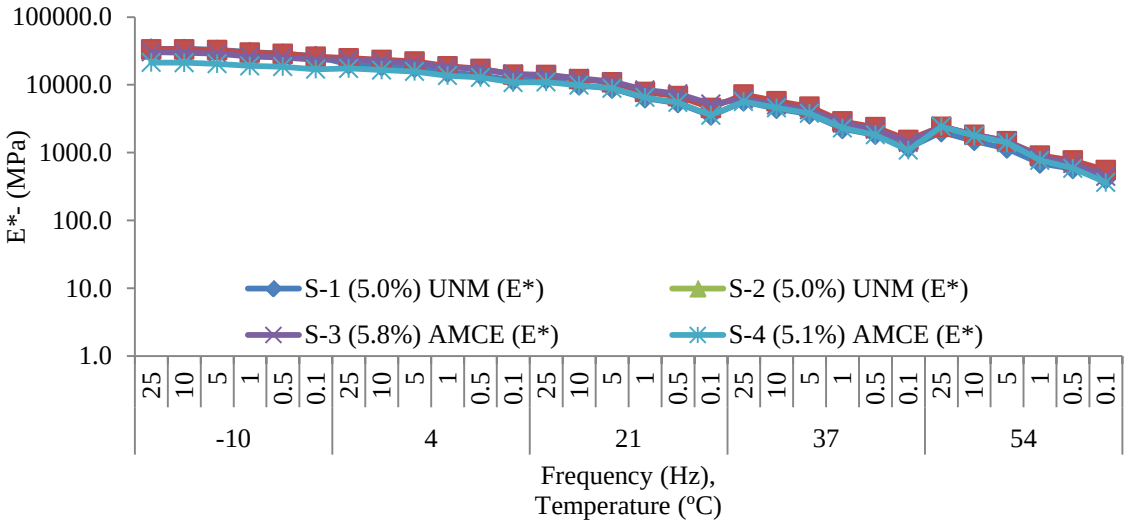


(a) SP-II with PG 64-22

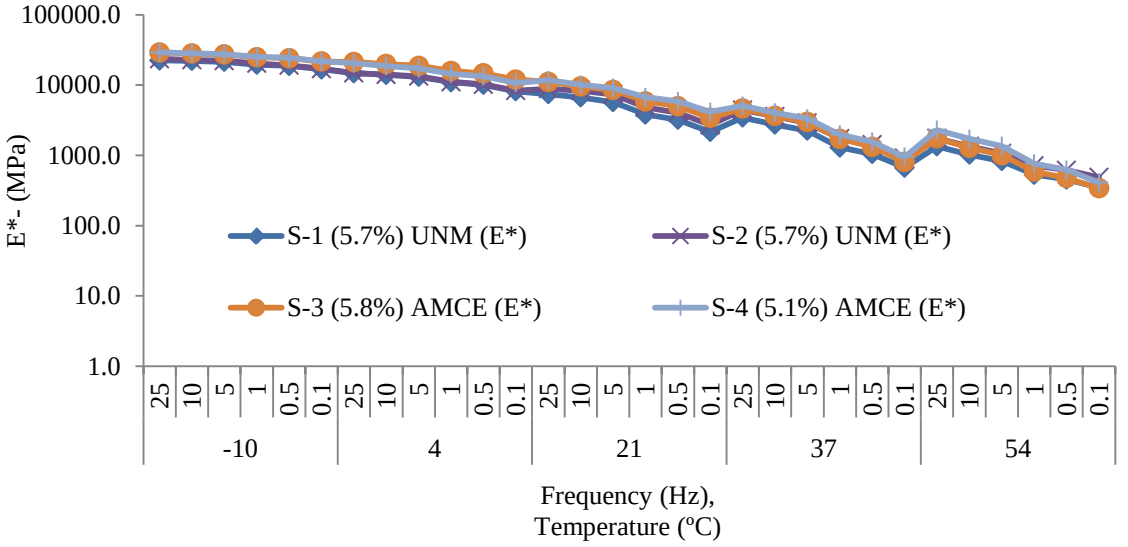


(b) SP-II with PG 70-22

Figure 4.2 (a-e) *E**-Trend Plots as A Function of Frequency and Temperature.

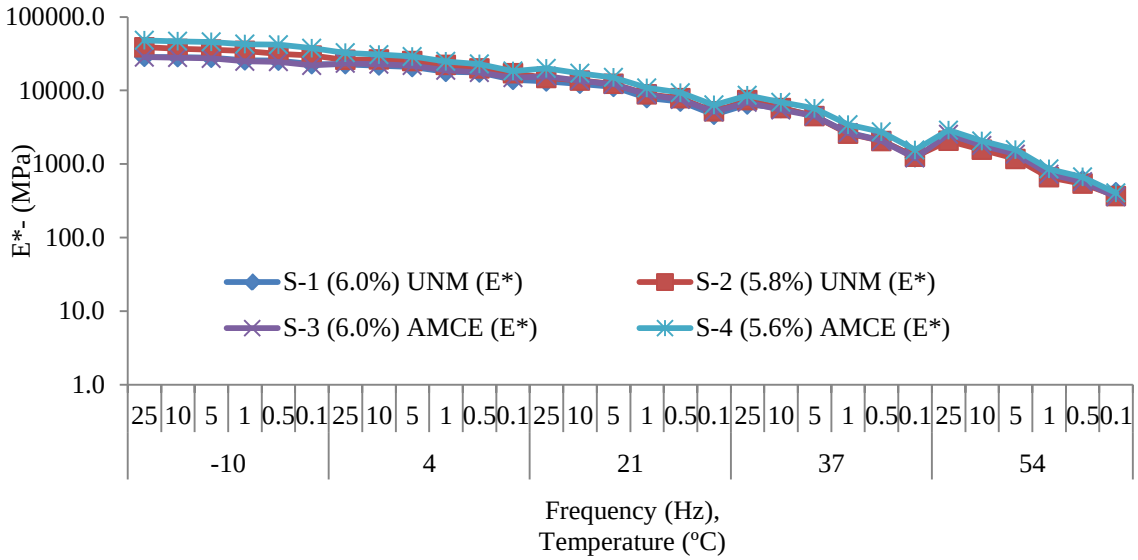


(c) SP-III with PG 64-22

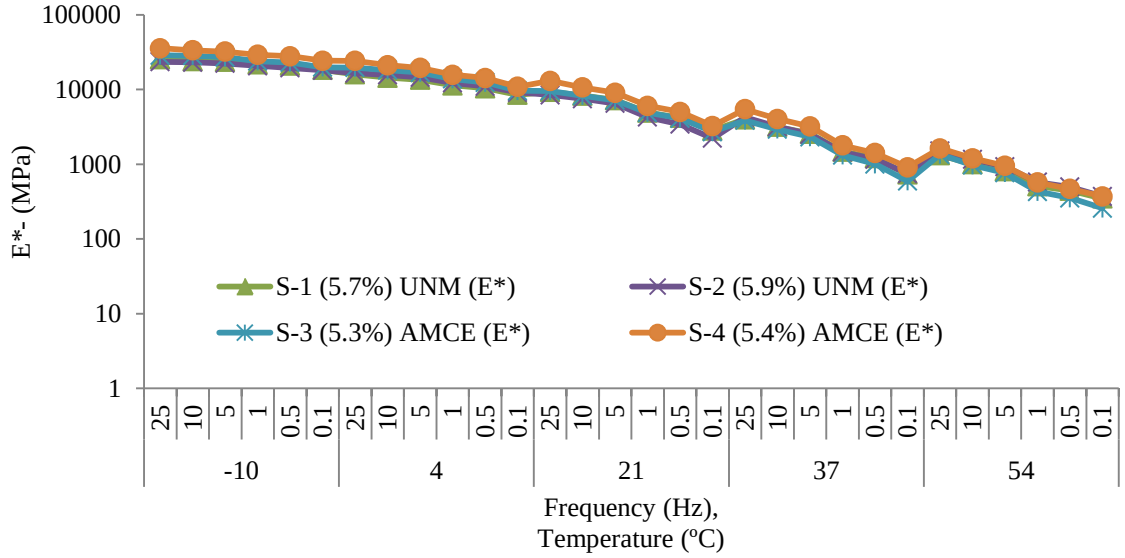


(d) SP-III with PG 70-22

Figure 4.2 (a-e) *E**- Trend Plots as A Function of Frequency and Temperature.

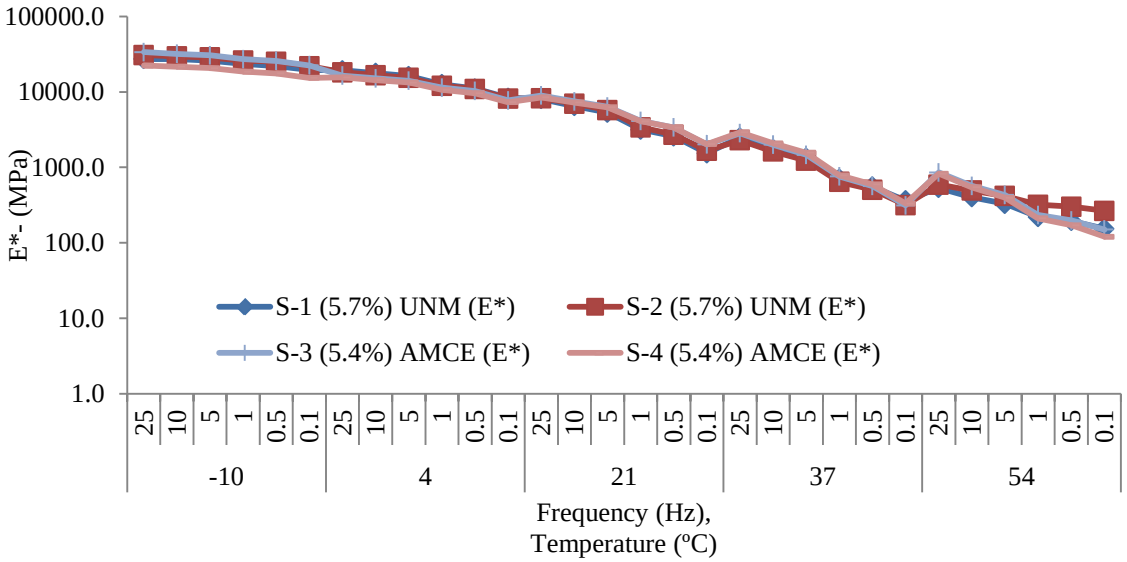


(e) SP-IV with PG 70-22

Figure 4.2 (a-e) *E**- Trend Plots as A Function of Frequency and Temperature.

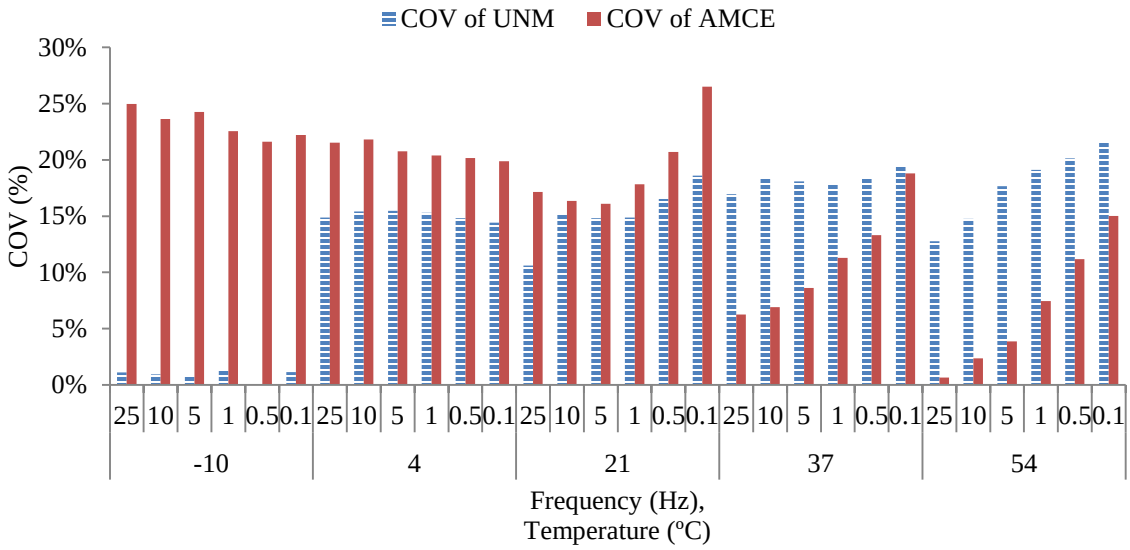


(a) SP-II with PG 64-22

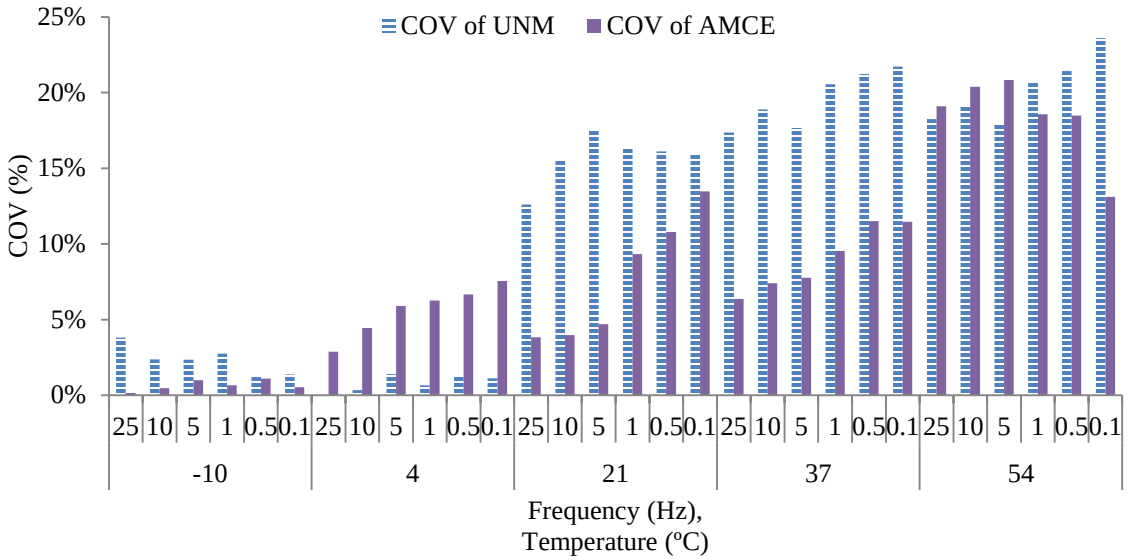


(b) SP-II with PG 70-22

Figure 4.3 (a-e) Coefficient of Variation (COV) Plots.

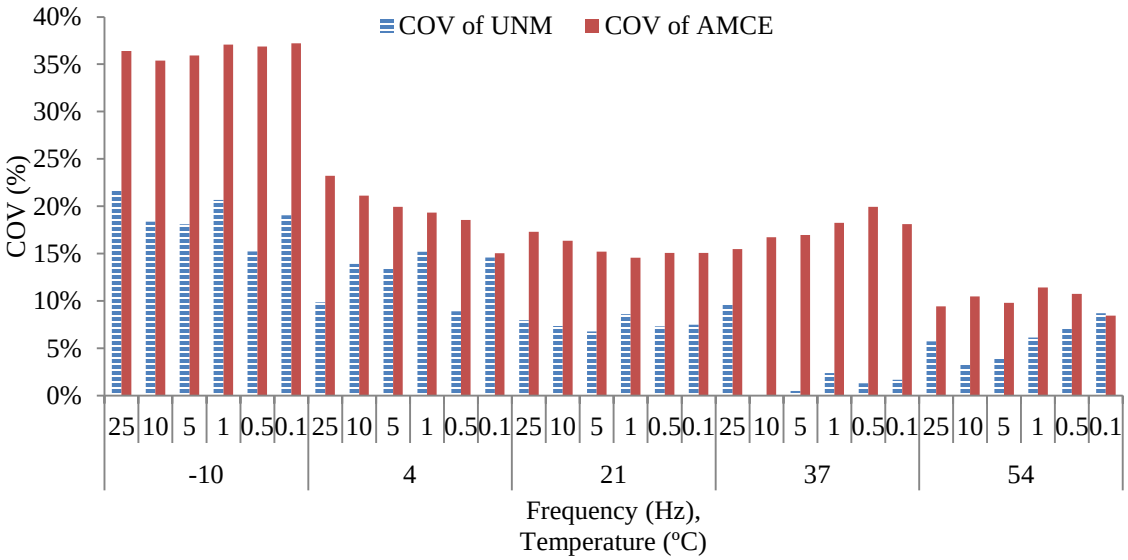


(c) SP-III with PG 64-22

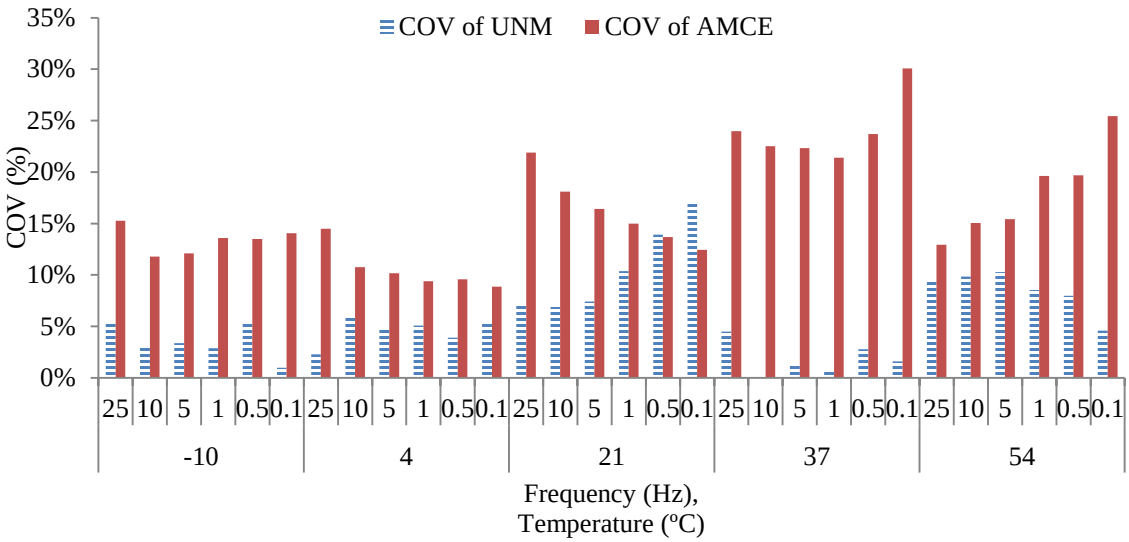


(d) SP-III with PG 70-22

Figure 4.3 (a-e) Coefficient of Variation (COV) Plots.

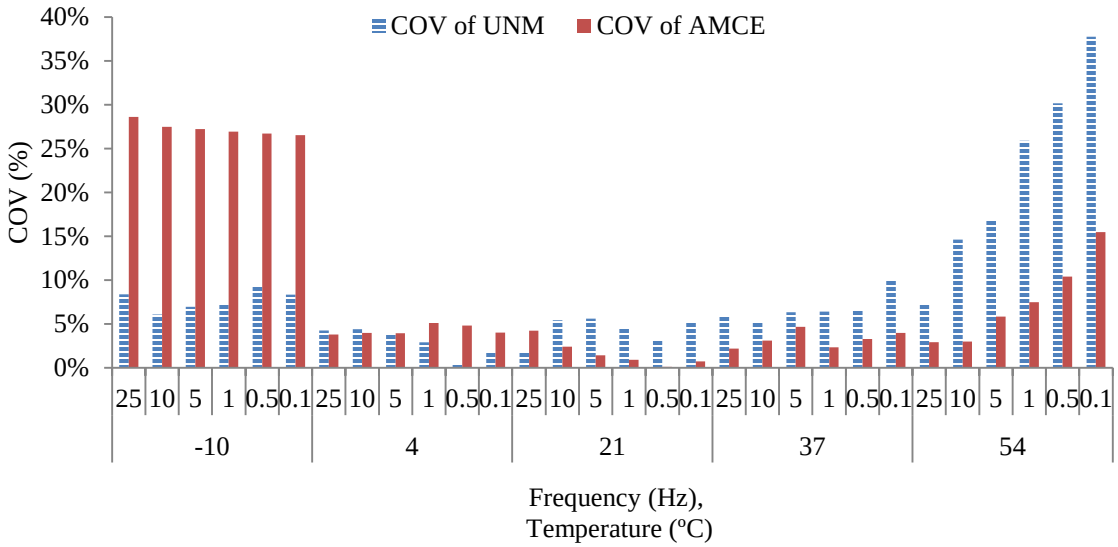


(e) SP-IV with PG 70-22

Figure 4.3 (a-e) Coefficient of Variation (COV) Plots.

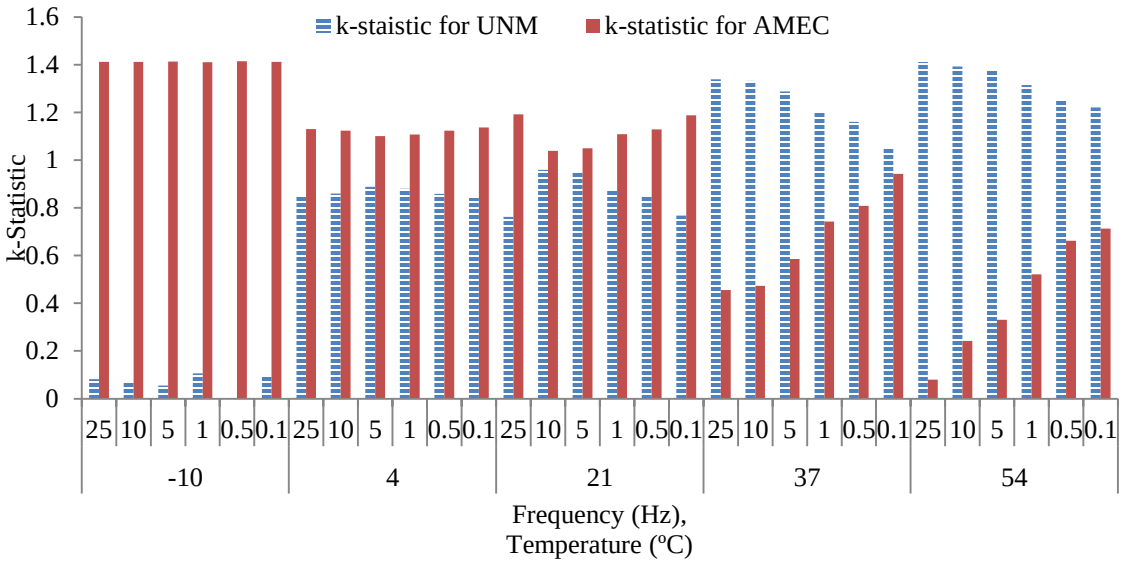


(a) SP-II with PG 64-22

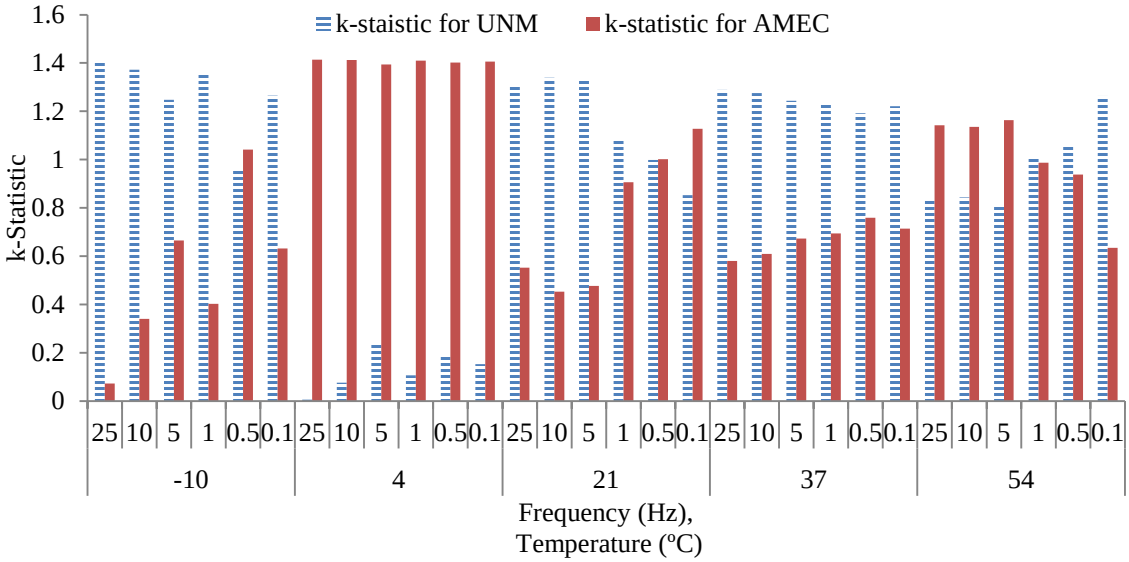


(b) SP-II with PG 70-22

Figure 4.4 (a-e) Within-Laboratory Consistency (*k*-Statistic) Plots.

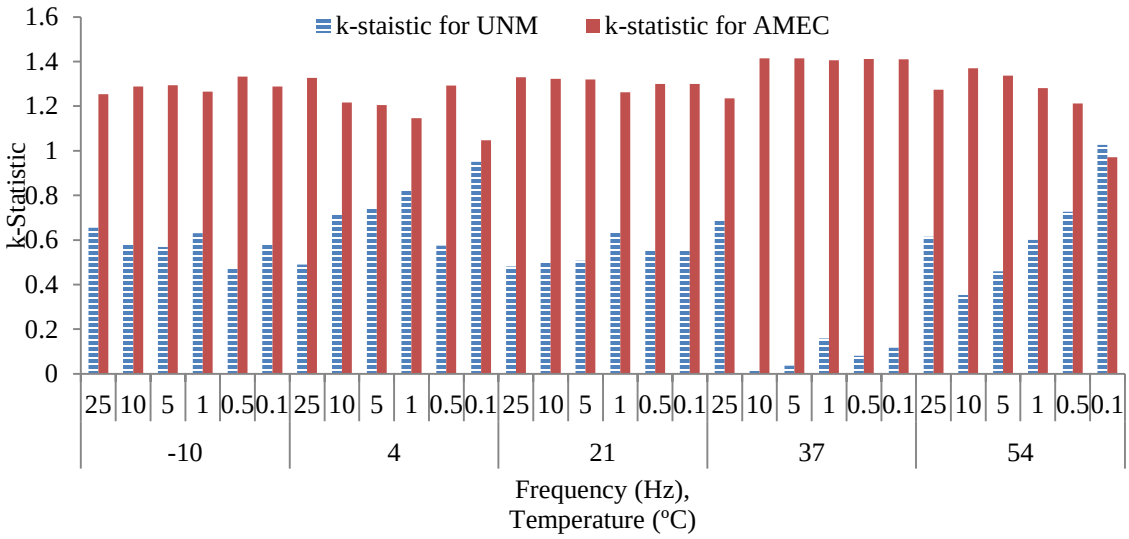


(c) SP-III with PG 64-22

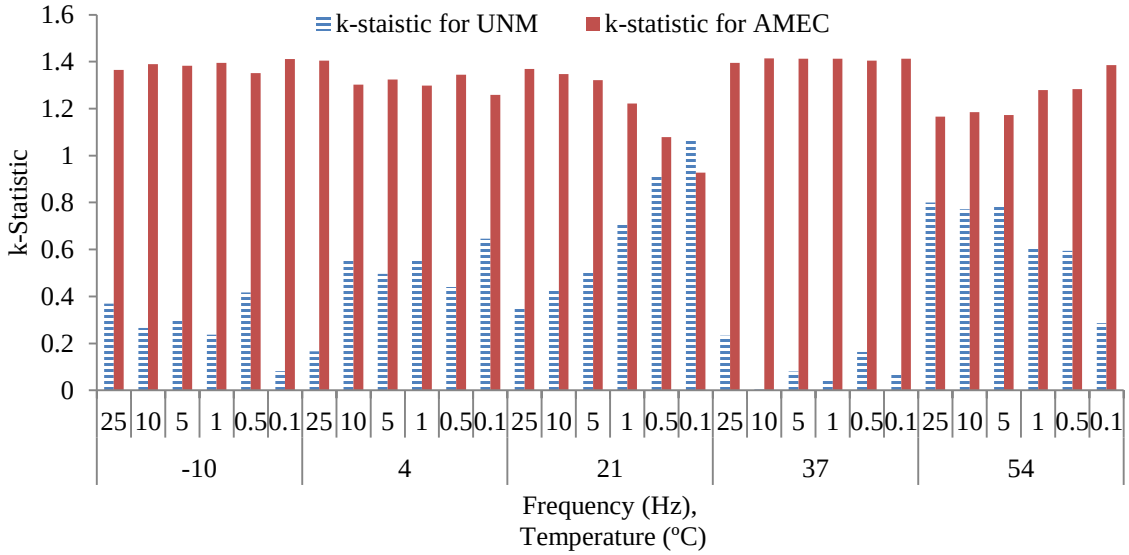


(d) SP-III with PG 70-22

Figure 4.4 (a-e) Within-Laboratory Consistency (*k*-Statistic) Plots.

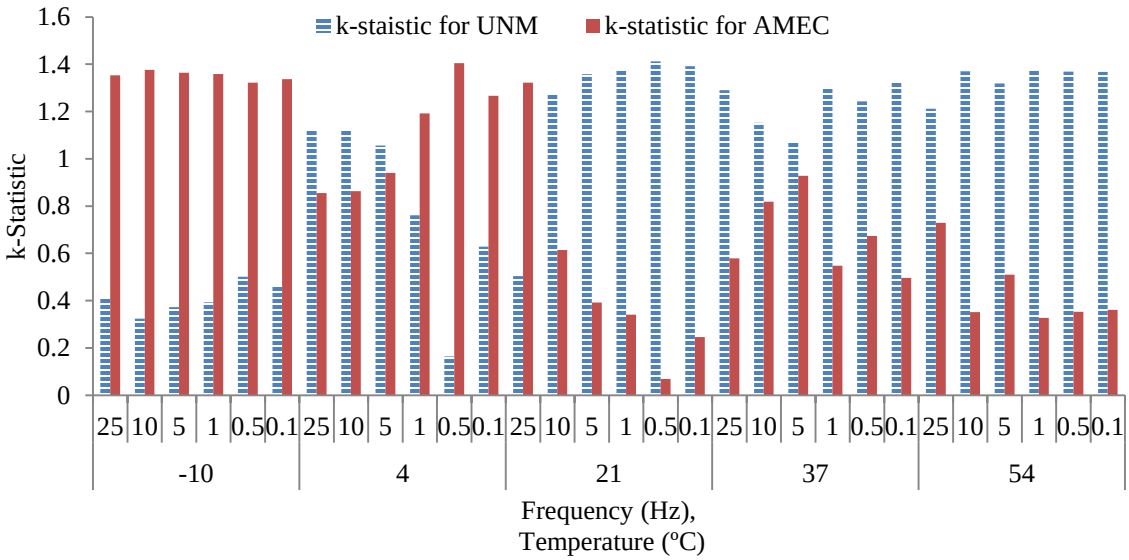


(e) SP-IV with PG 70-22

Figure 4.4 (a-e) Within-Laboratory Consistency (*k*-Statistic) Plots.

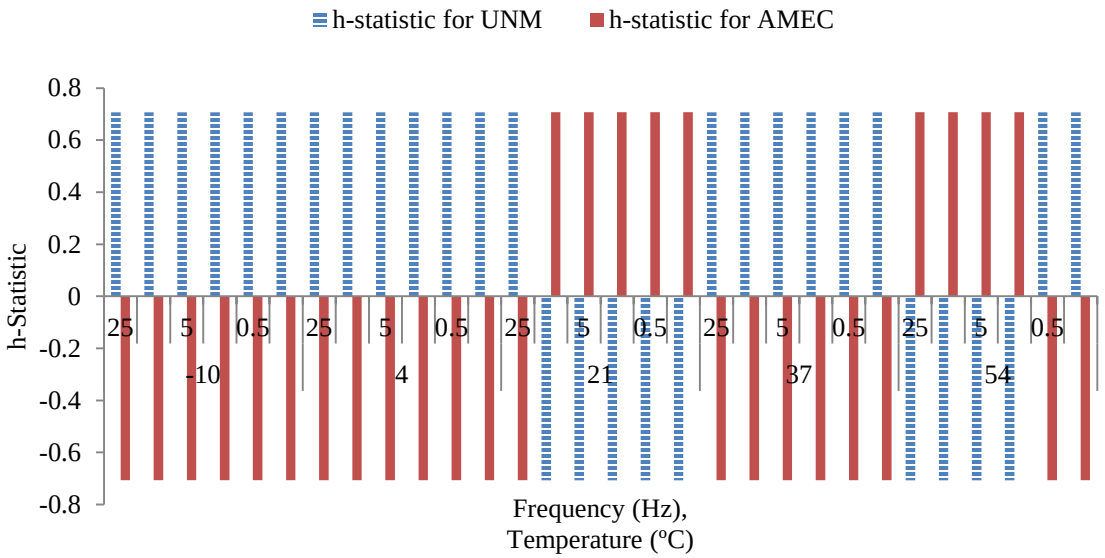


(a) SP-II with PG 64-22

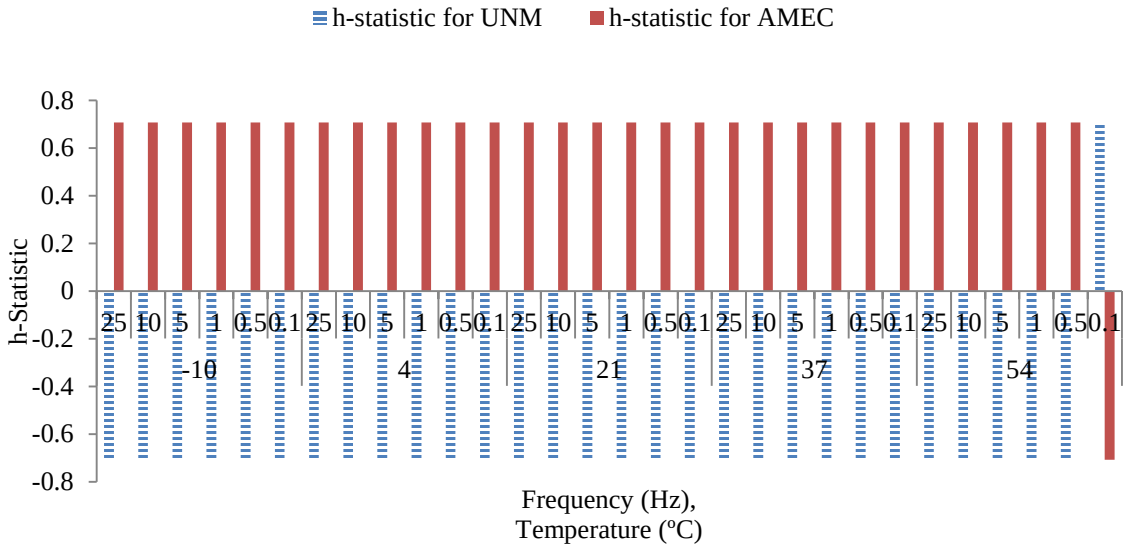


(b) SP-II with PG 70-22

Figure 4.5 (a-e) Between Laboratories *h*-statistic Plots.

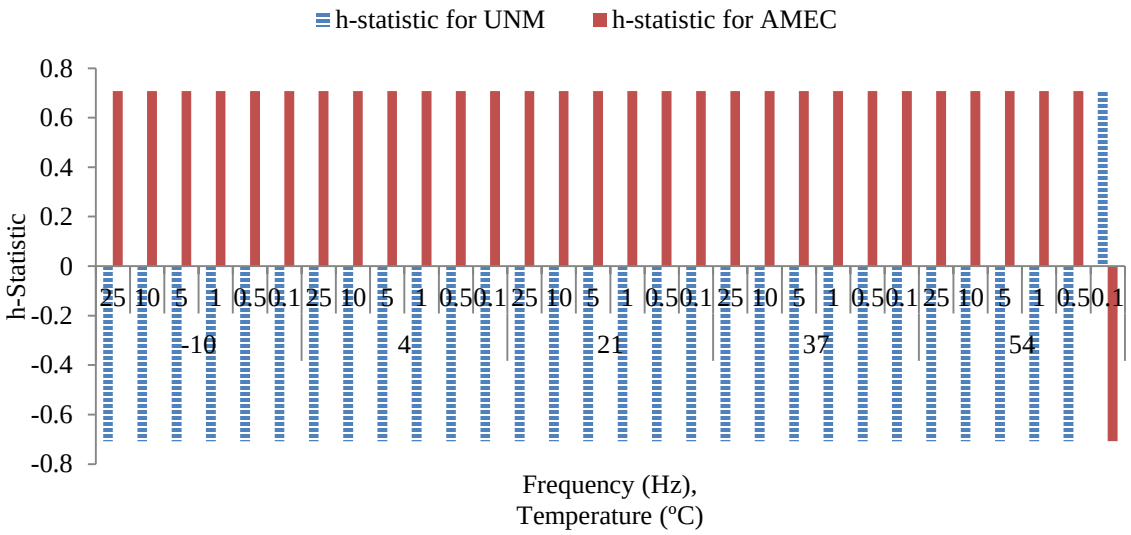


(c) SP-III with PG 64-22

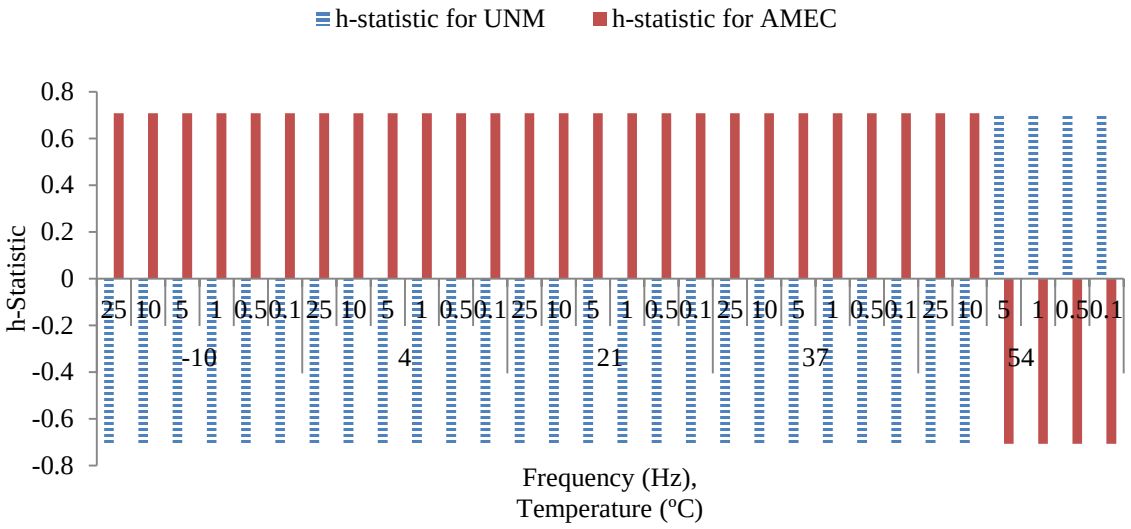


(d) SP-III with PG 70-22

Figure 4.5 (a-e) Between Laboratories *h*-statistic Plots.

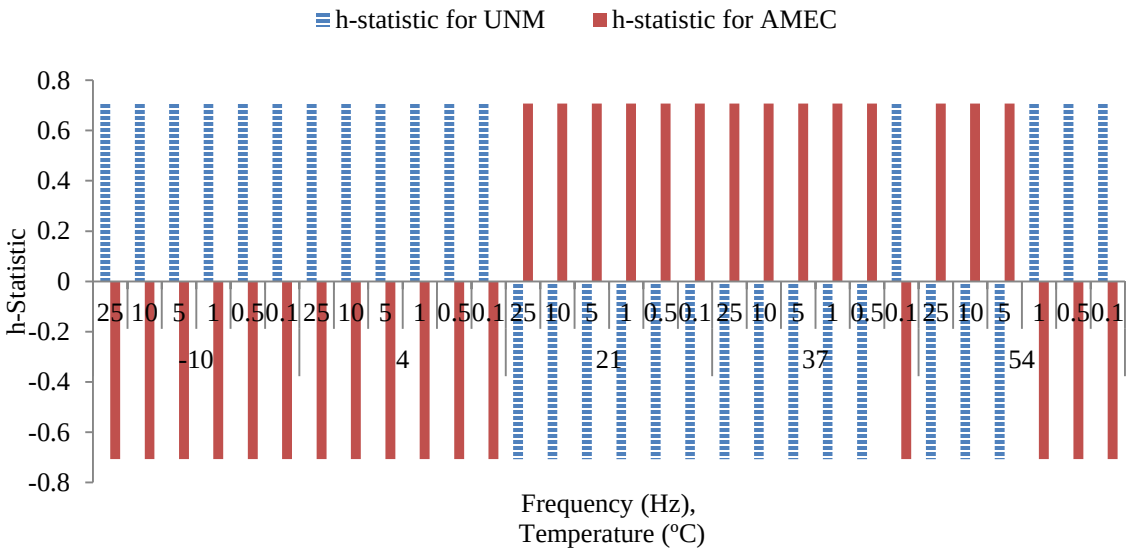


(e) SP-IV with PG 70-22

Figure 4.5 (a-e) Between Laboratories *h*-statistic Plots.

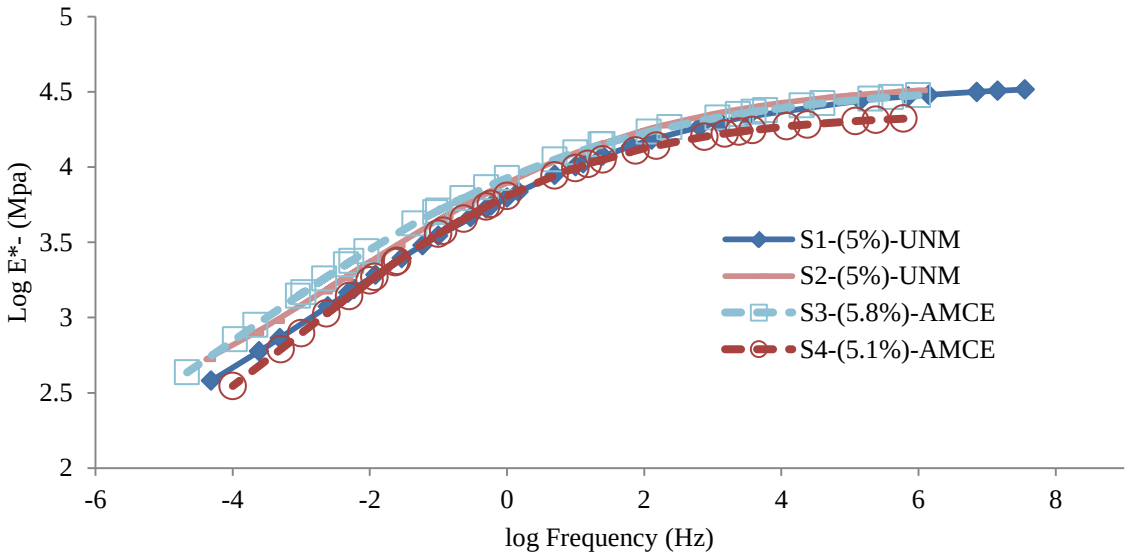


(a) SP-II with PG 64-22

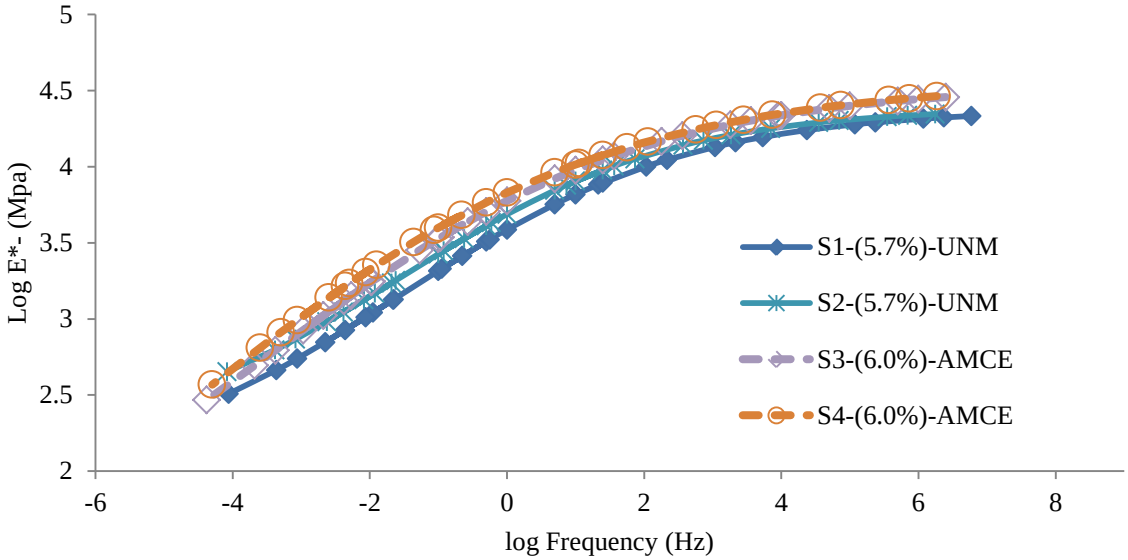


(b) SP-II with PG 70-22

Figure 4.6 (a-e) Mastercurve Plots.

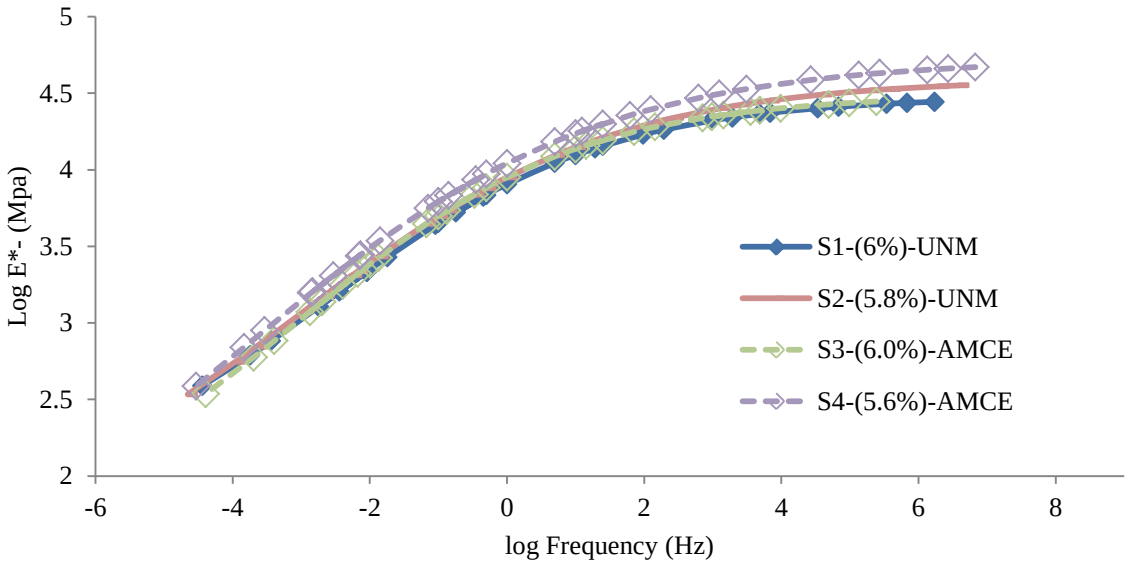


(c) SP-III with PG 64-22

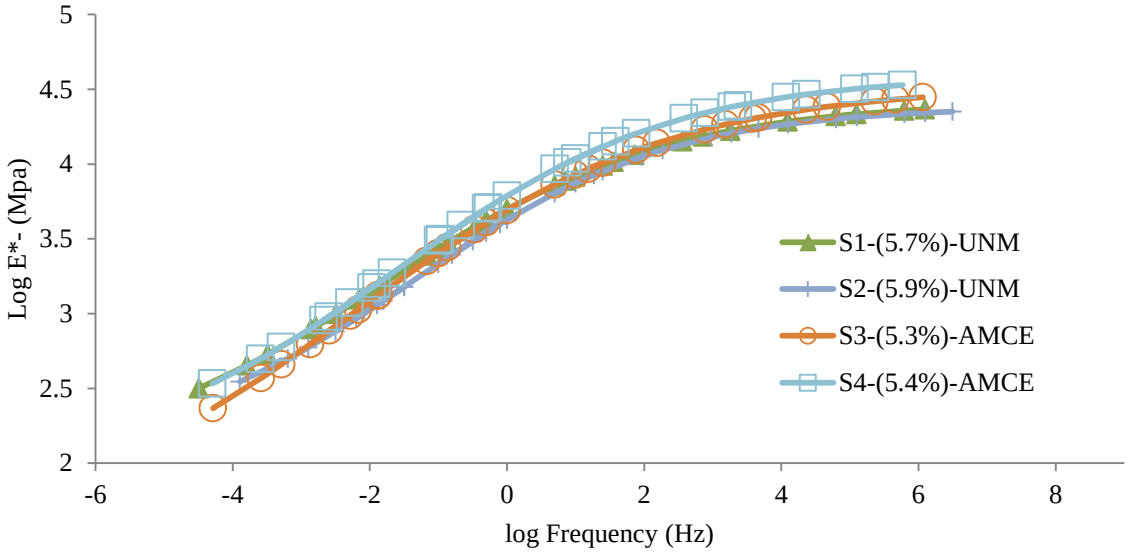


(d) SP-III with PG 70-22

Figure 4.6 (a-e) Mastercurve Plots.

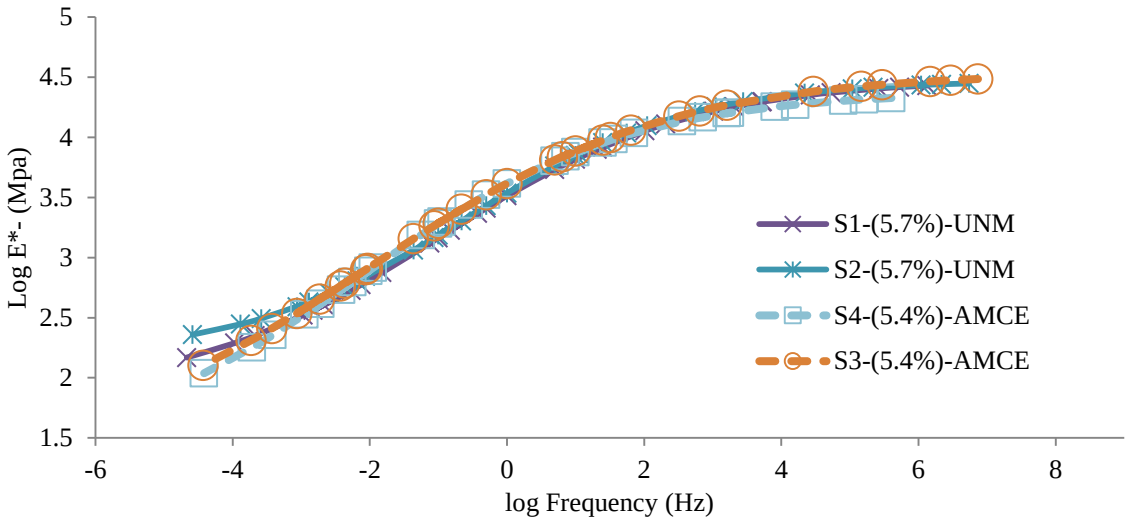


(e) SP-IV with PG 70-22

Figure 4.6 (a-e) Mastercurve Plots.

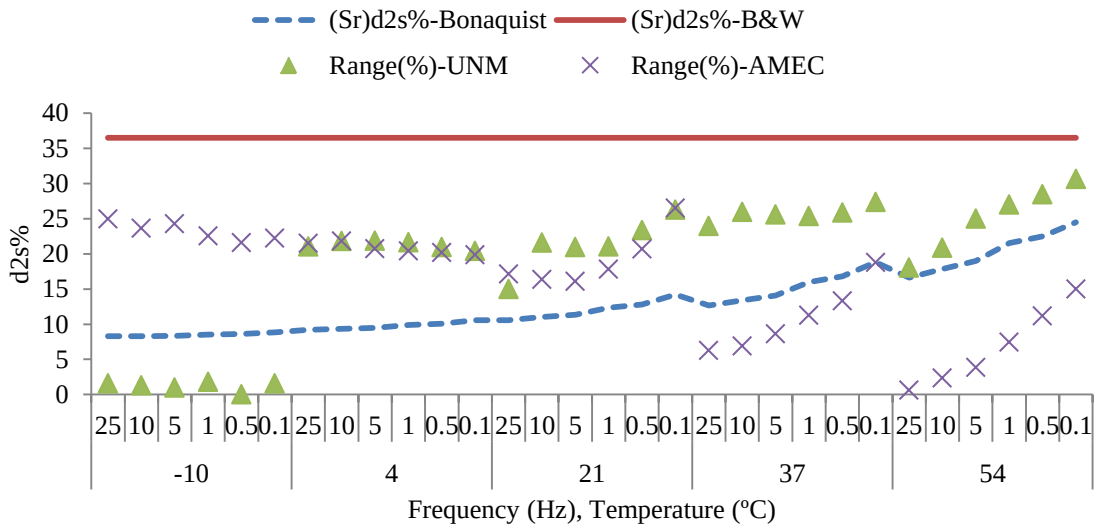


(a) SP-II with PG 64-22

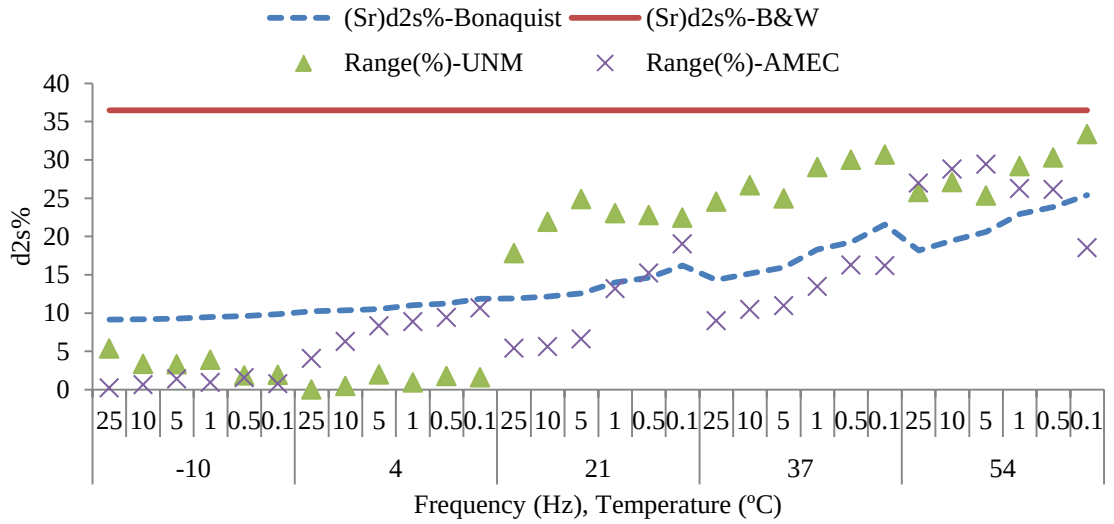


(b) SP-II with PG 70-22

Figure 4.7 (a-e) Repeatability Analysis of *E**-Results From UNM and AMEC Laboratories.

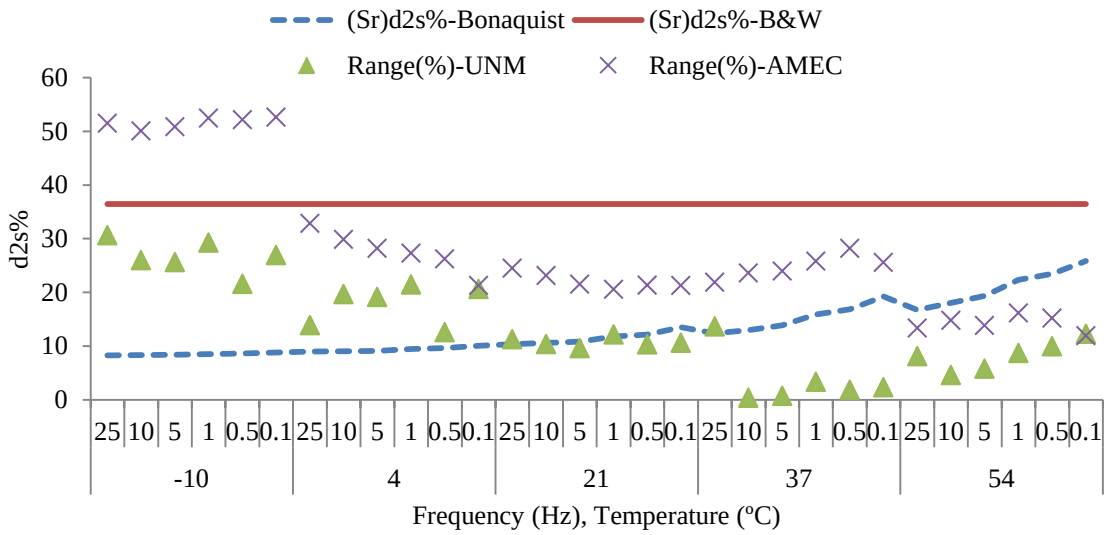


(c) SP-III with PG 64-22

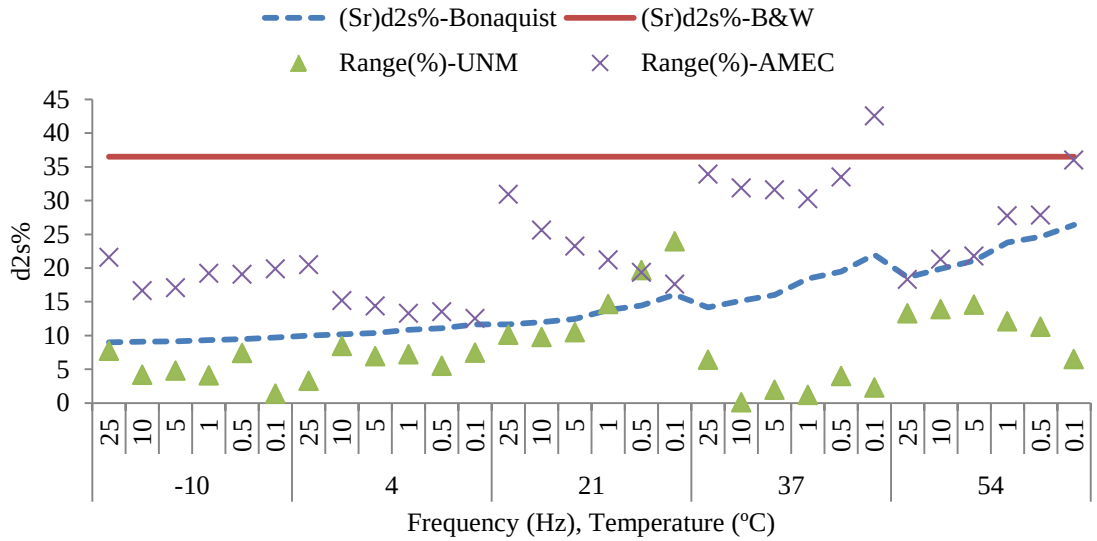


(d) SP-III with PG 70-22

Figure 4.7 (a-e) Repeatability Analysis of *E**-Results From UNM and AMEC Laboratories.

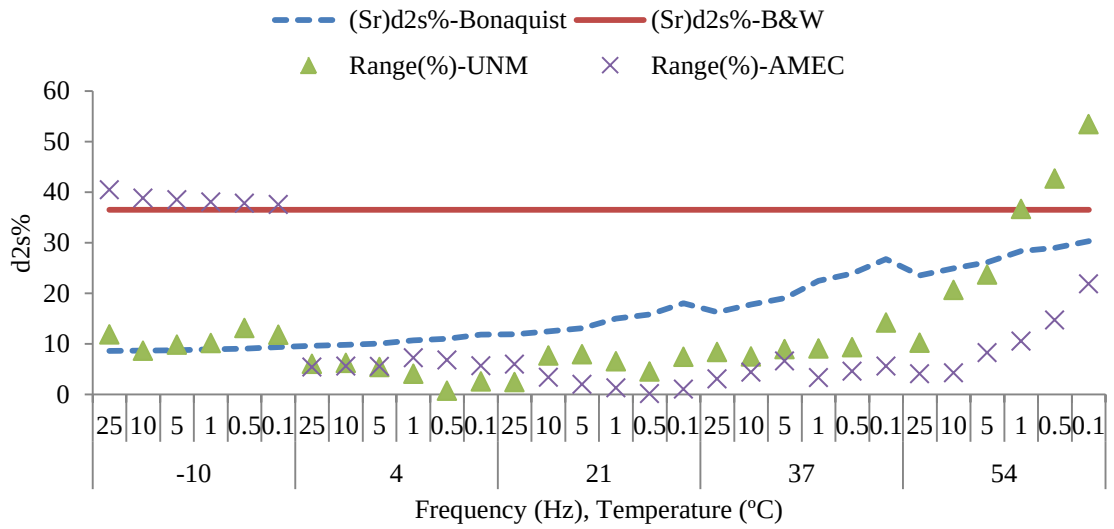


(e) SP-IV with PG 70-22

Figure 4.7 (a-e) Repeatability Analysis of *E**-Results From UNM and AMEC Laboratories.

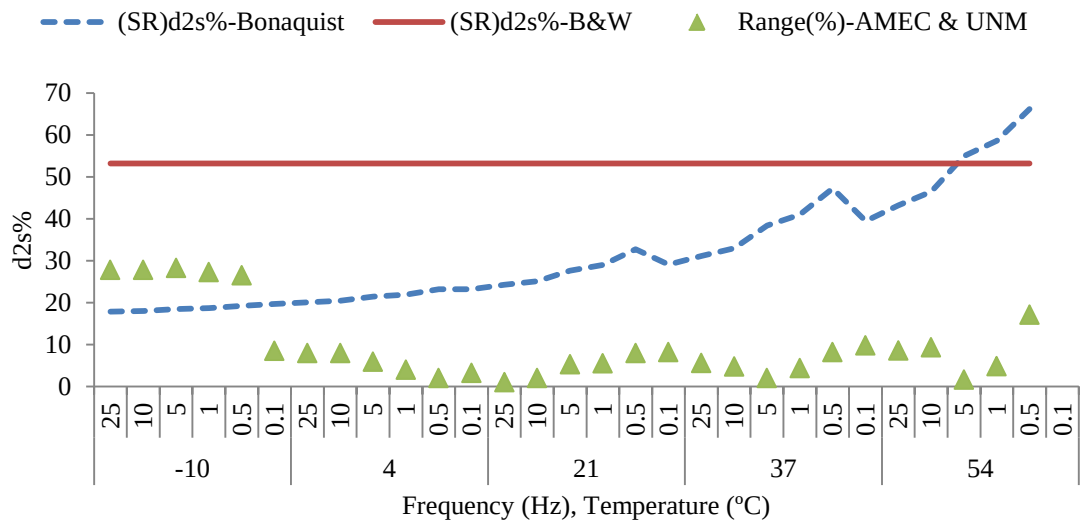


(a) SP-II with PG 64-22

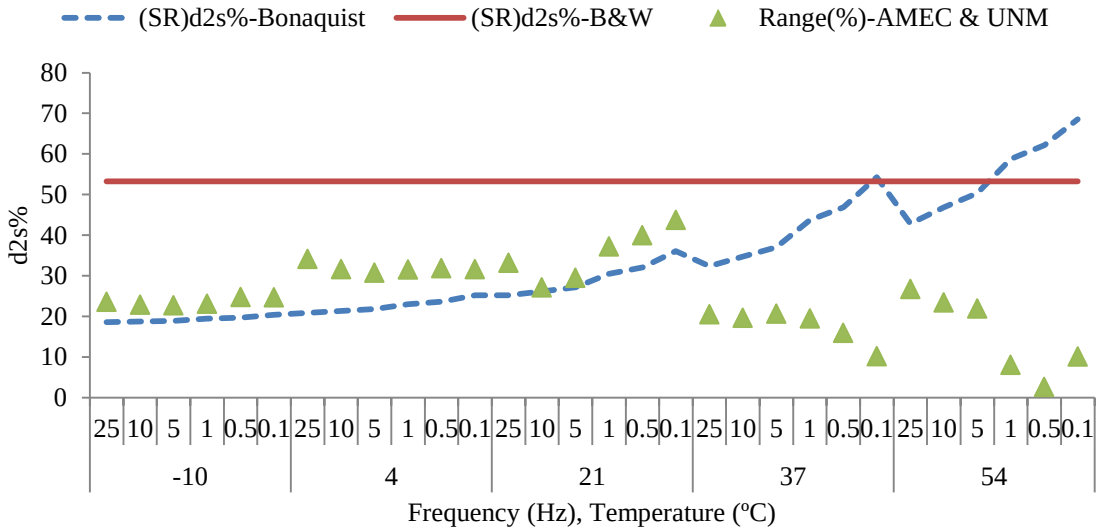


(b) SP-II with PG 70-22

Figure 4.8 (a-e) Reproducibility Analysis of *E**-Results From UNM and AMEC Laboratories.

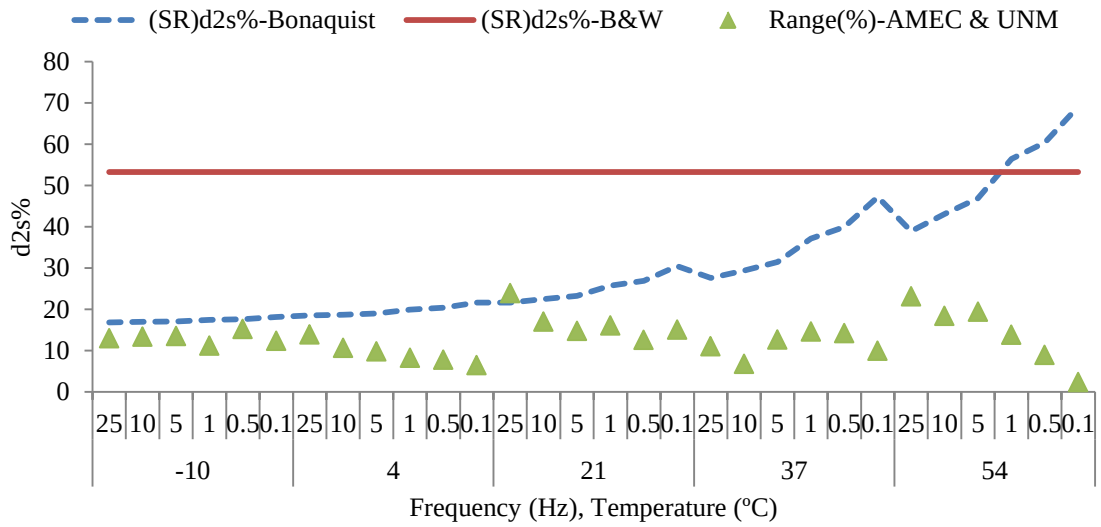


(c) SP-III with PG 64-22

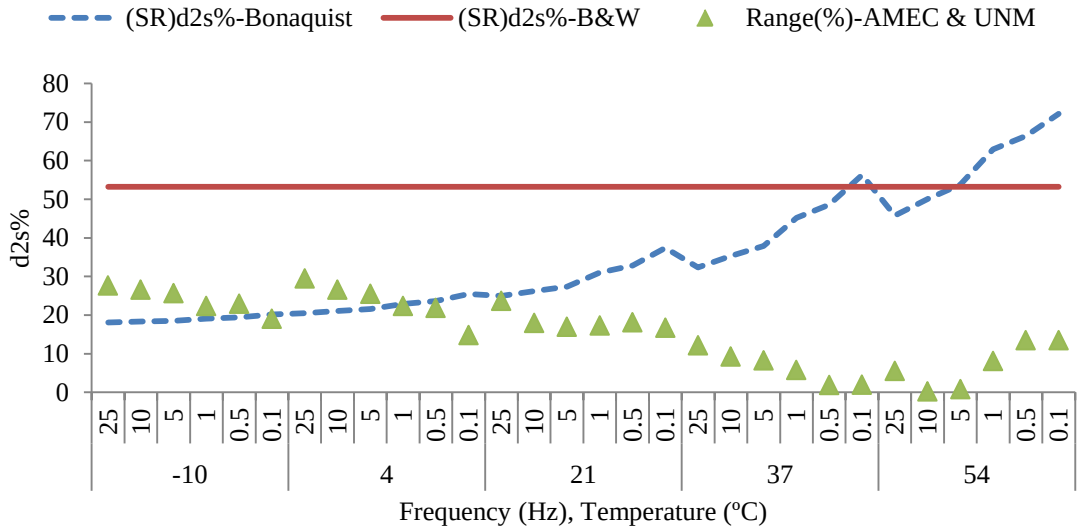


(d) SP-III with PG 70-22

Figure 4.8 (a-e) Reproducibility Analysis of *E**-Results From UNM and AMEC Laboratories.

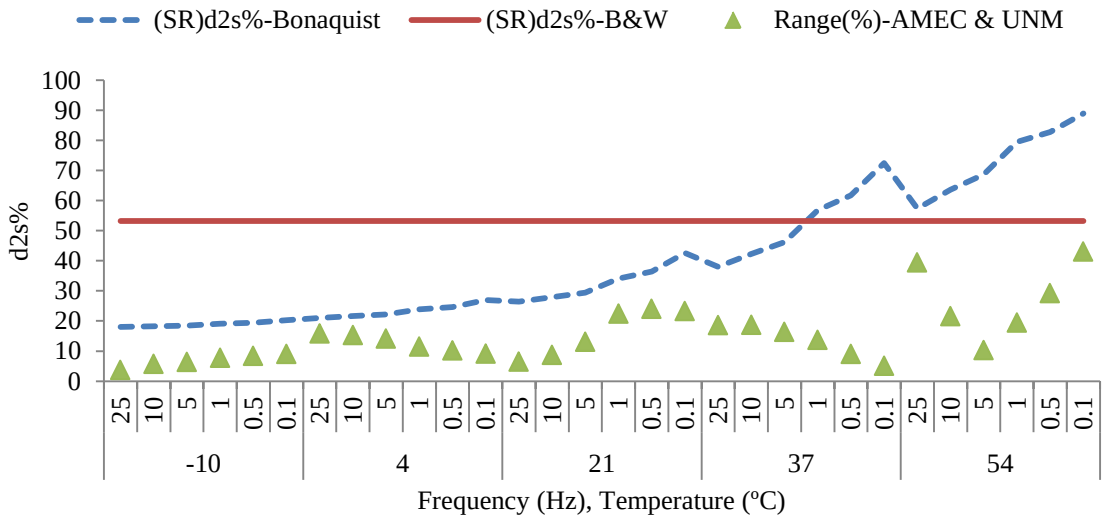


(e) SP-IV with PG 70-22

Figure 4.8 (a-e) Reproducibility Analysis of *E**-Results From UNM and AMEC Laboratories.

# Chapter 5

# Viscosity Based Witczak Model Application and Modification by Giving Emphasis to Mix Volumetrics

## 5.1. Introduction

The Viscosity based Witczak model is the primary dynamic modulus prediction model in MEPDG. The MEPDG levrl-3 analysis depends on the accuracy of this model. In this chapter the accuracy of viscosity based Witczak model is examined for predicting measured dynamic modulus values of typical New Mexico asphalt concrete. Moreover, the viscosity based model is also modified by giving more emphasis on mix volumetrics and eliminating coarse aggregate variables and introducing a modified version of aggregate contact factor developed by Hirsh. The model modification is based on the hypothesis that dynamic modulus test mostly influenced by mastic and mix volumetrics.

## 5.2. Objective

Specific objectives of this study are to:

- Apply viscosity based Witczak model for predicting measured dynamic modulus values of typical New Mexico Mixes
- Recalibrate the viscosity based Witczak model by giving more emphasis on mix volumetric properties

## 5.3. Viscosity Based Witczak Model

The viscosity based Witczak model, presented in Eq. (5.1), uses viscosity of binders as the main input parameter to capture the effect of binders. For developing this model 2750 dynamic modulus measurements from 205 different asphalt mixtures are tested in the laboratories of the Asphalt Institute, the University of Maryland, and the Federal Highway Administration. According to the developers, the model can predict the dynamic modulus of mixtures using both modified and conventional asphalt cements (ARA, Inc. 2004).

$$\begin{aligned}\log|E^*| &= -1.249937 + 0.029232\rho_{200} - 0.001767(\rho_{200})^2 - 0.002841\rho_4 \\ &- 0.058097V_a - 0.802208\left(\frac{V_{beff}}{V_{beff}+V_a}\right) \\ &+ \frac{3.871977 - 0.0021\rho_4 + 0.003958\rho_{38} - 0.000017(\rho_{38})^2 + 0.00547\rho_{34}}{1 + e^{(-603313 - 0.313351\log(f) - 0.393532\log(\eta))}}\end{aligned} \quad (5.1)$$

where: $|E^*|$ is dynamic modulus, $10^5$psi; $\eta$ is bitumen viscosity, $10^6$ Poise; f is loading frequency, Hz; $V_a$ is air void content, %; $V_{beff}$ is effective bitumen content, % by volume;

$\rho_{34}$ is cumulative % retained on the 19-mm (3/4-in.) sieve; $\rho_{38}$ is cumulative % retained on the 9.5-mm (3/8-in.) sieve; $\rho_4$ is cumulative % retained on the 4.76-mm (No. 4) sieve; $\rho_{200}$ is % passing the 0.075-mm (No. 200) sieve.

### 5.4. Analysis Method

It is possible to implement the viscosity based Witczak model in two different ways

- By using the default A and VTS values provided in MEPDG (method implemented in Level 3 input hierarchy of MEPDG)
- By determining the G* and phase angle of binder through a temperature sweep test, determining the A and VTS relationship for the binder and utilizing that for the model (method implemented in Level 2 input hierarchy of MEPDG)

In this study, both methods are implemented and the accuracy of the prediction is evaluated.

### 5.5. Application of Viscosity ($\eta$) based Witczak Model using Default *A* and *VTS* values

In this section the viscosity ($\eta$) based Witczak model is implemented using Microsoft excel to predict dynamic modulus mastercurves developed for the five mixes tested in this study. Default MEPDG A and VTS values are used in the temperature susceptibility relationship, given below in Eq. (5.2), to estimate the viscosity of each binder used. The default A and VTS values for PG 70-22 are 10.299 and -3.426 respectively and for PG 64-22 are A=10.98 and VTS=-3.68 (ARA, Inc. 2004).

$$\log\log\eta = A + VTS\log T_R \tag{5.2}$$

where: $\eta$ is viscosity (cP); $T_R$ is temperature (Rankine); A and VTS are regression intercept and regression slope of viscosity temperature susceptibility relationship.

Mastercurves are developed using predicted and measured data for the five mixes (SP-III-PG-64-22 (lab mix), SP-II-PG-70-22 (lab mix), SP-III-PG-70-22 (plant mix), SP-II-PG-64-22 (plant mix) and SP-IV-PG-70-22(plant mix)) and the results are presented in Figure 3.50 (a-e). The mastercurves developed using $\eta$-based Witczak model are found to underpredict mastercurves developed form measured data for all mixes except for the SP-IV mix. A scatter plot of raw $\eta$-based Witczak model $|E^*|$ prediction results in comparison with the measured $|E^*|$ data for all mixes tested in this study is presented in Figure 5.2. The result shows that $\eta$-based Witczak model predicts the $|E^*|$ test results of SP-IV mix with good accuracy but underpredicts $|E^*|$ of all other four mixes.

To quantitatively evaluate the accuracy of the $\eta$-based Witczak model the percent difference between predicted and tested data (the difference between the measured and predicted $|E^*|$ divided by the measured $|E^*|$) at each frequency and temperature are calculated. The average percent difference between predicted and tested data at each

temperature is tabulated in Table 5.1. Moreover, the trend of calculated percent of error with respect to temperature is presented in Figure 5.3(a) and the trend with respect to frequency is presented in Figure 5.3(b). Zero percent error for perfect prediction is shown in both figures. Positive sign of error indicates over prediction and negative sign indicates under prediction. It can be observed that the percent error of predicted $|E^*|$ is minimum for the cold temperature and increases with increasing temperature. However, no apparent trend is observed with respect to test frequency.

### 5.6. Level-3 $|E^*|$ Mastercurve prediction in MEPDG

For Level-3 input hierarchy MEPDG utilizes the viscosity ($\eta$) based Witczak model to predict the $|E^*|$ of asphalt mixes. At Level-3 input hierarchy no laboratory $|E^*|$ or binder viscosity test is required. Binder viscosity is determined using predetermined default A and VTS values specified based on previous test results. Mix data that are required for Level-3 MEPDG model prediction are: air void content ($V_a$) in %, effective bitumen content ($V_{beff}$) in % by volume, cumulative % retained on the 19 mm (3/4 in) sieve ($\rho_{34}$), cumulative % retained on the 9.5 mm (3/8 in) sieve ($\rho_{38}$ ), cumulative % retained on the 4.76 mm (No. 4) sieve ($\rho_4$) and % passing the 0.075 mm (No. 200) sieve ($\rho_{200}$) which are basically the inputs for viscosity ($\eta$) based Witczak model (ARA, Inc. 2004).

MEPDG software is also run to develop mastercurves for the SP-II, SP-III and SP-IV plant mixes tested this study. Figure 5.4 (a-c) present a comparison of Level-3 mastercurves developed using MEPDG software and laboratory test mastercurves. The results from the analysis show that the MEPDG software outputs are exactly the same as the excel calculations. The SP-II and SP-III mastercurves are under predicted while relatively better prediction accuracy is observed for SP-IV mix.

### 5.7. Application of Viscosity (η) Based Witczak Model using Actual *A* and *VTS* values

The A and VTS values for the binders used are determined by conducting dynamic shear,$|G^*|$, test on the binders and converting the results to viscosity using Eq. (5.3) and then using Eq. (5.2) on the viscosity data. For this purpose, the dynamic shear modulus test is conducted for binder grades PG 70-22 and PG 64-22. These binders are used for SP-II, SP-III and SP-IV mixes. For both binder grades dynamic shear modulus test is conducted on three replicate samples at different seven temperatures (40, 55, 70, 85, 100, 115, 130 $^oF$). These test temperature are selected based on MEPDG level two input requirements.

Table 5.2 present numeric dynamic shear modulus,$|G^*|$, and phase angle, δ, test results for binder grade PG 64-22 and PG 70-22. It can be observed that $|G^*|$ values decrease with increasing temperature while phase angle increases with increasing test temperature which confirms the rationality of the test results. The trends of dynamic shear

modulus,$|G^*|$, and phase angle, δ, for PG 64-22 and PG 70-22 are presented pictorially in Figure 5.5 (a), (b) and Figure 5.6 (a), (b) respectively. Then, the A and VTS relationships are developed and presented for PG 64-22 and PG 70-22 in Figure 5.5 (c) and Figure 5.6 (c) respectively.

$$\eta = \frac{G^*}{10}\left(\frac{1}{\sin\delta}\right)^{4.8628} \tag{5.3}$$

where: $G^*$ is binder shear modulus (Pa), $\delta$ is binder phase angle (deg), $\eta$ is viscosity (cP)

Then theses A and VTS values are used in the $\eta$-based Witczak model to predict dynamic modulus for the five mixes tested in this study. A scatter plot of raw $\eta$-based Witczak model $|E^*|$ prediction results in comparison with the measured $|E^*|$ data for all mixes is presented in Figure 5.7. The result shows that $\eta$-based Witczak model still predicts underpredicts $|E^*|$ of all other five mixes.

### 5.8. Level-2 $|E^*|$ Mastercurve Prediction in MEPDG

The viscosity ($\eta$) based Witczak model is still the primary model to predict the $|E^*|$ of asphalt mixes at the Level-2 input hierarchy of MEPDG. However, dynamic shear modulus,$|G^*|$, and phase angle, δ, test results are required to determine the binder viscosity. Binder viscosity is determined using the G* conversion and the temperature susceptibility relationships provided in Eq. (5.4) and Eq. (5.2). The A and VTS values determined by MEPDG software are compared with the values determined in this study and the results are found to match perfectly. Mix data that are required for Level-2 MEPDG model prediction are exactly the same as Level-3 input hierarchy (ARA, Inc. 2004). Then, MEPDG software is run to develop mastercurves for the SP-II, SP-III and SP-IV plant mixes at Level-2 input hierarchy and the results are presented in Figure 5.8 (a-c). The results from the analysis show that the MEPDG software outputs are exactly the same as the excel calculations and the MEPDG mastercurves under predicted all mixes.

### 5.9. Past Performance Evaluation of η-based Witczak Model

The performance of $\eta$-based Witczak model is evaluated by many researchers: Clyne et al. (2003) implemented the $\eta$-based Witczak model to predict $|E^*|$ mastercurves for MN/DOT mixes. The results indicated that $\eta$-based Witczak model always under predicted measured $|E^*|$ values of all mixes. The extent to which the model under predicted is also found to be different for different mixes. Christensen et al. (2003) also reported that the use of $\eta$-based Witczak predictive equation produced slightly less values than test results at higher modulus values. Birgisson et al. (2005) found predicted $|E^*|$ values to be largely dependent on the binder viscosity-temperature relationship. In their study, it is reported that the use A-VTS values proposed for mix/laydown condition by Witczak and Fonseca result in an over prediction of measured $|E^*|$ values. Kim et al. (2005) also investigated the accuracy of the $\eta$-based Witczak predictive model by calculating the percent of error at each frequency and temperature combination and then

averaging for different frequencies at the same temperature for each mixture. The findings implied that the $\eta$-based Witczak equation predicts better at cooler temperatures than at warmer temperatures. Schwartz (2005) employed sensitivity and validation analysis to evaluate the accuracy of $\eta$-based Witczak predictive equation. In conclusion, the Witczak model is found produce reasonable estimates in some cases and underpredict measured values at it worst performance. However, the model is also found to lack in predicting the performance variation of different mixes under varying design conditions. Tran and Hall (2005) used the coefficient of determination test statistic to evaluate the how well the $\eta$-based Witczak predictive equation estimates the measured $|E^*|$ and concluded that Witczak predictive equation have good correlation to the measured $|E^*|$ values. However, close observation of measured and predicted results indicated a tendency to underpredict $|E^*|$ values. Mohammad et al. (2005) investigated the accuracy of $\eta$-based Witczak model utilizing $|E^*|$ data collected at the FHWA mobile laboratory and the LTRC laboratory. They also found that predicted $|E^*|$ values are on the average 75% of measured $|E^*|$ values. Dongré et al. (2005) implemented the $\eta$-based Witczak model for original, RTFO and PAV aged binder cases. It is reported in their study that the $\eta$-based Witczak model produces unreasonable estimates for modulus below 700 MPa and underpredicts measured $|E^*|$ for air void and binder content higher than the mix design. Dongré et al. (2005) have also recommended to improve the sensitivity of $\eta$-based Witczak model to volumetric variables, such as the percentage of voids in mineral aggregate (VMA), the percentage of voids filled with asphalt (VFA), asphalt concrete percentage (AC), and Percentage of air voids by volume of mix (*Va*).

## 5.10. Maneuvering MEPDG inputs for Level-3 |E*| Mastercurve Predictions

In this section of the study the MEPDG mix input variables (air void content ($V_a$) in %, effective bitumen content ($V_{beff}$) in % by volume, cumulative % retained on the 19 mm (3/4 in) sieve ($\rho_{34}$), cumulative % retained on the 9.5 mm (3/8 in) sieve ($\rho_{38}$), cumulative % retained on the 4.76 mm (No. 4) sieve ($\rho_4$) and % passing the 0.075 mm (No. 200) sieve ($\rho_{200}$)) are optimized to minimize the error of predicted mastercurves and produce exact prediction of laboratory dynamic modulus tests results in level-3 input hierarchy. In other words, a solution for laboratory mastercurves are searched by changing mix input variables.

Optimization of mix input variables is performed by minimizing the sum of squared differences between predicted and test dynamic modulus values. To produce physically realistic optimized asphalt mix input data for Level-3 input hierarchy the following constraints are applied:

- All input values are physical quantities; therefore, the minimum value they can logically hold is zero.
- All input values are expressed in percentage; therefore, the maximum value they can hold is 100.

- The aggregate input values, cumulative % retained on the 19 mm (3/4 in) sieve ($\rho_{34}$), cumulative % retained on the 9.5 mm (3/8 in) sieve ($\rho_{38}$), cumulative % retained on the 4.76 mm (No. 4) sieve ($\rho_4$) are hierarchically related. Therefore, for physically logical results $\rho_{34} \leq \rho_{38} \leq \rho_4 \leq 100$.
- The model has air void content ($V_a$) in % and effective bitumen content ($V_{beff}$) in % by volume sum as a denominator, therefore, $V_a + V_{beff} > 0$.

Figure 5.9 (a-c) show a comparison of MEPDG Level-3 prediction of $|E^*|$ mastercurves using optimized input data and $|E^*|$ mastercurves developed from the actual $|E^*|$ test results for SP-II, SP-III and SP-IV plant mixes. The mastercurve plots show remarkable improvement of MEPDG Level-3 prediction when the optimized mix input values are used.

Original mix input values determined through laboratory test and optimized input values determined using Excel solver functions are presented in Table 5.3. The lab original values are actual laboratory test results while optimized values are obtained after minimizing the error between laboratory $|E^*|$ test results and model predicted $|E^*|$ values. Comparison of the optimized input data with original input values shows that the mix aggregate distribution variables, $\rho_{34}$, $\rho_{38}$ and $\rho_4$, are zero and the change in $V_a$, $V_{beff}$ and $\rho_{200}$ values are not very large. Therefore, the coarse aggregate influence on accuracy of $\eta$-based Witczak model is minimal and variables $\rho_{34}$, $\rho_{38}$ and $\rho_4$ can be eliminated without causing significant problems on model performance. Based on this finding and the it valid to make a hypothesis that dynamic modulus of asphalt concrete is influenced significantly by mastic properties and mix volumetrics and the η-based Witczak model can be modified by predominantly using mix volumetric variables and eliminating coarse aggregate variables.

## 5.11. Modification of η-based Witczak model

The $\eta$-based Witczak model is found to underpredict the laboratory measured $|E^*|$ for typical NMDOT mixes. Additionally, the performance evaluation of the $\eta$-based Witczak model by numerous researchers as described above also indicated the need for refining. Based on these evaluations and the findings of input optimization performed above, a modified version for $\eta$-based Witczak model is developed by eliminating the aggregate size variables and giving emphasis to mix volumetric indicators. For modification of this model the $|E^*|$ database developed by Bari (2005) is utilized. Bari's $|E^*|$ database includes 7400 sets of $|E^*|$ data from 346 asphalt mixes.
Main assumptions for the modification the $\eta$-based Witczak model are:

- $|E^*|$ of asphalt concrete is predominantly influenced by mix volumetric and mastic properties.
- The effect of aggregate distribution on $|E^*|$ can be captured by introducing aggregate contact factor which is dependent on mix volumetrics and viscosity of mastic in the mix.

- Coarse aggregate sizes variables in $\eta$-based Witczak model can be completely removed without causing significant problem and the effect of aggregate size distribution can be captured by
- The viscosity of binder can be accurately modeled using the viscosity temperature susceptibility liner regression model, Eq. (5.2), having intercept and regression slope of A and VTS.

Similar to the $\eta$-based Witczak model nonlinear regression analysis using the generalized reduced gradient optimization approach in Microsoft Excel's Solver is utilized for optimization. The sigmoidal function form as used for the $\eta$-based Witczak is also kept for the modification of the $\eta$-based Witczak model considering its proven performance in precious model developments. Therefore, the four sigmoidal function parameters α, β, γ and δ are utilized in the modification. The dependent variable is also kept as $\log|E^*|$ with a unit of pound per square inch (psi).

The $\eta$-based Witczak model has four sub models based on the four sigmoidal function parameters α, β, γ and δ. The δ –model in the $\eta$-based Witczak predictive equation is given by Eq. (5.4) (ARA, Inc. 2004). The modified δ –model given by Eq. (5.5) eliminates the coarse aggregate variable ($\rho_4$) and a new variable aggregate contact factor ($P_c$) given by Eq. (5.6) is introduced. $P_c$ is a modified version of the aggregate contact factor in the Hirsh model (Christensen et al. 2003). The regression constants in the $P_c$ ($P_0$, $P_1$ and $P_2$) are calibrated along the other regression constants of the modified model.

$$\delta = 3.750063 + 0.02932\rho_{200} - 0.001767(\rho_{200})^2 - 0.002841\rho_4 - 0.058097V_a - 0.802208\left(\frac{V_{beff}}{V_{beff}+V_a}\right) \quad (5.4)$$

$$\delta = a + b.\rho_{200} + c.(\rho_{200})^2 + d.\rho_4 + e.V_a + e.\left(\frac{V_{beff}}{V_{beff}+V_a}\right) + f.P_c \quad (5.5)$$

$$P_c = \frac{\left[P_o + \eta * \left(\frac{VFA}{VMA}\right)\right]^{P_1}}{P_2 + \left[\eta * \left(\frac{VFA}{VMA}\right)\right]^{P_1}} \quad (5.6)$$

$$VFA = \frac{V_{beff}}{V_{beff}+V_a} * 100 \quad (5.7)$$

$$VMA = \frac{Vol_{air}+Vol_{eff\ asphlt}}{Vol_{bulk}} * 100 = V_{beff}(\%)+V_a(\%) \quad (5.8)$$

where: $VFA$ is % voids filled with asphalt, $VMA$ is % voids in mineral aggregate, η is bitumen viscosity, $10^6$ Poise; $V_a$ is air void content, %; $V_{beff}$ is effective bitumen content, % by volume; $\rho_4$ is cumulative % retained on the 4.76-mm (No. 4) sieve; $\rho_{200}$ is % passing the 0.075-mm (No. 200) sieve, $P_c$ is aggregate contact factor, $a, b, c, d, e, f, P_o, P_1, P_2$ are regression constants to be determined with the modification.

The α –model in the $\eta$-based Witczak predictive equation is given by Eq. (5.9) (ARA, Inc. 2004). Similar to the δ –model the coarse aggregate variables $\rho_4$, $\rho_{38}$ and $\rho_{34}$ are removed and replaced with $P_c$ and VMA and the resulting form of the α –model for the modified model is given by Eq. (5.10).

$$\alpha = 3.871977 - 0.0021\rho_4 + 0.003958\rho_{38} - 0.000017(\rho_{38})^2 + 0.00547\rho_{34} \quad (5.9)$$

$$\alpha = g + h.P_c + i.(VMA) \quad (5.10)$$

where $\rho_{34}$ is cumulative % retained on the 19-mm (3/4-in.) sieve; $\rho_{38}$ is cumulative % retained on the 9.5-mm (3/8-in.) sieve; $\rho_4$ is cumulative % retained on the 4.76-mm (No. 4) sieve; $VMA$ is % voids in mineral aggregate, $P_c$ is aggregate contact factor, $g, h, i$ regression constants to be determined with the modification.

The exponential part of the sigmoidal function ($\beta + \gamma\, log(f)$) is modeled by Eq. (5.11) in the $\eta$-based Witczak predictive equation ARA, Inc. (2004). Similar functional form and variables are also used in the modified model as well. The exponent term in the modified model is given by Eq. (5.12).

$$\beta + \gamma \log(f) = -603313 - 0.313351\, log(f) - 0.393532\, log(\eta) \quad (5.11)$$

$$\beta + \gamma\, log(f) = j + k.log(f) + l.log(\eta) \quad (5.12)$$

The model optimization is performed using the Generalized Reduced Gradient (GRG nonlinear) algorism in the solver function of Microsoft Excel. The GRG nonlinear algorism is run with a convergence criterion of 0.0001. Initial staring values for recalibrating the model are chosen to avoid non-convergent solutions.

The modification is performed by determining the difference between the observed $\log|E^*|$ and predicted $\log|E^*|$ and minimizing the sum of the squared differences by optimizing the regression constants using the GRG nonlinear algorism in the solver function of Microsoft Excel. As mentioned earlier, the $|E^*|$ database developed by Bari (2005) is utilized for modification. The data base includes 7400 sets of $|E^*|$ data from 346 asphalt mixes. The modified model is presented in Eq. (5.13) and Eq. (5.14).

$$log|E^*| = 5.603 + 0.06045\rho_{200} - 0.00419(\rho_{200})^2 - 0.0847V_a - 1.602\left(\frac{V_{beff}}{V_{beff}+V_a}\right) - 0.0816P_c + \frac{-0.00896 + 2.1496P_c + 0.0185VMA}{1 + e^{-0.1765-0.6729log(\eta)-0.39985\, log(f)}} \quad (5.13)$$

$$P_c = \frac{\left[107.566 + \eta * \left(\frac{VFA}{VMA}\right)\right]^{0.0364}}{0.00008075 + \left[\eta * \left(\frac{VFA}{VMA}\right)\right]^{0.0364}} \quad (5.14)$$

where: $|E^*|$ is dynamic modulus, $10^5$psi; $VFA$ is % voids filled with asphalt, $VMA$ is % voids in mineral aggregate, $\eta$ is bitumen viscosity, $10^6$ Poise; $V_a$ is air void content, %; $V_{beff}$ is effective bitumen content, % by volume; $\rho_4$ is cumulative % retained on the 4.76-mm (No. 4) sieve; $\rho_{200}$ is % passing the 0.075-mm (No. 200) sieve, $P_c$ is aggregate contact factor.

Figure 5.10 (a) and (b) provided a scatter plot of all 7400 data points in logarithmic scale and in in arithmetic scale respectively. The measured $\log|E^*|$ is the abscissa and the predicted $\log|E^*|$ is the ordinate for both

Figure 5.10 (a) and (b). For an ideally perfect perdition all points in the scatter plots should lie on the line of equality. It can be observed
Figure 5.10 (a) that the scatter pots are closely populated along the line of equality for both models in the logarithmic scale, which shows a good prediction power of both models in the logarithmic scale. However, comparison of the scatter produced from the two models indicates that the $\eta$-based Witczak model tends to underpredict the measured $|E^*|$ more than the new modified model. Moreover, it is clearly visible that equality line passes right through the middle of the new modified model scatter plot but the center of scatter plot for the $\eta$-based Witczak model is slightly below the line of equality. The arithmetic plot,
Figure 5.10 (b), on the other hand, presents a scatter plot of observed $|E^*|$ on the abscissa verses predicted $|E^*|$ for both models. The arithmetic plot indicates that the predictions from both models decrease with increasing$|E^*|$. However, in the arithmetic sale also, the $\eta$-based Witczak model tends to underpredict the measured $|E^*|$ more than the new modified model. This indicates that the modified model has superior power than the $\eta$-based Witczak model.

## 5.12. Performance evaluation using Goodness of Fit Statistic

The goodness of fit of the new modified model is evaluated by calculating the coefficient of determination using Eq. (5.15). The coefficient of determination for the new modified model is determined both in the logarithm and arithmetic scale. For the arithmetic scale, observed and predicted $|E^*|$ values in $10^5$ Psi are used and for logarithmic scale observed and predicted log$|E^*|$ values in Psi are used. Table 5.4 presents the statistics for the newly modified model. The evaluation based on coefficient of determination shows that the new modified model have excellent prediction power with $R^2$= 0.89 in logarithmic scale. Great correlation is also found in the arithmetic scale as well, with $R^2$= 0.76. Goodness of fit for the $\eta$-based Witczak model is also determined to be 0.71 and 0.52 in logarithmic and arithmetic scales respectively. this clearly indicates the superior performance of the new modified model over the $\eta$-based Witczak model in predicting the 7400 data points populated by Bari (2005).

$$R^2 = 1 - \frac{n-p}{n-1}.\left(\frac{S_e}{S_y}\right)^2 \tag{5.15}$$

where: $n$ is number of data points, $p$ is number of regression constants, $n-p$ is degrees of freedom, $S_e$ is standard error of estimate, $S_y$ is standard deviation

### 5.12.1. Prediction Capacity of Modified $\eta$-Based Model

The prediction power of the new modified model is evaluated by using laboratory $|E^*|$ data collected for by testing NMDOT SP-II-PG 70-22 (lab mix), SP-II-PG 64-22 (plant mix), SP-III-PG 70-22 (plant mix) and SP-III-PG 64-22 (lab mix) asphalt mixes. Figure 5.11 shows the scatter plots for the new modified model predicted $|E^*|$ data. By Comparing Figure 5.11 and Figure 5.2, it clear that the new modified model is performing much better than the $\eta$ -based Witczak model. The most noticeable improvement is the prediction accuracy for high temperature dynamic modulus. The

average percent error of prediction for the new calibrated model at each temperature is also tabulated in Table 5.5. In addition, the difference in the absolute % error ($|\%\ \text{error of Witczak model}| - |\%\ \text{error of new model}|$) is shown in brackets. Positive values indicate improvement of prediction by the new model and negative values indicate the reverse. The results in Table 5.5 show remarkable improvement.

The trend of calculated percent of error with respect to temperature is presented in Figure 5.12 (a) and the trend with respect to frequency is presented in Figure 5.12 (b). The percent error of predicted $|E^*|$ is found to be much closer to the zero line for all temperatures and the trend is not as obvious for Witczak model and no apparent trend is also observed with respect to test frequency.

As described above, the aggregate size distribution and binder grades of SP-II and SP-III mixes are different. Moreover, Both SP-II and SP-III mixes are prepared using two binder grades (PG 64-22 and PG 70-22). However, the performance of the new modified model has improved in all cases and the predictions are with very good accuracy. This indicates the robust performance of the new modified model and its capability to take care of aggregate sizes variation as well as binder grade variation.

### 5.12.2. Frequency Distribution of Residuals

The dynamic modulus of asphalt concrete is assumed to normally distributed in the $\eta$-based Witczak model, therefore the same assumption is adopted in modification as well. The normality of the new modified model is checked by plotting a histogram of the residuals. For the normality assumption to be valid, the plot of the residuals should be similar to the normal distribution plot centered at zero (Bari 2005 and Montgomery 2001).

Figure 5.13 (a) shows the frequency distribution of the residuals of $|E^*|$ in logarithmic scale (predicted $\log|E^*|$ - observed $\log|E^*|$) for the new modified model. The distribution of residuals in logarithmic scale looks very much like a normal distribution. The average and standard deviation is found to be 0.00 and 0.22 respectively.

Figure 5.13 (b) shows the frequency distribution of the residuals of $|E^*|$ in arithmetic scale (predicted $|E^*|$ - observed $|E^*|$). The average of the residuals for the new modified model is $1.151*10^5$Psi and the standard deviation is equal to $7.114*10^5$Psi. The range and standard deviation of the base laboratory $|E^*|$ data is found to be $0.10*10^5$ - $86.45*10^5$ Psi and $14.59*10^5$psi respectively. Compared with variation observed in the base laboratory $|E^*|$ data, the mean and standard deviation of the residuals are very small. Moreover, Bari (2005) also indicated that it is impossible to find a mean value of zero for the residuals in arithmetic scale since base laboratory $|E^*|$ follow a logarithmic model. Therefore, the new modified model is an accurate predictive model that is normally distributed in both arithmetic and logarithmic scale.

## 5.13. Model Sensitivity Analysis

Sensitivity analysis is crucial for evaluation of new models since unrealistic model structure can result in unreasonable predictions even if the model calibration shows very

good coefficient determination. For a the new modified model to pass sensitivity test, the predicted dynamic modulus values must follow reasonably well the trend of laboratory measured$|E^*|$ data while one selected input variable is being varied (Bari 2005). In this study, the new modified model is developed based on the argument that mix volumetric properties (VMA, VFA) and aggregate contact variable are crucial in the model performance. As shown above all these variables are a function of % air voids, effective binder content therefore sensitively analysis is performed in these two input variables. In addition, sensitivity analysis of the model to percent of fines is also included.
The procedure adopted by Bari (2005) is followed in performing the sensitivity analysis. First, the maximum, minimum and average values input variables at -10, 21 and 54 ºC only for 10 Hz frequency are summarized. This allowed grasping the variability of each input. Then, the range of each selected variable is divided in to five subdivisions and for each sub division the input variables and the laboratory measured dynamic modulus values are averaged. For the sensitivity analysis, the average input values in each subdivision are used to predict the average dynamic modulus. It is important to note that the average value of all other variables is used in predicting the dynamic modulus and only the selected input variable is varied according to the subdivisions and corresponding average dynamic modulus of the subdivision are compared with the predicted data.

### 5.13.1. Model Sensitivity to $V_a$

The average air void values of all subdivisions of $V_a$ and corresponding observed dynamic modulus values are at -10, 21 and 54 ºC are calculated for 10 Hz frequency. Then the New modified model is utilized to predict the dynamic modulus of at each subdivision. The trend of both predicted and measured dynamic moduli with increasing air void is presented in
Figure 5.14 (a). The trend of predicted data is following the measured data closely which indicates the accurate prediction capability of the new modified model.

### 5.13.2. Model Sensitivity to $V_{eff}$

Effective binder content is used in the new modified model in combination with percent air voids to capture the effect of mixture density as explained in Bari (2005) and in combination with viscosity and percent air void to reflect the increasing effect of aggregate contact friction with increasing temperature as explained in Christensen et al. (2003). Average incremental values of effective binder content are calculated from each subdivision at -10, 21 and 54 ºC for 10 Hz frequency with corresponding average measured dynamic modulus. Dynamic moduli are also predicted using the new predicted model for each increment of effective binder. The trend of both predicted and measured dynamic moduli with increasing effective binder content is presented in
Figure 5.14 (b). The trend of predicted data is following the measured data closely which indicates the accurate prediction capability of the new modified model.

### 5.13.3. Model Sensitivity to $\rho_{200}$

The binding material in asphalt concrete is not pure asphalt; rather it is a mixture of asphalt binder with passing #200 sieve fines (% $\rho_{200}$). Average %$\rho_{200}$ values are also calculated for each subdivision with respective average measured dynamic modulus values at -10, 21 and 54 ºC for 10 Hz frequency. Predicted dynamic moduli are determined for each subdivision using the new modified model and the trend of predicted and measured dynamic moduli values are presented in
Figure 5.14 (c). The trend of predicted data is following the measured data closely which indicates the accurate prediction capability of the new modified model.

## 5.14. Conclusions

In this study, the viscosity based Witczak model is applied for predicting measured dynamic modulus values of typical New Mexico Mixes and a new modified viscosity based Witczak model is developed by giving more emphasis on mix volumetric properties. From this study, the following conclusions can be dawn:

- The viscosity based Witczak model is applied by using the default A and VTS values and the predicted dynamic modulus values are found to be less than the measured dynamic modulus values for all SP-III and SP-II mixes. However, better agreement is obtained between predicted and laboratory mastercurves for SP-IV mix.
- The application of viscosity based Witczak model using actual A and VTS valued determined using DSR test results is found to underpredict the dynamic modulus results of all typical NMDOT mixes.
- Mastercurve prediction at both Level-3 and Level-2 input hierarchy using viscosity based Witczak model in MEPDG are found to under predict the dynamic modulus of SP-III and SP-II mixes. However, better agreement is obtained between predicted and laboratory mastercurves for SP-IV mix.
- The percent error of prediction for viscosity based Witczak model is found to be minimum at the cold temperature and showed an increasing trend with increasing temperature. However, no apparent trend is observed with respect to test frequency.
- It is found that, by optimizing the mix variable values, it is possible to improve the viscosity based Witczak model prediction significantly and optimized solution showed that the coarse aggregate variables in the viscosity based model can be eliminated without huge change in the mastic and binder input variable values. This indicate the low significance of coarse aggregate variables( $\rho_{34}$, $\rho_{38}$ and $\rho_4$ ) on the model prediction accuracy.
- A new dynamic modulus predictive model is developed by eliminating the coarse aggregate variables in the viscosity based Witczak model and keeping the sigmoidal mathematical structure and introducing a modified aggregate contact factor from Hirsh model.

- The new dynamic modulus model showed significant improvement in predicting the dynamic modulus of typical NMDOT mixes.
- Sensitivity analysis of the new model showed the prediction of the model is rational to variations of air void, effective binder and percentage of fine aggregates.
- The New modified model has showed significant improvement in prediction accuracy over the viscosity based Witczak model.

## 5.15. References

ARA, Inc., ERES Consultants Division (2004). "Guide for Mechanistic-Empirical Design of New & Rehabilitated Pavement structures (Final Report)". NCHRP Project 1-37A, <http://onlinepubs.trb.org/onlinepubs/archive/mepdg/guide.htm> (July 19, 2013).

Bari, J. (2005). "Development of a New Revised Version of the Witczak E* Predictive Models for Hot Mix Asphalt Mixtures." Ph.D. Dissertation, Arizona State University, Phoenix, AZ.

Christensen, Jr., D.W., Pellinen, T.K., and Bonaquist, R.F. (2003). "Hirsch Model for Estimating the Modulus of Asphalt Concrete," *Journal of the Association of Asphalt Paving Technologists*, *72*, 97–121.

Clyne, T.R., Li, X., Marastenau, M.O., and Skok, E.L. (2003). "Dynamic and Resilient Modulus of Mn/DOT Asphalt Mixtures." Final Report MN/RC – 2003-09. University of Minnesota, Minneapolis, MN.

Christensen, D.W., Pellinen, T.K., and Bonaquist, R.F. (2003). "Hirsch Model for Estimating the Modulus of Asphalt Concrete." Journal of the Association of Asphalt Paving Technologists, Volume 72, Lexington, KY.

Birgisson, B., Sholar, G., and Roque, R. (2005). "Evaluation of Predicted Dynamic Modulus for Florida Mixtures." 84th Annual Meeting of the Transportation Research Board, Paper No. 05-1309, Ishington D.C.

Kim, Y.R., King, M., and Momen, M. (2005). "Typical Dynamic Moduli Values of Hot Mix Asphalt in North Carolina and Their Prediction." 84th Annual Meeting of the Transportation Research Board, Paper No. 05-2568, Ishington D.C.

Schwartz, C. W. (2005). "Evaluation of the Witczak Dynamic Modulus Prediction Model." 84th Annual Meeting of the Transportation Research Board, Paper No. 05-2112, Ishington D.C.

Tran, N.H., and Hall, K.D. (2005). "Evaluating the Predictive Equation in Determining Dynamic Moduli of Typical Asphalt Mixtures Used in Arkansas." Pre-Print of the Journal of the Association of Asphalt Paving Technologists, Volume 74, 2005.

Mohammad, L.N., Wu, Z., Myers, L., Cooper, S., and Abadie, C. (2005). "A Practical Look at Simple Performance Tests: Louisiana's Experience." Journal of the Association of Asphalt Paving Technologists, Volume 74, 2005 (in press).

Dongré, R., Myers, L., D'Angelo, J., Paugh, C., and Gudimettla, J. (2004). "Field Evaluation of Witczak and Hirsch Models for Predicting Dynamic Modulus of Hot-Mix Asphalt." Pre-Print of the Journal of the Association of Asphalt Paving Technologists, Volume 74, 2005.

Montgomery, D. C. (2001). " Design and Analysis of Experiments." John Wiley and Sons, Inc. New York.

Table 5.1: Average Percent Difference between Witczak predicted and tested E* data

| Temperature (ºC) | SP-III With PG 64-22 (lab mix) | SP-II With PG-70-22 (lab mix) | SP-III With PG-70-22 (plant mix) | SP-II With PG-64-22 (plant mix) | SP-III With PG-70-22 (plant mix) |
|---|---|---|---|---|---|
| -10 | -14% | 3% | -25% | -14% | -16% |
| 4 | -28% | 1% | -38% | -28% | -20% |
| 21 | -49% | -24% | -54% | -49% | -9% |
| 37 | -59% | -37% | -61% | -59% | 17% |
| 54 | -61% | -45% | -62% | -61% | 27% |

Table 5.2: DSR test Results for PG 64-22 and PG 70-22

| Binder | Temp. (°C) | Complex Modulus, \|G*\| (Kpa) | | | Phase Angle ,δ (Deg) | | | Avg. \|G*\| | Avg. δ |
|---|---|---|---|---|---|---|---|---|---|
| | | Test-1 | Test-2 | Test-3 | Test1 | Test2 | Test3 | (Kpa) | (Deg) |
| PG 64-22 | 4.4 | 12100 | 12100 | 12000 | 56.5 | 56.5 | 56 | 12066.7 | 56.3 |
| | 12.8 | 5380 | 5020 | 5230 | 58.8 | 59.7 | 58.5 | 5210.0 | 59.0 |
| | 21.1 | 1800 | 1760 | 1820 | 61.6 | 62.2 | 61.3 | 1793.3 | 61.7 |
| | 29.4 | 547 | 541 | 571 | 64.8 | 65.3 | 64.3 | 553.0 | 64.8 |
| | 37.8 | 155 | 150 | 165 | 68.8 | 69.4 | 68.3 | 156.7 | 68.8 |
| | 46.1 | 43.9 | 41.9 | 46.9 | 73.5 | 74.1 | 73.2 | 44.2 | 73.6 |
| | 54.4 | 13.1 | 12.3 | 14.2 | 78.9 | 78.9 | 78.3 | 13.2 | 78.7 |
| PG 70-22 | 4.4 | 9430 | 8840 | 9140 | 57.7 | 58.2 | 57.6 | 9136.7 | 57.8 |
| | 12.8 | 3050 | 2970 | 3050 | 60.2 | 60.4 | 60 | 3023.3 | 60.2 |
| | 21.1 | 939 | 910 | 962 | 62.2 | 62.3 | 61.9 | 937.0 | 62.1 |
| | 29.4 | 276 | 266 | 281 | 63.8 | 63.9 | 63.5 | 274.3 | 63.7 |
| | 37.8 | 81.2 | 78.7 | 84.3 | 65 | 65.1 | 64.8 | 81.4 | 65.0 |
| | 46.1 | 26.6 | 25.8 | 27.5 | 65.9 | 66 | 65.8 | 26.6 | 65.9 |
| | 54.4 | 9.98 | 9.67 | 10.3 | 67.1 | 67.2 | 67.1 | 10.0 | 67.1 |

Table 5.3: Original and Optimized Mix Variables for MEPDG Level-3 Analysis

| Mix Type | Mix Variables | LAB Original | LEVEL-3 Optimized Values |
|---|---|---|---|
| SP-II | VA (%) | 5.5 | 0.00026036 |
| | Vbeff (%) | 8.78 | 0.00402348 |
| | P34 (%) | 6 | 0 |
| | P38 (%) | 33 | 0 |
| | P4 (%) | 66 | 0 |
| | P200 (%) | 3.4 | 4.2263935 |
| SP-III | VA (%) | 5.5 | 0.0001 |
| | Vbeff (%) | 9.42 | 0.00047256 |
| | P34 (%) | 15 | 0 |
| | P38 (%) | 40 | 0 |
| | P4 (%) | 64 | 0 |
| | P200 (%) | 3.4 | 4.82795556 |
| SP-IV | VA (%) | 5.5 | 18.8964269 |
| | Vbeff (%) | 10.02 | 0 |
| | P34 (%) | 0 | 0 |
| | P38 (%) | 10 | 0 |
| | P4 (%) | 45 | 0 |
| | P200 (%) | 5.7 | 8.29808601 |

Table 5.4: Goodness of Fit of the Modified $\eta$-based Model

| Model | New Modified Model | | $\eta$-based Witczak model | |
|---|---|---|---|---|
| parameter | Logarithmic Scale | Arithmetic Scale | Logarithmic Scale | Arithmetic Scale |
| Data points | 7400 | 7400 | 7400 | 7400 |
| No. of Mixes | 346 | 346 | 346 | 346 |
| $S_e$ | 0.22 | 7.20 | 0.36 | 10.07 |
| $S_y$ | 0.66 | 14.59 | 0.66 | 14.59 |
| $S_e/S_y$ | 0.33 | 0.49 | 0.54 | 0.69 |
| $R^2$ | 0.89 | 0.76 | 0.71 | 0.52 |

Table 5.5: Average Percent Difference between Witczak predicted and tested E* data

| Temperature (ºC) | SP-III PG-64-22 (lab mix) | | SP-II PG-70-22 (lab mix) | | SP-III PG-70-22 (plant mix) | | SP-II PG-64-22 (plant mix) | |
|---|---|---|---|---|---|---|---|---|
| -10 | 7% | (+7%) | -11% | (-8%) | -3% | (22%) | -9% | (5%) |
| 4 | 32% | (-5%) | 1% | (0%) | 15% | (23%) | 1% | (27%) |
| 21 | 30% | (19%) | -11% | (13%) | 20% | (34%) | -7% | (42%) |
| 37 | 21% | (38%) | -20% | (17%) | 21% | (40%) | -16% | (43%) |
| 54 | 6% | (55%) | -22% | (23%) | 10% | (52%) | -19% | (42%) |

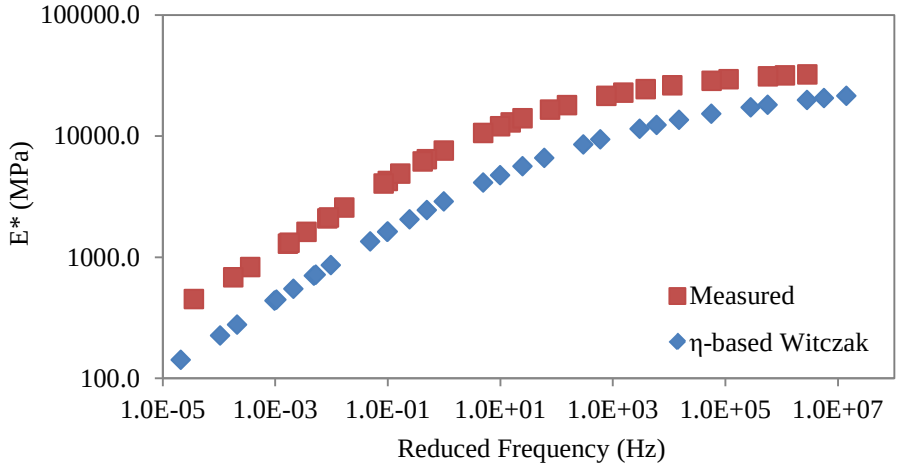


(a) SP-II plant

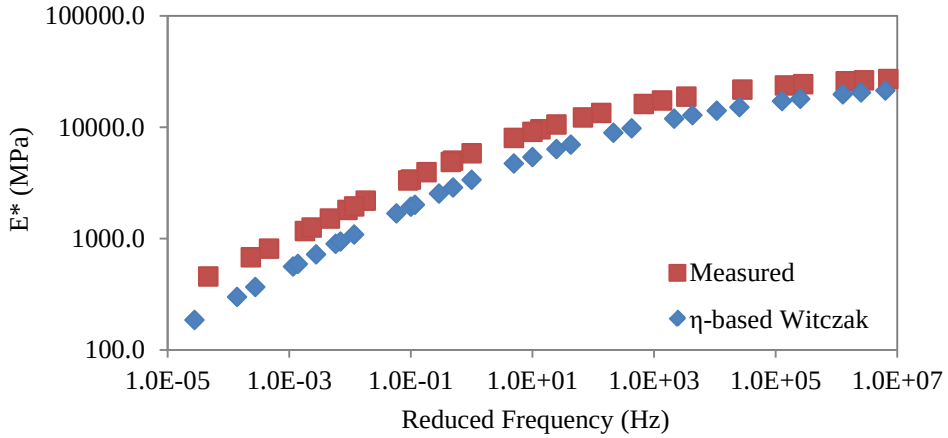


(b) SP-II Lab

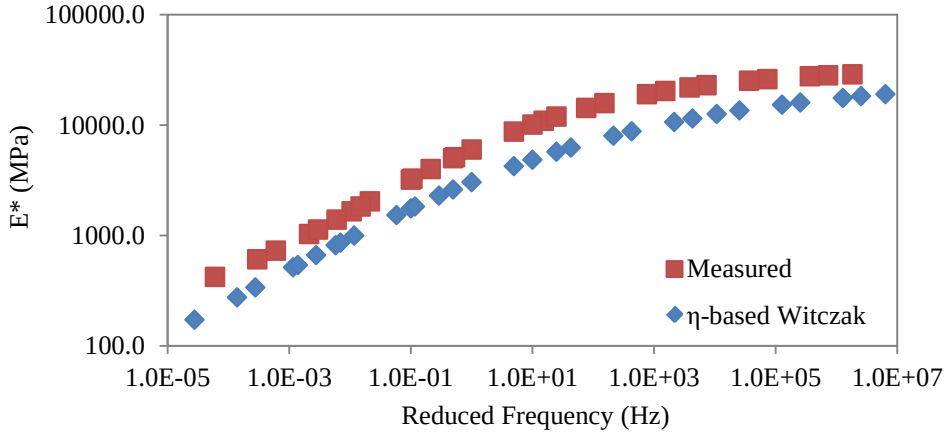


(c) SP-III plant

Figure 5.1(a-e): $\boldsymbol{\eta}$-based Witczak model predicted vs. Laboratory Measured $|\boldsymbol{E}^*|$

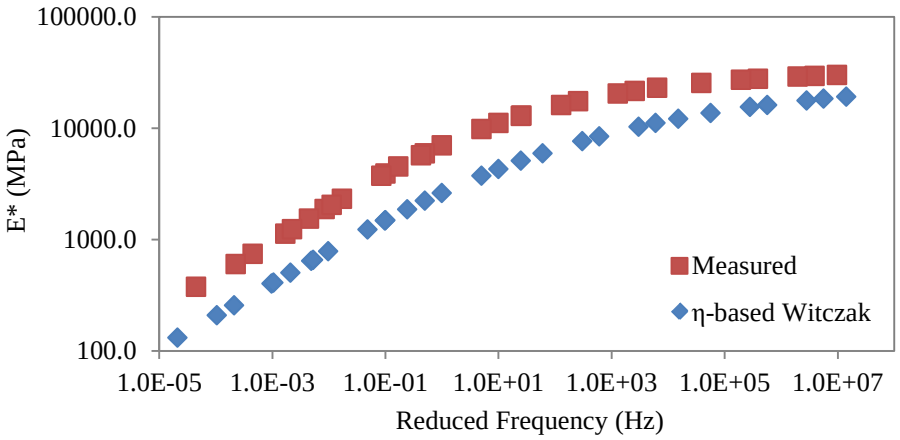


(d) SP-III lab

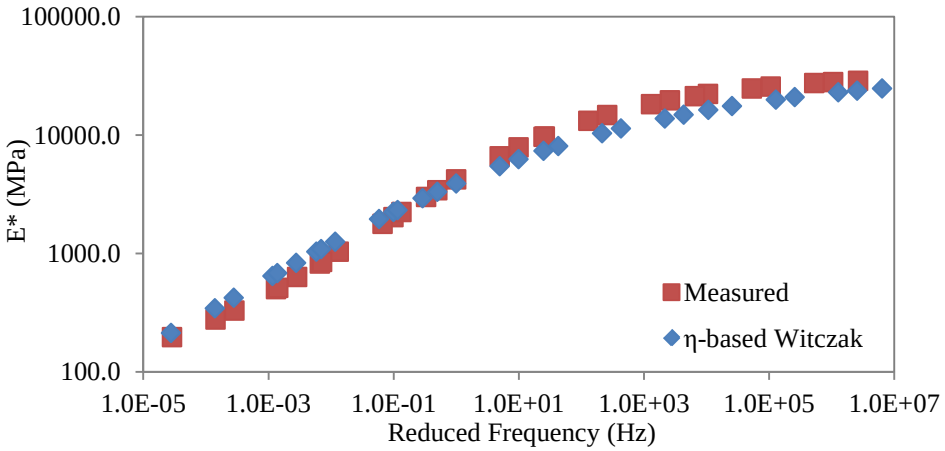


(e) SP-IV plant

Figure 5.1(a-e): $\boldsymbol{\eta}$-based Witczak model predicted vs. Laboratory Measured $|\boldsymbol{E}^*|$

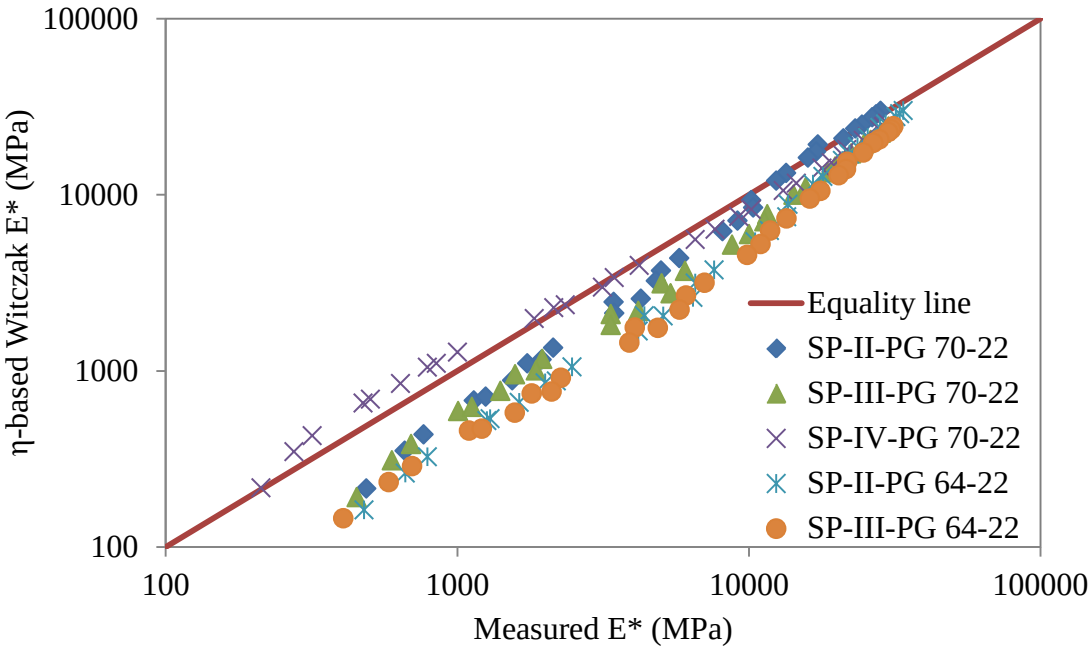


Figure 5.2: Scatter Plot for $\eta$-Based Witczak Model Predicted Vs. Laboratory Measured $|E^*|$ Data

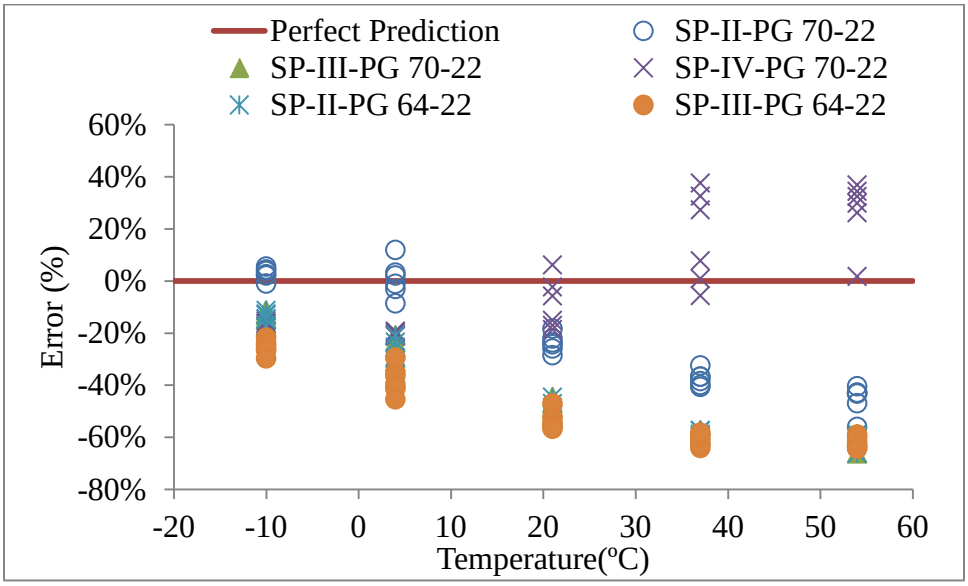


(a) Prediction error trend with temperature

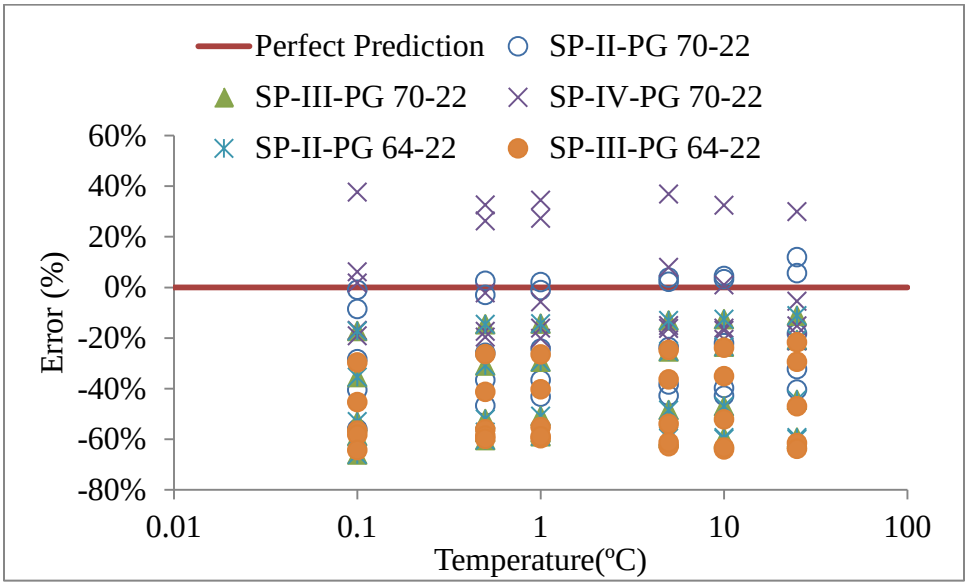


(b) Prediction error trend with frequency

Figure 5.3: Trend of Prediction % Error For $\eta$-Based Witczak Model

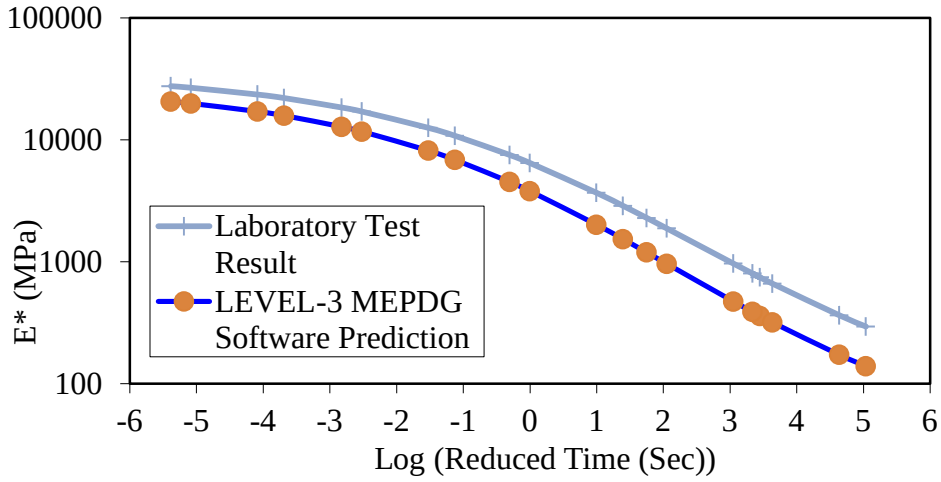


(a) SP-III mix

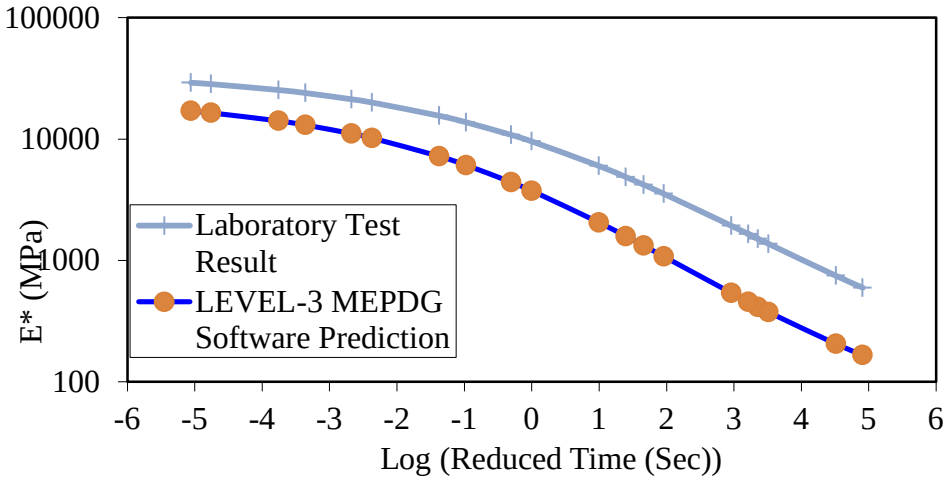


(b) SP-II mix

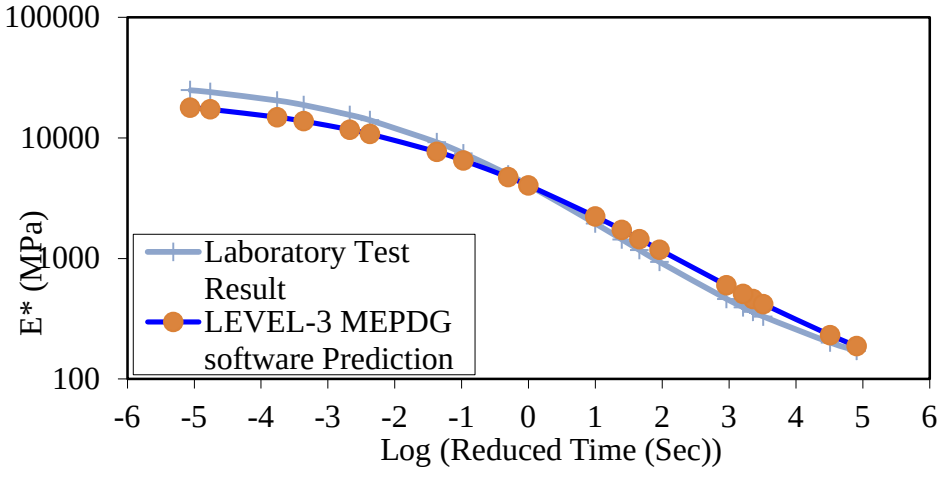


(c) SP-IV mix

Figure 5.4: MEPDG Level-3 Mastercurve Prediction vs. Mastercurve Developed for Laboratory $|E^*|$ Test Results

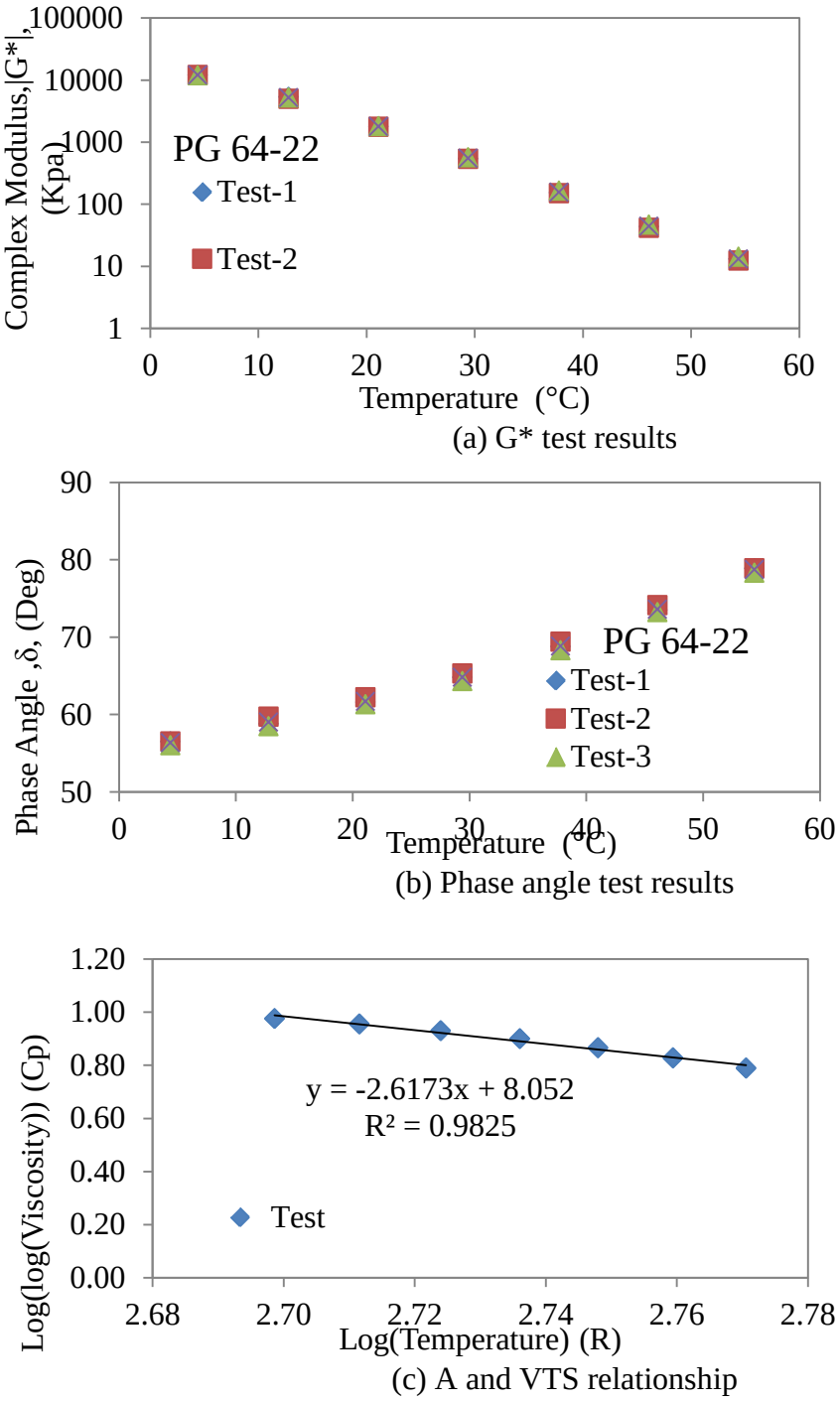


Figure 5.5: DSR Test Results and A and VTS Relationship for PG 64-22

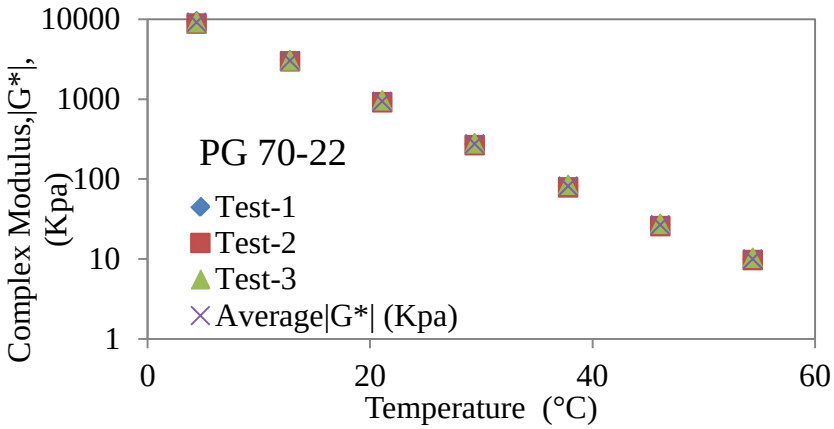


(a) G* test results

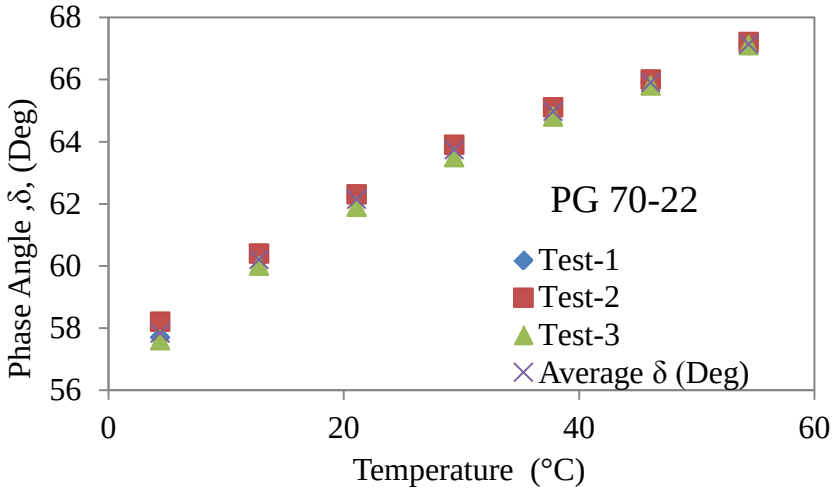


(b) Phase angle test results

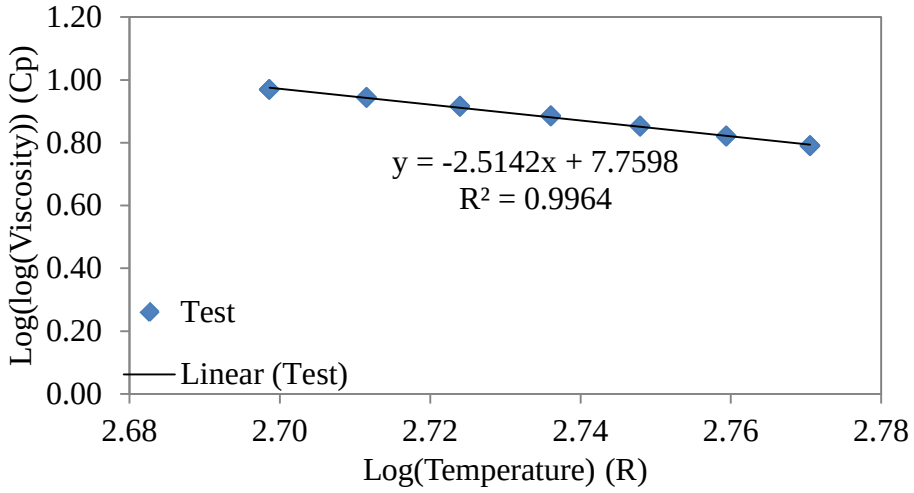


(c) A and VTS relationship

Figure 5.6: DSR Test Results and A and VTS Relationship for PG 70-22

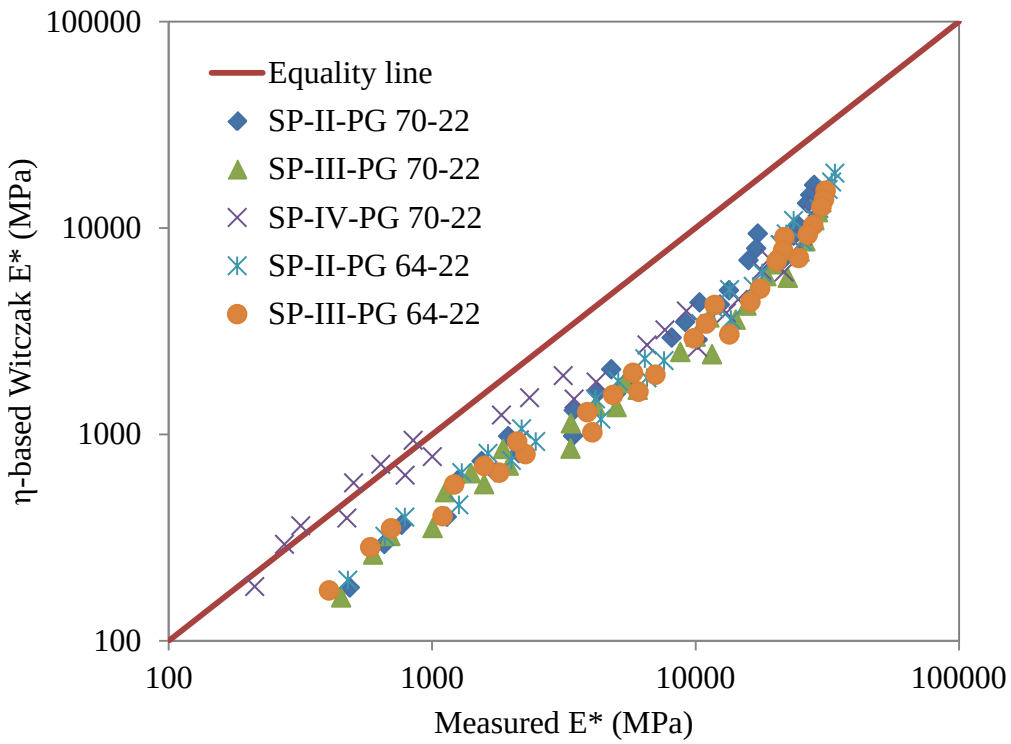


Figure 5.7: Scatter Plot for $\eta$-Based Witczak Model Prediction Using Actual *A* And *VTS* Developed Through Laboratory DSR Test

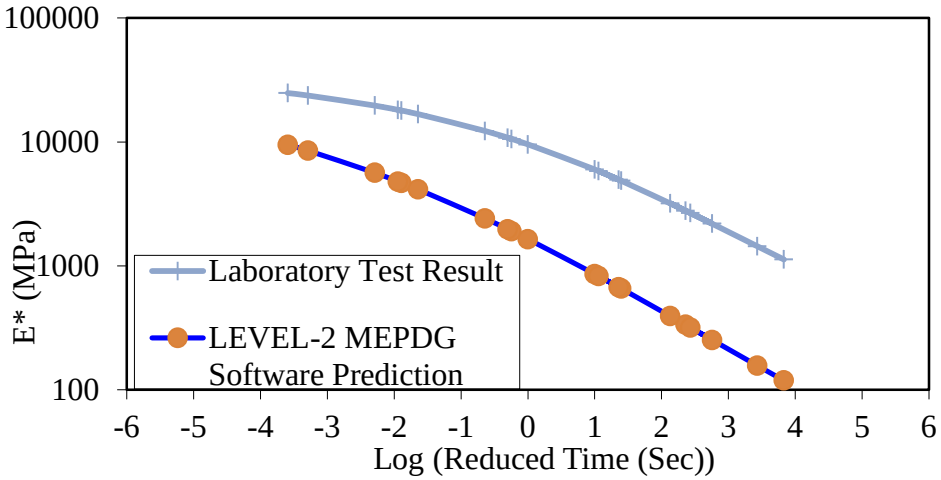


(a) SP-III Plant Mix

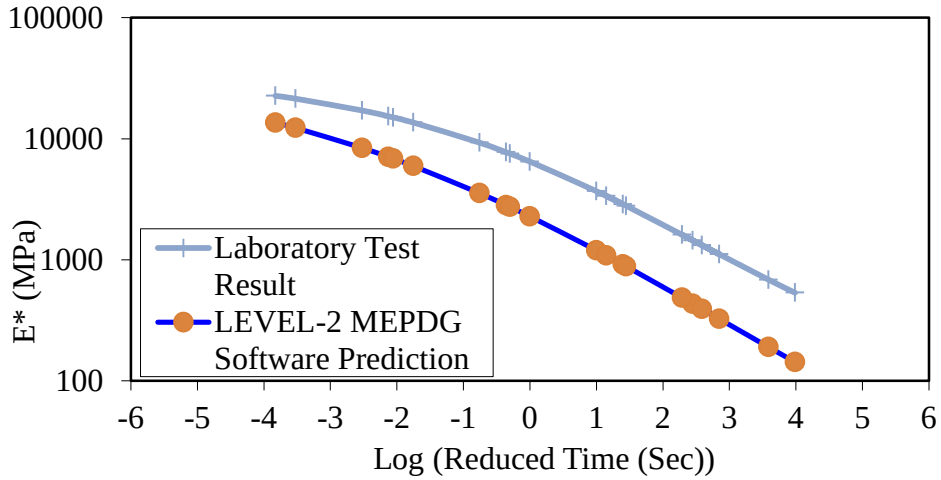


(b) SP-II Plant Mix

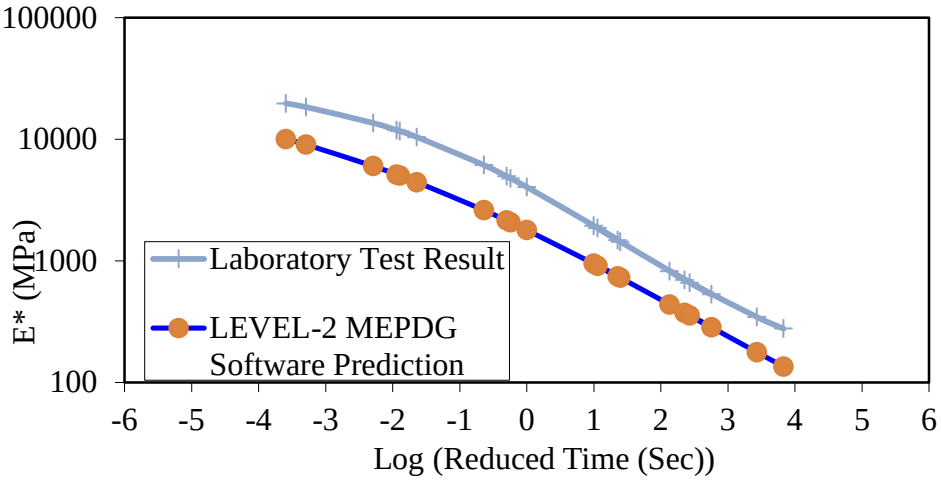


(c) SP-IV Plant Mix

Figure 5.8: MEPDG Level-2 Mastercurve Prediction vs. Mastercurve Developed for Laboratory $|E^*|$ Test Results

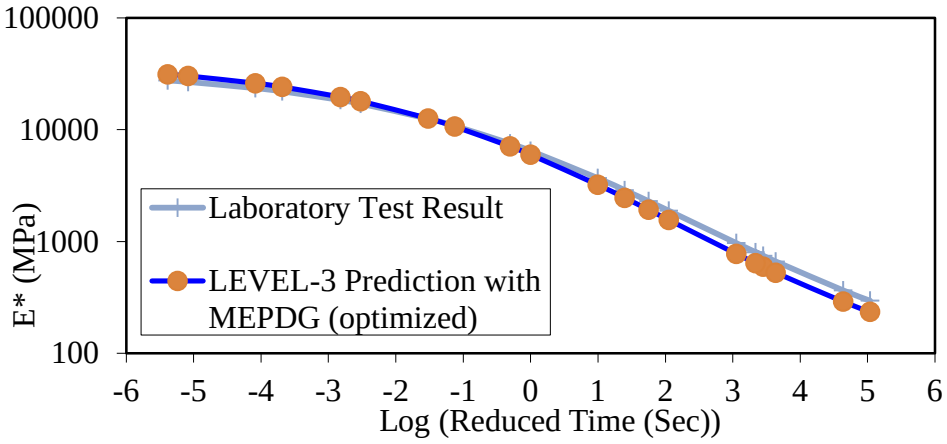


(a) SP-III Plant Mix

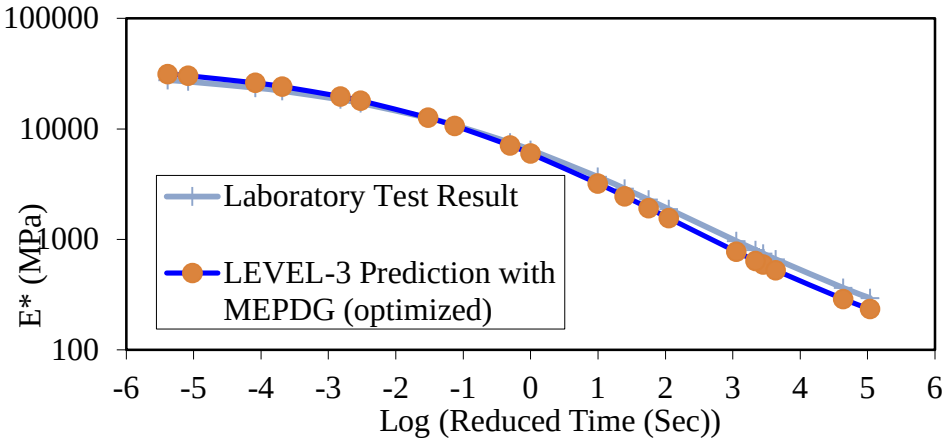


(b) SP-II Plant Mix

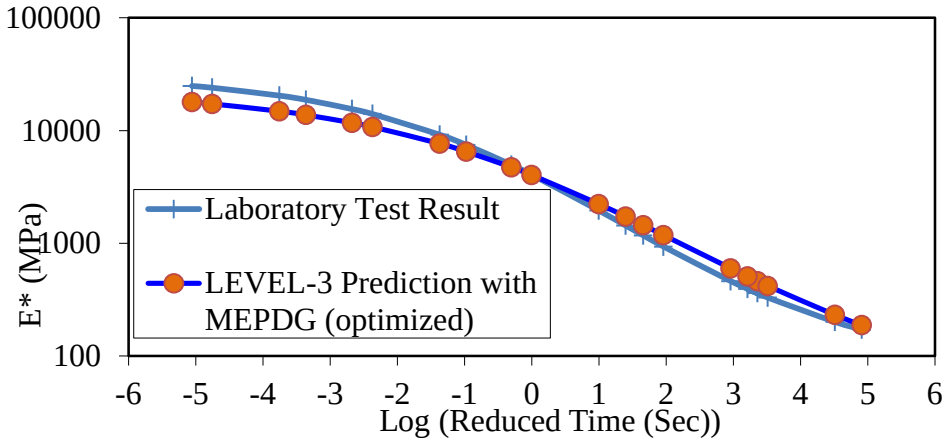


(c) SP-IV Plant Mix

Figure 5.9: MEPDG Level-3 Mastercurve Predictions Using Optimized Mix Data Vs. Mastercurve Developed for Laboratory $|E^*|$ Test Results.

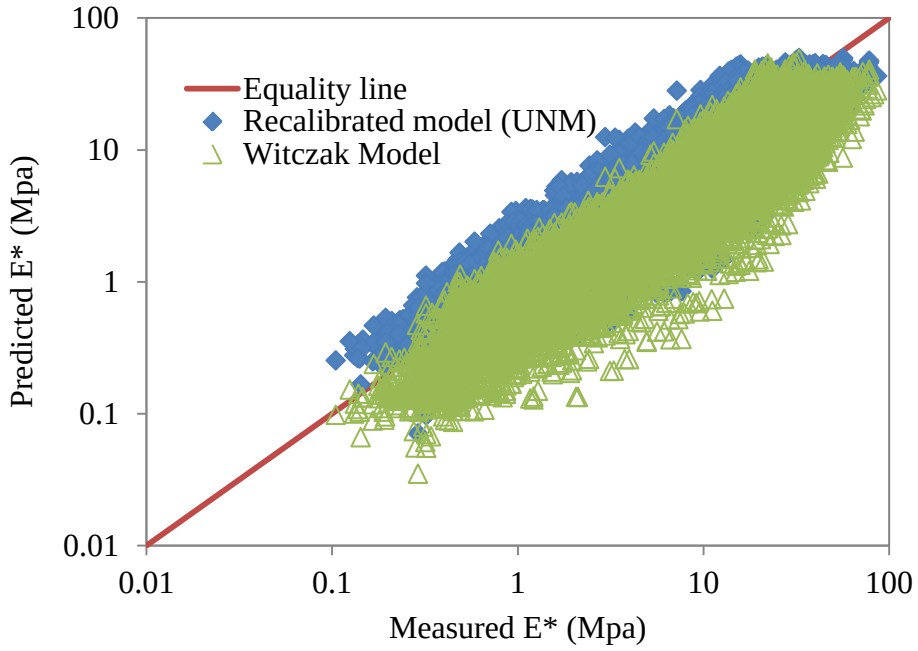


(a) Predicted Vs. Measured Scatter Plot (Logarithmic Scale)

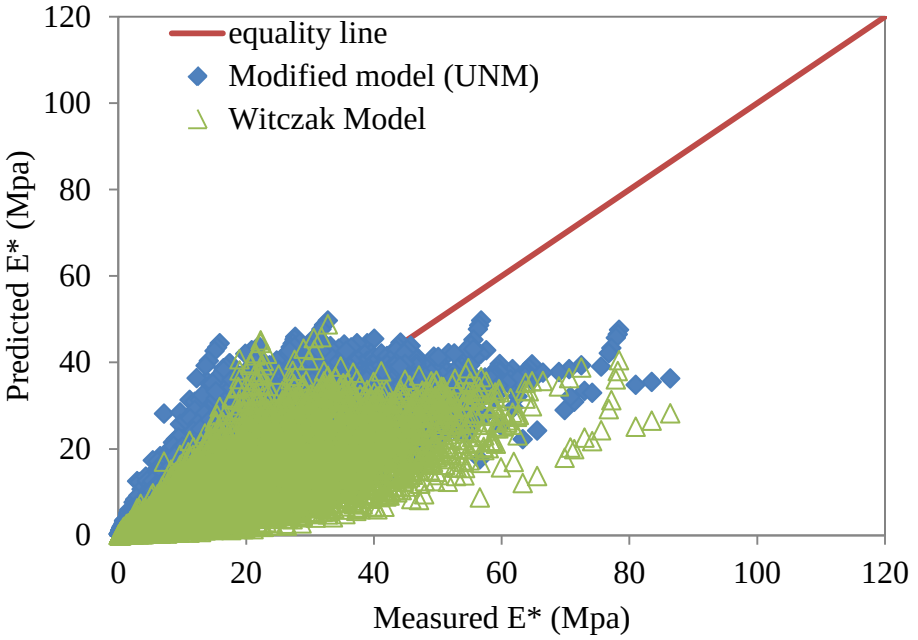


(b) Predicted Vs. Measured Scatter Plot (Arithmetic Scale)

Figure 5.10: Predicted Vs. Measured Scatter Plot

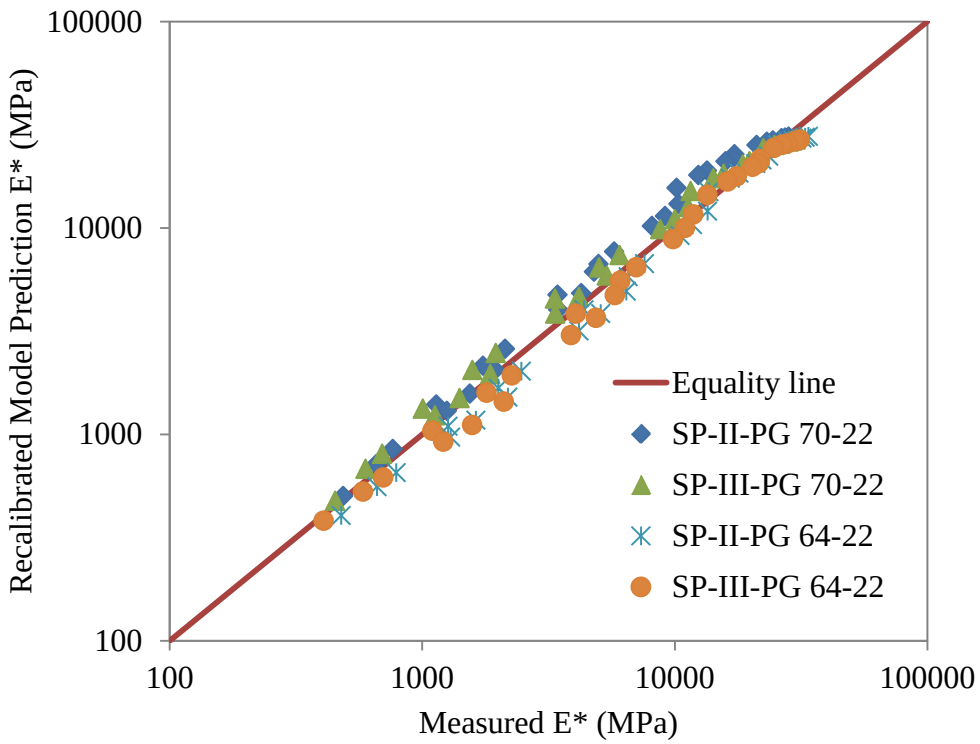


Figure 5.11: Scatter Plot for New Modified Model

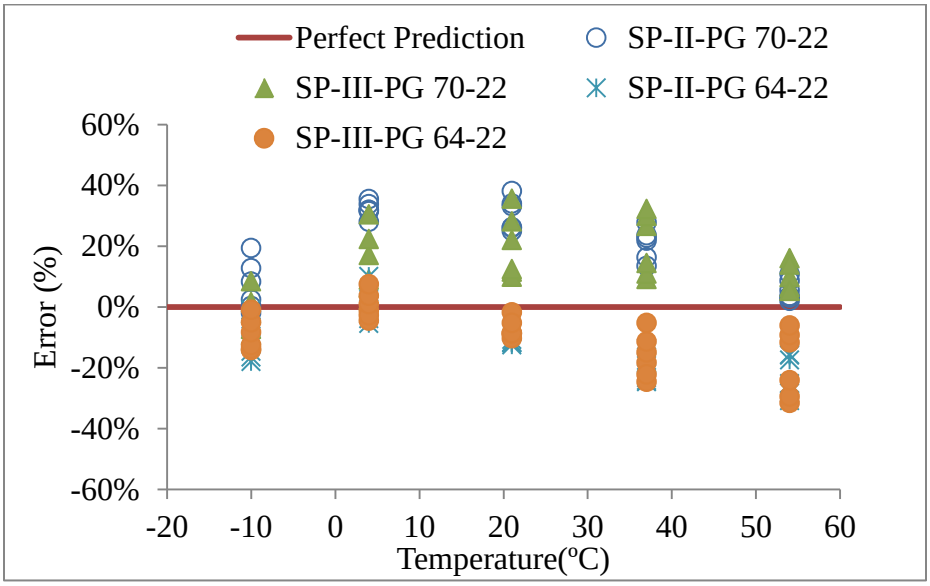


(a) Prediction Error Trend With Temperature

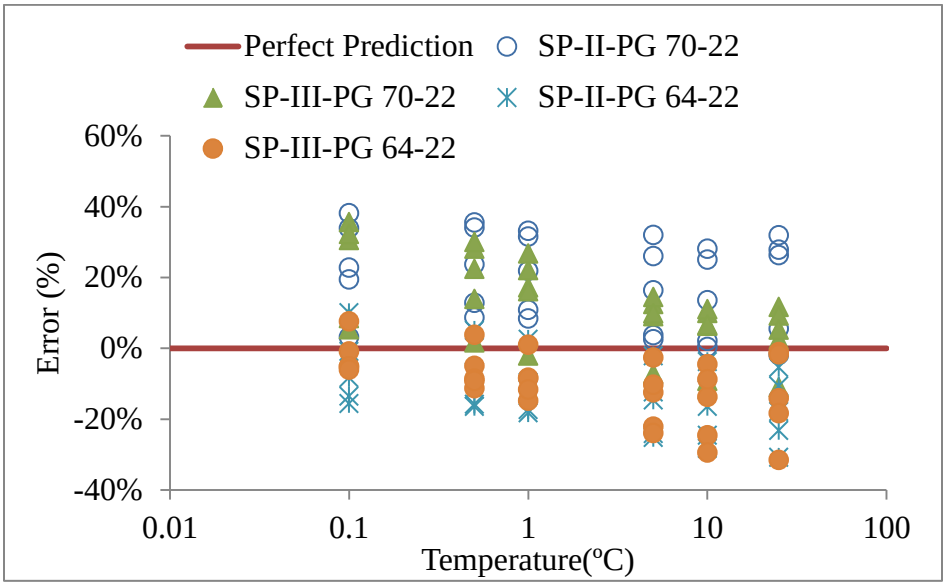


(b) Prediction Error Trend With Frequency

Figure 5.12: Trend of Prediction % Errors for New Modified Model

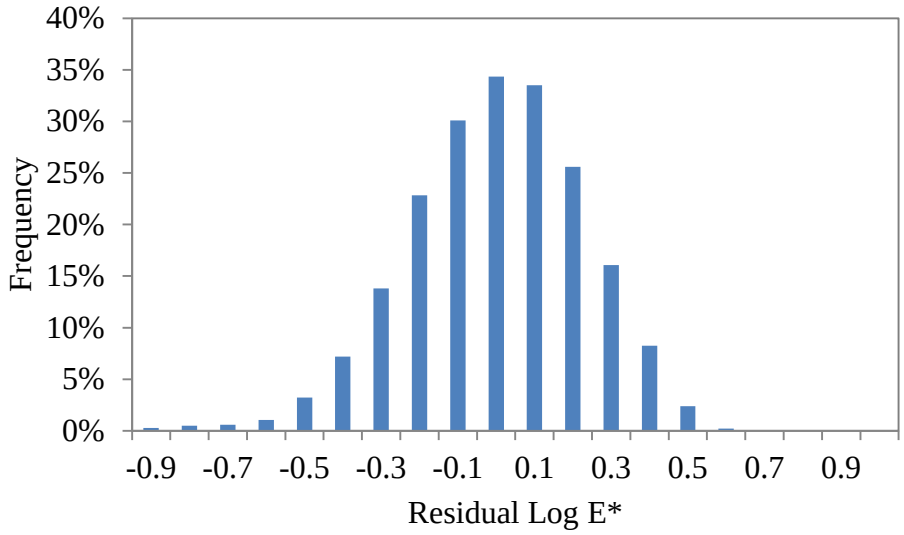


(a) Logarithmic Scale

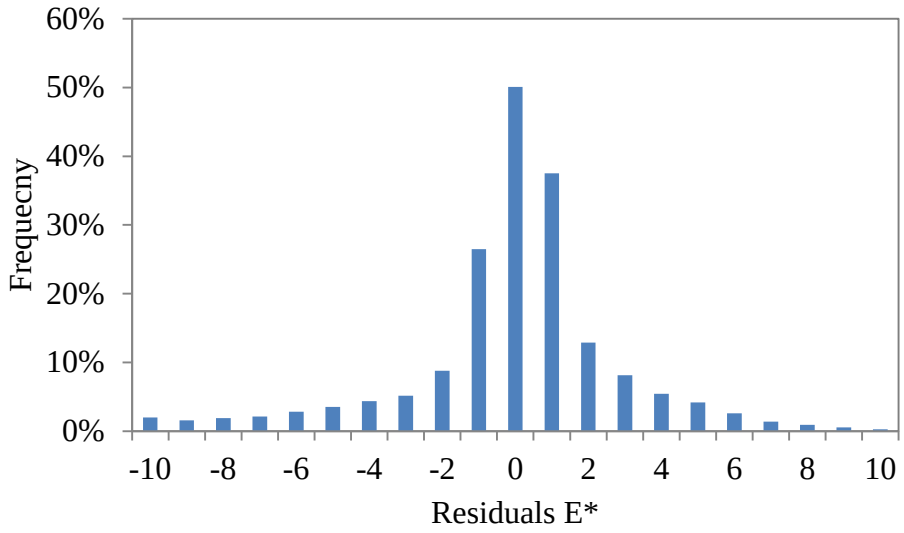


(b) Arithmetic Scale

Figure 5.13: Frequency Distribution of *E** Residuals

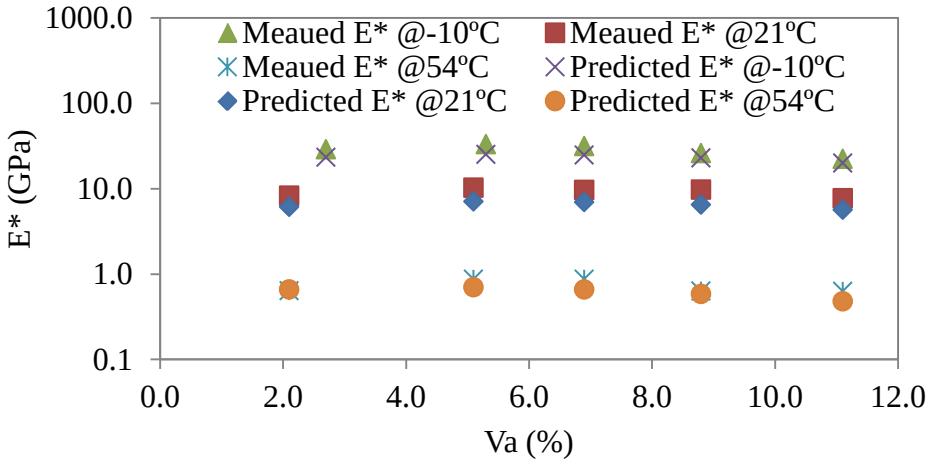


(a) Sensitivity to Mix Air Void

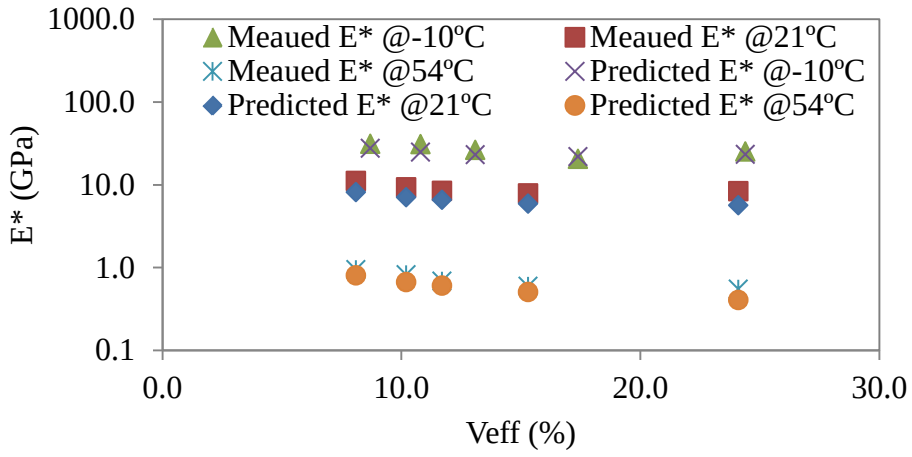


(b) Sensitivity to Mix Effective Binder Content

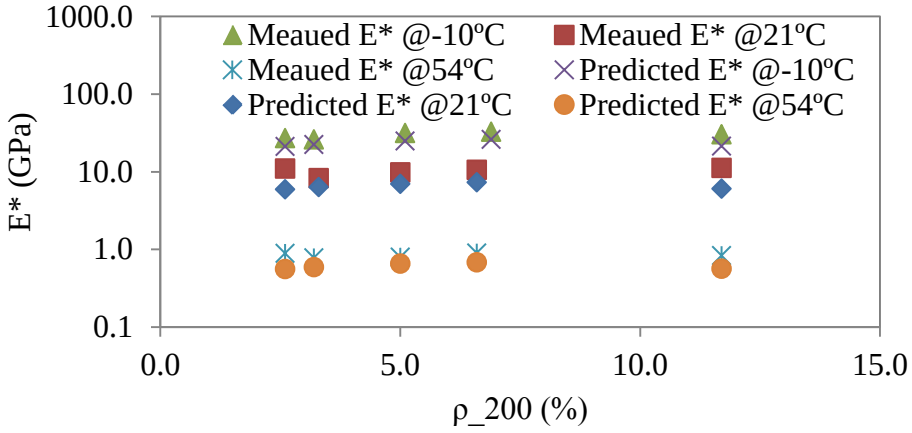


(c) Sensitivity to Percentage of Fines In The Mix

Figure 5.14: Sensitivity Analysis for the New Modified Model

# Chapter 6

# Dynamic Shear Modulus based Witczak Model Application to Typical NMDOT Mixes

## 6.1. Introduction

The dynamic shear modulus based Witczak model is the most advanced dynamic modulus prediction model in MEPDG. It is possible to utilize this model in the Level 2 and 3 design hierarchies of MEPDG. In this chapter the accuracy of dynamic shear modulus based Witczak model is investigated in predicting measured dynamic modulus values of typical New Mexico asphalt mixes.

## 6.2. Objectives

Specific objective is to:

- Apply dynamic shear modulus based Witczak model for predicting measured dynamic modulus values of typical New Mexico Mixes

## 6.3. Dynamic Shear Modulus Based Witczak Predictive Model

This model uses dynamic shear modulus test results as a parameter instead of viscosity. The model is also developed with larder database of dynamic modulus data. 7400 data points from 346 HMA mixtures are used to develop this revised version of the Witczak E* predictive model (Bari 2005).

$$log|E^*| = -0.349 + \tag{6.1}$$

$$\left\{0.754(|G_b^*|^{-0.0052}) * \begin{pmatrix} 6.65 - 0.032\rho_{200} + 0.0027(\rho_{200})^2 - 0.011\rho_4 \\ -0.0001(\rho_4)^2 + 0.006\rho_{38} - 0.00014(\rho_{38})^2 \\ -0.08V_a - 1.06\left(\frac{V_{beff}}{V_{beff}+V_a}\right) \end{pmatrix}\right\} +$$

$$\left\{\frac{2.558 + 0.032V_a + 0.713\left(\frac{V_{beff}}{V_{beff}+V_a}\right) + 0.0124\rho_{38} + 0.0001(\rho_{38})^2 + 0.00 - 0.0098\rho_{34}}{1 + e^{(-0.7814-0.5785\,log|G^*|_b-0.8834\,log(\delta_b))}}\right\}$$

where: $|E^*|$ is dynamic modulus, psi; $\rho_{200}$ is % (by weight of total aggregate) passing the 0.075-mm (No. 200) sieve; $\rho_4$ is cumulative % (by weight) retained on the 4.76-mm (No. 4) sieve; $\rho_{34}$ is cumulative % (by weight) retained on the 19-mm (3/4-in.) sieve; $\rho_{38}$

is cumulative % (by weight) retained on the 9.5-mm (3/8-in.) sieve; $V_a$ is air void content (by volume of the mix), %; $V_{beff}$ is effective binder content (by volume of the mix), %; $|G^*|_b$ is dynamic shear modulus of binder, psi; $\delta_b$ is phase angle of binder associated with $|G^*|_b$degree.

### 6.4. Analysis Method

It is possible to implement the dynamic shear modulus based Witczak model in three different ways

- By using the default A and VTS values provided in MEPDG (method implemented in Level 3 input hierarchy of MEPDG).
- By determining the $|G^*|_b$ and $\delta_b$ of binder through a temperature sweep test for a single frequency and determining the A and VTS relationship for the binder to be utilized for the model (method implemented in Level 2 input hierarchy of MEPDG).
- Conducting temperature and frequency weep $|G^*|_b$ testing and developing the mastercurve for G* and $\delta_b$ for the model prediction.

In this section of the report, all three methods are implemented and the accuracy of the prediction is evaluated. Afterwards, the possibility of using BBR data is investigated which is followed by the modification of the G* based model.

#### 6.4.1. Application of G* Based Model Using Default *A* and *VTS* Values Of MEPDG

In this section the viscosity ($G^*$) based Witczak model is implemented to predict dynamic modulus mastercurves developed for the five mixes tested in this study. The temperature susceptibility relationship, given in Eq. (5.2), is improved to consider loading frequency in addition to temperature (Bari, 2005). Specific viscosity values for each binder grade are determined for each test temperature and frequency combination which are in turn used to determine the dynamic shear modulus, $|G^*|_b$, and phase angle, $\delta_b$, of the binders. Eq. (6.5) and Eq. (6.6) are the relationships developed by Bari (2005) for predicting the dynamic shear modulus, $|G^*|_b$, and phase angle, $\delta_b$ from binder viscosity. The default A and VTS values given in MEPDG are to estimate the viscosity of each binder used. The default A and VTS values for PG 70-22 are 10.299 and -3.426 respectively and for PG 64-22 are A=10.98 and VTS=-3.68 (ARA, Inc. 2004).

$$\log\log \eta_{f,T} = A' + VTS' \log T_R \tag{6.2}$$

$$A' = 0.9699 f_s^{-0.0527} * A \tag{6.3}$$

$$VTS' = 0.9668 f_s^{-0.0575} * VTS \tag{6.4}$$

$$|G^*|_b = 0.0051 f_s \eta_{f,T} (\sin \delta_b)^{7.1542 - 0.4929 f_s + 0.0211 f_s^2} \tag{6.5}$$

$$\delta_b = 90 + (-7.3146 - 2.6162VTS') * \log(f_s * \eta_{f,T}) + (0.1124 + 0.2029VTS') * \log(f_s * \eta_{f,T})^2 \quad (6.6)$$

where: $\eta_{f,T}$ is viscosity as a function of both temperature and frequency (cP); $T_R$ is temperature (Rankine); A and VTS are regression intercept and regression slope of viscosity temperature susceptibility relationship; $A'$ and VTS$'$ are A and VTS values adjusted for frequency. $f_s$ is loading frequency in similar mode as for DSR testing (Hz); $|G^*|_b$ is dynamic shear modulus (Pa), $\delta_b$ phase angle (deg).

Figure 5.7 presents a scatter plot of raw $G^*$-based Witczak model $|E^*|$ prediction results in comparison with the measured $|E^*|$ data for all asphalt mixes (SP-III-PG-64-22 (lab mix), SP-II-PG-70-22 (lab mix), SP-III-PG-70-22 (plant mix), SP-II-PG-64-22 (plant mix) and SP-IV-PG-70-22(plant mix)) tested in this study. The result show that $G^*$-based Witczak model predicts the $|E^*|$ test results of SP-IV mix with better accuracy than the rest of mixes. For all asphalt mixes the predicted data is higher than measured $|E^*|$ at low temperatures and at high and intermediate temperatures measured $|E^*|$ are under predicted with the $G^*$-based Witczak model.

To quantitatively evaluate the accuracy of the $G^*$-based Witczak model the percent difference between predicted and tested data (the difference between the measured and predicted $|E^*|$ divided by the measured $|E^*|$) at each frequency and temperature are calculated. The average percent difference between predicted and tested data at each temperature is tabulated in Table 5.1. Moreover, the trend of calculated percent error with respect to temperature is presented in Figure 5.3 (a) and the trend with respect to frequency is presented in Figure 5.3 (b). Zero percent error for perfect prediction is shown in both figures. Positive sign of error indicates over prediction and negative sign indicates under prediction. The percent error of predicted $|E^*|$ at cold temperatures indicate significant over prediction. Minimum percent errors are observed at 21 ºC and as the temperature increases the percent errors go further below zero indicating under prediction of measured $|E^*|$ data. The trend of percent errors with respect to frequency, Figure 5.3 (b), shows a decrease in the range of percent error with increasing test frequency, which indicates an improvement in precision of predicted $|E^*|$ with increasing test frequency.

### 6.4.2. Application of G* Based Model Using Actual *A* and *VTS* Values of MEPDG

As mentioned in chapter five, Dynamic shear,$|G^*|$, test is conducted on three replicate samples of PG 70-22 and PG 64-22 at different seven temperatures (40, 55, 70, 85, 100, 115, 130 ºF) and 10 rsd/sec. The same test results and A and VTS calculations are utilized for $G^*$-based Witczak model in pave of the default values provided in MEPDG guide. The actual A and VTS values are determined to be 7.7598 and -2.5142 for PG 70-22 respectively and for PG 64-22 are A=8.052 and VTS=-2.6173.

A scatter plot of raw $G^*$-based Witczak model $|E^*|$ prediction results using actual A and VTS results in comparison with the measured $|E^*|$ data for all mixes is presented in Figure 6.3. The result show a significant improvement in the prediction accuracy of the $G^*$-based Witczak model, especially at cold temperatures, compared with the prediction using default A and VTS values. However, as the $|E^*|$ value decreases the $G^*$-based Witczak model is still under predicting measured $|E^*|$ of all five asphalt mixes. The average percent difference between predicted and tested data at each temperature is tabulated in Table 6.2. Comparing the results in Table 6.2 with those in Table 5.1, clearly shows the improvement in prediction accuracy of the $G^*$-based Witczak model at cold temperatures. However, at intermediate and high temperatures the prediction accuracy the $G^*$-based Witczak model does not show any improvement due to the use of actual A and VTS values and it still underpredicts the measured $|E^*|$.

Figure 6.4 (a) presents the trend of calculated percent error with respect to temperature. It can be observed that the percent error of predicted $|E^*|$ at -10 ºC is positive which indicate over prediction. Moreover, the range of percent prediction is very wide which indicates luck of precision. As the temperature increases, however, the range of percent error decreases indication an improvement in the prediction precision. Yet, even if there is an increase in precision, the model is significantly underpredicting measured $|E^*|$ at high and intermediate temperatures.

The trend with respect to frequency is presented in Figure 6.4 (b). Most of the percent errors are below the zero percent error for perfect prediction, which clearly shows the under perceive tendency of the model. However, similar to the results observed by using default A and VTS values, the range of percent error is found to decrease with increasing test frequency, which indicates an improvement in precision of predicted $|E^*|$ with increasing test frequency.

### 6.4.3. Application of G*-based model by using $|G^*|$ and δ Mastercurves

In this section dynamic shear modulus, $|G^*|$, and phase angle, $\delta$, mastercurves are to generate $|G^*|_b$ and $\delta_b$ inputs for the $G^*$-based Witczak model. Frequency sweep tests of dynamic shear modulus over a wide temperature and frequency range are conducted for developing dynamic shear modulus mastercurves. $G^*$- Mastercurves characterize binder rheological properties over a wide range of frequencies at a specific reduced temperature. This makes $G^*$- mastercurves very attractive to estimate binder G* and Φ values at any temperature and frequency point of interest. Therefore, in this study, $G^*$ and $\delta$ – mastercurves are developed at the same reference temperature at which $|E^*|$ - mastercurves are developed and $|G^*|_b$ and $\delta_b$ values corresponding to the reduced frequency of mix dynamic modulus are determined.

DSR test is conducted to determine dynamic shear modulus, $|G^*|$, and phase angle, $\delta$, for the two types of binders used in the asphalt mixes in this study. DSR test is conducted at seven test temperatures and 15 frequencies for each temperature. The seven testing temperatures are 130, 115, 100, 85, 70, 55, and 50°F. Two different sample sizes are used

for conducting these tests. 25mm diameter samples are tested at 130 and 115 °F. However, torsion force required to maintain a measurable strain level of a 25mm sample at lower temperatures exceeds the machine capacity. Therefore, the 8mm diameter sample size is used to conduct DSR testing 100, 85, 70, 55 and 50°F.

The DSR test is conducted in a stain controlled fashion. That is shear stress is measured while applying a preselected strain level. Appropriate strain level is selected to produce measureable strain amount according to the DSR compliance while taking in to consideration the maximum stress that can be applied by the machine. Therefore, the testing strain level is selected in such a way that it is large enough to be measured by the equipment and small enough so that the stress capacity of the machine is not exceeded. The applied stein level for the 8mm and 25mm sample is 1.0%.

DSR Test data of dynamic shear modulus, $|G^*|$, and phase angle, $\delta$, is provided in Appendix G. The mastercurve for the DSR test results is developed using the time temperature superposition principle. The Modified Sigmoidal Model is found to be the best function for fitting the shifted $G^*$- data to a mastercurve (Yusoff et al, 2010). The modified sigmoidal function is given in Eq. (6.7). Mastercurves for phase angle are also developed using the parameters determined for the |G*| mastercurves. Eq. (6.8) provides the mathematical relationship used for phase angle mastercurves (Chailleux et al. 2006). Figure 6.5 and Figure 6.6 present the $G^*$and $\delta$ – mastercurves developed for both binder grades, PG 64-22 and PG 70-22, used in this study. The mastercurve parameters for both binders are also given in Table 6.3.

$$\log(|G^*|) = \delta + \frac{\max - \delta}{1 + e^{\beta + \gamma \log(f_r)}} \tag{6.7}$$

$$\varphi = \frac{\pi}{2} * \frac{d log|G^*|}{d\, log(f_r)} = \frac{\pi}{2} * \alpha\gamma * \frac{e^{\beta+\gamma\, log(f_r)}}{(1 + e^{\beta+\gamma\, log(f_r)})^2} \tag{6.8}$$

where G* = dynamic modulus; $\delta$ = the minimum value of E*; max= the maximum value of $G^*$ which is taken as 1.0Gpa; $\beta$ and $\gamma$ are parameters that describe the shape of the sigmoidal function, $f_r$ is reduced frequency of loading at a reference temperature.

Figure 6.7 (a) is a scatter plot for $G^*$-based Witczak model prediction using G* and Phase angle mastercurves for SP-II, SP-III and SP-IV mixes. In all cases $G^*$-based Witczak model is found to under predict measured dynamic modulus here as well. Figure 6.7 (b) presents the percent difference between the predicted and test data over the entire reduced frequency range. The percent difference between predicted and measured dynamic modulus for all mixtures is found to be very close to 80% over the entire reduced frequency range. Applying 80% shift factor on the Witczak predicted results produced a good estimation of test results.

### 6.5. Conclusions

In this study the $G^*$-based Witczak model is implemented to predict measured dynamic modulus values for typical NMDOT mixes. Predictions are performed using MEPDG default binder properties and actual binder test data to simulate MEPDG software predictions at level 3 and Level 2 input hierarchy. Based on this study the following conclusions are drawn:

- The use of $G^*$-based Witczak model with MEPDG default binder properties indicated that the model underpredicts the dynamic modulus of NMDOT mixes
- $G^*$-based Witczak model application to using laboratory determined binder properties have shown improvement in the prediction accuracy, however, the model is found to underpredict measured dynamic modulus of NMDOT mixes in this case as well.
- $G^*$-based Witczak model is also implemented using $G^*$ and $\delta$ – mastercurves developed for binders used in the production of NMDOT mixes. This method completely replaced the use of A and VTS relationship with binder $G^*$ – mastercurves. The results however still underpredict measured dynamic modulus of typical NMDOT mixes.

### 6.6. References

ARA, Inc., ERES Consultants Division (2004). "Guide for Mechanistic-Empirical Design of New & Rehabilitated Pavement structures (Final Report)". NCHRP Project 1-37A, <http://onlinepubs.trb.org/onlinepubs/archive/mepdg/guide.htm> (July 19, 2013).

Bari, J. (2005). "Development of a New Revised Version of the Witczak E* Predictive Models for Hot Mix Asphalt Mixtures." Ph.D. Dissertation, Arizona State University, Phoenix, AZ.

Chailleux, E., Ramond, G.,Roche, C. D. L. (2006), "A mathematical-based master-curve construction method applied to complex modulus of bituminous materials." Road Materials and Pavement Design, EATA, pages 75-92.

Table 6.1: Average Percent Difference between Witczak Predicted and Measured E* Data Using Default *A* and *VTS* Values

| Temperature (ºC) | SP-III-PG-64-22 (lab mix) | SP-II-PG-70-22 (lab mix) | SP-III-PG-70-22 (plant mix) | SP-II-PG-64-22 (plant mix) | SP-III-PG-70-22 (plant mix) |
|---|---|---|---|---|---|
| -10 | 113% | 76% | 133% | 117% | 74% |
| 4 | 98% | 30% | 94% | 54% | 57% |
| 21 | -24% | -55% | -21% | -46% | -13% |
| 37 | -57% | -73% | -53% | -69% | -25% |
| 54 | -57% | -66% | -51% | -61% | -4% |

Table 6.2: Average Percent Difference between Witczak predicted and Tested *E** Data Using Actual *A* and *VTS* Values

| Temperature (ºC) | SP-III-PG-64-22 (lab mix) | SP-II-PG-70-22 (lab mix) | SP-III-PG-70-22 (plant mix) | SP-II-PG-64-22 (plant mix) | SP-III-PG-70-22 (plant mix) |
|---|---|---|---|---|---|
| -10 | 2% | 4% | 10% | 26% | -15% |
| 4 | -38% | -41% | -41% | -31% | -50% |
| 21 | -66% | -69% | -65% | -63% | -59% |
| 37 | -68% | -70% | -64% | -65% | -40% |
| 54 | -56% | -56% | -50% | -49% | -3% |

Table 6.3: Mastercurve Parameters for Binders (Ref. Temp = 21 ºc)

| Asphalt mix | Master curve parameters | | | |
|---|---|---|---|---|
| | $max$ | β | δ | γ |
| PG 70-22 | 9 | -1.27 | -1.27 | -1.27 |
| PG 64-22 | 9 | -0.73 | -0.26 | -0.32 |

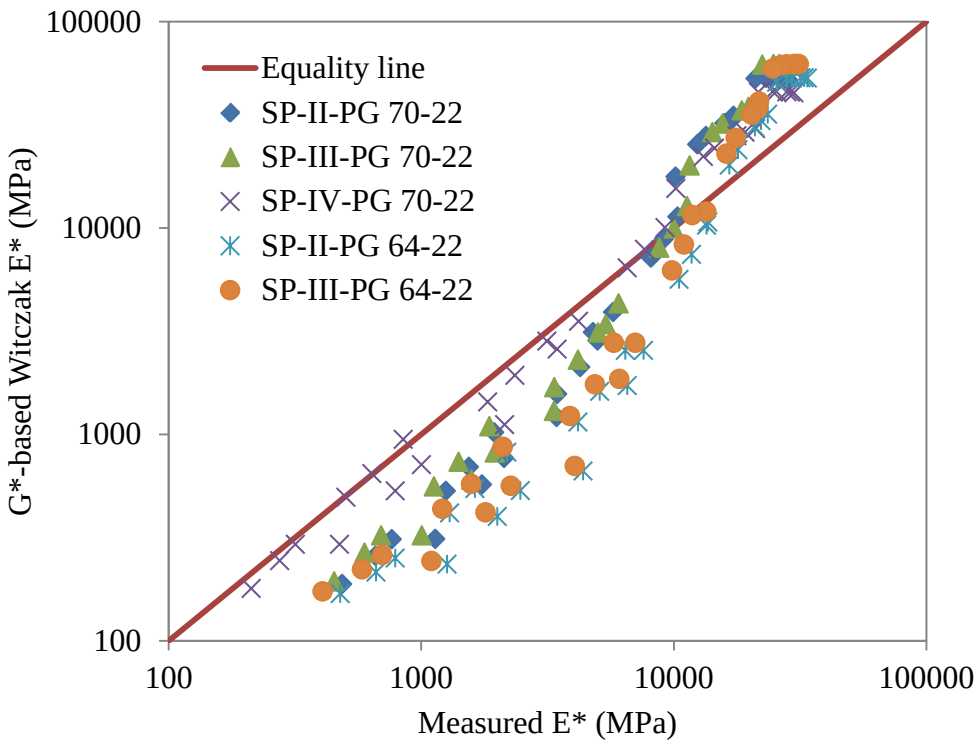


Figure 6.1: Scatter Plot for **G**$^*$-Based Witczak Model Prediction Using Default *A* and *VTS* Values From MEPDG.

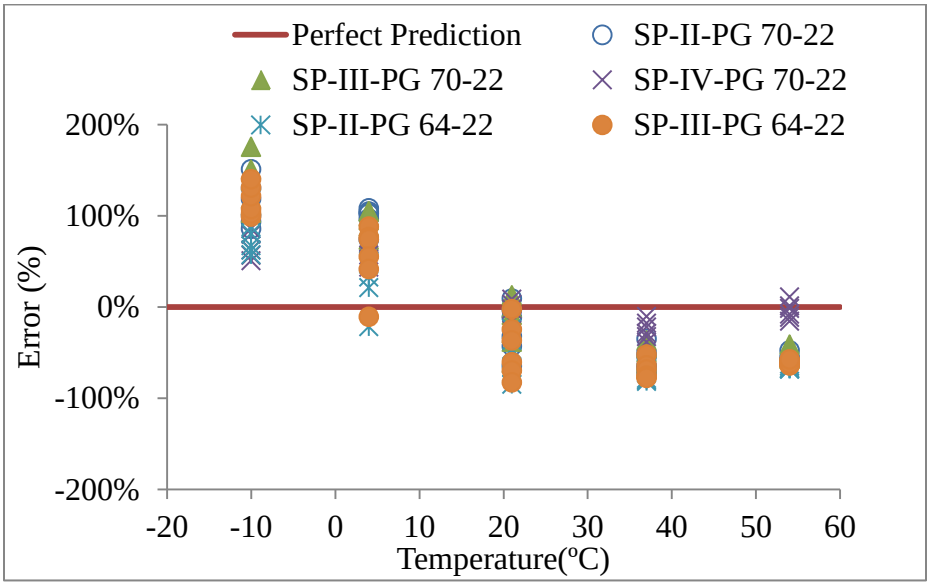


(a) Prediction error trend with temperature

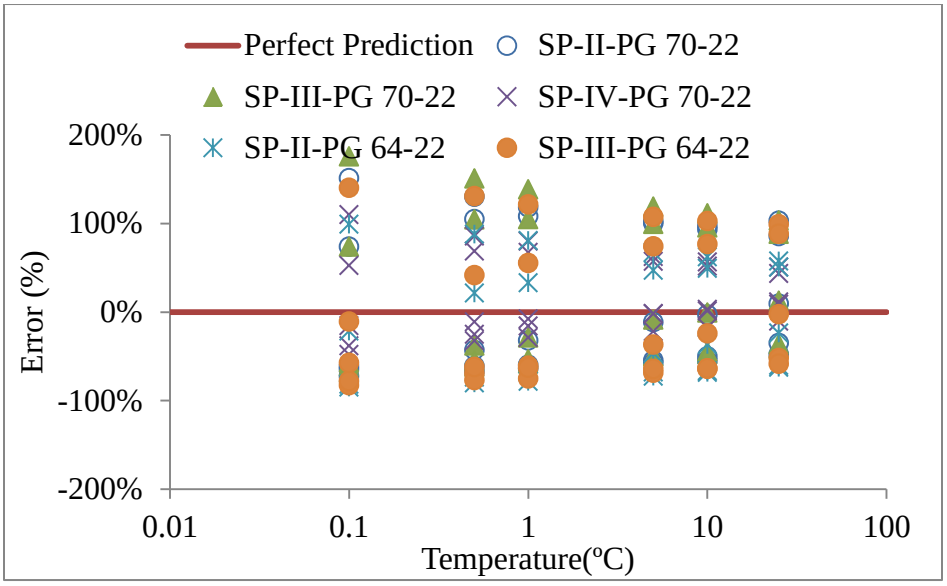


(b) Prediction error trend with frequency

Figure 6.2: Trend of Prediction % error for $G^*$-based Witczak model using default A and VTS values from MEPDG.

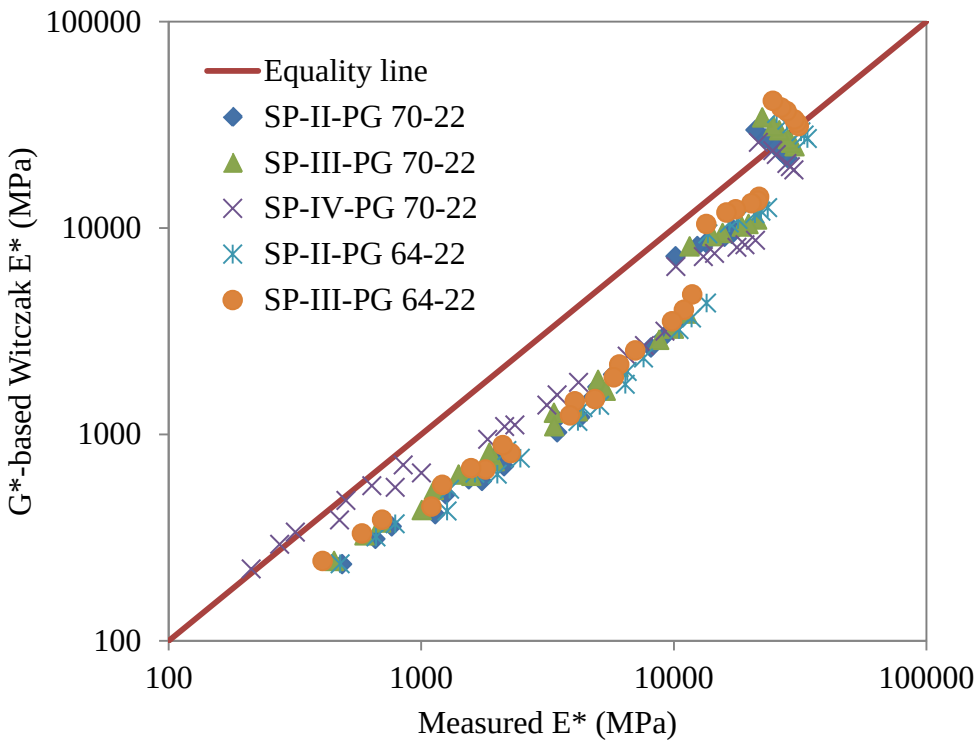


Figure 6.3: Scatter Plot For $G^*$-Based Witczak Model Prediction Using Actual *A* and *VTS* Values Determined From Laboratory DSR Test.

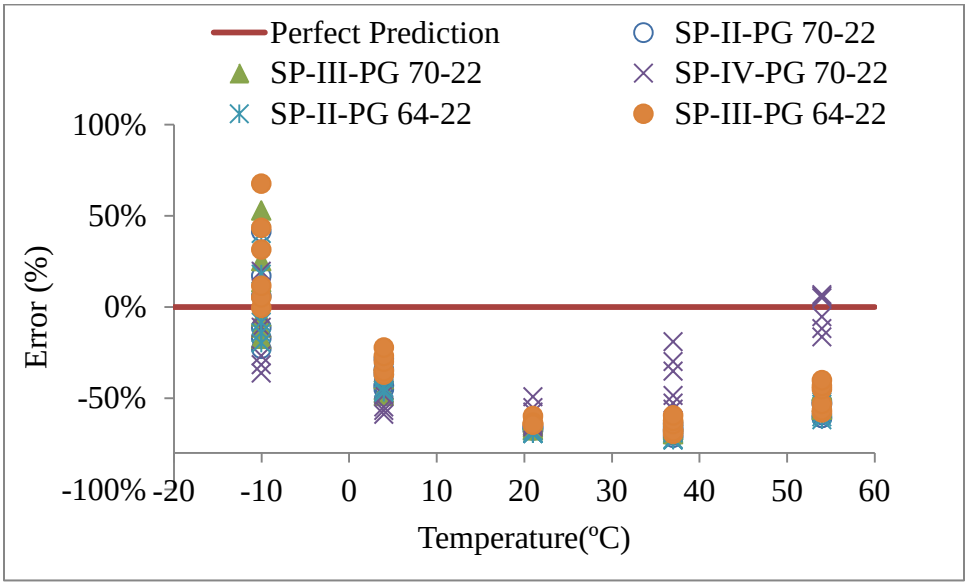


(a) Prediction Error Trend With Temperature

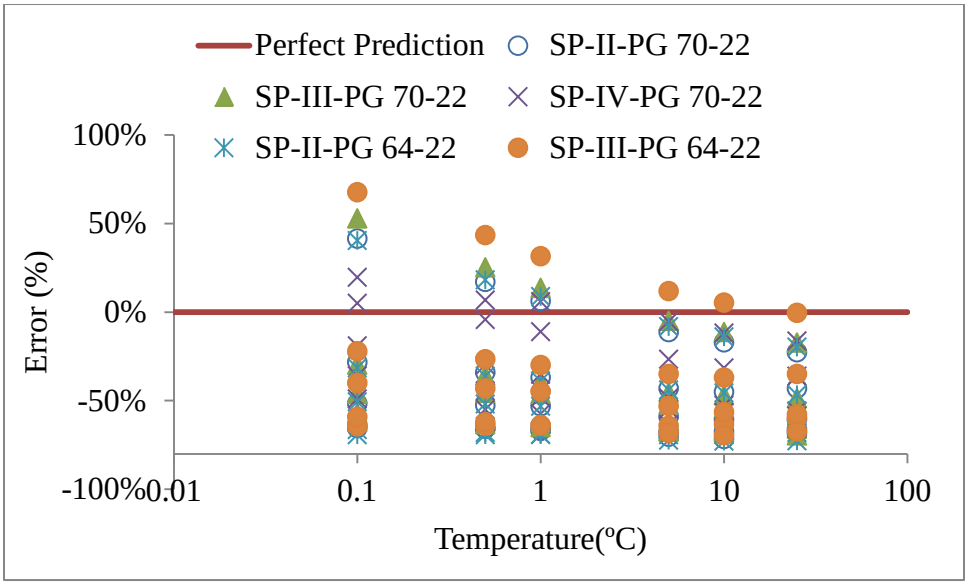


(b) Prediction Error Trend With Frequency

Figure 6.4: Trend of Prediction % Error for $G^*$-Based Witczak Model Using Default *A* and *VTS* Values from MEPDG

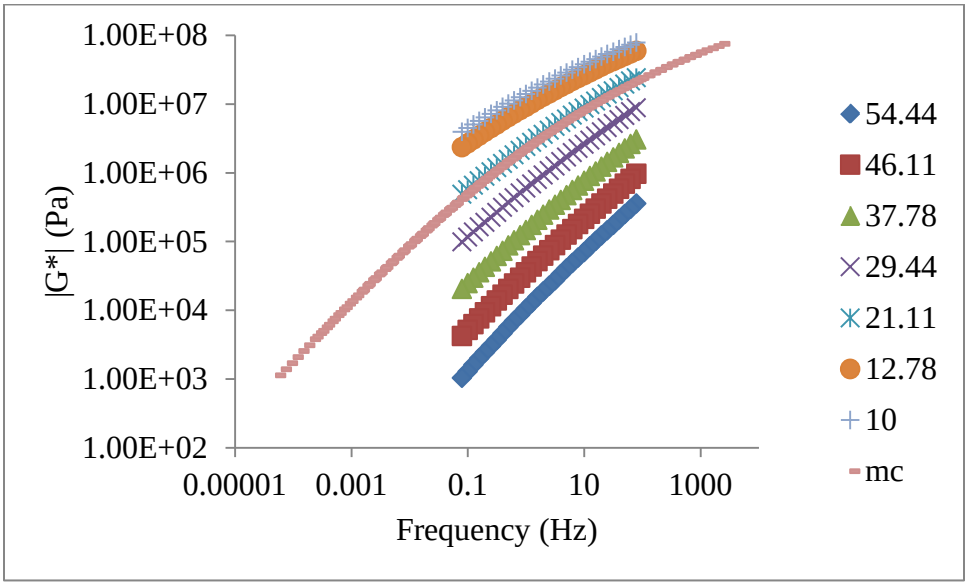


(a) *G** Mastercurve for PG 64-22

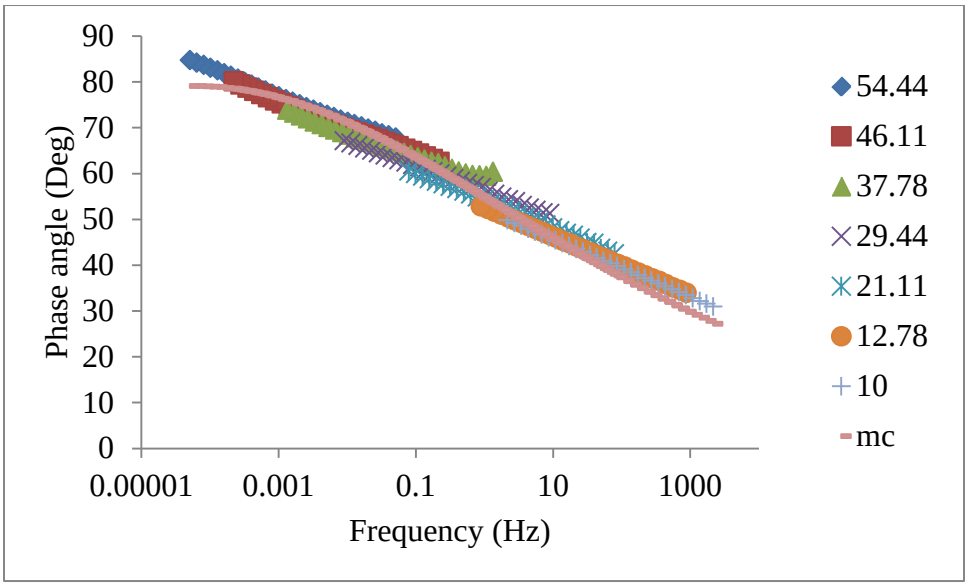


(b) Phase Angle Mastercurve for PG 64-22

Figure 6.5: *G** and Phase Angle Mastercurves For PG 64-22

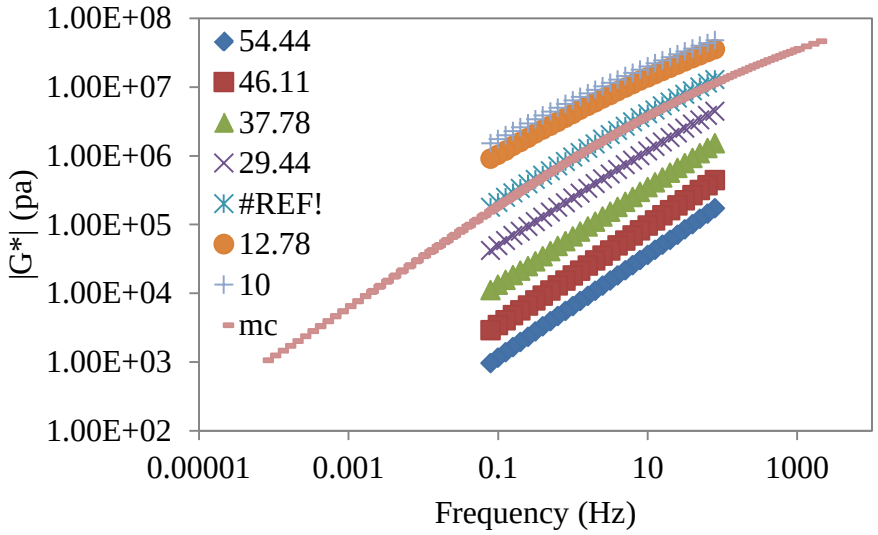


(a) G* mastercurve for PG 70-22

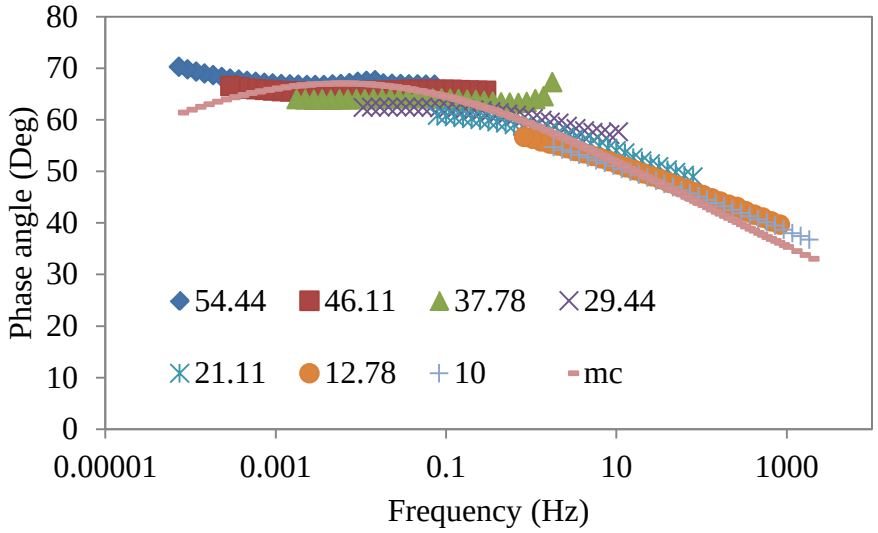


(b) Phase angle mastercurve for PG 70-22

Figure 6.6: G* and Phase angle mastercurves for PG 70-22

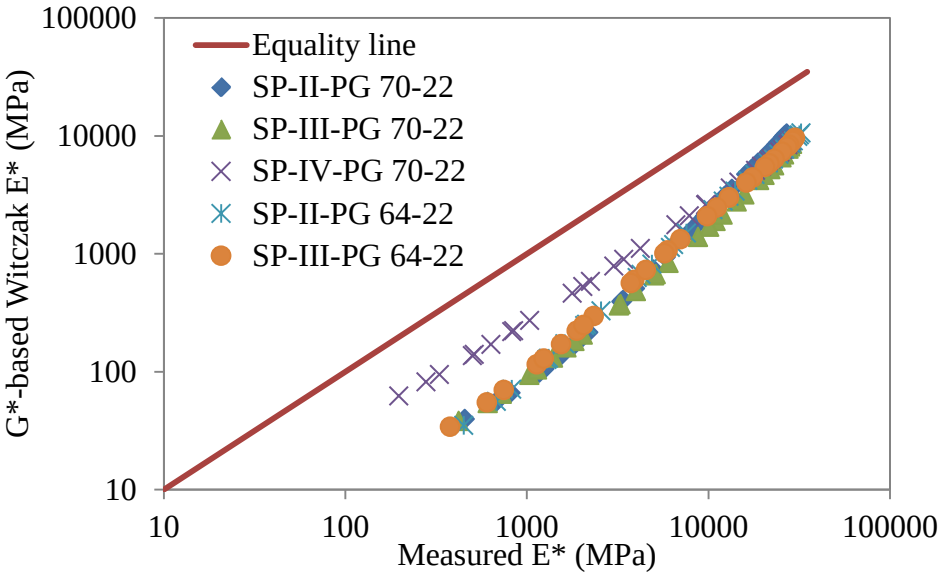


(a) scatter plot for G*-based Witczak model prediction

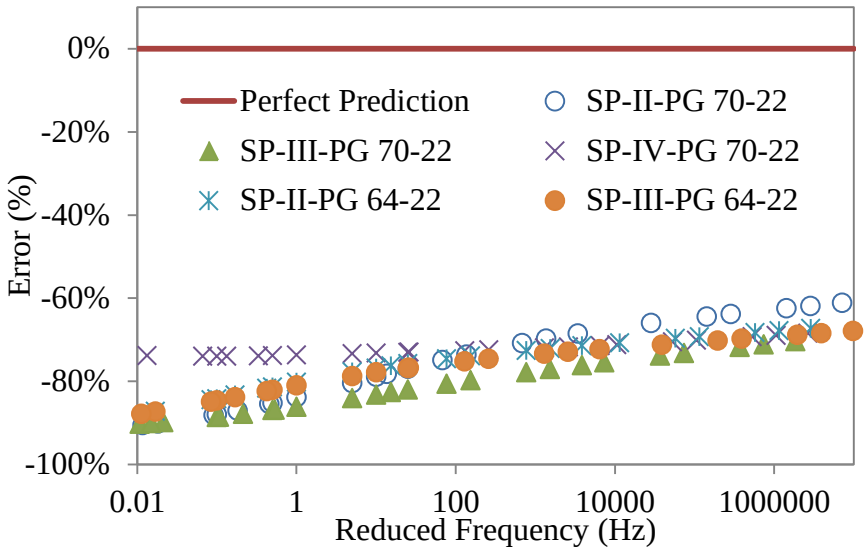


(b) Prediction error trend with frequency at 21ºC

Figure 6.7: Scatter Plot for G*-Based Witczak Model Prediction Using *G** and Phase Angle Mastercurves.

# Chapter 7

# Application and Modification of Hirsch Model for Typical New Mexico Asphalt Mixes

## 7.1. Introduction

The Hirsch model is the other well accepted dynamic modulus prediction model developed by Christensen et al. (2003). The Hirsch model is not adopted in the MEPDG design software, however, it is is used quite frequently for predicting dynamic modulus. In this chapter the accuracy of the Hirsch model is investigated in predicting measured dynamic modulus values of typical New Mexico asphalt concrete. Moreover, the Hirsch model is also modified by utilizing the dynamic modulus database developed by Bari (2005).

## 7.2. Objectives

Specific objectives of this study are:

- to apply Hirsch model for predicting measured dynamic modulus values of typical New Mexico Mixes
- to recalibrate the Hirsh model by using the extensive dynamic modulus database developed by Bari (2005).

## 7.3. Hirsch Model

The Hirsh model is different from Witczak model because it is based on rule of the mixtures for composite materials. Various forms of the mixture rule model are developed and the best model given in Eq. (7.1) is selected. The Hirsch model is calibrated using dynamic modulus database developed by compiling E* test results from Advanced Asphalt Technologists (AAC) and Arizona State university (ASU). The database included a total of 206 dynamic modulus measurements from 18 different mixtures Christensen et al. (2003).

$$|E^*| = P_c\left[4{,}200{,}000 * \left(1 - \frac{VMA}{100}\right) + 3|G^*|\left(\frac{VFA * VMA}{10{,}000}\right)\right] + (1 + P_c)\left[\frac{1 - \frac{VMA}{100}}{4{,}200{,}000} + \frac{VMA}{VFA * 3 * |G^*|}\right]^{-1} \quad (7.1)$$

$$P_c = \frac{\left(20 + \frac{VFA * 3 * |G_b^*|}{VMA}\right)^{0.58}}{650 + \left(\frac{VFA * 3 * |G_b^*|}{VMA}\right)^{0.58}} \quad (7.2)$$

$$\phi = -21(\log P_c)^2 - 55 \log P_c \quad (7.3)$$

where: $|E^*|$ is dynamic modulus, psi; $|G_b^*|$ is binder dynamic modulus, psi; VMA is voids in the mineral aggregate, %; VFA is voids filled with asphalt, %; $P_c$ is aggregate contact factor.

## 7.4. Analysis Method

It is possible to implement the Hirsh model in different ways based on how the binder G* data is obtained and utilized. In this study two methods are implemented:

- First, default A and VTS values are used to estimate the G* of the binder using the temperature susceptibly model developed by Bari (2005).
- Second actual the G* test is conducted at seven different temperatures (40, 55, 70, 85, 100, 115, 130 ºF) and 10 rsd/sec to determine the actual A and VTS values for the binders being used and then the G* of the binder is estimated by using the temperature susceptibly model developed by Bari (2005).
- Third, the G* mastercurves are utilized to estimate the G* values corresponding to the E* values at the same reduced frequency.

### 7.4.1. Application of Hirsch model using Default A and VTS values of MEPDG

The MEPDG default A and VTS values are used in Eq. (5.2) through Eq. (6.4) to determine temperature and frequency dependent viscosity for each binder. The default A and VTS values for PG 70-22 are 10.299 and -3.426 respectively and for PG 64-22 are A=10.98 and VTS=-3.68 (ARA, Inc. 2004). Then, the dynamic shear modulus, $|G^*|_b$, of the binders are determined using Eq. (6.5) for each temperature and frequency combination. Finally, the dynamic moduli of each mix at each test temperature and frequency combination are estimated using the Hirsh model.

Figure 7.1 presents a scatter plot of Hirsh model $|E^*|$ prediction results in comparison with the measured $|E^*|$ data for all asphalt mixes tested in this study. The result show that Hirsh model underpredicts the $|E^*|$ test results for all mixes at high and intermediate temperatures and over predicts for low temperature. The best prediction is observed for 4 ºC. Moreover, a clear bias for high temperature prediction is observed for all asphalt mixes.

Table 7.1 presents the average percent difference between predicted and tested data at each temperature. It can be observed that at -10 ºC the model is over predicting the measured $|E^*|$ by about 100% for all mixes and as the test temperature increases the model under predicts test results with increasing trend form 50% to 70%.

Figure 7.2 (a) presents the trend of all percent difference between predicted and tested data with temperature. The %error for -10 ºC is positive and ranges form 50-100% and as the temperature increases the model underpredicts the measured$|E^*|$. The % error is closest to zero (percent error for perfect prediction) at 4 ºC. The range of the error is also observed to decrease with increasing temperature. This indicates that the model is more precise at higher temperatures but the accuracy of the prediction is questionable.

Figure 7.2 (b) presents the trend of calculated percent error with respect frequency. The range of % error is observed to be from -100 to 150 % for all mixes. The maximum range is observed at the lowest test frequency and as the test frequency increases the range is observed to decrease. This indicates an increase in the precision of the model with increasing frequency.

### 7.4.2. Application of Hirsch model using Actual A and VTS determine through DSR testing

To determine actual A and VTS values for the binders G* test is conducted at seven different temperatures (40, 55, 70, 85, 100, 115, 130 ºF) and 10 rad/sec. the G* data is converted to viscosity using Eq. (5.3). Then, the relationship between viscosity and temperature is determined by plotting the logarithm of the logarithm of viscosity with respect to temperature in Rankin unit and fitting the linear regression line. This process provided the actual A and VTS values for the binders used in this study. The A and VTS values for PG 70-22 are determined are to be 7.759 and -2.514 respectively and for PG 64-22 are A=8.052 and VTS=-2.617. Following this, the dynamic shear modulus, $|G^*|_b$, of the binders are determined using Eq. (6.5) for each temperature and frequency combination. Finally, the dynamic moduli of each mix at each test temperature and frequency combination are estimated using the Hirsh model.

Figure 7.3 presents a scatter plot of Hirsh model $|E^*|$ prediction results using actual A and VTS values. The Hirsh model is under predicting in this case as well. The $|E^*|$ predictions are very close the line of equality at -10 ºC the trend of the prediction is not good. The prediction at 4 ºC and higher are observed to under predict measured $|E^*|$. The bias at high temperature prediction is still observed but the use of actual A and VTS values have improved the results.

Table 7.2 presents the average percent difference between predicted and tested data at each temperature for the case of using actual A and VTS values. There is a clear improvement in the accuracy of the predictions at -10 ºC resulting from the use of laboratory determined A and VTS values. However, the average percent difference remained very similar at intermediate and high temperature predictions. t

Figure 7.4 (a) presents the trend of all percent difference between predicted and tested data with temperature. The prediction at all temperatures is observed to under predict measured $|E^*|$. The %error for -10 ºC ranges from -50 to 0%. The trend of calculated percent error with respect to frequency is presented in Figure 7.4 (b). Similar to the previous case, the maximum range for % error is observed at the lowest test frequency and as the test frequency increases the range is observed to decrease. This indicates an increase in the precision of the model with increasing frequency.

### 7.4.3. Application of Hirsh Model by using $|G^*|$ and $\delta$ Mastercurves

For this method the $|E^*|$- mastercurves at reference temperature of 21 ºC is performed by using $|G^*|$and $\delta$ mastercurves at a reference temperature of 21 ºC in the Hirsch model. Therefore, $G^*$and $\delta$ – mastercurves replace the use of any type of model to predict $|G^*|_b$ and $\delta_b$ for use in the Hirsh model. The same $G^*$and $\delta$ – mastercurves developed for the case of G*-based Witczak model are utilized here as well.

Figure 7.5 (a) presents the scatter plot for the predicted and measured $|E^*|$ values. The Hirsch model is still under predicting measured $|E^*|$ values but the accuracy of the prediction is observed to be significantly improved. The bias at high temperature however, still remains. Figure 7.5 (b) presents the percent difference between the predicted and test data over the entire reduced frequency range at a reference temperature of 21 ºC. The percent difference between predicted and measured dynamic modulus is observed to decrease with increasing frequency.

## 7.5. Conclusion

In this study the Hirsch model is implemented to predict measured dynamic modulus values for typical NMDOT mixes. Predictions are performed using modes to predict $|G^*|_b$ and $\delta_b$ and using DSR binder test data. The A and VTS relations are used to simulate MEPDG software predictions at level 3 and Level 2 input hierarchy. Based on this study the following conclusions are drawn:

- The Hirsch model is found to under predict measured dynamic modulus values regardless model predicted or laboratory determined $|G^*|_b$ and $\delta_b$ are used. However, the accuracy of the model predictions has increased when laboratory determined G* values are used. Moreover the Hirsch model is found be biased at high temperatures.

## 7.6. References

Bari, J. (2005). “Development of a New Revised Version of the Witczak E* Predictive Models for Hot Mix Asphalt Mixtures.” Ph.D. Dissertation, Arizona State University, Phoenix, AZ.

Christensen, Jr., D.W., Pellinen, T.K., and Bonaquist, R.F. (2003). "Hirsch Model for Estimating the Modulus of Asphalt Concrete," *Journal of the Association of Asphalt Paving Technologists*, *72*, 97–121.

Table 7.1: Average Percent Difference between Hirsch Predicted and Measured *E** Data Using Default *A* and *VTS* Values

| Temperature (ºC) | SP-III-PG-64-22 (lab mix) | SP-II-PG-70-22 (lab mix) | SP-III-PG-70-22 (plant mix) | SP-II-PG-64-22 (plant mix) | SP-III-PG-70-22 (plant mix) |
|---|---|---|---|---|---|
| -10 | 129% | 84% | 123% | 102% | 134% |
| 4 | 41% | -7% | 19% | -4% | 26% |
| 21 | -45% | -68% | -49% | -65% | -32% |
| 37 | -74% | -83% | -74% | -82% | -53% |
| 54 | -70% | -73% | -68% | -70% | -30% |

Table 7.2: Average Percent Difference between Hirsch Predicted and Tested E* Data Using Actual A and VTS Values

| Temperature (ºc) | SP-III-PG-64-22 (Lab Mix) | SP-II-PG-70-22 (Lab Mix) | SP-III-PG-70-22 (Plant Mix) | SP-II-PG-64-22 (Plant Mix) | SP-III-PG-70-22 (Plant Mix) |
|---|---|---|---|---|---|
| -10 | -26% | -29% | -31% | -26% | -31% |
| 4 | -54% | -54% | -61% | -53% | -59% |
| 21 | -81% | -81% | -82% | -80% | -75% |
| 37 | -83% | -84% | -83% | -83% | -67% |
| 54 | -72% | -72% | -69% | -69% | -34% |

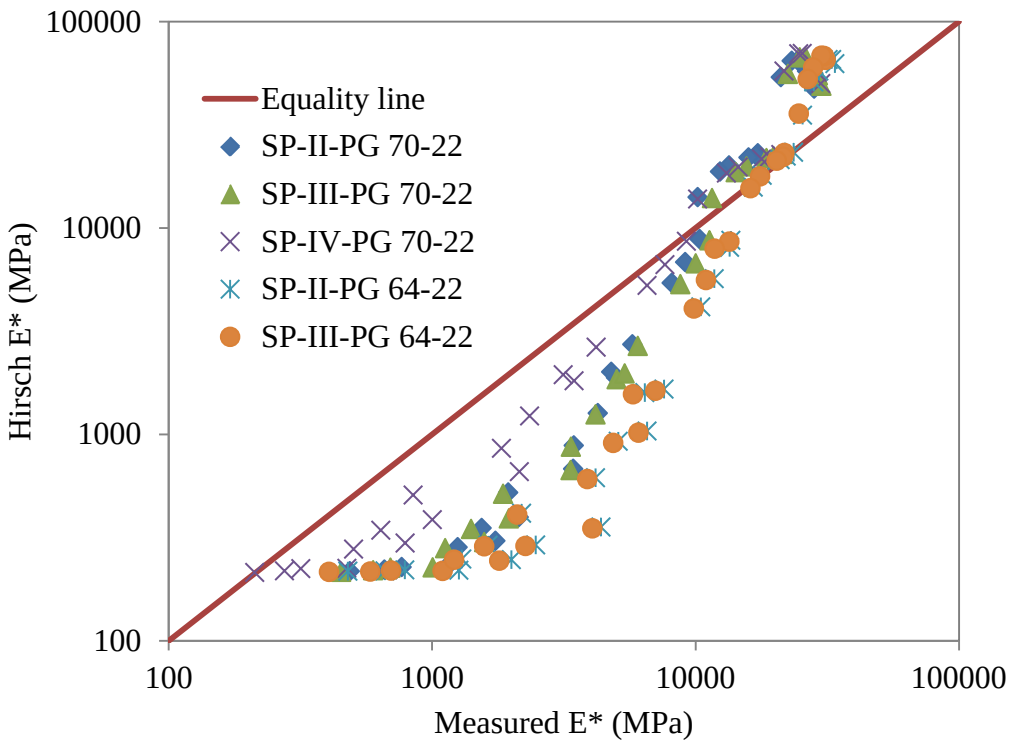


Figure 7.1: Scatter Plot for Hirsch Model Prediction Using Default *A* And *VTS* Values From MEPDG.

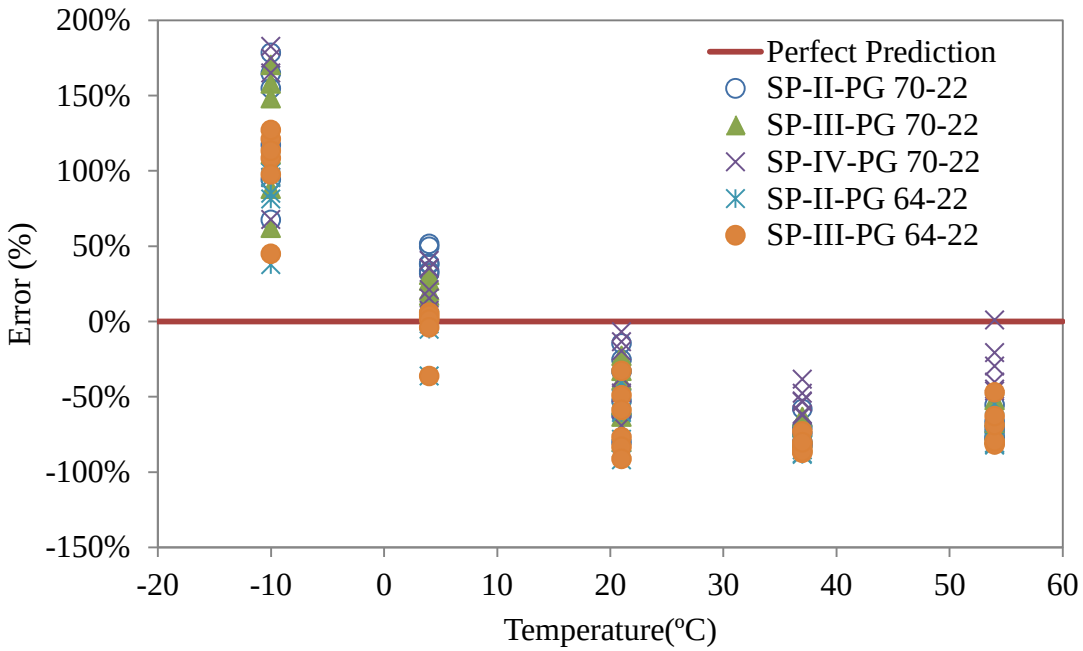


(a) Prediction Error Trend With Temperature

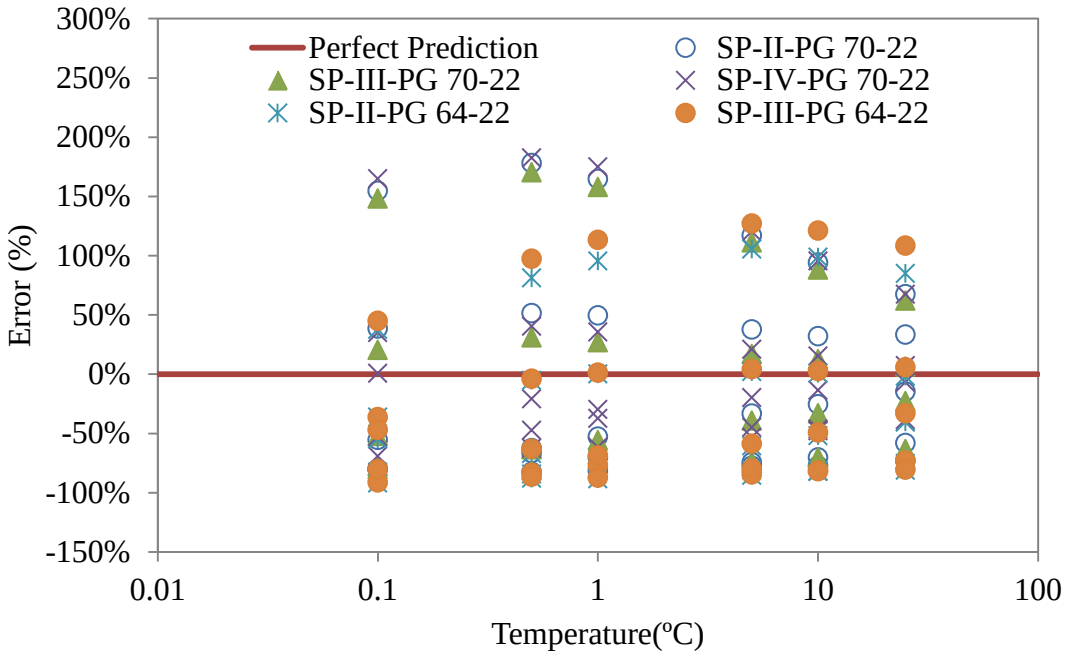


(b) Prediction Error Trend With Frequency

Figure 7.2: Trend of Prediction % Error for Hirsch Model Using Default *A* And *VTS* Values From MEPDG.

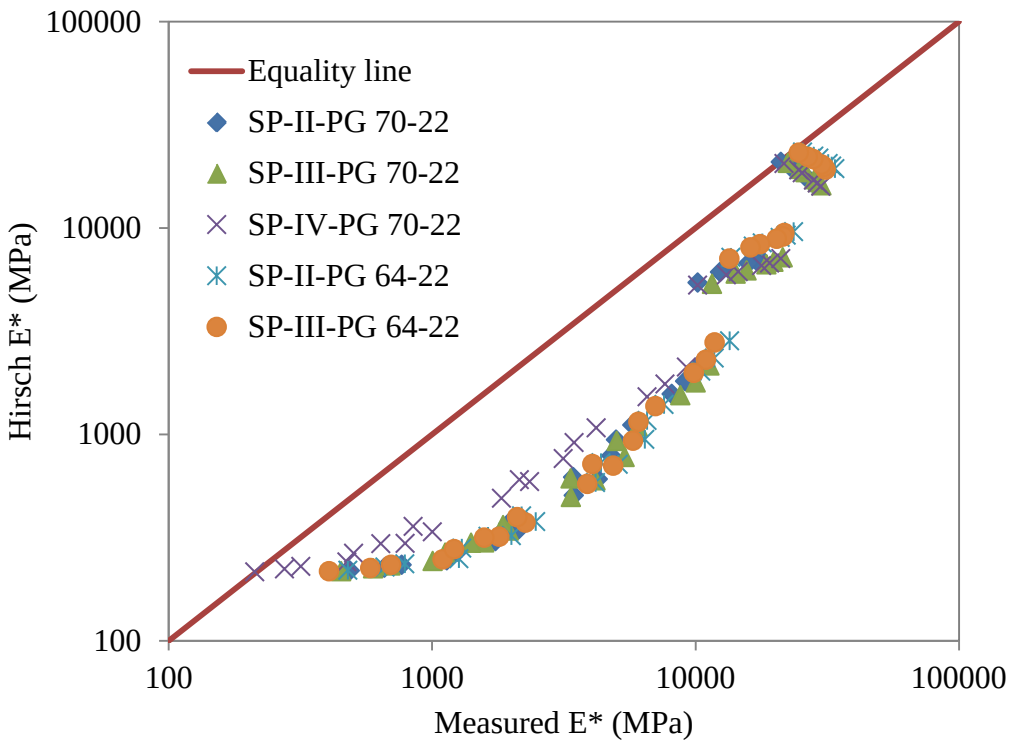


Figure 7.3: scatter plot for Hirsch model prediction using actual *A* and *VTS* values determined from laboratory DSR test.

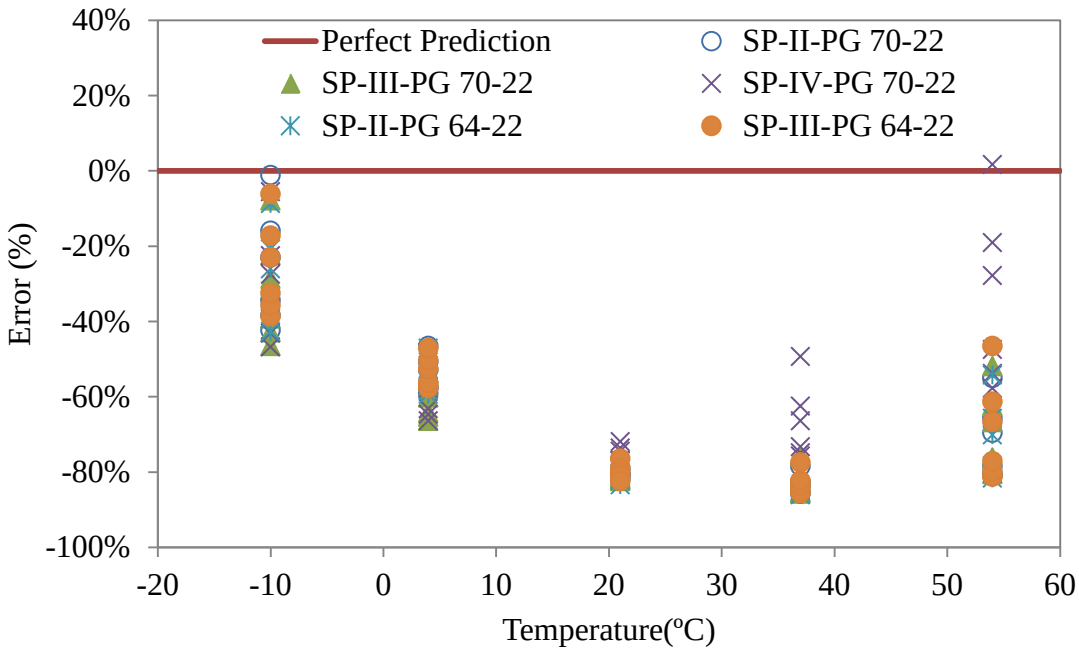


(a) Prediction error trend with temperature

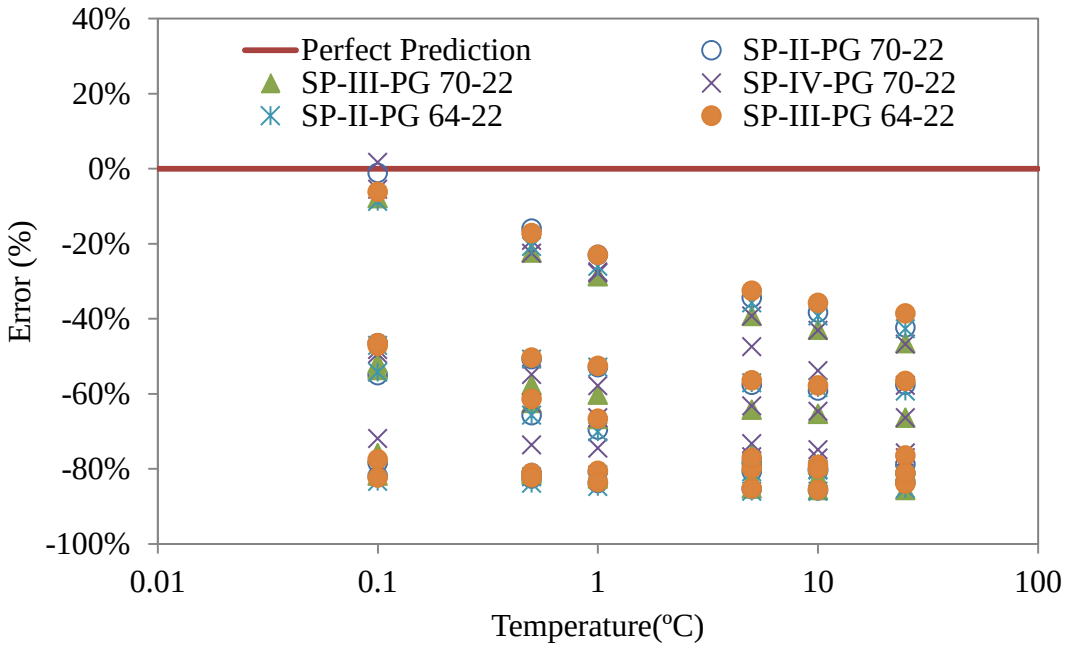


(b) Prediction error trend with frequency

Figure 7.4: Trend of Prediction % Error for Hirsch Model Using Default *A* and *VTS* Values From MEPDG

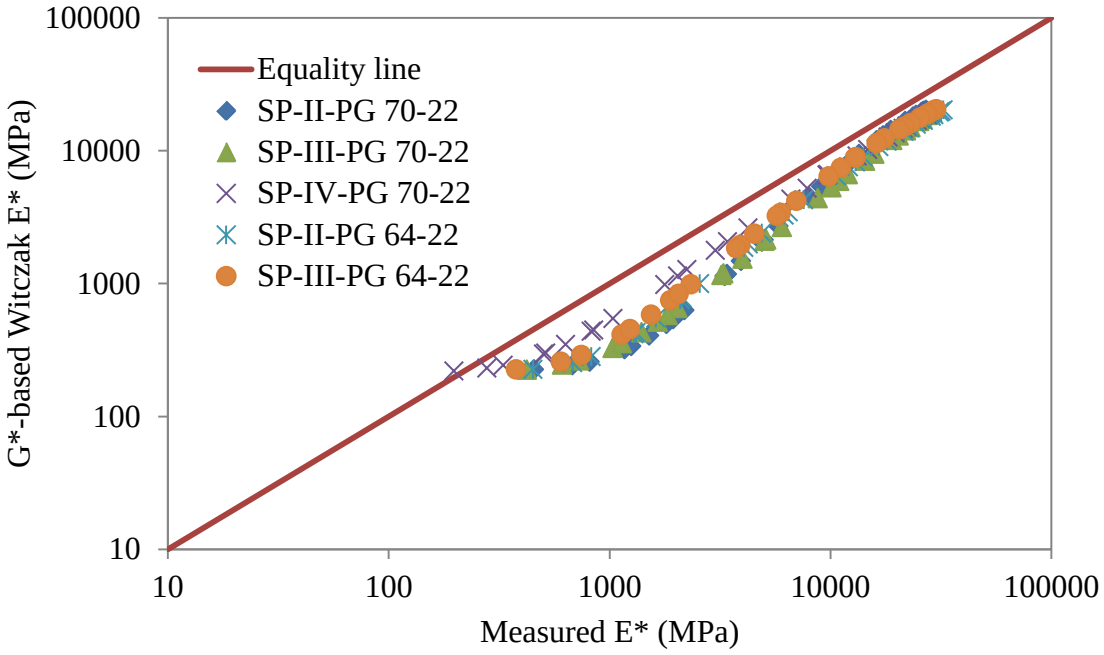


(a) scatter plot for Hirsch model prediction

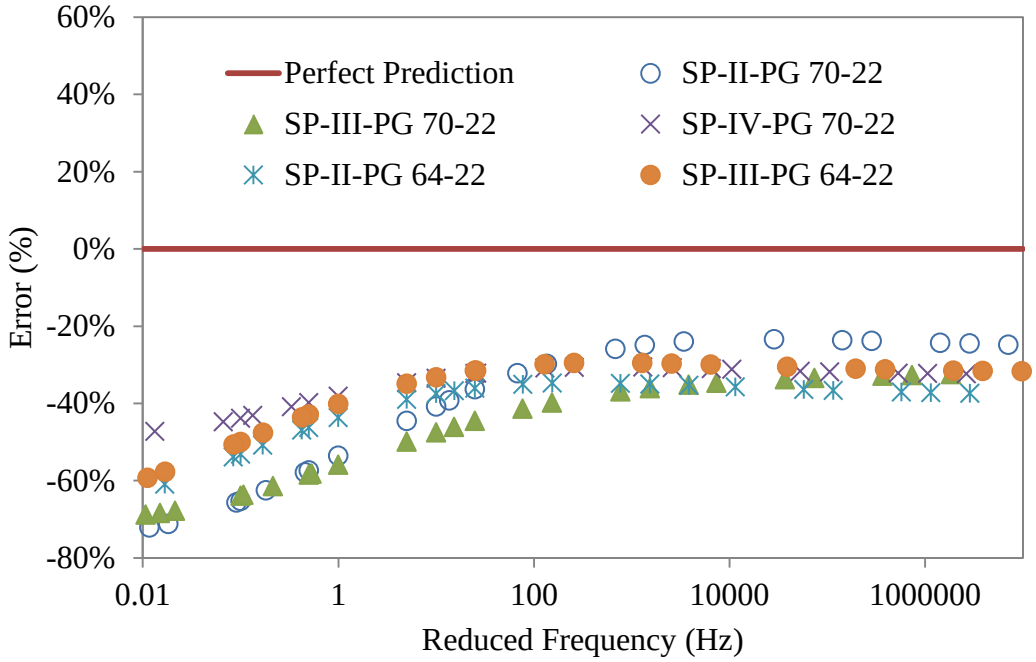


(b) Prediction error trend with frequency at 21ºC

Figure 7.5: Scatter plot for Hirsch model prediction using G* and Phase angle mastercurves.

# Chapter 8

# Conclusions and Recommendations

## 8.1. General

This study determines the dynamic modulus of five typical New Mexico asphalt mixes and analyzes test results to determine dynamic modulus mastercurves. In addition, this study implements dynamic modulus predictive models and evaluates the accuracy of the predictive models.

Dynamic modulus testing system was purchased from GCTS Testing Systems Company and installed at the University of New Mexico pavement Laboratory. Asphalt mixes are collected from actual construction sites in New Mexico. Using those mixes, dynamic modulus samples are prepared and laboratory testing is performed.

## 8.2. Conclusions

Dynamic modulus test data of each mix are evaluated. Based on the findings of this study, the following conclusions can be made:

- Isothermal plots of dynamic modulus test results show that dynamic modulus values of all mixes increase with increasing loading frequency, and $E^*$ values decrease with an increase in temperature.
- Isochronal plots indicate that the effects of change in loading frequency become more significant with increasing temperature for all mixes.
- Low and high temperature data quality analyses are performed using Cole and Cole plots and Black space plots; the results indicate good quality of dynamic modulus test data.
- Sigmoidal function is utilized to develop dynamic modulus mastercurves in Excel spreadsheets and a very good fit of data is found using sigmoidal function. A database of mastercurve parameters for all mixes is developed.
- Dynamic modulus mastercurve plots shows that SP II mixes have higher dynamic modulus than SP III mixes, and SP-IV mix exhibits lowest dynamic modulus among three mixes studied.

Independent assurance (IA) testing is performed in collaboration with AMEC laboratories to determine the precision of $E^*$-testing preformed in UNM pavement laboratory. The results from both laboratories are examined through statistical analysis. In addition, repeatability and reproducibility analysis are performed based on previous round-robin studies conducted in the past. From the IA study, the following conclusions are made:

- Coefficients of variation (COV) plots indicate that the results from UNM and AMEC laboratories are very similar.
- One-way ANOVA analysis performed at each test temperature and frequency combination. ANOVA results indicate no significant difference in the means as well as the variances of test results from UNM and AMEC laboratories, which indicates good accuracy of testing in both laboratories.
- Repeatability analysis of selected test results indicate acceptable repeatability of E*-testing in UNM and AMEC laboratories. This indicates good precision testing in both laboratories.
- Reproducibility analysis of selected test results indicate acceptable reproducibility of E*-testing in UNM and AMEC laboratories, which indicates good accuracy of test results.

The viscosity based Witczak model is applied for predicting measured dynamic modulus values of typical New Mexico Mixes and a new modified viscosity based Witczak model also developed by giving more emphasis on mix volumetric properties. From this study, the following conclusions can be dawn:

- The viscosity based Witczak model is applied by using the default A and VTS values and the predicted dynamic modulus values are found to be smaller than the measured dynamic modulus values for all SP-III and SP-II mix. However, better agreement is obtained between predicted and laboratory mastercurves for SP-IV mix.
- The application of viscosity based Witczak model using actual A and VTS valued determined using DSR test results is found to underpredict the dynamic modulus results of all typical NMDOT mixes.
- Mastercurve prediction at both Level-3 and Level-2 input hierarchy using viscosity based Witczak model in MEPDG are found to under predict the dynamic modulus of SP-III and SP-II mixes. However, better agreement is obtained between predicted and laboratory mastercurves for SP-IV mix.
- The percent error of prediction by viscosity based Witczak model is found to be low at the cold temperature, but error shows an increasing trend with increasing temperature. However, no apparent trend is observed with respect to test frequency.
- By optimizing the mix variable values, it is possible to improve the viscosity based Witczak model prediction significantly and optimized solution shows that the coarse aggregate variables in the viscosity based model can be eliminated without huge change in the mastic and binder input variable values. This indicates that the low significance of coarse aggregate variables( $\rho_{34}$, $\rho_{38}$ and $\rho_{4}$ ) on the model prediction accuracy.
- A new dynamic modulus predictive model is developed by eliminating the coarse aggregate variables in the viscosity based Witczak model and keeping the

sigmoidal mathematical structure and introducing a modified aggregate contact factor from Hirsh model.

- The new dynamic modulus model shows significant improvement in predicting the dynamic modulus of typical NMDOT mixes.
- Sensitivity analysis of the new model shows that new model prediction is rational to variations of air void, effective binder, and percentage of fine aggregates.

The $G^*$-based Witczak model is also implemented to predict measured dynamic modulus values for typical NMDOT mixes. Predictions are performed using MEPDG default binder properties and actual binder test data to simulate MEPDG software predictions at level 3. Based on this study the following conclusions are drawn:

- The use of $G^*$-based Witczak model with MEPDG default binder properties indicated that the model underpredicts the dynamic modulus of NMDOT mixes
- $G^*$-based Witczak model application by using laboratory determined binder properties have shown improvement in the prediction accuracy, however, the model is found to underpredict measured dynamic modulus of NMDOT mixes in this case as well.
- $G^*$-based Witczak model is also implemented using $G^*$ and $\delta$ – mastercurves developed for binders used in the production of NMDOT mixes. This method completely replaced the use of A and VTS relationship with binder $G^*$ – mastercurves. The results however still underpredict measured dynamic modulus of typical NMDOT mixes.

The Hirsch model is found to underpredict measured dynamic modulus values regardless model predicted or laboratory determined $|G^*|_b$ and $\delta_b$ are used. However, the accuracy of the model predictions increases when laboratory determined G* values are used. Moreover the Hirsch model is found be biased at high temperatures.

### 8.3. Recommendations

Based on this study, the following research recommendations are made:

- Dynamic modulus testing in University of New Mexico is found to be of good quality. However, the mixes tested in this study are only five. Therefore, it is recommended for NMDOT to perform dynamic modulus testing over a comprehensive state wide mixture types.
- Both Viscosity and G* based Witczak models are found to underpredict the measured dynamic modulus values of typical NMDOT mixes. Since these models are used in MEPDG, it is recommended to investigate the effect of dynamic modulus prediction error on the pavement performance prediction in MEPDG rutting and fatigue models.

- Recycled asphalt pavement (RAP) and Warm Mix Asphalt (WMA) are widely used by NMDOT. Further research is recommended to study the effects of RAP contents on dynamic modulus of asphalt mixes.
- The New model developed in this research has shown promising results in predicting dynamic modulus of NMDOT mixes. It is recommended for NMDOT to validate the accuracy of this model with further dynamic modulus test results in the future.

# APPENDIX A

DYNAMIC MODULUS TEST RESULTS FOR SP-III WITH PG 70-22 BINDER

Table A.1: E* test results for Sample 1 (SP-III with PG 70-22 binder)

| Temperature | Frequency | Stress | | Dynamic Modulus | Phase Angle | | Strain | | | |
|---|---|---|---|---|---|---|---|---|---|---|
| | | Amplitude (P-P) | SE | | | UC | (P-P) Recoverable | Permanent | SE | UC |
| (deg C) | (Hz) | (kPa) | (%) | (MPa) | (deg) | (deg) | (micro e) | (micro e) | (%) | (%) |
| -10 | 25 | 1899 | 7.7 | 33749.695 | 10.2 | 4.1 | 56.27 | 57.228 | 9.7 | 6.9 |
| -10 | 10 | 1953 | 7 | 33554.328 | 5.7 | 0.6 | 58.203 | 20.955 | 7.9 | 11.6 |
| -10 | 5 | 1948 | 5.9 | 32484.578 | 5.8 | 0.1 | 59.952 | 19.034 | 7 | 11.3 |
| -10 | 1 | 1741 | 2.1 | 29745.029 | 7 | 0.9 | 58.53 | 20.474 | 4 | 12.9 |
| -10 | 0.5 | 1611 | 1.3 | 28972.107 | 7.2 | 0.8 | 55.621 | 24.642 | 3.5 | 14.6 |
| -10 | 0.1 | 1543 | 0.5 | 25734.52 | 7.5 | 0.2 | 59.949 | 47.949 | 3 | 12.4 |
| 4 | 25 | 1350 | 6.2 | 29351.537 | 14.2 | 0.1 | 46.002 | 80.698 | 9.3 | 25.4 |
| 4 | 10 | 1329 | 6.8 | 26583.441 | 10.9 | 1.4 | 50.001 | 50.655 | 7.4 | 26.8 |
| 4 | 5 | 1266 | 5.5 | 25116.166 | 10.7 | 1.7 | 50.419 | 50.954 | 6.6 | 26.5 |
| 4 | 1 | 1066 | 2 | 21178.668 | 12 | 2.2 | 50.354 | 51.283 | 5.3 | 25.7 |
| 4 | 0.5 | 980 | 1.2 | 19158.592 | 13.3 | 2.1 | 51.162 | 56.562 | 2.8 | 26.9 |
| 4 | 0.1 | 883 | 0.6 | 15886.74 | 15.9 | 1.7 | 55.574 | 91.716 | 3.4 | 23.1 |
| 21 | 25 | 878 | 6 | 14279.107 | 20.7 | 1.5 | 61.477 | 186.417 | 8.1 | 2.7 |
| 21 | 10 | 756 | 6.2 | 12464.3 | 18.9 | 3.3 | 60.652 | 147.93 | 6.9 | 3 |
| 21 | 5 | 657 | 5.1 | 10947.893 | 19.9 | 3.7 | 60.022 | 136.691 | 5.7 | 3 |
| 21 | 1 | 464 | 2.6 | 7958.353 | 23.5 | 4.6 | 58.252 | 113.201 | 4.8 | 8.8 |
| 21 | 0.5 | 405 | 1.8 | 6771 | 25.2 | 5.2 | 59.849 | 117.486 | 4 | 11.7 |
| 21 | 0.1 | 629 | 0.5 | 4841.598 | 26 | 3.3 | 129.913 | 348.54 | 4 | 1.5 |
| 37 | 25 | 424 | 6.5 | 6867.026 | 25.1 | 2.3 | 61.718 | 336.534 | 6.2 | 13.6 |
| 37 | 10 | 303 | 6.8 | 5362.621 | 25 | 3 | 56.435 | 358.401 | 5.7 | 17.3 |
| 37 | 5 | 251 | 4.6 | 4345.317 | 25.9 | 1.7 | 57.688 | 362.349 | 5.4 | 18 |
| 37 | 1 | 155 | 3.1 | 2582.42 | 29.4 | 2.1 | 60.071 | 333.565 | 3.8 | 14.5 |
| 37 | 0.5 | 127 | 2.2 | 2087.269 | 30.1 | 2.3 | 60.989 | 337.311 | 3.4 | 12.6 |
| 37 | 0.1 | 85 | 1.3 | 1320.332 | 29.1 | 2.3 | 64.249 | 381.253 | 3.8 | 11.6 |
| 54 | 25 | 205 | 6.1 | 2553.447 | 30 | 0.3 | 80.181 | 335.349 | 5.7 | 2.4 |
| 54 | 10 | 158 | 4.7 | 1859.337 | 28.5 | 0.8 | 84.837 | 398.812 | 3.8 | 2.1 |
| 54 | 5 | 127 | 4.6 | 1417.013 | 28.1 | 0.9 | 89.928 | 409.597 | 3.6 | 4.3 |
| 54 | 1 | 74 | 3.2 | 795.796 | 27.1 | 0.7 | 93.044 | 394.694 | 3.7 | 0.9 |
| 54 | 0.5 | 59 | 2.8 | 645.422 | 25.5 | 0.5 | 90.892 | 391.743 | 4.3 | 0.5 |
| 54 | 0.1 | 39 | 3 | 426.353 | 20.6 | 0 | 92.122 | 415.725 | 5.5 | 7.9 |

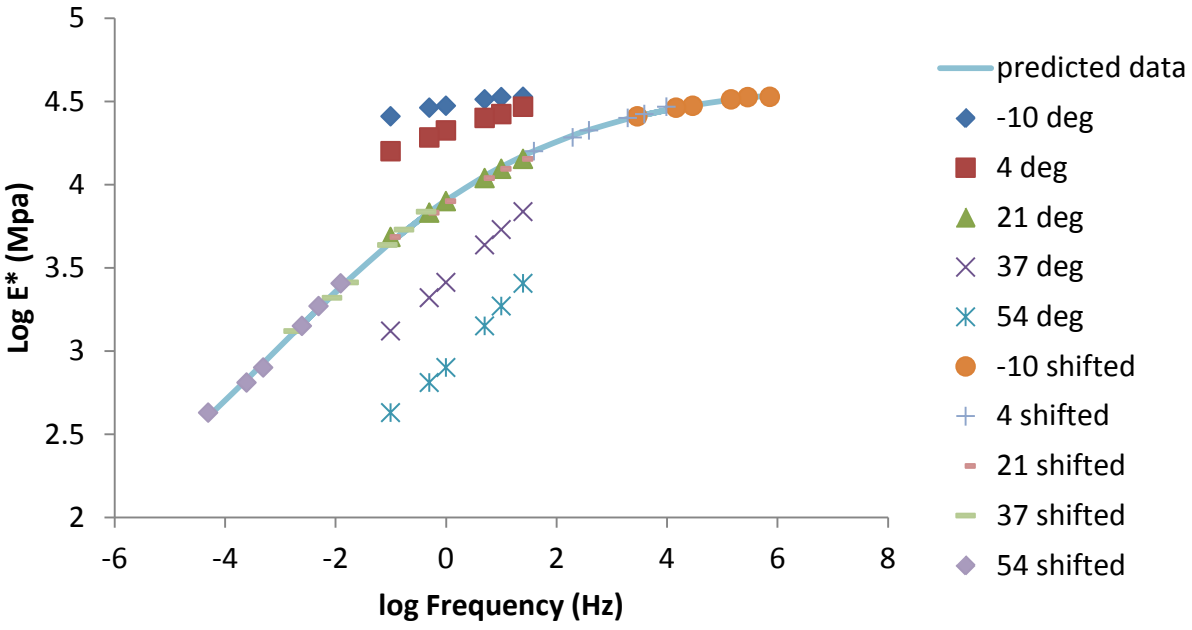


Figure A. 1: Master curve for Sample 1 (SP-III with PG 70-22 binder)

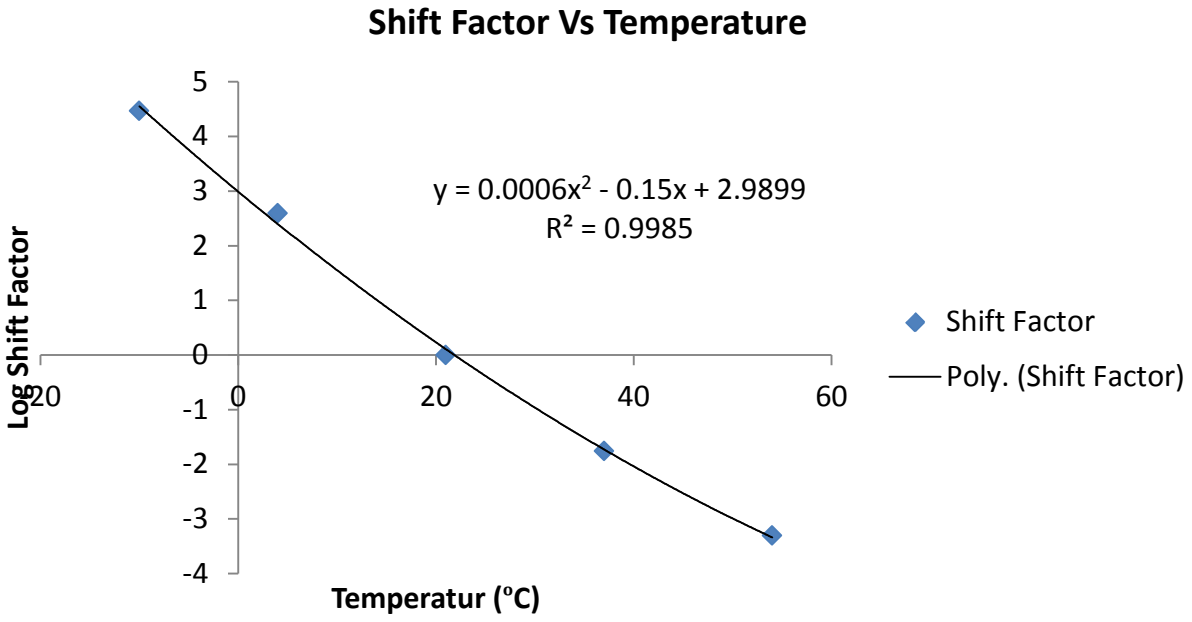


Figure A. 2: Shift factor for Sample 1 (SP-III with PG 70-22 binder)

Table A.2: E* test results for Sample 2 (SP-III with PG 70-22 binder)

| Temperature | Frequency | Stress | | Dynamic Modulus | Phase Angle | | Strain | | | |
|---|---|---|---|---|---|---|---|---|---|---|
| | | Amplitude (P-P) | SE | | | UC | (P-P) Recoverable | Permanent | SE | UC |
| (deg C) | (Hz) | (kPa) | (%) | (MPa) | (deg) | (deg) | (micro e) | (micro e) | (%) | (%) |
| -10 | 25 | 2038.0 | 6.1 | 36369.1 | 7.3 | 2.0 | 56.0 | 61.2 | 10.4 | 7.1 |
| -10 | 10 | 2067.0 | 6.1 | 35345.8 | 6.2 | 1.7 | 58.5 | 22.5 | 8.0 | 7.7 |
| -10 | 5 | 2011.0 | 5.2 | 34335.3 | 6.1 | 1.8 | 58.6 | 25.6 | 6.7 | 7.7 |
| -10 | 1 | 1804.0 | 1.5 | 32016.0 | 6.1 | 2.1 | 56.3 | 28.7 | 8.0 | 4.4 |
| -10 | 0.5 | 1697.0 | 0.9 | 30246.1 | 8.0 | 2.2 | 56.1 | 30.4 | 4.3 | 3.2 |
| -10 | 0.1 | 1543.0 | 0.5 | 27514.6 | 8.5 | 2.1 | 56.1 | 44.0 | 3.6 | 0.4 |
| 4 | 25 | 1521.0 | 6.3 | 24786.0 | 10.7 | 3.6 | 61.4 | 91.5 | 9.5 | 0.6 |
| 4 | 10 | 1490.0 | 6.5 | 23750.9 | 9.0 | 0.2 | 62.7 | 35.7 | 8.7 | 9.8 |
| 4 | 5 | 1420.0 | 5.2 | 22707.9 | 9.0 | 0.1 | 62.5 | 35.1 | 8.5 | 9.9 |
| 4 | 1 | 1201.0 | 1.7 | 19412.5 | 11.4 | 0.5 | 61.9 | 33.1 | 5.0 | 13.6 |
| 4 | 0.5 | 1103.0 | 1.0 | 17873.1 | 12.1 | 1.0 | 61.7 | 37.1 | 5.8 | 15.8 |
| 4 | 0.1 | 994.0 | 0.4 | 14309.3 | 15.3 | 0.2 | 69.4 | 82.4 | 3.9 | 17.2 |
| 21 | 25 | 855.0 | 7.3 | 12127.9 | 20.0 | 3.1 | 70.5 | 193.5 | 10.5 | 3.0 |
| 21 | 10 | 723.0 | 7.5 | 12137.9 | 17.5 | 0.3 | 59.5 | 161.3 | 7.7 | 28.9 |
| 21 | 5 | 626.0 | 6.8 | 10871.3 | 18.4 | 0.7 | 57.6 | 153.8 | 7.7 | 30.5 |
| 21 | 1 | 412.0 | 3.8 | 7686.1 | 23.0 | 0.4 | 53.6 | 124.5 | 4.2 | 30.6 |
| 21 | 0.5 | 348.0 | 2.5 | 6540.1 | 24.2 | 0.1 | 53.1 | 121.1 | 3.4 | 31.2 |
| 21 | 0.1 | 225.0 | 0.8 | 4174.9 | 27.3 | 0.2 | 53.9 | 154.9 | 3.1 | 32.1 |
| 37 | 25 | 485.0 | 8.9 | 7589.4 | 26.9 | 1.3 | 63.9 | 399.8 | 10.0 | 16.4 |
| 37 | 10 | 427.0 | 9.6 | 5981.9 | 26.5 | 2.2 | 71.3 | 498.9 | 7.8 | 22.8 |
| 37 | 5 | 364.0 | 9.1 | 4887.7 | 28.0 | 2.5 | 74.4 | 531.9 | 7.6 | 27.1 |
| 37 | 1 | 242.0 | 4.4 | 2706.5 | 31.0 | 2.2 | 89.2 | 514.2 | 6.7 | 36.7 |
| 37 | 0.5 | 200.0 | 3.2 | 2152.8 | 31.5 | 1.8 | 92.9 | 520.5 | 6.0 | 40.8 |
| 37 | 0.1 | 149.0 | 1.4 | 1343.0 | 30.3 | 0.5 | 110.7 | 606.6 | 5.7 | 44.2 |
| 54 | 25 | 137.0 | 9.1 | 2378.4 | 33.3 | 1.6 | 57.5 | 207.0 | 6.8 | 32.5 |
| 54 | 10 | 113.0 | 9.2 | 1770.0 | 30.2 | 1.1 | 64.0 | 262.8 | 6.0 | 25.5 |
| 54 | 5 | 97.0 | 8.7 | 1410.2 | 29.4 | 0.8 | 68.6 | 284.6 | 6.0 | 25.1 |
| 54 | 1 | 62.0 | 5.8 | 829.0 | 28.5 | 1.0 | 74.9 | 282.3 | 5.3 | 32.2 |
| 54 | 0.5 | 54.0 | 4.3 | 702.4 | 27.0 | 1.0 | 77.5 | 288.8 | 5.6 | 36.1 |
| 54 | 0.1 | 42.0 | 2.1 | 515.0 | 22.5 | 0.8 | 81.8 | 319.0 | 6.3 | 47.2 |

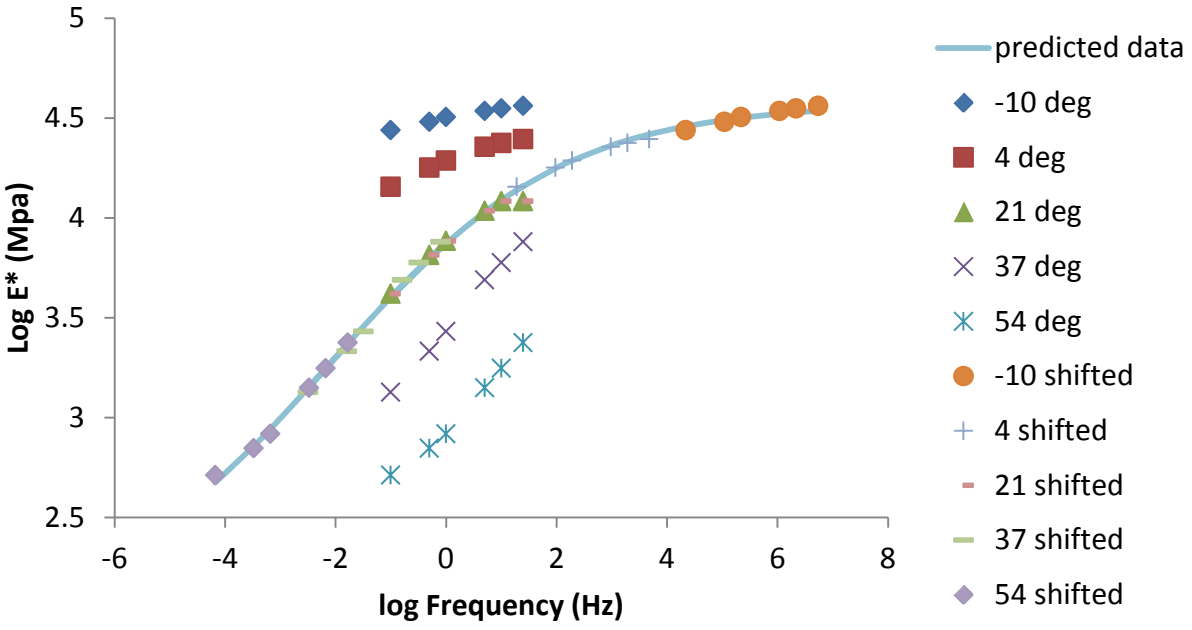


Figure A. 3: Master curve for Sample 2 (SP-III with PG 70-22 binder)

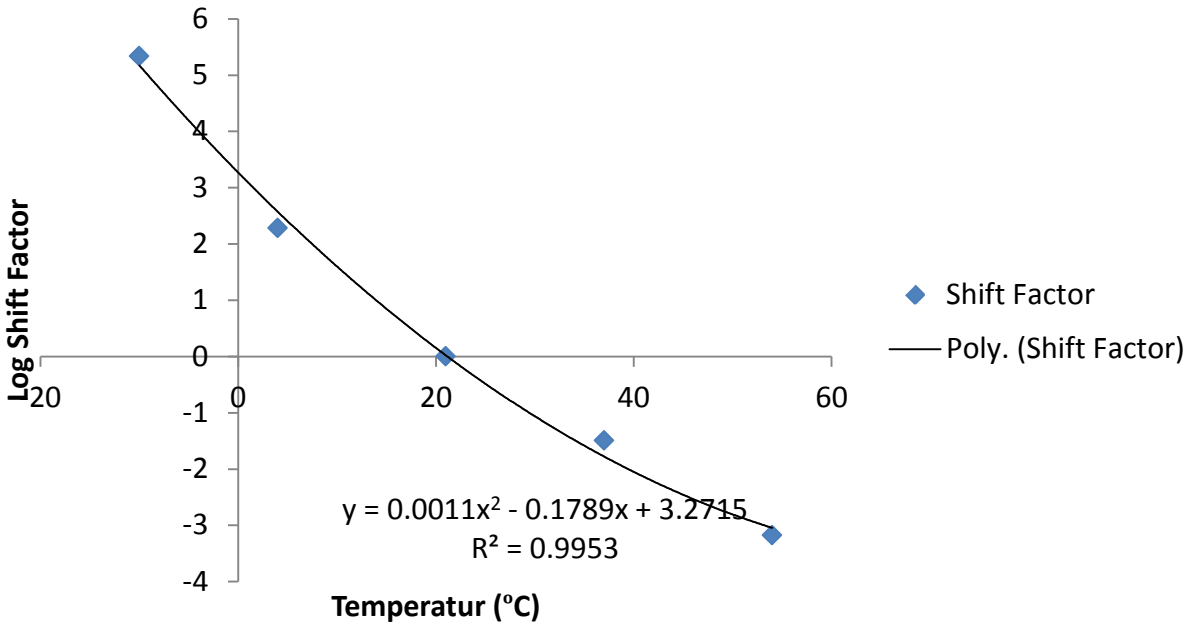


Figure A. 4: Shift factor for Sample 2 (SP-III with PG 70-22 binder)

Table A. 3: E* test results for Sample 3 (SP-III with PG 70-22 binder)

| Temperature | Frequency | Stress | | Dynamic Modulus | Phase Angle | | Strain | | | |
|---|---|---|---|---|---|---|---|---|---|---|
| | | Amplitude (P-P) | SE | | | UC | (P-P) Recoverable | Permanent | SE | UC |
| (deg C) | (Hz) | (kPa) | (%) | (MPa) | (deg) | (deg) | (micro e) | (micro e) | (%) | (%) |
| -10 | 25 | 2049 | 6.8 | 32667.498 | 7 | 1 | 62.734 | 72.951 | 9.5 | 19.5 |
| -10 | 10 | 1979 | 6.3 | 31308.1 | 6.6 | 0.6 | 63.2 | 18.07 | 8.3 | 18.3 |
| -10 | 5 | 1908 | 5.1 | 30411.125 | 6.2 | 0 | 62.741 | 16.513 | 7.2 | 16.9 |
| -10 | 1 | 1653 | 1.8 | 27615.971 | 6.4 | 0.1 | 59.846 | 15.778 | 5.8 | 13 |
| -10 | 0.5 | 1571 | 1 | 26189.592 | 8.8 | 1.9 | 60.003 | 17.994 | 3.7 | 10.8 |
| -10 | 0.1 | 1386 | 0.5 | 23250.439 | 9.1 | 1 | 59.618 | 33.955 | 4.4 | 7.9 |
| 4 | 25 | 1294 | 7.5 | 21708.938 | 10.7 | 3.4 | 59.621 | 131.618 | 9.8 | 3.9 |
| 4 | 10 | 1215 | 7.4 | 19684.326 | 11.4 | 0.7 | 61.746 | 76.446 | 7.4 | 6.4 |
| 4 | 5 | 1129 | 6.4 | 18147.914 | 12.2 | 0.8 | 62.188 | 75.79 | 6.2 | 5.4 |
| 4 | 1 | 886 | 2.8 | 14740.722 | 14.6 | 0.7 | 60.111 | 69.371 | 5.1 | 3.8 |
| 4 | 0.5 | 795 | 1.8 | 13102.343 | 16.6 | 2.3 | 60.662 | 74.204 | 4.3 | 0.8 |
| 4 | 0.1 | 608 | 0.9 | 10267.097 | 18.7 | 0.7 | 59.228 | 116.988 | 3.5 | 1.2 |
| 21 | 25 | 697 | 8 | 11424.726 | 17 | 6.6 | 60.965 | 240.313 | 11 | 20.4 |
| 21 | 10 | 574 | 8.3 | 9281.548 | 19.8 | 1.2 | 61.851 | 236.956 | 6.7 | 13.8 |
| 21 | 5 | 491 | 8.1 | 7974.197 | 21 | 1 | 61.521 | 233.081 | 6.6 | 13.3 |
| 21 | 1 | 310 | 5.4 | 5051.058 | 25.3 | 0.5 | 61.315 | 201.597 | 6.9 | 9.7 |
| 21 | 0.5 | 245 | 3.6 | 3978.456 | 26.6 | 1.9 | 61.697 | 195.752 | 5.2 | 10 |
| 21 | 0.1 | 158 | 1.5 | 2494.03 | 27.7 | 1.2 | 63.295 | 228.028 | 3.6 | 7.8 |
| 37 | 25 | 283 | 9.9 | 4857.816 | 27.8 | 4.2 | 58.202 | 168.393 | 8.1 | 9.2 |
| 37 | 10 | 225 | 9.3 | 3621.459 | 26.8 | 1.6 | 62.201 | 195.095 | 6.7 | 21.4 |
| 37 | 5 | 180 | 8.7 | 2896.652 | 26.9 | 1.7 | 62.259 | 202.194 | 6.4 | 23.6 |
| 37 | 1 | 114 | 5.8 | 1759.675 | 26.9 | 2.2 | 64.945 | 192.523 | 5.8 | 23.2 |
| 37 | 0.5 | 89 | 3.7 | 1441.959 | 26.2 | 2.2 | 62.038 | 193.184 | 5.5 | 23 |
| 37 | 0.1 | 61 | 1.5 | 986.215 | 24.6 | 1.3 | 61.874 | 217.7 | 7.7 | 22.4 |
| 54 | 25 | 102 | 9.7 | 1550.854 | 29.1 | 1.6 | 65.521 | 83.723 | 6.9 | 3.5 |
| 54 | 10 | 80 | 8.8 | 1201.377 | 26.6 | 2.3 | 66.285 | 111.038 | 5.7 | 8.6 |
| 54 | 5 | 64 | 8.1 | 973.169 | 25.4 | 2.5 | 66.066 | 118.016 | 5.5 | 2.1 |
| 54 | 1 | 44 | 5.6 | 685.538 | 23.4 | 3.5 | 64.2 | 114.045 | 5.1 | 4.5 |
| 54 | 0.5 | 40 | 4.1 | 613.822 | 22.4 | 3 | 64.429 | 115.623 | 5.8 | 6.7 |
| 54 | 0.1 | 38 | 2 | 511.312 | 19.8 | 3.4 | 74.378 | 136.762 | 7.3 | 12.3 |

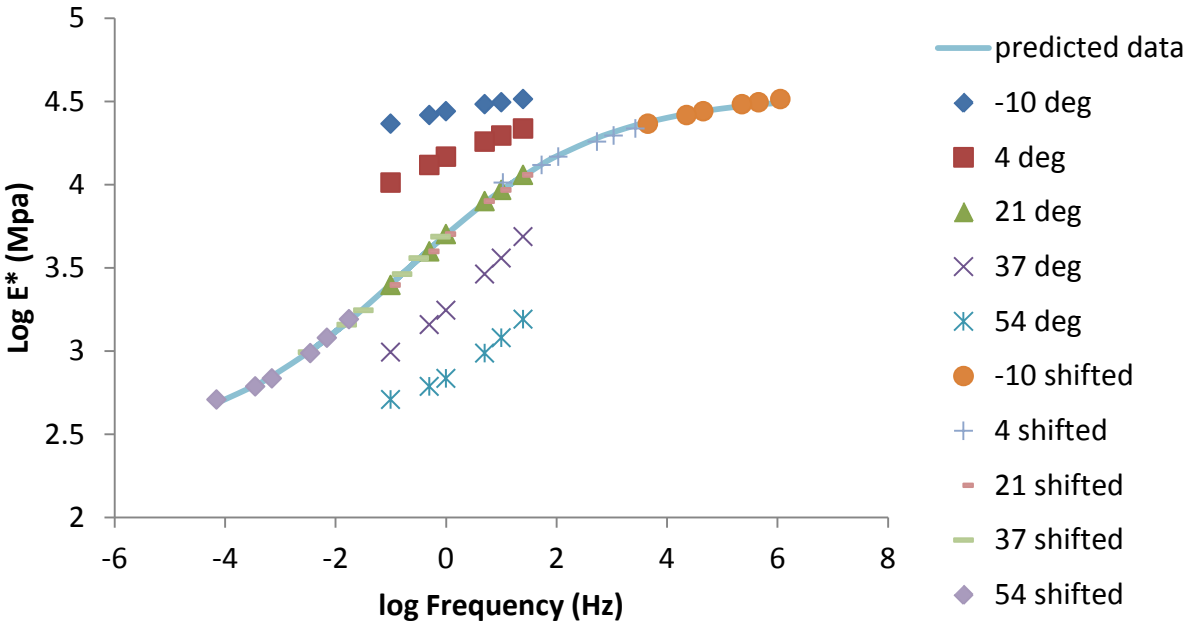


Figure A. 5: Master curve for Sample 3 (SP-III with PG 70-22 binder)

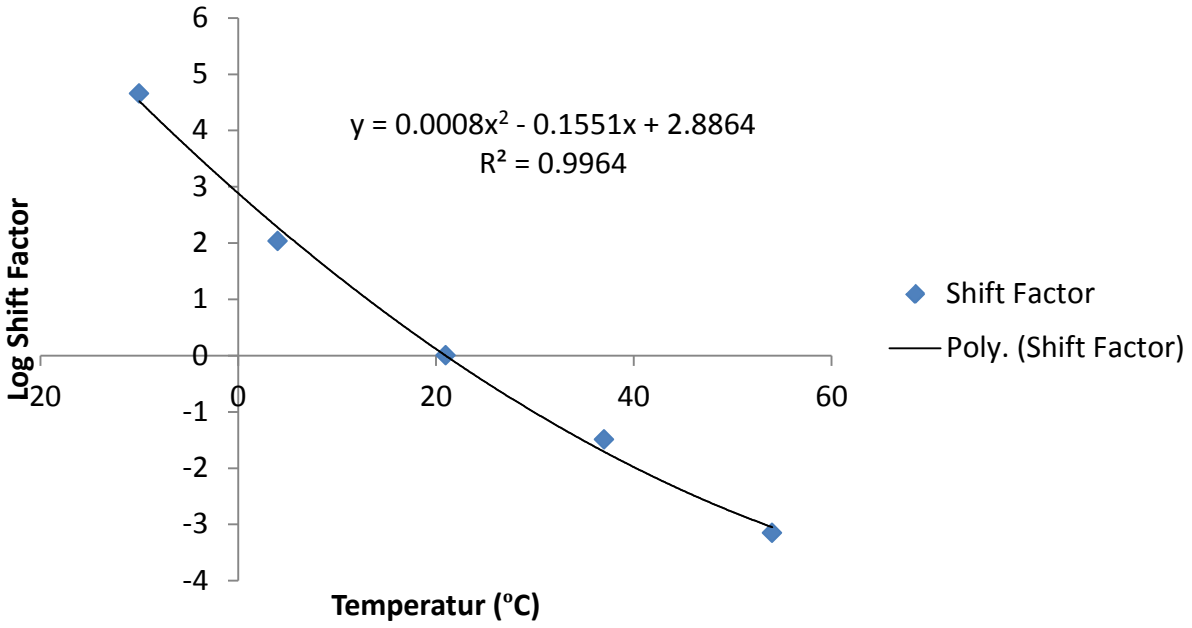


Figure A. 6: Shift factor for Sample 3 (SP-III with PG 70-22 binder)

Table A. 4: E* test results for Sample 4 (SP-III with PG 70-22 binder)

| Temperature | Frequency | Stress | | Dynamic Modulus | Phase Angle | | Strain | | | |
|---|---|---|---|---|---|---|---|---|---|---|
| | | Amplitude (P-P) | SE | | | UC | (P-P) Recoverable | Permanent | SE | UC |
| (deg C) | (Hz) | (kPa) | (%) | (MPa) | (deg) | (deg) | (micro e) | (micro e) | (%) | (%) |
| -10 | 25 | 1682 | 6.3 | 29150.547 | 8.6 | 4.4 | 57.697 | 53.002 | 9.7 | 4.9 |
| -10 | 10 | 1653 | 6.1 | 27856.824 | 7.6 | 2.1 | 59.332 | 12.374 | 8.9 | 1.9 |
| -10 | 5 | 1610 | 4.9 | 27035.098 | 7.3 | 2.2 | 59.544 | 12.917 | 7.4 | 2 |
| -10 | 1 | 1431 | 1.7 | 25229.08 | 8.3 | 2.3 | 56.739 | 11.417 | 6.1 | 4.8 |
| -10 | 0.5 | 1392 | 1 | 23516.889 | 7.8 | 3.4 | 59.182 | 13.598 | 4.9 | 3.2 |
| -10 | 0.1 | 1223 | 0.4 | 21690.828 | 9.3 | 2.8 | 56.405 | 26.508 | 4.7 | 6.8 |
| 4 | 25 | 1119 | 6.5 | 20288.385 | 12.2 | 8.2 | 55.164 | 45.561 | 9.7 | 3.3 |
| 4 | 10 | 1057 | 6.6 | 18643.26 | 12.7 | 3.9 | 56.677 | 2.701 | 9.2 | 0.2 |
| 4 | 5 | 989 | 5.4 | 17597.004 | 13 | 3.8 | 56.224 | 4.165 | 7.8 | 0.1 |
| 4 | 1 | 806 | 2.1 | 15001.527 | 15.8 | 4.4 | 53.741 | 3.156 | 6.2 | 1 |
| 4 | 0.5 | 739 | 1.3 | 13755.886 | 15.3 | 5.4 | 53.688 | 8.705 | 4.9 | 2.2 |
| 4 | 0.1 | 605 | 0.6 | 11377.559 | 18.5 | 3.8 | 53.216 | 38.133 | 5.4 | 6 |
| 21 | 25 | 664 | 6.3 | 12161.355 | 15.6 | 6.1 | 54.566 | 222.559 | 8.4 | 0.6 |
| 21 | 10 | 603 | 6.9 | 10465.024 | 17.9 | 1.4 | 57.588 | 231.192 | 6.5 | 7 |
| 21 | 5 | 518 | 5.6 | 9083.568 | 19.8 | 2.2 | 57.035 | 231.035 | 5.4 | 6.7 |
| 21 | 1 | 353 | 3.2 | 6414.058 | 25 | 3.2 | 55.075 | 203.765 | 4 | 3.8 |
| 21 | 0.5 | 294 | 2.1 | 5228.625 | 27.1 | 3.6 | 56.319 | 203.334 | 3.8 | 4.2 |
| 21 | 0.1 | 198 | 0.7 | 3592.041 | 27.8 | 2.5 | 55.073 | 241.806 | 3.7 | 8.3 |
| 37 | 25 | 423 | 6.7 | 4778.304 | 24.8 | 6.7 | 88.445 | 450.94 | 7 | 18.3 |
| 37 | 10 | 300 | 6.9 | 3759.005 | 26.1 | 2.1 | 79.864 | 471.986 | 4.5 | 11 |
| 37 | 5 | 249 | 4.5 | 2989.541 | 27 | 2 | 83.256 | 471.888 | 3.1 | 10.4 |
| 37 | 1 | 153 | 2.3 | 1782.164 | 29.6 | 2 | 86.067 | 435.573 | 3.6 | 7.7 |
| 37 | 0.5 | 126 | 1.5 | 1429.418 | 30.1 | 2.3 | 87.874 | 428.526 | 3.6 | 6.2 |
| 37 | 0.1 | 85 | 1 | 920.219 | 28.6 | 1.9 | 92.368 | 469.715 | 4.5 | 2.5 |
| 54 | 25 | 120 | 6.1 | 1868.617 | 31.8 | 0.5 | 64.402 | 191.509 | 5.8 | 16.4 |
| 54 | 10 | 95 | 6.2 | 1449.93 | 28.3 | 1.3 | 65.784 | 244.924 | 5.2 | 20.3 |
| 54 | 5 | 76 | 4 | 1208.933 | 27.1 | 0.9 | 62.681 | 259.605 | 5.1 | 20.9 |
| 54 | 1 | 48 | 4.5 | 775.469 | 26.6 | 1.9 | 61.715 | 256.523 | 6 | 22.9 |
| 54 | 0.5 | 42 | 4.4 | 684.54 | 24.7 | 2.1 | 60.869 | 265.624 | 6.4 | 26.9 |
| 54 | 0.1 | 32 | 4.9 | 540.118 | 20.9 | 2.6 | 59.3 | 291.875 | 8.1 | 35.5 |

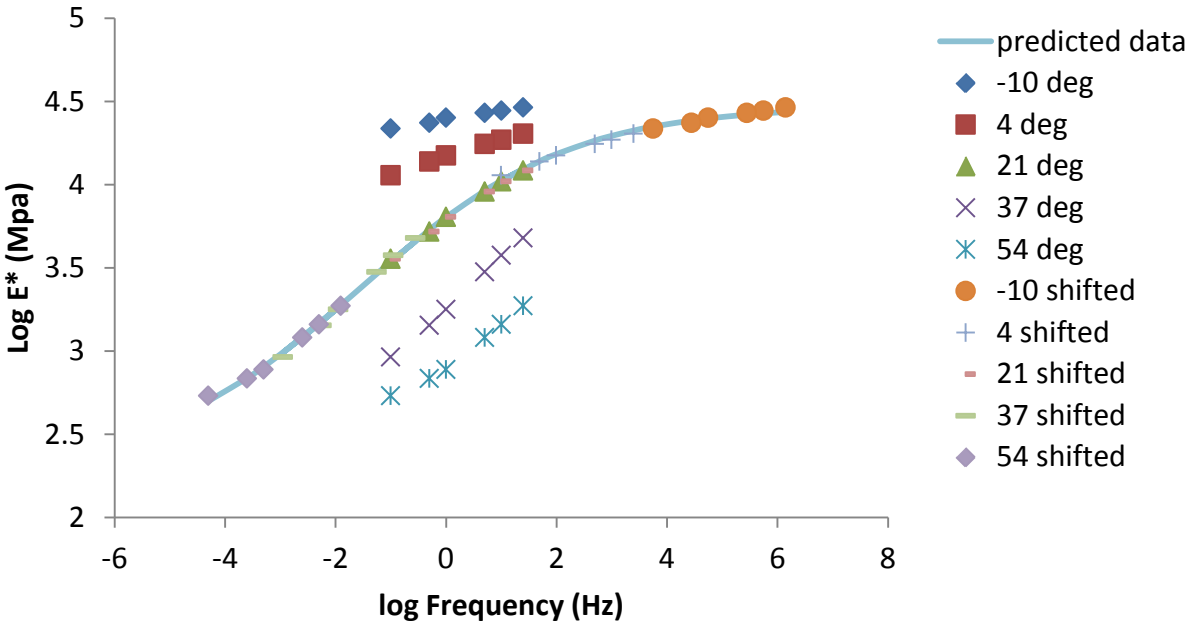


Figure A. 7: Master curve for Sample 4 (SP-III with PG 70-22 binder)

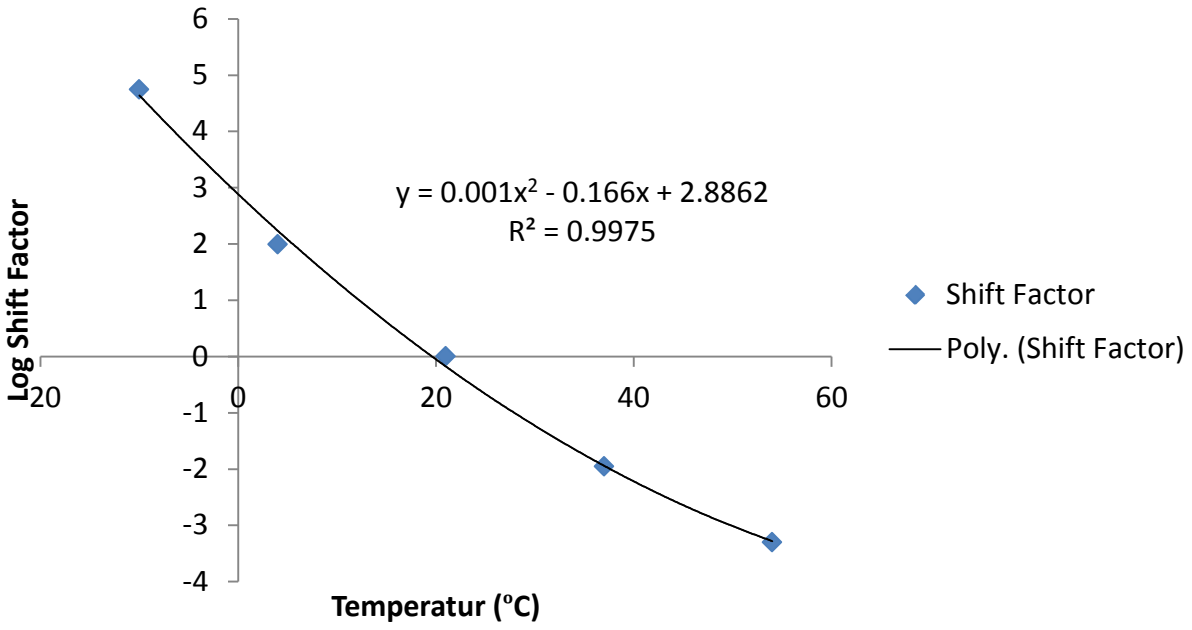


Figure A. 8: Shift factor for Sample 4 (SP-III with PG 70-22 binder)

Table A. 5: E* test results for Sample 5 (SP-III with PG 70-22 binder)

| Temperature | Frequency | Stress | | Dynamic Modulus | Phase Angle | | Strain | | | |
|---|---|---|---|---|---|---|---|---|---|---|
| | | Amplitude (P-P) | SE | | | UC | (P-P) Recoverable | Permanent | SE | UC |
| (deg C) | (Hz) | (kPa) | (%) | (MPa) | (deg) | (deg) | (micro e) | (micro e) | (%) | (%) |
| -10 | 25 | 1494 | 6.4 | 25315.043 | 7.4 | 0.9 | 59.025 | 39.872 | 12 | 4.9 |
| -10 | 10 | 1416 | 5.6 | 24060.75 | 5.6 | 0.2 | 58.851 | 8.067 | 9.8 | 4.7 |
| -10 | 5 | 1372 | 3.7 | 23369.6 | 5.4 | 0.1 | 58.702 | 7.018 | 8.3 | 4.6 |
| -10 | 1 | 1251 | 0.9 | 21594.982 | 6.2 | 0.2 | 57.938 | 8.517 | 5.5 | 4.4 |
| -10 | 0.5 | 1197 | 0.6 | 20879.859 | 6.4 | 0.8 | 57.35 | 7.775 | 5.2 | 2.9 |
| -10 | 0.1 | 1097 | 0.5 | 18319.586 | 7.6 | 0.2 | 59.897 | 23.579 | 4.7 | 4.8 |
| 4 | 25 | 914 | 6.3 | 15974.339 | 10.3 | 5.3 | 57.21 | 60.447 | 8.5 | 7.2 |
| 4 | 10 | 867 | 5.6 | 14368.625 | 10.1 | 0.5 | 60.358 | 52.587 | 9.1 | 6.7 |
| 4 | 5 | 823 | 4.1 | 13518.951 | 10.5 | 0.7 | 60.895 | 53.558 | 5.4 | 6.5 |
| 4 | 1 | 713 | 1.2 | 11344.43 | 12.1 | 0.3 | 62.886 | 51.313 | 3.2 | 5.4 |
| 4 | 0.5 | 623 | 0.9 | 10407.276 | 12.4 | 0.9 | 59.89 | 53.826 | 2.8 | 5.1 |
| 4 | 0.1 | 507 | 1.4 | 8478.356 | 15.9 | 0.3 | 59.839 | 91.809 | 3.1 | 1.1 |
| 21 | 25 | 490 | 6.5 | 9337.947 | 16.6 | 0.5 | 52.454 | 150.836 | 5.9 | 3.9 |
| 21 | 10 | 414 | 7.6 | 8265.17 | 16.4 | 0.5 | 50.11 | 167.021 | 5.6 | 5.2 |
| 21 | 5 | 356 | 6.9 | 7214.462 | 17.5 | 0.6 | 49.373 | 166.349 | 4.8 | 6.6 |
| 21 | 1 | 246 | 2.8 | 4920.59 | 20.7 | 1.3 | 50.089 | 149.907 | 3.1 | 9.5 |
| 21 | 0.5 | 206 | 1.9 | 4180.631 | 21.9 | 1.5 | 49.206 | 149.801 | 2.7 | 9.9 |
| 21 | 0.1 | 137 | 0.9 | 2827.762 | 23.9 | 1.4 | 48.58 | 180.482 | 2.9 | 10.4 |
| 37 | 25 | 219 | 5.4 | 3985.028 | 24.7 | 4.6 | 55.029 | 182.812 | 7.7 | 17.3 |
| 37 | 10 | 175 | 4 | 3164.449 | 24.5 | 0.2 | 55.332 | 199.029 | 5.8 | 19.1 |
| 37 | 5 | 147 | 3.8 | 2562.399 | 25.4 | 0.4 | 57.199 | 186.981 | 5.7 | 16.2 |
| 37 | 1 | 78 | 3.9 | 1472.059 | 28.8 | 1.3 | 52.757 | 140.493 | 6.8 | 24.2 |
| 37 | 0.5 | 87 | 4 | 1208.22 | 28.8 | 4.1 | 71.701 | 153.393 | 6.3 | 36.9 |
| 37 | 0.1 | 55 | 8.2 | 728.453 | 27.2 | 4.8 | 75.081 | 204.161 | 7.8 | 41.9 |
| 54 | 25 | 85 | 6.3 | 1314.608 | 29.5 | 1.2 | 64.726 | 202.678 | 6.1 | 5.2 |
| 54 | 10 | 69 | 5 | 1006.376 | 26.2 | 1.7 | 68.112 | 249.421 | 5.2 | 8.6 |
| 54 | 5 | 53 | 4.4 | 802.425 | 24.8 | 1.9 | 66.21 | 265.086 | 5.1 | 10.6 |
| 54 | 1 | 35 | 2.9 | 508.68 | 22 | 2.7 | 69.49 | 268.458 | 4.7 | 13.7 |
| 54 | 0.5 | 29 | 3 | 442.619 | 20.1 | 2.7 | 66.195 | 273.282 | 5.1 | 11.7 |
| 54 | 0.1 | 22 | 2.9 | 347.756 | 15.7 | 2.5 | 64.531 | 297.461 | 5.7 | 9.5 |

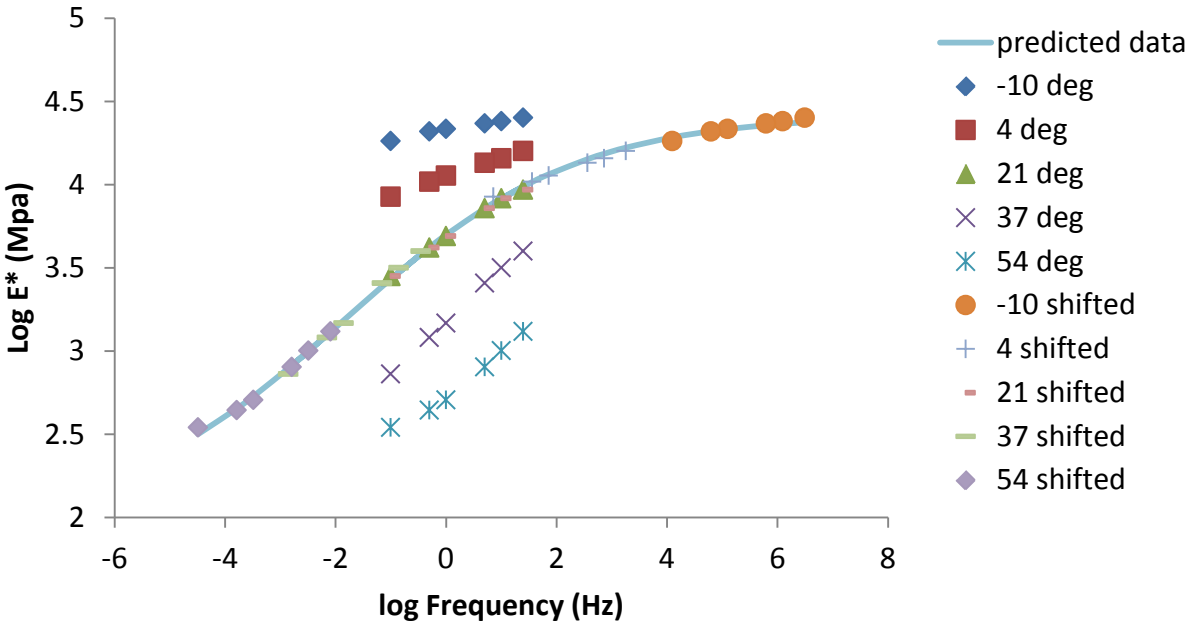


Figure A. 9: Master curve for Sample 5 (SP-III with PG 70-22 binder)

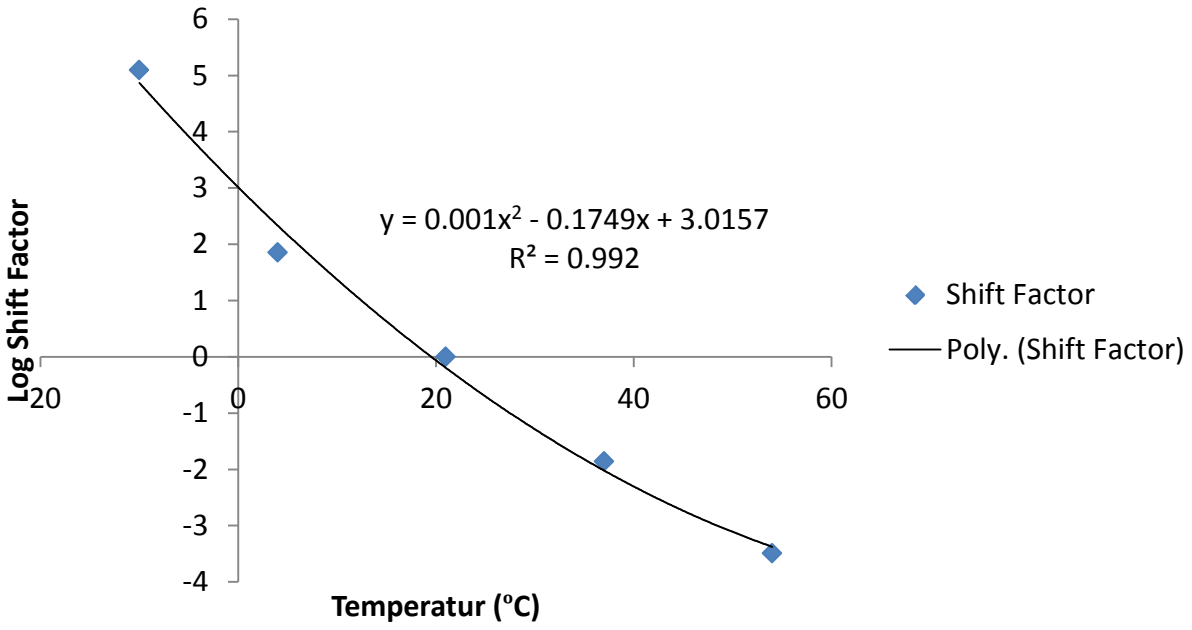


Figure A. 10: Shift factor for Sample 5 (SP-III with PG 70-22 binder)

Table A. 6: E* test results for Sample 6 (SP-III with PG 70-22 binder)

| Temperature | Frequency | Stress | | Dynamic Modulus | Phase Angle | | Strain | | | |
|---|---|---|---|---|---|---|---|---|---|---|
| | | Amplitude (P-P) | SE | | | UC | (P-P) Recoverable | Permanent | SE | UC |
| (deg C) | (Hz) | (kPa) | (%) | (MPa) | (deg) | (deg) | (micro e) | (micro e) | (%) | (%) |
| -10 | 25 | 1332 | 6.2 | 23431.807 | 10.5 | 0 | 56.859 | 38.507 | 6.2 | 12.7 |
| -10 | 10 | 1350 | 6.1 | 23077.113 | 7.9 | 0.9 | 58.484 | 2.989 | 5.7 | 12.7 |
| -10 | 5 | 1330 | 5.1 | 22279.92 | 7.7 | 1.1 | 59.693 | 1.3 | 5.1 | 12.6 |
| -10 | 1 | 1178 | 2 | 20731.375 | 8.5 | 1.2 | 56.84 | 0.988 | 3.7 | 10.4 |
| -10 | 0.5 | 1087 | 1.2 | 19385.332 | 8.6 | 1.7 | 56.072 | 1.904 | 3.9 | 12.7 |
| -10 | 0.1 | 1027 | 0.5 | 18065 | 9.3 | 1.3 | 56.861 | 13.22 | 3.9 | 11.4 |
| 4 | 25 | 1151 | 6.4 | 16503.855 | 13.5 | 3 | 69.717 | 101.957 | 6.3 | 40.3 |
| 4 | 10 | 1109 | 6.3 | 15632.985 | 11.4 | 3 | 70.955 | 51.629 | 5.7 | 41.4 |
| 4 | 5 | 1044 | 5.1 | 14492.424 | 12.4 | 3.3 | 72.034 | 48.558 | 5 | 41 |
| 4 | 1 | 838 | 2.1 | 12192.285 | 14.7 | 4.4 | 68.736 | 43.977 | 3.2 | 38.7 |
| 4 | 0.5 | 787 | 1.4 | 10998.2 | 15 | 5.4 | 71.518 | 49.394 | 3 | 39 |
| 4 | 0.1 | 634 | 0.6 | 9135.794 | 17.4 | 4.5 | 69.427 | 90.786 | 2.8 | 39.7 |
| 21 | 25 | 591 | 6.8 | 8439.486 | 19.3 | 1.3 | 70.074 | 207.386 | 7.2 | 17.5 |
| 21 | 10 | 537 | 7.3 | 7494.641 | 17 | 1 | 71.633 | 222.707 | 4.4 | 19 |
| 21 | 5 | 461 | 6.2 | 6494.875 | 18.3 | 0.8 | 70.994 | 216.123 | 4.6 | 19.3 |
| 21 | 1 | 299 | 3.4 | 4248.157 | 22.1 | 1.5 | 70.267 | 184.139 | 5.1 | 21.8 |
| 21 | 0.5 | 247 | 1.7 | 3431.381 | 24 | 1 | 71.892 | 177.453 | 3.4 | 19.4 |
| 21 | 0.1 | 158 | 0.7 | 2222.786 | 25.4 | 2.8 | 71.039 | 216.052 | 3.4 | 21.2 |
| 37 | 25 | 308 | 6.8 | 4248.188 | 25.4 | 1.7 | 72.595 | 245.525 | 5.4 | 18.1 |
| 37 | 10 | 249 | 5.5 | 3167.497 | 24.9 | 1 | 78.68 | 258.544 | 3.4 | 14.7 |
| 37 | 5 | 188 | 4.1 | 2512.946 | 26.4 | 1.7 | 74.825 | 250.028 | 2.6 | 14.5 |
| 37 | 1 | 103 | 2.1 | 1454.584 | 28.6 | 0.8 | 70.905 | 221.532 | 3.2 | 24.9 |
| 37 | 0.5 | 81 | 1.4 | 1161.21 | 28.7 | 0.4 | 70.178 | 219.39 | 3.4 | 29.6 |
| 37 | 0.1 | 49 | 1.6 | 745.322 | 27.1 | 0 | 65.909 | 245.547 | 3.7 | 38.6 |
| 54 | 25 | 121 | 7.1 | 1501.398 | 30.1 | 3.2 | 80.647 | 120.697 | 6.6 | 16.6 |
| 54 | 10 | 94 | 5.9 | 1156.913 | 27 | 2.4 | 81.46 | 155.73 | 5.9 | 11.9 |
| 54 | 5 | 77 | 5.8 | 928.563 | 25.6 | 2.7 | 82.397 | 157.843 | 5.4 | 10.4 |
| 54 | 1 | 49 | 4 | 574.108 | 23.2 | 2.5 | 84.768 | 155.05 | 5.2 | 8.8 |
| 54 | 0.5 | 43 | 4.1 | 495.56 | 20.9 | 2.4 | 85.784 | 161.4 | 6.9 | 8.1 |
| 54 | 0.1 | 32 | 4.9 | 371.193 | 17.3 | 2.4 | 84.903 | 192.221 | 6.9 | 3.4 |

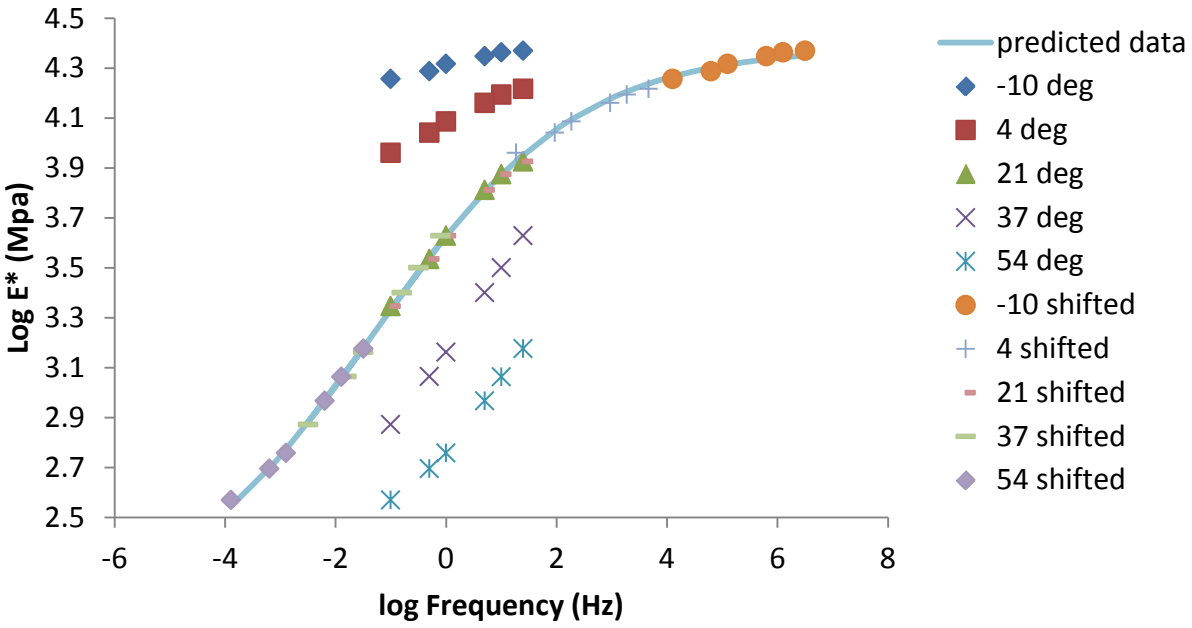


Figure A. 11: Master curve for Sample 6 (SP-III with PG 70-22 binder)

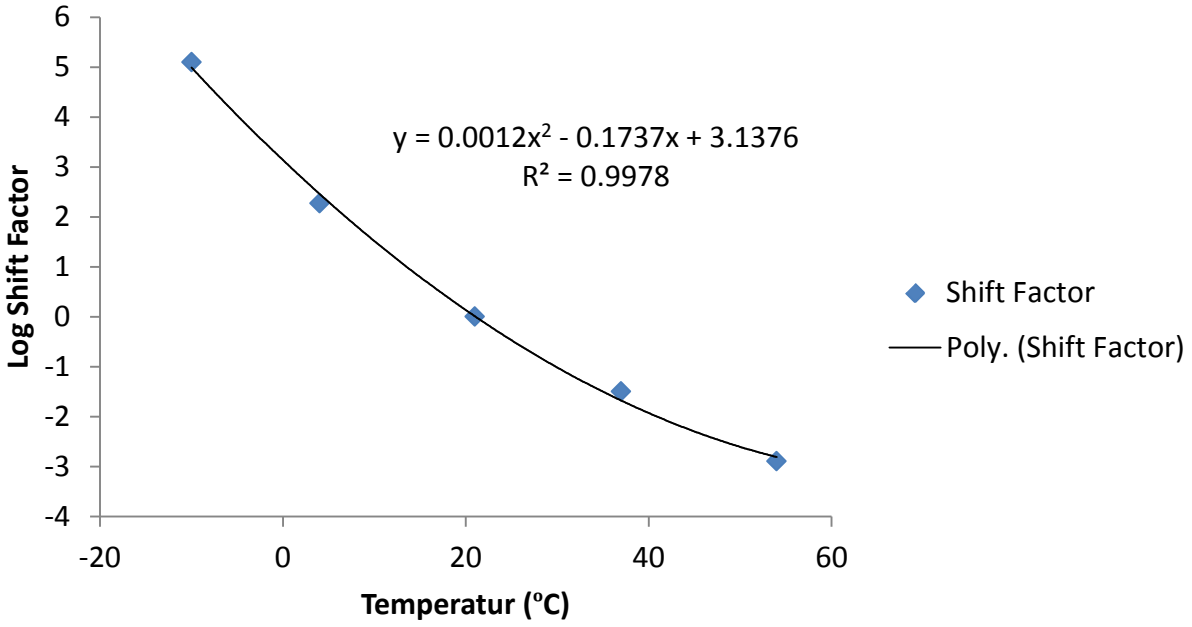


Figure A. 12: Shift factor for Sample 6 (SP-III with PG 70-22 binder)

# APPENDIX B

DYNAMIC MODULUS TEST RESULTS FOR SP-III WITH PG 64-22 BINDER

Table B. 1: E* test results for Sample 1 (SP-III with PG 64-22 binder)

| Temperature | Frequency | Stress | | Dynamic Modulus | Phase Angle | | Strain | | | |
|---|---|---|---|---|---|---|---|---|---|---|
| | | Amplitude (P-P) | SE | | | UC | (P-P) Recoverable | Permanent | SE | UC |
| (deg C) | (Hz) | (kPa) | (%) | (MPa) | (deg) | (deg) | (micro e) | (micro e) | (%) | (%) |
| -10 | 25 | 1692 | 5.4 | 31337.896 | 8.7 | 0 | 53.978 | 51.805 | 9 | 16.1 |
| -10 | 10 | 1646 | 5.5 | 30917.109 | 6.3 | 1.7 | 53.232 | 16.918 | 6.8 | 18.4 |
| -10 | 5 | 1599 | 4.4 | 30069.268 | 6.3 | 1.3 | 53.173 | 17.994 | 9.4 | 19.3 |
| -10 | 1 | 1426 | 1.1 | 27965.736 | 7.4 | 3.1 | 51.005 | 19.13 | 6.4 | 18.6 |
| -10 | 0.5 | 1387 | 0.6 | 27021.791 | 8.1 | 3.8 | 51.343 | 21.677 | 5.5 | 20.3 |
| -10 | 0.1 | 1221 | 0.4 | 24568.281 | 8.3 | 1.9 | 49.689 | 34.553 | 6.3 | 20 |
| 4 | 25 | 1114 | 6.3 | 19062.848 | 15.7 | 0.4 | 58.43 | 69.156 | 9.9 | 8.1 |
| 4 | 10 | 1137 | 7 | 19328.514 | 9.1 | 0.5 | 58.829 | 46.958 | 8.2 | 8.1 |
| 4 | 5 | 1071 | 5.8 | 18027.525 | 9.7 | 0 | 59.402 | 49.703 | 6.6 | 5.5 |
| 4 | 1 | 874 | 2.1 | 15269.101 | 11.3 | 0.3 | 57.25 | 49.216 | 3.7 | 3.5 |
| 4 | 0.5 | 794 | 1.3 | 14043.222 | 12.1 | 1.2 | 56.574 | 54.39 | 2.6 | 2.4 |
| 4 | 0.1 | 642 | 0.7 | 11343.323 | 15.3 | 0.1 | 56.627 | 92.254 | 3.4 | 3.7 |
| 21 | 25 | 656 | 7.8 | 9663.283 | 21.5 | 2.2 | 67.886 | 303.004 | 13 | 17.7 |
| 21 | 10 | 580 | 8.3 | 9486.148 | 17.2 | 1.5 | 61.158 | 390.839 | 8.7 | 18.6 |
| 21 | 5 | 500 | 6.9 | 8529.991 | 18.5 | 1.2 | 58.575 | 442.694 | 7.2 | 15.7 |
| 21 | 1 | 347 | 3.8 | 6125.399 | 23.1 | 1.9 | 56.72 | 447.293 | 5.3 | 9.9 |
| 21 | 0.5 | 281 | 2 | 5094.076 | 25.2 | 1.4 | 55.103 | 472.697 | 5.5 | 1.6 |
| 21 | 0.1 | 192 | 0.9 | 3413.253 | 28 | 3.3 | 56.376 | 552.326 | 5.3 | 9.3 |
| 37 | 25 | 259 | 7.6 | 4714.375 | 34.1 | 7.9 | 54.851 | 347.461 | 11 | 17.5 |
| 37 | 10 | 227 | 7.4 | 3945.555 | 26.7 | 1.5 | 57.447 | 535.292 | 6.2 | 7.9 |
| 37 | 5 | 184 | 6.2 | 3177.973 | 27.7 | 2 | 57.814 | 610.915 | 5.2 | 8.2 |
| 37 | 1 | 108 | 2.9 | 1807.236 | 29.8 | 4.8 | 59.605 | 608.898 | 3.7 | 4.1 |
| 37 | 0.5 | 86 | 2.1 | 1431.4 | 29.6 | 5.4 | 59.951 | 626.89 | 3.7 | 9.7 |
| 37 | 0.1 | 52 | 1.6 | 851.621 | 27.3 | 6.2 | 60.775 | 676.02 | 2.9 | 23.7 |
| 54 | 25 | 106 | 6.5 | 1777.092 | 33.4 | 10.3 | 59.382 | 168.863 | 7.2 | 29.5 |
| 54 | 10 | 82 | 5.7 | 1315.882 | 30.6 | 3.2 | 62.524 | 267.143 | 5.8 | 19.9 |
| 54 | 5 | 65 | 4.7 | 1023.748 | 29.1 | 4.3 | 63.5 | 303.366 | 5.6 | 12.7 |
| 54 | 1 | 45 | 2.3 | 580.03 | 26.1 | 6.4 | 76.893 | 312.06 | 3.8 | 9.3 |
| 54 | 0.5 | 40 | 2.3 | 489.127 | 23.9 | 6.1 | 81.084 | 329.09 | 6 | 15.8 |
| 54 | 0.1 | 37 | 1.7 | 369.198 | 17.9 | 4.3 | 100.621 | 399.629 | 7.7 | 25.3 |

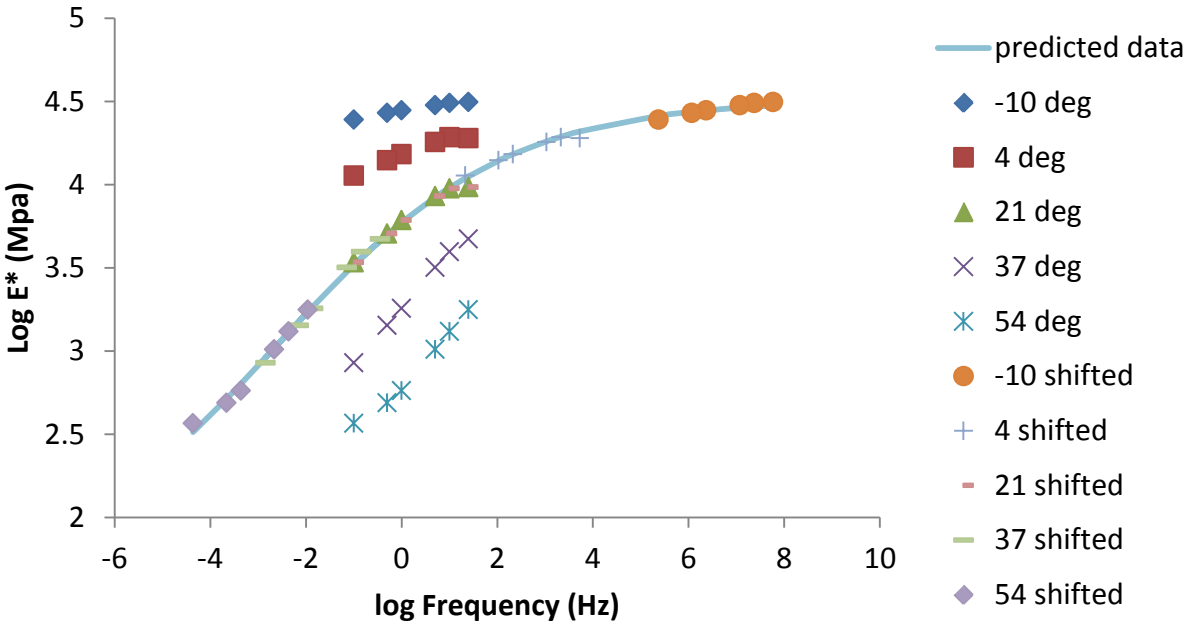


Figure B. 1: Master curve for Sample 1 (SP-III with PG 64-22 binder)

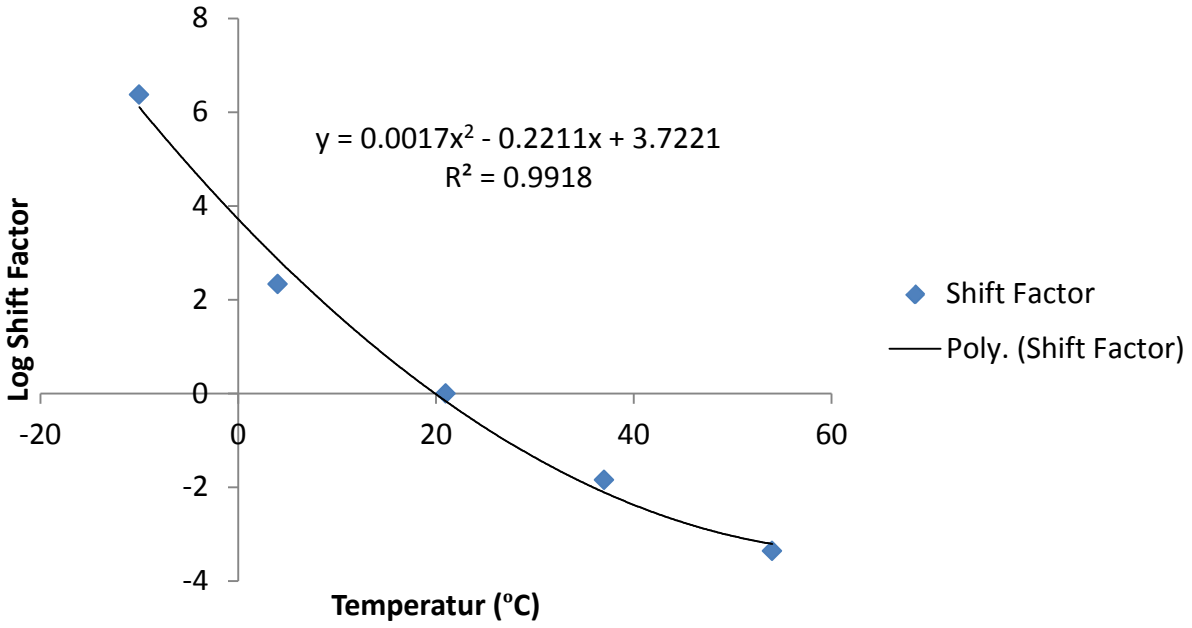


Figure B. 2: Shift factor for Sample 1 (SP-III with PG 64-22 binder)

Table B. 2: E* test results for Sample 2 (SP-III with PG 64-22 binder)

| Temperature | Frequency | Stress | | Dynamic Modulus | Phase Angle | | Strain | | | |
|---|---|---|---|---|---|---|---|---|---|---|
| | | Amplitude (P-P) | SE | | | UC | (P-P) Recoverable | Permanent | SE | UC |
| (deg C) | (Hz) | (kPa) | (%) | (MPa) | (deg) | (deg) | (micro e) | (micro e) | (%) | (%) |
| -10 | 25 | 1684 | 6.1 | 39516.027 | 8.9 | 0.4 | 42.61 | 37.892 | 8.1 | 21.3 |
| -10 | 10 | 1636 | 6.9 | 39410.977 | 5.5 | 0.4 | 41.512 | 11.03 | 7.6 | 23.2 |
| -10 | 5 | 1589 | 5.1 | 38824.109 | 4.7 | 0.1 | 40.929 | 12.448 | 7.1 | 23.1 |
| -10 | 1 | 1424 | 1.4 | 34941.195 | 7.1 | 0.8 | 40.746 | 13.37 | 5.5 | 24 |
| -10 | 0.5 | 1387 | 0.8 | 34042.211 | 6.8 | 0 | 40.75 | 15.708 | 6.8 | 22.6 |
| -10 | 0.1 | 1218 | 0.5 | 31414.158 | 7 | 0 | 38.766 | 23.558 | 6.7 | 24.9 |
| 4 | 25 | 1506 | 6.2 | 24130.764 | 12.2 | 2.7 | 62.427 | 93.1 | 8.9 | 21.6 |
| 4 | 10 | 1449 | 7.2 | 22428.479 | 9.3 | 0.1 | 64.608 | 44.845 | 8.5 | 12.9 |
| 4 | 5 | 1356 | 5.6 | 20991.328 | 9.7 | 0.5 | 64.589 | 45.512 | 6.4 | 13.2 |
| 4 | 1 | 1144 | 1.9 | 17791.613 | 11.2 | 0 | 64.308 | 45.277 | 4.5 | 13.2 |
| 4 | 0.5 | 1065 | 1.1 | 16397.324 | 12.3 | 0.5 | 64.972 | 51.53 | 3 | 10.1 |
| 4 | 0.1 | 838 | 0.5 | 13484.795 | 14.6 | 0.6 | 62.139 | 88.915 | 3.5 | 8.3 |
| 21 | 25 | 664 | 6.7 | 11463.028 | 22.7 | 6.9 | 57.959 | 210.758 | 11 | 23.7 |
| 21 | 10 | 578 | 6.9 | 11011.873 | 17.3 | 1 | 52.475 | 265.408 | 6.7 | 33.4 |
| 21 | 5 | 500 | 5.9 | 9854.926 | 17.9 | 0.6 | 50.765 | 299.03 | 6.4 | 33.5 |
| 21 | 1 | 348 | 3 | 7012.647 | 21.8 | 1.9 | 49.695 | 298.292 | 5.3 | 36.7 |
| 21 | 0.5 | 282 | 2 | 5800.085 | 24.3 | 0.4 | 48.667 | 317.822 | 5.1 | 36.5 |
| 21 | 0.1 | 194 | 0.7 | 3820.879 | 26.8 | 1.5 | 50.789 | 394.336 | 3.8 | 39 |
| 37 | 25 | 320 | 7.7 | 5212.354 | 31.8 | 14.9 | 61.46 | 363.564 | 15 | 30.3 |
| 37 | 10 | 275 | 6.6 | 4033.591 | 26.5 | 3.4 | 68.189 | 522.086 | 8.3 | 45.5 |
| 37 | 5 | 228 | 5.4 | 3302.319 | 27.8 | 3 | 68.925 | 588.309 | 7.8 | 45.2 |
| 37 | 1 | 135 | 2.5 | 1894.822 | 30.3 | 3.9 | 71.114 | 573.641 | 5.8 | 47.7 |
| 37 | 0.5 | 107 | 1.6 | 1494.127 | 30.6 | 3.7 | 71.339 | 585.409 | 4.9 | 49.3 |
| 37 | 0.1 | 65 | 1 | 898.829 | 28.8 | 2.3 | 71.922 | 625.897 | 4.8 | 53.6 |
| 54 | 25 | 112 | 7.1 | 1852.333 | 45.5 | 25.5 | 60.432 | 255.664 | 14 | 9.3 |
| 54 | 10 | 80 | 6.6 | 1358.079 | 32.2 | 7.3 | 59.113 | 348.747 | 8.9 | 19 |
| 54 | 5 | 61 | 5.3 | 1034.453 | 31.1 | 7.5 | 59.117 | 377.314 | 9.1 | 24.8 |
| 54 | 1 | 34 | 3.1 | 564.193 | 27.3 | 8.6 | 59.62 | 366.493 | 8.8 | 46.2 |
| 54 | 0.5 | 28 | 3.3 | 471.387 | 23.6 | 8.5 | 59.281 | 373.442 | 13 | 57.9 |
| 54 | 0.1 | 23 | 2.5 | 318.732 | 19 | 4.8 | 71.133 | 410.3 | 7.3 | 68.8 |

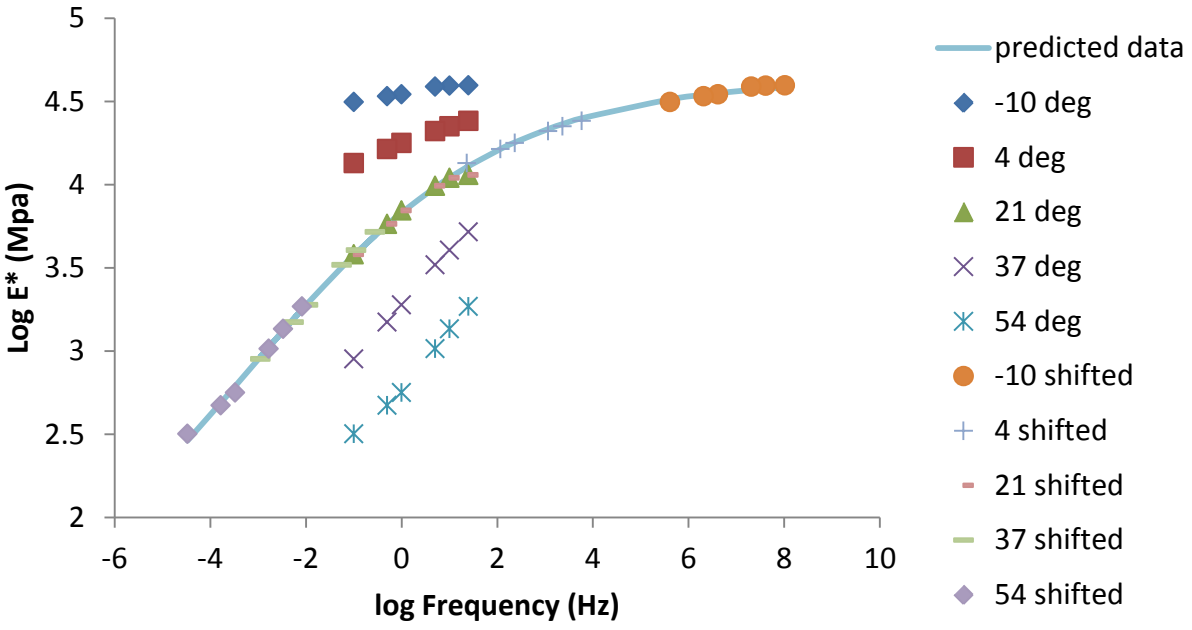


Figure B. 3: Master curve for sample 2 (SP-III with PG 64-22 binder)

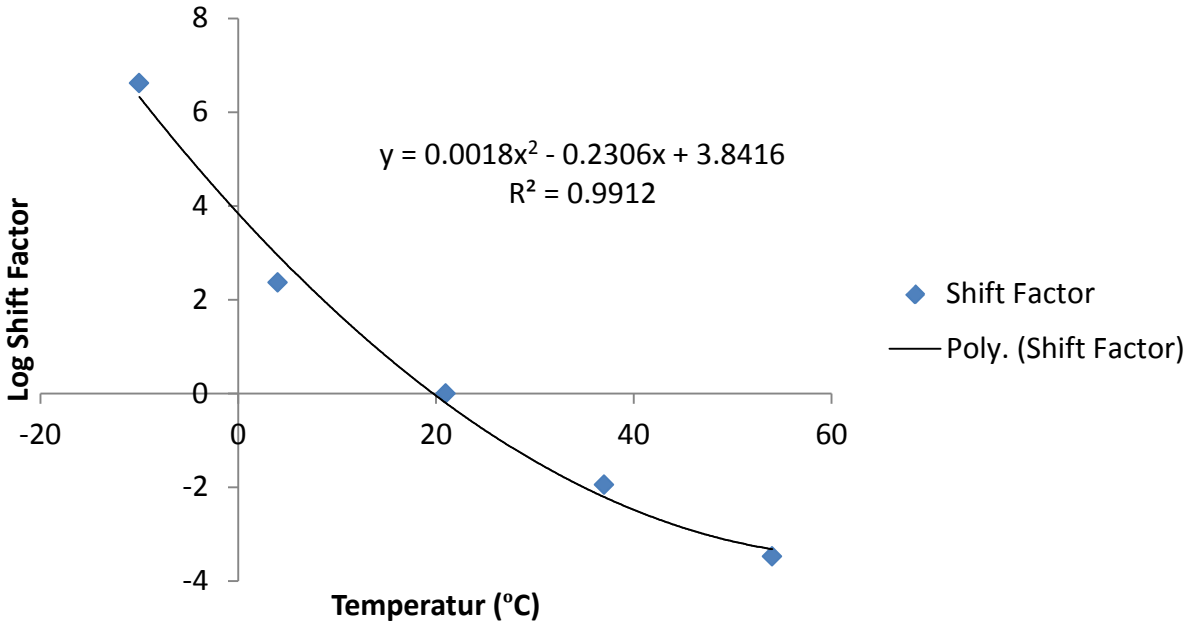


Figure B. 4: Shift factor for sample 2 (SP-III with PG 64-22 binder)

Table B. 3: E* test results for Sample 3 (SP-III with PG 64-22 binder)

| Temperature | Frequency | Stress | | Dynamic Modulus | Phase Angle | | Strain | | | |
|---|---|---|---|---|---|---|---|---|---|---|
| | | Amplitude (P-P) | SE | | | UC | (P-P) Recoverable | Permanent | SE | UC |
| (deg C) | (Hz) | (kPa) | (%) | (MPa) | (deg) | (deg) | (micro e) | (micro e) | (%) | (%) |
| -10 | 25 | 1429 | 6.8 | 24301.539 | 4.9 | 2.7 | 58.805 | 52.445 | 8.3 | 24.8 |
| -10 | 10 | 1442 | 7.3 | 22754.941 | 5.4 | 0.7 | 63.351 | 20.351 | 8.5 | 18.8 |
| -10 | 5 | 1408 | 5.8 | 22090.209 | 4.7 | 0.2 | 63.748 | 22.041 | 8.7 | 19.2 |
| -10 | 1 | 1266 | 1.8 | 20305.637 | 4.8 | 0 | 62.338 | 22.718 | 5.6 | 18.3 |
| -10 | 0.5 | 1189 | 1.1 | 19241.973 | 5.3 | 0.1 | 61.774 | 24.801 | 4.7 | 16.4 |
| -10 | 0.1 | 1080 | 0.5 | 17721.838 | 7.8 | 0.9 | 60.927 | 41.729 | 6.1 | 18 |
| 4 | 25 | 953 | 8.1 | 18866.928 | 10.8 | 6.4 | 50.497 | 50.451 | 17 | 16.4 |
| 4 | 10 | 927 | 7.9 | 18478.998 | 10.4 | 1.5 | 50.186 | 40.853 | 12 | 25.8 |
| 4 | 5 | 882 | 6.7 | 17472.617 | 10.8 | 1.5 | 50.488 | 42.111 | 11 | 27.3 |
| 4 | 1 | 752 | 2.7 | 15062.924 | 12.4 | 0.9 | 49.931 | 41.418 | 9.4 | 24.9 |
| 4 | 0.5 | 691 | 1.7 | 13657.909 | 15.1 | 1.8 | 50.627 | 47.003 | 7.7 | 25 |
| 4 | 0.1 | 621 | 0.6 | 10957.547 | 17.4 | 2.4 | 56.712 | 89.554 | 6.7 | 22.5 |
| 21 | 25 | 857 | 7.8 | 10678.063 | 20.1 | 3 | 80.218 | 444.809 | 11 | 38.6 |
| 21 | 10 | 727 | 8.2 | 9272.583 | 18.4 | 0.8 | 78.391 | 466.628 | 8.6 | 24 |
| 21 | 5 | 630 | 7.6 | 8148.166 | 19.2 | 0.6 | 77.258 | 489.383 | 7.7 | 21.7 |
| 21 | 1 | 415 | 4.5 | 5614.063 | 24.4 | 0.9 | 73.875 | 457.89 | 4.6 | 18.6 |
| 21 | 0.5 | 349 | 3.2 | 4731.282 | 26.3 | 1.3 | 73.801 | 465.705 | 4 | 17.2 |
| 21 | 0.1 | 226 | 1.2 | 3025.313 | 28.6 | 1.9 | 74.771 | 530.577 | 3.2 | 17.7 |
| 37 | 25 | 254 | 9.9 | 4981.711 | 35.9 | 14.4 | 50.901 | 303.246 | 14 | 41.6 |
| 37 | 10 | 215 | 9.8 | 3732.825 | 28.4 | 3.1 | 57.608 | 369.513 | 8.5 | 21.2 |
| 37 | 5 | 186 | 9.2 | 2988.708 | 29.6 | 3.7 | 62.213 | 376.951 | 8.2 | 20.1 |
| 37 | 1 | 126 | 5.9 | 1644.457 | 32.4 | 4.2 | 76.579 | 344.634 | 6.4 | 20 |
| 37 | 0.5 | 106 | 4.2 | 1283.537 | 32.8 | 4.1 | 82.532 | 349.247 | 4.7 | 20.9 |
| 37 | 0.1 | 73 | 1.6 | 782.056 | 30.5 | 4.3 | 93.949 | 414.95 | 3.8 | 18.8 |
| 54 | 25 | 82 | 9.7 | 1578.961 | 33.7 | 2.5 | 51.729 | 119.921 | 8.5 | 0.3 |
| 54 | 10 | 67 | 8.6 | 1193.614 | 29.8 | 1.7 | 56.399 | 177.158 | 6.3 | 2.5 |
| 54 | 5 | 57 | 8.1 | 948.844 | 28.5 | 1.9 | 59.672 | 198.294 | 5.9 | 4 |
| 54 | 1 | 36 | 5.7 | 580.198 | 26.3 | 2.5 | 62.144 | 197.478 | 5 | 5.9 |
| 54 | 0.5 | 32 | 4.5 | 500.923 | 23.6 | 1.9 | 62.954 | 204.956 | 5 | 6.4 |
| 54 | 0.1 | 24 | 2 | 364.013 | 19.8 | 1.4 | 67.084 | 234.518 | 5.3 | 11.8 |

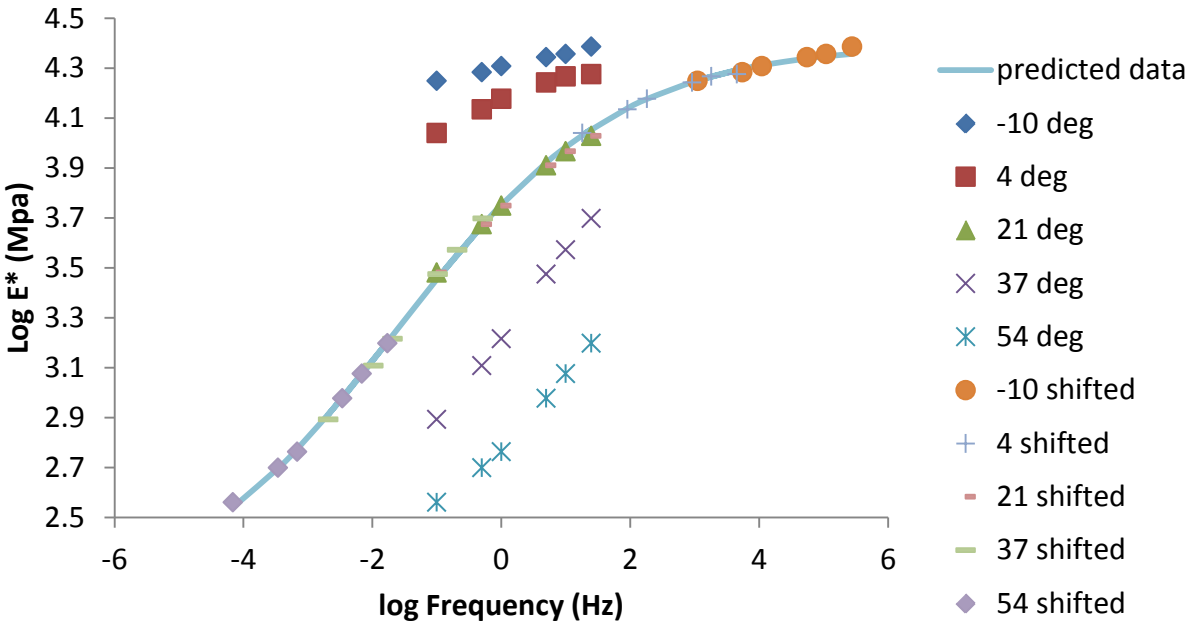


Figure B. 5: Master curve for sample 3 (SP-III with PG 64-22 binder)

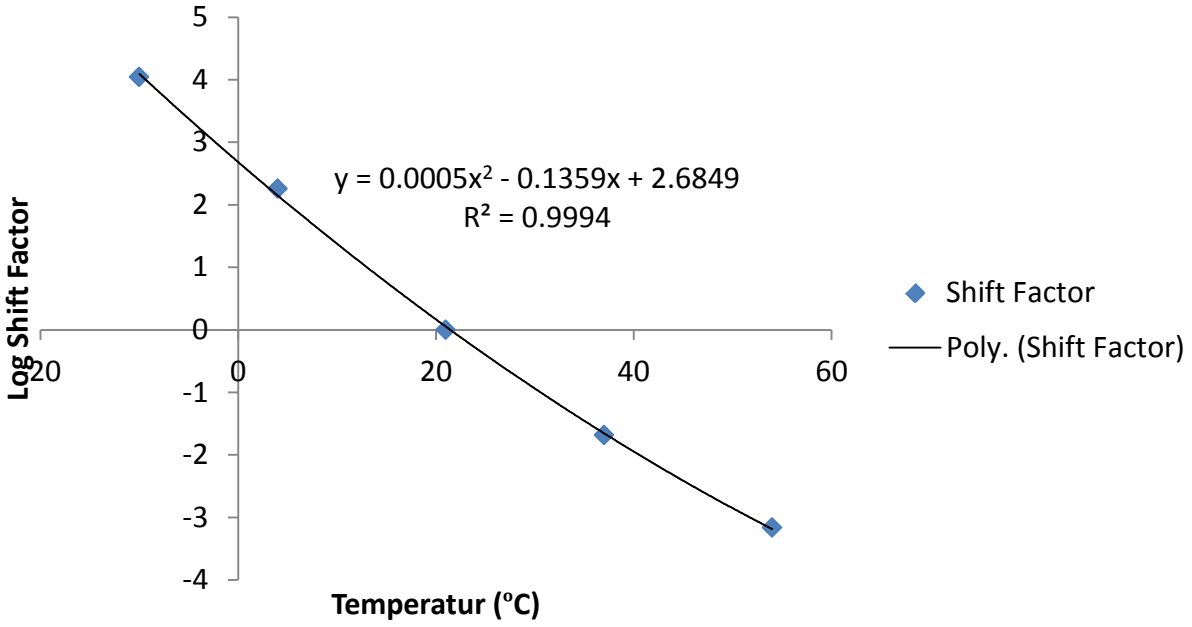


Figure B. 6: Shift factor for sample 3 (SP-III with PG 64-22 binder)

Table B. 4: E* test results for Sample 4 (SP-III with PG 64-22 binder)

| Temperature | Frequency | Stress | | Dynamic Modulus | Phase Angle | | Strain | | | |
|---|---|---|---|---|---|---|---|---|---|---|
| | | Amplitude (P-P) | SE | | | UC | (P-P) Recoverable | Permanent | SE | UC |
| (deg C) | (Hz) | (kPa) | (%) | (MPa) | (deg) | (deg) | (micro e) | (micro e) | (%) | (%) |
| -10 | 25 | 2187 | 6.6 | 28456.047 | 5.5 | 0.5 | 76.859 | 62.24 | 8.3 | 20.1 |
| -10 | 10 | 2177 | 6.4 | 28372.594 | 5.2 | 0.8 | 76.717 | 2.745 | 6.5 | 1.5 |
| -10 | 5 | 2102 | 5.2 | 27799.273 | 4.8 | 0.7 | 75.63 | 4.019 | 6.1 | 1.4 |
| -10 | 1 | 1878 | 1.8 | 25733.543 | 4.5 | 0.7 | 72.976 | 0.97 | 6.6 | 1.5 |
| -10 | 0.5 | 1796 | 1 | 25433.66 | 6.7 | 1.3 | 70.598 | 2.879 | 9 | 0.8 |
| -10 | 0.1 | 1681 | 0.4 | 22739.225 | 6.6 | 0.7 | 73.925 | 16.537 | 5.1 | 2.1 |
| 4 | 25 | 1520 | 7.8 | 22645.568 | 10.3 | 2.6 | 67.135 | 91.752 | 8.9 | 6.5 |
| 4 | 10 | 1481 | 8 | 21738.816 | 8 | 0.6 | 68.125 | 40.728 | 9.1 | 8.4 |
| 4 | 5 | 1418 | 6.8 | 20769.295 | 8.4 | 0.3 | 68.295 | 41.186 | 7 | 9.1 |
| 4 | 1 | 1207 | 3 | 17927.912 | 10.5 | 1 | 67.348 | 40.327 | 11 | 10.3 |
| 4 | 0.5 | 1106 | 1.9 | 17511.275 | 10.2 | 0.4 | 63.156 | 45.375 | 6.7 | 14 |
| 4 | 0.1 | 994 | 0.6 | 13964.575 | 12.4 | 0.6 | 71.148 | 83.804 | 4.7 | 13 |
| 21 | 25 | 863 | 8.9 | 13227.816 | 12.9 | 4.4 | 65.274 | 201.785 | 16 | 51.6 |
| 21 | 10 | 728 | 8.3 | 12289.354 | 15.3 | 0.2 | 59.264 | 186.334 | 7.3 | 25.4 |
| 21 | 5 | 629 | 7.7 | 11166.761 | 16 | 0.6 | 56.302 | 190.617 | 8.5 | 21.3 |
| 21 | 1 | 432 | 4.3 | 7879.575 | 19.8 | 0.9 | 54.794 | 168.735 | 5 | 13.2 |
| 21 | 0.5 | 381 | 2.8 | 7059.471 | 21.9 | 0.3 | 54.012 | 171.617 | 5.2 | 7.2 |
| 21 | 0.1 | 302 | 1.6 | 4674.593 | 24.2 | 0.4 | 64.687 | 249.973 | 4.6 | 2 |
| 37 | 25 | 375 | 9.3 | 6440.611 | 17.6 | 17.8 | 58.249 | 282.743 | 27 | 63.6 |
| 37 | 10 | 320 | 11 | 5783.175 | 24.4 | 0.4 | 55.292 | 393.382 | 8.9 | 35 |
| 37 | 5 | 273 | 8.4 | 4508.117 | 25.9 | 0.7 | 60.568 | 439.345 | 7.2 | 27.4 |
| 37 | 1 | 183 | 4.9 | 2673.577 | 29.5 | 0.8 | 68.273 | 425.222 | 4.7 | 24.1 |
| 37 | 0.5 | 151 | 3.3 | 2097.048 | 30 | 1.1 | 72.095 | 432.399 | 4.1 | 22.3 |
| 37 | 0.1 | 112 | 2 | 1232.507 | 28.9 | 1.5 | 90.821 | 509.339 | 4 | 20.2 |
| 54 | 25 | 138 | 9 | 2241.489 | 36.1 | 7.8 | 61.533 | 276.176 | 12 | 11.9 |
| 54 | 10 | 120 | 11 | 1633.508 | 32.6 | 3.8 | 73.189 | 435.834 | 8.7 | 26.5 |
| 54 | 5 | 96 | 9.8 | 1244.183 | 31.5 | 3.5 | 77.034 | 511.597 | 7.9 | 24.4 |
| 54 | 1 | 65 | 7 | 719.161 | 28.8 | 2.6 | 90.103 | 538.588 | 7.7 | 29.2 |
| 54 | 0.5 | 58 | 5.3 | 595.869 | 26.3 | 2.7 | 98.107 | 564.89 | 8 | 27 |
| 54 | 0.1 | 46 | 2.4 | 415.15 | 20.7 | 2.3 | 111.389 | 633.451 | 7.5 | 28.8 |

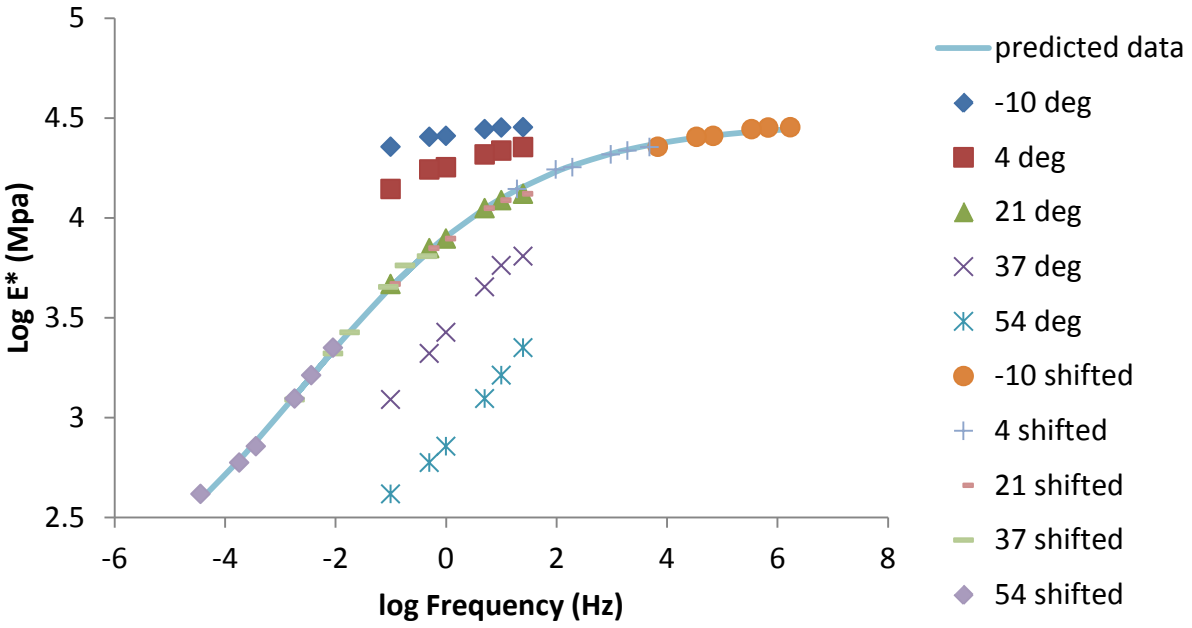


Figure B. 7: Master curve for sample 4 (SP-III with PG 64-22 binder)

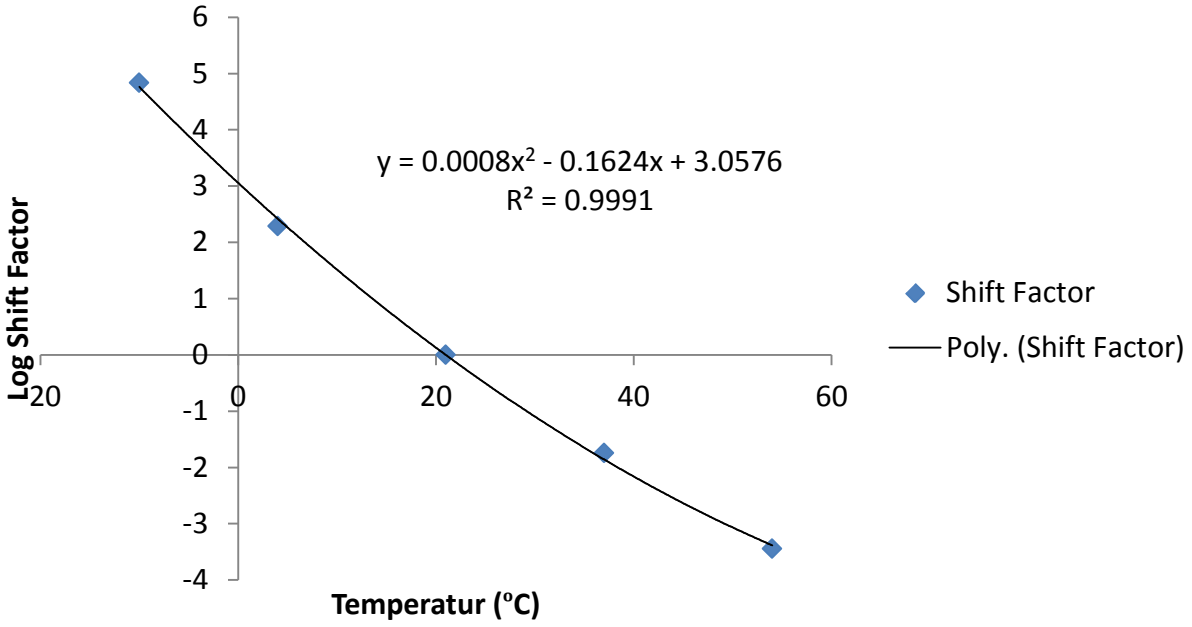


Figure B. 8: Shift factor for sample 4 (SP-III with PG 64-22 binder)

Table B. 5: E* test results for Sample 5 (SP-III with PG 64-22 binder)

| Temperature | Frequency | Stress | | Dynamic Modulus | Phase Angle | | Strain | | | |
|---|---|---|---|---|---|---|---|---|---|---|
| | | Amplitude (P-P) | SE | | | UC | (P-P) Recoverable | Permanent | SE | UC |
| (deg C) | (Hz) | (kPa) | (%) | (MPa) | (deg) | (deg) | (micro e) | (micro e) | (%) | (%) |
| -10 | 25 | 2192 | 6.4 | 38748.406 | 1.9 | 1.9 | 56.563 | 52.91 | 12 | 14.3 |
| -10 | 10 | 2176 | 5.8 | 36853.953 | 4.4 | 0.4 | 59.036 | 9.812 | 9.2 | 19.8 |
| -10 | 5 | 2097 | 4.7 | 35965.59 | 4.3 | 0.4 | 58.292 | 9.775 | 8.3 | 19.6 |
| -10 | 1 | 1874 | 1.4 | 34554.699 | 2.6 | 1.9 | 54.238 | 8.273 | 10 | 23.7 |
| -10 | 0.5 | 1794 | 0.8 | 31582.086 | 5.3 | 0.3 | 56.803 | 9.792 | 8.9 | 20.3 |
| -10 | 0.1 | 1680 | 0.4 | 29829.203 | 7.3 | 1 | 56.322 | 16.376 | 11 | 23.6 |
| 4 | 25 | 1524 | 7.5 | 26037.035 | 8.9 | 0.4 | 58.539 | 73.61 | 8.4 | 3.3 |
| 4 | 10 | 1483 | 7.6 | 26481.822 | 8 | 0.2 | 56.007 | 33.148 | 9.3 | 2 |
| 4 | 5 | 1417 | 6.3 | 25162.861 | 7.6 | 0.5 | 56.331 | 32.932 | 7.7 | 2.6 |
| 4 | 1 | 1205 | 2.7 | 22245.033 | 8.6 | 0.2 | 54.156 | 32.577 | 8.6 | 4.3 |
| 4 | 0.5 | 1104 | 1.7 | 19868.914 | 10 | 0 | 55.565 | 36.347 | 5.4 | 3.1 |
| 4 | 0.1 | 994 | 0.6 | 17175.463 | 13.1 | 0.2 | 57.85 | 65.689 | 6.6 | 7 |
| 21 | 25 | 862 | 8.2 | 14808.646 | 14.3 | 1.5 | 58.219 | 172.062 | 8.3 | 19.7 |
| 21 | 10 | 722 | 8.6 | 13637.328 | 16.1 | 0.2 | 52.962 | 166.569 | 8.8 | 35.8 |
| 21 | 5 | 628 | 7.9 | 12292.71 | 16.9 | 0.1 | 51.053 | 170.177 | 7.9 | 35.8 |
| 21 | 1 | 432 | 4.5 | 8902.611 | 21 | 0.2 | 48.521 | 158.188 | 5.1 | 35.6 |
| 21 | 0.5 | 383 | 3 | 7830.484 | 23.9 | 1.6 | 48.887 | 166.822 | 3.9 | 40.5 |
| 21 | 0.1 | 303 | 1.5 | 5199.132 | 25 | 0.9 | 58.201 | 239.084 | 5.8 | 40.2 |
| 37 | 25 | 373 | 10 | 7385.051 | 25.9 | 6 | 50.51 | 342.779 | 9.3 | 2.4 |
| 37 | 10 | 319 | 11 | 5762.308 | 24.6 | 1.1 | 55.29 | 467.933 | 7.9 | 14.9 |
| 37 | 5 | 268 | 8.6 | 4475.339 | 26.1 | 1 | 59.975 | 526.967 | 6.9 | 22.4 |
| 37 | 1 | 183 | 4.8 | 2584.46 | 28.9 | 1.2 | 70.854 | 529.718 | 4.7 | 30.5 |
| 37 | 0.5 | 152 | 3.2 | 2058.192 | 28.9 | 1.6 | 73.648 | 547.601 | 3.8 | 31.5 |
| 37 | 0.1 | 113 | 1.6 | 1262.099 | 26.8 | 1.3 | 89.684 | 631.441 | 4.9 | 30.3 |
| 54 | 25 | 136 | 8.4 | 2066.465 | 33.2 | 9.3 | 65.925 | 415.987 | 7.1 | 18.2 |
| 54 | 10 | 120 | 7.6 | 1559.874 | 31.4 | 0.8 | 77.222 | 620.206 | 4.5 | 28.1 |
| 54 | 5 | 96 | 7.1 | 1174.072 | 30.6 | 1.5 | 82.168 | 709.648 | 4 | 30.6 |
| 54 | 1 | 65 | 5.2 | 659.145 | 28.6 | 2.6 | 98.148 | 734.073 | 4.3 | 30 |
| 54 | 0.5 | 59 | 3.8 | 539.239 | 26.4 | 3.4 | 108.816 | 767.766 | 5.2 | 26.9 |
| 54 | 0.1 | 46 | 1.7 | 366.955 | 21.3 | 3.9 | 125.853 | 855.931 | 7.6 | 19 |

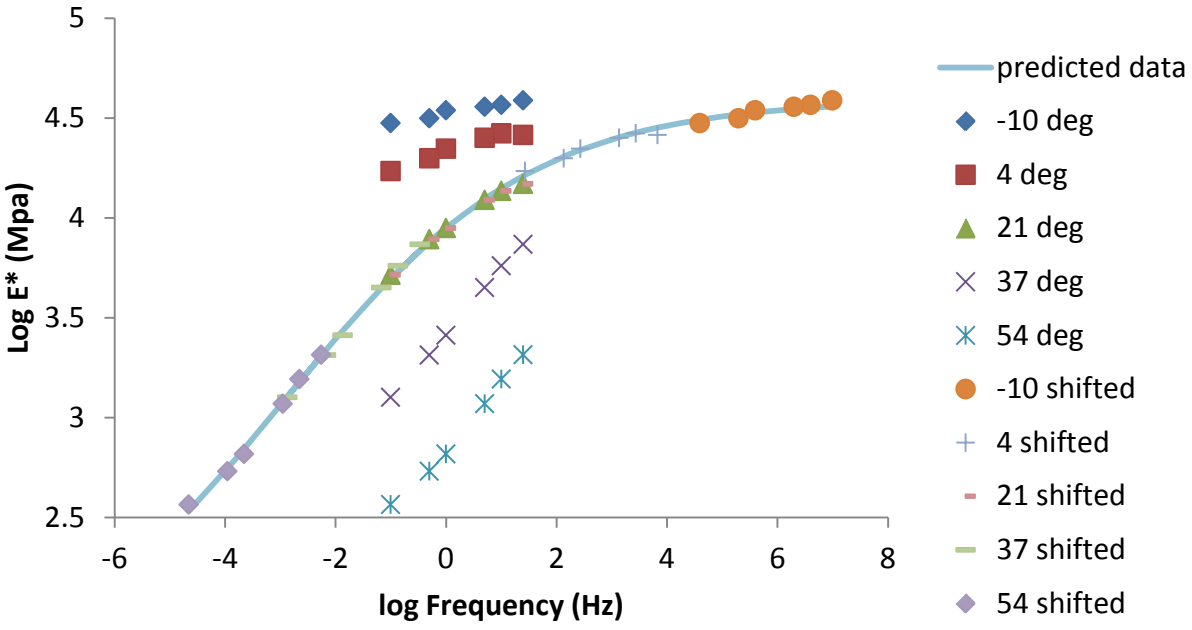


Figure B. 9: Master curve for sample 5 (SP-III with PG 64-22 binder)

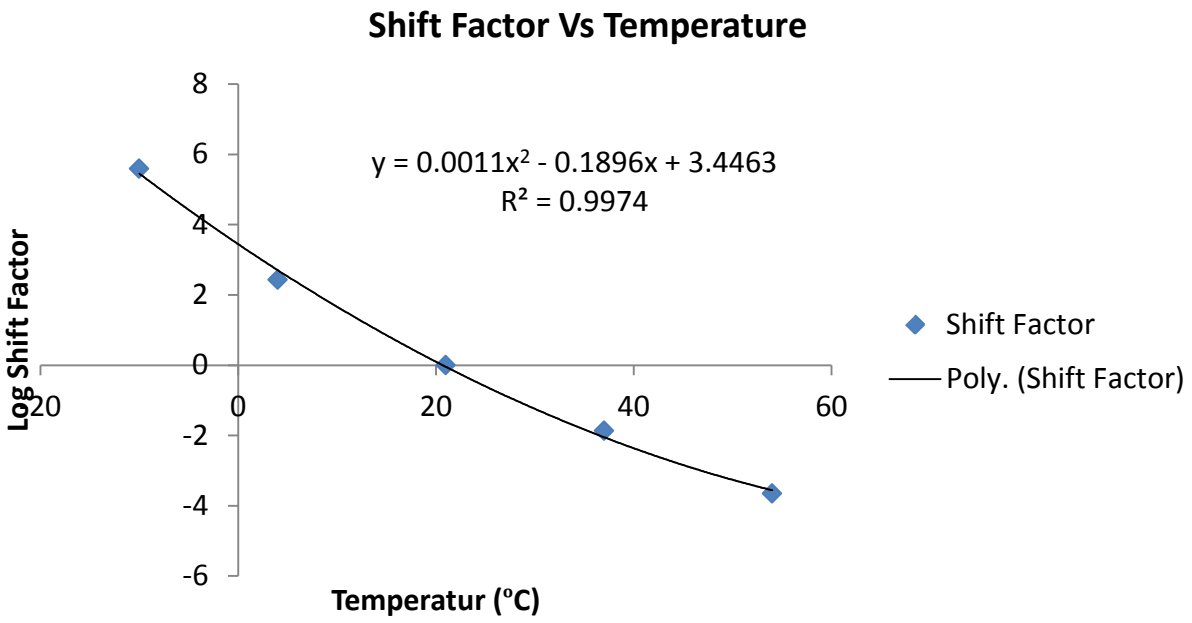


Figure B. 10: Shift factor for sample 5 (SP-III with PG 64-22 binder)

Table B. 6: E* test results for Sample 6 (SP-III with PG 64-22 binder)

| Temperature | Frequency | Stress | | Dynamic Modulus | Phase Angle | | Strain | | | |
|---|---|---|---|---|---|---|---|---|---|---|
| | | Amplitude (P-P) | SE | | | UC | (P-P) Recoverable | Permanent | SE | UC |
| (deg C) | (Hz) | (kPa) | (%) | (MPa) | (deg) | (deg) | (micro e) | (micro e) | (%) | (%) |
| -10 | 25 | 1684 | 6.1 | 39516.027 | 8.9 | 0.4 | 42.61 | 37.892 | 8.1 | 21.3 |
| -10 | 10 | 1636 | 6.9 | 39410.977 | 5.5 | 0.4 | 41.512 | 11.03 | 7.6 | 23.2 |
| -10 | 5 | 1589 | 5.1 | 38824.109 | 4.7 | 0.1 | 40.929 | 12.448 | 7.1 | 23.1 |
| -10 | 1 | 1424 | 1.4 | 34941.195 | 7.1 | 0.8 | 40.746 | 13.37 | 5.5 | 24 |
| -10 | 0.5 | 1387 | 0.8 | 34042.211 | 6.8 | 0 | 40.75 | 15.708 | 6.8 | 22.6 |
| -10 | 0.1 | 1218 | 0.5 | 31414.158 | 7 | 0 | 38.766 | 23.558 | 6.7 | 24.9 |
| 4 | 25 | 1506 | 6.2 | 24130.764 | 12.2 | 2.7 | 62.427 | 93.1 | 8.9 | 21.6 |
| 4 | 10 | 1449 | 7.2 | 22428.479 | 9.3 | 0.1 | 64.608 | 44.845 | 8.5 | 12.9 |
| 4 | 5 | 1356 | 5.6 | 20991.328 | 9.7 | 0.5 | 64.589 | 45.512 | 6.4 | 13.2 |
| 4 | 1 | 1144 | 1.9 | 17791.613 | 11.2 | 0 | 64.308 | 45.277 | 4.5 | 13.2 |
| 4 | 0.5 | 1065 | 1.1 | 16397.324 | 12.3 | 0.5 | 64.972 | 51.53 | 3 | 10.1 |
| 4 | 0.1 | 838 | 0.5 | 13484.795 | 14.6 | 0.6 | 62.139 | 88.915 | 3.5 | 8.3 |
| 21 | 25 | 664 | 6.7 | 11463.028 | 22.7 | 6.9 | 57.959 | 210.758 | 11 | 23.7 |
| 21 | 10 | 578 | 6.9 | 11011.873 | 17.3 | 1 | 52.475 | 265.408 | 6.7 | 33.4 |
| 21 | 5 | 500 | 5.9 | 9854.926 | 17.9 | 0.6 | 50.765 | 299.03 | 6.4 | 33.5 |
| 21 | 1 | 348 | 3 | 7012.647 | 21.8 | 1.9 | 49.695 | 298.292 | 5.3 | 36.7 |
| 21 | 0.5 | 282 | 2 | 5800.085 | 24.3 | 0.4 | 48.667 | 317.822 | 5.1 | 36.5 |
| 21 | 0.1 | 194 | 0.7 | 3820.879 | 26.8 | 1.5 | 50.789 | 394.336 | 3.8 | 39 |
| 37 | 25 | 320 | 7.7 | 5212.354 | 31.8 | 14.9 | 61.46 | 363.564 | 15 | 30.3 |
| 37 | 10 | 275 | 6.6 | 4033.591 | 26.5 | 3.4 | 68.189 | 522.086 | 8.3 | 45.5 |
| 37 | 5 | 228 | 5.4 | 3302.319 | 27.8 | 3 | 68.925 | 588.309 | 7.8 | 45.2 |
| 37 | 1 | 135 | 2.5 | 1894.822 | 30.3 | 3.9 | 71.114 | 573.641 | 5.8 | 47.7 |
| 37 | 0.5 | 107 | 1.6 | 1494.127 | 30.6 | 3.7 | 71.339 | 585.409 | 4.9 | 49.3 |
| 37 | 0.1 | 65 | 1 | 898.829 | 28.8 | 2.3 | 71.922 | 625.897 | 4.8 | 53.6 |
| 54 | 25 | 112 | 7.1 | 1852.333 | 45.5 | 25.5 | 60.432 | 255.664 | 14 | 9.3 |
| 54 | 10 | 80 | 6.6 | 1358.079 | 32.2 | 7.3 | 59.113 | 348.747 | 8.9 | 19 |
| 54 | 5 | 61 | 5.3 | 1034.453 | 31.1 | 7.5 | 59.117 | 377.314 | 9.1 | 24.8 |
| 54 | 1 | 34 | 3.1 | 564.193 | 27.3 | 8.6 | 59.62 | 366.493 | 8.8 | 46.2 |
| 54 | 0.5 | 28 | 3.3 | 471.387 | 23.6 | 8.5 | 59.281 | 373.442 | 13 | 57.9 |
| 54 | 0.1 | 23 | 2.5 | 318.732 | 19 | 4.8 | 71.133 | 410.3 | 7.3 | 68.8 |

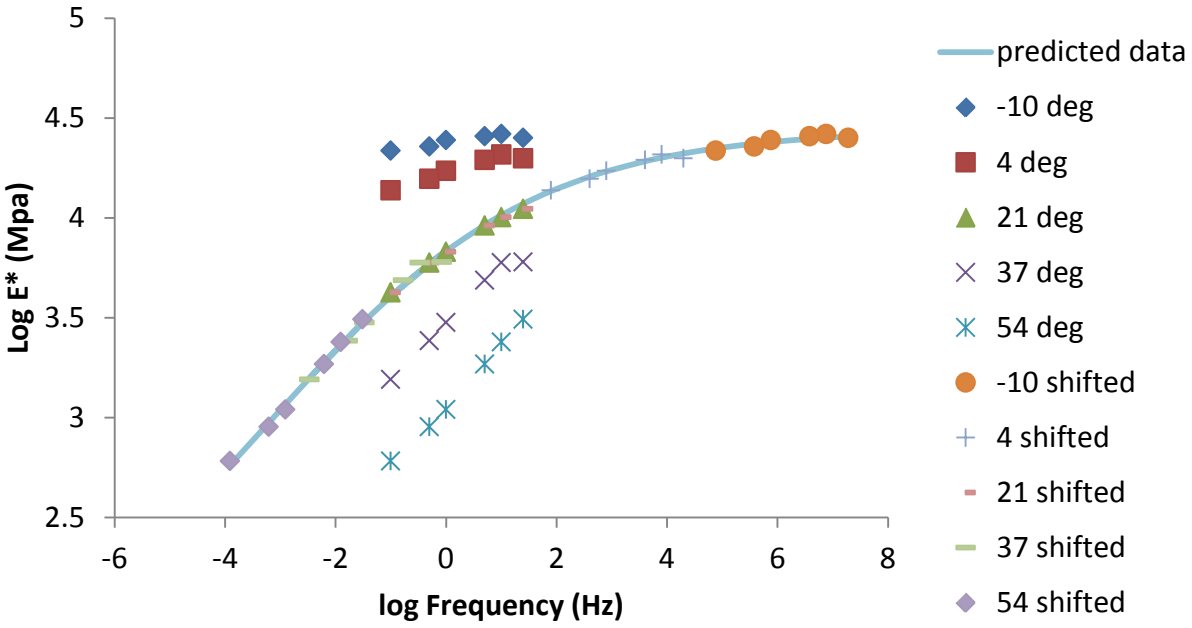


Figure B. 11: Master curve for sample 6 (SP-III with PG 64-22 binder)

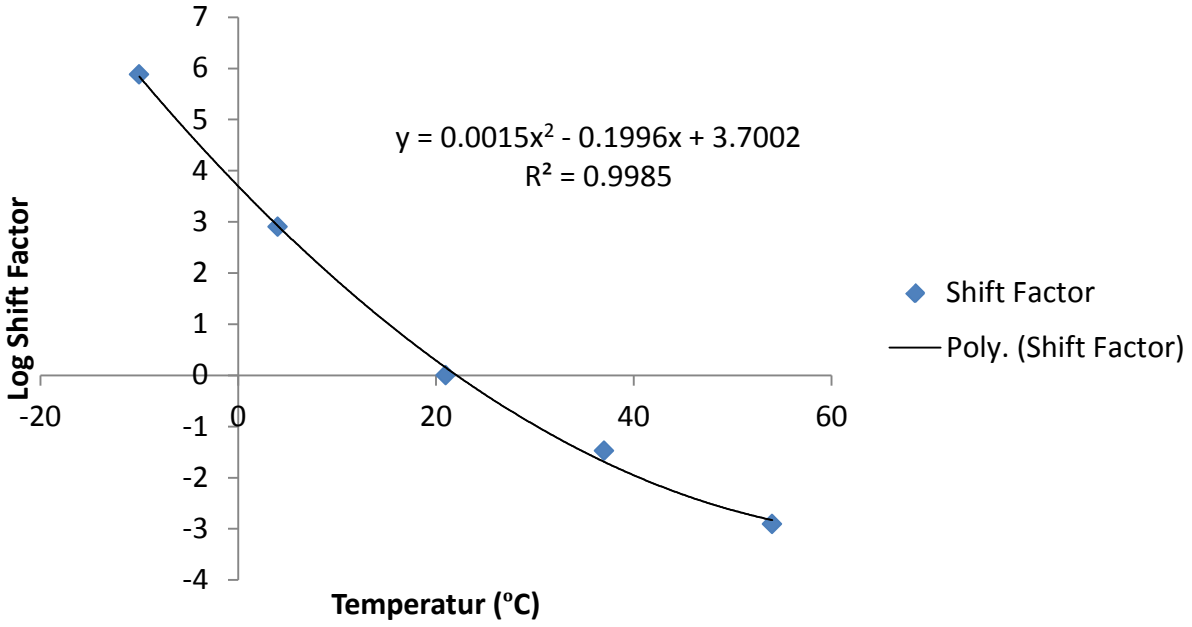


Figure B. 12: Shift factor for sample 6 (SP-III with PG 64-22 binder)

# APPENDIX C

DYNAMIC MODULUS TEST RESULTS FOR SP-II WITH PG 64-22 BINDER

**Table C. 1: E* test results for Sample 1 (SP-II with PG 64-22 binder)**

| Temperature | Frequency | Stress | | Dynamic Modulus | Phase Angle | | Strain | | | |
|---|---|---|---|---|---|---|---|---|---|---|
| | | Amplitude (P-P) | SE | | | UC | (P-P) Recoverable | Permanent | SE | UC |
| (deg C) | (Hz) | (kPa) | (%) | (MPa) | (deg) | (deg) | (micro e) | (micro e) | (%) | (%) |
| -10 | 25 | 2078 | 5.6 | 35496.758 | 7.3 | 1.3 | 58.541 | 56.55 | 8.5 | 36.2 |
| -10 | 10 | 2042 | 5.6 | 33913.875 | 5.4 | 2.1 | 60.222 | 13.497 | 7.7 | 34 |
| -10 | 5 | 1982 | 4.7 | 32930.559 | 5.4 | 2 | 60.196 | 13.227 | 5.7 | 34.1 |
| -10 | 1 | 1732 | 1.4 | 30479.164 | 6 | 2.6 | 56.811 | 12.795 | 4.7 | 35.9 |
| -10 | 0.5 | 1743 | 0.7 | 28896.313 | 7 | 2.7 | 60.329 | 14.955 | 2.7 | 36.9 |
| -10 | 0.1 | 1561 | 0.5 | 27275.375 | 7.5 | 2.6 | 57.228 | 22.703 | 3.3 | 35.1 |
| 4 | 25 | 1508 | 6.4 | 23246.865 | 10 | 0.3 | 64.869 | 107.336 | 7.3 | 22.2 |
| 4 | 10 | 1376 | 6.4 | 21961.838 | 8.5 | 1.8 | 62.634 | 53.261 | 7.1 | 21.3 |
| 4 | 5 | 1301 | 5.4 | 20698 | 8.9 | 1.5 | 62.858 | 58.107 | 5.9 | 21.3 |
| 4 | 1 | 1082 | 1.9 | 17775.93 | 10.2 | 0.7 | 60.858 | 58.883 | 7.7 | 21.1 |
| 4 | 0.5 | 977 | 1.1 | 16000.103 | 13.2 | 3 | 61.067 | 65.299 | 2.8 | 25.2 |
| 4 | 0.1 | 831 | 0.5 | 13364.011 | 14.6 | 1.7 | 62.172 | 105.128 | 3.1 | 25.4 |
| 21 | 25 | 856 | 6.4 | 15431.851 | 18.8 | 2.8 | 55.467 | 305.593 | 7.4 | 30.6 |
| 21 | 10 | 723 | 7.3 | 13307.329 | 18.4 | 3.2 | 54.358 | 346.984 | 7.1 | 23.9 |
| 21 | 5 | 625 | 6.5 | 11741.616 | 20 | 3.3 | 53.215 | 374.976 | 5.6 | 25.9 |
| 21 | 1 | 413 | 3.4 | 8275.877 | 24.9 | 3.4 | 49.889 | 363.451 | 4.2 | 27.7 |
| 21 | 0.5 | 348 | 2.4 | 7028.054 | 25.9 | 2.7 | 49.504 | 373.565 | 4.6 | 27 |
| 21 | 0.1 | 225 | 0.9 | 4524.876 | 28.5 | 2.8 | 49.807 | 426.507 | 4.2 | 26.1 |
| 37 | 25 | 499 | 7.2 | 7437.835 | 25.6 | 1.1 | 67.04 | 310.707 | 6.3 | 41.6 |
| 37 | 10 | 397 | 9 | 5847.632 | 25.6 | 1 | 67.903 | 354.776 | 5.7 | 38.2 |
| 37 | 5 | 295 | 8.4 | 4619.726 | 27.6 | 0.7 | 63.84 | 348.035 | 5.3 | 37.5 |
| 37 | 1 | 178 | 4.1 | 2600.065 | 31.4 | 0.2 | 68.319 | 311.343 | 4.8 | 33 |
| 37 | 0.5 | 140 | 2.9 | 2030.515 | 31.7 | 0.3 | 68.99 | 299.929 | 5 | 30.4 |
| 37 | 0.1 | 87 | 1.4 | 1197.621 | 30.7 | 1.1 | 72.597 | 322.399 | 4.4 | 27.4 |
| 54 | 25 | 109 | 8.4 | 2309.902 | 33.4 | 5.6 | 47.291 | 182.05 | 6 | 55.3 |
| 54 | 10 | 88 | 7.7 | 1673.724 | 29.7 | 6.2 | 52.38 | 231.082 | 5 | 43.9 |
| 54 | 5 | 75 | 7 | 1312.287 | 28.5 | 5.6 | 57.232 | 250.212 | 4.7 | 38.5 |
| 54 | 1 | 48 | 4 | 819.836 | 24.5 | 4.8 | 58.821 | 250.634 | 4.5 | 29.1 |
| 54 | 0.5 | 42 | 2.9 | 682.787 | 23.5 | 3.6 | 62.182 | 254.361 | 3.8 | 26.2 |
| 54 | 0.1 | 34 | 1.4 | 514.518 | 17.7 | 3.2 | 66.433 | 274.787 | 5 | 19.3 |

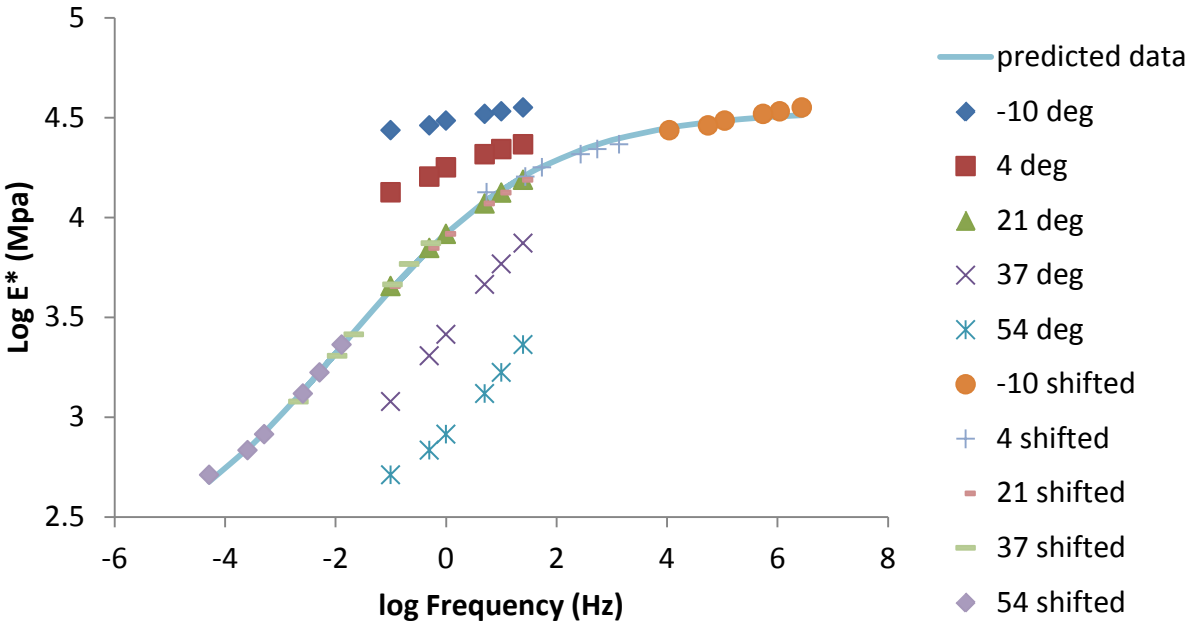


Figure C. 1: Master curve for sample 1 (SP-II with PG 64-22 binder)

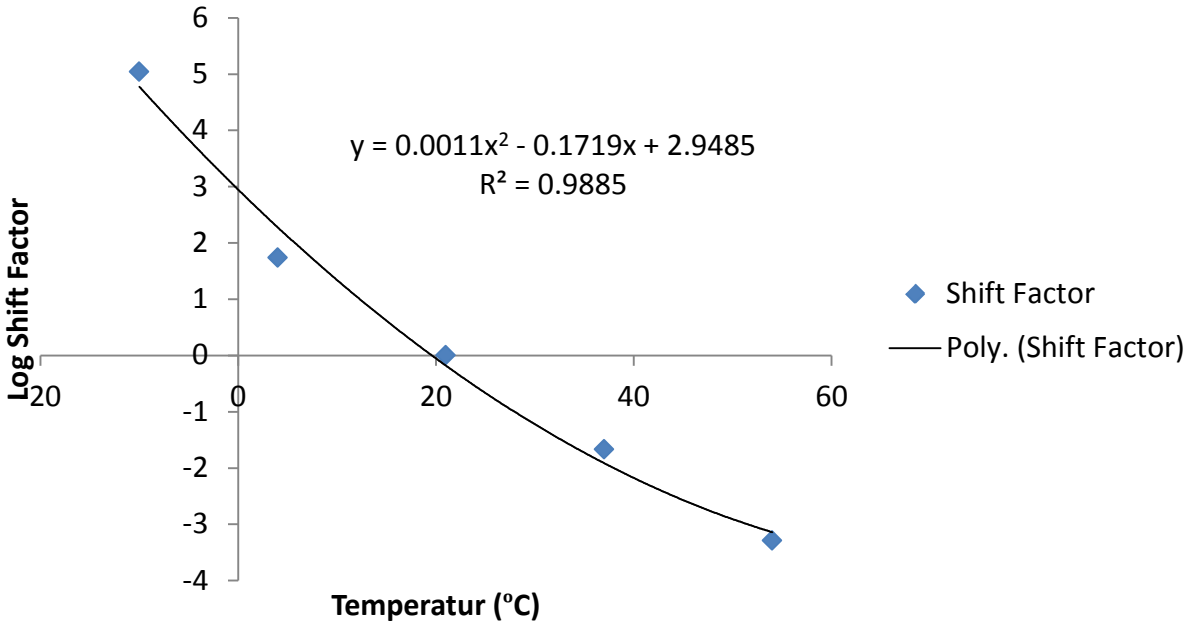


Figure C. 2: Shift factor for sample 1 (SP-II with PG 64-22 binder)

Table C. 2: E* test results for Sample 2 (SP-II with PG 64-22 binder)

| Temperature | Frequency | Stress | | Dynamic Modulus | Phase Angle | | Strain | | | |
|---|---|---|---|---|---|---|---|---|---|---|
| | | Amplitude (P-P) | SE | | | UC | (P-P) Recoverable | Permanent | SE | UC |
| (deg C) | (Hz) | (kPa) | (%) | (MPa) | (deg) | (deg) | (micro e) | (micro e) | (%) | (%) |
| -10 | 25 | 2038 | 6.1 | 36369.063 | 7.3 | 2 | 56.043 | 61.216 | 10 | 7.1 |
| -10 | 10 | 2067 | 6.1 | 35345.848 | 6.2 | 1.7 | 58.487 | 22.472 | 8 | 7.7 |
| -10 | 5 | 2011 | 5.2 | 34335.277 | 6.1 | 1.8 | 58.564 | 25.55 | 6.7 | 7.7 |
| -10 | 1 | 1804 | 1.5 | 32015.998 | 6.1 | 2.1 | 56.339 | 28.728 | 8 | 4.4 |
| -10 | 0.5 | 1697 | 0.9 | 30246.063 | 8 | 2.2 | 56.119 | 30.371 | 4.3 | 3.2 |
| -10 | 0.1 | 1543 | 0.5 | 27514.568 | 8.5 | 2.1 | 56.093 | 43.954 | 3.6 | 0.4 |
| 4 | 25 | 1521 | 6.3 | 24786.035 | 10.7 | 3.6 | 61.382 | 91.459 | 9.5 | 0.6 |
| 4 | 10 | 1490 | 6.5 | 23750.865 | 9 | 0.2 | 62.729 | 35.671 | 8.7 | 9.8 |
| 4 | 5 | 1420 | 5.2 | 22707.852 | 9 | 0.1 | 62.537 | 35.125 | 8.5 | 9.9 |
| 4 | 1 | 1201 | 1.7 | 19412.52 | 11.4 | 0.5 | 61.883 | 33.095 | 5 | 13.6 |
| 4 | 0.5 | 1103 | 1 | 17873.082 | 12.1 | 1 | 61.714 | 37.145 | 5.8 | 15.8 |
| 4 | 0.1 | 994 | 0.4 | 14309.274 | 15.3 | 0.2 | 69.443 | 82.434 | 3.9 | 17.2 |
| 21 | 25 | 855 | 7.3 | 12127.919 | 20 | 3.1 | 70.486 | 193.465 | 11 | 3 |
| 21 | 10 | 723 | 7.5 | 12137.903 | 17.5 | 0.3 | 59.534 | 161.287 | 7.7 | 28.9 |
| 21 | 5 | 626 | 6.8 | 10871.323 | 18.4 | 0.7 | 57.595 | 153.848 | 7.7 | 30.5 |
| 21 | 1 | 412 | 3.8 | 7686.097 | 23 | 0.4 | 53.6 | 124.476 | 4.2 | 30.6 |
| 21 | 0.5 | 348 | 2.5 | 6540.138 | 24.2 | 0.1 | 53.134 | 121.11 | 3.4 | 31.2 |
| 21 | 0.1 | 225 | 0.8 | 4174.866 | 27.3 | 0.2 | 53.915 | 154.915 | 3.1 | 32.1 |
| 37 | 25 | 485 | 8.9 | 7589.415 | 26.9 | 1.3 | 63.948 | 399.819 | 10 | 16.4 |
| 37 | 10 | 427 | 9.6 | 5981.912 | 26.5 | 2.2 | 71.301 | 498.915 | 7.8 | 22.8 |
| 37 | 5 | 364 | 9.1 | 4887.654 | 28 | 2.5 | 74.414 | 531.908 | 7.6 | 27.1 |
| 37 | 1 | 242 | 4.4 | 2706.521 | 31 | 2.2 | 89.236 | 514.193 | 6.7 | 36.7 |
| 37 | 0.5 | 200 | 3.2 | 2152.753 | 31.5 | 1.8 | 92.881 | 520.457 | 6 | 40.8 |
| 37 | 0.1 | 149 | 1.4 | 1342.989 | 30.3 | 0.5 | 110.685 | 606.569 | 5.7 | 44.2 |
| 54 | 25 | 137 | 9.1 | 2378.366 | 33.3 | 1.6 | 57.491 | 207.035 | 6.8 | 32.5 |
| 54 | 10 | 113 | 9.2 | 1769.989 | 30.2 | 1.1 | 64.014 | 262.814 | 6 | 25.5 |
| 54 | 5 | 97 | 8.7 | 1410.177 | 29.4 | 0.8 | 68.554 | 284.598 | 6 | 25.1 |
| 54 | 1 | 62 | 5.8 | 828.981 | 28.5 | 1 | 74.867 | 282.276 | 5.3 | 32.2 |
| 54 | 0.5 | 54 | 4.3 | 702.35 | 27 | 1 | 77.488 | 288.831 | 5.6 | 36.1 |
| 54 | 0.1 | 42 | 2.1 | 515.047 | 22.5 | 0.8 | 81.784 | 318.995 | 6.3 | 47.2 |

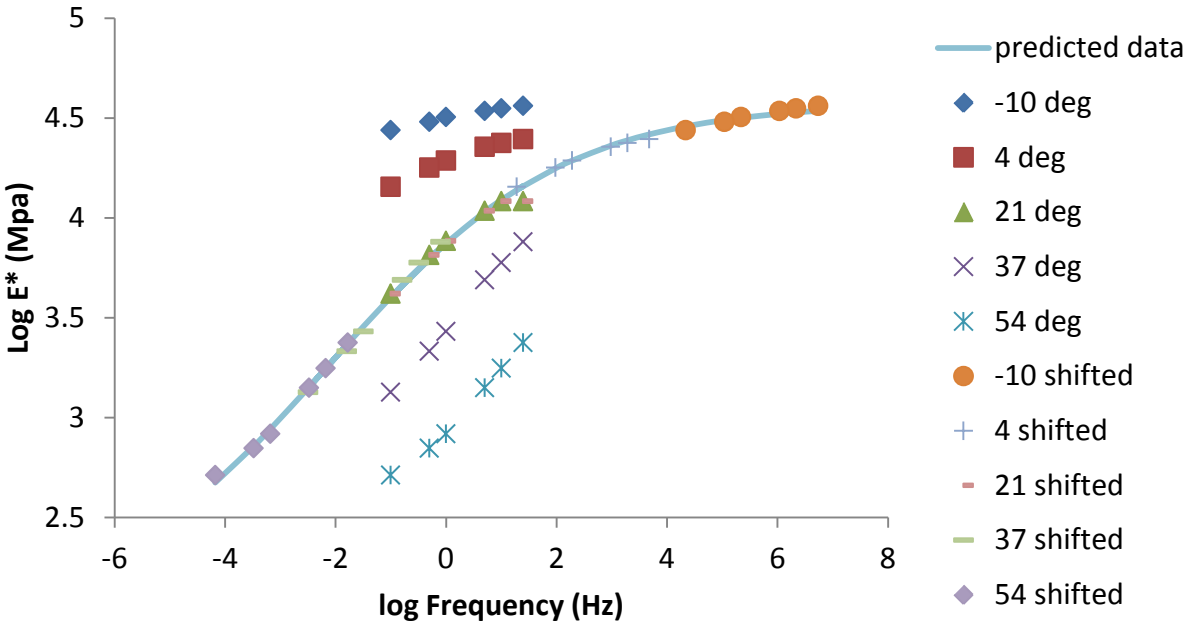


Figure C. 3: Master curve for sample 2 (SP-II with PG 64-22 binder)

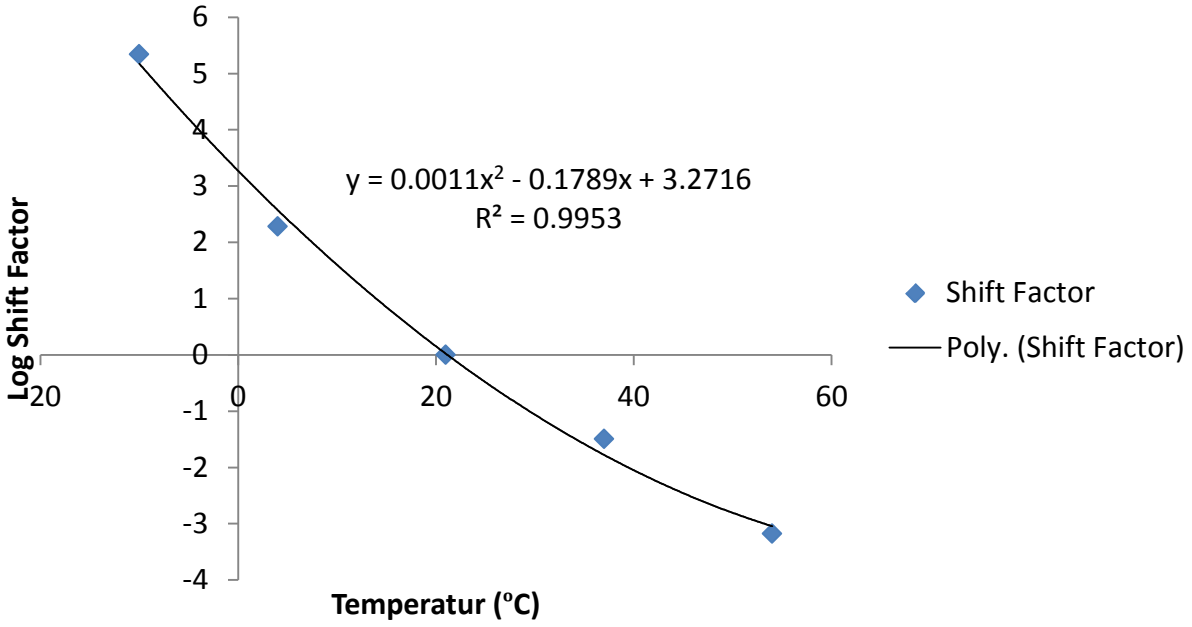


Figure C. 4: Shift factor for sample 2 (SP-II with PG 64-22 binder)

Table C. 3: E* test results for Sample 3 (SP-II with PG 64-22 binder)

| Temperature | Frequency | Stress | | Dynamic Modulus | Phase Angle | | Strain | | | |
|---|---|---|---|---|---|---|---|---|---|---|
| | | Amplitude (P-P) | SE | | | UC | (P-P) Recoverable | Permanent | SE | UC |
| (deg C) | (Hz) | (kPa) | (%) | (MPa) | (deg) | (deg) | (micro e) | (micro e) | (%) | (%) |
| -10 | 25 | 2479 | 5.7 | 34573.656 | 5.5 | 0.7 | 71.714 | 86.201 | 23 | 15 |
| -10 | 10 | 2435 | 5 | 33187.059 | 5.9 | 0.1 | 73.366 | 17.756 | 11 | 20.8 |
| -10 | 5 | 2333 | 4.6 | 31952.471 | 6 | 1 | 73.027 | 16.391 | 12 | 19.4 |
| -10 | 1 | 2052 | 1.1 | 29044.682 | 6.9 | 0.1 | 70.657 | 15.813 | 11 | 13.1 |
| -10 | 0.5 | 1984 | 0.6 | 27750.891 | 7 | 1.1 | 71.507 | 18.27 | 12 | 11.3 |
| -10 | 0.1 | 1742 | 0.4 | 24475.203 | 8.6 | 0.2 | 71.19 | 37.512 | 11 | 3.3 |
| 4 | 25 | 1598 | 8.1 | 31442.223 | 9.4 | 1.4 | 50.83 | 77.984 | 12 | 14.7 |
| 4 | 10 | 1586 | 7.8 | 28853.557 | 9 | 0.8 | 54.952 | 35.017 | 10 | 17.1 |
| 4 | 5 | 1505 | 6.6 | 27215.047 | 9.3 | 1.1 | 55.292 | 38.321 | 8.7 | 15.9 |
| 4 | 1 | 1259 | 2.7 | 23551.484 | 11.3 | 1.7 | 53.455 | 36.858 | 6.4 | 11 |
| 4 | 0.5 | 1137 | 1.6 | 22387.742 | 11.7 | 1.3 | 50.799 | 38.163 | 3.5 | 12.1 |
| 4 | 0.1 | 964 | 0.7 | 18269.055 | 14.1 | 1 | 52.779 | 70.114 | 3.3 | 6.9 |
| 21 | 25 | 1025 | 7.9 | 17994.422 | 15.5 | 1.5 | 56.95 | 251.191 | 12 | 6.3 |
| 21 | 10 | 952 | 7.7 | 15031.265 | 16.6 | 0.3 | 63.317 | 260.974 | 9.5 | 5.5 |
| 21 | 5 | 843 | 7.1 | 13415.535 | 17.6 | 0.4 | 62.813 | 285.964 | 8.5 | 6 |
| 21 | 1 | 593 | 3.9 | 10171.664 | 21.7 | 0.4 | 58.284 | 278.22 | 5.9 | 8.3 |
| 21 | 0.5 | 495 | 2.8 | 8995.204 | 23.1 | 0.5 | 55.027 | 290.251 | 5.7 | 11.1 |
| 21 | 0.1 | 341 | 1.5 | 6375.208 | 26.2 | 0.5 | 53.494 | 355.567 | 5.8 | 1.8 |
| 37 | 25 | 527 | 11 | 6204.32 | 25.7 | 3.1 | 84.889 | 347.693 | 14 | 16.3 |
| 37 | 10 | 426 | 11 | 5025.318 | 23.7 | 0.7 | 84.792 | 417.214 | 11 | 17.3 |
| 37 | 5 | 343 | 12 | 4218.61 | 24.8 | 0.7 | 81.292 | 432.946 | 10 | 18.5 |
| 37 | 1 | 223 | 8.2 | 2636.639 | 28 | 1.9 | 84.761 | 397.499 | 8.7 | 17.7 |
| 37 | 0.5 | 182 | 6.4 | 2178.816 | 28.8 | 2.6 | 83.528 | 398.814 | 7.4 | 13.2 |
| 37 | 0.1 | 116 | 2.7 | 1421.049 | 28.3 | 3.9 | 81.771 | 443.279 | 5.8 | 15.3 |
| 54 | 25 | 202 | 13 | 2388.001 | 30 | 3.3 | 84.564 | 382.143 | 20 | 11 |
| 54 | 10 | 164 | 12 | 1730.44 | 28.6 | 3.6 | 94.774 | 543.447 | 11 | 3 |
| 54 | 5 | 137 | 11 | 1395.827 | 28 | 3.6 | 98.056 | 621.081 | 9.1 | 3 |
| 54 | 1 | 87 | 7.7 | 855.588 | 27.2 | 3.7 | 101.416 | 625.51 | 7 | 18.2 |
| 54 | 0.5 | 79 | 5.5 | 715.444 | 25.7 | 3.6 | 110.018 | 647.736 | 5.6 | 24.7 |
| 54 | 0.1 | 59 | 2.4 | 490.544 | 22.1 | 1.6 | 119.715 | 713.906 | 4.8 | 38.1 |

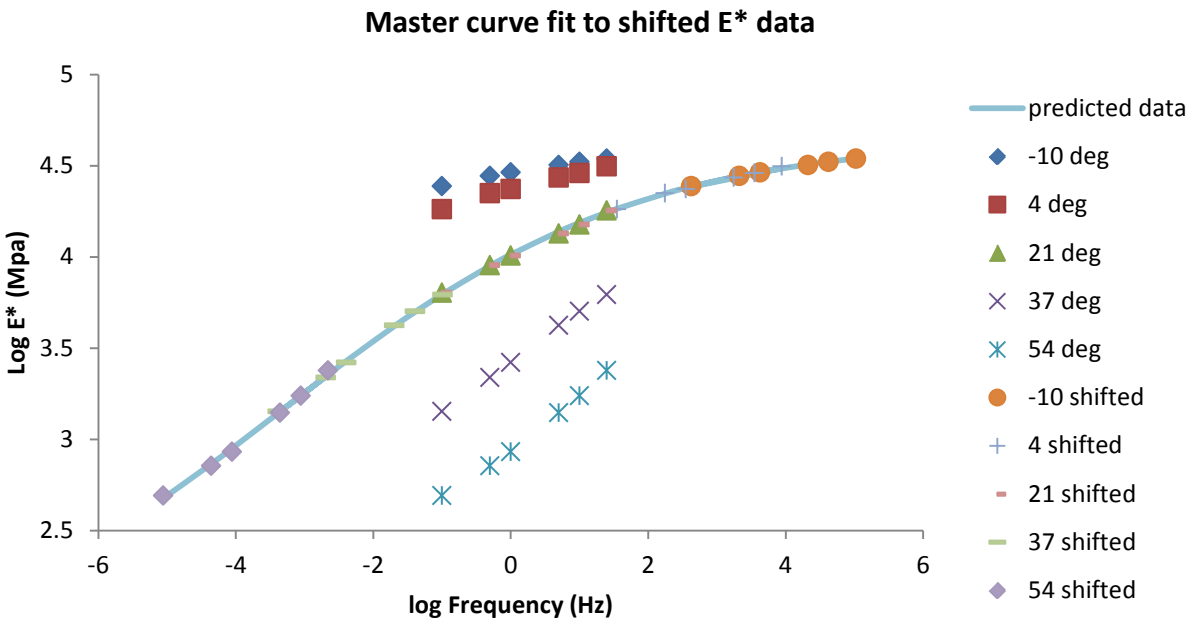


Figure C. 5: Master curve for sample 3 (SP-II with PG 64-22 binder)

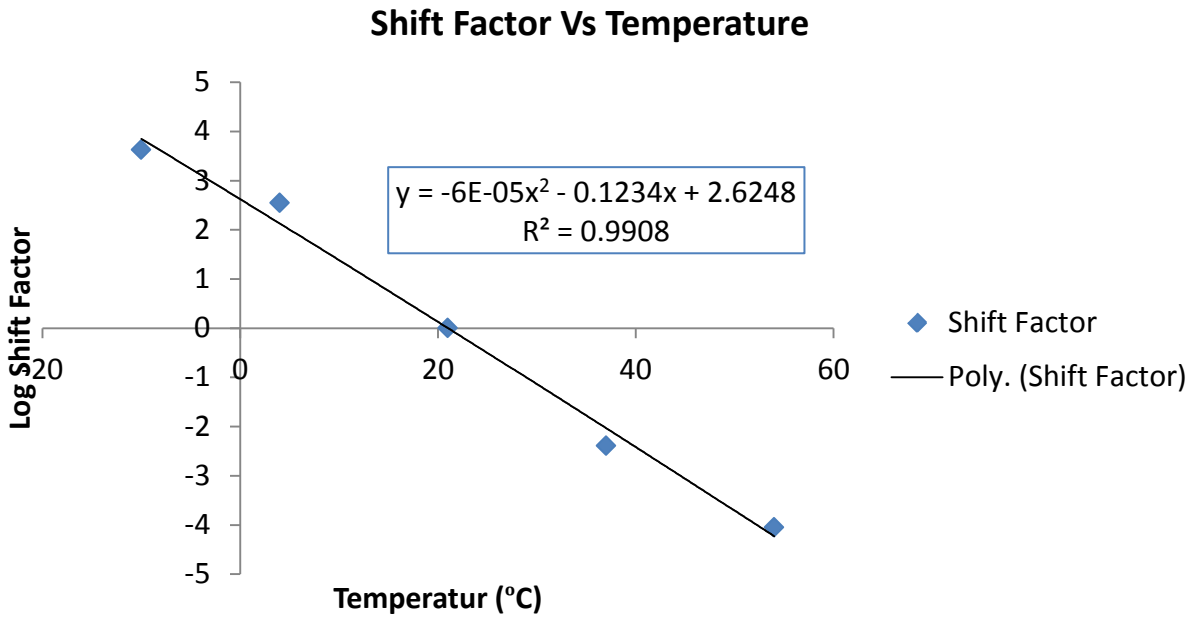


Figure C. 6: Shift factor for sample 3 (SP-II with PG 64-22 binder)

Table C. 4: E* test results for Sample 4 (SP-II with PG 64-22 binder)

| Temperature | Frequency | Stress | | Dynamic Modulus | Phase Angle | | Strain | | | |
|---|---|---|---|---|---|---|---|---|---|---|
| | | Amplitude (P-P) | SE | | | UC | (P-P) Recoverable | Permanent | SE | UC |
| (deg C) | (Hz) | (kPa) | (%) | (MPa) | (deg) | (deg) | (micro e) | (micro e) | (%) | (%) |
| -10 | 25 | 1887 | 7.2 | 33972.43 | 9.4 | 5.1 | 55.555 | 59.167 | 9 | 14.3 |
| -10 | 10 | 1902 | 6.8 | 33861.215 | 6.2 | 1.3 | 56.169 | 19.538 | 8.6 | 19.2 |
| -10 | 5 | 1839 | 6 | 32843.027 | 6.2 | 1.3 | 56.001 | 18.243 | 7.4 | 19.1 |
| -10 | 1 | 1619 | 2.2 | 30343.51 | 6.6 | 1 | 53.372 | 17.318 | 4.7 | 17.4 |
| -10 | 0.5 | 1530 | 1.3 | 28768.539 | 7.2 | 0.9 | 53.184 | 18.294 | 4.2 | 13 |
| -10 | 0.1 | 1413 | 0.5 | 26568.941 | 8.5 | 2.5 | 53.201 | 29.325 | 5.8 | 15.5 |
| 4 | 25 | 1125 | 8.4 | 20015.885 | 8.9 | 0.1 | 56.216 | 67.392 | 10 | 5.3 |
| 4 | 10 | 1105 | 8.4 | 18820.432 | 8.5 | 0.5 | 58.736 | 39.119 | 8.3 | 1.9 |
| 4 | 5 | 1051 | 7.3 | 17770.1 | 8.7 | 0.4 | 59.148 | 44.233 | 7.7 | 0.7 |
| 4 | 1 | 885 | 3.1 | 15128.261 | 10.6 | 0.4 | 58.521 | 43.869 | 5.6 | 2.5 |
| 4 | 0.5 | 800 | 1.9 | 13955.012 | 10.9 | 0.4 | 57.308 | 47.224 | 6.3 | 3.2 |
| 4 | 0.1 | 681 | 0.8 | 11559.654 | 12.7 | 0.8 | 58.869 | 79.411 | 5.1 | 7.4 |
| 21 | 25 | 721 | 8.5 | 11983.729 | 13.8 | 3.6 | 60.192 | 192.87 | 12 | 23.2 |
| 21 | 10 | 610 | 8.1 | 9832.118 | 16.4 | 0.8 | 62.022 | 203.279 | 7.8 | 8.1 |
| 21 | 5 | 536 | 7.7 | 8796.159 | 17.3 | 1.2 | 60.94 | 212.099 | 7.9 | 4.4 |
| 21 | 1 | 381 | 5 | 6343.747 | 21 | 1.3 | 59.996 | 192.696 | 5.2 | 2.7 |
| 21 | 0.5 | 326 | 3.5 | 5378.944 | 22.5 | 1.2 | 60.673 | 199.908 | 4.2 | 6 |
| 21 | 0.1 | 213 | 1.6 | 3517.992 | 24.9 | 0.1 | 60.473 | 267.376 | 5.2 | 12.7 |
| 37 | 25 | 450 | 9.2 | 7204.163 | 23.6 | 2.4 | 62.5 | 274.341 | 8.2 | 12.9 |
| 37 | 10 | 346 | 9.8 | 5762.231 | 23.3 | 2 | 60.062 | 346.43 | 6 | 14.6 |
| 37 | 5 | 281 | 8.8 | 4762.981 | 24.4 | 2 | 59.024 | 388.28 | 5.6 | 13.6 |
| 37 | 1 | 183 | 5 | 2890.281 | 26.9 | 2.3 | 63.212 | 385.7 | 4.6 | 9 |
| 37 | 0.5 | 152 | 3.4 | 2378.358 | 27.4 | 2.2 | 63.862 | 400.287 | 4.4 | 7.1 |
| 37 | 0.1 | 101 | 1.4 | 1547.319 | 26.6 | 2.3 | 65.293 | 447.842 | 3.6 | 3 |
| 54 | 25 | 121 | 10 | 2009.607 | 32.2 | 0.4 | 60.246 | 113.792 | 8 | 17.9 |
| 54 | 10 | 90 | 9 | 1489.218 | 29.5 | 2.1 | 60.676 | 170.54 | 5.8 | 22.2 |
| 54 | 5 | 70 | 8.1 | 1147.843 | 28.7 | 2 | 60.769 | 183.257 | 6.2 | 21.2 |
| 54 | 1 | 40 | 4.8 | 691.214 | 27 | 2.7 | 58.543 | 174.755 | 4.5 | 19.6 |
| 54 | 0.5 | 33 | 3.8 | 575.674 | 25.8 | 2.1 | 57.157 | 175.359 | 4 | 20.1 |
| 54 | 0.1 | 22 | 3 | 406.99 | 21.8 | 4 | 55.153 | 194.022 | 4.9 | 20.3 |

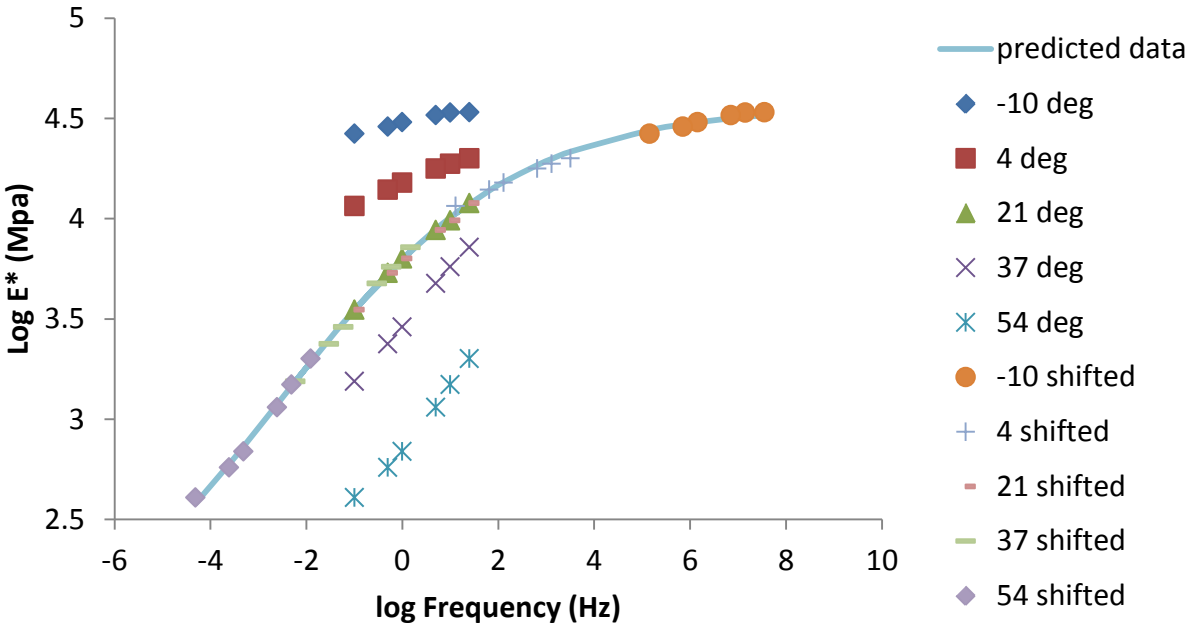


Figure C. 7: Master curve for sample 4 (SP-II with PG 64-22 binder)

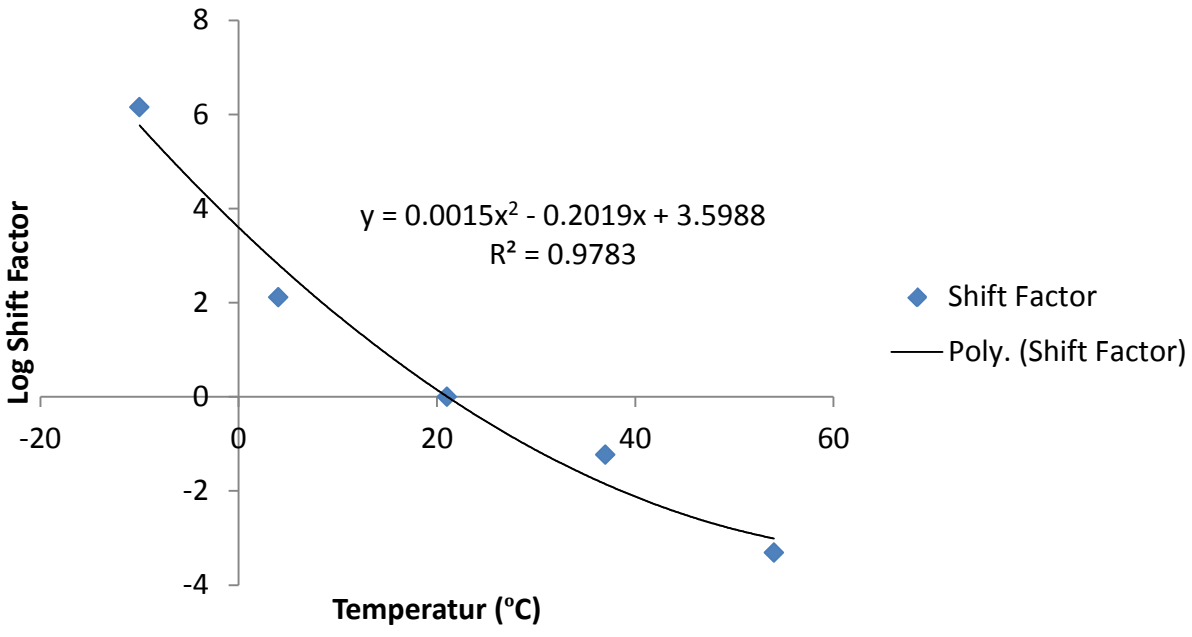


Figure C. 8: Shift factor for sample 4 (SP-II with PG 64-22 binder)

Table C. 5: E* test results for Sample 5 (SP-II with PG 64-22 binder)

| Temperature | Frequency | Stress | | Dynamic Modulus | Phase Angle | | Strain | | | |
|---|---|---|---|---|---|---|---|---|---|---|
| | | Amplitude (P-P) | SE | | | UC | (P-P) Recoverable | Permanent | SE | UC |
| (deg C) | (Hz) | (kPa) | (%) | (MPa) | (deg) | (deg) | (micro e) | (micro e) | (%) | (%) |
| -10 | 25 | 1875 | 6.9 | 33439.43 | 6.7 | 1.9 | 56.085 | 51.823 | 9.9 | 13 |
| -10 | 10 | 1886 | 6.7 | 33413.246 | 5.1 | 0.2 | 56.445 | 11.296 | 6.5 | 18.1 |
| -10 | 5 | 1820 | 5.4 | 32511.082 | 4.9 | 0.1 | 55.969 | 9.707 | 6.3 | 19.3 |
| -10 | 1 | 1613 | 1.9 | 29800.637 | 5.6 | 0.2 | 54.124 | 8.388 | 4.7 | 22.3 |
| -10 | 0.5 | 1527 | 1 | 28775.555 | 4.4 | 1.5 | 53.063 | 9.357 | 5.7 | 23 |
| -10 | 0.1 | 1412 | 0.5 | 26145.514 | 6.6 | 0.1 | 54.003 | 18.588 | 4.6 | 24.3 |
| 4 | 25 | 1646 | 7.1 | 24721.539 | 9.4 | 0.2 | 66.585 | 108.927 | 6.3 | 14.5 |
| 4 | 10 | 1499 | 7.6 | 23427.918 | 8.6 | 0.5 | 63.979 | 41.457 | 6.5 | 19.1 |
| 4 | 5 | 1418 | 6.4 | 22134.037 | 8.8 | 0.4 | 64.065 | 40.604 | 5.8 | 19.9 |
| 4 | 1 | 1187 | 2.6 | 18799.396 | 10 | 0.6 | 63.156 | 39.566 | 5.8 | 20.5 |
| 4 | 0.5 | 1072 | 1.6 | 17219.402 | 11.2 | 0.2 | 62.282 | 42.726 | 3.8 | 18 |
| 4 | 0.1 | 912 | 0.6 | 14186.721 | 13.2 | 0.1 | 64.263 | 74.565 | 3.9 | 18.3 |
| 21 | 25 | 844 | 7.8 | 13929.848 | 15.1 | 0.9 | 60.566 | 158.88 | 8.8 | 8.6 |
| 21 | 10 | 754 | 7.6 | 12212.933 | 15.5 | 0.3 | 61.776 | 161.313 | 6 | 13.2 |
| 21 | 5 | 675 | 6.9 | 10855.43 | 16.6 | 0.4 | 62.211 | 167.51 | 5.4 | 12.1 |
| 21 | 1 | 477 | 3.7 | 7835.529 | 19.8 | 0.4 | 60.82 | 151.398 | 4.3 | 6.2 |
| 21 | 0.5 | 408 | 2.8 | 6802.162 | 21.1 | 0.1 | 59.912 | 160.693 | 3.9 | 7.8 |
| 21 | 0.1 | 275 | 0.9 | 4582.961 | 23.1 | 0.4 | 60.024 | 215.225 | 3.6 | 6.9 |
| 37 | 25 | 450 | 9.2 | 7204.163 | 23.6 | 2.4 | 62.5 | 274.341 | 8.2 | 12.9 |
| 37 | 10 | 346 | 9.8 | 5762.231 | 23.3 | 2 | 60.062 | 346.43 | 6 | 14.6 |
| 37 | 5 | 281 | 8.8 | 4762.981 | 24.4 | 2 | 59.024 | 388.28 | 5.6 | 13.6 |
| 37 | 1 | 183 | 5 | 2890.281 | 26.9 | 2.3 | 63.212 | 385.7 | 4.6 | 9 |
| 37 | 0.5 | 152 | 3.4 | 2378.358 | 27.4 | 2.2 | 63.862 | 400.287 | 4.4 | 7.1 |
| 37 | 0.1 | 101 | 1.4 | 1547.319 | 26.6 | 2.3 | 65.293 | 447.842 | 3.6 | 3 |
| 54 | 25 | 141 | 9.6 | 2408.435 | 30.9 | 2.3 | 58.427 | 187.687 | 7.3 | 6 |
| 54 | 10 | 114 | 9 | 1836.391 | 28.7 | 1.1 | 61.885 | 236.423 | 6.4 | 0.7 |
| 54 | 5 | 93 | 8.2 | 1475.662 | 28.2 | 1.3 | 62.788 | 247.882 | 6 | 3.5 |
| 54 | 1 | 57 | 5.2 | 907.126 | 27.6 | 2.1 | 62.463 | 236.64 | 4.8 | 10.5 |
| 54 | 0.5 | 47 | 3.4 | 766.731 | 26.6 | 2.8 | 61.267 | 233.877 | 3.7 | 11.5 |
| 54 | 0.1 | 35 | 1.8 | 554.261 | 23.4 | 4.3 | 63.029 | 248.731 | 4.3 | 19.2 |

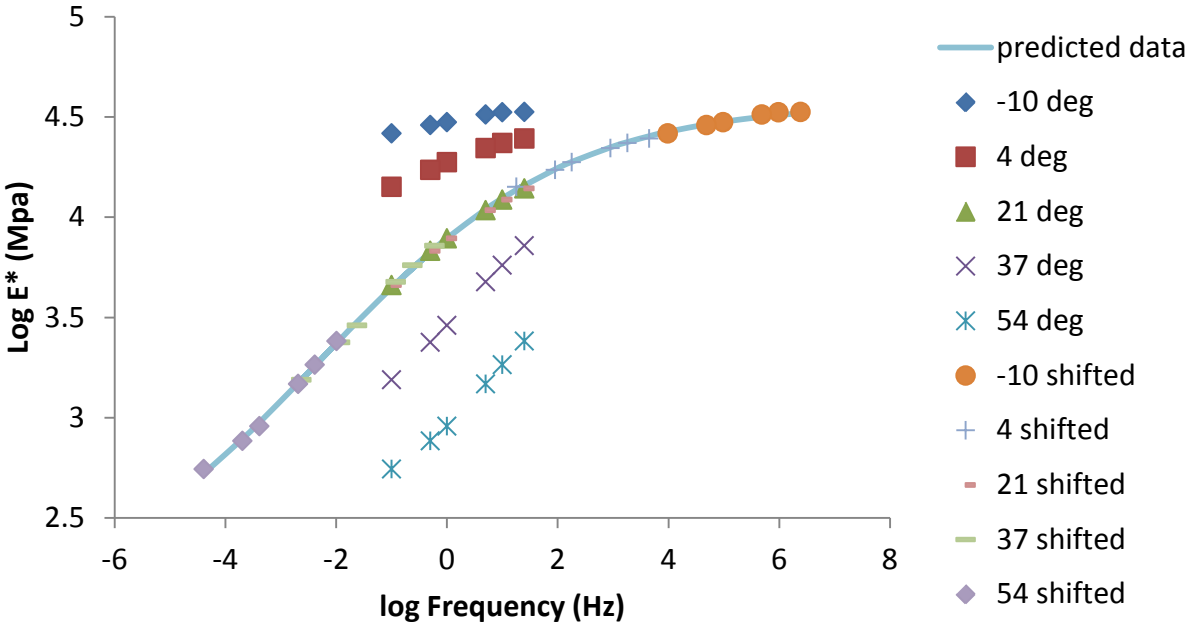


Figure C. 9: Master curve for sample 5 (SP-II with PG 64-22 binder)

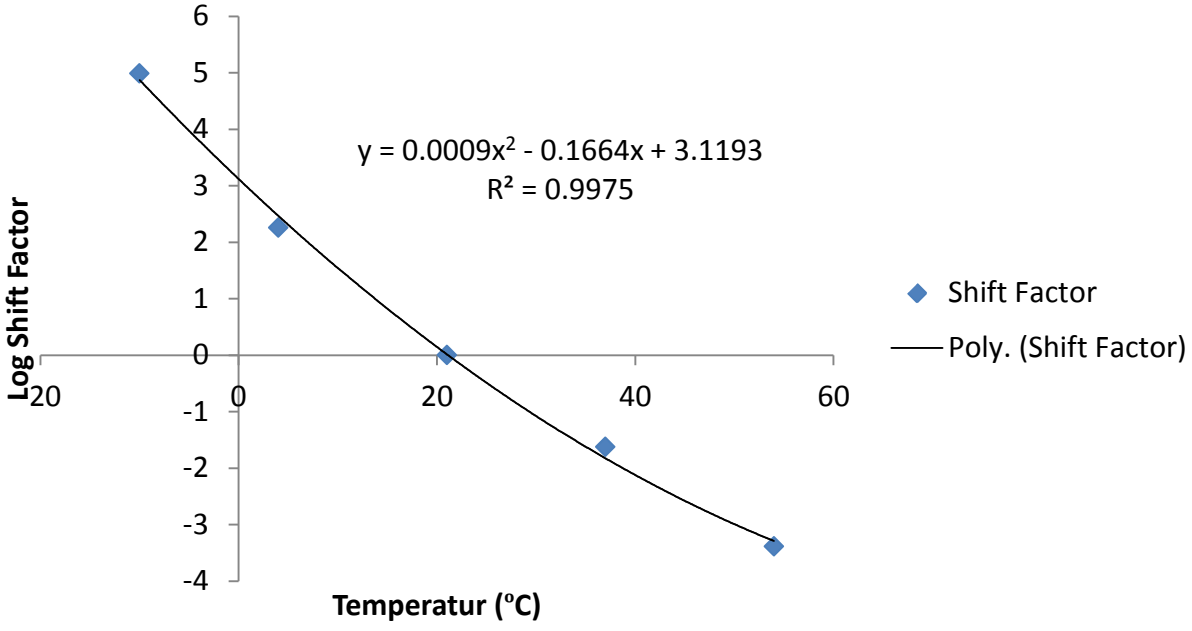


Figure C. 10: Shift factor for sample 5 (SP-II with PG 64-22 binder)

Table C. 6: E* test results for Sample 6 (SP-II with PG 64-22 binder)

| Temperature | Frequency | Stress | | Dynamic Modulus | Phase Angle | | Strain | | | |
|---|---|---|---|---|---|---|---|---|---|---|
| | | Amplitude (P-P) | SE | | | UC | (P-P) Recoverable | Permanent | SE | UC |
| (deg C) | (Hz) | (kPa) | (%) | (MPa) | (deg) | (deg) | (micro e) | (micro e) | (%) | (%) |
| -10 | 25 | 1745 | 6.4 | 29015.891 | 7 | 0.2 | 60.144 | 33.169 | 12 | 19.9 |
| -10 | 10 | 1698 | 6.3 | 27568.977 | 5.6 | 1.2 | 61.606 | 4.417 | 9.1 | 8.8 |
| -10 | 5 | 1622 | 5.3 | 26854.023 | 5.2 | 1.8 | 60.392 | -10.451 | 7.6 | 6.4 |
| -10 | 1 | 1461 | 1.6 | 24833.041 | 5.7 | 1.9 | 58.836 | -16.993 | 4.8 | 6.4 |
| -10 | 0.5 | 1335 | 0.9 | 24290.967 | 6.3 | 1.6 | 54.963 | -11.164 | 4.9 | 8.7 |
| -10 | 0.1 | 1227 | 0.4 | 21284.256 | 7.6 | 1.4 | 57.636 | -1.926 | 4.7 | 5.7 |
| 4 | 25 | 942 | 9.2 | 17343.375 | 9.3 | 0.4 | 54.295 | 33.88 | 11 | 3.3 |
| 4 | 10 | 832 | 9.5 | 16111.846 | 9.1 | 0.6 | 51.663 | 17.384 | 9.6 | 1 |
| 4 | 5 | 778 | 8.5 | 15249.849 | 9.4 | 0.7 | 51.008 | 16.156 | 8.4 | 1.4 |
| 4 | 1 | 712 | 4.1 | 13103.287 | 10.1 | 0.1 | 54.314 | 15.273 | 6 | 2.1 |
| 4 | 0.5 | 604 | 2.8 | 12133.614 | 11.4 | 1.3 | 49.793 | 17.226 | 3 | 4.6 |
| 4 | 0.1 | 499 | 1.1 | 10161.441 | 12.9 | 0.6 | 49.09 | 37.761 | 2.6 | 3.9 |
| 21 | 25 | 672 | 9.7 | 9523.605 | 14.7 | 1.5 | 70.552 | 163.279 | 15 | 16.4 |
| 21 | 10 | 605 | 9.7 | 8150.564 | 15.8 | 0.2 | 74.203 | 179.549 | 8.7 | 10.6 |
| 21 | 5 | 536 | 9.1 | 7279.357 | 16.8 | 0.2 | 73.634 | 193.177 | 8 | 9.4 |
| 21 | 1 | 376 | 6.4 | 5319.224 | 20.1 | 0.5 | 70.629 | 178.546 | 5.5 | 13.4 |
| 21 | 0.5 | 325 | 4.3 | 4572.022 | 21.5 | 0.3 | 71.155 | 192.086 | 4 | 14.9 |
| 21 | 0.1 | 226 | 1.5 | 3120.064 | 23.7 | 0.6 | 72.497 | 273.505 | 3 | 15.4 |
| 37 | 25 | 303 | 10 | 4503.634 | 22.3 | 4.1 | 67.386 | 298.372 | 15 | 11.5 |
| 37 | 10 | 252 | 10 | 3500.4 | 23.5 | 0.5 | 72.015 | 382.682 | 8.5 | 11.3 |
| 37 | 5 | 208 | 10 | 2888.458 | 24.7 | 0.6 | 72.116 | 413.889 | 8.7 | 8.9 |
| 37 | 1 | 127 | 8 | 1773.825 | 27.7 | 0.8 | 71.833 | 395.473 | 7.1 | 10.6 |
| 37 | 0.5 | 103 | 5.9 | 1444.666 | 28.3 | 1.4 | 71.329 | 403.658 | 6.3 | 10.4 |
| 37 | 0.1 | 65 | 2.3 | 912.941 | 27.9 | 2 | 70.839 | 453.616 | 4.6 | 12.6 |
| 54 | 25 | 102 | 11 | 1635.277 | 30.7 | 0.1 | 62.472 | 287.448 | 8.8 | 11.6 |
| 54 | 10 | 76 | 8.9 | 1290.741 | 27.7 | 2.6 | 59.013 | 386.887 | 6.2 | 0.6 |
| 54 | 5 | 65 | 7.4 | 1048.568 | 26.6 | 2.5 | 62.011 | 437.416 | 5.7 | 2.7 |
| 54 | 1 | 33 | 4.9 | 635.182 | 25 | 1.9 | 51.977 | 436.915 | 5 | 3 |
| 54 | 0.5 | 31 | 5 | 535.703 | 23.7 | 2.7 | 57.12 | 449.24 | 4 | 1.6 |
| 54 | 0.1 | 27 | 4.6 | 391.945 | 19.7 | 2.3 | 68.03 | 500.66 | 4.4 | 1.8 |

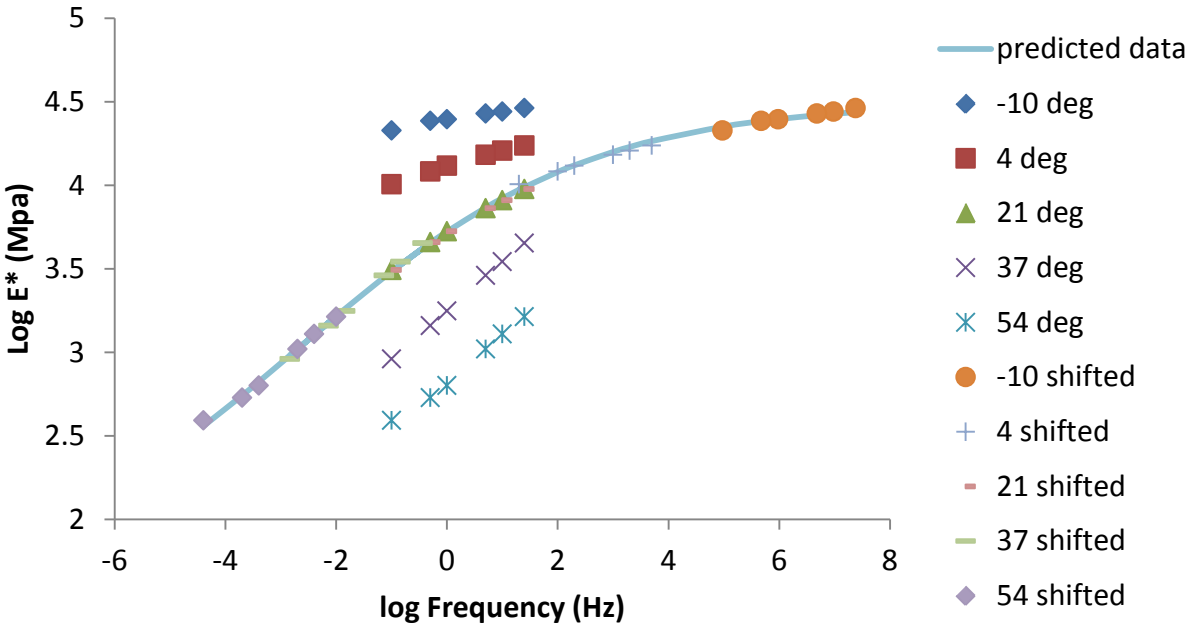


Figure C. 11: Master curve for sample 6 (SP-II with PG 64-22 binder)

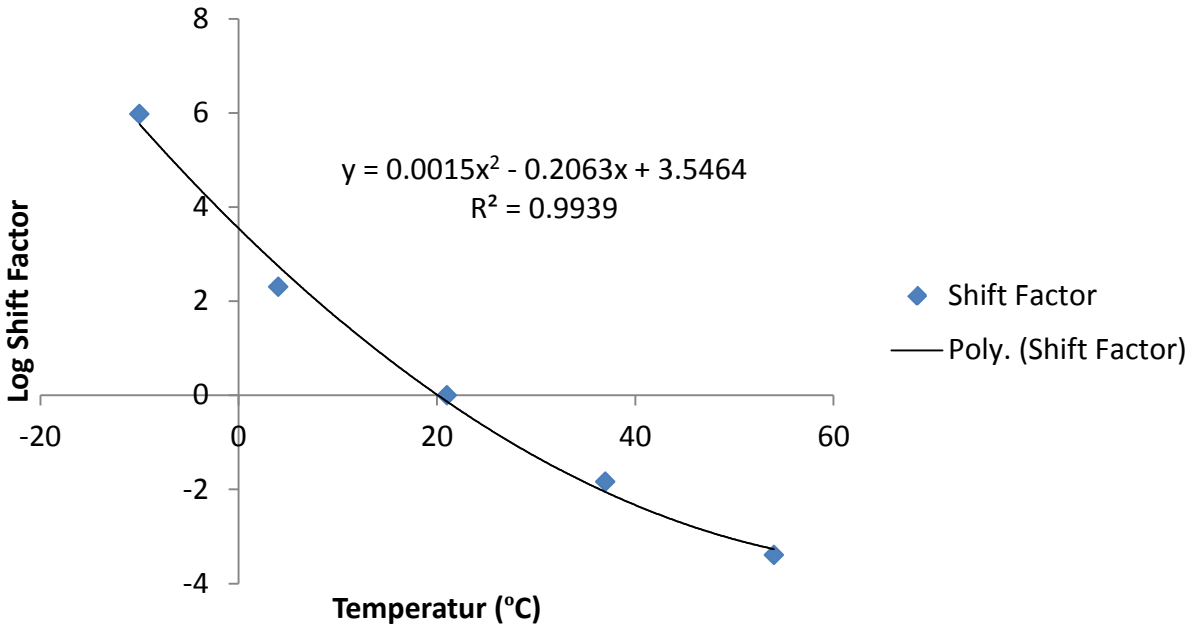


Figure C. 12: Shift factor for sample 6 (SP-II with PG 64-22 binder)

# APPENDIX D

DYNAMIC MODULUS TEST RESULTS FOR SP-II WITH PG 70-22 BINDER

**Table D. 1: E* test results for Sample 1 (SP-II with PG 70-22 binder)**

| Temperature | Frequency | Stress | | Dynamic Modulus | Phase Angle | | Strain | | | |
|---|---|---|---|---|---|---|---|---|---|---|
| | | Amplitude (P-P) | SE | | | UC | (P-P) Recoverable | Permanent | SE | UC |
| (deg C) | (Hz) | (kPa) | (%) | (MPa) | (deg) | (deg) | (micro e) | (micro e) | (%) | (%) |
| -10 | 25 | 1309 | 5.8 | 22393.246 | 9.9 | 1.5 | 58.435 | 35.645 | 8.4 | 14.2 |
| -10 | 10 | 1334 | 5.9 | 22022.662 | 6.9 | 1.3 | 60.57 | 8.519 | 8.3 | 10.4 |
| -10 | 5 | 1307 | 4.6 | 21429.338 | 6.4 | 1 | 60.998 | 7.7 | 7.4 | 10.1 |
| -10 | 1 | 1181 | 1.4 | 19482.635 | 7.7 | 2.4 | 60.599 | 6.355 | 4.7 | 7.3 |
| -10 | 0.5 | 1126 | 0.9 | 18753.098 | 9 | 3.5 | 60.033 | 7.1 | 5.7 | 7.9 |
| -10 | 0.1 | 1037 | 0.5 | 16745.855 | 9.5 | 2.2 | 61.901 | 20.585 | 5 | 7.2 |
| 4 | 25 | 837 | 6.3 | 14776.076 | 11.4 | 1.5 | 56.626 | 54.003 | 8.1 | 6.3 |
| 4 | 10 | 755 | 6.7 | 13962.789 | 10.1 | 0.2 | 54.063 | 51.347 | 8.6 | 2.9 |
| 4 | 5 | 708 | 5.7 | 13052.636 | 10.5 | 0.2 | 54.236 | 55.71 | 7.4 | 2.2 |
| 4 | 1 | 591 | 2.5 | 11001.224 | 12.3 | 0.7 | 53.702 | 56.753 | 6 | 3.7 |
| 4 | 0.5 | 535 | 1.5 | 10042.3 | 13.4 | 0.2 | 53.282 | 62.565 | 4.5 | 3.6 |
| 4 | 0.1 | 456 | 0.7 | 8173.402 | 15.9 | 0.6 | 55.768 | 102.081 | 4.8 | 11.8 |
| 21 | 25 | 672 | 9.7 | 9523.605 | 14.7 | 1.5 | 70.552 | 163.279 | 15 | 16.4 |
| 21 | 10 | 605 | 9.7 | 8150.564 | 15.8 | 0.2 | 74.203 | 179.549 | 8.7 | 10.6 |
| 21 | 5 | 536 | 9.1 | 7279.357 | 16.8 | 0.2 | 73.634 | 193.177 | 8 | 9.4 |
| 21 | 1 | 376 | 6.4 | 5319.224 | 20.1 | 0.5 | 70.629 | 178.546 | 5.5 | 13.4 |
| 21 | 0.5 | 325 | 4.3 | 4572.022 | 21.5 | 0.3 | 71.155 | 192.086 | 4 | 14.9 |
| 21 | 0.1 | 226 | 1.5 | 3120.064 | 23.7 | 0.6 | 72.497 | 273.505 | 3 | 15.4 |
| 37 | 25 | 206 | 6.9 | 3457.687 | 26.2 | 0.3 | 59.721 | 192.878 | 6.3 | 43.1 |
| 37 | 10 | 165 | 5.7 | 2738.074 | 25.6 | 2.3 | 60.443 | 283.361 | 4.1 | 33.8 |
| 37 | 5 | 136 | 4.7 | 2244.93 | 26.7 | 1.7 | 60.545 | 309.935 | 4.1 | 27.7 |
| 37 | 1 | 77 | 2.3 | 1294.376 | 28.5 | 0.9 | 59.393 | 296.506 | 3.4 | 15.9 |
| 37 | 0.5 | 62 | 1.4 | 1045.145 | 28.5 | 0.7 | 59.664 | 306.558 | 3.5 | 11.7 |
| 37 | 0.1 | 39 | 1.7 | 671.566 | 26.8 | 0.3 | 57.787 | 347.994 | 3.8 | 3.7 |
| 54 | 25 | 87 | 7.1 | 1345.157 | 29.8 | 3.5 | 64.617 | 154.001 | 6.8 | 27.9 |
| 54 | 10 | 68 | 6.3 | 1024.803 | 26.1 | 2.1 | 66.766 | 231.246 | 6.9 | 22.3 |
| 54 | 5 | 53 | 5.1 | 828.984 | 25.7 | 1.9 | 63.447 | 254.506 | 4 | 26.6 |
| 54 | 1 | 31 | 4.7 | 532.754 | 22.8 | 2.2 | 59.069 | 251.941 | 4.8 | 34.9 |
| 54 | 0.5 | 27 | 3.9 | 453.839 | 21.8 | 2 | 60.369 | 260.976 | 6 | 36.2 |
| 54 | 0.1 | 21 | 4.2 | 346.742 | 17.9 | 1.8 | 60.601 | 294.036 | 5.4 | 43.7 |

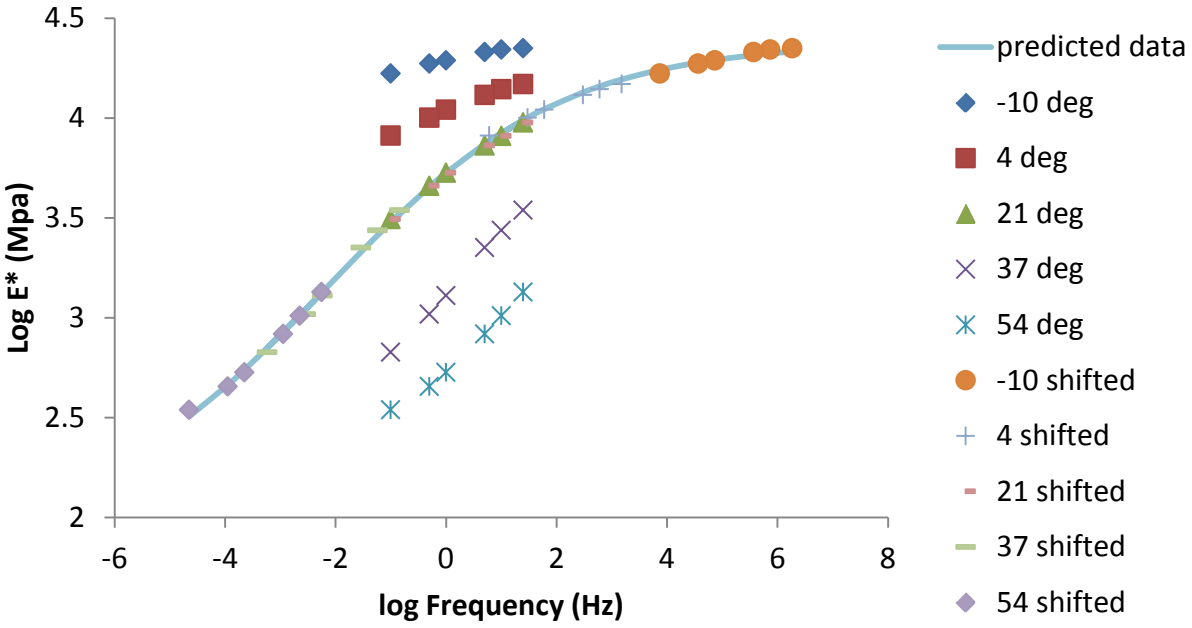


Figure D. 1: Master curve for sample 1 (SP-II with PG 70-22 binder)

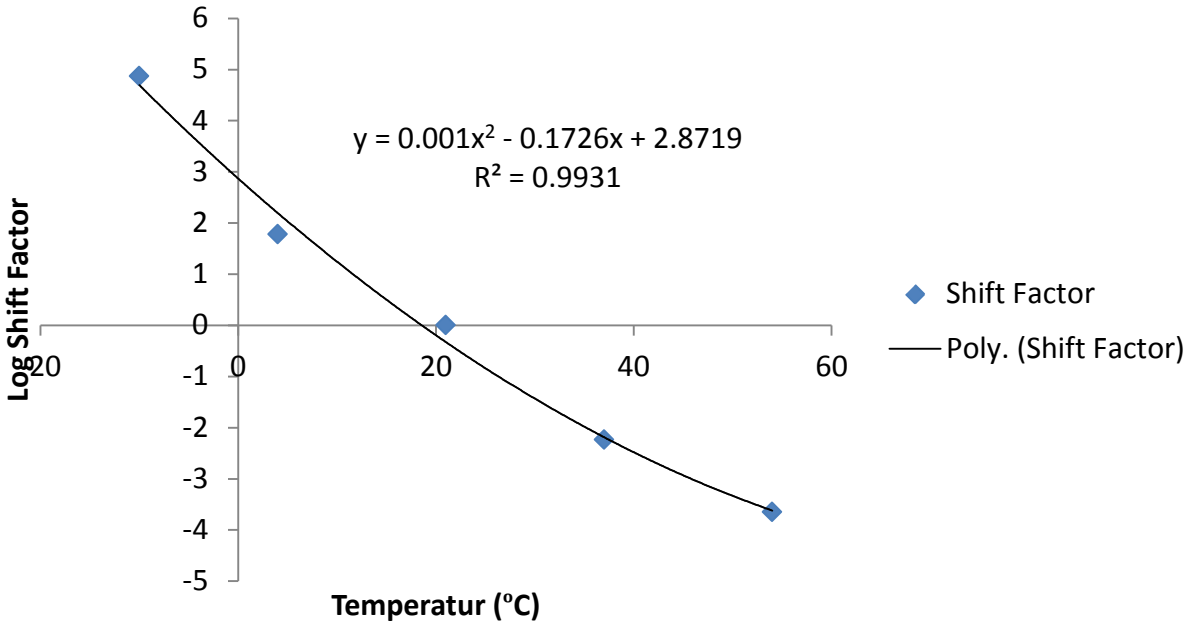


Figure D. 2: Shift factor for sample 1 (SP-II with PG 70-22 binder)

Table D. 2: E* test results for Sample 2 (SP-II with PG 70-22 binder)

| Temperature | Frequency | Stress | | Dynamic Modulus | Phase Angle | | Strain | | | |
|---|---|---|---|---|---|---|---|---|---|---|
| | | Amplitude (P-P) | SE | | | UC | (P-P) Recoverable | Permanent | SE | UC |
| (deg C) | (Hz) | (kPa) | (%) | (MPa) | (deg) | (deg) | (micro e) | (micro e) | (%) | (%) |
| -10 | 25 | 2293 | 5.4 | 25258.293 | 7 | 0.4 | 90.778 | 100.005 | 7 | 19.6 |
| -10 | 10 | 2255 | 5.3 | 24166.85 | 5.1 | 0.6 | 93.328 | 28.164 | 6.3 | 16.7 |
| -10 | 5 | 2186 | 4.8 | 23551.881 | 4.8 | 0.4 | 92.797 | 28.869 | 5.8 | 16.6 |
| -10 | 1 | 1906 | 1.3 | 21527.123 | 5.1 | 0.1 | 88.549 | 27.505 | 3.8 | 18 |
| -10 | 0.5 | 1734 | 0.7 | 21126.848 | 4.6 | 0.6 | 82.072 | 29.139 | 3.1 | 17.3 |
| -10 | 0.1 | 1574 | 0.5 | 18821.896 | 6.8 | 0.5 | 83.608 | 47.255 | 5 | 18.6 |
| 4 | 25 | 904 | 9.1 | 13652.99 | 6.7 | 5.8 | 66.232 | 38.866 | 15 | 20.6 |
| 4 | 10 | 816 | 10 | 15243.325 | 8.4 | 0.3 | 53.556 | 28.526 | 11 | 12.9 |
| 4 | 5 | 769 | 9.2 | 14473.225 | 8.3 | 0.1 | 53.158 | 26.487 | 9.3 | 12.2 |
| 4 | 1 | 652 | 4.7 | 12188.368 | 9.6 | 0.2 | 53.522 | 28.616 | 9.1 | 10.6 |
| 4 | 0.5 | 586 | 3.2 | 11317.236 | 6.8 | 1.2 | 51.805 | 31.219 | 8 | 10.1 |
| 4 | 0.1 | 497 | 1.2 | 9888.192 | 12.6 | 0 | 50.3 | 52.529 | 8.6 | 5 |
| 21 | 25 | 863 | 7.9 | 9231.69 | 15.9 | 1.5 | 93.506 | 279.318 | 6.9 | 42 |
| 21 | 10 | 729 | 8.9 | 8468.601 | 15.2 | 0.1 | 86.084 | 283.014 | 7.2 | 34.1 |
| 21 | 5 | 630 | 8.2 | 7608.027 | 16 | 0.6 | 82.865 | 300.203 | 8.5 | 32.7 |
| 21 | 1 | 432 | 4.6 | 5456.587 | 18.4 | 1.3 | 79.249 | 285.252 | 6.7 | 23.4 |
| 21 | 0.5 | 382 | 2.9 | 4716.106 | 20.2 | 0.4 | 81.073 | 298.301 | 4.8 | 19.9 |
| 21 | 0.1 | 304 | 1.4 | 3431.923 | 22.7 | 0.3 | 88.643 | 402.179 | 5.9 | 13.2 |
| 37 | 25 | 370 | 14 | 4328.697 | 24.5 | 12.9 | 85.392 | 397.899 | 17 | 0.2 |
| 37 | 10 | 319 | 11 | 4297.676 | 20.9 | 1.1 | 74.205 | 560.796 | 6.9 | 9.9 |
| 37 | 5 | 271 | 8.1 | 3436.286 | 22.5 | 0.8 | 78.936 | 635.377 | 5.9 | 10.4 |
| 37 | 1 | 183 | 4.8 | 2123.081 | 26 | 2 | 86.366 | 636.383 | 5.3 | 6.6 |
| 37 | 0.5 | 152 | 3.6 | 1720.912 | 26.7 | 2.7 | 88.14 | 661.869 | 4.1 | 2.2 |
| 37 | 0.1 | 113 | 2.2 | 1119.979 | 25.8 | 3.1 | 100.891 | 781.356 | 5.1 | 9.4 |
| 54 | 25 | 137 | 8.2 | 1918.862 | 31.5 | 5.4 | 71.487 | 357.352 | 6.6 | 13 |
| 54 | 10 | 121 | 7.4 | 1502.492 | 29.4 | 2.7 | 80.33 | 569.945 | 4.3 | 20.7 |
| 54 | 5 | 97 | 6.7 | 1187.823 | 29.3 | 3.4 | 81.598 | 665.377 | 4 | 22.8 |
| 54 | 1 | 65 | 4.8 | 715.493 | 29 | 3.5 | 91.259 | 691.578 | 5.4 | 23.1 |
| 54 | 0.5 | 58 | 3.5 | 622.655 | 28.2 | 4.6 | 93.595 | 729.052 | 5.7 | 26.1 |
| 54 | 0.1 | 46 | 1.7 | 435.285 | 25.1 | 5.1 | 106.44 | 829.028 | 7.8 | 24 |

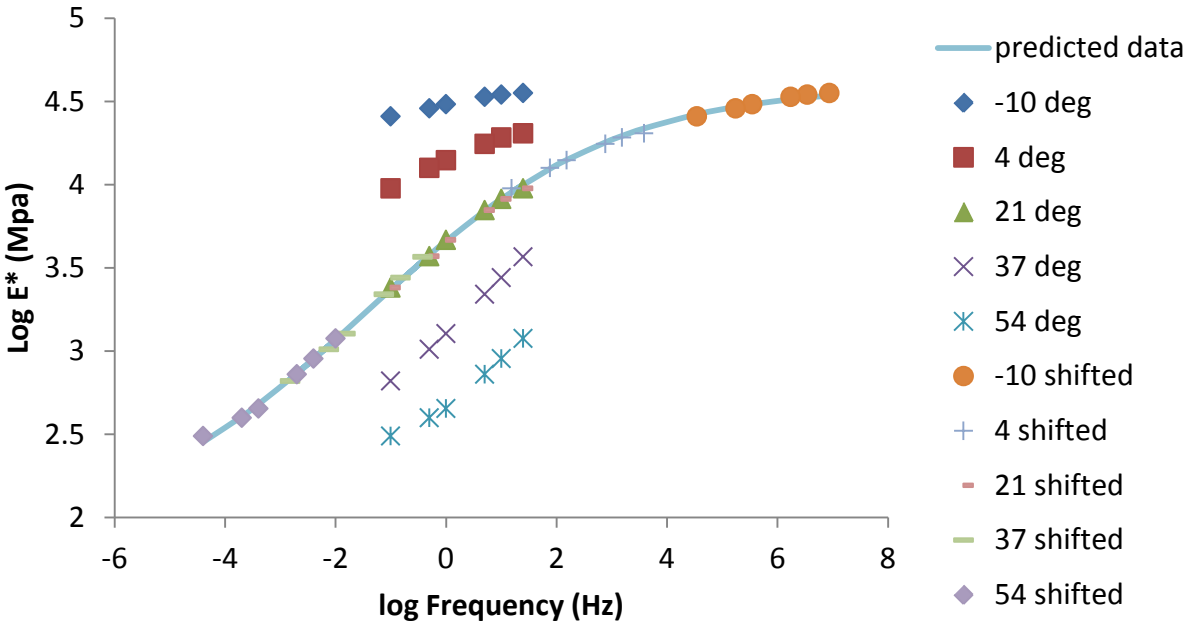


Figure D. 3: Master curve for sample 2 (SP-II with PG 70-22 binder)

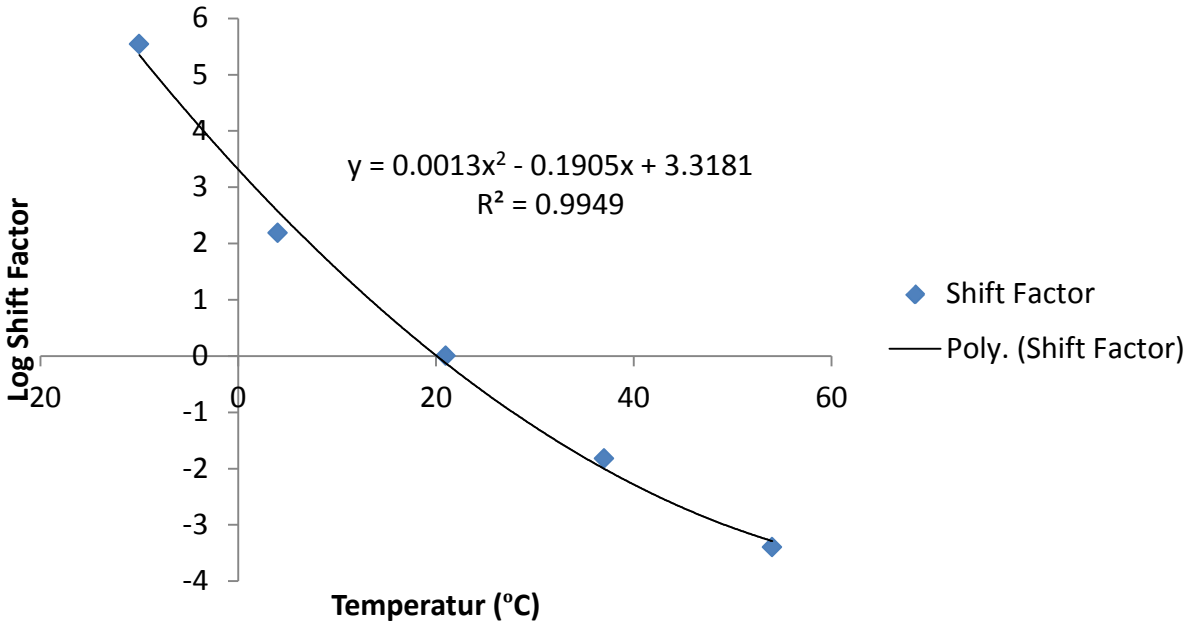


Figure D. 4: Shift factor for sample 2 (SP-II with PG 70-22 binder)

Table D. 3: E* test results for Sample 3 (SP-II with PG 70-22 binder)

| Temperature | Frequency | Stress | | Dynamic Modulus | Phase Angle | | Strain | | | |
|---|---|---|---|---|---|---|---|---|---|---|
| | | Amplitude (P-P) | SE | | | UC | (P-P) Recoverable | Permanent | SE | UC |
| (deg C) | (Hz) | (kPa) | (%) | (MPa) | (deg) | (deg) | (micro e) | (micro e) | (%) | (%) |
| -10 | 25 | 2030 | 5.2 | 35461.676 | 10.4 | 2.8 | 57.243 | 68.967 | 13 | 14.4 |
| -10 | 10 | 2100 | 4.7 | 34736.535 | 8.2 | 2.9 | 60.459 | 22.957 | 9.3 | 9.3 |
| -10 | 5 | 2034 | 3.8 | 33632.422 | 8 | 3.1 | 60.481 | 23.367 | 7.8 | 6.7 |
| -10 | 1 | 1734 | 1 | 30427.633 | 9.1 | 3.4 | 56.999 | 22.515 | 6.5 | 1 |
| -10 | 0.5 | 1663 | 0.6 | 28684.082 | 9.4 | 3.3 | 57.981 | 24.997 | 6.2 | 5.3 |
| -10 | 0.1 | 1462 | 0.4 | 25689.592 | 11 | 3.4 | 56.893 | 44.367 | 6.1 | 8.8 |
| 4 | 25 | 1654 | 5.4 | 20311.299 | 15.5 | 2.3 | 81.414 | 223.152 | 11 | 7.5 |
| 4 | 10 | 1503 | 5.3 | 19208.438 | 13.5 | 2.3 | 78.262 | 142.399 | 7.7 | 6.7 |
| 4 | 5 | 1416 | 4.2 | 17549.875 | 14.1 | 2.5 | 80.657 | 155.691 | 6.3 | 3 |
| 4 | 1 | 1181 | 1.2 | 14042.968 | 16.8 | 2.4 | 84.107 | 159.672 | 4.9 | 5.6 |
| 4 | 0.5 | 1069 | 0.7 | 12625.292 | 17.9 | 2.7 | 84.651 | 176.166 | 4 | 8.4 |
| 4 | 0.1 | 913 | 0.4 | 9496.972 | 21.3 | 2.3 | 96.088 | 276.243 | 2.5 | 6.9 |
| 21 | 25 | 627 | 6.1 | 9485.652 | 27.7 | 1.6 | 66.068 | 319.316 | 14 | 14.7 |
| 21 | 10 | 529 | 7.3 | 8204.207 | 21.2 | 0.1 | 64.418 | 393.351 | 7.4 | 7.7 |
| 21 | 5 | 457 | 6.4 | 7040.788 | 22.4 | 0.3 | 64.946 | 433.399 | 5.6 | 7.7 |
| 21 | 1 | 324 | 3.1 | 4657.685 | 26.4 | 0.7 | 69.574 | 423.541 | 4.3 | 5.3 |
| 21 | 0.5 | 279 | 1.4 | 3723.819 | 27.9 | 0.1 | 74.865 | 449.912 | 4.1 | 1.8 |
| 21 | 0.1 | 185 | 0.7 | 2405.771 | 30.1 | 0.3 | 76.728 | 546.803 | 3.1 | 6 |
| 37 | 25 | 207 | 6.5 | 3687.917 | 30.2 | 11.1 | 56.165 | 217.873 | 11 | 40.8 |
| 37 | 10 | 164 | 6.2 | 2763.598 | 28.6 | 1 | 59.517 | 295.966 | 6.5 | 28.9 |
| 37 | 5 | 135 | 5.4 | 2191.872 | 29 | 1 | 61.724 | 318.496 | 6.1 | 25.3 |
| 37 | 1 | 77 | 2 | 1273.728 | 30 | 0.3 | 60.633 | 301.766 | 3.5 | 12.4 |
| 37 | 0.5 | 63 | 1.5 | 1026.285 | 29.5 | 0.1 | 60.97 | 310.802 | 3.1 | 8.3 |
| 37 | 0.1 | 39 | 1.4 | 661.555 | 26.6 | 0.6 | 58.975 | 348.957 | 3 | 0.8 |
| 54 | 25 | 71 | 6.3 | 1191.62 | 32.6 | 1.7 | 59.274 | 254.294 | 6.3 | 33.3 |
| 54 | 10 | 50 | 4.6 | 900.586 | 29.1 | 2.3 | 55.615 | 310.819 | 3.8 | 17.7 |
| 54 | 5 | 39 | 3.6 | 724.882 | 27.1 | 2 | 54.323 | 331.515 | 3.6 | 12.1 |
| 54 | 1 | 24 | 2.7 | 451.474 | 23.5 | 1.4 | 52.978 | 335.279 | 4.8 | 1.8 |
| 54 | 0.5 | 18 | 3.1 | 397.848 | 20.7 | 1 | 45.77 | 338.627 | 4.1 | 2.6 |
| 54 | 0.1 | 15 | 2.9 | 308.37 | 16.8 | 0.1 | 49.54 | 361.393 | 6.5 | 6.7 |

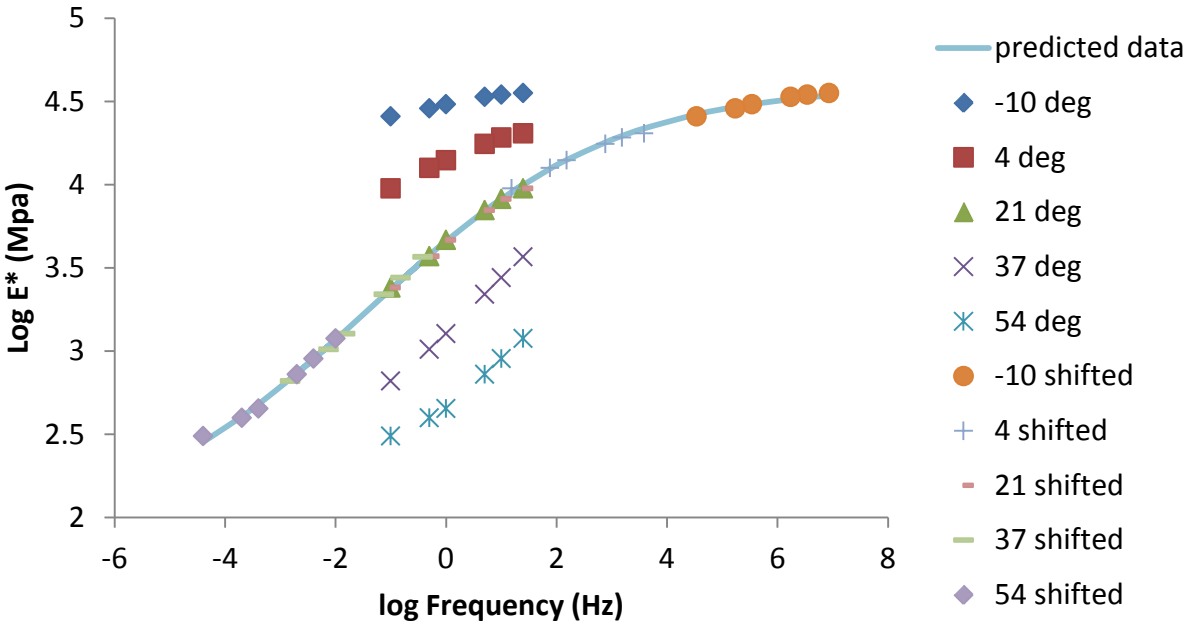


Figure D. 5: Master curve for sample 3 (SP-II with PG 70-22 binder)

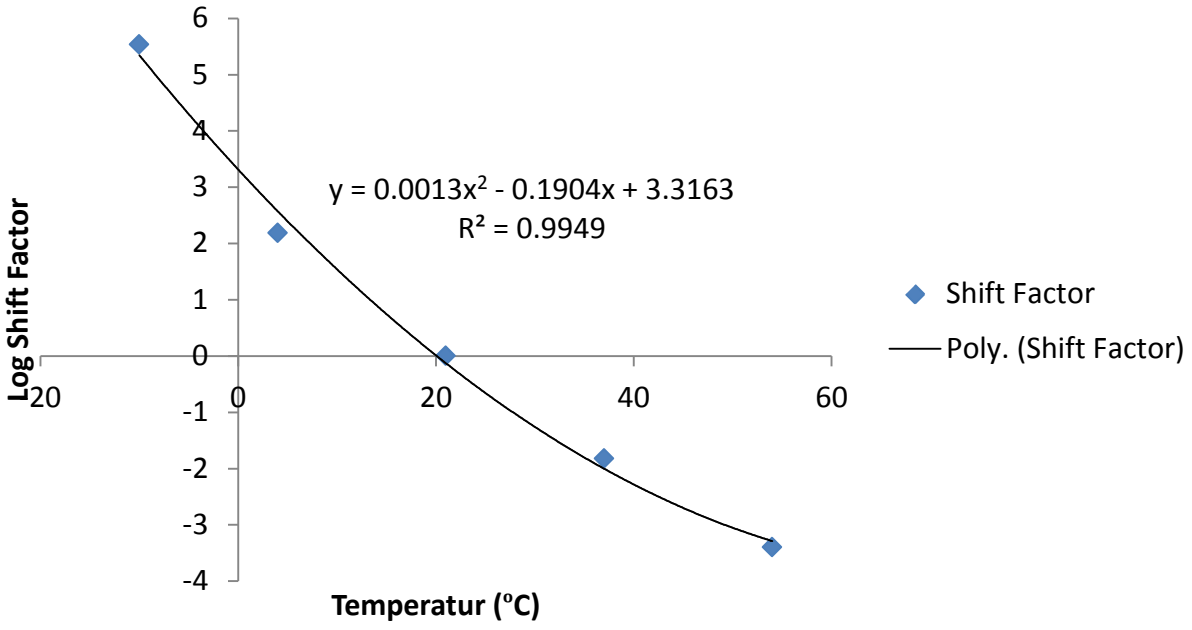


Figure D. 6: Shift factor for sample 3 (SP-II with PG 70-22 binder)

Table D. 4: E* test results for Sample 4 (SP-II with PG 70-22 binder)

| Temperature | Frequency | Stress | | Dynamic Modulus | Phase Angle | | Strain | | | |
|---|---|---|---|---|---|---|---|---|---|---|
| | | Amplitude (P-P) | SE | | | UC | (P-P) Recoverable | Permanent | SE | UC |
| (deg C) | (Hz) | (kPa) | (%) | (MPa) | (deg) | (deg) | (micro e) | (micro e) | (%) | (%) |
| -10 | 25 | 1303 | 6 | 23630.602 | 8.7 | 4.1 | 55.156 | 43.798 | 11 | 23 |
| -10 | 10 | 1324 | 5.8 | 22770.619 | 7.1 | 0.7 | 58.153 | 18.703 | 8.4 | 26.2 |
| -10 | 5 | 1306 | 4.7 | 22154.896 | 6.9 | 0.5 | 58.946 | 19.698 | 8.6 | 26.3 |
| -10 | 1 | 1181 | 1.4 | 20257.17 | 7.2 | 0.1 | 58.279 | 20.874 | 8.2 | 26.5 |
| -10 | 0.5 | 1126 | 0.8 | 19101.023 | 7.3 | 1.1 | 58.972 | 23.866 | 5.7 | 24 |
| -10 | 0.1 | 1038 | 0.5 | 17075.572 | 9.3 | 0.3 | 60.796 | 41.42 | 4.2 | 26.5 |
| 4 | 25 | 839 | 6.4 | 14779.32 | 11.3 | 5.2 | 56.762 | 64.47 | 10 | 28.1 |
| 4 | 10 | 750 | 6.4 | 14028.559 | 10.6 | 1.7 | 53.467 | 64.522 | 6.8 | 26.6 |
| 4 | 5 | 704 | 5.5 | 13311.586 | 10.7 | 1.3 | 52.891 | 70.3 | 5.9 | 26.1 |
| 4 | 1 | 593 | 2.3 | 11103.771 | 12.9 | 1.9 | 53.364 | 72.029 | 3.2 | 22.5 |
| 4 | 0.5 | 535 | 1.5 | 10221.488 | 13.7 | 3 | 52.371 | 78.738 | 3.3 | 20.6 |
| 4 | 0.1 | 456 | 0.7 | 8304.708 | 16.3 | 2.4 | 54.911 | 121.379 | 3.3 | 13.5 |
| 21 | 25 | 541 | 6.8 | 8869.354 | 25.2 | 4 | 60.945 | 202.226 | 12 | 3.6 |
| 21 | 10 | 506 | 7.5 | 8312.87 | 18.9 | 2.8 | 60.816 | 276.14 | 6.8 | 1 |
| 21 | 5 | 436 | 6.9 | 7336.928 | 20 | 3.3 | 59.387 | 301.378 | 5.4 | 5.6 |
| 21 | 1 | 278 | 2.8 | 4810.072 | 23.8 | 5.1 | 57.788 | 279.822 | 3.5 | 25.4 |
| 21 | 0.5 | 234 | 1.9 | 4035.469 | 25.8 | 6.3 | 57.937 | 288.888 | 3.8 | 18.2 |
| 21 | 0.1 | 156 | 1.1 | 2696.693 | 28.4 | 8 | 57.878 | 351.739 | 3.2 | 0.1 |
| 37 | 25 | 283 | 7.1 | 4425.193 | 29.4 | 8.7 | 64.019 | 187.466 | 8.2 | 26.5 |
| 37 | 10 | 230 | 7 | 3581.793 | 26.2 | 7 | 64.168 | 217.801 | 6 | 19.4 |
| 37 | 5 | 184 | 6.3 | 2885.143 | 26.8 | 7.7 | 63.765 | 217.768 | 6.3 | 10 |
| 37 | 1 | 109 | 3.1 | 1734.764 | 27.7 | 9.8 | 62.693 | 196.071 | 5.1 | 15.4 |
| 37 | 0.5 | 86 | 2 | 1414.211 | 26.5 | 10.9 | 61.012 | 196.045 | 4.1 | 29.2 |
| 37 | 0.1 | 55 | 1.4 | 915.261 | 21.6 | 12.5 | 60.546 | 223.873 | 6.4 | 61.3 |
| 54 | 25 | 71 | 7.7 | 1743.423 | 30.2 | 3.4 | 40.897 | 99.511 | 6.2 | 7.8 |
| 54 | 10 | 51 | 6.2 | 1346.024 | 27.3 | 3.2 | 38.021 | 116.195 | 7.7 | 8.7 |
| 54 | 5 | 41 | 5.8 | 1069.521 | 25.3 | 3.3 | 38.031 | 122.194 | 5.7 | 16 |
| 54 | 1 | 24 | 3.7 | 714.917 | 21.4 | 3.5 | 33.618 | 122.258 | 5.8 | 32.9 |
| 54 | 0.5 | 18 | 3.4 | 615.903 | 19.4 | 3.8 | 29.846 | 125.62 | 5.1 | 36.2 |
| 54 | 0.1 | 15 | 3 | 485.561 | 14.9 | 2.9 | 31.365 | 141.025 | 5.4 | 43.8 |

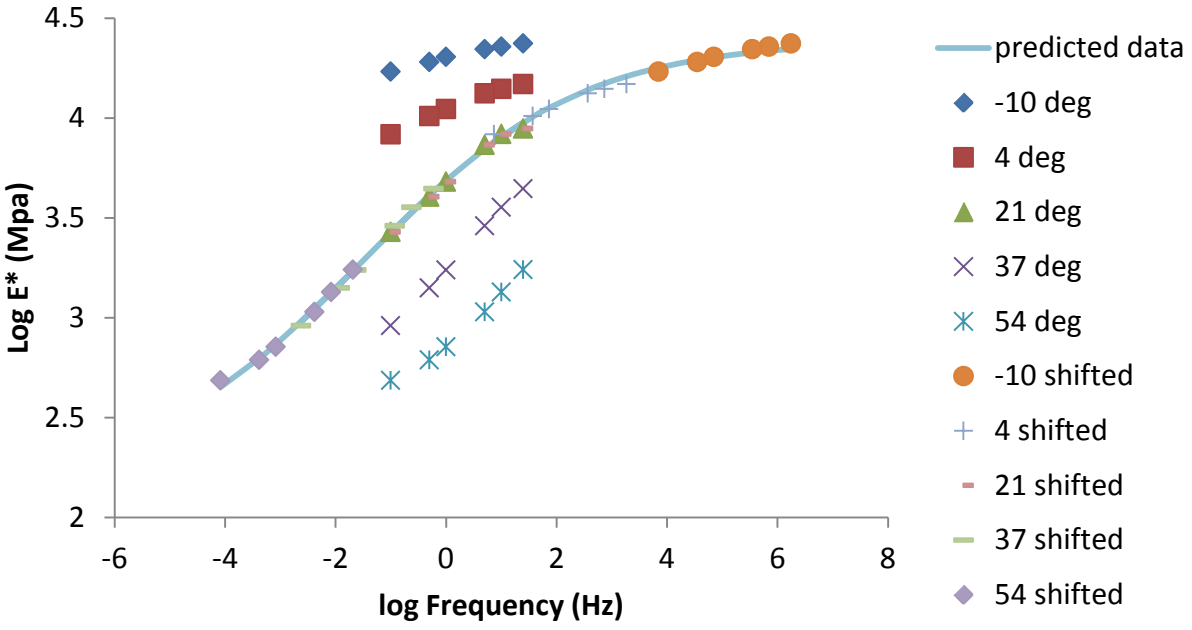


Figure D. 7: Master curve for sample 4 (SP-II with PG 70-22 binder)

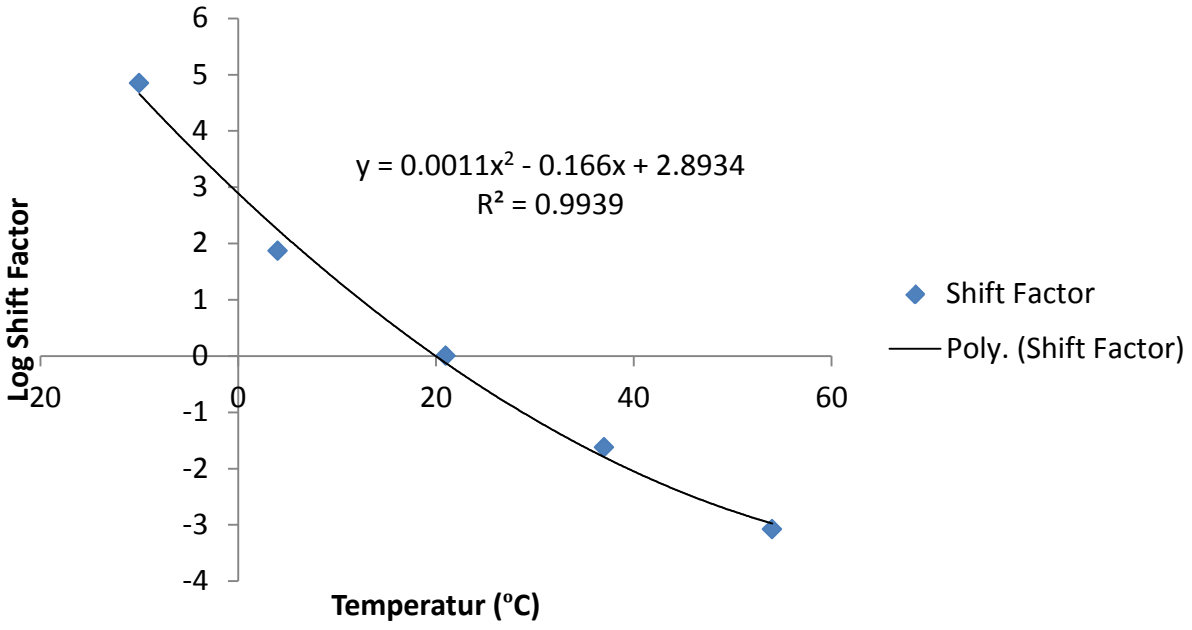


Figure D. 8: Shift factor for sample 4 (SP-II with PG 70-22 binder)

Table D. 5: E* test results for Sample 5 (SP-II with PG 70-22 binder)

| Temperature | Frequency | Stress | | Dynamic Modulus | Phase Angle | | Strain | | | |
|---|---|---|---|---|---|---|---|---|---|---|
| | | Amplitude (P-P) | SE | | | UC | (P-P) Recoverable | Permanent | SE | UC |
| (deg C) | (Hz) | (kPa) | (%) | (MPa) | (deg) | (deg) | (micro e) | (micro e) | (%) | (%) |
| -10 | 25 | 2294 | 6.3 | 29461.037 | 9.3 | 2 | 77.859 | 79.036 | 7.7 | 27.9 |
| -10 | 10 | 2248 | 6 | 28249.523 | 4.7 | 0.7 | 79.566 | 18.938 | 6.9 | 21 |
| -10 | 5 | 2189 | 5.4 | 27618.645 | 4.5 | 0.7 | 79.243 | 18.577 | 6.8 | 19.6 |
| -10 | 1 | 1910 | 1.7 | 25694.252 | 5.4 | 0.9 | 74.333 | 15.1 | 4.1 | 19.8 |
| -10 | 0.5 | 1735 | 1 | 24770.588 | 3.9 | 0.3 | 70.027 | 16.195 | 4.1 | 20 |
| -10 | 0.1 | 1574 | 0.5 | 23076.516 | 5.2 | 0.8 | 68.213 | 27.921 | 6.3 | 20.6 |
| 4 | 25 | 1269 | 7.9 | 21310.27 | 2.3 | 7.4 | 59.562 | 55.535 | 11 | 44.1 |
| 4 | 10 | 1333 | 7.7 | 22349.805 | 7.2 | 0.6 | 59.66 | 32.521 | 9.7 | 29.6 |
| 4 | 5 | 1306 | 6.4 | 21095.498 | 7.3 | 0.3 | 61.9 | 34.254 | 7.1 | 29.2 |
| 4 | 1 | 1115 | 2.8 | 18714.902 | 8.6 | 0.4 | 59.572 | 35.232 | 6.3 | 26.9 |
| 4 | 0.5 | 999 | 1.8 | 17643.465 | 10.2 | 0.1 | 56.633 | 37.837 | 4.8 | 24.5 |
| 4 | 0.1 | 860 | 0.7 | 15234.109 | 11.1 | 0.3 | 56.423 | 58.152 | 6.2 | 20.3 |
| 21 | 25 | 864 | 8.9 | 14017.16 | 11 | 8.2 | 61.658 | 90.759 | 22 | 47.8 |
| 21 | 10 | 738 | 8.7 | 12668.365 | 13.6 | 1.4 | 58.234 | 70.106 | 9.5 | 17 |
| 21 | 5 | 638 | 8.4 | 11794.512 | 14.5 | 1.1 | 54.106 | 65.132 | 9.5 | 15.1 |
| 21 | 1 | 436 | 4.8 | 8935.9 | 19.3 | 0 | 48.765 | 49.133 | 10 | 12.4 |
| 21 | 0.5 | 384 | 3.2 | 8444.93 | 17.4 | 2.1 | 45.524 | 52.787 | 6 | 7.1 |
| 21 | 0.1 | 304 | 1.3 | 5990.656 | 20.9 | 1.1 | 50.784 | 94.169 | 5 | 3.6 |
| 37 | 25 | 373 | 13 | 7376.699 | 26.4 | 10.1 | 50.616 | 173.983 | 21 | 4.5 |
| 37 | 10 | 321 | 11 | 7476.621 | 19.1 | 2 | 42.936 | 245.694 | 8.9 | 4.2 |
| 37 | 5 | 270 | 8.2 | 6294.983 | 19.9 | 2.5 | 42.96 | 272.439 | 8.6 | 9.9 |
| 37 | 1 | 183 | 4.9 | 4136.012 | 23.6 | 2.8 | 44.277 | 262.082 | 6.9 | 20.8 |
| 37 | 0.5 | 152 | 3.8 | 3437.292 | 25.7 | 2 | 44.299 | 272.424 | 6.1 | 21.7 |
| 37 | 0.1 | 112 | 1.9 | 2325.957 | 27.1 | 2.6 | 48.185 | 342.888 | 5.2 | 24.9 |
| 54 | 25 | 228 | 8.4 | 3754.338 | 28.4 | 6.4 | 60.608 | 367.061 | 8.6 | 3 |
| 54 | 10 | 204 | 8.3 | 3049.85 | 24.5 | 3 | 66.783 | 570.796 | 7 | 6 |
| 54 | 5 | 161 | 7.5 | 2527.257 | 25.7 | 2.7 | 63.866 | 641.863 | 6.2 | 8.5 |
| 54 | 1 | 109 | 5.6 | 1484.48 | 27.5 | 3.4 | 73.585 | 652.611 | 4.9 | 1.3 |
| 54 | 0.5 | 99 | 4.1 | 1269.382 | 27.7 | 4 | 77.8 | 693.33 | 6.4 | 2.7 |
| 54 | 0.1 | 78 | 1.7 | 897.949 | 25.8 | 3.9 | 87.349 | 820.33 | 8.6 | 6.8 |

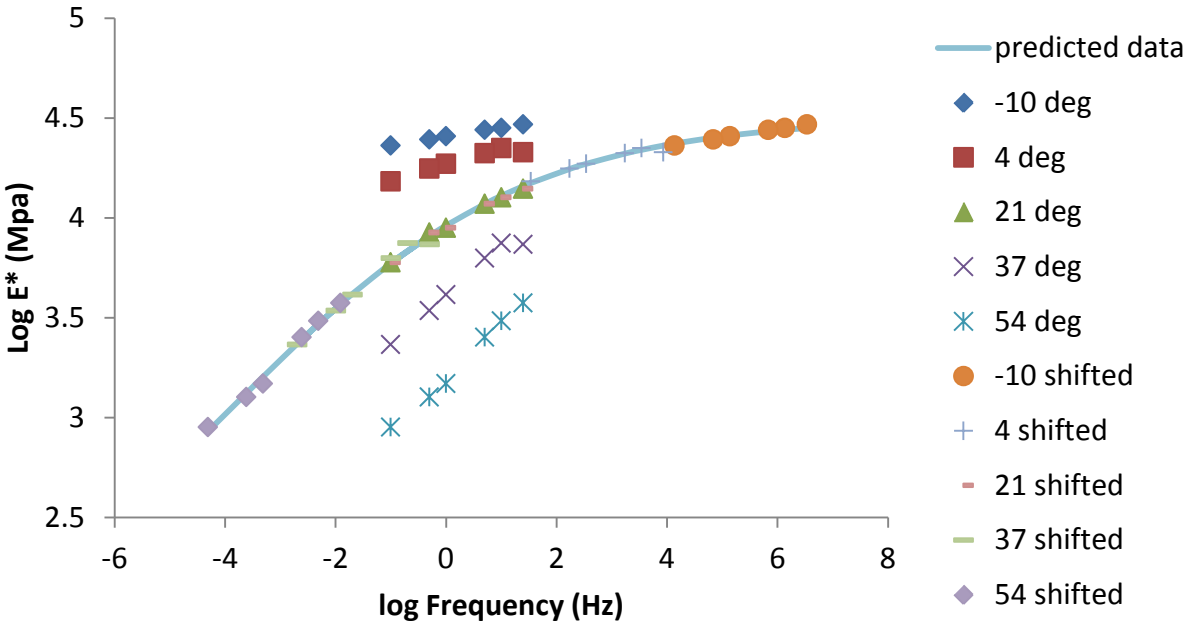


Figure D. 9: Master curve for sample 5 (SP-II with PG 70-22 binder)

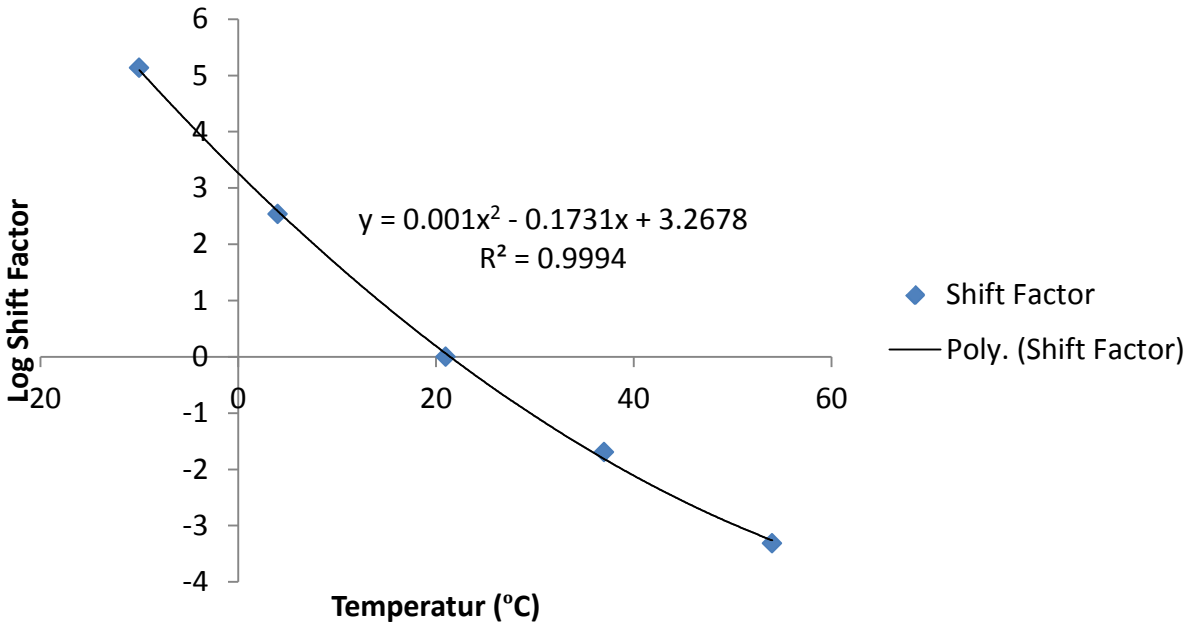


Figure D. 10: Shift factor for sample 5 (SP-II with PG 70-22 binder)

Table D. 6: E* test results for Sample 6 (SP-II with PG 70-22 binder)

| Temperature | Frequency | Stress | | Dynamic Modulus | Phase Angle | | Strain | | | |
|---|---|---|---|---|---|---|---|---|---|---|
| | | Amplitude (P-P) | SE | | | UC | (P-P) Recoverable | Permanent | SE | UC |
| (deg C) | (Hz) | (kPa) | (%) | (MPa) | (deg) | (deg) | (micro e) | (micro e) | (%) | (%) |
| -10 | 25 | 2298 | 6.2 | 33331.75 | 4.7 | 1 | 68.929 | 74.001 | 11 | 19.7 |
| -10 | 10 | 2254 | 6.3 | 32001.172 | 5.7 | 0.9 | 70.446 | 14.833 | 9 | 12.3 |
| -10 | 5 | 2192 | 5.4 | 30705.807 | 6.2 | 1.4 | 71.375 | 14.831 | 8.2 | 13.4 |
| -10 | 1 | 1909 | 1.7 | 29331.199 | 6 | 1.7 | 65.078 | 13.881 | 6.2 | 12.8 |
| -10 | 0.5 | 1733 | 1 | 26629.072 | 6.8 | 1 | 65.068 | 14.763 | 5.8 | 15.6 |
| -10 | 0.1 | 1574 | 0.5 | 25160.848 | 7.8 | 1.2 | 62.54 | 25.96 | 5.7 | 14.4 |
| 4 | 25 | 1266 | 8.9 | 18566.732 | 10.1 | 2.5 | 68.193 | 100.22 | 10 | 2 |
| 4 | 10 | 1326 | 9 | 17287.932 | 9.5 | 1.6 | 76.705 | 66.962 | 11 | 6.1 |
| 4 | 5 | 1307 | 7.7 | 16042.076 | 10 | 1.2 | 81.449 | 73.844 | 8.8 | 6.9 |
| 4 | 1 | 1117 | 3.5 | 13465.104 | 11.5 | 1.9 | 82.944 | 74.867 | 6 | 0.7 |
| 4 | 0.5 | 1001 | 2.3 | 12531.27 | 13.7 | 2.1 | 79.842 | 82.75 | 4.7 | 3.2 |
| 4 | 0.1 | 860 | 0.9 | 9997.458 | 15.2 | 2.8 | 86.035 | 140.225 | 4.2 | 7.9 |
| 21 | 25 | 860 | 9.5 | 13111.93 | 22.3 | 4.8 | 65.566 | 306.371 | 34 | 25.6 |
| 21 | 10 | 731 | 8.9 | 10558.581 | 18.2 | 0.2 | 69.269 | 339.97 | 11 | 21.3 |
| 21 | 5 | 629 | 8.1 | 9235.335 | 19.1 | 0.1 | 68.123 | 371.019 | 9.1 | 20.9 |
| 21 | 1 | 433 | 4.8 | 6917.416 | 21.9 | 0.6 | 62.609 | 354.494 | 7.2 | 22 |
| 21 | 0.5 | 383 | 3.3 | 5858.501 | 25.5 | 2.8 | 65.409 | 367.747 | 4.7 | 19.1 |
| 21 | 0.1 | 305 | 1.6 | 3950.138 | 26.7 | 1.8 | 77.142 | 468.614 | 4 | 16 |
| 37 | 25 | 378 | 13 | 5492.263 | 23.2 | 9 | 68.797 | 357.979 | 20 | 21.9 |
| 37 | 10 | 323 | 11 | 4713.86 | 24.6 | 1 | 68.503 | 486.454 | 8.9 | 18.3 |
| 37 | 5 | 270 | 9 | 3693.346 | 25.7 | 0.5 | 73.047 | 536.667 | 8.5 | 14.9 |
| 37 | 1 | 182 | 5.5 | 2232.767 | 28.8 | 0.1 | 81.694 | 523.027 | 6.3 | 3.8 |
| 37 | 0.5 | 152 | 4.1 | 1792.959 | 29.1 | 0.4 | 84.923 | 532.893 | 4.8 | 2.3 |
| 37 | 0.1 | 113 | 1.8 | 1139.466 | 27 | 0.6 | 99.484 | 617.198 | 4.3 | 1.9 |
| 54 | 25 | 114 | 9 | 1736.376 | 33.2 | 11.6 | 65.785 | 121.472 | 13 | 25.8 |
| 54 | 10 | 95 | 8.3 | 1441.434 | 27.1 | 0.4 | 65.879 | 175.315 | 6.4 | 5.8 |
| 54 | 5 | 78 | 8 | 1169.751 | 26.1 | 0.9 | 66.966 | 202.065 | 6.6 | 4.2 |
| 54 | 1 | 53 | 6.7 | 696.871 | 24.4 | 1.7 | 76.175 | 204.421 | 5.3 | 9.3 |
| 54 | 0.5 | 49 | 5.4 | 600.584 | 22.4 | 1.9 | 81.634 | 220.213 | 5 | 6.8 |
| 54 | 0.1 | 41 | 2.8 | 449.943 | 18.5 | 2.1 | 90.75 | 256.086 | 6.1 | 6.7 |

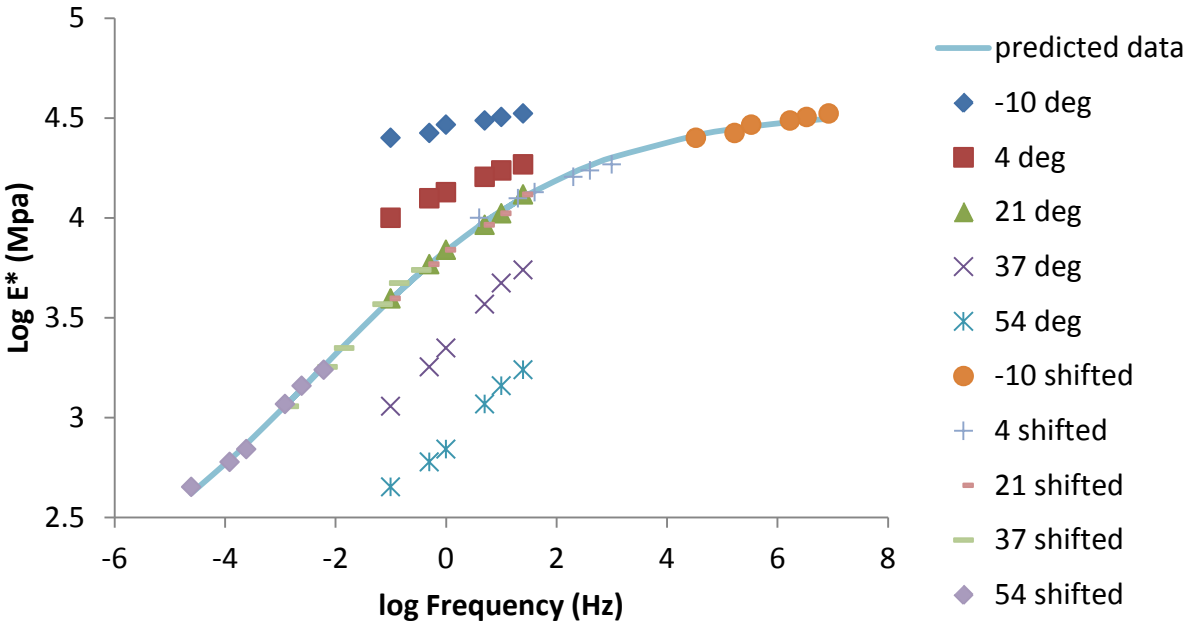


Figure D. 11: Master curve for sample 6 (SP-II with PG 70-22 binder)

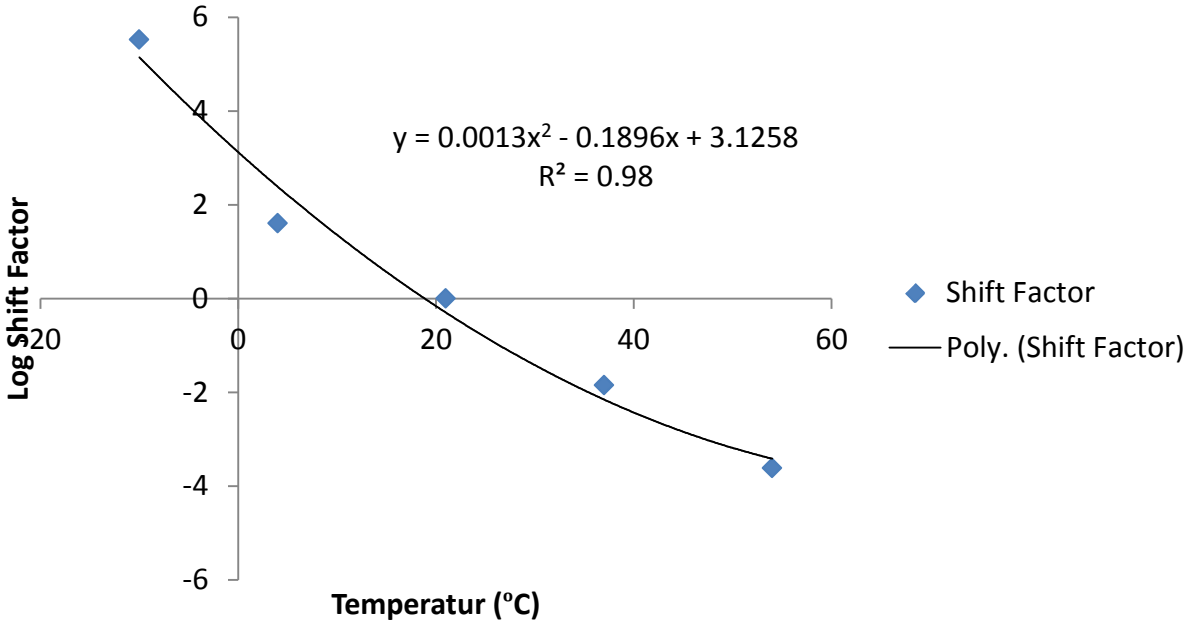


Figure D. 12: Shift factor for sample 6 (SP-II with PG 70-22 binder)

# APPENDIX E

DYNAMIC MODULUS TEST RESULTS FOR SP-IV WITH PG 70-22 BINDER

Table E. 7: E* test results for Sample 1 (SP-IV with PG 70-22 binder)

| Temperature | Frequency | Stress | | Dynamic Modulus | Phase Angle | | Strain | | | |
|---|---|---|---|---|---|---|---|---|---|---|
| | | Amplitude (P-P) | SE | | | UC | (P-P) Recoverable | Permanent | SE | UC |
| (deg C) | (Hz) | (kPa) | (%) | (MPa) | (deg) | (deg) | (micro e) | (micro e) | (%) | (%) |
| -10 | 25 | 1539 | 7.1 | 27403.5 | 12.1 | 1.7 | 56.1 | 62.5 | 13.5 | 15.8 |
| -10 | 10 | 1552 | 7.7 | 27150.6 | 6.8 | 0.8 | 57.1 | 27.2 | 9.6 | 32.1 |
| -10 | 5 | 1517 | 5.9 | 26043.9 | 6.7 | 1.2 | 58.2 | 26.7 | 9.0 | 33.1 |
| -10 | 1 | 1364 | 1.8 | 23503.2 | 8.2 | 0.3 | 58.0 | 28.9 | 9.0 | 35.8 |
| -10 | 0.5 | 1284 | 1.0 | 22032.2 | 6.9 | 1.0 | 58.3 | 31.9 | 5.1 | 36.7 |
| -10 | 0.1 | 1166 | 0.5 | 19524.5 | 11.0 | 0.1 | 59.7 | 52.9 | 9.8 | 36.3 |
| 4 | 25 | 1113 | 8.1 | 19352.5 | 19.7 | 11.1 | 57.5 | 169.1 | 13.2 | 20.6 |
| 4 | 10 | 1024 | 8.3 | 17755.1 | 13.9 | 2.6 | 57.7 | 152.0 | 8.7 | 8.3 |
| 4 | 5 | 936 | 6.7 | 16204.3 | 14.6 | 2.5 | 57.8 | 169.1 | 6.9 | 6.6 |
| 4 | 1 | 715 | 2.9 | 12627.4 | 17.5 | 2.7 | 56.6 | 173.6 | 4.6 | 3.9 |
| 4 | 0.5 | 633 | 1.8 | 11057.0 | 21.3 | 4.7 | 57.2 | 191.1 | 7.5 | 1.8 |
| 4 | 0.1 | 448 | 0.9 | 8347.5 | 22.9 | 2.5 | 53.6 | 261.2 | 3.9 | 0.9 |
| 21 | 25 | 429 | 9.8 | 8068.7 | 23.7 | 1.9 | 53.2 | 404.6 | 11.5 | 23.3 |
| 21 | 10 | 356 | 11.2 | 6493.9 | 24.6 | 2.6 | 54.8 | 570.2 | 9.3 | 18.2 |
| 21 | 5 | 297 | 10.0 | 5331.0 | 26.3 | 3.0 | 55.7 | 655.6 | 8.1 | 14.6 |
| 21 | 1 | 202 | 5.1 | 3175.9 | 30.8 | 3.4 | 63.6 | 659.4 | 5.3 | 13.7 |
| 21 | 0.5 | 170 | 3.3 | 2589.5 | 32.4 | 4.1 | 65.7 | 703.7 | 4.5 | 14.4 |
| 21 | 0.1 | 112 | 1.2 | 1543.2 | 33.7 | 4.8 | 72.7 | 819.3 | 3.5 | 11.9 |
| 37 | 25 | 146 | 9.9 | 2484.5 | 36.7 | 0.4 | 58.7 | 460.0 | 8.2 | 1.9 |
| 37 | 10 | 124 | 9.8 | 1752.4 | 35.4 | 3.0 | 70.6 | 751.5 | 7.5 | 10.7 |
| 37 | 5 | 91 | 9.3 | 1343.2 | 35.9 | 3.5 | 68.0 | 846.9 | 7.4 | 11.5 |
| 37 | 1 | 53 | 5.7 | 703.8 | 35.2 | 4.4 | 75.4 | 852.8 | 5.9 | 13.9 |
| 37 | 0.5 | 41 | 4.1 | 555.1 | 34.2 | 5.0 | 73.0 | 864.2 | 4.7 | 10.5 |
| 37 | 0.1 | 25 | 1.8 | 364.5 | 29.6 | 6.3 | 67.7 | 886.7 | 4.9 | 2.9 |
| 54 | 25 | 28 | 6.7 | 534.709 | 35.3 | 6.2 | 52.074 | 310.572 | 7 | 19.3 |
| 54 | 10 | 23 | 5.4 | 401.472 | 29.9 | 0.1 | 56.448 | 434.176 | 4.8 | 1.2 |
| 54 | 5 | 19 | 5.8 | 329.095 | 27.6 | 0.8 | 56.339 | 468.307 | 9 | 0.7 |
| 54 | 1 | 11 | 6.2 | 220.836 | 20.7 | 0.5 | 51.886 | 466.481 | 11.6 | 2 |
| 54 | 0.5 | 10 | 8.2 | 195.123 | 18.7 | 0.7 | 51.153 | 469.821 | 9.3 | 1.2 |
| 54 | 0.1 | 8 | 9.8 | 153.339 | 16 | 0.7 | 52.708 | 486.686 | 14.8 | 3.2 |

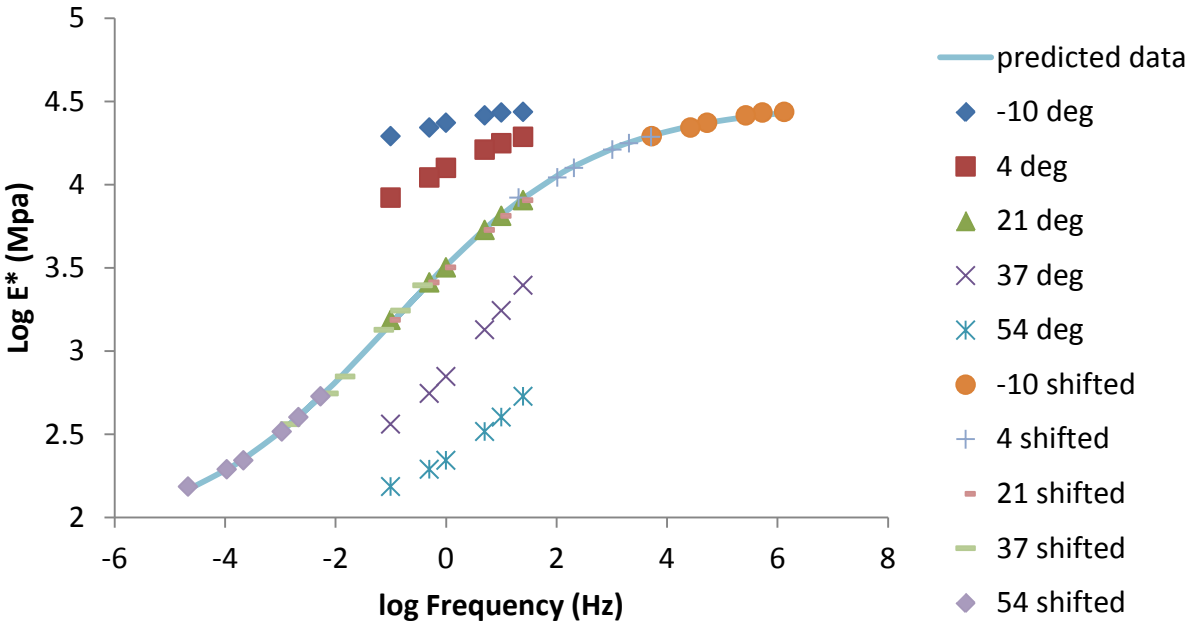


Figure E. 13: Master curve for sample 1 (SP-IV with PG 70-22 binder)

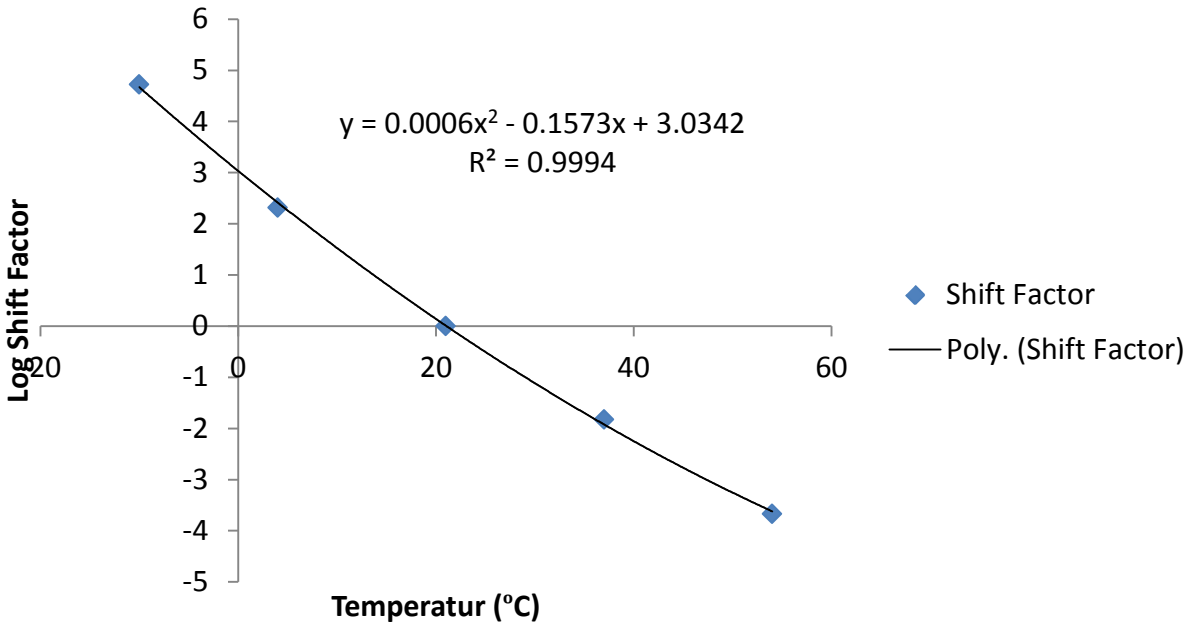


Figure E. 14: Shift factor for sample 1 (SP-IV with PG 70-22 binder)

Table E. 8: E* test results for Sample 2 (SP-IV with PG 70-22 binder)

| Temperature | Frequency | Stress | | Dynamic Modulus | Phase Angle | | Strain | | | |
|---|---|---|---|---|---|---|---|---|---|---|
| | | Amplitude (P-P) | SE | | | UC | (P-P) Recoverable | Permanent | SE | UC |
| (deg C) | (Hz) | (kPa) | (%) | (MPa) | (deg) | (deg) | (micro e) | (micro e) | (%) | (%) |
| -10 | 25 | 1760 | 5.7 | 30858.7 | 6.0 | 1.7 | 57.0 | 57.8 | 6.9 | 29.9 |
| -10 | 10 | 1782 | 5.7 | 29603.5 | 5.6 | 0.1 | 60.2 | 23.5 | 6.8 | 33.1 |
| -10 | 5 | 1728 | 4.5 | 28745.9 | 5.4 | 0.3 | 60.1 | 16.4 | 5.5 | 33.5 |
| -10 | 1 | 1557 | 1.2 | 26027.2 | 6.0 | 0.7 | 59.8 | 13.9 | 5.1 | 33.6 |
| -10 | 0.5 | 1468 | 0.7 | 25135.9 | 7.3 | 0.3 | 58.4 | 18.0 | 4.1 | 35.7 |
| -10 | 0.1 | 1335 | 0.4 | 21973.2 | 8.6 | 0.1 | 60.8 | 29.3 | 3.3 | 35.7 |
| 4 | 25 | 1113 | 7.7 | 18215.0 | 18.4 | 4.0 | 61.1 | 166.1 | 10.3 | 2.9 |
| 4 | 10 | 1027 | 7.8 | 16676.0 | 13.2 | 1.7 | 61.6 | 146.5 | 8.5 | 10.9 |
| 4 | 5 | 938 | 6.6 | 15346.3 | 13.9 | 1.2 | 61.1 | 164.2 | 6.6 | 11.3 |
| 4 | 1 | 715 | 2.9 | 12117.5 | 17.6 | 2.3 | 59.0 | 168.4 | 6.9 | 12.0 |
| 4 | 0.5 | 634 | 1.8 | 10977.4 | 17.4 | 1.1 | 57.7 | 183.8 | 4.0 | 10.0 |
| 4 | 0.1 | 448 | 1.0 | 8134.9 | 22.1 | 2.4 | 55.0 | 249.8 | 3.7 | 2.6 |
| 21 | 25 | 422 | 10.9 | 8268.7 | 29.4 | 1.4 | 51.1 | 485.7 | 35.0 | 22.1 |
| 21 | 10 | 358 | 10.6 | 7015.3 | 25.5 | 3.1 | 51.0 | 687.5 | 8.5 | 36.6 |
| 21 | 5 | 297 | 9.3 | 5772.3 | 27.0 | 3.3 | 51.5 | 786.6 | 6.7 | 32.2 |
| 21 | 1 | 202 | 4.5 | 3391.9 | 32.2 | 3.7 | 59.4 | 796.6 | 4.7 | 27.4 |
| 21 | 0.5 | 170 | 3.0 | 2709.9 | 33.5 | 3.5 | 62.8 | 841.1 | 3.8 | 27.8 |
| 21 | 0.1 | 112 | 1.1 | 1662.3 | 33.7 | 3.7 | 67.4 | 946.0 | 4.4 | 25.1 |
| 37 | 25 | 131 | 9.8 | 2284.8 | 33.6 | 1.8 | 57.5 | 382.8 | 8.2 | 2.0 |
| 37 | 10 | 110 | 9.4 | 1625.9 | 32.8 | 0.7 | 67.6 | 556.6 | 6.8 | 7.4 |
| 37 | 5 | 82 | 9.0 | 1227.7 | 32.9 | 0.8 | 67.0 | 608.9 | 6.9 | 13.5 |
| 37 | 1 | 47 | 5.7 | 642.6 | 31.7 | 0.6 | 73.7 | 604.9 | 5.0 | 20.8 |
| 37 | 0.5 | 37 | 4.4 | 505.5 | 29.9 | 0.7 | 72.6 | 610.5 | 3.9 | 23.7 |
| 37 | 0.1 | 21 | 2.2 | 316.1 | 24.0 | 1.2 | 67.5 | 624.7 | 3.5 | 22.8 |
| 54 | 25 | 41 | 9.2 | 592.4 | 28.1 | 34.3 | 68.5 | 196.4 | 10.7 | 42.0 |
| 54 | 10 | 32 | 7.4 | 494.1 | 31.1 | 3.6 | 65.4 | 296.2 | 5.8 | 13.9 |
| 54 | 5 | 27 | 6.8 | 417.7 | 27.0 | 3.2 | 65.8 | 340.8 | 4.2 | 3.2 |
| 54 | 1 | 18 | 4.9 | 320.0 | 19.3 | 0.8 | 55.6 | 336.0 | 4.2 | 18.1 |
| 54 | 0.5 | 15 | 4.4 | 301.0 | 16.6 | 0.9 | 51.4 | 334.0 | 3.6 | 25.2 |
| 54 | 0.1 | 11 | 2.9 | 265.1 | 10.4 | 0.6 | 42.2 | 330.5 | 5.1 | 39.6 |

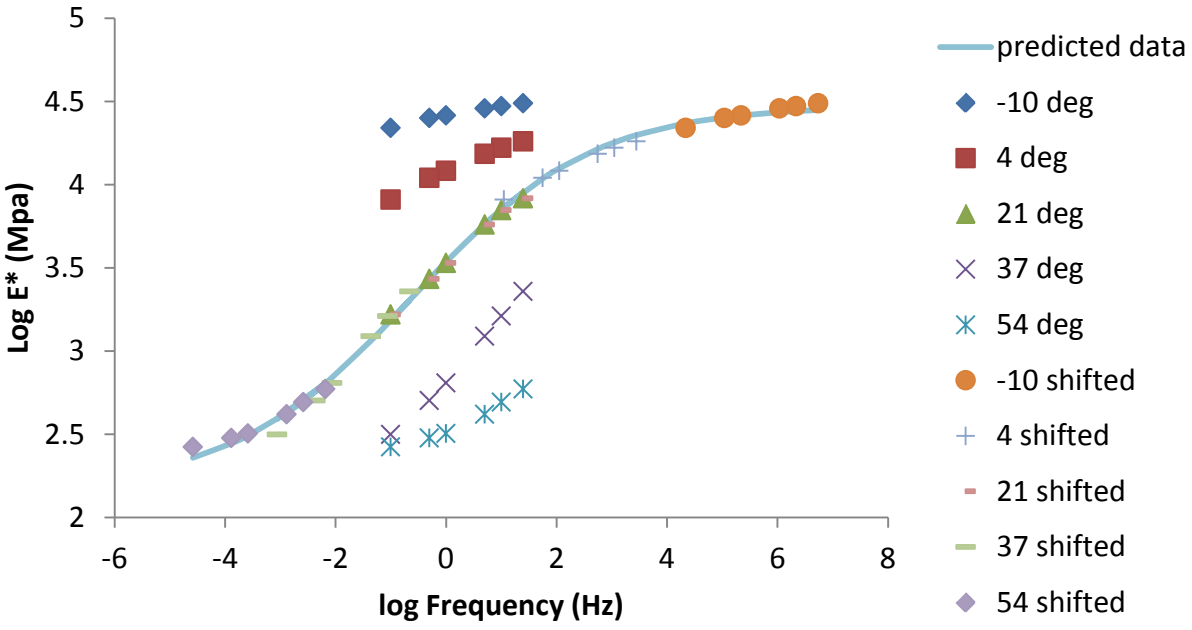


Figure E. 15: Master curve for sample 2 (SP-IV with PG 70-22 binder)

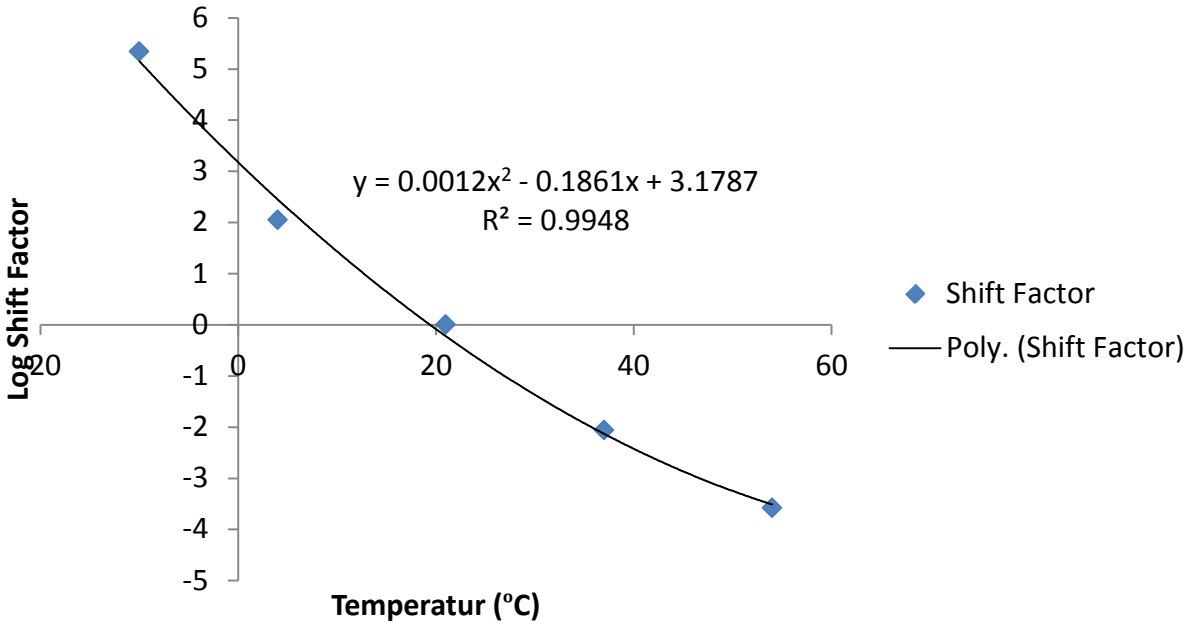


Figure E. 16: Shift factor for sample 2 (SP-IV with PG 70-22 binder)

Table E. 9: E* test results for Sample 3 (SP-IV with PG 70-22 binder)

| Temperature | Frequency | Stress | | Dynamic Modulus | Phase Angle | | Strain | | | |
|---|---|---|---|---|---|---|---|---|---|---|
| | | Amplitude (P-P) | SE | | | UC | (P-P) Recoverable | Permanent | SE | UC |
| (deg C) | (Hz) | (kPa) | (%) | (MPa) | (deg) | (deg) | (micro e) | (micro e) | (%) | (%) |
| -10 | 25 | 2288 | 5.9 | 30190.744 | 5.8 | 1.1 | 75.793 | 79.415 | 8.8 | 18.9 |
| -10 | 10 | 2188 | 6.1 | 29133.283 | 5.4 | 0.3 | 75.12 | 14.926 | 8.7 | 18.3 |
| -10 | 5 | 2116 | 5.2 | 28118.191 | 5.2 | 0.5 | 75.271 | 13.198 | 9.4 | 17.4 |
| -10 | 1 | 1858 | 1.6 | 25860.313 | 6.1 | 0.5 | 71.84 | 12.66 | 7.6 | 20 |
| -10 | 0.5 | 1731 | 0.9 | 25818.975 | 6.6 | 0.3 | 67.057 | 13.633 | 5.2 | 18.7 |
| -10 | 0.1 | 1604 | 0.5 | 22382.008 | 6.9 | 0.4 | 71.68 | 29.73 | 6.2 | 21.2 |
| 4 | 25 | 1469 | 6.5 | 21625.295 | 10.3 | 0.2 | 67.915 | 105.896 | 7.4 | 1.7 |
| 4 | 10 | 1365 | 7 | 20020.873 | 9.1 | 0.2 | 68.183 | 40.994 | 8.4 | 8.4 |
| 4 | 5 | 1281 | 6 | 18700.885 | 9.3 | 0.2 | 68.479 | 38.165 | 7.4 | 9.9 |
| 4 | 1 | 1072 | 2.3 | 15911.765 | 10.7 | 0 | 67.39 | 36.452 | 8.4 | 12.3 |
| 4 | 0.5 | 952 | 1.4 | 14191.255 | 11.6 | 0.1 | 67.101 | 42.252 | 4.2 | 15.3 |
| 4 | 0.1 | 785 | 0.5 | 11744.354 | 15.2 | 0.6 | 66.823 | 84.539 | 7.7 | 13.5 |
| 21 | 25 | 655 | 9.3 | 9905.348 | 19.3 | 2.3 | 66.118 | 317.902 | 13 | 8.8 |
| 21 | 10 | 550 | 9.5 | 8288.413 | 18.7 | 0.3 | 66.375 | 379.002 | 8.6 | 6 |
| 21 | 5 | 467 | 9.5 | 7255.802 | 20.1 | 0 | 64.315 | 416.217 | 7.8 | 6.2 |
| 21 | 1 | 303 | 5.5 | 4909.348 | 24.1 | 0.1 | 61.746 | 399.884 | 4.9 | 0.1 |
| 21 | 0.5 | 257 | 3.1 | 3999.884 | 25.7 | 0 | 64.319 | 420.825 | 3.6 | 1.1 |
| 21 | 0.1 | 169 | 1.3 | 2551.361 | 28.3 | 0.3 | 66.094 | 509.56 | 2.9 | 2.7 |
| 37 | 25 | 261 | 9.5 | 4214.005 | 26.6 | 7.1 | 62.027 | 413.907 | 19 | 14.3 |
| 37 | 10 | 218 | 9.7 | 3270.401 | 27.4 | 0.6 | 66.632 | 629.521 | 9.3 | 10.8 |
| 37 | 5 | 162 | 8.8 | 2577.224 | 28.1 | 0.1 | 62.724 | 680.179 | 7.1 | 9.2 |
| 37 | 1 | 96 | 5.6 | 1419.351 | 31.4 | 1.2 | 67.542 | 659.897 | 8.1 | 1.9 |
| 37 | 0.5 | 76 | 3.9 | 1126.01 | 31.2 | 0.5 | 67.113 | 674.609 | 5 | 3.8 |
| 37 | 0.1 | 43 | 2.7 | 658.969 | 29 | 0.2 | 65.315 | 722.468 | 4 | 8.5 |
| 54 | 25 | 71 | 9.3 | 1298.131 | 34.3 | 1.3 | 54.908 | 339.206 | 7.6 | 2.4 |
| 54 | 10 | 59 | 7.8 | 936.152 | 31.3 | 0.9 | 63.199 | 500.488 | 5.2 | 1.1 |
| 54 | 5 | 49 | 6.7 | 724.029 | 29.8 | 0.9 | 67.219 | 563.521 | 5.4 | 0.9 |
| 54 | 1 | 32 | 5.6 | 428.028 | 27.2 | 0.9 | 74.435 | 573.882 | 4.7 | 4.3 |
| 54 | 0.5 | 28 | 4.2 | 358.361 | 24.7 | 0.7 | 78.344 | 595.17 | 4.8 | 3.4 |
| 54 | 0.1 | 23 | 3.3 | 265.662 | 19.6 | 0.1 | 86.741 | 648.351 | 7.4 | 2.5 |

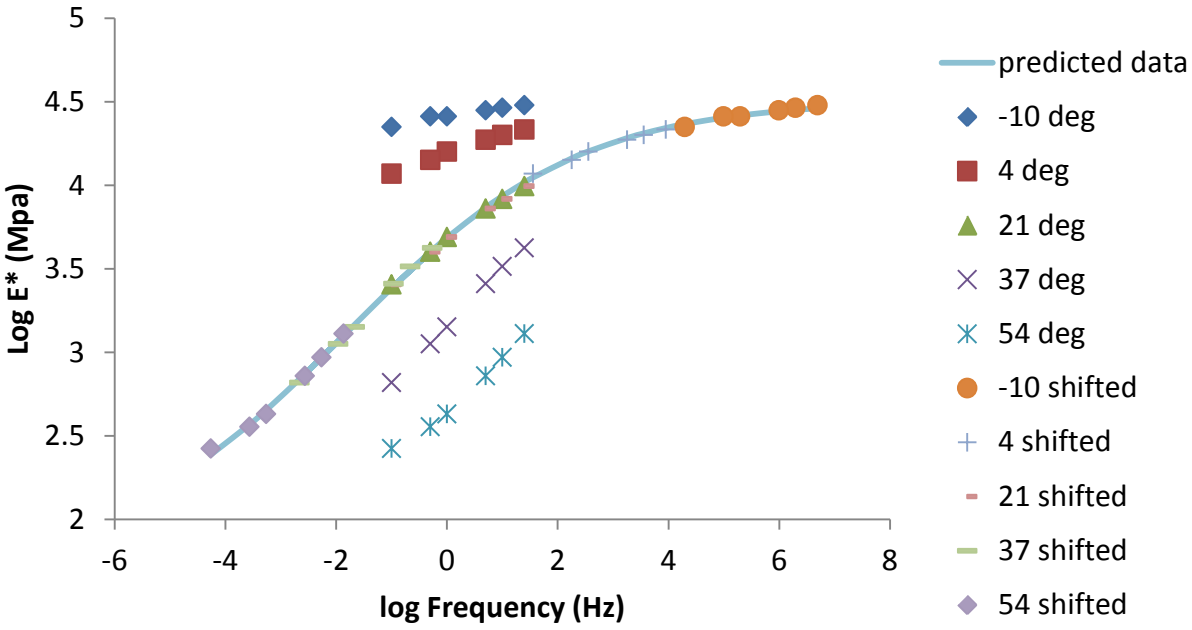


Figure E. 17: Master curve for Sample 3 (SP-IV with PG 70-22 binder)

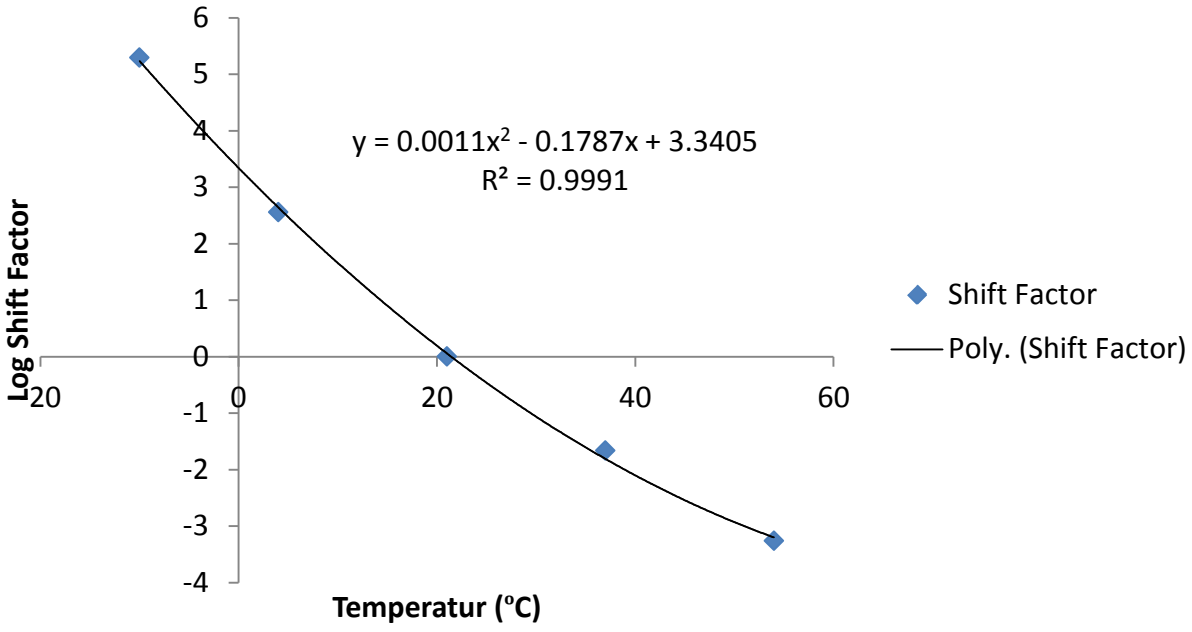


Figure E. 18: Shift factor for Sample 3 (SP-IV with PG 70-22 binder)

Table E. 10: E* test results for Sample 4 (SP-IV with PG 70-22 binder)

| Temperature | Frequency | Stress | | Dynamic Modulus | Phase Angle | | Strain | | | |
|---|---|---|---|---|---|---|---|---|---|---|
| | | Amplitude (P-P) | SE | | | UC | (P-P) Recoverable | Permanent | SE | UC |
| (deg C) | (Hz) | (kPa) | (%) | (MPa) | (deg) | (deg) | (micro e) | (micro e) | (%) | (%) |
| -10 | 25 | 2284 | 6.1 | 27870.521 | 8.2 | 6 | 81.941 | 95.201 | 7.3 | 5.2 |
| -10 | 10 | 2182 | 6.1 | 26863.889 | 5.4 | 0 | 81.239 | 28.557 | 7.6 | 2.5 |
| -10 | 5 | 2125 | 5.4 | 26322.541 | 5 | 0.2 | 80.714 | 26.048 | 6.6 | 1.2 |
| -10 | 1 | 1860 | 1.7 | 24133.479 | 5.5 | 0.6 | 77.062 | 25.203 | 6.3 | 1 |
| -10 | 0.5 | 1733 | 0.9 | 22164.762 | 6.4 | 0.1 | 78.181 | 26.649 | 4.5 | 1.8 |
| -10 | 0.1 | 1605 | 0.4 | 20529.926 | 7.9 | 0.3 | 78.177 | 41.239 | 6 | 0.3 |
| 4 | 25 | 1473 | 7 | 20316.455 | 9.8 | 3.3 | 72.499 | 144.386 | 7.5 | 32.3 |
| 4 | 10 | 1367 | 7.8 | 18166.545 | 10 | 0.7 | 75.256 | 80.528 | 8.5 | 21.9 |
| 4 | 5 | 1279 | 6.7 | 17364.184 | 9.4 | 0.1 | 73.665 | 82.893 | 13 | 22.8 |
| 4 | 1 | 1073 | 2.6 | 14095.119 | 13.3 | 1.5 | 76.123 | 85.158 | 4.4 | 18.8 |
| 4 | 0.5 | 952 | 1.6 | 13090.8 | 13.9 | 1.5 | 72.694 | 92.668 | 4.7 | 19.2 |
| 4 | 0.1 | 784 | 0.6 | 10328.222 | 15.7 | 1.2 | 75.924 | 145.136 | 4.4 | 19.1 |
| 21 | 25 | 585 | 9.1 | 9268.237 | 17.9 | 2.4 | 63.172 | 237.591 | 8.4 | 2.4 |
| 21 | 10 | 492 | 10 | 7775.177 | 18.4 | 0.6 | 63.325 | 305.267 | 9.6 | 3.5 |
| 21 | 5 | 418 | 10 | 6926.833 | 19.6 | 0.7 | 60.413 | 336.126 | 8.6 | 3.3 |
| 21 | 1 | 274 | 5 | 4546.571 | 23.5 | 1 | 60.358 | 322.434 | 5.2 | 9.1 |
| 21 | 0.5 | 231 | 3.3 | 3849.597 | 25 | 0.8 | 60.12 | 338.254 | 4.6 | 9.9 |
| 21 | 0.1 | 153 | 1.2 | 2528.231 | 27.8 | 0.6 | 60.589 | 411.707 | 3.3 | 10.8 |
| 37 | 25 | 219 | 9.6 | 3357.617 | 28.1 | 2 | 65.172 | 559.408 | 9.3 | 16.3 |
| 37 | 10 | 183 | 9.6 | 2587.447 | 27.5 | 0.5 | 70.612 | 804.307 | 7.2 | 7.3 |
| 37 | 5 | 137 | 8.7 | 2067.036 | 28.6 | 0.9 | 66.126 | 867.508 | 6.3 | 7.7 |
| 37 | 1 | 79 | 5.8 | 1142.5 | 31.1 | 1 | 69.239 | 853.743 | 4.8 | 6.7 |
| 37 | 0.5 | 62 | 4 | 899.356 | 30.9 | 1.2 | 68.855 | 868.386 | 4.7 | 6 |
| 37 | 0.1 | 36 | 2.7 | 522.808 | 29.2 | 1.2 | 68.292 | 916.359 | 3.8 | 4.7 |
| 54 | 25 | 55 | 8.5 | 937.895 | 36.2 | 8 | 59.013 | 96.009 | 8.6 | 11.4 |
| 54 | 10 | 45 | 6.8 | 689.88 | 32.4 | 2.5 | 65.924 | 145.164 | 7.7 | 2.5 |
| 54 | 5 | 36 | 5.3 | 539.367 | 31.3 | 3.7 | 67.517 | 159.838 | 6.2 | 4.1 |
| 54 | 1 | 24 | 3.9 | 310.104 | 27.8 | 3.3 | 76.478 | 157.602 | 7.2 | 10.6 |
| 54 | 0.5 | 22 | 3.7 | 256.901 | 25.3 | 3 | 85.14 | 168.054 | 4.8 | 13.5 |
| 54 | 0.1 | 18 | 2.6 | 181.758 | 19.8 | 2.5 | 96.953 | 209.564 | 5.2 | 20.3 |

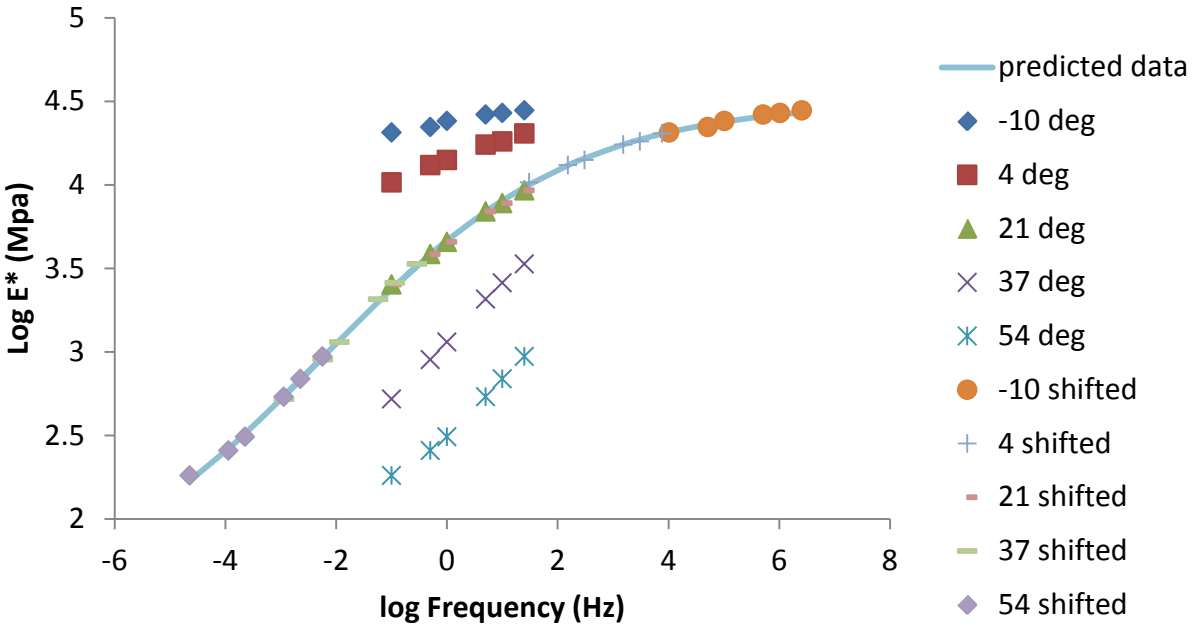


Figure E. 19: Master curve for Sample 4 (SP-IV with PG 70-22 binder)

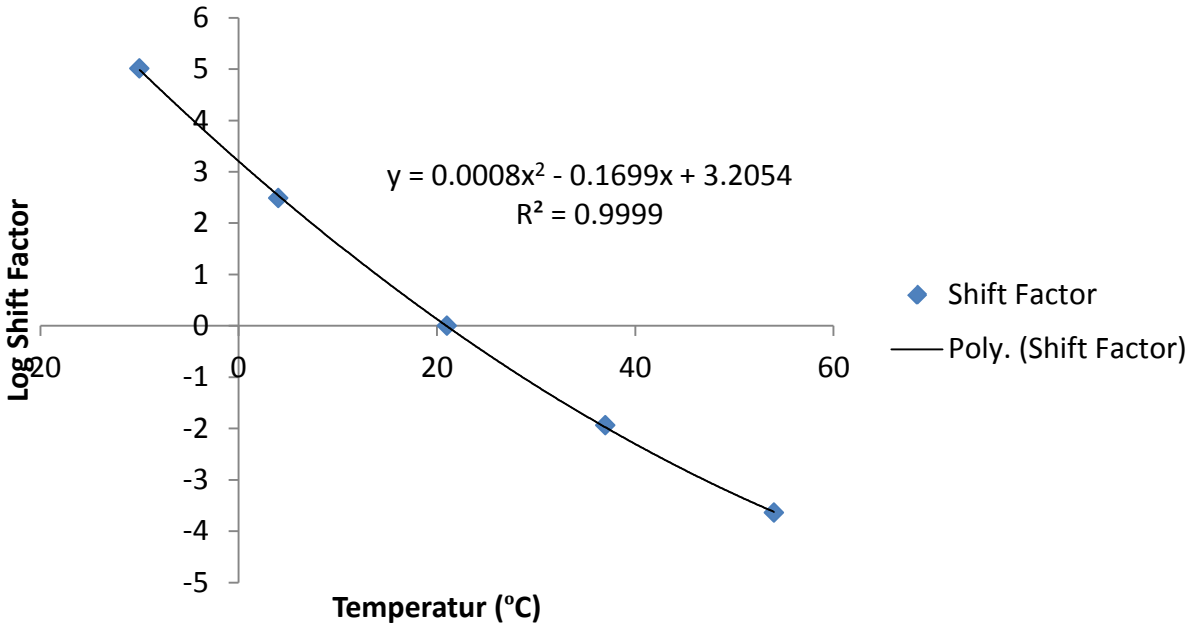


Figure E. 20: Shift factor for Sample 4 (SP-IV with PG 70-22 binder)

Table E. 11: E* test results for Sample 5 (SP-IV with PG 70-22 binder)

| Temperature | Frequency | Stress | | Dynamic Modulus | Phase Angle | | Strain | | | |
|---|---|---|---|---|---|---|---|---|---|---|
| | | Amplitude (P-P) | SE | | | UC | (P-P) Recoverable | Permanent | SE | UC |
| (deg C) | (Hz) | (kPa) | (%) | (MPa) | (deg) | (deg) | (micro e) | (micro e) | (%) | (%) |
| -10 | 25 | 1539.0 | 5.5 | 24367.8 | 5.7 | 0.8 | 63.1 | 70.0 | 6.1 | 17.3 |
| -10 | 10 | 1554.0 | 5.3 | 23665.4 | 5.6 | 0.2 | 65.7 | 30.4 | 5.6 | 24.3 |
| -10 | 5 | 1506.0 | 4.2 | 22811.3 | 5.8 | 0.2 | 66.0 | 34.2 | 4.7 | 24.3 |
| -10 | 1 | 1357.0 | 1.2 | 20487.9 | 7.0 | 0.3 | 66.2 | 33.3 | 4.4 | 24.8 |
| -10 | 0.5 | 1281.0 | 0.7 | 19221.9 | 7.1 | 0.1 | 66.6 | 35.7 | 6.0 | 22.7 |
| -10 | 0.1 | 1166.0 | 0.4 | 17009.3 | 8.3 | 0.1 | 68.5 | 59.4 | 6.6 | 23.3 |
| 4 | 25 | 1217.0 | 7.0 | 19924.6 | 14.3 | 2.0 | 61.1 | 185.7 | 6.8 | 0.7 |
| 4 | 10 | 1191.0 | 7.6 | 18009.6 | 13.5 | 2.7 | 66.1 | 157.1 | 7.5 | 8.3 |
| 4 | 5 | 1136.0 | 6.3 | 16418.0 | 14.2 | 2.9 | 69.2 | 178.4 | 6.2 | 8.6 |
| 4 | 1 | 963.0 | 2.3 | 12831.3 | 16.8 | 2.8 | 75.0 | 189.2 | 4.2 | 7.3 |
| 4 | 0.5 | 885.0 | 1.3 | 11478.9 | 19.7 | 3.5 | 77.1 | 217.9 | 3.0 | 7.3 |
| 4 | 0.1 | 796.0 | 0.7 | 8169.4 | 23.4 | 3.4 | 97.5 | 376.0 | 3.2 | 6.1 |
| 21 | 25 | 430.0 | 9.9 | 7528.9 | 25.6 | 0.9 | 57.1 | 389.0 | 21.0 | 27.2 |
| 21 | 10 | 357.0 | 10.2 | 6115.1 | 24.0 | 0.4 | 58.3 | 549.8 | 8.1 | 27.8 |
| 21 | 5 | 297.0 | 9.2 | 4965.0 | 25.4 | 0.5 | 59.8 | 628.8 | 5.8 | 27.8 |
| 21 | 1 | 202.0 | 4.6 | 2873.1 | 30.2 | 1.1 | 70.3 | 625.4 | 4.4 | 27.7 |
| 21 | 0.5 | 170.0 | 3.1 | 2268.7 | 31.7 | 1.2 | 75.1 | 664.1 | 3.5 | 26.2 |
| 21 | 0.1 | 112.0 | 1.1 | 1309.1 | 32.1 | 1.4 | 85.5 | 778.0 | 3.9 | 22.9 |
| 37 | 25 | 133.0 | 9.9 | 2197.8 | 33.9 | 0.7 | 60.3 | 557.9 | 8.2 | 25.7 |
| 37 | 10 | 110.0 | 9.6 | 1521.4 | 33.1 | 0.7 | 72.6 | 805.3 | 7.0 | 19.3 |
| 37 | 5 | 83.0 | 9.3 | 1133.4 | 33.2 | 0.8 | 72.9 | 882.3 | 6.8 | 20.5 |
| 37 | 1 | 47.0 | 6.0 | 592.6 | 31.3 | 1.8 | 79.9 | 879.3 | 5.2 | 27.9 |
| 37 | 0.5 | 37.0 | 4.3 | 463.0 | 29.6 | 1.7 | 79.9 | 887.4 | 4.4 | 30.6 |
| 37 | 0.1 | 22.0 | 2.0 | 284.6 | 23.6 | 1.4 | 75.9 | 906.6 | 3.6 | 39.8 |
| 54 | 25 | 41.0 | 9.4 | 469.2 | 30.9 | 31.4 | 86.4 | 539.6 | 11.4 | 39.5 |
| 54 | 10 | 33.0 | 7.7 | 378.7 | 28.3 | 0.7 | 86.4 | 735.0 | 6.3 | 31.3 |
| 54 | 5 | 28.0 | 7.4 | 305.4 | 26.0 | 0.2 | 91.7 | 827.1 | 5.1 | 30.6 |
| 54 | 1 | 18.0 | 5.4 | 208.4 | 19.7 | 0.0 | 85.4 | 836.2 | 6.6 | 37.6 |
| 54 | 0.5 | 15.0 | 4.3 | 184.0 | 18.2 | 0.2 | 83.6 | 850.0 | 5.3 | 35.3 |
| 54 | 0.1 | 11.0 | 3.2 | 150.0 | 13.0 | 0.4 | 74.5 | 873.7 | 7.1 | 34.9 |

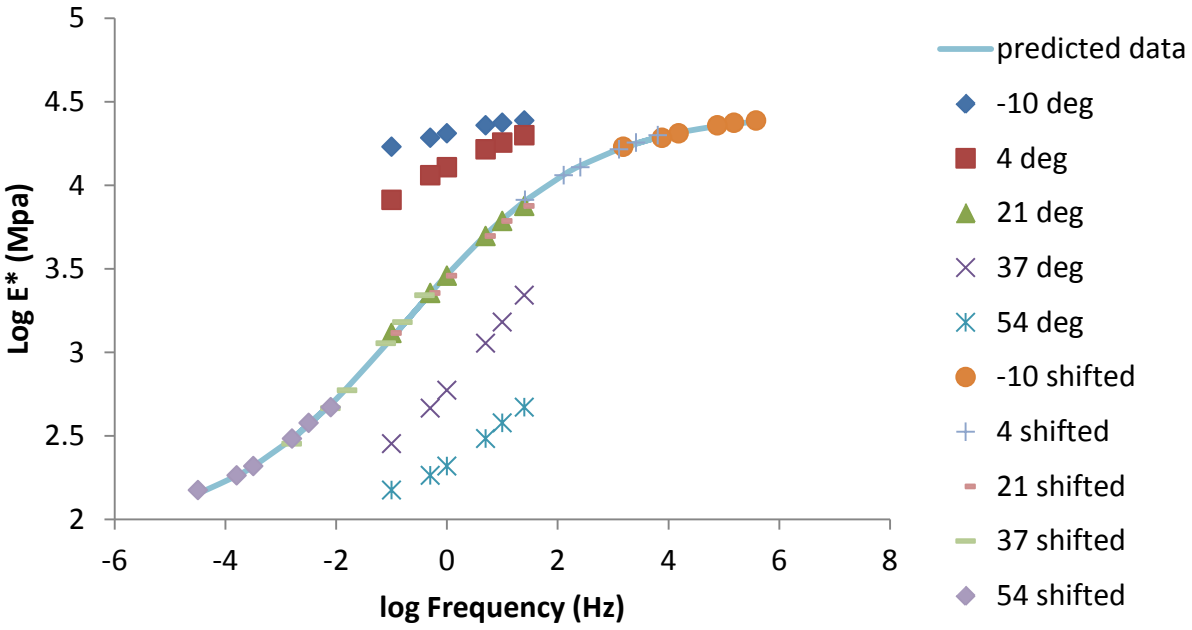


Figure E. 21: Master curve for Sample 5 (SP-IV with PG 70-22 binder)

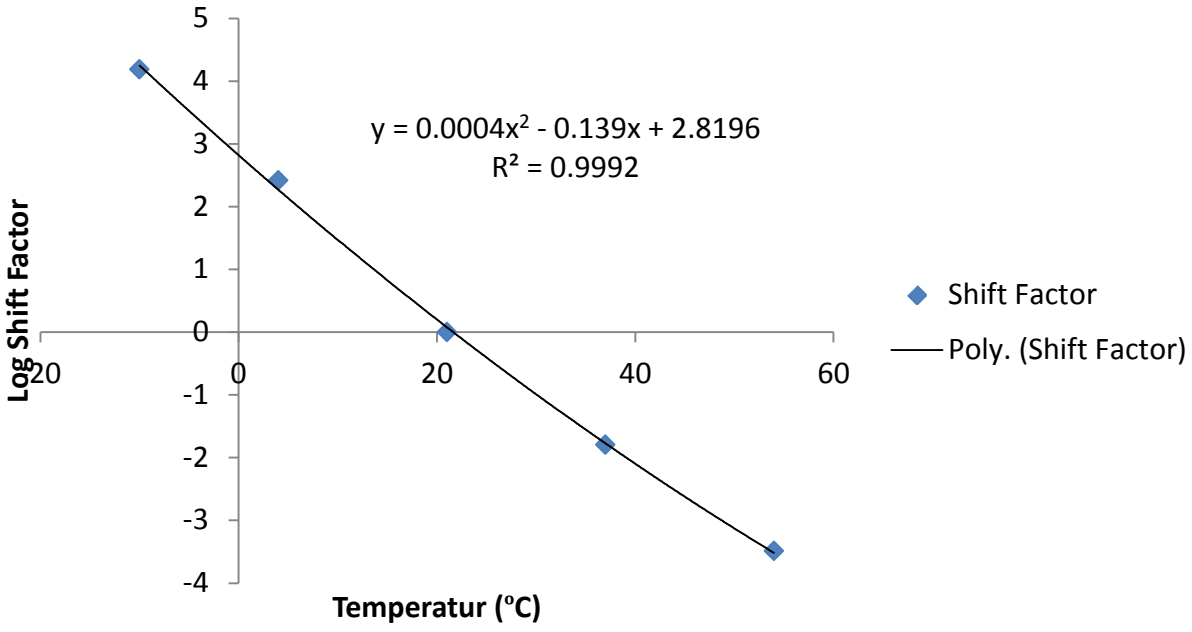


Figure E. 22: Shift factor for Sample 5 (SP-IV with PG 70-22 binder)

Table E. 12: E* test results for Sample 6 (SP-IV with PG 70-22 binder)

| Temperature | Frequency | Stress | | Dynamic Modulus | Phase Angle | | Strain | | | |
|---|---|---|---|---|---|---|---|---|---|---|
| | | Amplitude (P-P) | SE | | | UC | (P-P) Recoverable | Permanent | SE | UC |
| (deg C) | (Hz) | (kPa) | (%) | (MPa) | (deg) | (deg) | (micro e) | (micro e) | (%) | (%) |
| -10 | 25 | 2289.0 | 6.4 | 38885.2 | 6.0 | 1.0 | 58.9 | 63.6 | 8.5 | 11.3 |
| -10 | 10 | 2189.0 | 6.5 | 37536.6 | 5.1 | 0.4 | 58.3 | 13.8 | 8.6 | 5.8 |
| -10 | 5 | 2121.0 | 5.6 | 36217.8 | 5.2 | 0.0 | 58.6 | 19.1 | 7.6 | 5.6 |
| -10 | 1 | 1858.0 | 1.7 | 32822.5 | 7.1 | 0.4 | 56.6 | 20.6 | 10.6 | 4.6 |
| -10 | 0.5 | 1732.0 | 1.0 | 33693.9 | 4.1 | 2.3 | 51.4 | 17.8 | 8.8 | 9.0 |
| -10 | 0.1 | 1604.0 | 0.5 | 28712.2 | 7.5 | 0.4 | 55.9 | 24.9 | 7.3 | 5.8 |
| 4 | 25 | 1473.0 | 7.4 | 27304.4 | 7.6 | 2.2 | 53.9 | 98.5 | 10.6 | 29.5 |
| 4 | 10 | 1361.0 | 7.7 | 24327.9 | 9.5 | 0.1 | 55.9 | 51.1 | 10.0 | 39.7 |
| 4 | 5 | 1275.0 | 6.5 | 22900.6 | 9.8 | 0.2 | 55.7 | 52.4 | 8.3 | 41.1 |
| 4 | 1 | 1073.0 | 2.6 | 19680.2 | 11.7 | 0.0 | 54.5 | 52.4 | 5.8 | 43.6 |
| 4 | 0.5 | 952.0 | 1.6 | 17955.7 | 9.5 | 0.9 | 53.0 | 56.0 | 5.6 | 45.8 |
| 4 | 0.1 | 784.0 | 0.6 | 14465.5 | 14.9 | 0.1 | 54.2 | 91.8 | 4.8 | 47.3 |
| 21 | 25 | 782.0 | 7.7 | 12364.9 | 17.8 | 1.0 | 63.3 | 296.0 | 8.0 | 11.8 |
| 21 | 10 | 658.0 | 8.3 | 10328.6 | 18.1 | 0.8 | 63.7 | 361.5 | 8.4 | 21.2 |
| 21 | 5 | 565.0 | 8.3 | 9085.9 | 19.1 | 1.3 | 62.2 | 403.3 | 8.2 | 21.4 |
| 21 | 1 | 367.0 | 5.1 | 6329.9 | 22.4 | 1.0 | 58.0 | 415.2 | 6.7 | 28.8 |
| 21 | 0.5 | 308.0 | 3.4 | 5340.4 | 24.9 | 1.4 | 57.7 | 464.1 | 5.0 | 29.4 |
| 21 | 0.1 | 202.0 | 1.4 | 3277.9 | 28.3 | 1.4 | 61.7 | 537.4 | 3.5 | 31.9 |
| 37 | 25 | 263.0 | 9.2 | 4372.4 | 27.4 | 2.0 | 60.2 | 611.3 | 8.5 | 9.2 |
| 37 | 10 | 220.0 | 9.7 | 3341.2 | 27.4 | 1.4 | 65.7 | 873.1 | 7.8 | 0.1 |
| 37 | 5 | 162.0 | 8.8 | 2672.5 | 28.5 | 1.3 | 60.7 | 938.0 | 6.8 | 1.2 |
| 37 | 1 | 95.0 | 5.7 | 1520.2 | 31.6 | 1.4 | 62.7 | 918.5 | 5.4 | 9.4 |
| 37 | 0.5 | 75.0 | 4.0 | 1196.0 | 31.9 | 1.8 | 62.7 | 930.7 | 4.6 | 13.7 |
| 37 | 0.1 | 45.0 | 1.9 | 709.3 | 30.0 | 1.3 | 62.9 | 968.6 | 3.4 | 18.0 |
| 54 | 25 | 70.0 | 9.9 | 1292.0 | 34.5 | 7.1 | 54.4 | 156.1 | 9.3 | 0.8 |
| 54 | 10 | 59.0 | 8.1 | 940.7 | 31.3 | 0.4 | 62.2 | 272.7 | 8.3 | 10.6 |
| 54 | 5 | 48.0 | 6.9 | 720.0 | 30.5 | 0.0 | 66.7 | 311.6 | 7.5 | 4.7 |
| 54 | 1 | 31.0 | 6.1 | 425.5 | 28.3 | 0.9 | 73.5 | 311.5 | 7.6 | 0.0 |
| 54 | 0.5 | 29.0 | 5.0 | 356.7 | 25.8 | 0.8 | 80.6 | 321.1 | 5.5 | 0.8 |
| 54 | 0.1 | 22.0 | 4.3 | 255.9 | 20.7 | 1.2 | 87.1 | 369.5 | 6.1 | 1.4 |

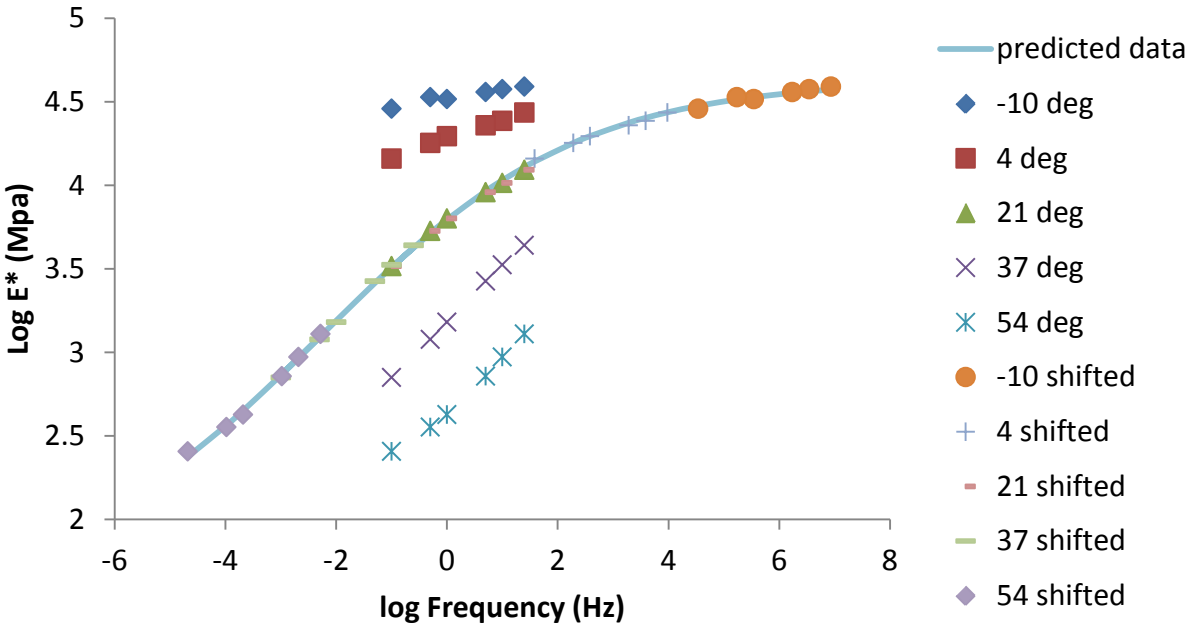


Figure E. 23: Master curve for Sample 6 (SP-IV with PG 70-22 binder)

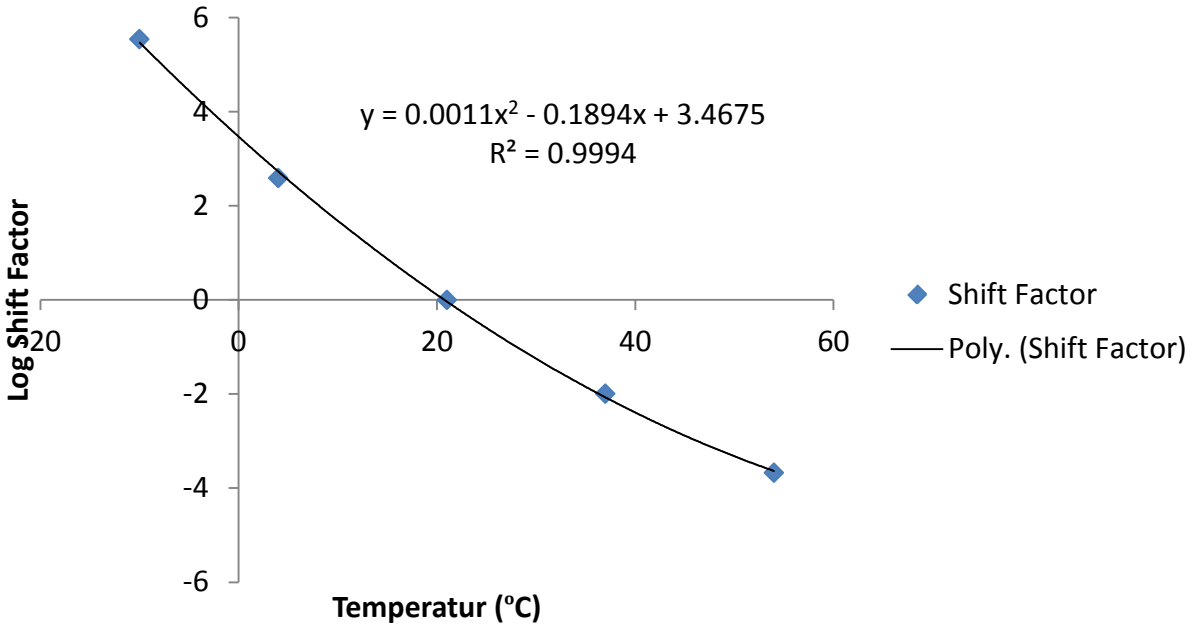


Figure E. 24: Shift factor for Sample 6 (SP-IV with PG 70-22 binder)

# APPENDIX F

AMEC LABORTORY DYNAMIC MODULUS TEST RESULTS

FOR

SP-II WITH PG 64-22 BINDER

SP-II WITH PG 70-22 BINDER

SP-III WITH PG 64-22 BINDER

SP-III WITH PG 70-22 BINDER

SP-IV WITH PG 70-22 BINDER

MIXES

**SP-II WITH PG 64-22 BINDER - Samples**

Table F. 13: E* test results for Sample 1 (SP-II with PG 64-22 binder)

| Temperature | Frequency | Stress | | Dynamic Modulus | Phase Angle | | Strain | | | |
|---|---|---|---|---|---|---|---|---|---|---|
| | | Amplitude (P-P) | SE | | | UC | (P-P) Recoverable | Permanent | SE | UC |
| (deg C) | (Hz) | (kPa) | (%) | (MPa) | (deg) | (deg) | (micro e) | (micro e) | (%) | (%) |
| -10 | 25 | 1439.5 | 6.6 | 30474.2 | 5.3 | 1.6 | 47.237 | -9.148 | 14 | 47.1 |
| -10 | 10 | 1356.1 | 4.2 | 29670.5 | 4.8 | 0.9 | 45.705 | -15.7 | 8 | 38.9 |
| -10 | 5 | 1255.8 | 2.1 | 28941.1 | 4.3 | 0.6 | 43.39 | -18.674 | 7.1 | 38.7 |
| -10 | 1 | 1110 | 0.4 | 26219.3 | 5.4 | 0.3 | 42.335 | -20.688 | 5.8 | 39.5 |
| -10 | 0.5 | 1050.7 | 0.3 | 25208.1 | 5.5 | 0.6 | 41.682 | -21.056 | 6 | 40.3 |
| -10 | 0.1 | 908.4 | 0.2 | 23361.1 | 5.9 | 0.2 | 38.885 | -16.345 | 5.7 | 42.2 |
| 4 | 25 | 1212.7 | 6 | 23668.0 | 8.7 | 2.1 | 51.237 | 15.442 | 9.6 | 53.1 |
| 4 | 10 | 1089.9 | 4 | 22520.6 | 9.2 | 2 | 48.397 | 15.315 | 7.7 | 48.5 |
| 4 | 5 | 976.8 | 2.1 | 21126.1 | 9.8 | 2.3 | 46.236 | 14.051 | 7.4 | 48.2 |
| 4 | 1 | 880.2 | 0.4 | 18292.3 | 10.2 | 1.8 | 48.12 | 12.294 | 7 | 49.2 |
| 4 | 0.5 | 799.9 | 0.3 | 17108.3 | 11.8 | 1.6 | 46.753 | 13.59 | 9 | 50 |
| 4 | 0.1 | 697.9 | 0.2 | 14392.7 | 13.5 | 2.2 | 48.491 | 34.858 | 6.6 | 47.7 |
| 21 | 25 | 653.6 | 5.7 | 14062.2 | 13.1 | 1.3 | 46.476 | 108.367 | 7.2 | 47.1 |
| 21 | 10 | 591.5 | 3.9 | 12427.5 | 14 | 0.5 | 47.6 | 142.111 | 5.6 | 44.6 |
| 21 | 5 | 529.8 | 2.2 | 11170.3 | 14.8 | 0.5 | 47.427 | 151.444 | 4.7 | 43.8 |
| 21 | 1 | 378.7 | 0.5 | 8415.5 | 18.1 | 0.8 | 44.997 | 141.069 | 4.8 | 45.7 |
| 21 | 0.5 | 318.3 | 0.4 | 7377.7 | 19.6 | 0.5 | 43.145 | 142.645 | 5.7 | 45.7 |
| 21 | 0.1 | 237.7 | 0.2 | 5210.6 | 22.8 | 1.2 | 45.611 | 184.179 | 3.3 | 43.8 |
| 37 | 25 | 329.9 | 5.6 | 6188.3 | 22.7 | 3.6 | 53.312 | 337.727 | 6.7 | 32.4 |
| 37 | 10 | 273.5 | 4.4 | 5056.8 | 24.2 | 2.6 | 54.095 | 429.362 | 6.2 | 29.1 |
| 37 | 5 | 224.7 | 2.8 | 4270.5 | 25.3 | 2.7 | 52.622 | 448.156 | 4.2 | 27.9 |
| 37 | 1 | 148.4 | 0.8 | 2715.2 | 28.7 | 2.5 | 54.648 | 423.158 | 4.5 | 27.7 |
| 37 | 0.5 | 108.7 | 0.8 | 2206.1 | 30.2 | 2 | 49.26 | 412.945 | 3.8 | 28.3 |
| 37 | 0.1 | 68.9 | 0.6 | 1420.3 | 30.7 | 2.1 | 48.5 | 444.599 | 5 | 28.8 |
| 54 | 25 | 127.7 | 6 | 2448.0 | 28.1 | 3.6 | 52.179 | 575.348 | 7.2 | 16.4 |
| 54 | 10 | 100.3 | 4.9 | 1842.1 | 27.7 | 2 | 54.438 | 714.831 | 5.9 | 14.3 |
| 54 | 5 | 84.6 | 3.3 | 1479.8 | 27.6 | 1.3 | 57.176 | 769.609 | 4.7 | 12.2 |
| 54 | 1 | 48.7 | 1.1 | 855.5 | 27.9 | 0.1 | 56.981 | 757.162 | 4.1 | 6.7 |
| 54 | 0.5 | 39 | 0.8 | 689.8 | 27.1 | 0.2 | 56.6 | 759.398 | 3.6 | 5.1 |
| 54 | 0.1 | 29.3 | 1.3 | 447.9 | 24.5 | 0.3 | 65.461 | 795.26 | 4.5 | 5.4 |

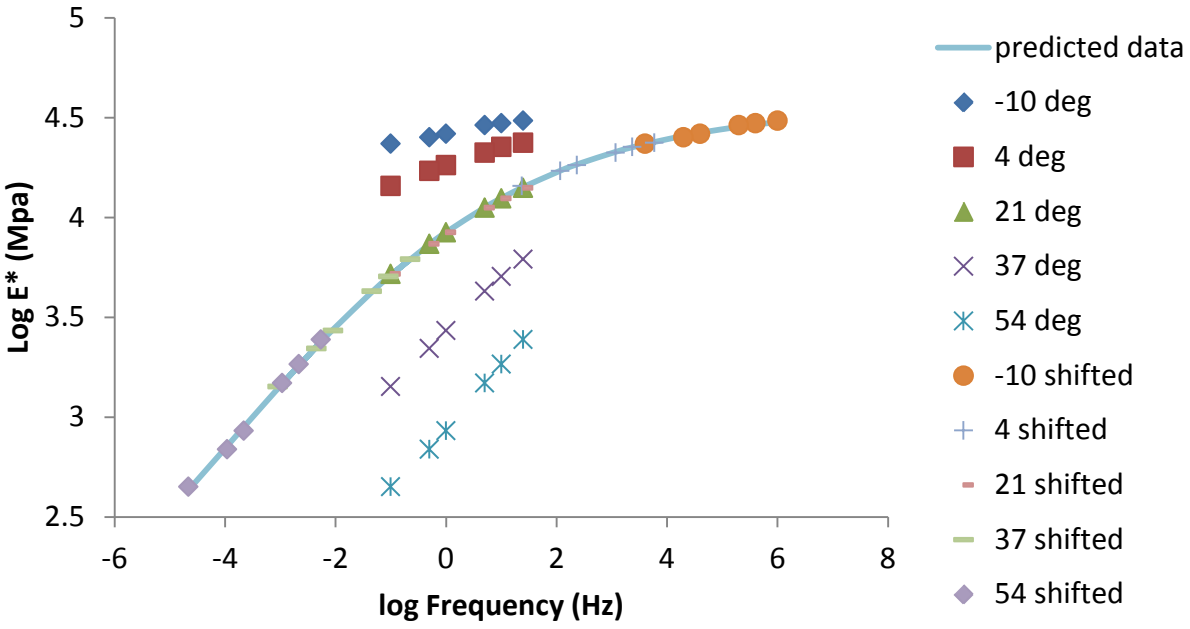


Figure F. 25: Master curve for Sample 1 (SP-II with PG 64-22 binder)

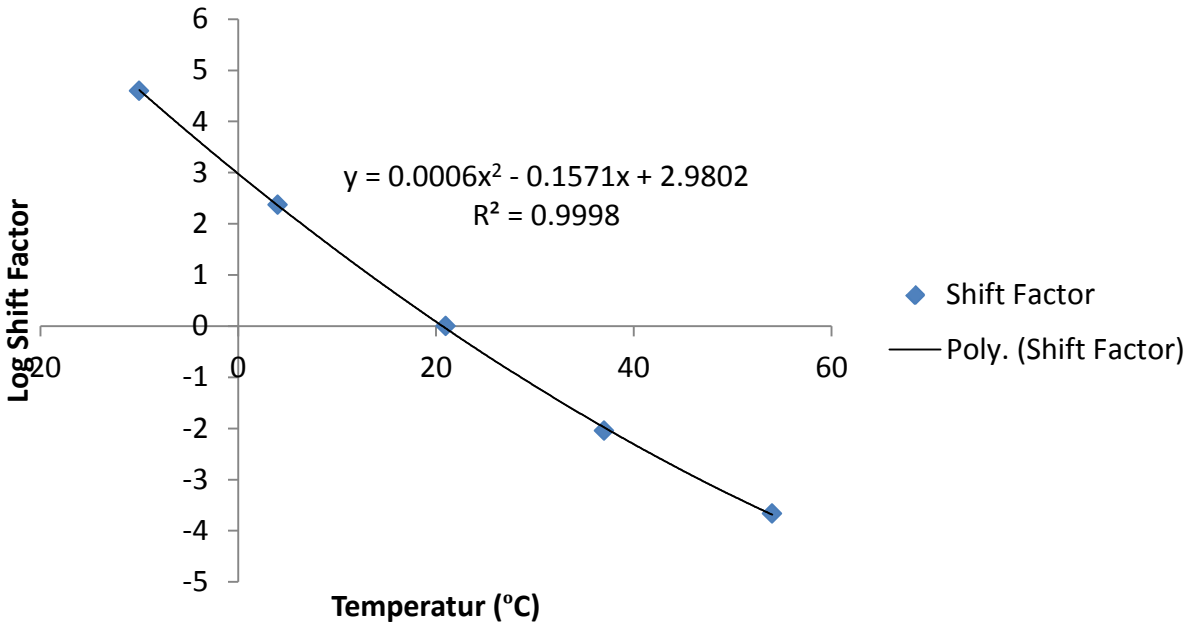


Figure F. 26: Shift factor for Sample 1 (SP-II with PG 64-22 binder)

Table F. 14: E* test results for Sample 2 (SP-II with PG 64-22 binder)

| Temperature | Frequency | Stress | | Dynamic Modulus | Phase Angle | | Strain | | | |
|---|---|---|---|---|---|---|---|---|---|---|
| | | Amplitude (P-P) | SE | | | UC | (P-P) Recoverable | Permanent | SE | UC |
| (deg C) | (Hz) | (kPa) | (%) | (MPa) | (deg) | (deg) | (micro e) | (micro e) | (%) | (%) |
| -10 | 25 | 1174.3 | 5.9 | 21325.5 | 3.9 | 0.8 | 55.066 | -40.377 | 13 | 85.2 |
| -10 | 10 | 1113 | 3.8 | 21173.8 | 3.7 | 0.3 | 52.563 | -52.739 | 8.3 | 85.1 |
| -10 | 5 | 1057.5 | 2 | 20462.5 | 4.2 | 0.2 | 51.68 | -57.884 | 7.2 | 84.4 |
| -10 | 1 | 949.7 | 0.4 | 19009.1 | 4.9 | 1.3 | 49.962 | -61.702 | 7.7 | 86.3 |
| -10 | 0.5 | 900.1 | 0.3 | 18523.2 | 124.1 | 207 | 48.593 | -63.3 | 6.3 | 88.1 |
| -10 | 0.1 | 818.5 | 0.2 | 17017.7 | 5.3 | 0.4 | 48.098 | -58.066 | 6.3 | 88.5 |
| 4 | 25 | 914.6 | 5.9 | 17416.6 | 7.6 | 2.3 | 52.513 | -36.468 | 7.1 | 45 |
| 4 | 10 | 844 | 4.1 | 16502.7 | 7.9 | 1 | 51.145 | -50.547 | 5.7 | 42.9 |
| 4 | 5 | 797.6 | 2.2 | 15718.6 | 8.1 | 0.7 | 50.743 | -52.623 | 5.6 | 42.9 |
| 4 | 1 | 699.6 | 0.5 | 13679.6 | 9.2 | 0.8 | 51.145 | -55.637 | 4.7 | 44.5 |
| 4 | 0.5 | 649.8 | 0.4 | 12836.4 | 10.4 | 0.5 | 50.619 | -54.446 | 4 | 44.2 |
| 4 | 0.1 | 547 | 0.3 | 10844.0 | 11.9 | 0.5 | 50.447 | -33.017 | 4 | 42.2 |
| 21 | 25 | 539.8 | 5.7 | 11019.3 | 13.3 | 1.9 | 48.989 | 165.104 | 6.2 | 1.6 |
| 21 | 10 | 497.6 | 4.2 | 9851.8 | 14.3 | 0.6 | 50.506 | 224.924 | 4.9 | 2 |
| 21 | 5 | 439.3 | 2.3 | 8888.1 | 15.5 | 0.1 | 49.422 | 258.529 | 4.4 | 0.5 |
| 21 | 1 | 338.4 | 0.5 | 6531.5 | 19.1 | 0.4 | 51.815 | 314.903 | 4.4 | 1.5 |
| 21 | 0.5 | 298 | 0.4 | 5493.2 | 20.5 | 0.9 | 54.25 | 383.798 | 4.1 | 2.7 |
| 21 | 0.1 | 208.1 | 0.2 | 3564.9 | 24.8 | 0.5 | 58.388 | 476.701 | 3.8 | 5 |
| 37 | 25 | 299.1 | 5.7 | 5663.2 | 20.1 | 0.1 | 52.821 | 459.606 | 6.6 | 21.9 |
| 37 | 10 | 245 | 4.5 | 4586.3 | 21.7 | 0.5 | 53.428 | 581.537 | 4.6 | 21.2 |
| 37 | 5 | 195 | 3.1 | 3779.7 | 23.3 | 0.5 | 51.603 | 611.742 | 4.8 | 22.1 |
| 37 | 1 | 128.9 | 0.8 | 2313.5 | 26.6 | 0.9 | 55.702 | 598.556 | 3.9 | 26.4 |
| 37 | 0.5 | 88.9 | 0.6 | 1826.2 | 28.5 | 1.1 | 48.689 | 593.153 | 3.7 | 30.2 |
| 37 | 0.1 | 49.2 | 0.5 | 1087.0 | 28.8 | 1.1 | 45.241 | 619.495 | 3.8 | 32 |
| 54 | 25 | 128.8 | 6.1 | 2425.5 | 27.6 | 0.5 | 53.091 | 505.021 | 6.4 | 10.5 |
| 54 | 10 | 102.3 | 5.2 | 1781.9 | 28.5 | 0.2 | 57.39 | 659.034 | 5 | 10.2 |
| 54 | 5 | 85.5 | 3.9 | 1400.8 | 28.9 | 0.3 | 61.059 | 727.464 | 5.1 | 8.9 |
| 54 | 1 | 53.9 | 1.4 | 769.8 | 29 | 1.1 | 69.957 | 725.481 | 4.5 | 12.5 |
| 54 | 0.5 | 39.1 | 1 | 588.7 | 28.7 | 1.2 | 66.409 | 721.448 | 4.8 | 13.6 |
| 54 | 0.1 | 27.4 | 1.3 | 361.9 | 25.3 | 2.3 | 75.573 | 753.168 | 4.8 | 16.5 |

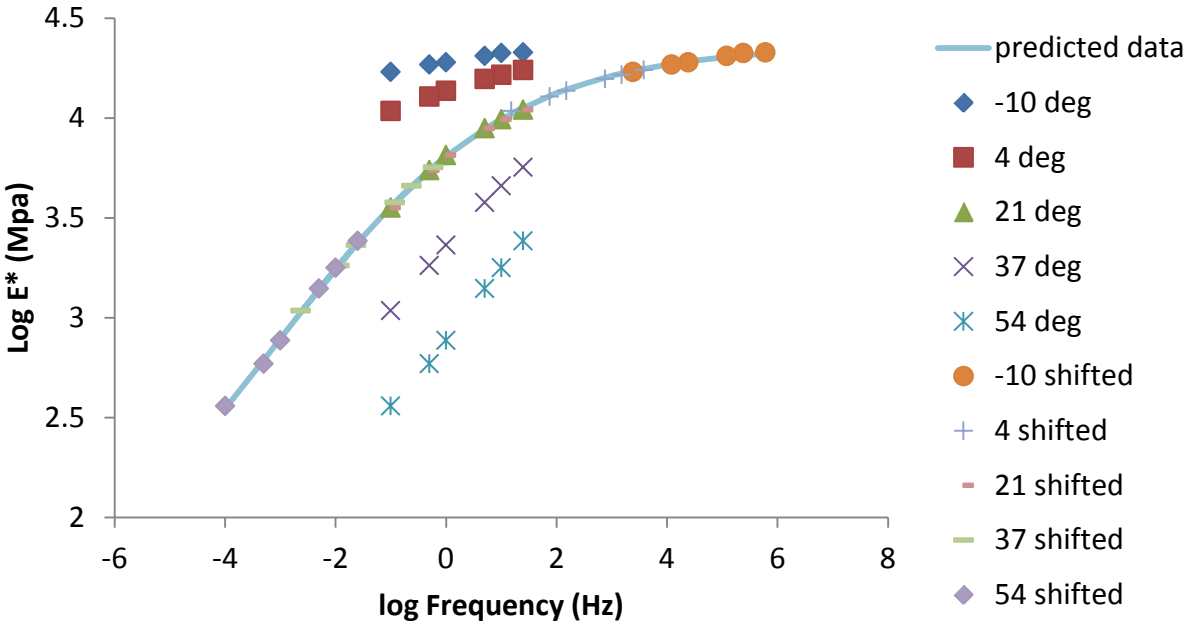


Figure F. 27: Master curve for Sample 2 (SP-II with PG 64-22 binder)

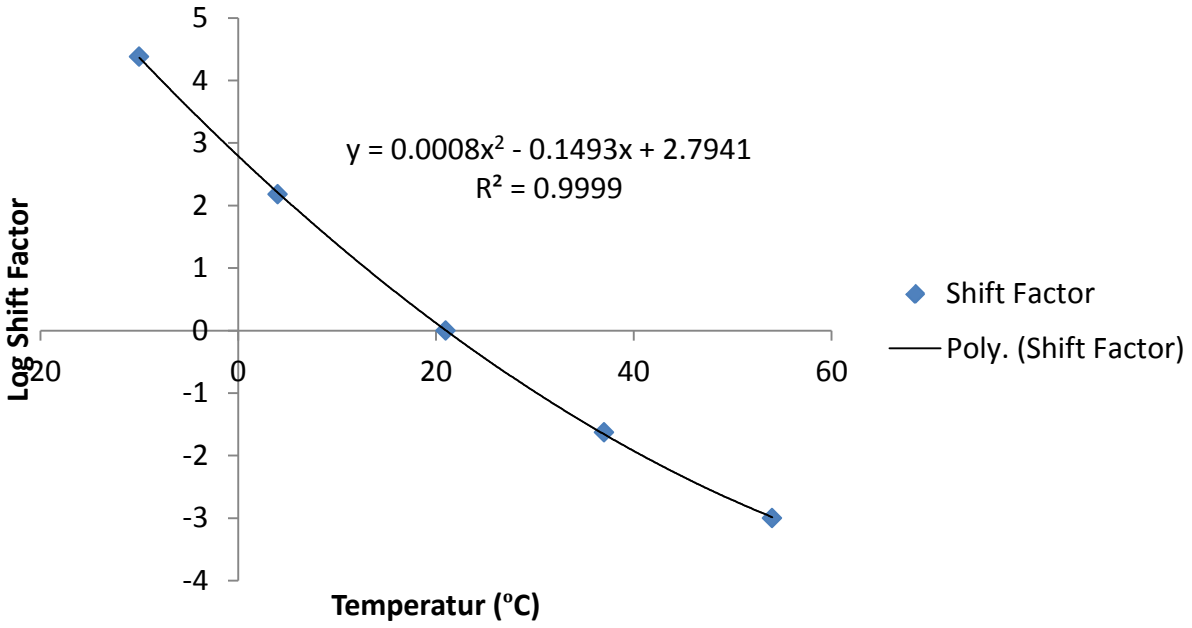


Figure F. 28: Shift factor for Sample 2 (SP-II with PG 64-22 binder)

**SP-II WITH PG 70-22 BINDER - Samples**

Table F. 15: E* test results for Sample 1 (SP-II with PG 70-22 binder)

| Temperature | Frequency | Stress | | Dynamic Modulus | Phase Angle | | Strain | | | |
|---|---|---|---|---|---|---|---|---|---|---|
| | | Amplitude (P-P) | SE | | | UC | (P-P) Recoverable | Permanent | SE | UC |
| (deg C) | (Hz) | (kPa) | (%) | (MPa) | (deg) | (deg) | (micro e) | (micro e) | (%) | (%) |
| -10 | 25 | 1171.6 | 6 | 29126.2 | 5.6 | 2.7 | 40.226 | -49.751 | 11 | 16 |
| -10 | 10 | 1111.7 | 3.9 | 28092.4 | 5.9 | 2.4 | 39.574 | -64.516 | 9.6 | 13.9 |
| -10 | 5 | 1054.2 | 2 | 27174.7 | 6 | 1.3 | 38.794 | -70.332 | 8.9 | 15.7 |
| -10 | 1 | 950.1 | 0.4 | 24946.3 | 6.3 | 2.1 | 38.085 | -74.961 | 9.5 | 18.4 |
| -10 | 0.5 | 900 | 0.3 | 24080.6 | 7.5 | 1 | 37.373 | -76.597 | 8.3 | 20.3 |
| -10 | 0.1 | 818.5 | 0.2 | 21588.8 | 7.6 | 0.6 | 37.915 | -70.64 | 8.8 | 22.8 |
| 4 | 25 | 1220.4 | 6 | 21289.1 | 7.7 | 0.6 | 57.324 | 17.179 | 7.9 | 25.8 |
| 4 | 10 | 1091.1 | 3.8 | 19857.9 | 8.2 | 0.4 | 54.946 | 24.681 | 5.4 | 27.1 |
| 4 | 5 | 1005.9 | 2 | 18726.2 | 9.2 | 0.3 | 53.715 | 29.41 | 4 | 27.5 |
| 4 | 1 | 899.7 | 0.4 | 15868.7 | 10.6 | 0.9 | 56.695 | 30.767 | 4.2 | 28.1 |
| 4 | 0.5 | 819.2 | 0.3 | 14628.3 | 11.8 | 1 | 56.002 | 36.19 | 3.3 | 28.9 |
| 4 | 0.1 | 717.9 | 0.2 | 11939.7 | 14.1 | 1.5 | 60.127 | 76.26 | 3.6 | 33 |
| 21 | 25 | 608.5 | 5.4 | 11077.8 | 16.5 | 1 | 54.927 | 217.436 | 8.2 | 51.6 |
| 21 | 10 | 541.9 | 3.7 | 9564.1 | 17.2 | 0.3 | 56.663 | 297.255 | 6.2 | 49.5 |
| 21 | 5 | 481 | 2.2 | 8488.4 | 18.2 | 0.4 | 56.66 | 328.063 | 5.1 | 49.7 |
| 21 | 1 | 348.3 | 0.5 | 5869.7 | 22.4 | 0.6 | 59.333 | 322.72 | 4 | 51.3 |
| 21 | 0.5 | 298.3 | 0.4 | 5019.9 | 23.7 | 0.4 | 59.419 | 335.784 | 4.6 | 52.1 |
| 21 | 0.1 | 217.7 | 0.2 | 3421.2 | 26.7 | 0.8 | 63.638 | 412.048 | 4.4 | 51.4 |
| 37 | 25 | 329.8 | 5.6 | 4624.7 | 23.4 | 0.7 | 71.31 | 733.518 | 5.5 | 26.4 |
| 37 | 10 | 272.5 | 4.1 | 3646.6 | 24.5 | 0.7 | 74.737 | 893.987 | 4.1 | 24.7 |
| 37 | 5 | 222.3 | 2.5 | 2982.8 | 25.4 | 1.1 | 74.526 | 933.179 | 4.1 | 25.2 |
| 37 | 1 | 147.8 | 0.7 | 1717.8 | 27.9 | 1.8 | 86.047 | 911.834 | 3.7 | 28.3 |
| 37 | 0.5 | 108.3 | 0.6 | 1325.4 | 28.5 | 2 | 81.703 | 905.267 | 4.5 | 31.8 |
| 37 | 0.1 | 68.8 | 0.4 | 807.2 | 27.2 | 1.5 | 85.29 | 952.352 | 4.2 | 35.9 |
| 54 | 25 | 108 | 5.9 | 1748.3 | 29.6 | 1.6 | 61.792 | 322.677 | 5.5 | 17.6 |
| 54 | 10 | 85.1 | 4.3 | 1283.5 | 28.1 | 0.3 | 66.311 | 377.081 | 4.9 | 16.3 |
| 54 | 5 | 69.8 | 3.2 | 1008.9 | 27.5 | 0.7 | 69.224 | 377.141 | 4.5 | 16.1 |
| 54 | 1 | 38.7 | 1.4 | 587.5 | 26.2 | 1.3 | 65.825 | 349.997 | 4.9 | 16.8 |
| 54 | 0.5 | 29.1 | 1.2 | 477.3 | 25.3 | 1.9 | 60.959 | 332.135 | 4.1 | 17 |
| 54 | 0.1 | 23.3 | 1.6 | 341.2 | 20.8 | 1.8 | 68.347 | 326.619 | 5 | 17.7 |

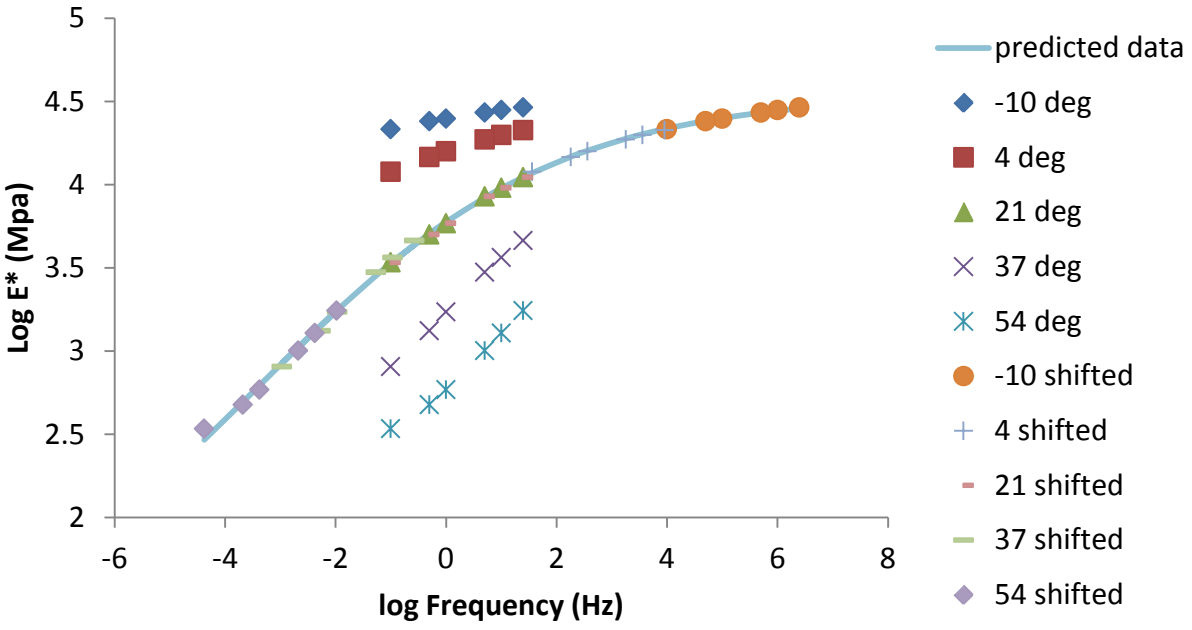


Figure F. 29: Master curve for Sample 1 (SP-II with PG 70-22 binder)

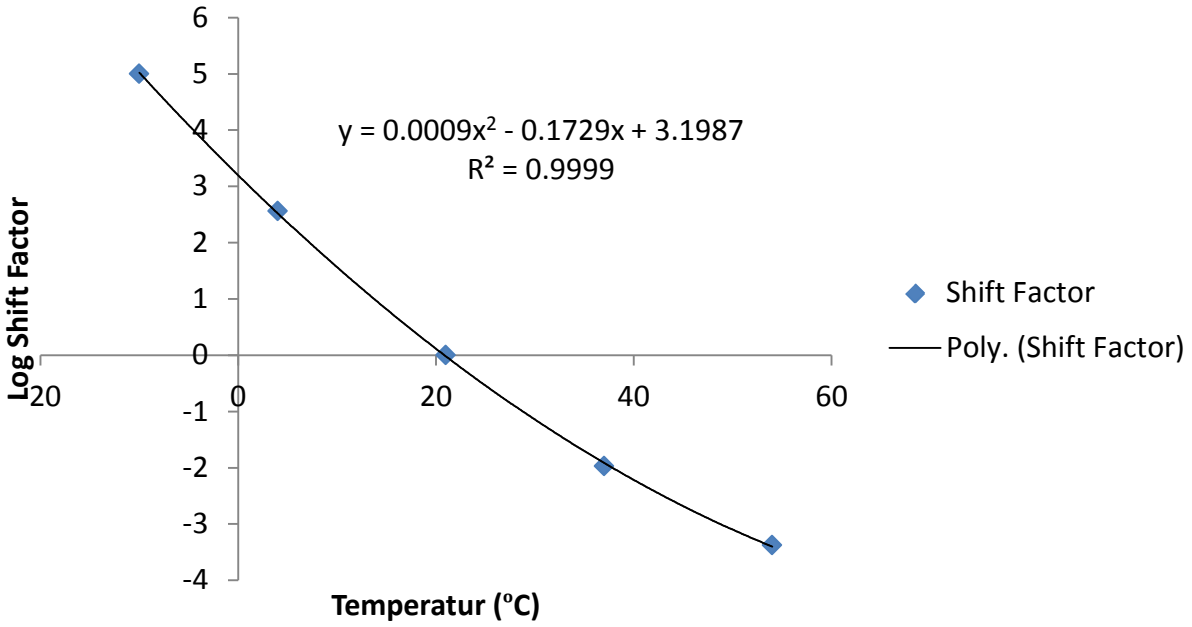


Figure F. 30: Shift factor for Sample 1 (SP-II with PG 70-22 binder)

Table F. 16: E* test results for Sample 2 (SP-II with PG 70-22 binder)

| Temperature | Frequency | Stress | | Dynamic Modulus | Phase Angle | | Strain | | | |
|---|---|---|---|---|---|---|---|---|---|---|
| | | Amplitude (P-P) | SE | | | UC | (P-P) Recoverable | Permanent | SE | UC |
| (deg C) | (Hz) | (kPa) | (%) | (MPa) | (deg) | (deg) | (micro e) | (micro e) | (%) | (%) |
| -10 | 25 | 1443.2 | 6.9 | 29189.7 | 20.4 | 27.3 | 49.441 | -27.301 | 29 | 124 |
| -10 | 10 | 1357.3 | 4.8 | 28277.5 | 7.1 | 3.9 | 48 | -39.721 | 19 | 120 |
| -10 | 5 | 1260.1 | 2.7 | 27560.8 | 6.2 | 2.4 | 45.72 | -38.842 | 21 | 122 |
| -10 | 1 | 1153.3 | 0.7 | 25176.0 | 7.7 | 2.1 | 45.811 | -32.899 | 21 | 125 |
| -10 | 0.5 | 1101.2 | 0.4 | 24459.2 | 126.5 | 204.8 | 45.021 | -38.626 | 25 | 127 |
| -10 | 0.1 | 998.3 | 0.2 | 21753.6 | 8.6 | 2.6 | 45.892 | -31.187 | 26 | 125 |
| 4 | 25 | 1279.4 | 6.1 | 20443.2 | 8.6 | 1.4 | 62.581 | 2.14 | 8.6 | 31.9 |
| 4 | 10 | 1153.2 | 3.9 | 18650.0 | 8.3 | 0.5 | 61.834 | -2.274 | 6 | 28.6 |
| 4 | 5 | 1066.5 | 2 | 17227.4 | 9.4 | 0.2 | 61.906 | -5.039 | 4.4 | 27.7 |
| 4 | 1 | 959.4 | 0.4 | 14522.8 | 10.9 | 0.2 | 66.061 | -9.946 | 3 | 27.5 |
| 4 | 0.5 | 880.1 | 0.3 | 13310.4 | 11.9 | 0.2 | 66.125 | -9.61 | 2.9 | 26.9 |
| 4 | 0.1 | 777.9 | 0.2 | 10729.4 | 14.5 | 0.3 | 72.503 | 29.748 | 2.9 | 23.4 |
| 21 | 25 | 621.6 | 5.8 | 11694.0 | 14.9 | 2 | 53.159 | 141.616 | 6.7 | 15.8 |
| 21 | 10 | 560.3 | 4.2 | 10118.2 | 15.9 | 2.2 | 55.376 | 189.511 | 5.8 | 18.6 |
| 21 | 5 | 500.1 | 2.4 | 9070.1 | 17 | 2.3 | 55.134 | 204.915 | 4.9 | 20.9 |
| 21 | 1 | 348.2 | 0.5 | 6699.4 | 20.5 | 2.9 | 51.978 | 192.903 | 3.1 | 21.7 |
| 21 | 0.5 | 297.9 | 0.4 | 5847.9 | 22 | 2.4 | 50.95 | 199.512 | 3.6 | 22.9 |
| 21 | 0.1 | 218.1 | 0.2 | 4141.3 | 24.6 | 3.2 | 52.656 | 270.133 | 4.6 | 25.2 |
| 37 | 25 | 298.9 | 5.7 | 5060.3 | 21.9 | 1.2 | 59.06 | 404.828 | 5.9 | 32.5 |
| 37 | 10 | 253.9 | 4.3 | 4049.4 | 22.7 | 0.4 | 62.697 | 519.682 | 4.7 | 27.5 |
| 37 | 5 | 193 | 2.9 | 3329.5 | 24.3 | 0.7 | 57.981 | 521.841 | 4.2 | 29.9 |
| 37 | 1 | 113.6 | 0.8 | 1966.0 | 28.9 | 1.5 | 57.765 | 469.87 | 3.5 | 38.4 |
| 37 | 0.5 | 88.8 | 0.6 | 1560.3 | 29.9 | 1.8 | 56.89 | 457.025 | 5.7 | 41.7 |
| 37 | 0.1 | 54.1 | 0.5 | 949.6 | 30.3 | 2.7 | 56.923 | 480.744 | 5.7 | 43 |
| 54 | 25 | 128.3 | 6.1 | 2293.7 | 28.1 | 1.2 | 55.955 | 406.434 | 6.1 | 36.1 |
| 54 | 10 | 100.6 | 4.6 | 1715.8 | 28 | 1 | 58.605 | 510.425 | 5.4 | 35.3 |
| 54 | 5 | 79.1 | 3.2 | 1357.2 | 28.4 | 1.3 | 58.302 | 535.748 | 6.6 | 36.1 |
| 54 | 1 | 40.9 | 1.1 | 765.0 | 28.8 | 1.3 | 53.403 | 509.695 | 3.9 | 40.5 |
| 54 | 0.5 | 31.1 | 1 | 620.9 | 27.8 | 1.4 | 50.134 | 502.976 | 4.3 | 43.4 |
| 54 | 0.1 | 21.4 | 1.5 | 410.9 | 23.9 | 1.9 | 52.002 | 518.524 | 4.7 | 46.4 |

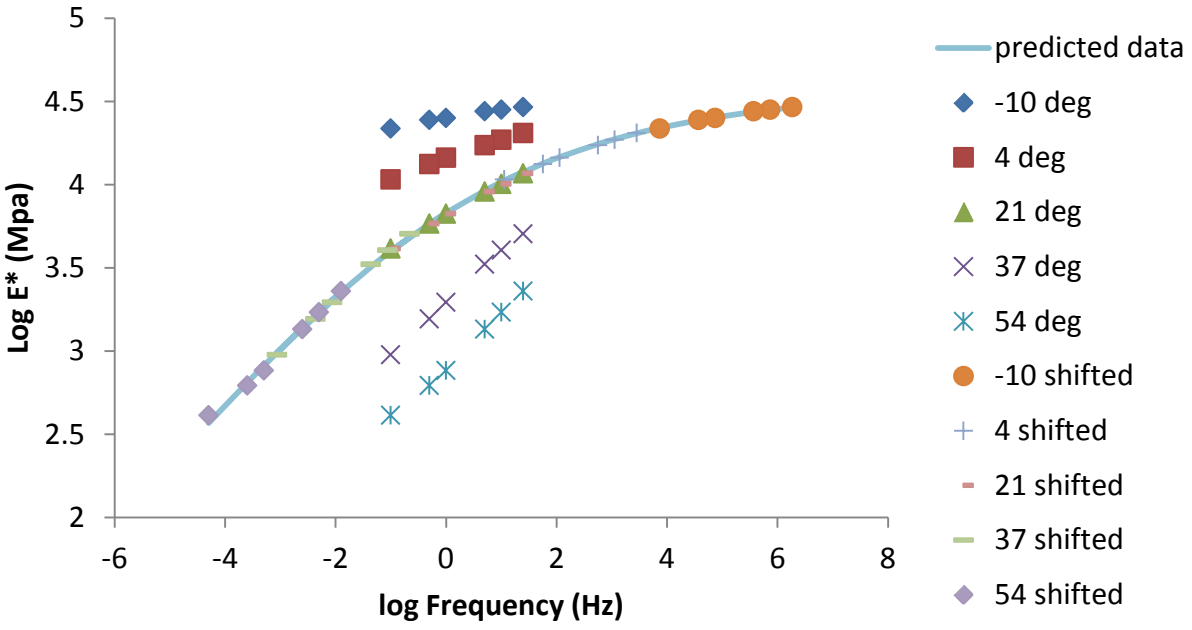


Figure F. 31: Master curve for Sample 2 (SP-II with PG 70-22 binder)

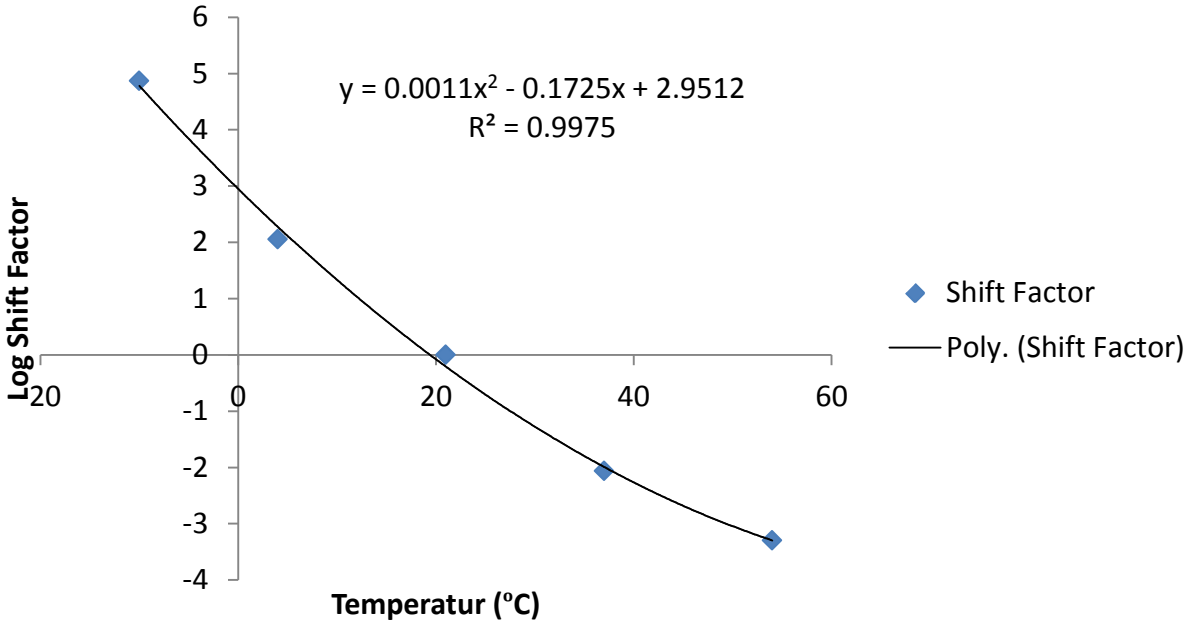


Figure F. 32: Shift factor for Sample 2 (SP-II with PG 70-22 binder)

**SP-III WITH PG 64-22 BINDER - Samples**

Table F. 17: E* test results for Sample 1 (SP-III with PG 64-22 binder)

| Temperature | Frequency | Stress | | Dynamic Modulus | Phase Angle | | Strain | | | |
|---|---|---|---|---|---|---|---|---|---|---|
| | | Amplitude (P-P) | SE | | | UC | (P-P) Recoverable | Permanent | SE | UC |
| (deg C) | (Hz) | (kPa) | (%) | (MPa) | (deg) | (deg) | (micro e) | (micro e) | (%) | (%) |
| -10 | 25 | 1437.4 | 6.5 | 28409.1 | 7.7 | 7.5 | 50.595 | -59.154 | 30 | 93.1 |
| -10 | 10 | 1356.8 | 4.6 | 27961.9 | 5.5 | 2.1 | 48.523 | -78.339 | 18 | 89.8 |
| -10 | 5 | 1256.5 | 2.5 | 27220.4 | 3.4 | 2.1 | 46.161 | -87.045 | 18 | 91.1 |
| -10 | 1 | 1150.2 | 0.5 | 24882.2 | 8.2 | 5.8 | 46.225 | -92.074 | 35 | 91.1 |
| -10 | 0.5 | 1080.8 | 0.3 | 24542.8 | 6.8 | 2.1 | 44.037 | -94.534 | 26 | 95 |
| -10 | 0.1 | 948.2 | 0.2 | 21918.7 | 11.9 | 9.7 | 43.26 | -89.287 | 54 | 94.3 |
| 4 | 25 | 1226.6 | 6.1 | 23386.3 | 7.4 | 3 | 52.448 | -2.94 | 9.5 | 79.2 |
| 4 | 10 | 1092.5 | 4.1 | 22811.8 | 7.9 | 1.8 | 47.891 | -6.165 | 6.9 | 76.1 |
| 4 | 5 | 1007.7 | 2.2 | 21770.6 | 9.1 | 1.6 | 46.285 | -6.732 | 6.9 | 74.9 |
| 4 | 1 | 899.5 | 0.4 | 18826.3 | 9.9 | 2.2 | 47.781 | -8.684 | 4.9 | 76 |
| 4 | 0.5 | 819.4 | 0.3 | 17553.8 | 11.3 | 2 | 46.68 | -6.276 | 5.7 | 76.2 |
| 4 | 0.1 | 718.1 | 0.2 | 14845.2 | 13.4 | 2 | 48.37 | 19.961 | 5.7 | 74 |
| 21 | 25 | 814.3 | 6 | 15647.4 | 13.1 | 1.3 | 52.039 | 204.909 | 7.1 | 36.3 |
| 21 | 10 | 755.2 | 4.4 | 13590.4 | 14.7 | 0.7 | 55.566 | 262.581 | 5.9 | 35.2 |
| 21 | 5 | 690.4 | 2.5 | 12137.0 | 15.8 | 0.7 | 56.88 | 281.725 | 5.6 | 33 |
| 21 | 1 | 589.7 | 0.5 | 8842.9 | 19.5 | 1.3 | 66.691 | 288.311 | 3.6 | 34.5 |
| 21 | 0.5 | 529.8 | 0.4 | 7543.1 | 21.1 | 1.2 | 70.241 | 309.799 | 4.2 | 33.9 |
| 21 | 0.1 | 387.1 | 0.3 | 5130.8 | 24.5 | 1.4 | 75.438 | 406.191 | 3.8 | 34.1 |
| 37 | 25 | 357.7 | 5.9 | 6872.4 | 22.4 | 0.4 | 52.05 | 444.668 | 6.9 | 13.2 |
| 37 | 10 | 282.9 | 4.7 | 5446.4 | 24.2 | 0.3 | 51.936 | 554.327 | 6.1 | 13.9 |
| 37 | 5 | 235.2 | 2.9 | 4488.4 | 26 | 0.6 | 52.403 | 584.668 | 4.9 | 12.9 |
| 37 | 1 | 138.4 | 0.8 | 2649.9 | 29.7 | 1.4 | 52.23 | 545.3 | 4.5 | 17.9 |
| 37 | 0.5 | 98.7 | 0.6 | 2058.5 | 30.9 | 1.6 | 47.938 | 529.125 | 5 | 21.6 |
| 37 | 0.1 | 69 | 0.4 | 1201.9 | 30.9 | 2.3 | 57.404 | 566.399 | 4.2 | 24.2 |
| 54 | 25 | 127.8 | 6.2 | 2535.3 | 32.1 | 1.6 | 50.402 | 379.599 | 6.8 | 6.5 |
| 54 | 10 | 99.8 | 4.8 | 1778.0 | 32.2 | 1.5 | 56.119 | 462.267 | 5.4 | 6.1 |
| 54 | 5 | 84.2 | 3.3 | 1366.9 | 32.2 | 1.4 | 61.61 | 494.06 | 4.7 | 6 |
| 54 | 1 | 48.6 | 1.2 | 727.6 | 31.7 | 1.8 | 66.822 | 461.204 | 4 | 3.9 |
| 54 | 0.5 | 39 | 0.8 | 573.3 | 30.5 | 1.7 | 67.983 | 444.271 | 4 | 4.3 |
| 54 | 0.1 | 27.3 | 0.8 | 359.0 | 25.8 | 1.7 | 76.159 | 449.279 | 4.5 | 4.8 |

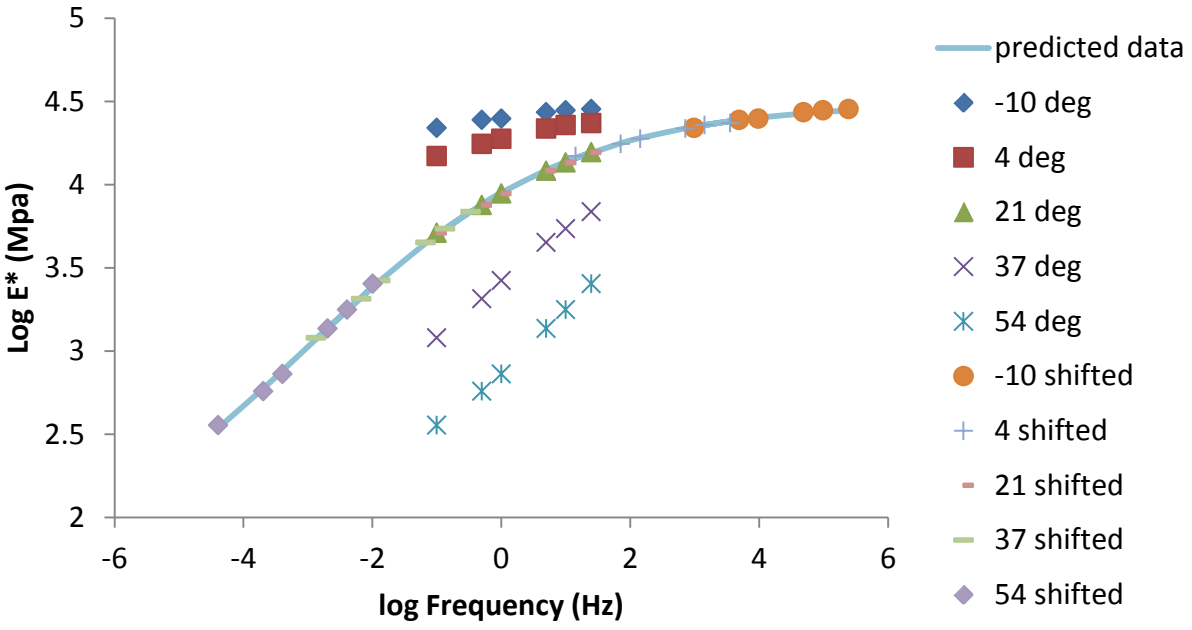


Figure F. 33: Master curve for Sample 1 (SP-III with PG 64-22 binder)

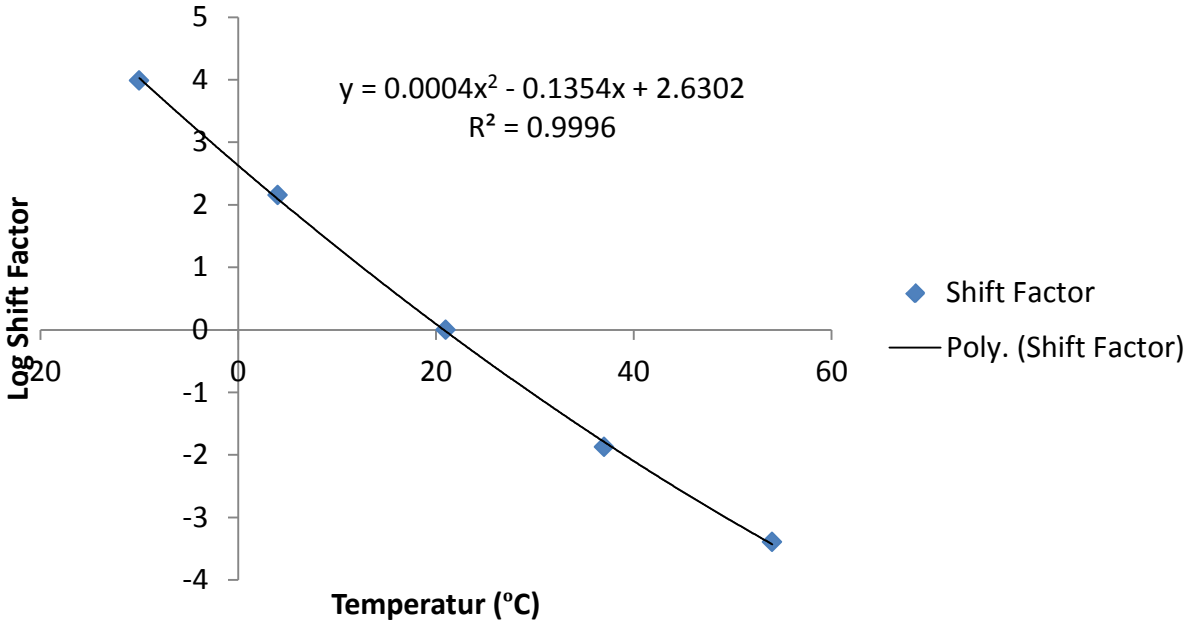


Figure F. 34: Shift factor for Sample 1 (SP-III with PG 64-22 binder)

Table F. 18: E* test results for Sample 2 (SP-III with PG 64-22 binder)

| Temperature | Frequency | Stress | | Dynamic Modulus | Phase Angle | | Strain | | | |
|---|---|---|---|---|---|---|---|---|---|---|
| | | Amplitude (P-P) | SE | | | UC | (P-P) Recoverable | Permanent | SE | UC |
| (deg C) | (Hz) | (kPa) | (%) | (MPa) | (deg) | (deg) | (micro e) | (micro e) | (%) | (%) |
| -10 | 25 | 1435.7 | 6.5 | 48110.0 | 7.5 | 4 | 29.843 | -57.701 | 26 | 100 |
| -10 | 10 | 1359.5 | 4.7 | 46624.2 | 5.5 | 1.7 | 29.16 | -71.607 | 20 | 90.8 |
| -10 | 5 | 1258.6 | 2.6 | 45764.7 | 6.1 | 3.1 | 27.501 | -75.745 | 25 | 92 |
| -10 | 1 | 1150 | 0.5 | 42565.3 | 7.1 | 3.2 | 27.018 | -77.894 | 23 | 98.6 |
| -10 | 0.5 | 1099.9 | 0.4 | 41863.6 | 125.5 | 205.5 | 26.274 | -77.925 | 20 | 102 |
| -10 | 0.1 | 999 | 0.2 | 37570.8 | 6.2 | 0.6 | 26.59 | -72.746 | 20 | 103 |
| 4 | 25 | 1443.3 | 7.1 | 32572.3 | 14.7 | 8.7 | 44.311 | -54.551 | 41 | 125 |
| 4 | 10 | 1364.6 | 5.3 | 30817.2 | 7.3 | 0.3 | 44.279 | -61.548 | 24 | 112 |
| 4 | 5 | 1269.8 | 3.3 | 28910.8 | 9 | 1.7 | 43.921 | -63.535 | 25 | 108 |
| 4 | 1 | 1152.2 | 0.7 | 24786.8 | 10.1 | 1.3 | 46.483 | -63.559 | 28 | 113 |
| 4 | 0.5 | 1111.4 | 0.5 | 22856.3 | 12.1 | 2 | 48.625 | -57.393 | 28 | 112 |
| 4 | 0.1 | 998.2 | 0.2 | 18379.3 | 13.1 | 0.9 | 54.31 | -26.329 | 29 | 111 |
| 21 | 25 | 1121.6 | 5.9 | 20012.9 | 15.1 | 4.1 | 56.043 | 187.582 | 6.5 | 36.1 |
| 21 | 10 | 1027.4 | 3.8 | 17146.4 | 16.6 | 3.4 | 59.919 | 269.093 | 4.6 | 37.8 |
| 21 | 5 | 947.2 | 2 | 15061.3 | 17.7 | 3.7 | 62.887 | 317.096 | 4.7 | 38.6 |
| 21 | 1 | 799.4 | 0.4 | 10870.7 | 22.2 | 3.4 | 73.538 | 338.906 | 4.2 | 38.5 |
| 21 | 0.5 | 708.8 | 0.4 | 9344.7 | 23.3 | 3.2 | 75.855 | 377.709 | 2.6 | 37.7 |
| 21 | 0.1 | 627.2 | 0.3 | 6354.1 | 27.2 | 3 | 98.716 | 576.722 | 3.6 | 36.2 |
| 37 | 25 | 452.4 | 5.9 | 8562.7 | 22.2 | 1.3 | 52.83 | 501.039 | 6.7 | 43.8 |
| 37 | 10 | 377.5 | 4.6 | 6906.3 | 23.8 | 0.7 | 54.667 | 591.8 | 5.9 | 44.8 |
| 37 | 5 | 328.2 | 3.1 | 5712.4 | 25.7 | 0.8 | 57.445 | 646.667 | 4.9 | 45.5 |
| 37 | 1 | 218.2 | 0.8 | 3435.7 | 29.5 | 1.5 | 63.508 | 618.597 | 3.9 | 47 |
| 37 | 0.5 | 173.3 | 0.6 | 2733.6 | 30.2 | 1.8 | 63.392 | 602.821 | 4.6 | 47.8 |
| 37 | 0.1 | 88.8 | 0.7 | 1554.8 | 30.9 | 3.1 | 57.139 | 590.014 | 5.5 | 54.2 |
| 54 | 25 | 147.5 | 6.6 | 2897.9 | 32.8 | 0.6 | 50.885 | 573.531 | 8.5 | 27 |
| 54 | 10 | 114.7 | 5.5 | 2062.4 | 32.9 | 1.5 | 55.596 | 687.403 | 7.2 | 26.7 |
| 54 | 5 | 95.3 | 3.9 | 1570.2 | 33.1 | 1.9 | 60.697 | 695.075 | 6.4 | 27.5 |
| 54 | 1 | 63.3 | 1.2 | 855.4 | 32.3 | 1.5 | 73.973 | 653.607 | 6 | 27.9 |
| 54 | 0.5 | 53.7 | 0.8 | 667.7 | 31.5 | 0.8 | 80.417 | 643.854 | 5.8 | 27.4 |
| 54 | 0.1 | 34.2 | 1.2 | 404.6 | 27.6 | 0.9 | 84.422 | 656.19 | 6.3 | 28.4 |

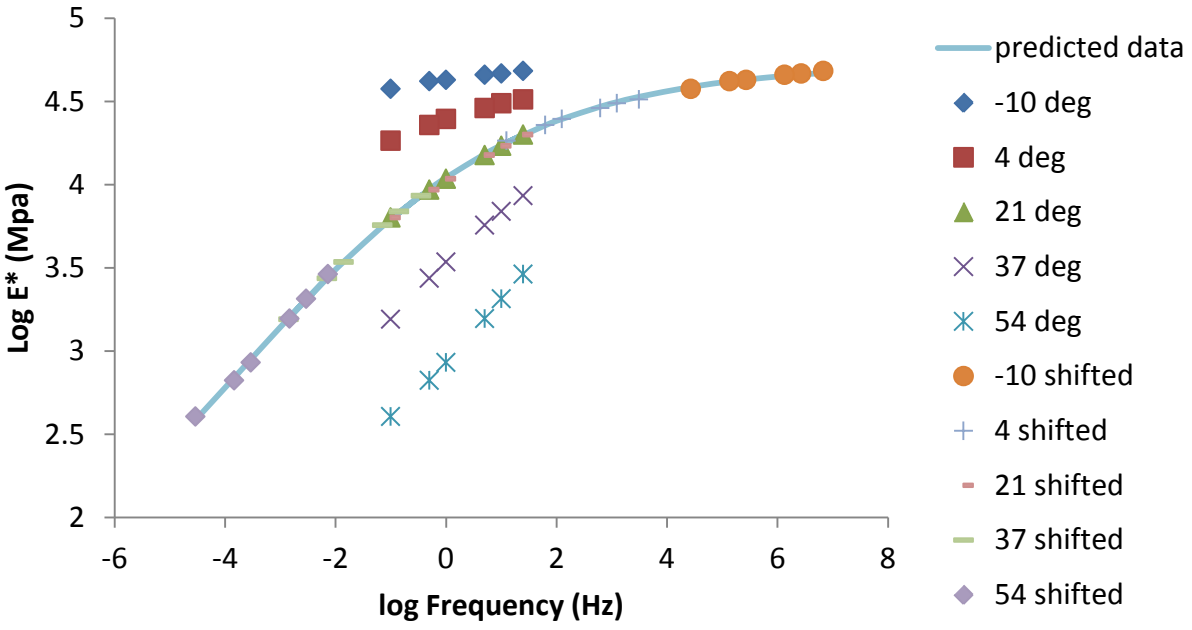


Figure F. 35: Master curve for Sample 2 (SP-III with PG 64-22 binder)

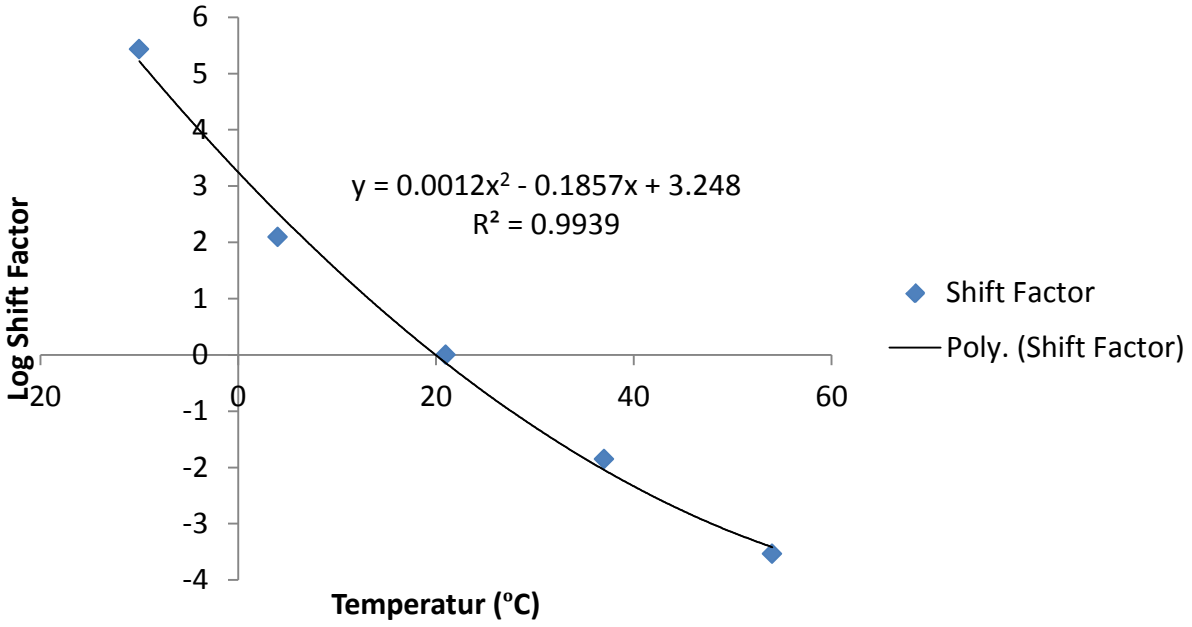


Figure F. 36: Shift factor for Sample 2 (SP-III with PG 64-22 binder)

**SP-III WITH PG 70-22 BINDER - Samples**

Table F. 19: E* test results for Sample 1 (SP-III with PG 70-22 binder)

| Temperature | Frequency | Stress | | Dynamic Modulus | Phase Angle | | Strain | | | |
|---|---|---|---|---|---|---|---|---|---|---|
| | | Amplitude (P-P) | SE | | | UC | (P-P) Recoverable | Permanent | SE | UC |
| (deg C) | (Hz) | (kPa) | (%) | (MPa) | (deg) | (deg) | (micro e) | (micro e) | (%) | (%) |
| -10 | 25 | 1171 | 5.7 | 28726.0 | 8.6 | 4 | 40.764 | -47.598 | 7.2 | 20.4 |
| -10 | 10 | 1113.1 | 3.6 | 28241.1 | 8.7 | 4.1 | 39.414 | -68.569 | 5 | 20.5 |
| -10 | 5 | 1056.6 | 1.8 | 27029.0 | 9.1 | 4.5 | 39.09 | -78.544 | 5.5 | 20.4 |
| -10 | 1 | 950.6 | 0.3 | 23942.1 | 9.4 | 4 | 39.703 | -85.025 | 5.5 | 19.6 |
| -10 | 0.5 | 899.9 | 0.3 | 22940.9 | 9.8 | 4.1 | 39.226 | -86.559 | 5.4 | 20.2 |
| -10 | 0.1 | 818.5 | 0.2 | 19830.6 | 11.3 | 3.3 | 41.275 | -75.716 | 4.2 | 19.8 |
| 4 | 25 | 1068.4 | 5.8 | 19615.5 | 9.7 | 2.1 | 54.467 | 31.466 | 7.1 | 39.2 |
| 4 | 10 | 1003.6 | 3.6 | 18102.7 | 10.4 | 1.1 | 55.437 | 40.352 | 4.4 | 38.4 |
| 4 | 5 | 948.3 | 1.9 | 16806.7 | 11 | 1.2 | 56.422 | 46.336 | 4 | 38 |
| 4 | 1 | 859.5 | 0.4 | 13748.5 | 13.2 | 0.6 | 62.516 | 48.377 | 2.7 | 38.1 |
| 4 | 0.5 | 800 | 0.3 | 12423.1 | 14.6 | 0.7 | 64.395 | 58.375 | 2.6 | 38.2 |
| 4 | 0.1 | 707.8 | 0.2 | 9579.6 | 17.2 | 0.7 | 73.886 | 126.194 | 2.6 | 38 |
| 21 | 25 | 551 | 5.7 | 9534.8 | 17.7 | 2.1 | 57.785 | 344.397 | 6.1 | 41.9 |
| 21 | 10 | 492.4 | 3.9 | 8227.2 | 18.4 | 1 | 59.852 | 448.857 | 5.3 | 38.9 |
| 21 | 5 | 430.9 | 2.5 | 7180.5 | 20 | 1.3 | 60.005 | 485.857 | 4.5 | 37.6 |
| 21 | 1 | 328.6 | 0.6 | 4874.5 | 23.7 | 0.8 | 67.41 | 487.864 | 3.7 | 38.5 |
| 21 | 0.5 | 288.3 | 0.4 | 4121.4 | 24.6 | 0.4 | 69.962 | 508.554 | 5.2 | 39.1 |
| 21 | 0.1 | 197.8 | 0.3 | 2722.7 | 27.5 | 1.7 | 72.661 | 588.604 | 4.7 | 43.6 |
| 37 | 25 | 298.7 | 5.6 | 3863.1 | 26 | 3.6 | 77.311 | 930.954 | 5.7 | 7.9 |
| 37 | 10 | 244.5 | 4.3 | 2919.8 | 26.7 | 2.6 | 83.734 | 1074.152 | 4.2 | 10.5 |
| 37 | 5 | 193.6 | 3.1 | 2321.5 | 27.9 | 2.6 | 83.388 | 1101.466 | 4.2 | 11.9 |
| 37 | 1 | 128.1 | 0.9 | 1315.3 | 29.8 | 2.7 | 97.428 | 1073.225 | 3.8 | 14.9 |
| 37 | 0.5 | 88.5 | 0.7 | 1004.8 | 30.7 | 2.7 | 88.103 | 1053.952 | 4 | 15.6 |
| 37 | 0.1 | 49.1 | 0.5 | 591.6 | 29 | 2.5 | 82.937 | 1072.005 | 3.9 | 17.8 |
| 54 | 25 | 108.1 | 5.9 | 1352.1 | 33.2 | 4.5 | 79.954 | 634.408 | 5.4 | 7.9 |
| 54 | 10 | 79.7 | 4.6 | 968.8 | 31.9 | 3.3 | 82.32 | 698.325 | 4.2 | 6.9 |
| 54 | 5 | 64.5 | 3.7 | 764.8 | 31.2 | 2.9 | 84.392 | 712.556 | 4.7 | 8.2 |
| 54 | 1 | 33.7 | 1.6 | 430.0 | 29.8 | 1.6 | 78.435 | 688.969 | 4.6 | 10.6 |
| 54 | 0.5 | 24.2 | 1.3 | 352.8 | 28.2 | 0.8 | 68.541 | 678.366 | 4.2 | 14.8 |
| 54 | 0.1 | 17.4 | 1.2 | 257.5 | 22.8 | 2.3 | 67.425 | 689.667 | 4.8 | 26.1 |

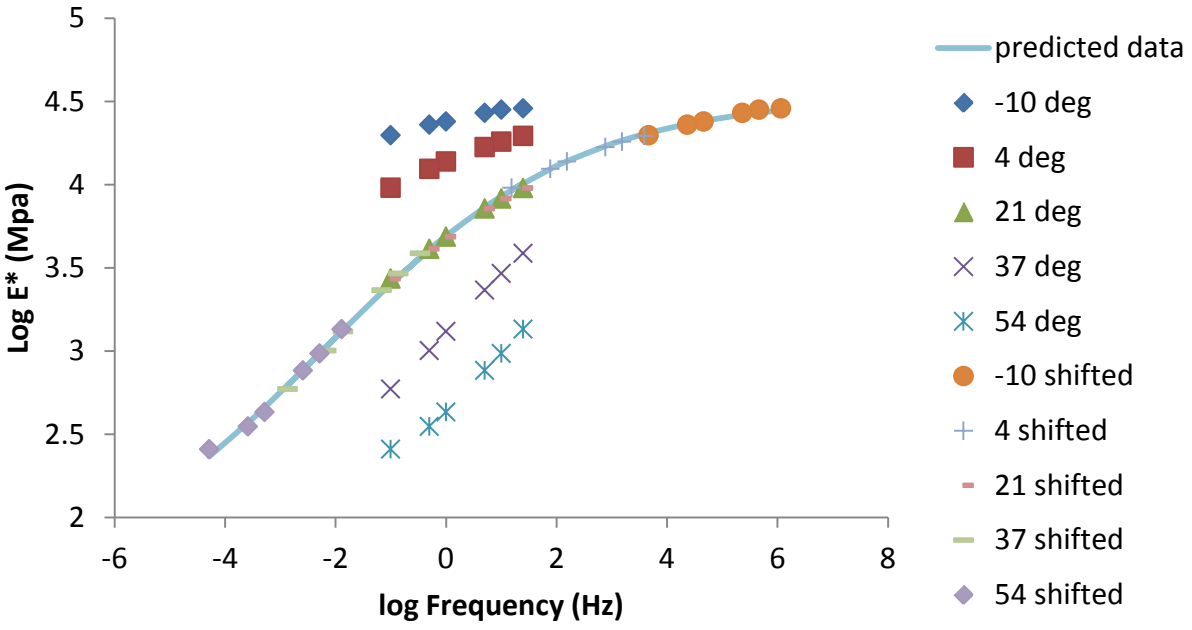


Figure F. 37: Master curve for Sample 1 (SP-III with PG 70-22 binder)

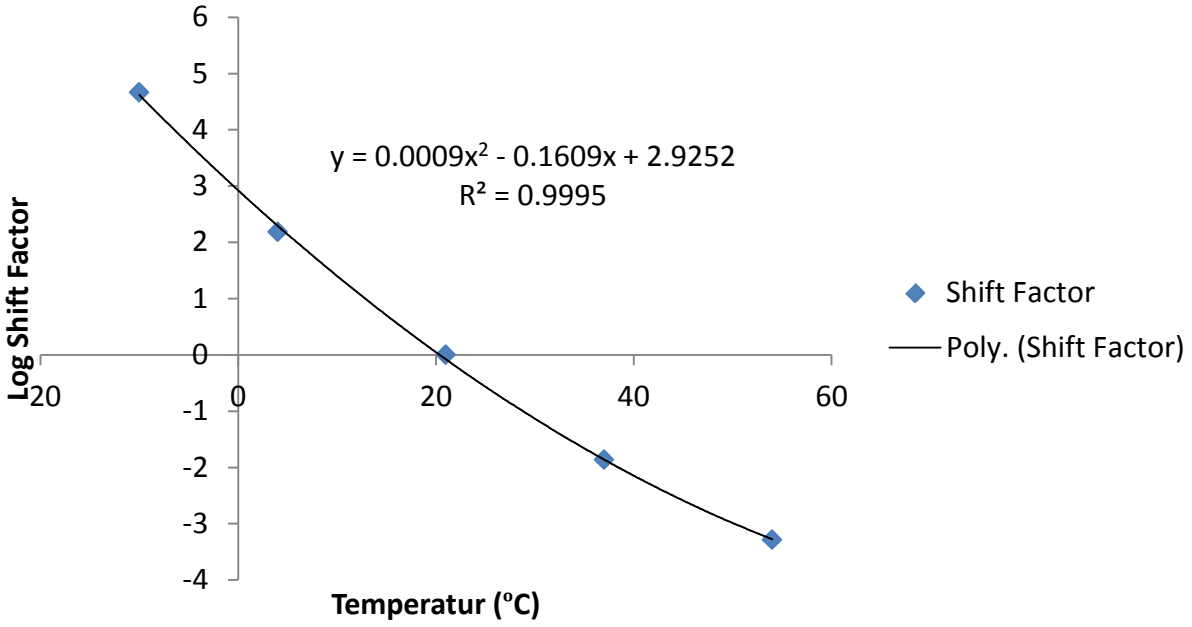


Figure F. 38: Shift factor for Sample 1 (SP-III with PG 70-22 binder)

Table F. 20: E* test results for Sample 2 (SP-III with PG 70-22 binder)

| Temperature | Frequency | Stress | | Dynamic Modulus | Phase Angle | | Strain | | | |
|---|---|---|---|---|---|---|---|---|---|---|
| | | Amplitude (P-P) | SE | | | UC | (P-P) Recoverable | Permanent | SE | UC |
| (deg C) | (Hz) | (kPa) | (%) | (MPa) | (deg) | (deg) | (micro e) | (micro e) | (%) | (%) |
| -10 | 25 | 1430 | 6.1 | 35672.0 | 9.5 | 6.6 | 40.087 | -7.789 | 33 | 85 |
| -10 | 10 | 1350.6 | 3.8 | 33370.5 | 11.3 | 9.4 | 40.473 | -14.475 | 44 | 81.8 |
| -10 | 5 | 1253 | 1.9 | 32080.2 | 5.6 | 0.8 | 39.059 | -15.641 | 24 | 82.3 |
| -10 | 1 | 1110 | 0.3 | 29025.4 | 7.2 | 0.7 | 38.244 | -16.311 | 32 | 82.8 |
| -10 | 0.5 | 1050.6 | 0.3 | 27775.0 | 7.9 | 1.3 | 37.827 | -15.11 | 25 | 83.4 |
| -10 | 0.1 | 908.1 | 0.2 | 24208.3 | 10.9 | 4.3 | 37.511 | -4.404 | 21 | 82.5 |
| 4 | 25 | 1122.7 | 5.9 | 24090.7 | 10.2 | 1.7 | 46.603 | 7.234 | 8.3 | 24.8 |
| 4 | 10 | 1054.9 | 3.7 | 21081.1 | 10.9 | 0.3 | 50.042 | 15.783 | 5.5 | 33.5 |
| 4 | 5 | 978 | 2 | 19405.8 | 11.9 | 0.5 | 50.398 | 19.402 | 4 | 34.8 |
| 4 | 1 | 880.2 | 0.4 | 15706.3 | 14.4 | 0.8 | 56.043 | 20.862 | 3.6 | 33.2 |
| 4 | 0.5 | 799.8 | 0.3 | 14226.4 | 14.9 | 0.3 | 56.219 | 30.045 | 5.6 | 33 |
| 4 | 0.1 | 697.7 | 0.2 | 10860.1 | 18.4 | 0.9 | 64.247 | 93.445 | 3.6 | 33.9 |
| 21 | 25 | 651.6 | 5.6 | 13026.0 | 18.7 | 4 | 50.026 | 319.127 | 6.8 | 39.5 |
| 21 | 10 | 591.4 | 3.8 | 10642.5 | 20.3 | 3.7 | 55.566 | 428.324 | 7 | 39.3 |
| 21 | 5 | 531 | 2.1 | 9067.9 | 21.9 | 3.5 | 58.554 | 478.221 | 5.1 | 40.9 |
| 21 | 1 | 399.9 | 0.5 | 6029.9 | 26.2 | 3.6 | 66.314 | 483.459 | 4.3 | 47.2 |
| 21 | 0.5 | 348.5 | 0.4 | 5004.9 | 27.1 | 3.8 | 69.641 | 505.711 | 5 | 48.6 |
| 21 | 0.1 | 267.3 | 0.3 | 3248.4 | 28.6 | 3.2 | 82.277 | 608.073 | 4.8 | 48.8 |
| 37 | 25 | 327.4 | 5.8 | 5440.0 | 29.3 | 3.7 | 60.183 | 833.293 | 7 | 59 |
| 37 | 10 | 270.7 | 4.5 | 4026.2 | 30.5 | 5.4 | 67.232 | 973.982 | 6.4 | 60.4 |
| 37 | 5 | 222.7 | 2.8 | 3192.1 | 31 | 5.4 | 69.764 | 1004.743 | 7.8 | 62.5 |
| 37 | 1 | 148.3 | 0.9 | 1784.5 | 32.8 | 4.5 | 83.081 | 979.693 | 7.2 | 63.5 |
| 37 | 0.5 | 108 | 0.6 | 1409.2 | 33 | 3.3 | 76.656 | 965.443 | 6 | 65.9 |
| 37 | 0.1 | 68.8 | 0.4 | 911.3 | 29.4 | 1.7 | 75.506 | 985.886 | 6 | 63.4 |
| 54 | 25 | 127.2 | 6.7 | 1624.4 | 35.5 | 2.4 | 78.317 | 569.412 | 7.1 | 58.7 |
| 54 | 10 | 99.1 | 5.8 | 1199.8 | 32.9 | 3.5 | 82.579 | 653.613 | 6.2 | 56.7 |
| 54 | 5 | 84.1 | 4.5 | 951.9 | 32 | 2.6 | 88.392 | 670.411 | 6.4 | 53.7 |
| 54 | 1 | 52.7 | 1.8 | 568.6 | 30.1 | 1.9 | 92.632 | 646.21 | 7.5 | 51.3 |
| 54 | 0.5 | 38.7 | 1.1 | 466.9 | 29 | 2.2 | 82.807 | 626.121 | 6.7 | 49.1 |
| 54 | 0.1 | 27.2 | 0.8 | 370.5 | 24.1 | 3.1 | 73.39 | 608.726 | 5.8 | 41.4 |

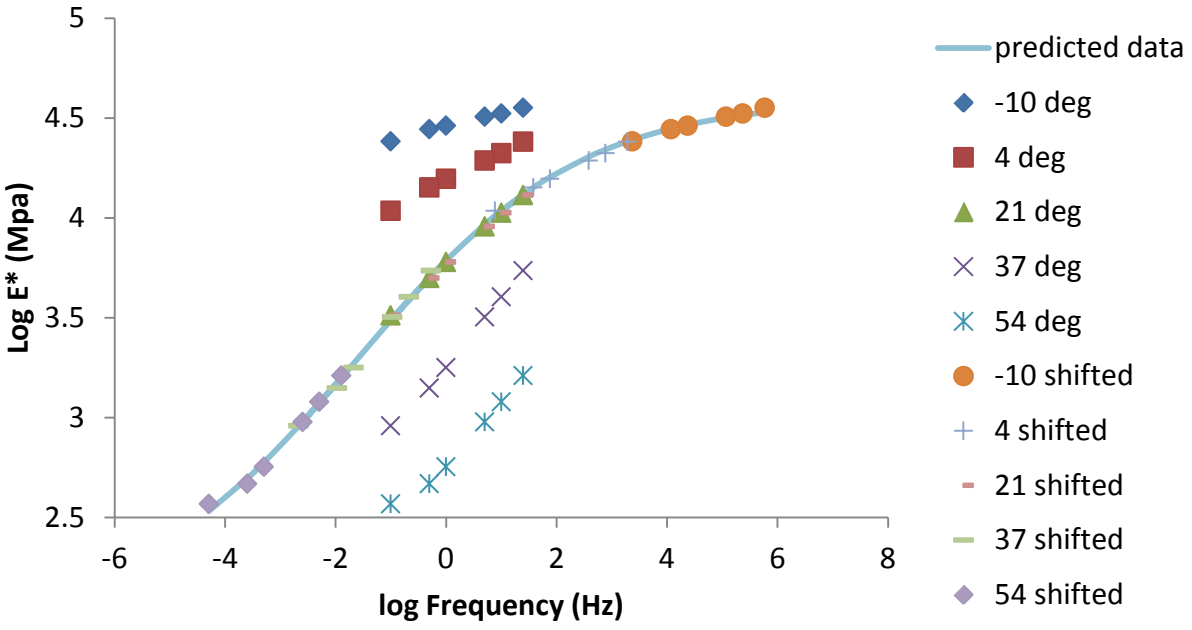


Figure F. 39: Master curve for Sample 2 (SP-III with PG 70-22 binder)

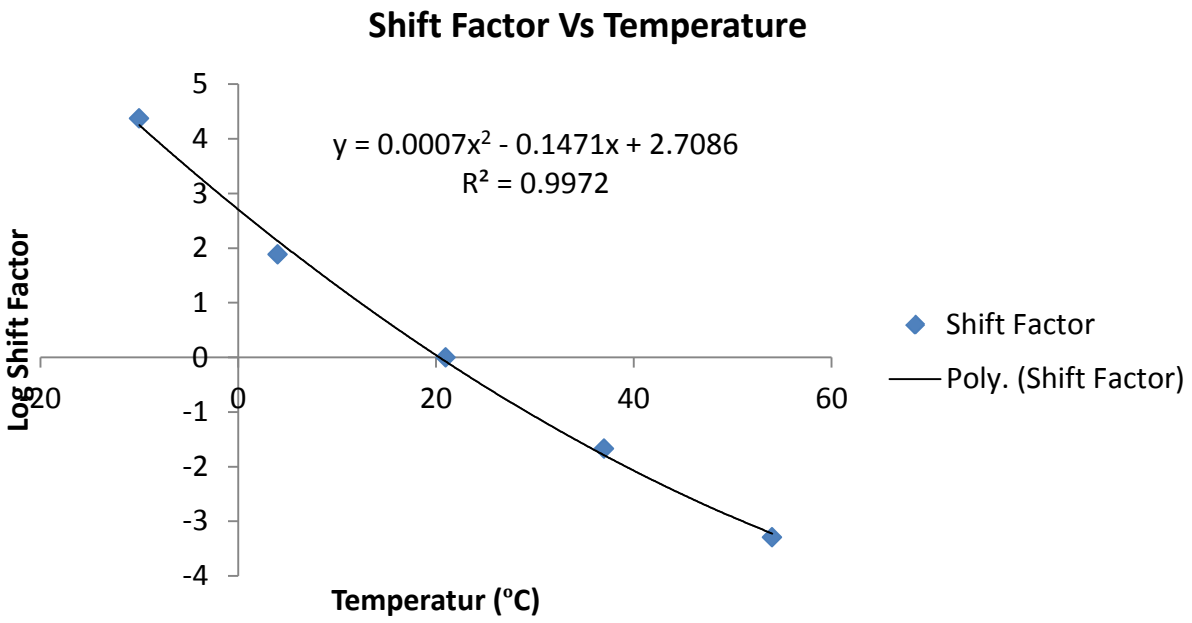


Figure F. 40: Shift factor for Sample 2 (SP-III with PG 70-22 binder)

Table F. 21: E* test results for Sample 3 (SP-III with PG 70-22 binder)

| Temperature | Frequency | Stress | | Dynamic Modulus | Phase Angle | | Strain | | | |
|---|---|---|---|---|---|---|---|---|---|---|
| | | Amplitude (P-P) | SE | | | UC | (P-P) Recoverable | Permanent | SE | UC |
| (deg C) | (Hz) | (kPa) | (%) | (MPa) | (deg) | (deg) | (micro e) | (micro e) | (%) | (%) |
| -10 | 25 | 1173.6 | 5.9 | 18871.2 | 5.9 | 0.8 | 62.189 | -18.957 | 6.8 | 16.3 |
| -10 | 10 | 1113.1 | 3.8 | 18102.3 | 6.2 | 0.4 | 61.487 | -24.079 | 4.8 | 14.4 |
| -10 | 5 | 1055.2 | 1.9 | 17521.9 | 6.2 | 0.5 | 60.223 | -16.127 | 3.8 | 14.8 |
| -10 | 1 | 950.4 | 0.4 | 15841.3 | 7.4 | 0.4 | 59.995 | -4.38 | 3.7 | 16 |
| -10 | 0.5 | 900.2 | 0.3 | 15124.2 | 7.7 | 0.3 | 59.518 | 6.165 | 3.3 | 15.5 |
| -10 | 0.1 | 818.6 | 0.2 | 13534.8 | 8.5 | 0.7 | 60.481 | 28.431 | 3.6 | 14.6 |
| 4 | 25 | 913.3 | 5.8 | 13693.5 | 9.2 | 0.3 | 66.693 | 29.305 | 5.7 | 9.3 |
| 4 | 10 | 844.6 | 3.7 | 12908.0 | 10.3 | 0.6 | 65.431 | 40.105 | 3.9 | 8.2 |
| 4 | 5 | 797.5 | 2 | 12057.7 | 11 | 0.7 | 66.138 | 40.177 | 3.4 | 9.3 |
| 4 | 1 | 699.1 | 0.4 | 9860.7 | 13.2 | 1 | 70.901 | 37.635 | 3.4 | 10.1 |
| 4 | 0.5 | 649.5 | 0.3 | 9000.4 | 14.6 | 1 | 72.161 | 47.584 | 3.5 | 11.1 |
| 4 | 0.1 | 548.2 | 0.2 | 7097.3 | 17.2 | 1.2 | 77.246 | 118.17 | 4.5 | 13.5 |
| 21 | 25 | 518.8 | 5.6 | 8128.2 | 17.2 | 0.4 | 63.829 | 334.237 | 5.6 | 18 |
| 21 | 10 | 459.9 | 3.4 | 7011.6 | 18.5 | 0.9 | 65.591 | 410.852 | 4.1 | 18.2 |
| 21 | 5 | 399.5 | 2.1 | 5954.8 | 20.2 | 1.2 | 67.09 | 490.916 | 3.2 | 17.7 |
| 21 | 1 | 278.6 | 0.5 | 3902.4 | 24.9 | 1.8 | 71.396 | 474.193 | 2.9 | 16.5 |
| 21 | 0.5 | 247.5 | 0.4 | 3212.7 | 26.3 | 1.4 | 77.028 | 496.673 | 3.8 | 16.1 |
| 21 | 0.1 | 158.2 | 0.3 | 2075.7 | 28.4 | 1.8 | 76.195 | 568.377 | 3.3 | 16 |
| 37 | 25 | 220.4 | 5.6 | 3096.7 | 27.6 | 0.4 | 71.163 | 443.457 | 5.4 | 21.6 |
| 37 | 10 | 163.6 | 4.4 | 2310.0 | 28.8 | 0.9 | 70.821 | 469.686 | 3.9 | 17.5 |
| 37 | 5 | 121.4 | 3.5 | 1797.9 | 30 | 0.9 | 67.532 | 446.732 | 4.2 | 16 |
| 37 | 1 | 68.6 | 1.2 | 985.5 | 31.7 | 0.7 | 69.64 | 400.174 | 3.1 | 9.3 |
| 37 | 0.5 | 48.9 | 0.9 | 769.7 | 31.3 | 0.9 | 63.59 | 377.459 | 3.2 | 6.3 |
| 37 | 0.1 | 29.3 | 0.8 | 473.1 | 28.1 | 2.1 | 61.88 | 378.396 | 4.2 | 8.7 |
| 54 | 25 | 78.8 | 5.9 | 1009.0 | 31.1 | 2.3 | 78.144 | 141.032 | 5.6 | 27.1 |
| 54 | 10 | 59.5 | 4.8 | 736.1 | 28.3 | 2.5 | 80.876 | 150.366 | 3.6 | 13.1 |
| 54 | 5 | 43.9 | 4.1 | 575.3 | 27.3 | 2.6 | 76.375 | 140.191 | 3.8 | 10.5 |
| 54 | 1 | 23.8 | 2.1 | 346.0 | 24.3 | 2.2 | 68.794 | 118.479 | 4.5 | 7.8 |
| 54 | 0.5 | 19.2 | 1.9 | 288.3 | 22.8 | 2.1 | 66.472 | 94.361 | 4.2 | 7.4 |
| 54 | 0.1 | 14.4 | 1.3 | 212.8 | 18.4 | 1.7 | 67.72 | 73.424 | 5.4 | 7.9 |

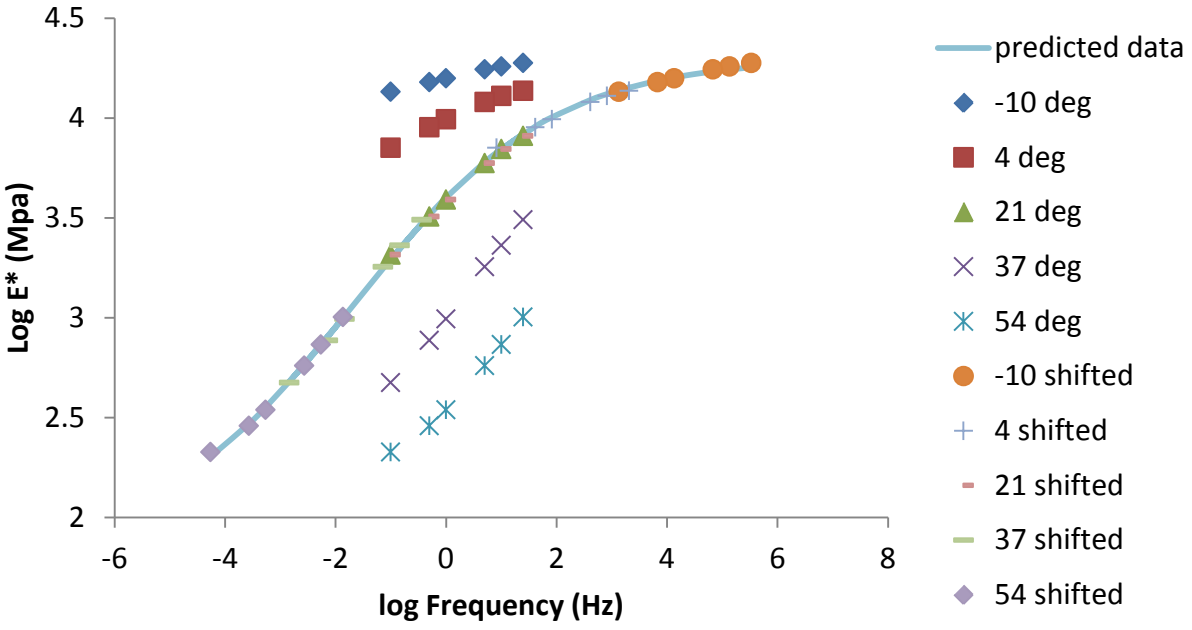


Figure F. 41: Master curve for Sample 3 (SP-III with PG 70-22 binder)

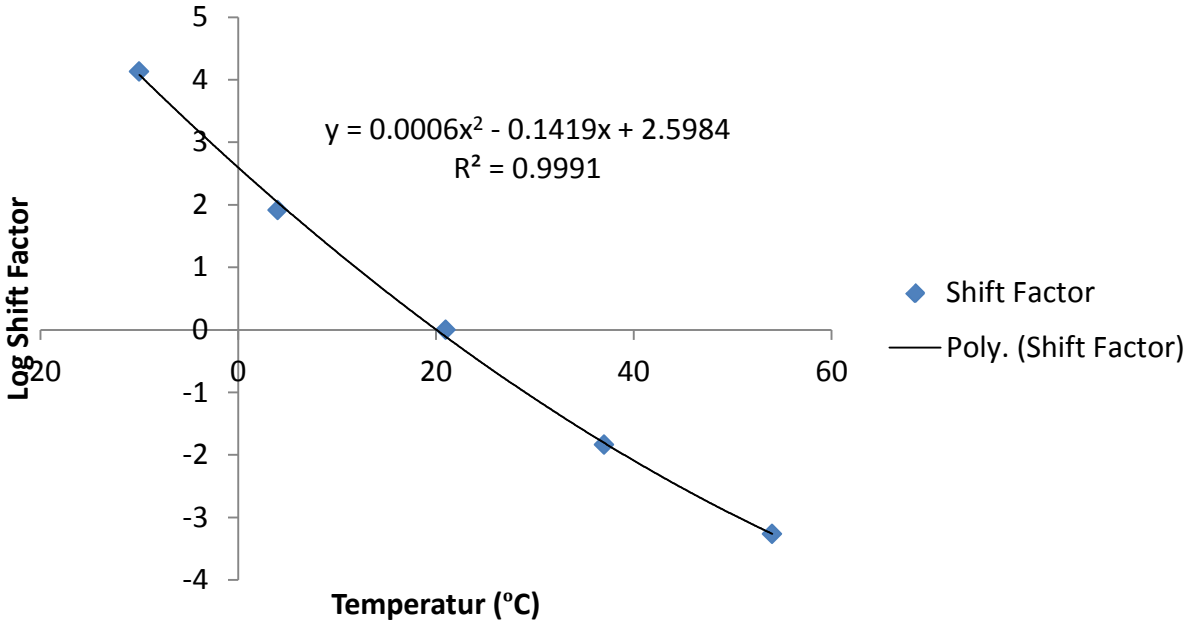


Figure F. 42: Shift factor for Sample 3 (SP-III with PG 70-22 binder)

Table F. 22: E* test results for Sample 4 (SP-III with PG 70-22 binder)

| Temperature | Frequency | Stress | | Dynamic Modulus | Phase Angle | | Strain | | | |
|---|---|---|---|---|---|---|---|---|---|---|
| | | Amplitude (P-P) | SE | | | UC | (P-P) Recoverable | Permanent | SE | UC |
| (deg C) | (Hz) | (kPa) | (%) | (MPa) | (deg) | (deg) | (micro e) | (micro e) | (%) | (%) |
| -10 | 25 | 1175.0 | 5.9 | 16488.0 | 5.6 | 0.9 | 71.3 | -82.3 | 6.1 | 4.4 |
| -10 | 10 | 1113.4 | 3.7 | 16338.1 | 6.2 | 0.6 | 68.1 | -120.8 | 3.3 | 2.7 |
| -10 | 5 | 1056.2 | 1.9 | 15982.5 | 6.3 | 0.7 | 66.1 | -143.5 | 2.7 | 2.6 |
| -10 | 1 | 950.4 | 0.4 | 14531.8 | 7.3 | 0.9 | 65.4 | -158.7 | 2.6 | 3.9 |
| -10 | 0.5 | 900.0 | 0.3 | 14045.5 | 7.3 | 1.1 | 64.1 | -167.4 | 3.2 | 4.6 |
| -10 | 0.1 | 818.4 | 0.2 | 12851.1 | 8.2 | 0.9 | 63.7 | -160.7 | 2.8 | 5.0 |
| 4 | 25 | 910.8 | 5.7 | 13161.1 | 8.7 | 0.8 | 69.2 | 0.8 | 5.5 | 10.9 |
| 4 | 10 | 845.1 | 3.6 | 12513.8 | 9.3 | 0.3 | 67.5 | 1.1 | 3.9 | 10.3 |
| 4 | 5 | 798.7 | 1.9 | 11795.1 | 10.0 | 0.7 | 67.7 | 4.6 | 3.1 | 9.8 |
| 4 | 1 | 700.0 | 0.4 | 9794.9 | 12.3 | 0.9 | 71.5 | 4.6 | 3.2 | 9.1 |
| 4 | 0.5 | 649.5 | 0.3 | 9013.0 | 13.4 | 0.8 | 72.1 | 14.1 | 3.3 | 8.8 |
| 4 | 0.1 | 548.1 | 0.2 | 7390.5 | 15.8 | 1.0 | 74.2 | 75.1 | 3.2 | 7.4 |
| 21 | 25 | 523.6 | 5.7 | 8808.1 | 15.4 | 1.1 | 59.4 | 252.4 | 6.2 | 22.6 |
| 21 | 10 | 461.5 | 3.8 | 7887.3 | 16.6 | 0.4 | 58.5 | 325.8 | 4.4 | 19.8 |
| 21 | 5 | 398.9 | 2.4 | 6761.6 | 18.0 | 0.4 | 59.0 | 338.0 | 4.7 | 17.4 |
| 21 | 1 | 248.3 | 0.6 | 4410.4 | 22.8 | 0.4 | 56.3 | 312.9 | 5.2 | 26.8 |
| 21 | 0.5 | 208.3 | 0.5 | 3696.6 | 23.4 | 0.6 | 56.4 | 317.3 | 5.9 | 29.6 |
| 21 | 0.1 | 148.3 | 0.2 | 2448.1 | 26.5 | 0.4 | 60.6 | 380.8 | 5.0 | 34.4 |
| 37 | 25 | 281.3 | 5.6 | 4240.8 | 24.5 | 2.0 | 66.3 | 739.9 | 5.8 | 18.5 |
| 37 | 10 | 216.0 | 4.2 | 3261.6 | 25.7 | 0.9 | 66.2 | 850.2 | 4.4 | 17.6 |
| 37 | 5 | 162.0 | 3.1 | 2580.5 | 27.1 | 0.9 | 62.8 | 855.3 | 3.9 | 17.6 |
| 37 | 1 | 88.6 | 1.0 | 1373.6 | 31.1 | 1.7 | 64.5 | 799.9 | 3.9 | 23.2 |
| 37 | 0.5 | 68.8 | 0.7 | 1068.8 | 31.3 | 1.9 | 64.3 | 789.4 | 3.7 | 24.9 |
| 37 | 0.1 | 39.2 | 0.6 | 618.2 | 30.5 | 2.3 | 63.4 | 813.4 | 3.7 | 26.3 |
| 54 | 25 | 109.9 | 6.0 | 1511.7 | 30.1 | 2.8 | 72.7 | 364.6 | 5.9 | 21.5 |
| 54 | 10 | 80.4 | 4.7 | 1085.0 | 28.8 | 2.9 | 74.1 | 397.5 | 4.4 | 14.6 |
| 54 | 5 | 64.9 | 4.0 | 851.0 | 28.0 | 3.0 | 76.3 | 393.2 | 4.6 | 14.4 |
| 54 | 1 | 33.8 | 1.9 | 478.1 | 26.9 | 3.0 | 70.6 | 356.7 | 4.8 | 13.4 |
| 54 | 0.5 | 24.2 | 1.4 | 382.4 | 26.0 | 3.3 | 63.2 | 337.3 | 3.9 | 13.2 |
| 54 | 0.1 | 17.4 | 1.0 | 265.8 | 21.7 | 3.0 | 65.3 | 341.5 | 3.9 | 14.5 |

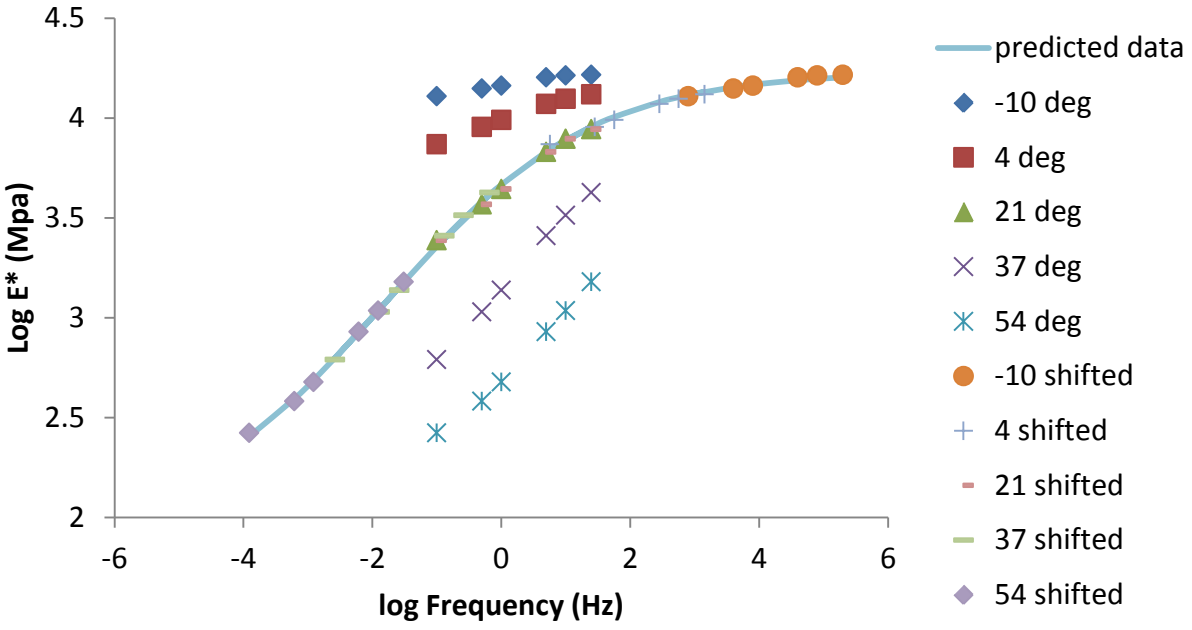


Figure F. 43: Master curve for Sample 4 (SP-III with PG 70-22 binder)

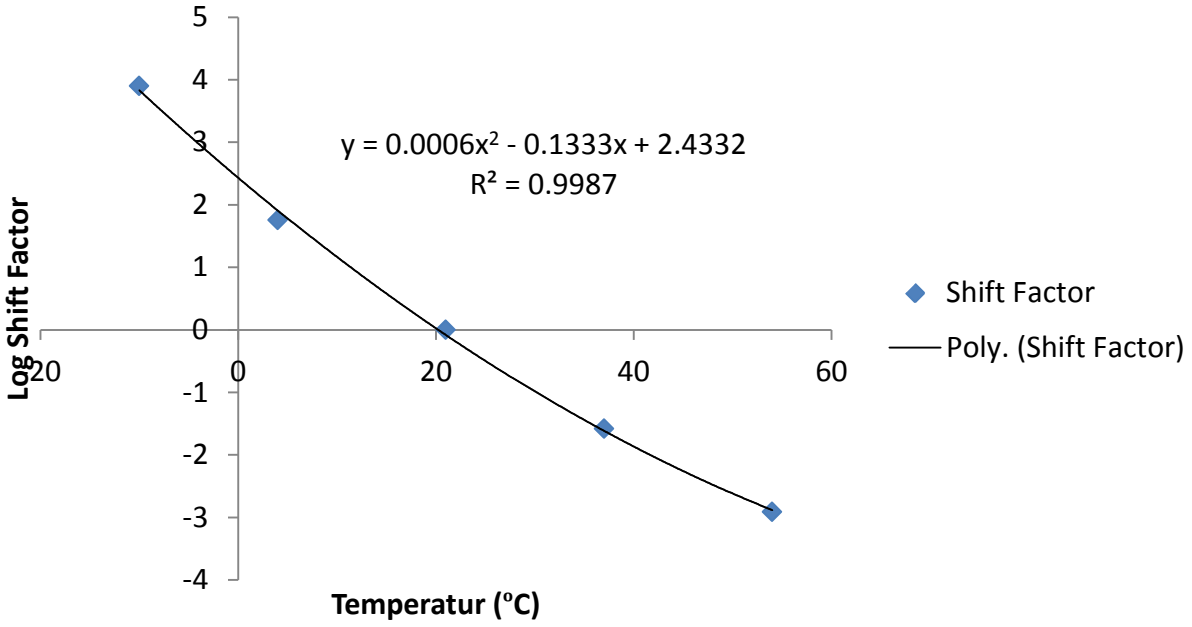


Figure F. 44: Shift factor for Sample 4 (SP-III with PG 70-22 binder)

**SP-IV WITH PG 70-22 BINDER - Samples**

Table F. 23: E* test results for Sample 1 (SP-IV with PG 70-22 binder)

| Temperature | Frequency | Stress | | Dynamic Modulus | Phase Angle | | Strain | | | |
|---|---|---|---|---|---|---|---|---|---|---|
| | | Amplitude (P-P) | SE | | | UC | (P-P) Recoverable | Permanent | SE | UC |
| (deg C) | (Hz) | (kPa) | (%) | (MPa) | (deg) | (deg) | (micro e) | (micro e) | (%) | (%) |
| -10 | 25 | 1172.7 | 5.8 | 33728.5 | 7.1 | 2.1 | 34.8 | -41.6 | 9.1 | 40.7 |
| -10 | 10 | 1115.8 | 3.7 | 32000.4 | 6.4 | 1.0 | 34.9 | -57.3 | 6.1 | 35.0 |
| -10 | 5 | 1056.5 | 1.9 | 30637.3 | 6.8 | 1.1 | 34.5 | -62.7 | 5.0 | 35.0 |
| -10 | 1 | 950.5 | 0.4 | 27276.1 | 8.1 | 0.9 | 34.8 | -67.4 | 3.6 | 35.7 |
| -10 | 0.5 | 900.0 | 0.3 | 25772.9 | 8.7 | 0.9 | 34.9 | -68.4 | 3.8 | 34.3 |
| -10 | 0.1 | 818.5 | 0.2 | 22499.7 | 10.1 | 1.4 | 36.4 | -59.1 | 3.9 | 31.7 |
| 4 | 25 | 1125.4 | 6.0 | 16449.9 | 10.1 | 3.0 | 68.4 | 73.0 | 7.9 | 33.8 |
| 4 | 10 | 1059.1 | 3.7 | 15180.2 | 10.5 | 0.7 | 69.8 | 101.5 | 4.8 | 27.1 |
| 4 | 5 | 1006.5 | 1.9 | 14076.1 | 11.2 | 0.4 | 71.5 | 118.5 | 4.1 | 25.0 |
| 4 | 1 | 859.6 | 0.4 | 11427.0 | 14.0 | 0.9 | 75.2 | 123.6 | 3.5 | 26.6 |
| 4 | 0.5 | 789.9 | 0.3 | 10291.1 | 15.1 | 0.5 | 76.8 | 142.9 | 3.4 | 26.5 |
| 4 | 0.1 | 697.3 | 0.3 | 7733.7 | 18.8 | 0.9 | 90.2 | 253.0 | 3.1 | 24.0 |
| 21 | 25 | 599.9 | 5.5 | 8979.3 | 18.4 | 1.1 | 66.8 | 650.3 | 5.9 | 15.3 |
| 21 | 10 | 541.2 | 3.4 | 7500.2 | 20.3 | 0.8 | 72.2 | 920.6 | 3.7 | 14.8 |
| 21 | 5 | 489.4 | 1.9 | 6389.9 | 22.1 | 0.8 | 76.6 | 1073.2 | 3.4 | 13.8 |
| 21 | 1 | 389.1 | 0.4 | 4140.4 | 26.9 | 1.3 | 94.0 | 1141.9 | 2.9 | 10.8 |
| 21 | 0.5 | 338.1 | 0.4 | 3375.5 | 28.5 | 1.2 | 100.2 | 1236.3 | 2.6 | 9.1 |
| 21 | 0.1 | 257.5 | 0.2 | 2015.8 | 30.9 | 1.0 | 127.7 | 1532.4 | 2.8 | 7.4 |
| 37 | 25 | 189.9 | 5.6 | 2829.8 | 30.4 | 1.7 | 67.1 | 861.0 | 5.6 | 5.7 |
| 37 | 10 | 131.0 | 4.3 | 1993.1 | 31.9 | 0.6 | 65.7 | 978.2 | 5.0 | 8.0 |
| 37 | 5 | 89.9 | 3.1 | 1464.4 | 33.3 | 1.0 | 61.4 | 988.2 | 3.7 | 10.2 |
| 37 | 1 | 53.3 | 1.2 | 759.3 | 34.0 | 1.8 | 70.2 | 956.6 | 3.2 | 10.0 |
| 37 | 0.5 | 38.9 | 0.9 | 567.2 | 33.3 | 2.5 | 68.5 | 934.2 | 3.6 | 10.1 |
| 37 | 0.1 | 19.3 | 1.0 | 314.1 | 29.5 | 2.5 | 61.5 | 916.7 | 3.5 | 6.7 |
| 54 | 25 | 73.0 | 5.6 | 858.4 | 35.6 | 2.4 | 85.0 | 973.3 | 5.1 | 3.9 |
| 54 | 10 | 49.3 | 4.4 | 567.8 | 34.3 | 1.0 | 86.8 | 1048.4 | 4.2 | 4.0 |
| 54 | 5 | 38.5 | 3.9 | 431.1 | 33.1 | 2.0 | 89.4 | 1037.5 | 3.9 | 6.5 |
| 54 | 1 | 18.6 | 2.3 | 234.1 | 30.2 | 3.3 | 79.4 | 940.2 | 4.2 | 17.8 |
| 54 | 0.5 | 16.1 | 1.8 | 198.4 | 27.3 | 3.6 | 81.2 | 881.3 | 5.5 | 25.1 |
| 54 | 0.1 | 11.4 | 2.5 | 149.8 | 19.4 | 1.8 | 76.2 | 811.3 | 5.3 | 44.7 |

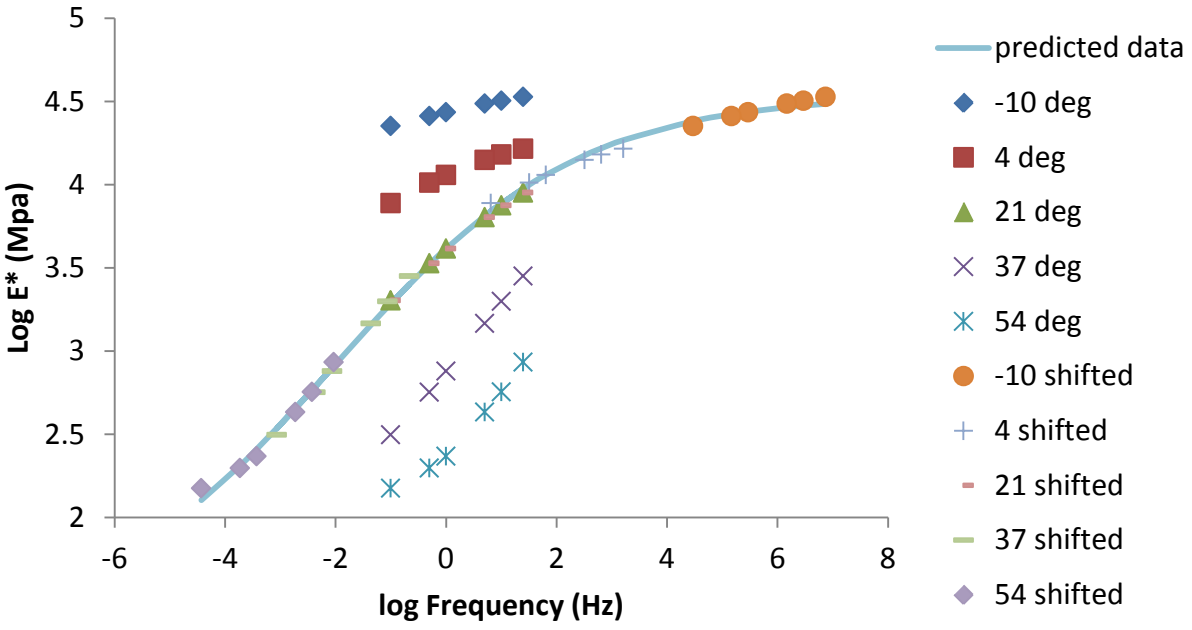


Figure F. 45: Master curve for Sample 1 (SP-IV with PG 70-22 binder)

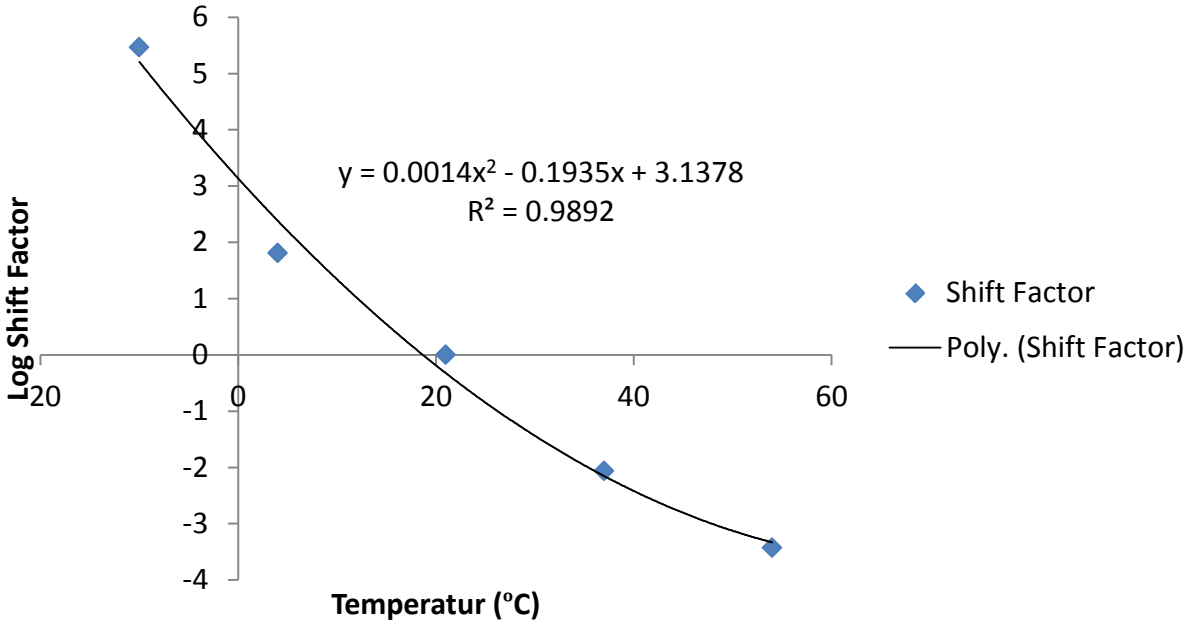


Figure F. 46: Shift factor for Sample 1 (SP-IV with PG 70-22 binder)

Table F. 24: E* test results for Sample 2 (SP-IV with PG 70-22 binder)

| Temperature | Frequency | Stress | | Dynamic Modulus | Phase Angle | | Strain | | | |
|---|---|---|---|---|---|---|---|---|---|---|
| | | Amplitude (P-P) | SE | | | UC | (P-P) Recoverable | Permanent | SE | UC |
| (deg C) | (Hz) | (kPa) | (%) | (MPa) | (deg) | (deg) | (micro e) | (micro e) | (%) | (%) |
| -10 | 25 | 1172.5 | 5.8 | 22379.3 | 5.7 | 1.7 | 52.4 | -40.6 | 6.6 | 20.9 |
| -10 | 10 | 1114.1 | 3.6 | 21593.3 | 6.0 | 1.6 | 51.6 | -57.4 | 4.6 | 19.6 |
| -10 | 5 | 1056.5 | 1.7 | 20746.7 | 6.4 | 1.6 | 50.9 | -65.4 | 4.0 | 19.0 |
| -10 | 1 | 949.8 | 0.3 | 18551.5 | 7.3 | 1.2 | 51.2 | -71.9 | 3.8 | 16.7 |
| -10 | 0.5 | 900.0 | 0.3 | 17584.0 | 7.7 | 1.5 | 51.2 | -73.6 | 2.5 | 16.0 |
| -10 | 0.1 | 818.4 | 0.2 | 15389.6 | 9.4 | 1.7 | 53.2 | -60.6 | 2.7 | 16.5 |
| 4 | 25 | 965.8 | 5.8 | 15585.6 | 10.0 | 2.2 | 62.0 | 40.3 | 7.8 | 27.9 |
| 4 | 10 | 910.2 | 3.6 | 14349.4 | 10.6 | 1.1 | 63.4 | 57.8 | 5.2 | 24.4 |
| 4 | 5 | 859.8 | 1.9 | 13312.4 | 11.4 | 1.2 | 64.6 | 69.7 | 4.4 | 22.9 |
| 4 | 1 | 779.7 | 0.4 | 10628.7 | 14.5 | 1.6 | 73.4 | 76.7 | 3.7 | 19.9 |
| 4 | 0.5 | 728.9 | 0.3 | 9612.0 | 15.8 | 1.8 | 75.8 | 95.2 | 3.1 | 18.5 |
| 4 | 0.1 | 638.0 | 0.2 | 7306.1 | 19.0 | 1.3 | 87.3 | 201.3 | 2.5 | 15.5 |
| 21 | 25 | 548.2 | 5.5 | 8454.8 | 18.1 | 2.1 | 64.8 | 596.3 | 6.2 | 16.4 |
| 21 | 10 | 488.7 | 3.6 | 7248.7 | 19.6 | 1.7 | 67.4 | 837.7 | 4.8 | 14.7 |
| 21 | 5 | 429.7 | 2.0 | 6262.9 | 21.8 | 1.9 | 68.6 | 954.3 | 3.6 | 14.5 |
| 21 | 1 | 298.6 | 0.5 | 4086.9 | 26.6 | 1.6 | 73.1 | 974.3 | 3.0 | 13.1 |
| 21 | 0.5 | 258.5 | 0.4 | 3369.7 | 27.6 | 1.8 | 76.7 | 1024.9 | 5.2 | 12.9 |
| 21 | 0.1 | 168.0 | 0.3 | 2036.7 | 30.9 | 1.3 | 82.5 | 1157.1 | 3.9 | 9.8 |
| 37 | 25 | 199.8 | 5.6 | 2919.3 | 31.5 | 5.1 | 68.4 | 931.1 | 5.4 | 12.7 |
| 37 | 10 | 140.6 | 4.1 | 2083.0 | 32.8 | 3.6 | 67.5 | 1068.6 | 4.2 | 8.0 |
| 37 | 5 | 110.2 | 2.9 | 1564.8 | 34.2 | 3.5 | 70.4 | 1120.0 | 3.8 | 5.4 |
| 37 | 1 | 58.3 | 0.9 | 785.0 | 35.9 | 3.1 | 74.2 | 1083.6 | 3.2 | 4.5 |
| 37 | 0.5 | 43.8 | 0.8 | 594.1 | 35.1 | 3.0 | 73.7 | 1073.2 | 3.5 | 4.3 |
| 37 | 0.1 | 24.2 | 1.0 | 332.3 | 31.4 | 2.9 | 72.9 | 1083.0 | 4.0 | 0.6 |
| 54 | 25 | 77.5 | 5.6 | 823.7 | 37.7 | 4.4 | 94.1 | 736.0 | 5.7 | 13.2 |
| 54 | 10 | 58.7 | 4.3 | 544.1 | 35.3 | 2.9 | 108.0 | 890.4 | 4.1 | 7.1 |
| 54 | 5 | 43.7 | 3.9 | 396.9 | 34.2 | 2.7 | 110.2 | 913.3 | 4.1 | 5.8 |
| 54 | 1 | 23.3 | 3.4 | 210.6 | 30.7 | 3.0 | 110.4 | 856.5 | 5.5 | 8.1 |
| 54 | 0.5 | 19.0 | 1.9 | 171.2 | 28.3 | 3.1 | 110.7 | 814.1 | 4.8 | 10.6 |
| 54 | 0.1 | 14.3 | 1.6 | 120.2 | 22.2 | 3.4 | 119.0 | 792.7 | 6.0 | 15.2 |

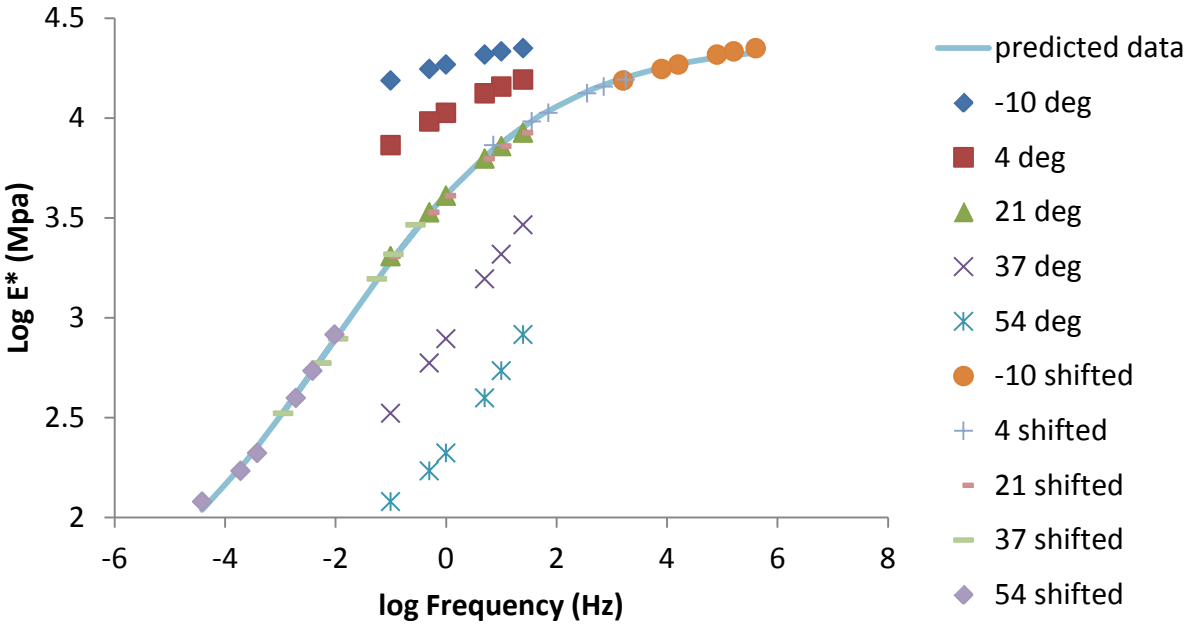


Figure F. 47: Master curve for Sample 2 (SP-IV with PG 70-22 binder)

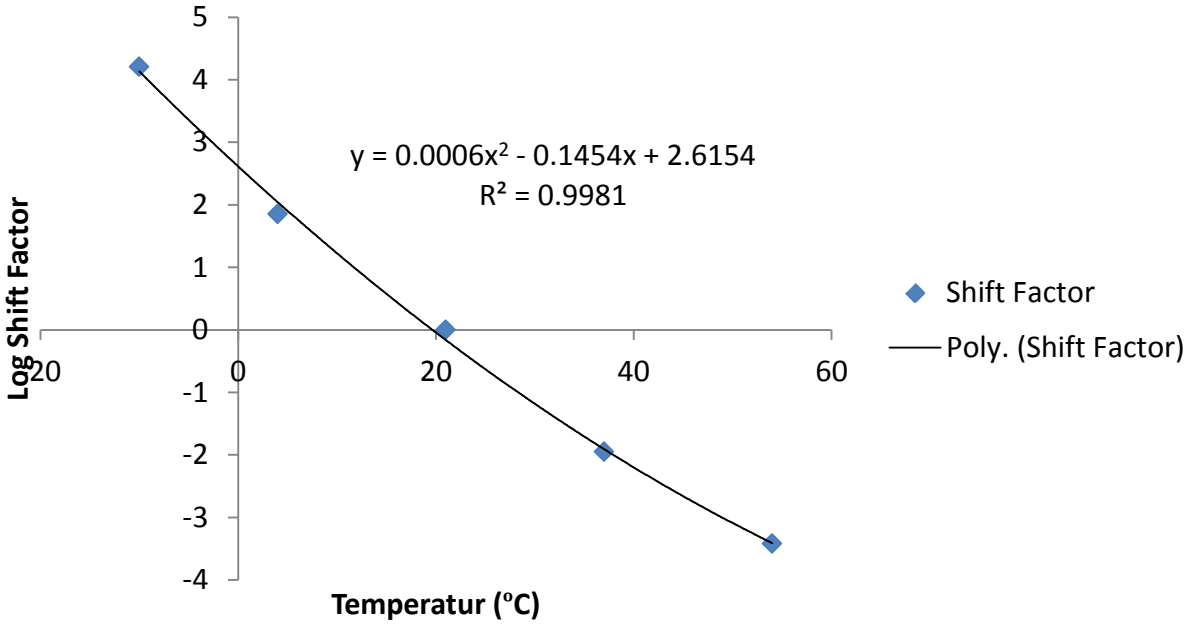


Figure F. 48: Shift factor for Sample 2 (SP-IV with PG 70-22 binder)

# APPENDIX G

## DYNAMIC SHEAR MODULUS TEST RESULTS FOR PG 64-22 and PG 70-22 BINDERs

Table G. 25: DSR test result PG 64-22 at 54 ºC

| Meas. Pts. | Binder Grade | Temperature | Angular Frequency | Storage Modulus | Loss Modulus | Phase Angle |
|---|---|---|---|---|---|---|
| | | ºC | [rad/s] | [Pa] | [Pa] | [°] |
| 1 | PG 64-22 | 54.44 | 5.00E+02 | 1.35E+05 | 3.30E+05 | 67.84 |
| 2 | | 54.44 | 3.97E+02 | 1.10E+05 | 2.77E+05 | 68.3 |
| 3 | | 54.44 | 3.16E+02 | 9.07E+04 | 2.33E+05 | 68.77 |
| 4 | | 54.44 | 2.51E+02 | 7.42E+04 | 1.96E+05 | 69.27 |
| 5 | | 54.44 | 1.99E+02 | 6.06E+04 | 1.64E+05 | 69.76 |
| 6 | | 54.44 | 1.58E+02 | 4.93E+04 | 1.38E+05 | 70.26 |
| 7 | | 54.44 | 1.26E+02 | 4.02E+04 | 1.15E+05 | 70.76 |
| 8 | | 54.44 | 9.98E+01 | 3.27E+04 | 9.65E+04 | 71.26 |
| 9 | | 54.44 | 7.92E+01 | 2.65E+04 | 8.05E+04 | 71.77 |
| 10 | | 54.44 | 6.30E+01 | 2.14E+04 | 6.69E+04 | 72.29 |
| 11 | | 54.44 | 5.00E+01 | 1.72E+04 | 5.58E+04 | 72.82 |
| 12 | | 54.44 | 3.97E+01 | 1.39E+04 | 4.65E+04 | 73.35 |
| 13 | | 54.44 | 3.16E+01 | 1.12E+04 | 3.88E+04 | 73.92 |
| 14 | | 54.44 | 2.51E+01 | 8.91E+03 | 3.21E+04 | 74.48 |
| 15 | | 54.44 | 1.99E+01 | 7.05E+03 | 2.64E+04 | 75.06 |
| 16 | | 54.44 | 1.58E+01 | 5.61E+03 | 2.19E+04 | 75.64 |
| 17 | | 54.44 | 1.26E+01 | 4.49E+03 | 1.83E+04 | 76.21 |
| 18 | | 54.44 | 9.98E+00 | 3.55E+03 | 1.51E+04 | 76.81 |
| 19 | | 54.44 | 7.92E+00 | 2.78E+03 | 1.25E+04 | 77.43 |
| 20 | | 54.44 | 6.30E+00 | 2.16E+03 | 1.02E+04 | 78.08 |
| 21 | | 54.44 | 5.00E+00 | 1.67E+03 | 8.38E+03 | 78.72 |
| 22 | | 54.44 | 3.97E+00 | 1.29E+03 | 6.85E+03 | 79.37 |
| 23 | | 54.44 | 3.16E+00 | 9.89E+02 | 5.61E+03 | 80 |
| 24 | | 54.44 | 2.51E+00 | 7.49E+02 | 4.55E+03 | 80.66 |
| 25 | | 54.44 | 1.99E+00 | 5.62E+02 | 3.68E+03 | 81.31 |
| 26 | | 54.44 | 1.58E+00 | 4.27E+02 | 2.99E+03 | 81.89 |
| 27 | | 54.44 | 1.26E+00 | 3.22E+02 | 2.43E+03 | 82.47 |
| 28 | | 54.44 | 9.98E-01 | 2.39E+02 | 1.97E+03 | 83.08 |
| 29 | | 54.44 | 7.92E-01 | 1.78E+02 | 1.60E+03 | 83.66 |
| 30 | | 54.44 | 6.30E-01 | 1.30E+02 | 1.28E+03 | 84.2 |
| 31 | | 54.44 | 5.00E-01 | 9.58E+01 | 1.04E+03 | 84.72 |

Table G. 26: DSR test result PG 64-22 at 46 ºC

| Meas. Pts. | Binder Grade | Temperature | Angular Frequency | Storage Modulus | Loss Modulus | Phase Angle |
|---|---|---|---|---|---|---|
| | | ºC | [rad/s] | [Pa] | [Pa] | [°] |
| 1 | PG 64-22 | 46.11 | 5.00E+02 | 4.45E+05 | 8.57E+05 | 62.55 |
| 2 | | 46.11 | 3.97E+02 | 3.69E+05 | 7.30E+05 | 63.17 |
| 3 | | 46.11 | 3.16E+02 | 3.06E+05 | 6.21E+05 | 63.74 |
| 4 | | 46.11 | 2.51E+02 | 2.55E+05 | 5.29E+05 | 64.31 |
| 5 | | 46.11 | 1.99E+02 | 2.12E+05 | 4.51E+05 | 64.86 |
| 6 | | 46.11 | 1.58E+02 | 1.75E+05 | 3.83E+05 | 65.4 |
| 7 | | 46.11 | 1.26E+02 | 1.45E+05 | 3.25E+05 | 65.93 |
| 8 | | 46.11 | 9.98E+01 | 1.20E+05 | 2.75E+05 | 66.45 |
| 9 | | 46.11 | 7.92E+01 | 9.90E+04 | 2.33E+05 | 66.95 |
| 10 | | 46.11 | 6.30E+01 | 8.16E+04 | 1.97E+05 | 67.45 |
| 11 | | 46.11 | 5.00E+01 | 6.74E+04 | 1.66E+05 | 67.94 |
| 12 | | 46.11 | 3.97E+01 | 5.56E+04 | 1.41E+05 | 68.43 |
| 13 | | 46.11 | 3.16E+01 | 4.54E+04 | 1.18E+05 | 68.94 |
| 14 | | 46.11 | 2.51E+01 | 3.72E+04 | 9.93E+04 | 69.44 |
| 15 | | 46.11 | 1.99E+01 | 3.06E+04 | 8.37E+04 | 69.94 |
| 16 | | 46.11 | 1.58E+01 | 2.49E+04 | 7.02E+04 | 70.47 |
| 17 | | 46.11 | 1.26E+01 | 2.02E+04 | 5.86E+04 | 71.02 |
| 18 | | 46.11 | 9.98E+00 | 1.63E+04 | 4.91E+04 | 71.58 |
| 19 | | 46.11 | 7.92E+00 | 1.32E+04 | 4.10E+04 | 72.15 |
| 20 | | 46.11 | 6.30E+00 | 1.06E+04 | 3.41E+04 | 72.75 |
| 21 | | 46.11 | 5.00E+00 | 8.51E+03 | 2.85E+04 | 73.35 |
| 22 | | 46.11 | 3.97E+00 | 6.78E+03 | 2.36E+04 | 73.99 |
| 23 | | 46.11 | 3.16E+00 | 5.40E+03 | 1.96E+04 | 74.62 |
| 24 | | 46.11 | 2.51E+00 | 4.28E+03 | 1.63E+04 | 75.28 |
| 25 | | 46.11 | 1.99E+00 | 3.36E+03 | 1.34E+04 | 75.96 |
| 26 | | 46.11 | 1.58E+00 | 2.64E+03 | 1.11E+04 | 76.64 |
| 27 | | 46.11 | 1.26E+00 | 2.06E+03 | 9.13E+03 | 77.32 |
| 28 | | 46.11 | 9.98E-01 | 1.58E+03 | 7.48E+03 | 78.04 |
| 29 | | 46.11 | 7.92E-01 | 1.23E+03 | 6.14E+03 | 78.72 |
| 30 | | 46.11 | 6.30E-01 | 9.48E+02 | 5.07E+03 | 79.4 |
| 31 | | 46.11 | 5.00E-01 | 7.26E+02 | 4.15E+03 | 80.09 |

Table G. 27: DSR test result PG 64-22 at 37 ºC

| Meas. Pts. | Binder Grade | Temperature ºC | Angular Frequency [rad/s] | Storage Modulus [Pa] | Loss Modulus [Pa] | Phase Angle [°] |
|---|---|---|---|---|---|---|
| 1 | PG 64-22 | 37.78 | 5.00E+02 | 1.52E+06 | 2.66E+06 | 60.34 |
| 2 | | 37.78 | 3.97E+02 | 1.33E+06 | 2.26E+06 | 59.45 |
| 3 | | 37.78 | 3.16E+02 | 1.14E+06 | 1.94E+06 | 59.6 |
| 4 | | 37.78 | 2.51E+02 | 9.85E+05 | 1.69E+06 | 59.68 |
| 5 | | 37.78 | 1.99E+02 | 8.41E+05 | 1.46E+06 | 60.02 |
| 6 | | 37.78 | 1.58E+02 | 7.11E+05 | 1.25E+06 | 60.45 |
| 7 | | 37.78 | 1.26E+02 | 5.98E+05 | 1.08E+06 | 60.96 |
| 8 | | 37.78 | 9.98E+01 | 5.01E+05 | 9.23E+05 | 61.51 |
| 9 | | 37.78 | 7.92E+01 | 4.16E+05 | 7.91E+05 | 62.26 |
| 10 | | 37.78 | 6.30E+01 | 3.52E+05 | 6.77E+05 | 62.54 |
| 11 | | 37.78 | 5.00E+01 | 2.96E+05 | 5.82E+05 | 63.01 |
| 12 | | 37.78 | 3.97E+01 | 2.50E+05 | 5.00E+05 | 63.48 |
| 13 | | 37.78 | 3.16E+01 | 2.08E+05 | 4.26E+05 | 63.98 |
| 14 | | 37.78 | 2.51E+01 | 1.74E+05 | 3.64E+05 | 64.46 |
| 15 | | 37.78 | 1.99E+01 | 1.45E+05 | 3.10E+05 | 64.93 |
| 16 | | 37.78 | 1.58E+01 | 1.21E+05 | 2.64E+05 | 65.43 |
| 17 | | 37.78 | 1.26E+01 | 9.99E+04 | 2.24E+05 | 65.93 |
| 18 | | 37.78 | 9.98E+00 | 8.29E+04 | 1.90E+05 | 66.4 |
| 19 | | 37.78 | 7.92E+00 | 6.85E+04 | 1.61E+05 | 66.9 |
| 20 | | 37.78 | 6.30E+00 | 5.63E+04 | 1.35E+05 | 67.42 |
| 21 | | 37.78 | 5.00E+00 | 4.65E+04 | 1.15E+05 | 67.93 |
| 22 | | 37.78 | 3.97E+00 | 3.84E+04 | 9.71E+04 | 68.44 |
| 23 | | 37.78 | 3.16E+00 | 3.14E+04 | 8.18E+04 | 68.99 |
| 24 | | 37.78 | 2.51E+00 | 2.55E+04 | 6.86E+04 | 69.56 |
| 25 | | 37.78 | 1.99E+00 | 2.09E+04 | 5.78E+04 | 70.14 |
| 26 | | 37.78 | 1.58E+00 | 1.69E+04 | 4.83E+04 | 70.73 |
| 27 | | 37.78 | 1.26E+00 | 1.37E+04 | 4.04E+04 | 71.33 |
| 28 | | 37.78 | 9.98E-01 | 1.10E+04 | 3.38E+04 | 71.99 |
| 29 | | 37.78 | 7.92E-01 | 8.84E+03 | 2.83E+04 | 72.64 |
| 30 | | 37.78 | 6.30E-01 | 7.11E+03 | 2.37E+04 | 73.27 |
| 31 | | 37.78 | 5.00E-01 | 5.66E+03 | 1.96E+04 | 73.93 |

Table G. 28: DSR test result PG 64-22 at 29 ºC

| Meas. Pts. | Binder Grade | Temperature | Angular Frequency | Storage Modulus | Loss Modulus | Phase Angle |
|---|---|---|---|---|---|---|
| | | ºC | [rad/s] | [Pa] | [Pa] | [°] |
| 1 | PG 64-22 | 29.44 | 5.00E+02 | 5.53E+06 | 6.89E+06 | 51.25 |
| 2 | | 29.44 | 3.97E+02 | 4.84E+06 | 6.06E+06 | 51.42 |
| 3 | | 29.44 | 3.16E+02 | 4.19E+06 | 5.35E+06 | 51.95 |
| 4 | | 29.44 | 2.51E+02 | 3.62E+06 | 4.71E+06 | 52.46 |
| 5 | | 29.44 | 1.99E+02 | 3.12E+06 | 4.15E+06 | 53.04 |
| 6 | | 29.44 | 1.58E+02 | 2.67E+06 | 3.66E+06 | 53.87 |
| 7 | | 29.44 | 1.26E+02 | 2.31E+06 | 3.21E+06 | 54.26 |
| 8 | | 29.44 | 9.98E+01 | 1.98E+06 | 2.82E+06 | 54.86 |
| 9 | | 29.44 | 7.92E+01 | 1.70E+06 | 2.47E+06 | 55.48 |
| 10 | | 29.44 | 6.30E+01 | 1.45E+06 | 2.16E+06 | 56.11 |
| 11 | | 29.44 | 5.00E+01 | 1.24E+06 | 1.90E+06 | 56.9 |
| 12 | | 29.44 | 3.97E+01 | 1.06E+06 | 1.65E+06 | 57.35 |
| 13 | | 29.44 | 3.16E+01 | 9.01E+05 | 1.43E+06 | 57.83 |
| 14 | | 29.44 | 2.51E+01 | 7.66E+05 | 1.24E+06 | 58.34 |
| 15 | | 29.44 | 1.99E+01 | 6.49E+05 | 1.08E+06 | 58.88 |
| 16 | | 29.44 | 1.58E+01 | 5.49E+05 | 9.29E+05 | 59.41 |
| 17 | | 29.44 | 1.26E+01 | 4.65E+05 | 8.03E+05 | 59.93 |
| 18 | | 29.44 | 9.98E+00 | 3.93E+05 | 6.94E+05 | 60.45 |
| 19 | | 29.44 | 7.92E+00 | 3.36E+05 | 6.04E+05 | 60.92 |
| 20 | | 29.44 | 6.30E+00 | 2.85E+05 | 5.23E+05 | 61.4 |
| 21 | | 29.44 | 5.00E+00 | 2.39E+05 | 4.48E+05 | 61.92 |
| 22 | | 29.44 | 3.97E+00 | 2.00E+05 | 3.83E+05 | 62.45 |
| 23 | | 29.44 | 3.16E+00 | 1.68E+05 | 3.28E+05 | 62.93 |
| 24 | | 29.44 | 2.51E+00 | 1.41E+05 | 2.81E+05 | 63.45 |
| 25 | | 29.44 | 1.99E+00 | 1.16E+05 | 2.38E+05 | 63.97 |
| 26 | | 29.44 | 1.58E+00 | 9.65E+04 | 2.02E+05 | 64.51 |
| 27 | | 29.44 | 1.26E+00 | 8.05E+04 | 1.73E+05 | 65.02 |
| 28 | | 29.44 | 9.98E-01 | 6.74E+04 | 1.48E+05 | 65.53 |
| 29 | | 29.44 | 7.92E-01 | 5.56E+04 | 1.25E+05 | 66.05 |
| 30 | | 29.44 | 6.30E-01 | 4.60E+04 | 1.07E+05 | 66.62 |
| 31 | | 29.44 | 5.00E-01 | 3.85E+04 | 9.14E+04 | 67.15 |

Table G. 29: DSR test result PG 64-22 at 21 ºC

| Meas. Pts. | Binder Grade | Temperature ºC | Angular Frequency [rad/s] | Storage Modulus [Pa] | Loss Modulus [Pa] | Phase Angle [°] |
|---|---|---|---|---|---|---|
| 1 | PG 64-22 | 21.11 | 5.00E+02 | 1.79E+07 | 1.64E+07 | 42.5 |
| 2 | | 21.11 | 3.97E+02 | 1.59E+07 | 1.49E+07 | 43.06 |
| 3 | | 21.11 | 3.16E+02 | 1.41E+07 | 1.35E+07 | 43.69 |
| 4 | | 21.11 | 2.51E+02 | 1.23E+07 | 1.22E+07 | 44.8 |
| 5 | | 21.11 | 1.99E+02 | 1.11E+07 | 1.10E+07 | 44.94 |
| 6 | | 21.11 | 1.58E+02 | 9.70E+06 | 1.00E+07 | 45.92 |
| 7 | | 21.11 | 1.26E+02 | 8.55E+06 | 9.02E+06 | 46.51 |
| 8 | | 21.11 | 9.98E+01 | 7.54E+06 | 8.07E+06 | 46.95 |
| 9 | | 21.11 | 7.92E+01 | 6.62E+06 | 7.23E+06 | 47.52 |
| 10 | | 21.11 | 6.30E+01 | 5.82E+06 | 6.49E+06 | 48.14 |
| 11 | | 21.11 | 5.00E+01 | 5.10E+06 | 5.82E+06 | 48.75 |
| 12 | | 21.11 | 3.97E+01 | 4.47E+06 | 5.21E+06 | 49.37 |
| 13 | | 21.11 | 3.16E+01 | 3.90E+06 | 4.65E+06 | 49.99 |
| 14 | | 21.11 | 2.51E+01 | 3.40E+06 | 4.14E+06 | 50.6 |
| 15 | | 21.11 | 1.99E+01 | 2.96E+06 | 3.68E+06 | 51.22 |
| 16 | | 21.11 | 1.58E+01 | 2.57E+06 | 3.26E+06 | 51.83 |
| 17 | | 21.11 | 1.26E+01 | 2.22E+06 | 2.88E+06 | 52.44 |
| 18 | | 21.11 | 9.98E+00 | 1.92E+06 | 2.55E+06 | 53.05 |
| 19 | | 21.11 | 7.92E+00 | 1.65E+06 | 2.24E+06 | 53.65 |
| 20 | | 21.11 | 6.30E+00 | 1.42E+06 | 1.97E+06 | 54.25 |
| 21 | | 21.11 | 5.00E+00 | 1.21E+06 | 1.73E+06 | 54.85 |
| 22 | | 21.11 | 3.97E+00 | 1.04E+06 | 1.50E+06 | 55.47 |
| 23 | | 21.11 | 3.16E+00 | 8.79E+05 | 1.31E+06 | 56.06 |
| 24 | | 21.11 | 2.51E+00 | 7.53E+05 | 1.14E+06 | 56.64 |
| 25 | | 21.11 | 1.99E+00 | 6.46E+05 | 1.00E+06 | 57.16 |
| 26 | | 21.11 | 1.58E+00 | 5.51E+05 | 8.73E+05 | 57.73 |
| 27 | | 21.11 | 1.26E+00 | 4.69E+05 | 7.58E+05 | 58.28 |
| 28 | | 21.11 | 9.98E-01 | 3.96E+05 | 6.55E+05 | 58.85 |
| 29 | | 21.11 | 7.92E-01 | 3.36E+05 | 5.68E+05 | 59.36 |
| 30 | | 21.11 | 6.30E-01 | 2.84E+05 | 4.90E+05 | 59.95 |
| 31 | | 21.11 | 5.00E-01 | 2.40E+05 | 4.25E+05 | 60.49 |

Table G. 30: DSR test result PG 64-22 at 12 ºC

| Meas. Pts. | Binder Grade | Temperature ºC | Angular Frequency [rad/s] | Storage Modulus [Pa] | Loss Modulus [Pa] | Phase Angle [°] |
|---|---|---|---|---|---|---|
| 1 | PG 64-22 | 12.78 | 5.00E+02 | 4.94E+07 | 3.33E+07 | 33.94 |
| 2 | | 12.78 | 3.97E+02 | 4.51E+07 | 3.11E+07 | 34.55 |
| 3 | | 12.78 | 3.16E+02 | 4.12E+07 | 2.90E+07 | 35.17 |
| 4 | | 12.78 | 2.51E+02 | 3.75E+07 | 2.70E+07 | 35.81 |
| 5 | | 12.78 | 1.99E+02 | 3.39E+07 | 2.51E+07 | 36.56 |
| 6 | | 12.78 | 1.58E+02 | 3.08E+07 | 2.33E+07 | 37.13 |
| 7 | | 12.78 | 1.26E+02 | 2.79E+07 | 2.16E+07 | 37.72 |
| 8 | | 12.78 | 9.98E+01 | 2.51E+07 | 1.99E+07 | 38.36 |
| 9 | | 12.78 | 7.92E+01 | 2.27E+07 | 1.83E+07 | 39 |
| 10 | | 12.78 | 6.30E+01 | 2.03E+07 | 1.69E+07 | 39.65 |
| 11 | | 12.78 | 5.00E+01 | 1.83E+07 | 1.55E+07 | 40.27 |
| 12 | | 12.78 | 3.97E+01 | 1.64E+07 | 1.42E+07 | 40.9 |
| 13 | | 12.78 | 3.16E+01 | 1.47E+07 | 1.30E+07 | 41.52 |
| 14 | | 12.78 | 2.51E+01 | 1.31E+07 | 1.19E+07 | 42.14 |
| 15 | | 12.78 | 1.99E+01 | 1.17E+07 | 1.08E+07 | 42.76 |
| 16 | | 12.78 | 1.58E+01 | 1.04E+07 | 9.83E+06 | 43.4 |
| 17 | | 12.78 | 1.26E+01 | 9.21E+06 | 8.91E+06 | 44.04 |
| 18 | | 12.78 | 9.98E+00 | 8.16E+06 | 8.07E+06 | 44.68 |
| 19 | | 12.78 | 7.92E+00 | 7.23E+06 | 7.31E+06 | 45.3 |
| 20 | | 12.78 | 6.30E+00 | 6.37E+06 | 6.58E+06 | 45.94 |
| 21 | | 12.78 | 5.00E+00 | 5.61E+06 | 5.93E+06 | 46.57 |
| 22 | | 12.78 | 3.97E+00 | 4.94E+06 | 5.33E+06 | 47.2 |
| 23 | | 12.78 | 3.16E+00 | 4.34E+06 | 4.79E+06 | 47.84 |
| 24 | | 12.78 | 2.51E+00 | 3.80E+06 | 4.29E+06 | 48.46 |
| 25 | | 12.78 | 1.99E+00 | 3.31E+06 | 3.82E+06 | 49.12 |
| 26 | | 12.78 | 1.58E+00 | 2.89E+06 | 3.41E+06 | 49.73 |
| 27 | | 12.78 | 1.26E+00 | 2.52E+06 | 3.04E+06 | 50.34 |
| 28 | | 12.78 | 9.98E-01 | 2.19E+06 | 2.70E+06 | 51 |
| 29 | | 12.78 | 7.92E-01 | 1.90E+06 | 2.40E+06 | 51.63 |
| 30 | | 12.78 | 6.30E-01 | 1.65E+06 | 2.13E+06 | 52.24 |
| 31 | | 12.78 | 5.00E-01 | 1.43E+06 | 1.89E+06 | 52.84 |

Table G. 31: DSR test result PG 64-22 at 10ºF

| Meas. Pts. | Binder Grade | Temperature | Angular Frequency | Storage Modulus | Loss Modulus | Phase Angle |
|---|---|---|---|---|---|---|
| | | ºC | [rad/s] | [Pa] | [Pa] | [°] |
| 1 | PG 64-22 | 10 | 5.00E+02 | 6.77E+07 | 4.06E+07 | 30.93 |
| 2 | | 10 | 3.97E+02 | 6.23E+07 | 3.82E+07 | 31.55 |
| 3 | | 10 | 3.16E+02 | 5.74E+07 | 3.61E+07 | 32.16 |
| 4 | | 10 | 2.51E+02 | 5.27E+07 | 3.39E+07 | 32.79 |
| 5 | | 10 | 1.99E+02 | 4.82E+07 | 3.19E+07 | 33.49 |
| 6 | | 10 | 1.58E+02 | 4.41E+07 | 2.98E+07 | 34.06 |
| 7 | | 10 | 1.26E+02 | 4.03E+07 | 2.79E+07 | 34.69 |
| 8 | | 10 | 9.98E+01 | 3.67E+07 | 2.60E+07 | 35.33 |
| 9 | | 10 | 7.92E+01 | 3.34E+07 | 2.42E+07 | 35.95 |
| 10 | | 10 | 6.30E+01 | 3.03E+07 | 2.25E+07 | 36.58 |
| 11 | | 10 | 5.00E+01 | 2.75E+07 | 2.09E+07 | 37.19 |
| 12 | | 10 | 3.97E+01 | 2.50E+07 | 1.94E+07 | 37.8 |
| 13 | | 10 | 3.16E+01 | 2.25E+07 | 1.78E+07 | 38.43 |
| 14 | | 10 | 2.51E+01 | 2.02E+07 | 1.64E+07 | 39.08 |
| 15 | | 10 | 1.99E+01 | 1.81E+07 | 1.50E+07 | 39.72 |
| 16 | | 10 | 1.58E+01 | 1.62E+07 | 1.38E+07 | 40.35 |
| 17 | | 10 | 1.26E+01 | 1.46E+07 | 1.26E+07 | 40.97 |
| 18 | | 10 | 9.98E+00 | 1.30E+07 | 1.15E+07 | 41.6 |
| 19 | | 10 | 7.92E+00 | 1.16E+07 | 1.05E+07 | 42.23 |
| 20 | | 10 | 6.30E+00 | 1.03E+07 | 9.56E+06 | 42.88 |
| 21 | | 10 | 5.00E+00 | 9.15E+06 | 8.69E+06 | 43.51 |
| 22 | | 10 | 3.97E+00 | 8.10E+06 | 7.86E+06 | 44.15 |
| 23 | | 10 | 3.16E+00 | 7.19E+06 | 7.14E+06 | 44.78 |
| 24 | | 10 | 2.51E+00 | 6.38E+06 | 6.46E+06 | 45.39 |
| 25 | | 10 | 1.99E+00 | 5.64E+06 | 5.84E+06 | 46.01 |
| 26 | | 10 | 1.58E+00 | 4.96E+06 | 5.26E+06 | 46.66 |
| 27 | | 10 | 1.26E+00 | 4.35E+06 | 4.71E+06 | 47.31 |
| 28 | | 10 | 9.98E-01 | 3.81E+06 | 4.22E+06 | 47.95 |
| 29 | | 10 | 7.92E-01 | 3.33E+06 | 3.77E+06 | 48.61 |
| 30 | | 10 | 6.30E-01 | 2.93E+06 | 3.39E+06 | 49.21 |
| 31 | | 10 | 5.00E-01 | 2.55E+06 | 3.03E+06 | 49.84 |

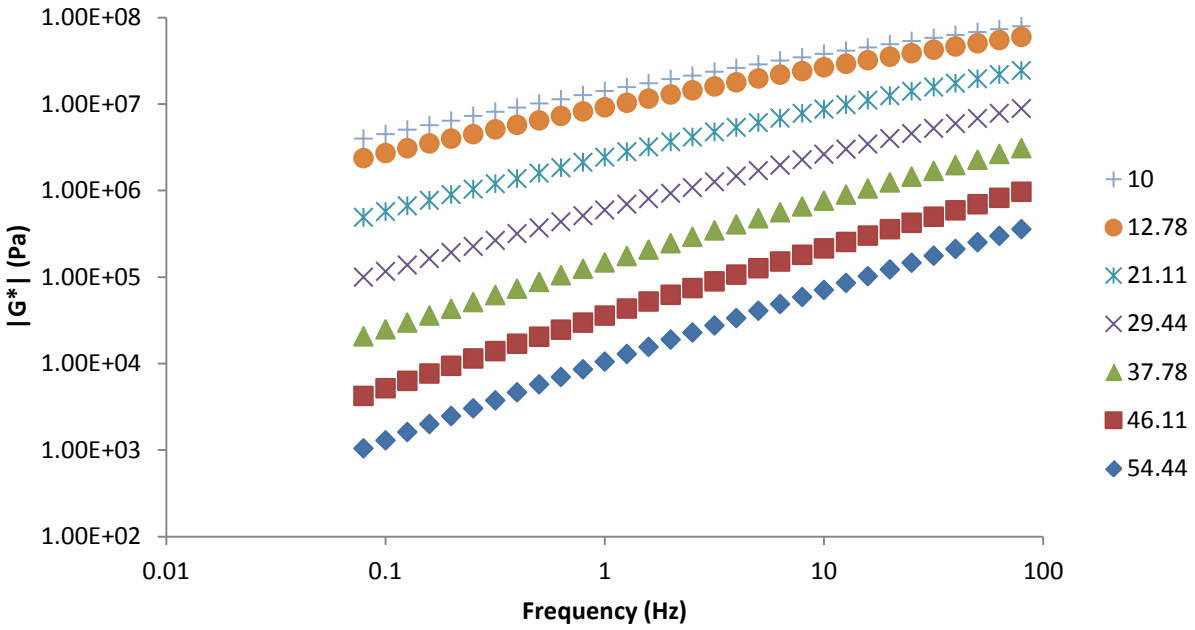


Figure G. 49: |G*| test results PG 64-22

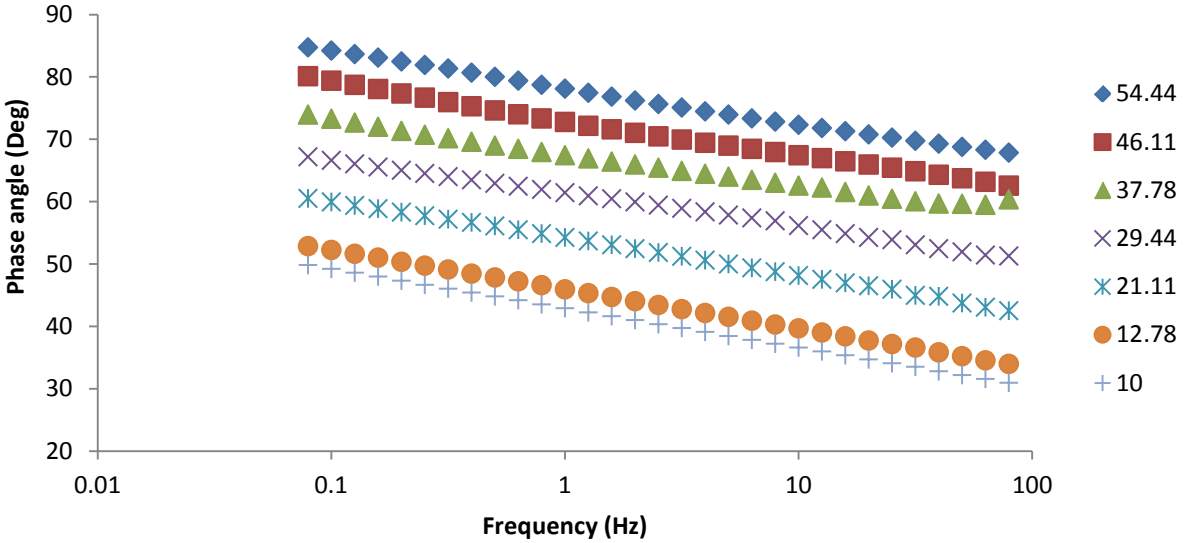


Figure G. 50: Phase angle test results PG 64-22

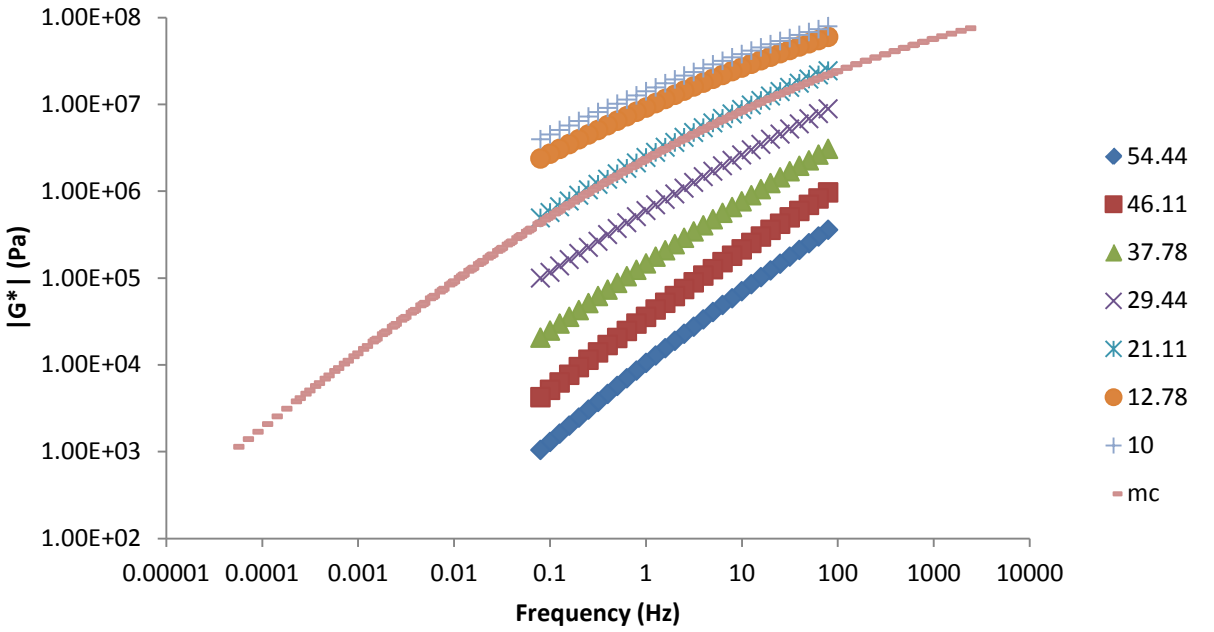


Figure G. 51: G* mastercurve for PG 64-22

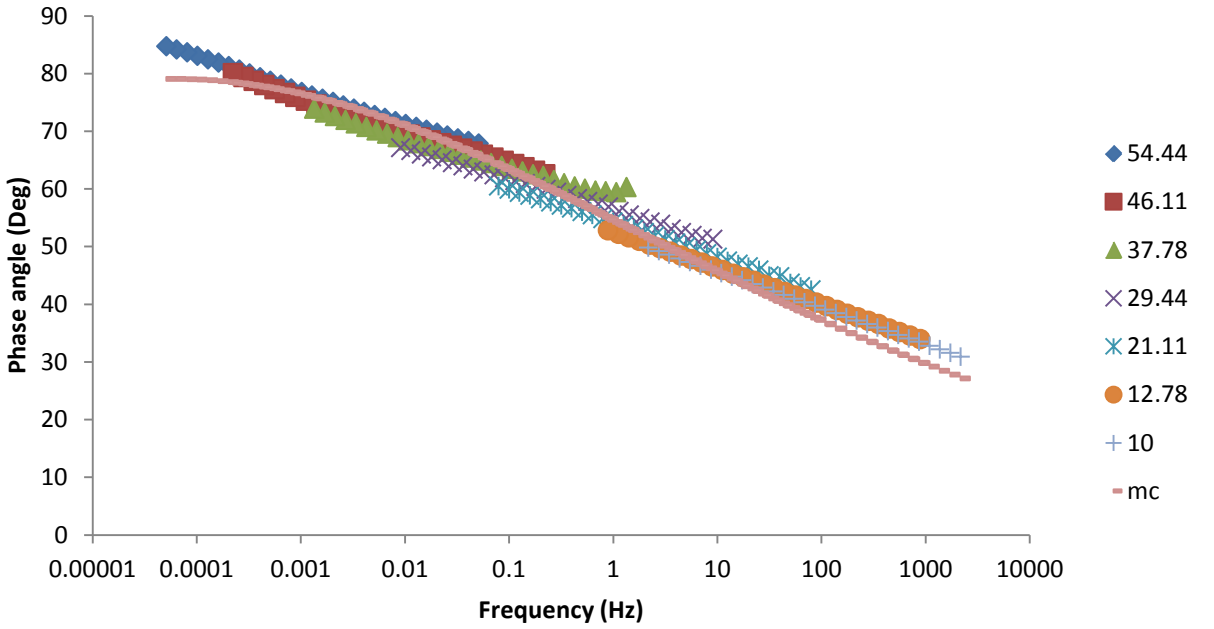


Figure G. 52: Phase angle mastercurve for PG 64-22

Table G. 32: DSR test result PG 70-22 at 54 ºC

| Meas. Pts. | Binder Grade | Temperature | Angular Frequency | Storage Modulus | Loss Modulus | Phase Angle |
|---|---|---|---|---|---|---|
| | | ºC | [rad/s] | [Pa] | [Pa] | [°] |
| 1 | PG 70-22 | 54.44 | 5.00E+02 | 6.78E+04 | 1.58E+05 | 66.81 |
| 2 | | 54.44 | 3.97E+02 | 5.69E+04 | 1.33E+05 | 66.78 |
| 3 | | 54.44 | 3.16E+02 | 4.74E+04 | 1.11E+05 | 66.89 |
| 4 | | 54.44 | 2.51E+02 | 3.96E+04 | 9.29E+04 | 66.9 |
| 5 | | 54.44 | 1.99E+02 | 3.31E+04 | 7.79E+04 | 66.96 |
| 6 | | 54.44 | 1.58E+02 | 2.78E+04 | 6.54E+04 | 67 |
| 7 | | 54.44 | 1.26E+02 | 2.33E+04 | 5.51E+04 | 67.07 |
| 8 | | 54.44 | 9.98E+01 | 1.92E+04 | 4.68E+04 | 67.66 |
| 9 | | 54.44 | 7.92E+01 | 1.63E+04 | 3.94E+04 | 67.54 |
| 10 | | 54.44 | 6.30E+01 | 1.39E+04 | 3.33E+04 | 67.36 |
| 11 | | 54.44 | 5.00E+01 | 1.18E+04 | 2.79E+04 | 67.12 |
| 12 | | 54.44 | 3.97E+01 | 1.00E+04 | 2.35E+04 | 66.96 |
| 13 | | 54.44 | 3.16E+01 | 8.46E+03 | 1.98E+04 | 66.85 |
| 14 | | 54.44 | 2.51E+01 | 7.13E+03 | 1.66E+04 | 66.76 |
| 15 | | 54.44 | 1.99E+01 | 6.02E+03 | 1.40E+04 | 66.75 |
| 16 | | 54.44 | 1.58E+01 | 5.08E+03 | 1.18E+04 | 66.77 |
| 17 | | 54.44 | 1.26E+01 | 4.28E+03 | 9.98E+03 | 66.8 |
| 18 | | 54.44 | 9.98E+00 | 3.61E+03 | 8.44E+03 | 66.86 |
| 19 | | 54.44 | 7.92E+00 | 3.03E+03 | 7.11E+03 | 66.95 |
| 20 | | 54.44 | 6.30E+00 | 2.54E+03 | 6.00E+03 | 67.05 |
| 21 | | 54.44 | 5.00E+00 | 2.14E+03 | 5.08E+03 | 67.18 |
| 22 | | 54.44 | 3.97E+00 | 1.78E+03 | 4.27E+03 | 67.36 |
| 23 | | 54.44 | 3.16E+00 | 1.49E+03 | 3.61E+03 | 67.54 |
| 24 | | 54.44 | 2.51E+00 | 1.25E+03 | 3.05E+03 | 67.78 |
| 25 | | 54.44 | 1.99E+00 | 1.04E+03 | 2.57E+03 | 68.01 |
| 26 | | 54.44 | 1.58E+00 | 8.60E+02 | 2.16E+03 | 68.33 |
| 27 | | 54.44 | 1.26E+00 | 7.14E+02 | 1.83E+03 | 68.65 |
| 28 | | 54.44 | 9.98E-01 | 5.90E+02 | 1.54E+03 | 68.99 |
| 29 | | 54.44 | 7.92E-01 | 4.88E+02 | 1.29E+03 | 69.34 |
| 30 | | 54.44 | 6.30E-01 | 4.00E+02 | 1.09E+03 | 69.8 |
| 31 | | 54.44 | 5.00E-01 | 3.26E+02 | 9.10E+02 | 70.27 |

Table G. 33: DSR test result PG 70-22 at 46 ºC

| Meas. Pts. | Binder Grade | Temperature ºC | Angular Frequency [rad/s] | Storage Modulus [Pa] | Loss Modulus [Pa] | Phase Angle [°] |
|---|---|---|---|---|---|---|
| 1 | PG 70-22 | 46.11 | 5.00E+02 | 1.83E+05 | 4.05E+05 | 65.65 |
| 2 | | 46.11 | 3.97E+02 | 1.55E+05 | 3.42E+05 | 65.65 |
| 3 | | 46.11 | 3.16E+02 | 1.30E+05 | 2.89E+05 | 65.7 |
| 4 | | 46.11 | 2.51E+02 | 1.10E+05 | 2.43E+05 | 65.74 |
| 5 | | 46.11 | 1.99E+02 | 9.27E+04 | 2.06E+05 | 65.79 |
| 6 | | 46.11 | 1.58E+02 | 7.82E+04 | 1.74E+05 | 65.82 |
| 7 | | 46.11 | 1.26E+02 | 6.59E+04 | 1.47E+05 | 65.83 |
| 8 | | 46.11 | 9.98E+01 | 5.56E+04 | 1.24E+05 | 65.84 |
| 9 | | 46.11 | 7.92E+01 | 4.70E+04 | 1.05E+05 | 65.83 |
| 10 | | 46.11 | 6.30E+01 | 3.98E+04 | 8.85E+04 | 65.8 |
| 11 | | 46.11 | 5.00E+01 | 3.37E+04 | 7.49E+04 | 65.76 |
| 12 | | 46.11 | 3.97E+01 | 2.85E+04 | 6.31E+04 | 65.71 |
| 13 | | 46.11 | 3.16E+01 | 2.41E+04 | 5.33E+04 | 65.66 |
| 14 | | 46.11 | 2.51E+01 | 2.05E+04 | 4.52E+04 | 65.63 |
| 15 | | 46.11 | 1.99E+01 | 1.73E+04 | 3.81E+04 | 65.55 |
| 16 | | 46.11 | 1.58E+01 | 1.46E+04 | 3.21E+04 | 65.5 |
| 17 | | 46.11 | 1.26E+01 | 1.24E+04 | 2.72E+04 | 65.45 |
| 18 | | 46.11 | 9.98E+00 | 1.05E+04 | 2.30E+04 | 65.41 |
| 19 | | 46.11 | 7.92E+00 | 8.89E+03 | 1.94E+04 | 65.39 |
| 20 | | 46.11 | 6.30E+00 | 7.53E+03 | 1.64E+04 | 65.38 |
| 21 | | 46.11 | 5.00E+00 | 6.39E+03 | 1.39E+04 | 65.38 |
| 22 | | 46.11 | 3.97E+00 | 5.40E+03 | 1.18E+04 | 65.4 |
| 23 | | 46.11 | 3.16E+00 | 4.55E+03 | 9.96E+03 | 65.43 |
| 24 | | 46.11 | 2.51E+00 | 3.83E+03 | 8.41E+03 | 65.5 |
| 25 | | 46.11 | 1.99E+00 | 3.25E+03 | 7.14E+03 | 65.57 |
| 26 | | 46.11 | 1.58E+00 | 2.74E+03 | 6.06E+03 | 65.69 |
| 27 | | 46.11 | 1.26E+00 | 2.32E+03 | 5.15E+03 | 65.81 |
| 28 | | 46.11 | 9.98E-01 | 1.95E+03 | 4.37E+03 | 65.92 |
| 29 | | 46.11 | 7.92E-01 | 1.64E+03 | 3.71E+03 | 66.08 |
| 30 | | 46.11 | 6.30E-01 | 1.38E+03 | 3.14E+03 | 66.32 |
| 31 | | 46.11 | 5.00E-01 | 1.15E+03 | 2.65E+03 | 66.58 |

Table G. 34: DSR test result PG 70-22 at 37 ºC

| Meas. Pts. | Binder Grade | Temperature | Angular Frequency | Storage Modulus | Loss Modulus | Phase Angle |
|---|---|---|---|---|---|---|
| | | ºC | [rad/s] | [Pa] | [Pa] | [°] |
| 1 | PG 70-22 | 37.78 | 5.00E+02 | 5.84E+05 | 1.40E+06 | 67.3 |
| 2 | | 37.78 | 3.97E+02 | 5.56E+05 | 1.17E+06 | 64.55 |
| 3 | | 37.78 | 3.16E+02 | 4.79E+05 | 9.84E+05 | 64.04 |
| 4 | | 37.78 | 2.51E+02 | 4.14E+05 | 8.29E+05 | 63.47 |
| 5 | | 37.78 | 1.99E+02 | 3.53E+05 | 7.01E+05 | 63.3 |
| 6 | | 37.78 | 1.58E+02 | 2.99E+05 | 5.95E+05 | 63.31 |
| 7 | | 37.78 | 1.26E+02 | 2.55E+05 | 5.09E+05 | 63.37 |
| 8 | | 37.78 | 9.98E+01 | 2.15E+05 | 4.31E+05 | 63.53 |
| 9 | | 37.78 | 7.92E+01 | 1.83E+05 | 3.70E+05 | 63.67 |
| 10 | | 37.78 | 6.30E+01 | 1.55E+05 | 3.15E+05 | 63.83 |
| 11 | | 37.78 | 5.00E+01 | 1.31E+05 | 2.68E+05 | 63.92 |
| 12 | | 37.78 | 3.97E+01 | 1.10E+05 | 2.27E+05 | 64.01 |
| 13 | | 37.78 | 3.16E+01 | 9.31E+04 | 1.92E+05 | 64.09 |
| 14 | | 37.78 | 2.51E+01 | 7.89E+04 | 1.63E+05 | 64.14 |
| 15 | | 37.78 | 1.99E+01 | 6.68E+04 | 1.38E+05 | 64.17 |
| 16 | | 37.78 | 1.58E+01 | 5.65E+04 | 1.17E+05 | 64.2 |
| 17 | | 37.78 | 1.26E+01 | 4.78E+04 | 9.89E+04 | 64.22 |
| 18 | | 37.78 | 9.98E+00 | 4.06E+04 | 8.40E+04 | 64.2 |
| 19 | | 37.78 | 7.92E+00 | 3.44E+04 | 7.10E+04 | 64.17 |
| 20 | | 37.78 | 6.30E+00 | 2.93E+04 | 6.03E+04 | 64.13 |
| 21 | | 37.78 | 5.00E+00 | 2.49E+04 | 5.13E+04 | 64.09 |
| 22 | | 37.78 | 3.97E+00 | 2.13E+04 | 4.37E+04 | 64.05 |
| 23 | | 37.78 | 3.16E+00 | 1.80E+04 | 3.70E+04 | 64.02 |
| 24 | | 37.78 | 2.51E+00 | 1.51E+04 | 3.10E+04 | 64.01 |
| 25 | | 37.78 | 1.99E+00 | 1.28E+04 | 2.62E+04 | 63.98 |
| 26 | | 37.78 | 1.58E+00 | 1.09E+04 | 2.23E+04 | 63.94 |
| 27 | | 37.78 | 1.26E+00 | 9.37E+03 | 1.91E+04 | 63.92 |
| 28 | | 37.78 | 9.98E-01 | 8.05E+03 | 1.64E+04 | 63.93 |
| 29 | | 37.78 | 7.92E-01 | 6.88E+03 | 1.41E+04 | 63.92 |
| 30 | | 37.78 | 6.30E-01 | 5.85E+03 | 1.20E+04 | 63.95 |
| 31 | | 37.78 | 5.00E-01 | 4.87E+03 | 1.00E+04 | 64.04 |

Table G. 35: DSR test result PG 70-22 at 29 ºC

| Meas. Pts. | Binder Grade | Temperature ºC | Angular Frequency [rad/s] | Storage Modulus [Pa] | Loss Modulus [Pa] | Phase Angle [°] |
|---|---|---|---|---|---|---|
| 1 | PG 70-22 | 29.44 | 5.00E+02 | 2.38E+06 | 3.76E+06 | 57.69 |
| 2 | | 29.44 | 3.97E+02 | 2.10E+06 | 3.25E+06 | 57.13 |
| 3 | | 29.44 | 3.16E+02 | 1.80E+06 | 2.81E+06 | 57.37 |
| 4 | | 29.44 | 2.51E+02 | 1.55E+06 | 2.44E+06 | 57.56 |
| 5 | | 29.44 | 1.99E+02 | 1.33E+06 | 2.12E+06 | 57.88 |
| 6 | | 29.44 | 1.58E+02 | 1.13E+06 | 1.83E+06 | 58.29 |
| 7 | | 29.44 | 1.26E+02 | 9.61E+05 | 1.58E+06 | 58.71 |
| 8 | | 29.44 | 9.98E+01 | 8.11E+05 | 1.37E+06 | 59.35 |
| 9 | | 29.44 | 7.92E+01 | 6.92E+05 | 1.18E+06 | 59.52 |
| 10 | | 29.44 | 6.30E+01 | 5.87E+05 | 1.01E+06 | 59.89 |
| 11 | | 29.44 | 5.00E+01 | 5.00E+05 | 8.73E+05 | 60.23 |
| 12 | | 29.44 | 3.97E+01 | 4.25E+05 | 7.52E+05 | 60.55 |
| 13 | | 29.44 | 3.16E+01 | 3.60E+05 | 6.45E+05 | 60.85 |
| 14 | | 29.44 | 2.51E+01 | 3.05E+05 | 5.52E+05 | 61.12 |
| 15 | | 29.44 | 1.99E+01 | 2.59E+05 | 4.75E+05 | 61.36 |
| 16 | | 29.44 | 1.58E+01 | 2.20E+05 | 4.06E+05 | 61.59 |
| 17 | | 29.44 | 1.26E+01 | 1.86E+05 | 3.46E+05 | 61.77 |
| 18 | | 29.44 | 9.98E+00 | 1.58E+05 | 2.96E+05 | 61.93 |
| 19 | | 29.44 | 7.92E+00 | 1.34E+05 | 2.52E+05 | 62.07 |
| 20 | | 29.44 | 6.30E+00 | 1.14E+05 | 2.15E+05 | 62.19 |
| 21 | | 29.44 | 5.00E+00 | 9.67E+04 | 1.84E+05 | 62.28 |
| 22 | | 29.44 | 3.97E+00 | 8.23E+04 | 1.57E+05 | 62.34 |
| 23 | | 29.44 | 3.16E+00 | 7.00E+04 | 1.34E+05 | 62.41 |
| 24 | | 29.44 | 2.51E+00 | 5.94E+04 | 1.14E+05 | 62.45 |
| 25 | | 29.44 | 1.99E+00 | 5.07E+04 | 9.73E+04 | 62.48 |
| 26 | | 29.44 | 1.58E+00 | 4.33E+04 | 8.31E+04 | 62.48 |
| 27 | | 29.44 | 1.26E+00 | 3.68E+04 | 7.08E+04 | 62.5 |
| 28 | | 29.44 | 9.98E-01 | 3.20E+04 | 6.14E+04 | 62.48 |
| 29 | | 29.44 | 7.92E-01 | 2.70E+04 | 5.18E+04 | 62.48 |
| 30 | | 29.44 | 6.30E-01 | 2.27E+04 | 4.35E+04 | 62.44 |
| 31 | | 29.44 | 5.00E-01 | 1.93E+04 | 3.70E+04 | 62.42 |

Table G. 36: DSR test result PG 70-22 at 21 ºC

| Meas. Pts. | Binder Grade | Temperature | Angular Frequency | Storage Modulus | Loss Modulus | Phase Angle |
|---|---|---|---|---|---|---|
| | | ºC | [rad/s] | [Pa] | [Pa] | [°] |
| 1 | PG 70-22 | 21.11 | 5.00E+02 | 8.39E+06 | 9.64E+06 | 48.95 |
| 2 | | 21.11 | 3.97E+02 | 7.43E+06 | 8.62E+06 | 49.24 |
| 3 | | 21.11 | 3.16E+02 | 6.49E+06 | 7.68E+06 | 49.78 |
| 4 | | 21.11 | 2.51E+02 | 5.66E+06 | 6.82E+06 | 50.32 |
| 5 | | 21.11 | 1.99E+02 | 4.94E+06 | 6.08E+06 | 50.93 |
| 6 | | 21.11 | 1.58E+02 | 4.30E+06 | 5.40E+06 | 51.48 |
| 7 | | 21.11 | 1.26E+02 | 3.73E+06 | 4.78E+06 | 52.04 |
| 8 | | 21.11 | 9.98E+01 | 3.22E+06 | 4.23E+06 | 52.67 |
| 9 | | 21.11 | 7.92E+01 | 2.77E+06 | 3.75E+06 | 53.58 |
| 10 | | 21.11 | 6.30E+01 | 2.40E+06 | 3.31E+06 | 54.04 |
| 11 | | 21.11 | 5.00E+01 | 2.08E+06 | 2.91E+06 | 54.45 |
| 12 | | 21.11 | 3.97E+01 | 1.79E+06 | 2.54E+06 | 54.89 |
| 13 | | 21.11 | 3.16E+01 | 1.53E+06 | 2.22E+06 | 55.36 |
| 14 | | 21.11 | 2.51E+01 | 1.32E+06 | 1.94E+06 | 55.82 |
| 15 | | 21.11 | 1.99E+01 | 1.12E+06 | 1.68E+06 | 56.29 |
| 16 | | 21.11 | 1.58E+01 | 9.55E+05 | 1.46E+06 | 56.77 |
| 17 | | 21.11 | 1.26E+01 | 8.09E+05 | 1.26E+06 | 57.23 |
| 18 | | 21.11 | 9.98E+00 | 6.86E+05 | 1.08E+06 | 57.67 |
| 19 | | 21.11 | 7.92E+00 | 5.88E+05 | 9.42E+05 | 58.04 |
| 20 | | 21.11 | 6.30E+00 | 5.04E+05 | 8.19E+05 | 58.39 |
| 21 | | 21.11 | 5.00E+00 | 4.30E+05 | 7.07E+05 | 58.73 |
| 22 | | 21.11 | 3.97E+00 | 3.64E+05 | 6.07E+05 | 59.06 |
| 23 | | 21.11 | 3.16E+00 | 3.08E+05 | 5.20E+05 | 59.38 |
| 24 | | 21.11 | 2.51E+00 | 2.64E+05 | 4.51E+05 | 59.63 |
| 25 | | 21.11 | 1.99E+00 | 2.28E+05 | 3.92E+05 | 59.86 |
| 26 | | 21.11 | 1.58E+00 | 1.95E+05 | 3.38E+05 | 60.04 |
| 27 | | 21.11 | 1.26E+00 | 1.66E+05 | 2.91E+05 | 60.22 |
| 28 | | 21.11 | 9.98E-01 | 1.42E+05 | 2.50E+05 | 60.43 |
| 29 | | 21.11 | 7.92E-01 | 1.22E+05 | 2.16E+05 | 60.59 |
| 30 | | 21.11 | 6.30E-01 | 1.03E+05 | 1.83E+05 | 60.7 |
| 31 | | 21.11 | 5.00E-01 | 8.72E+04 | 1.56E+05 | 60.82 |

Table G. 37: DSR test result PG 70-22 at 12 ºC

| Meas. Pts. | Binder Grade | Temperature ºC | Angular Frequency [rad/s] | Storage Modulus [Pa] | Loss Modulus [Pa] | Phase Angle [°] |
|---|---|---|---|---|---|---|
| 1 | PG 70-22 | 12.78 | 5.00E+02 | 2.74E+07 | 2.27E+07 | 39.65 |
| 2 | | 12.78 | 3.97E+02 | 2.46E+07 | 2.08E+07 | 40.29 |
| 3 | | 12.78 | 3.16E+02 | 2.19E+07 | 1.91E+07 | 41.06 |
| 4 | | 12.78 | 2.51E+02 | 1.96E+07 | 1.74E+07 | 41.58 |
| 5 | | 12.78 | 1.99E+02 | 1.75E+07 | 1.59E+07 | 42.28 |
| 6 | | 12.78 | 1.58E+02 | 1.56E+07 | 1.45E+07 | 43.07 |
| 7 | | 12.78 | 1.26E+02 | 1.39E+07 | 1.32E+07 | 43.54 |
| 8 | | 12.78 | 9.98E+01 | 1.23E+07 | 1.20E+07 | 44.15 |
| 9 | | 12.78 | 7.92E+01 | 1.09E+07 | 1.08E+07 | 44.77 |
| 10 | | 12.78 | 6.30E+01 | 9.72E+06 | 9.84E+06 | 45.37 |
| 11 | | 12.78 | 5.00E+01 | 8.62E+06 | 8.92E+06 | 45.97 |
| 12 | | 12.78 | 3.97E+01 | 7.63E+06 | 8.06E+06 | 46.56 |
| 13 | | 12.78 | 3.16E+01 | 6.69E+06 | 7.22E+06 | 47.2 |
| 14 | | 12.78 | 2.51E+01 | 5.84E+06 | 6.45E+06 | 47.84 |
| 15 | | 12.78 | 1.99E+01 | 5.09E+06 | 5.75E+06 | 48.47 |
| 16 | | 12.78 | 1.58E+01 | 4.46E+06 | 5.14E+06 | 49.06 |
| 17 | | 12.78 | 1.26E+01 | 3.90E+06 | 4.59E+06 | 49.64 |
| 18 | | 12.78 | 9.98E+00 | 3.39E+06 | 4.08E+06 | 50.24 |
| 19 | | 12.78 | 7.92E+00 | 2.96E+06 | 3.63E+06 | 50.8 |
| 20 | | 12.78 | 6.30E+00 | 2.56E+06 | 3.20E+06 | 51.38 |
| 21 | | 12.78 | 5.00E+00 | 2.21E+06 | 2.82E+06 | 51.95 |
| 22 | | 12.78 | 3.97E+00 | 1.90E+06 | 2.48E+06 | 52.52 |
| 23 | | 12.78 | 3.16E+00 | 1.64E+06 | 2.18E+06 | 53.04 |
| 24 | | 12.78 | 2.51E+00 | 1.43E+06 | 1.93E+06 | 53.55 |
| 25 | | 12.78 | 1.99E+00 | 1.24E+06 | 1.71E+06 | 53.99 |
| 26 | | 12.78 | 1.58E+00 | 1.06E+06 | 1.49E+06 | 54.51 |
| 27 | | 12.78 | 1.26E+00 | 9.08E+05 | 1.30E+06 | 55 |
| 28 | | 12.78 | 9.98E-01 | 7.89E+05 | 1.14E+06 | 55.41 |
| 29 | | 12.78 | 7.92E-01 | 6.70E+05 | 9.88E+05 | 55.83 |
| 30 | | 12.78 | 6.30E-01 | 5.75E+05 | 8.62E+05 | 56.3 |
| 31 | | 12.78 | 5.00E-01 | 4.97E+05 | 7.56E+05 | 56.69 |

Table G. 38: DSR test result PG 70-22 at 10 ºC

| Meas. Pts. | Binder Grade | Temperature ºC | Angular Frequency [rad/s] | Storage Modulus [Pa] | Loss Modulus [Pa] | Phase Angle [°] |
|---|---|---|---|---|---|---|
| 1 | PG 70-22 | 10 | 5.00E+02 | 3.84E+07 | 2.87E+07 | 36.76 |
| 2 | | 10 | 3.97E+02 | 3.47E+07 | 2.66E+07 | 37.42 |
| 3 | | 10 | 3.16E+02 | 3.14E+07 | 2.46E+07 | 38.03 |
| 4 | | 10 | 2.51E+02 | 2.83E+07 | 2.27E+07 | 38.69 |
| 5 | | 10 | 1.99E+02 | 2.54E+07 | 2.09E+07 | 39.52 |
| 6 | | 10 | 1.58E+02 | 2.29E+07 | 1.93E+07 | 40.13 |
| 7 | | 10 | 1.26E+02 | 2.05E+07 | 1.76E+07 | 40.65 |
| 8 | | 10 | 9.98E+01 | 1.85E+07 | 1.62E+07 | 41.27 |
| 9 | | 10 | 7.92E+01 | 1.65E+07 | 1.48E+07 | 41.92 |
| 10 | | 10 | 6.30E+01 | 1.47E+07 | 1.35E+07 | 42.56 |
| 11 | | 10 | 5.00E+01 | 1.31E+07 | 1.23E+07 | 43.2 |
| 12 | | 10 | 3.97E+01 | 1.16E+07 | 1.12E+07 | 43.83 |
| 13 | | 10 | 3.16E+01 | 1.03E+07 | 1.01E+07 | 44.47 |
| 14 | | 10 | 2.51E+01 | 9.10E+06 | 9.13E+06 | 45.11 |
| 15 | | 10 | 1.99E+01 | 8.05E+06 | 8.25E+06 | 45.72 |
| 16 | | 10 | 1.58E+01 | 7.08E+06 | 7.43E+06 | 46.35 |
| 17 | | 10 | 1.26E+01 | 6.23E+06 | 6.68E+06 | 46.97 |
| 18 | | 10 | 9.98E+00 | 5.48E+06 | 6.00E+06 | 47.58 |
| 19 | | 10 | 7.92E+00 | 4.80E+06 | 5.36E+06 | 48.19 |
| 20 | | 10 | 6.30E+00 | 4.20E+06 | 4.80E+06 | 48.78 |
| 21 | | 10 | 5.00E+00 | 3.69E+06 | 4.29E+06 | 49.35 |
| 22 | | 10 | 3.97E+00 | 3.21E+06 | 3.82E+06 | 49.94 |
| 23 | | 10 | 3.16E+00 | 2.79E+06 | 3.39E+06 | 50.51 |
| 24 | | 10 | 2.51E+00 | 2.42E+06 | 3.00E+06 | 51.1 |
| 25 | | 10 | 1.99E+00 | 2.10E+06 | 2.66E+06 | 51.64 |
| 26 | | 10 | 1.58E+00 | 1.82E+06 | 2.34E+06 | 52.18 |
| 27 | | 10 | 1.26E+00 | 1.58E+06 | 2.07E+06 | 52.7 |
| 28 | | 10 | 9.98E-01 | 1.36E+06 | 1.82E+06 | 53.24 |
| 29 | | 10 | 7.92E-01 | 1.18E+06 | 1.60E+06 | 53.75 |
| 30 | | 10 | 6.30E-01 | 1.02E+06 | 1.42E+06 | 54.23 |
| 31 | | 10 | 5.00E-01 | 8.78E+05 | 1.24E+06 | 54.7 |

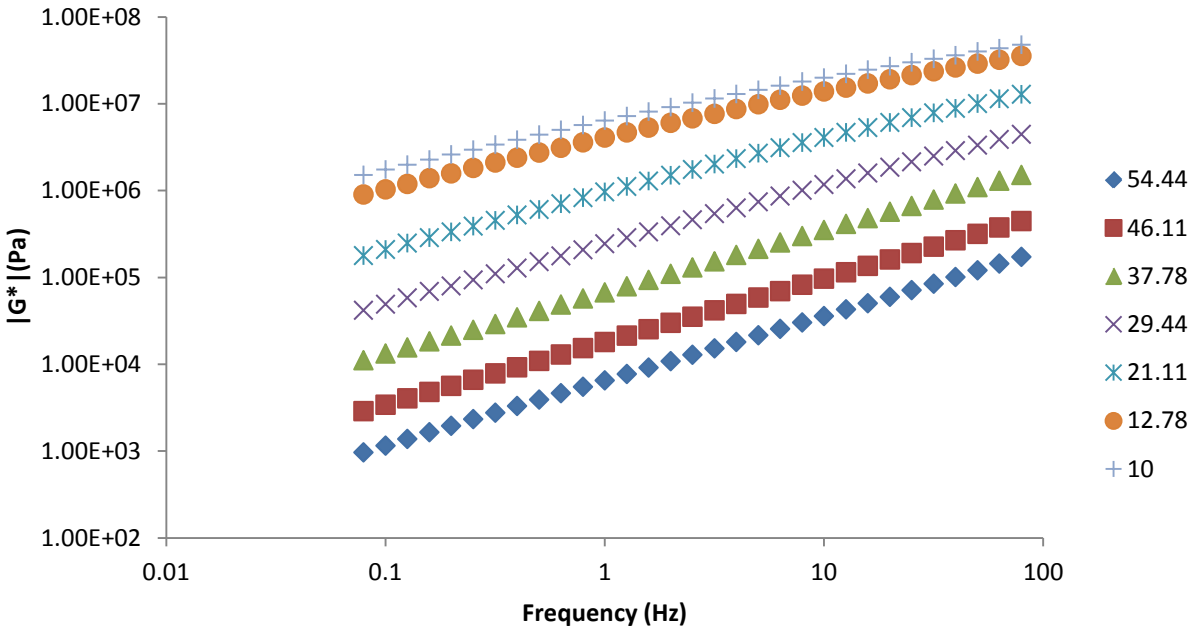


Figure G. 53: G* test result for PG 70-22

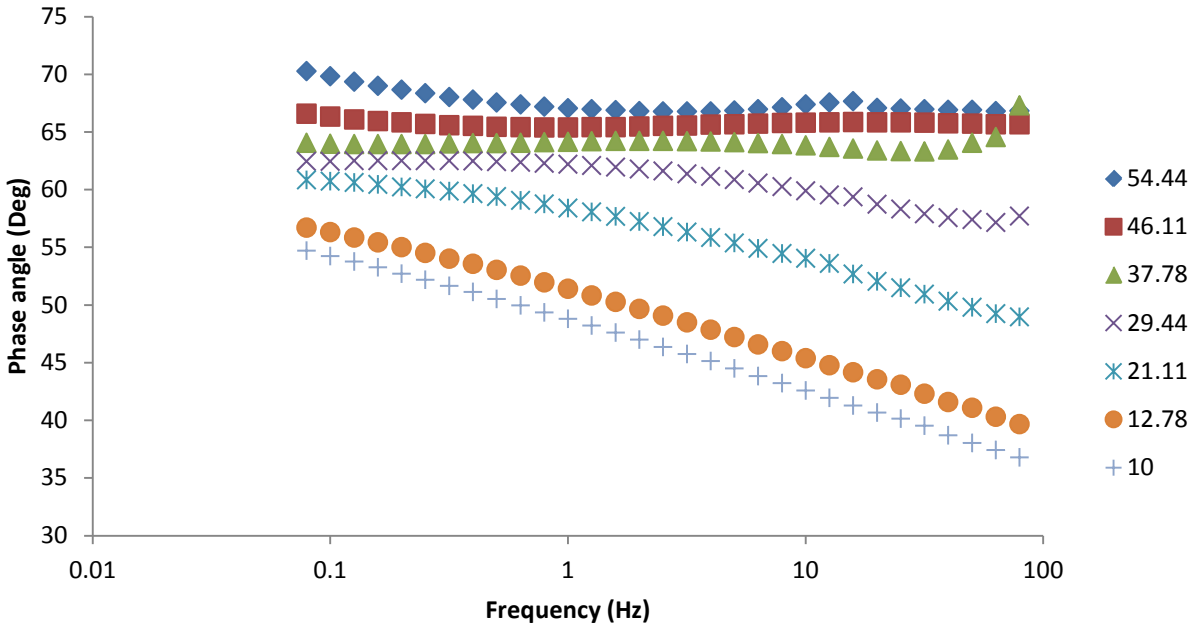


Figure G. 54: phase angle result for PG 70-22

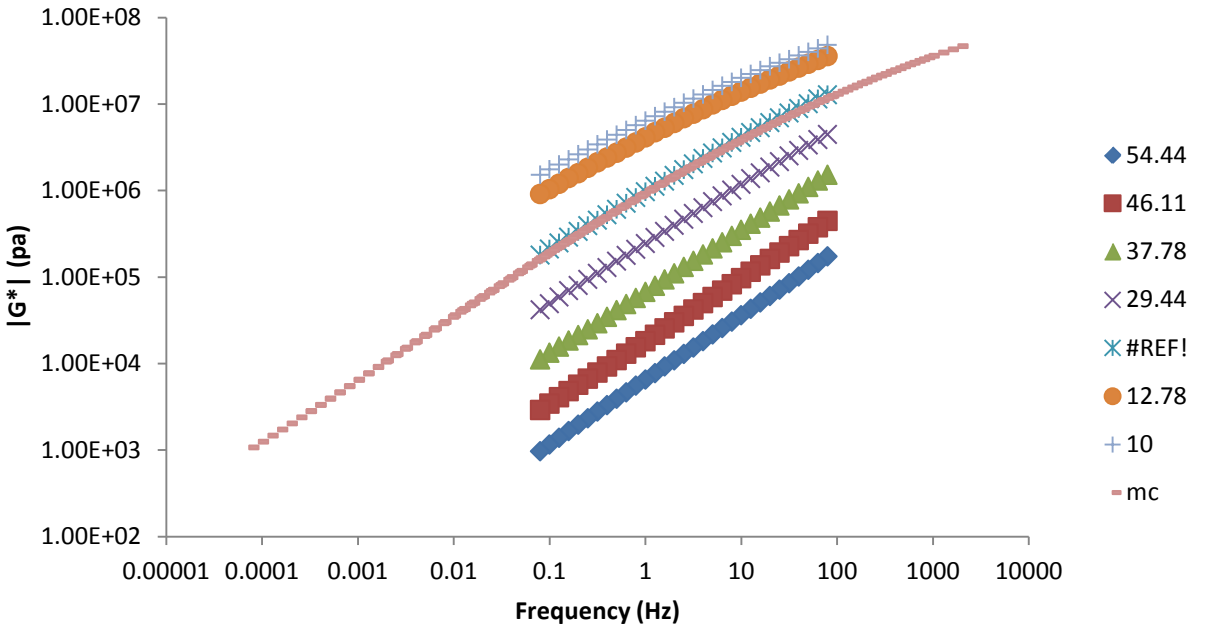


Figure G. 55: G* mastercurve PG 70-22

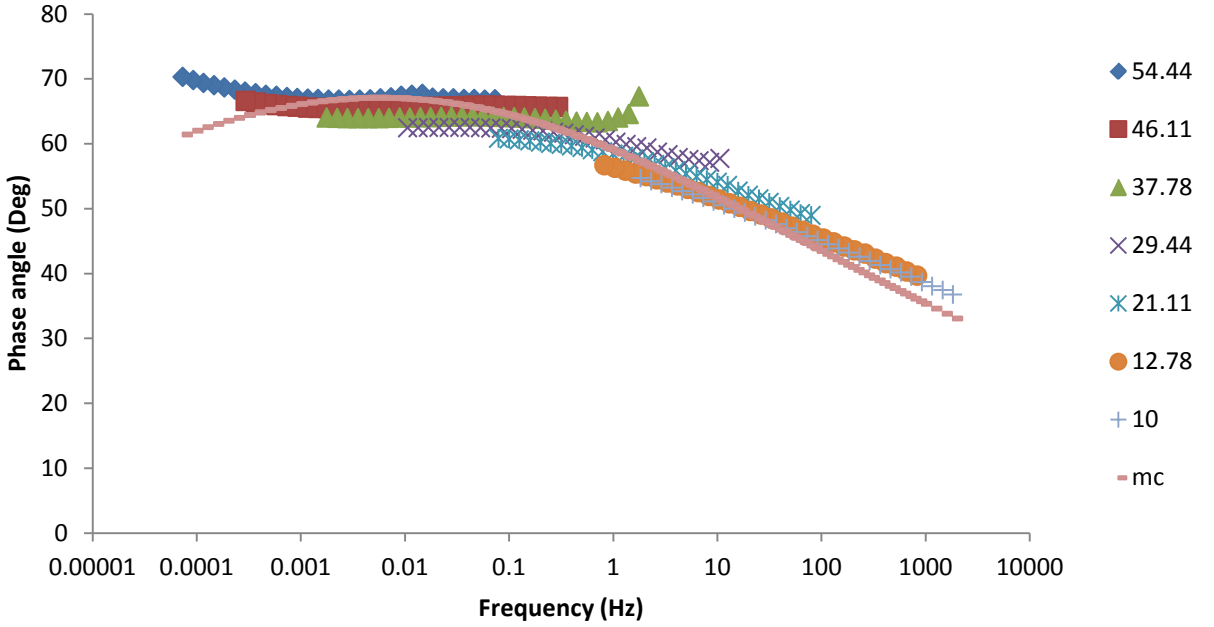


Figure G. 56: Phase angle mastercurve for PG 70-22